Mémoires de Géologie (Lausanne) No. 24, 1994

Three-dimensional sequence stratigraphy offshore Louisiana, Gulf of Mexico (West Cameron 3D seismic data)

by Benoît Reymond

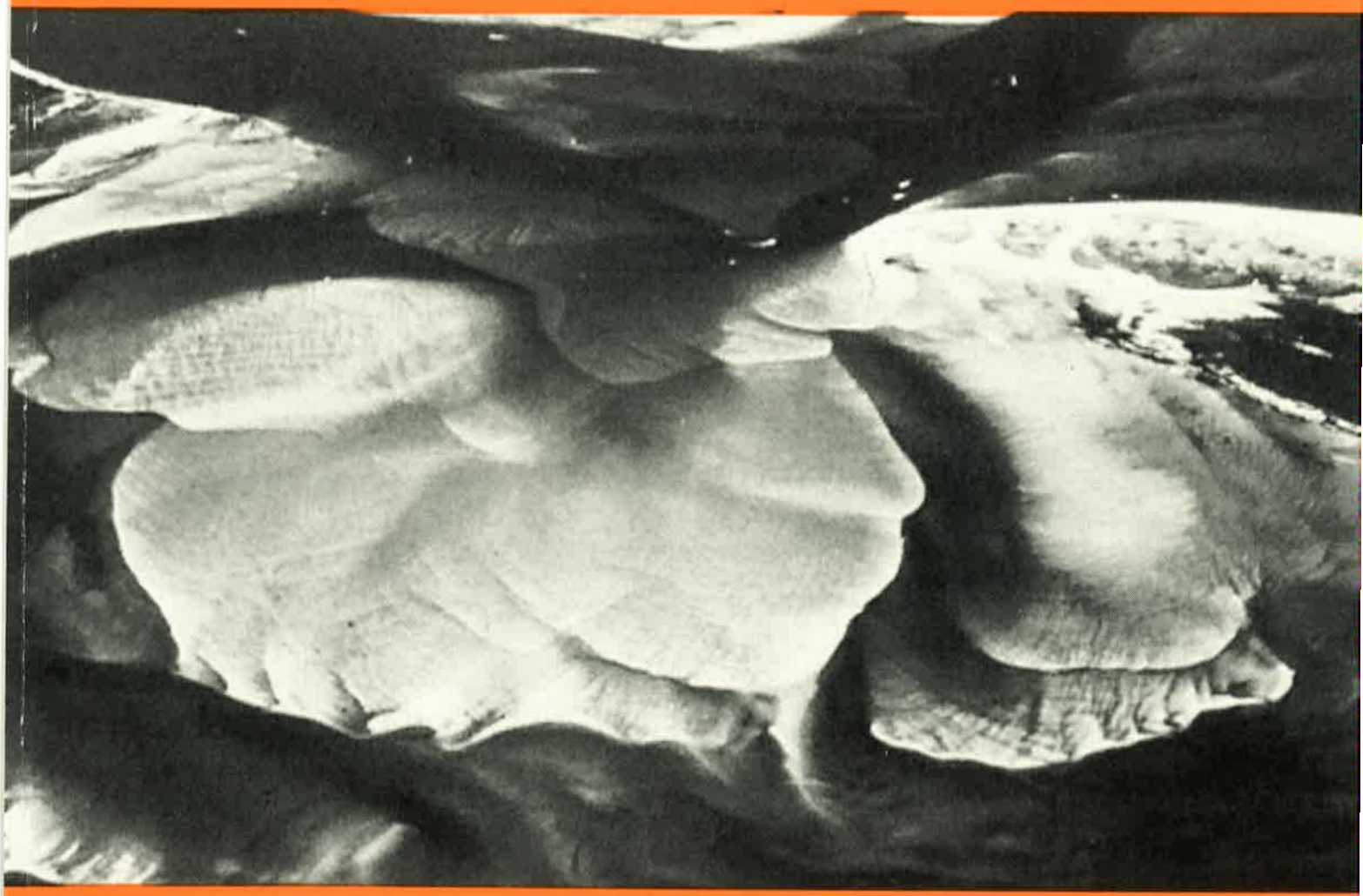

IMPRIVITE S.A., LAUSANNE

ISSN 1015-3578

Mémoires de Géologie (Lausanne)

Mémoires de Géologie (Lausanne)
Section des Sciences de la Terre
Institut de Géologie et Paléontologie
Université de Lausanne
BFSH-2, CH-1015 Lausanne

REYMOND, Benoît
Three-dimensional sequence stratigraphy offshore Louisiana, Gulf of Mexico (West Cameron 3D seismic data).
Mém. Géol. (Lausanne), n° 24, 1994, 215 p., 161 figs., 49 pls.

Dépôt légal: 4ème trimestre 1994
ISSN: 1015-3578

Imprimeur: Imprivite Lausanne

Cover image: A comparison of the present aspect of the flood-tidal delta of the Chatham Harbor, Massachussetts with the reconstructed horizontal sedimentary facies presented in this study. Note on this image the well-developed transverse reworked sand bars intersected by a shallow flood channel and compare them with similar bars and channels obtained on 3D horizontal seismic images of lower Pliocene sediments in figs. 5-51 and 5-52, (p. 144 -145). Compare also the flood-current dominated silty fans with highstand low angle progradation in fig. 5-39 (p. 124) and in fig. 5-21 (p. 96).
(after a photograph from Boothroyd J.C., Tidal inlets and tidal deltas. In: Richard A. Davis (Eds), Coastal and Sedimentary Environments, Spinger-Verlag, 1985).

Université de Lausanne
Faculté des Sciences

Institut de Géologie
et de Paléontologie

Three-Dimensional Sequence Stratigraphy offshore Louisiana, Gulf of Mexico (West Cameron 3D Seismic Data)

Thèse de doctorat
présentée à la Faculté des Sciences
de l'Université de Lausanne
par **Benoît REYMOND**
géologue diplômé

Jury de thèse:
Prof. Gérard Stampfli (Directeur)
Prof. Albert.W. Bally (Houston, Texas)
Prof. Henri Masson (Lausanne)
Dr. Lars Sonneland (Stavanger, Norway)

Mémoires de Géologie (Lausanne) No. 24, 1994

Table of Contents

Abstract 1
Résumé 1
Extended abstract 2
Acknowledgements 7
1. General Introduction 8
1.1 Foreword 8
1.2 Three-dimensional seismic data: history 8
1.3 This research: history and objectives 9
History 9
Objectives 10
1.4 Geographical and geological framework 11
Introduction 11
Geographical situation 11
Geological Framework 12
Cenozoic 15
Miocene 15
Pliocene 17
Plio-Pleistocene limit 17
Pleistocene 18
1.5 Summary 20
2. Sequence stratigraphy 21
2.1 Introduction 21
2.2 General concepts in sequence stratigraphy 21
2.3 From the model back to reality 26
2.4 What causes eustasy ? 28
2.5 Sea level changes: a key for future climate predictions ? 31
2.6 Summary 31
3. Well log interpretation (formation evaluation and sequential analysis) 33
3.1 Introduction 33
3.2 Well log formation evaluation: main tools 33
Spontaneous Potential (SP) 33
Natural Gamma Ray (GR) 34
Electrode resistivity tools 35
Total porosity logs (Sonic, Density, Neutron porosity logs) 35
3.3 Well log formation evaluation: paleo-water-depth 35
Introduction 35
Lithofacies and paleo-water-depth 37
3.4 Well log formation sequential analysis 37
Introduction 37
3.5 Synthetic log, velocity law and porosity curves. 30
Synthetic log 48
Velocity law 48
Porosity curves 51
3.6 Summary 52
4. Three-D seismic acquisition, interpretation methods and applications. 53
4.1 Introduction 53
4.2 Three-D seismic acquisition 53
Introduction 53
3D marine seismic: this survey, acquisition and seismic data. 53
Conclusions to 3D seismic acquisition 54
4.3 3D seismic interpretation methods 56
4.3.1 Interpretation procedure and main tools 56

4.3.2 Attributes and Maps....60
Introduction....60
a. Seismic attributes....60
b. Attribute Maps....65
c. Volume related attributes....68
Attributes and maps: conclusion....68
4.3.3 Fault interpretation and annexes to 3D seismic interpretation....69
Fault interpretation....69
Annexes to 3D seismic interpretation....71
4.4 Conclusions....71
5. THREE DIMENSIONAL SEQUENCE STRATIGRAPHY....73
5.1 Introduction....73
5.2 Upper Pleistocene (0 to SB 0.8 Ma)....76
Introduction....76
Observation....81
Conclusion....85
An additional tool....86
5.3 Lower Pleistocene (SB 0.8 to SB 1.46 Ma)....87
Introduction....87
Observation....87
HP2 interpreted horizon: a minor sequence boundary (SB 1.25) or a condensed section between SB 1.46 and SB 1.1 ?....89
Conclusion....98
5.4 Plio-Pleistocene limit (a 4th order sequence from SB1.46 to SB 1.85)....99
Introduction....99
Observation....99
Conclusion....103
Introduction to § 5.5 and § 5.6....109
5.5 SB 1.85 to SB 2.4: a large 4th order sequence....110
Introduction....110
Observation....110
Well log data....110
Vertical seismic section and amplitude maps....113
Conclusion....118
5.6 Top Gulf coast Pliocene hiatus (2.6 to 3.0 Ma)....126
Introduction....126
Observation....126
Conclusion....135
Gulf coast Pleistocene (0 to 2.8 Ma) synthesis and conclusions....135
5.7 Top Messinian lowstand and base Pliocene series....136
Introduction....136
5.7.1: Base Pliocene....137
Introduction....137
Observation....137
Conclusion....147
5.7 2: An alternative interpretation to the SB 5.5 to SB 4.2 interval....148
Introduction....148
Observation....149
Conclusion....149
5.7.3: Middle and top Pliocene hiatuses (SB 4.2 to SB 3.0 Ma)....150
Conclusion....150
5.8 Middle and Late Miocene 3rd order sequences....153
Introduction....153
Observation....153
Conclusion....154
5.9 Synthesis....161

6. THREE-D SEQUENCE STRATIGRAPHY AND THE SEARCH FOR HYDROCARBONS 163
6.1 Introduction 163
6.2 Three-D sequence stratigraphy in clastic rocks: a composite sequence 164
Conclusions 166
6.3 Application of 3D sequence stratigraphy to early Middle Miocene productive Cibicides opima sands 170
Introduction 170
Observation. 170
Conclusions 175
6.4 Summary 175

7. DEFORMATION, GROWTH FAULTS AND ASSOCIATED SEDIMENTATION 179
7.1 Salt and growth faults in the Gulf of Mexico, history 179
7.2 Deformation versus sedimentation 181
7.3 Total subsidence, relation to sedimentation and eustasy 183
Total subsidence calculation: introduction 183
Decompaction principle 183
Total subsidence versus sedimentation and eustasy. 184
Conclusion 187
Total subsidence versus local deformation and sedimentation 188
7.4 An application of 3D fault analysis to subtle potential traps 189
7.5 Conclusions 191
8. DISCUSSION AND CONCLUSIONS. 192
REFERENCES: 194
ANNEXE 1: PROCEDURE OF ROTATION OF SEISMIC DATA 202
ANNEXE 2: COMPILED TABLES AND MAPS OF BIOSTRATIGRAPHIC HORIZONS 204
ANNEXE 3: WELL LOG SEQUENTIAL INTERPRETATION PROCEDURE 209
ANNEXE 4: SUBSIDENCE AND FAULT THROW CALCULATION TABLES AND MEASURES. 213

Indeed it would be impious to believe that, having taken pains, they wrote lies. Therefore there is another sense than what is given in the words, a sense concealed by various mysteries but up to now expounded by none of the masters which sense I doubt whether anyone can attain solely by the mere reading of books, without a skilled and trusty master unless he be illuminated by a divine spirit, a thing which is granted to very few; and so many strive in vain who pursue these most recondite secrets of Nature applying their mind to a mere course of reading.

Cornelius d'Agrippa "De Occulta Philosophia" (1527)

ABSTRACT

3D sequence stratigraphy is defined as the sequential analysis of chronostratigraphic maps interpreted on 3D seismic data. It results from the combination of three pre-existent methods of analysis of detritic sediments: sequence stratigraphy on 2D vertical seismic sections, well log sequence stratigraphy analysis and vertical and horizontal high resolution sequence stratigraphy interpretation of 3D seismic data sets. It aims at identifying the changes of relative sea level recorded in the fossil and constitutes a new potent exploration and development tool for subtle hydrocarbons stratigraphic traps discovery. Reservoir morphology, heterogeneity and subtle stratigraphic trapping mechanisms can be better understood through systematic horizontal identification of sedimentary facies of systems tracts provided by 3D attribute maps. On new prospects as well as on already producing fields the additional input of 3D sequence stratigraphy enables to locate and identify new productive zones.

In a clastic shelf environment such as offshore Louisiana (northern Gulf of Mexico), it becomes possible to directly infer the sedimentation facies from the lateral variations in seismic reflection along a time consistent reflector interpreted on the entire surface of a 3D survey. These amplitude anomalies observed along a flattened horizon enhance subtle and continuous geological objects (inferior to 20 m) invisible on the vertical seismic lines. Successive paleosurfaces of sedimentation can be reconstructed every 4 milliseconds (every 4 m in the sub-surface, 0-2500 m) and show the vertical evolution in the deposition conditions through time and space. The relationship between deformation (subsidence, salt tectonic) and sedimentation is deduced from these reconstructed paleosurfaces.

Offshore Louisiana, regular eustatic cycles of 0.1 Ma extend over the entire Gulf Coast Pleistocene (0 to 3.0 Ma) and 0.8 Ma cycles are identified from the upper Neogene to the present (0 to 10.5 Ma). 0.1 Ma cycles are correlated to the eccentricity period of the Earth orbit around the sun (96'000 years) and the 0.8 Ma cycles coincide with major inversions of the magnetic field around the Earth.

RÉSUMÉ

La stratigraphie séquentielle à 3 dimensions est l'analyse séquentielle de cartes chronostratigraphiques interprétées sur la base d'un volume de données sismiques 3D. Elle intègre trois méthodes d'analyse de sédiments détritiques: la stratigraphie séquentielle sur profil sismiques verticaux, l'analyse séquentielle sur diagraphies et la stratigraphie séquentielle appliquée aux plans verticaux et horizontaux de la sismique 3D. Son but est d'identifier les variations relatives du niveau marin et constitue un nouvel outil pour la recherche de pièges stratigraphiques à hydrocarbures. Les cartes d'attributs sismiques à 3D permettent de caractériser la morphologie et l'hétérogénéité d'un réservoir et de mieux comprendre les mécanismes à l'origine de leur formation. Aussi bien sur d'anciennes zones productives qu'en exploration, la stratigraphie séquentielle à 3D est d'un intérêt économique certain.

Dans un environnement de plate-forme détritique tel qu'au large de la Louisiane (nord du Golfe du Mexique), il est directement possible de déduire le milieu de sédimentation des variations latérales du signal sismique enregistrées le long d'un réflecteur sismique donné interprété sur la totalité des données sismiques 3D. Ces anomalies d'amplitude observées le long du réflecteur ramené à l'horizontale mettent en évidence des objets géologiques (inférieurs à 20 m) invisibles sur les sections sismiques verticales. Des reconstructions de paléosurfaces de sédimentation sont obtenues toutes les 4 millisecondes (tous les 4 m en sub-surface, 0 à 2500 m) et permettent de suivre l'évolution des conditions de sédimentation au cours du temps. Les relations entre la déformation (subsidence, tectonique salifère) et la sédimentation sont mises en évidence par ces reconstructions.

Au large de la Louisiane, des cycles eustatiques réguliers de 0.1 Ma sont présents sur la totalité du Pléistocène du Golfe du Mexique (0 à 3.0 Ma) et des cycles de 0.8 Ma sont observés du Néogène moyen à l'actuel (0 à 10.5 Ma). Les cycles de 0.1 Ma sont corrélés à l'excentricité de la trajectoire de la Terre autour du Soleil d'une période de 96'000 ans et les cycles de 0.8 Ma coïncident avec les inversions majeures du champ magnétique terrestre.

EXTENDED ABSTRACT

Nowadays, who has the time to read a thesis from corner to corner ? This extended abstract is a summary of the results presented in this research. If more information is required on any particular aspect, the corresponding conclusion and even the entire development of the argument can be found within each of the following chapters.

1. GENERAL INTRODUCTION

This research is based on the sequential and tectonic analysis of a 225 sq. km cube of 3D seismic reflection data situated 40 km offshore from the Louisiana and Texas border (West Cameron region). The concept of 3D seismic reflection data (Walton 1972) really became fully operative when the first interactive interpretation workstation appeared on the market in 1984 (Brown *et al.* 1984).

In the studied area, the Neogene and Pleistocene total thickness reaches 6 to 7 km. The Cenozoic sediments of the northern Gulf of Mexico are dominated by clastic input coming from the broad drainage basins of central North America. They are arranged in offshore migrating depocentres. The result of the massive sediment loading on the subjacent Louann salt enables large sheets of allochtonous salt to be driven basinward and to converge under the present foot of the continental slope (Sigsbee escarpment). Important mainly down-to-the-basin growth fault are connected to salt movements over the northern portion of the Gulf coast shelf. All Cenozoic sedimentation patterns on the shelf are directly related to mainly salt driven tectonic subsidence, rate of sedimentation input and eustasy. This research illustrates the top Miocene, Pliocene and Pleistocene local sedimentation history and relation to deformation based on horizontal three-dimensional displays.

2. SEQUENCE STRATIGRAPHY

Sequence stratigraphy was defined for the first time in 1987 as: "the study of rock relationships within a chronostratigraphic framework of repetitive, genetically related strata bounded by surfaces of erosion or non deposition, or their correlative conformities"(Van Wagoner *et al.*, 1987). Based on the concepts of cyclic sedimentation and climatic influences on sequences deposition observed on seismic reflection data, Vail et al (1977) proposed their first eustatic cycle chart leading to global correlation of stratigraphic events.

Depositional sequences are mainly controlled by accommodation space and sediment flux. The determination of lithofacies leading to the identification of paleoenvironments and of erosional surfaces interpreted as sequence boundaries allow understanding the organisation of the sediment record into sequences. Based on clastic shelf models, a sequence is organised in systems tracts related to changes in relative sea level. Most simplified models of sequences deposition lack the integration of the local tectonic component being a major controlling factor on the sequences morphologies and development.

Eustasy is the world-wide sea level fluctuations caused by absolutes changes in the volume of free sea-water and is thereby directly related to climate and tectonic movements at the planetary scale. The various causes at the origin of eustasy are not clearly understood except for the shortest orbitally forced cycles (< 0.5 Ma).

Sea level changes observations at a historic scale (centuries) leading to predictions for the near future are difficult to relate to the time resolution of eustasy as observed from the resolution proposed by sequence stratigraphy applied to the sediment record (100 to 1000 times larger cycles).

3. WELL LOG INTERPRETATION

Well log data from combined tools are used in this study to correlate lithological, sequential and chronological information derived from well log data to the seismic 3D volume via synthetic logs. The biostratigraphic correlations are based on benthic foraminifers paleo-tops. 6 logs out of 40 drilled in the survey have been obtained for this study. The sequential interpretation on logs is realised on SP and GR curves after the depositional environments have been determined. A single velocity law is used for all time/depth transformations within the limited area of the 3D survey. Lithology and porosity are the two main parameters needed to identify the presence of hydrocarbons on logs. They are obtained from the sonic, density and neutron curves available on only one log in this research.

4. THREE-D SEISMIC REFLECTION: ACQUISITION METHODS AND APPLICATIONS.

Ever more 3D seismic surveys are shot both on land and offshore for improved hydrocarbons recovery due to the rapid evolution of computer possibilities and the lower costs of acquisition. The visualisation of the spatial distribution of seismic attributes such as amplitude, reflection strength, instantaneous phase or frequency on vertical and horizontal planes enables to precisely delimit and characterise seismic facies and to interpret them as sedimentary facies. Structure (faults and micro-fractures), morphology, lithology and even porosity and fluid content of sedimentary bodies can be directly derived from attributes maps calculated along interpreted horizons (amplitude, dip and azimuth maps). Volume related attributes (reflection heterogeneity, reflection intensity and acoustic impedance) expressing the seismic component between two interpreted horizons are designed for precise reservoir characterisation. The combined usage of all the interpretation tools provided by 3D seismic interpretation techniques facilitates the search for subtle stratigraphic and structural traps but has also many different fields of applications like environmental or purely academic (waste sites characterisation, sedimentology, sequence stratigraphy, micro-tectonic, etc...).

5. THREE-D SEQUENCE STRATIGRAPHY

Systematically mapping depositional environments from the interpretation of horizontal 3D images in the studied area, from Early Miocene to the present (17 Ma, 4500 m) shows a definite periodicity in sequences of deposition. The cyclic character of sedimentation is mainly related to eustasy, sediment influx and total subsidence. This study leads to the understanding of the relation between sedimentation, deformation and eustasy on a limited portion of the northern central Gulf Coast.

5.2 On the Upper Pleistocene interval (0-0.8Ma), seven distinct erosional events are recognised in the studied area. A representative sequence of the inner shelf condition is composed of (1) an erosional basal unconformity filled by (2) transgressive thinning up sands on which (3) highstand sands prograde. Hst sands can be partially reworked into elongated sand bars constituting good potential reservoirs. Time structure map of interpreted horizons is an additional tool that can specify sediment assemblage morphology and enhance lateral differences in lithology and compaction rates.

5.3 Two sequence boundaries (SB 1.1 and SB 1.25) are identified in the interval between the global SB 0.8 and SB 1.46 Ma sequence boundaries by 2 erosional surfaces and 3 highstand prograding fans intercalated. This is confirmed by the nanno-fossils abundance curves (Schaffer, 1990) and various oxygen isotope curves (Haddad & Vail 1992). Thus, 0.1 Ma 4th order sequences are not limited to the Upper Pleistocene but extend down to the 1.46 Ma sequence boundary (Earth orbital eccentricity related cycles, Milankovitch 1941).

5.4 The international base Pleistocene limit (1.65 Ma) corresponds to a maximum of relative low sea level in the Gulf of Mexico (global prolonged cold period) and to a major inversion in the Earth magnetic field. The long 4th order sequence from SB 1.46 to SB 1.85 Ma comprises four shorter 4th order (0.1 Ma long) sequences bordered by 5 distinct erosional surfaces (C5, C6, C7, C8 and C9, C10). This implies that in the studied area, 0.1 Ma cycles can be identified down to the base of the Pleistocene (sensus stricto). During the transgressive period of the large 4th order sequence (C8 and C9), shorter cycles are better preserved on the inner shelf and 5 additional 5th order parasequences are identified as the superposition of closely spaced generation of erosional features.

5.5 The 0.55 Ma long 4th order sequence (from SB 1.85 to SB 2.4) is identified on logs and vertical seismic sections by lowstand incised valleys at the base, massive sandy progradation and transgressive and highstand silt and shale on top. This sequence coincides exactly with the reverse Earth magnetic field period between the Olduvai and Gauss periods. Three dimensional sequence stratigraphy allows to subdivide this interval into three distinct shorter 0.1 to 0.25 Ma long 4th order sequence by recognising two distinct erosional surfaces (SB 2.1 and SB 2.3). An additional sequence boundary (SB 2.5) is identified in the interval below the SB 2.4 erosional surface subdividing in two the 0.2 Ma long 4th order sequence described in the literature between SB 2.4 and SB 2.6 (3.72, Wornardt &Vail 1991).

The observation of more than 21 erosional surfaces and sequence boundaries over the Gulf coast Pleistocene (0-2.8 Ma) enables to conclude that:

- Successive erosional surfaces can be distinguished by the difference in their channels depth, orientation, size and degree of sinuosity.

- Major lowstand periods can be subdivided into 2 distinct erosional phases:

1) beginning of sea level fall recorded on the shelf as shallow meanders developing fan lobes on the hanging wall of major growth faults.

2) maximum of lowstand recorded as deep rectilinear thin channels and wide incised valleys.

- Volume related attributes and in particular reflection intensity maps can help to distinguish successive closely spaced erosional phases by superposing several channels generation
- Isopach maps calculated between closely spaced interpreted datum indicate sand bodiy thicknesses and reveal detailed morphologies of subtle objects unnoticed on vertical sections or on amplitude maps.
- On the inner shelf, the cyclic alternation of thick and coarse deltaic sands and homogeneous strata of shale sealing them at their base and top gather the perfect condition for potential subtle hydrocarbon stratigraphic traps.
- Exact location and lateral extension of potential traps can be foreseen and then identified from the consistent sequential interpretation of a 3D data set.

5.6 The top Gulf Coast Pliocene hiatus is mainly related to the SB 3.0 erosional surface composed of at least two superimposed channels generations. The potentially missing 0.1 Ma cycles at the base of the Pleistocene (2.6 to 3.0 Ma) are probably contained in the unconformity (one loop) situated above the MPLIO interpreted horizon. Unconformities are missed on well log data lacking high resolution fauna data, identified on vertical sections and their paleomorphology and potential paleogeomorphic traps are depicted on 3D horizontal images. Transgressive coastal onlaps and abrasions leading to the formation of elongated reworked sand bodies, parallel to the paleoshoreline are identified on 3D images and characterised on logs by sharp peaks (gamma ray curves).

Gulf coast Pleistocene, synthesis: In the studied area, at least 23 distinct erosional surfaces are identified within the 3.1 Ma before present time. They are interpreted as regional 4th order sequence boundaries proposing the existence of 0.1 Ma orbitally forced cycles over the entire Gulf coast Pleistocene. Major regional sequence boundaries marked by deeper erosions (mainly north-south oriented channels) are registered approximately every 0.8 Ma (0.8, 1.65 to 1.85, 2.3 to 2.5, 3.0 to 3.1). A systematic 0.2 to 0.3 Ma gap or hiatus is recorded below each of these major erosions and can explain the lacking seven or eight 0.1 Ma cycles. A comparison can be made with the magnetostratigraphic major inversions recorded over that interval at 0.79, 1.67, 2.48 and 3.2 Ma before present. It strongly suggests that the extended Gulf coast Pleistocene (0 to 3.2 Ma) is composed of four 0.8 Ma cycles each bearing eight 0.1 Ma orbitally forced eustatic cycles.

5.7 The Pliocene, in the Gulf coast sense (2.8 to 5.5 Ma) is limited on top and base by two major unconformities. The Mio-Pliocene limit is associated with two important marine regressions (SB 5.5 and SB 6.3) contributing to the mainly tectonically related Messinian Mediterranean salinity crisis. In the studied area, the base Pliocene shows a complete 3rd order sequence (SB 5.5 to SB 4.2; 3.4 Wornardt & Vail 1991) recorded in middle neritic condition that can be subdivided in two shorter 4th order sequences by the identification of an additional erosional surface at 5.1 Ma. This is supported and dated by paleo-temperature curves based on oxygen isotopes. On this type of data, 0.1 Ma cycles are not recognised below the Gulf coast Pleistocene limit but 8 of them have been identified and dated at the Mio-Pliocene transition in the south Pacific by Aharon (1993) on the basis of oxygen, carbon and strontium isotopes.

The top Pliocene hiatus is marked by two important erosional phases (SB 4.2 and SB 3.8) whose dating is uncertain due to the large sedimentary gap recorded.

On the inner shelf, highstand progradation or top lowstand outer shelf fan progradation can be reworked by transgressive abrasion into elongated porous sand bodies commonly sealed by conformable shale of the main flooding surfaces. In such a setting, large surfaces of shallow water lagoon or estuarine, rich in organic matter (source rock) can develop landward of the reworked sand bars to constitute high potential subtle stratigraphic traps.

5.8 The curve of coastal onlap (that cannot be directly checked by this study) shows a constant increase in relative marine transgression rate over the entire Tortonian and Messinian stages. In this interval (SB 5.5 to SB 10.5), where 4 distinct erosional surfaces are recognised on the Haq et al. curve (1988), 8 are now identified on the vertical seismic sections, the well log data sequential analysis and the horizontal facies reconstruction of this 3D data. They all fit colder paleo-climate intervals as indicated by oxygen isotopic curves. The 0.8 Ma periodicity in stronger erosions can also be observed on the almost totality of this interval.

5.9 The synoptic view of all the characteristics of the erosional surfaces and associated sequence boundaries observed in the studied area via three-dimensional sequence stratigraphy show that:
- the local Gulf coast Pleistocene sedimentation is dominated by short (0.1Ma) sequences and longer 4th order sequences (0.2 to 0.4 Ma) marked by relatively shallow lowstand erosions oriented mainly from the NE to the SW. This indicates a main sediment input from Louisiana, (Mississippi drainage basin).
- the Neogene in the studied area is dominated by deeper and less frequent erosions oriented NW-SE (4th and 3rd order sequences) indicating a dominant influence from the Texan drainage basin.
- The 0.8 Ma periodicity in the recurrence of stronger incision of the central northern Gulf coast is observed on the entire Pleistocene and upper Neogene (0.8, 1.65 to 1.85, 2.3 to 2.5, 3.0 to 3.1, 3.8, hiatus, 5.5, 6.3, 7.1, 8.2, 8.8, 9.7 and 10.5).

The interpretation of seismic features displayed in various attributes and enhanced by sometimes extensive colour scale manipulation into sedimentary bodies is based on their lateral continuity and coherence recognised on reconstituted horizontal surfaces of deposition or erosion. This study provides a vast number of different typical stratigraphic and morphologic templates of horizontal seismic responses to sedimentary facies in an inner to outer shelf clastic environment.

6. Application to hydrocarbon research

6.1 Three-D sequence stratigraphy integrates sequential analysis of regional 2D lines, well log data, 3D horizontal sample and volume related attributes maps to locate, define and understand sedimentary facies of subtle stratigraphic traps. It is a potent tool for the discovery of stratigraphic traps, their exploration and development. It leads to the better understanding of reservoir morphology, heterogeneity and subtle stratigraphic trapping mechanisms. On new prospects as well as on already producing fields the additional input of sequential analysis on logs and on 3D data allows to identify and locate new potential productive zones.

6.2 The observed periodicity in sedimentary facies derived from sequential analysis in clastic rocks allows to look directly at the right place through time and space for the hidden potential stratigraphic traps associated with definite systems tracts

- basal lowstand systems tract reservoirs associated with erosional surfaces or sequence boundaries are mainly found in the porous sands of the incised valley beds and associated lateral crevasse splays.
- upper lowstand (prograding complex) potential reservoir on the outer shelf are found in distributary mouth bars and proximal deltaic lobes. On the inner shelf, occasional productive lowstand fans are developed on the footwall of growth faults (increased accommodation space by locally higher tectonic subsidence rate).
- top lowstand sands and transgressive silts can be reworked during marine transgression in elongated sand bodies likely to become good reservoir rocks.
- inner shelf low angle highstand progradation rarely constitutes good reservoir.
- inner shelf shallow erosional surfaces interpreted as type 2 sequence boundary do not constitute deep and coarse enough material to present interesting reservoirs.

6.3 An application of 3D sequence stratigraphy to the Cibicides opima gas condensate productive interval in the studied area reveals that previously interpreted stacked structural traps associated with a faulted anticline are in fact deformed stratigraphic traps limited by definite sedimentary bodies organised in sequences. The sequential analysis of pay sands and the visualisation of their morphology and lateral extend on horizontal 3D images enables to avoid drilling dry holes that look for the lateral shaling out of the reservoirs.

7. Relation between deformation, sedimentation and eustasy .

Growth faults in the studied area are of relative short lateral extension and present curved morphologies delimiting small rim-synclines or mini-basins showing higher rate of subsidence and sedimentation than the rest of the shelf. Major growth faults are initiated near the shelf break during periods of relative low sea level due to the combined effects of aquatic overburden and concentrated sedimentation lateral differences and increased pore fluid expulsion in the fault plane.

The salt tectonic style of the northern Gulf coast is governed by gravitational processes. The main driving forces inducing basinward and lateral salt movements are:

- offshore progressive migration of main depocentres at the basin scale.
- sedimentary loading: 1) during periods of lowstand when large volumes of sediments are brought to the outer shelf generating instabilities at the origin of major growth faults; 2) during periods of high sea level (highstand proximal progradation).
- differential erosional loading/unloading (inner shelf incisions or erosion of pre-existent topographies).

If the total subsidence is propitious then sedimentation influenced by eustasy will contribute to differential loading on the shelf. The curve of tectonic subsidence cannot be evaluated because of complex factors such as 3rd and 4th order eustatic changes in water load, allochtonous salt napes movements, Gulf coast basement tectonic response to basin loading and lithospheric thermal subsidence. The rate of total subsidence is mainly governed by depocentre migration on the shelf. Very high rate of total subsidence (≈ 700 m/Ma) are recorded over the Early Miocene interval in the studied area due the proximity of the shelf break and of the main depocentre. In such conditions no eustatic erosional surfaces have any chances to be recorded. Much lower rate of total subsidence is registered over the Middle and Late Miocene and basal Pliocene (130 m/Ma). During that interval, only 3rd order major erosions are identifiable on the shelf. Short cycles are absent or not recorded. Rapid and episodic increase in subsidence rate are related to instantaneous responses to lowstand differential loading and unloading on the shelf. During the Gulf coast Pleistocene in the studied area, the rate of total subsidence is increasing (210 m/Ma) even if the corresponding depocentre is located more than 300 Km offshore. This is related to the important volume of sediment trapped in the mini-basins on the inner shelf. This differential loading on the shelf is at the origin of a third phase of salt activity (Plio-Pleistocene allochtonous or detached allochtonous salt napes, Wu *et al.* 1990b).

The type of sedimentation on the inner shelf is related to total subsidence, local fault and salt tectonic related subsidence, volume of sediment influx and eustasy. Lowstand sedimentation on the inner shelf is concentrated on the footwalls of major growth faults (superposition of lobes).This perpetuates and even increases their rate of activity. Highstand progradation on the inner shelf spreads over large areas and deposits thin large mainly juxtaposed lobes not affecting tectonic local subsidence but rather global total subsidence. Delta lobes shift laterally on the shelf break during period of lowstand and migrate laterally on the inner shelf during period of highstand. Faults possibly trigger salt tectonic rather than the opposite. Secondary normal and antithetic faults parallel to major growth faults develop progressively in the basinward direction. Pre-existing antithetic faults of a major growth fault can be shifted by a second generation of faults. Transfer zones between juxtaposed growth faults of different generation form dome-like structures liable to constitute potential well confined structural traps.

8. Discussion.

This research leads to three major conclusions:

- the development of a rapid procedure of how to apply 3D sequence stratigraphy in order to find, delimit and characterise new potential stratigraphic or tectonic traps based on 3D data sets shot on new or older prospects.
- the proposition that 0.1 Ma orbitally forced eustatic cycles can be identified on the entire Gulf coast Pleistocene and that a 0.8 Ma periodicity in the recurrence of stronger and deeper erosions is recorded on the Pleistocene and top Neogene periods and coincides with major Earth magnetic field inversions.
- the sedimentation on the inner shelf is mainly governed by the rate of total subsidence, local tectonic subsidence, volume of sediment influx and eustasy. Salt basinward and lateral displacement under the northern Gulf coast shelf is controlled by growth faults generation near the shelf break and by rim-synclines formation on the inner shelf.

Annexe 1: Procedure of rotation of seismic data and interpretation grids

Annexe 2: Compiled tables of mostly used biostratigraphic horizons(Early Miocene to present)

Annexe 3: Well log 2D and 3D data set sequential interpretation procedure

Annexe 4: Subsidence calculation tables and fault throw measures in the studied area

ACKNOWLEDGEMENTS

The interpretation of the 3D seismic data has been realised on a CHARISMA S (Schlumberger-Geoquest™) workstation acquired by the Geological Institute of the University of Lausanne in 1989. This challenging research could not have been realised without the constant support of Henri Masson, director of the Geological Institute of the University of Lausanne, the financial help of the Herbette Foundation in Lausanne and the Swiss National Fund for Scientific Research (projects 2975-088, 20-28943.90, 20-394.93).

To deal with the new, rapidly evolving computer technology used for modern seismic interpretation, involved the help and efficient support of Geco-Prakla (Schlumberger-Geoquest) in London, Stavanger and Hannover. I am deeply obliged to Alison Spice, Jan Westergaard, Reidar Haavik, Rich Lozier and Lars Wiborg (amongst others) for the hardware and software maintenance and to Albrecht Glocke and Kjell Erik Fagertun for giving me the opportunity to be formed on the CHARISMA S System in Stavanger in summer 1993.

Michel Muller and Daniel Henchoz from the Computing Centre of the University of Lausanne have always been instantaneously available to solve any kind of computer problems and has always been greatly appreciated.

All my gratitude goes to Professor A.W. Bally from Rice University in Houston-Texas for his help in getting the necessary well log and regional seismic data and welcoming me to Rice University during summer 1992 to learn the basics of well log interpretation and of the Gulf Coast geology. I am deeply honoured and grateful to have him reading and correcting my PhD dissertation and accepting to be a member of the examination board. We are grateful to TGS-CALIBRE Geophysical Company and Geco-Prakla that provided the regional line 1036-6 to Dr S. Wu in order to correlate the studied 3D data set across the northern Gulf of Mexico shelf.

Many thanks also to David Scolman from Corpus Christi Oil and Gas Company in Houston who helped in providing me with the rest of the well log data necessary for this study. The velocity law used in this research and the synthetic log were realised in his office.

I am equally grateful to Lars Sonneland (Geco-Prakla in Stavanger) for accepting to be part of my examination board and to take the time to read and correct the geophysical aspects of this work.

I wish to thank Professor Dominique M. Chapellier for correcting some theoretical aspects in the chapter on well logging.

A solitary research within a team work:

To my friend and teacher Gérard Stampfli, I owe the silent, patient and generous communication of knowledge. He knows how to guide without influencing, to motivate without forcing and to criticise without being critical.

So many English or software problems have been diligently solved by my office partner without hesitation to spend time to help ? For all the laughter shared together in the Himalayas, Costa Rica or during the work classes with the students in Lausanne during the last 4 years, for making geological life easy and happy, and for all the rest, thank you Robin.

In our working team there was another extremely competent person from whom we all learned an incredible lot. The one that knows a lot of things about a lot of things and shares it with you quietly if you ask. To Philippe Favre and his "subsiding" Hewlet Packard, all my gratitude.

The friendly smoking computer moaner next door could answer and solve any Macintosh problems, if you dared to ask. Did you recognise Alain Pillevuit ?

Many thanks to the official team translator and English corrector (Preeta Muthalali) finding her way through a myriad of geological terms.

I would like to thank two friends for taking me from behind the computer screens to the outer wilderness in order not to loose contact with the field work: Jean-Claude Vannay in the pure and elevated Indian Himalayas and François Bujan in the unknown and impenetrable Costa-Rican jungle.

To be a PhD student in the Geological Institute of the University of Lausanne is a great privilege for more than one reason and I would like to express my love and gratitude to all its members who have not been explicitly mentioned here.

And finally, let me dedicate this work to the One that knows how to be present in her absence and absent in her loving presence, that lives and thereby teaches another application of the great mysteries of the natural cycles, the Great Silent Bitter Sea, Katia.

1. General Introduction

"The world three-dimensionality is not its own property, but merely the property of our perception of the world. The three-dimensionality of the world is the property of its reflection in our consciousness"

P.D. Ouspensky "Tertium Organum" (1920)

1.1 Foreword

Isn't it strange that a nature-loving geologist decided to sit behind screens for 4 years trying to learn to talk to a computer. Fortunately, there was colour, the third,... and the fourth dimensions. Field geologists commonly work with all 4 dimensions at a time without always being quite aware of it. For instance: the three co-ordinates of space where a rock has been sampled and the type of rock sampled. This very simple analogy sums up the principle of three-dimensional seismic data interpretation: "A localised point in space with an attribute". The main natural limitation of field geology is the restricted outcropping surfaces, both in the vertical and horizontal planes. The gentle relief on this planet (compared to Mars) never provides more than 3000 m of vertical continuous outcrop and most of the horizontal surface we are living on is covered by water, vegetation or towns. The constant desire of a surface geologist is to always see more. He tries to extrapolate the surface information to understand the underground and plays with time trying to reconstitute ancient and deformed morphologies. Imagine the immense joy of such a geologist suddenly discovering the existence of three-dimensional seismic data providing :

"almost infinite vertical outcrop and limitless possibilities to reconstruct paleosurfaces through time and space"

The shimmering aspect of such perspectives was enough to trap one more field geologist and send him on the track of deep buried Earth history.

This research consists of 7 independent chapters, comprising an introduction and a conclusion or summary. After a general introduction presenting the historical and geological framework, three chapters discuss the theoretical principles and techniques of analysis as applied in this study. Reflections on uses of sequence stratigraphy and its limitations (2) is followed by a summary of well log interpretation procedure in terms of lithology and sequential analysis. This third chapter presents the wells and synthetic seismograms used for further correlation with the 3D seismic data. Chapter 4 presents the basics of 3D seismic interpretation and the main tools available on modern software with examples taken from this study. Chapter 5, 6 and 7 present three different types of possible integration and application of the tools and techniques described above. Chapter 5 discusses the time interval between Early Miocene and the present from the point of view of three dimensional sequence stratigraphy. Every 4th and 3rd order sequences known today in the Gulf of Mexico for that period are illustrated and discussed on the base of horizontal reconstruction of sedimentary facies. Chapter 6 shows an application of 3D seismic data and three dimensional sequence stratigraphy to locate, identify and circumscribe a gas field. And finally chapter 7 discusses the sedimentation versus deformation relations as observed in the studied area, related to gravity induced salt movements occurring below the Gulf coast shelf.

In order to facilitate the reading of this volume, a special care has been given to provide every chapter with an exhaustive conclusion of the argument presented.

1.2 Three-dimensional seismic data: history

"The Whole is more than the sum of the parts" (Aristotle)

Three-dimensional extrapolation or interpolation on the basis of two-dimensional information is realised through the interpreter's memory and imagination. The gap between two wells, two slopes, two galleries or two vertical seismic lines can be filled by contour maps showing the most probable trend. Limitation occurs when natural discontinuities, invisible on the available data make the interpolation differ from reality. The most secure way to prevent this from happening, is to increase the density of information.

Based on that principle, Walton presented for the first time in November 1970, the new concept of three-dimensional seismic method at the 40th Annual International SEG Meeting held in New Orleans, Louisiana (Walton, 1972). He wrote: "Instead of showing the subsurface beneath a profile line, 3-D displays give an **areal picture** from the shallowest reflector to the deepest one that can be found seismically". The concept of surface visualisation provided by high density data was there already but no computer facilities were available at that time to apply true 3D migration nor to realise true slicing through a 3D volume of seismic reflection data. Nevertheless, 3-D surveys were shot on normal contractual basis since 1975 and Bone, Giles and Tegland (Bone *et al.*, 1976) and Tegland; 1977) demonstrated that this method could considerably contribute to discovery, development and production of hydrocarbons.

But real 3-D display of a volumetric image remained the main problem until late in 1983 when the first true interactive system or seismic interpretation workstation became available on the market (Sonneland, 1983 and Gerhardstein & Brown 1984). The first commercialised interpretation workstation was a CHARISMA I sytem, the direct predecessor of the "machine" used in this study. Before that, and for almost 10 years, the interpreter had to work with non automatic systems such as the "Seismodel display unit" consisting of a series of transparent plastic plates on which the seismic was printed and the interpretation drawn manually. Thus a physical hologram of the interpreted zone was visible when illumined from the back. From it, constant time slice sections could be projected onto a transparent paper to contour the seismic response of successive time-slices. Because of the ever increasing numbers of vertical slices to consider at once, quicker modes of access to the seismic data were devised. The images were stored on film and displayed separately on television screens. The interpreter could then superpose transparent films to vertical or horizontal displays and rapidly follow an object (fault plane, local amplitude swell, salt dome, etc...) and generate manually an accurate contour map. The first published horizontal display is shown in Bone *et al.*, (1983) on a Seiscrop Interpretation Table, but in 1981 already, Prakla realised horizontal seiscrops on a 3D survey offshore Brunei (Stampfli, oral comm.).

In 1984, with the elaboration of the first interactive computer, a new generation of seismic interpretation techniques was born allowing the interpreter to work without paper, getting the seismic data on screen and simultaneously storing the interpretation on the database. The three first options added to the Seiscrop Interpretation Table were the possibility to adapt colour scale to enhance or mask seismic objects, to compose vertical with horizontal planes on one screen and to apply automatic tracking of horizons within a given amplitude range (this last option was already used on 2D lines since the early seventies. From all this resulted a very considerable gain in time and visualisation possibilities helping the interpreter to have a rapid and complete understanding of the local geological complexity.

During the 10 years separating today from this major step taken in the field of seismic reflection, incredible improvements have been brought to this basic idea. Due to the rapid expansion of calculation and storage capacities of computers, modern seismic interactive workstations will provide ever more developed and effective interpretation possibilities (seismic data attributes maps, treatment facilities, true 3D visualisation, integration of well-log data, etc...). The development of the applications used in this research will be discussed in Chapter 4.

1.3 This research: history and objectives

History

Earlier in 1990, a vacant seat appeared behind the screens of a revolutionary machine acquired in 1989 by the Geological Institute of the University of Lausanne, Switzerland. Already widely used in the oil industry since the middle eighties, it was very uncommon and even unknown for a University in Europe to be equipped with such a seismic interpretation system. A 3 Dimensional seismic speculative survey offshore Louisiana (Gulf of Mexico U.S.A.), was generously provided by Geco (London) as the CHARISMA VME^{TM} (Schlumberger-Geoquest) interpretation system supported by a SUN Vicom hardware was bought by the University of Lausanne. The primary objective after mastering the software and hardware configuration was to extend the research done by Professor Stampfli with Shell international (Dalley *et al.*, 1989 ; Stampfli & Höcker, 1989) try to develop the possibilities of geological interpretation provided by the horizontal surfaces and attributes of 3D data sets.

After a year of interpretation and experiencing of the different possibilities of data handling provided by such a software on both onshore and offshore 3D data set (onshore spec. survey in Holland

and offshore 3D in the West-Cameron area, Gulf of Mexico) it was decided to concentrate the research on a detailed geological description of the offshore West-Cameron survey. The excellent quality of the 3D survey situated on the present inner shelf of the northern central Gulf of Mexico showed a good potential to develop systematic description of vertical evolution of sedimentary facies observed along the horizontal plane via the multiple attributes available on seismic interpretation workstations.

Rapidly, the primary geological conclusions reached from seismic interpretation of major fault trends and sedimentary facies revealed that the seismic data were stored on the computer with a rotation error of 90° and in a mirror position (the data set was loaded before this research started). It was an easy task to reload the seismic data in the correct orientation but in order to save the already done interpretation, a small procedure had to be written to switch the interpretation grids back to their correct position. Data loading on seismic interactive workstation was very complex and time consuming in the early days of seismic workstations but is slowly becoming easier as software progress (the inversion and rotation procedure is developed in Annexe 1).

Over the last 4 years, we have had to adapt the local hardware configuration several times to the frequent software changes. We started on a Sun Vicom station with a 4 Gigabits memory configuration and a complicated remote plotting interface operated by a micro-VAX system making a first rasterisation of the data. In 1992, the first micro-VAX was removed and the plotting configuration adapted. In 1993, a new software version could not be supported anymore by the "obsolete, 4 years old" Vicom station which had to be replaced by a powerful Sun Sparc station (Model 20) belonging to the new generation of workstation. At the beginning of 1994, the next software version was not compatible anymore with the ancient plotting configuration nor with the new colour plotter purchased by the University of Lausanne ! An additional plotting interface had to be purchased to replace the VAX interface. All these modifications are supposed to converge towards standard formats making the geologist or interpreter task easy and interactive. New hardware and improved software are already in preparation and will replace the present configuration... Geologists should persevere to keep up with computer science or else geology will become exclusively a matter for computer scientists !

The second conclusion reached, was that well-log data were absolutely necessary to confirm the geological interpretation realised in terms of sequence stratigraphy and deformation, even if assumptions on the correlation with the pre-existing eustatic curves were made on the basis of vertical succession and cyclic character of seismic facies. Two months at Rice University (Houston-Texas), in the team of Professor Bally were enough to confirm the idea that the data set was "upside down", to get in contact with the oil industry in order to obtain well-log data, to learn the basics of well-log interpretation technique as well as basic knowledge on the Gulf Coast geology. The dating assumptions made on the base of the sequence stratigraphy analysis of the 3D seismic data, revealed themselves almost correct after comparison with the correlation effectuated on the base of well log data.

Objectives

After having achieved the sequence stratigraphic interpretation of well-log data based on lithology and faunal assemblages and having correlated it to the 3D data set, the next objective became clear:

- to recognise and systematically represent the various cyclic sedimentary features developing in relation to changes in relative sea level on 3D horizontal images
- to systematically represent subtle potential stratigraphic traps in relation to systems tracts using high horizontal resolution and the imaging possibilities of 3D seismic data.

Up to very recently nothing has ever been published on the subject even if this type of research must be common in the oil industry. Brown and others (Brown, 1979; Brown & McBeath, 1980; Brown *et al.*, 1981; Brown *et al.*, 1982; Brown, 1983; Brown, 1983b; Brown *et al.*, 1984; Brown, 1985; Brown, 1986a; Brown, 1986b; Brown, 1990; Brown, 1992; Bone *et al.*, 1976; Tegland, 1977; Bone *et al.*, 1983; Gerhardstein & Brown, 1984) have published many papers on the usage and advantages of 3D horizontal images but up to now and to our present knowledge, nothing was ever published on the systematic description of systems tracts with 3D images and their use for exploration purposes.

1.4 Geographical and geological framework

Introduction

The deep structures of the Gulf of Mexico have always been a source of questioning and uncertainty due to the very thick sediment package masking its basement. From the time when geologists tried to reconstruct paleomorphologies of drifting continents (Bullard *et al.*, 1965) , up to today, the Gulf of Mexico still remains a delicate zone to interpret. And this, despite of probably being one of the most studied and explored region in the world. Recent synthesis on the Gulf of Mexico structure and stratigraphy have been presented by Winker, (1982); Curtis, (1987); Winker & Buffler, (1988); Worral & Snelson, (1989). An extensive review and discussion of the origin of the Gulf of Mexico is beyond the scope of this study, but a presentation of the main geological framework is needed to understand the sedimentation and deformation processes affecting the younger sediments. This research effectively concentrates on the sediments between Early Miocene and Upper Pleistocene, on a limited portion of the continental shelf, 15 by 15 km offshore Louisiana, in the West-Cameron region.

Geographical situation

The studied area is located on the north central coast of the Gulf of Mexico, 40 Km offshore Sabine Lake, on the marine border between Texas and Louisiana (see fig. 1-1).
Its present latitude is 29° north and did not change position very much throughout the Cenozoic. The present climate is continental sub-tropical. Water depth is less than 20 m on this inner portion of the

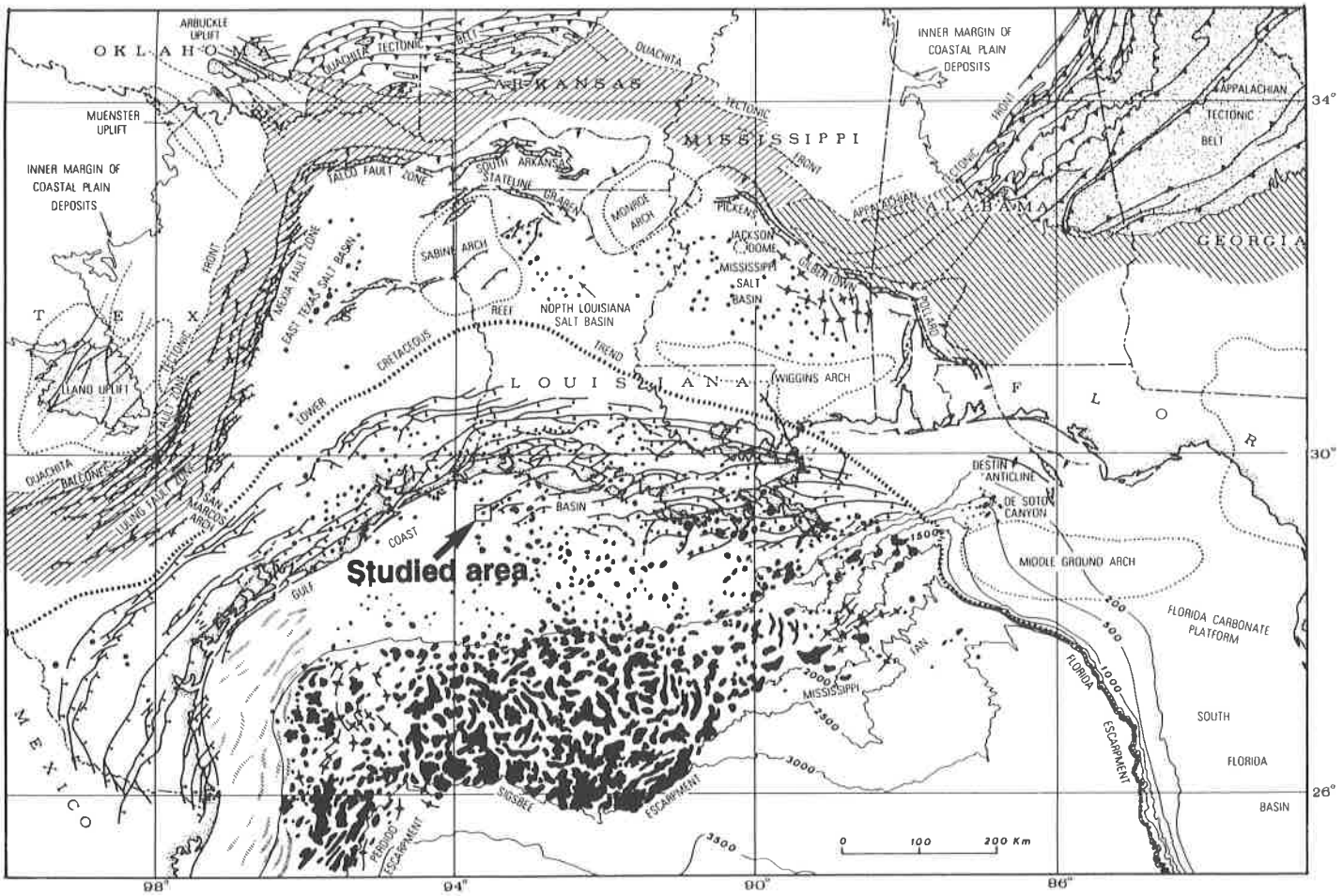

Fig. 1-1: Geographical situation of studied 3D speculative seismic survey on a tectonic map of the northern Gulf of Mexico (modified from Martin 1978).

continental shelf. The main present clastic input to the Gulf is the Mississippi delta whose sediments are transported laterally to the west, as far as offshore Corpus Christi region affecting the studied area. The minor local sediment input is done through the Sabine, Trinity, Brazos and Texan Colorado rivers. They drain the Texan plateau up to the Sacramento, Marathon and Ouachita mountains.

The sea floor morphology of the Gulf was first studied by Treadwell (1949) , who described it as formed of numerous irregular basins, knobs, ridges and trough-like valleys attributed to slumping and faulting. The most recent description of the north slope Gulf physiography was done by Martin and Bouma (1978) . They divided the Gulf into different types of shelves and slopes intersected by submarine canyons. The northern part of the Texas-Louisiana slope is limited by the Sigsbee escarpment to the south, by the Mississippi foldbelt to the west (offshore Mississippi delta) and by the Perdido foldbelt to the east (offshore north Mexico, see fig. 1-1). The discovery of these three inversion features marking the transition between the slope and the abyssal plain is what led to so much research done on the deep structure and deformation of the Gulf shelf. They are connected to the important movement of deep lying salt masses whose mechanism will be summarised in Chapter 7.

Geological Framework

In the early Carboniferous, Gondwana and the American portion of Laurussia were separated by the proto-Atlantic ocean. From late Mississippian to Middle Permian, this ocean closed by subducting the north American plate towards the south-east under south America. Two blocks of Palaeozoic continental crust (Yucatan and Florida straits blocks) drifted laterally, to fill in part of the gap between north and south America. The Ouachita, Marathon and Huastecans foldbelts are interpreted as an accretionary prism thrusted onto the North American margin at the time of oceanic closure (Pindell, 1985; fig. 1-2) .

Marine sediments from Late Permian to Late Triassic are absent in the central Gulf preceding the period of continental crustal thinning and rifting between the North and South American plates.

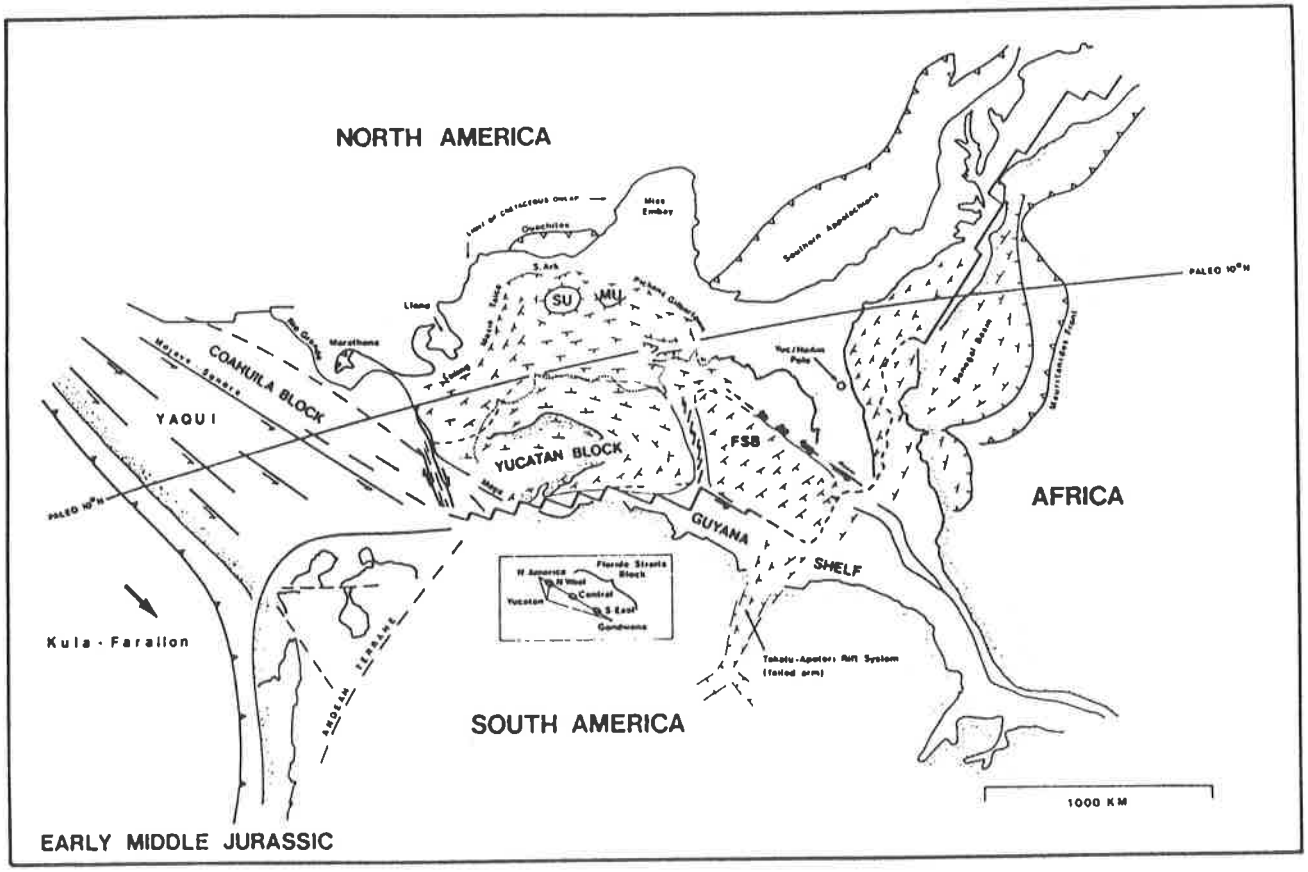

Fig. 1-2: Early Middle Jurassic reconstruction (≈ 180 Ma). Beginning of divergence between North America and Africa causing rifting in the proto-gulf of Mexico and beginning of salt accumulation. FSB, Florida Straits block; SU, Sabine uplift; MU, Monroe uplift (modified from Pindell, 1985).

In the central Gulf, the syn-rift sedimentation consists of non-marine red beds (Eagle Mills Formation, upper Triassic, lower Jurassic) and is associated with dike emplacement ranging from 180 to 200 Ma (Scott *et al.*, 1961; Dooley and Wampler, 1983; Salvador, 1987). The maximum opening between the Texas-Louisiana margin and the Yucatan block has been estimated as 500 Km by Sawyer (1985) and Pindell (1985).

Thermal subsidence started in Middle Jurassic and was associated with episodic marine incursions resulting in deposition of thick evaporite layers in the central Gulf region. Two major salt basins have been identified on the basis of deep reflection seismic data and wells : the Northern Gulf salt basin and the Campeche salt basin. Separating these two major zones of salt accumulation the Sigsbee abyssal plain is underlined by presumed oceanic crust estimated by gravity and magnetic data (Buffler, 1989; Humphris, 1978; Humphris, 1979). They suggested that these two areas previously contiguous were later separated by north-south oceanic spreading (see fig. 1-3).

The age of the Louann Salt has been estimated from preserved palynomorphs from Late Triassic to Middle Jurassic (Jux, 1961; Kirkland & Gerhard, 1971). The original thickness of salt in the Northern Gulf

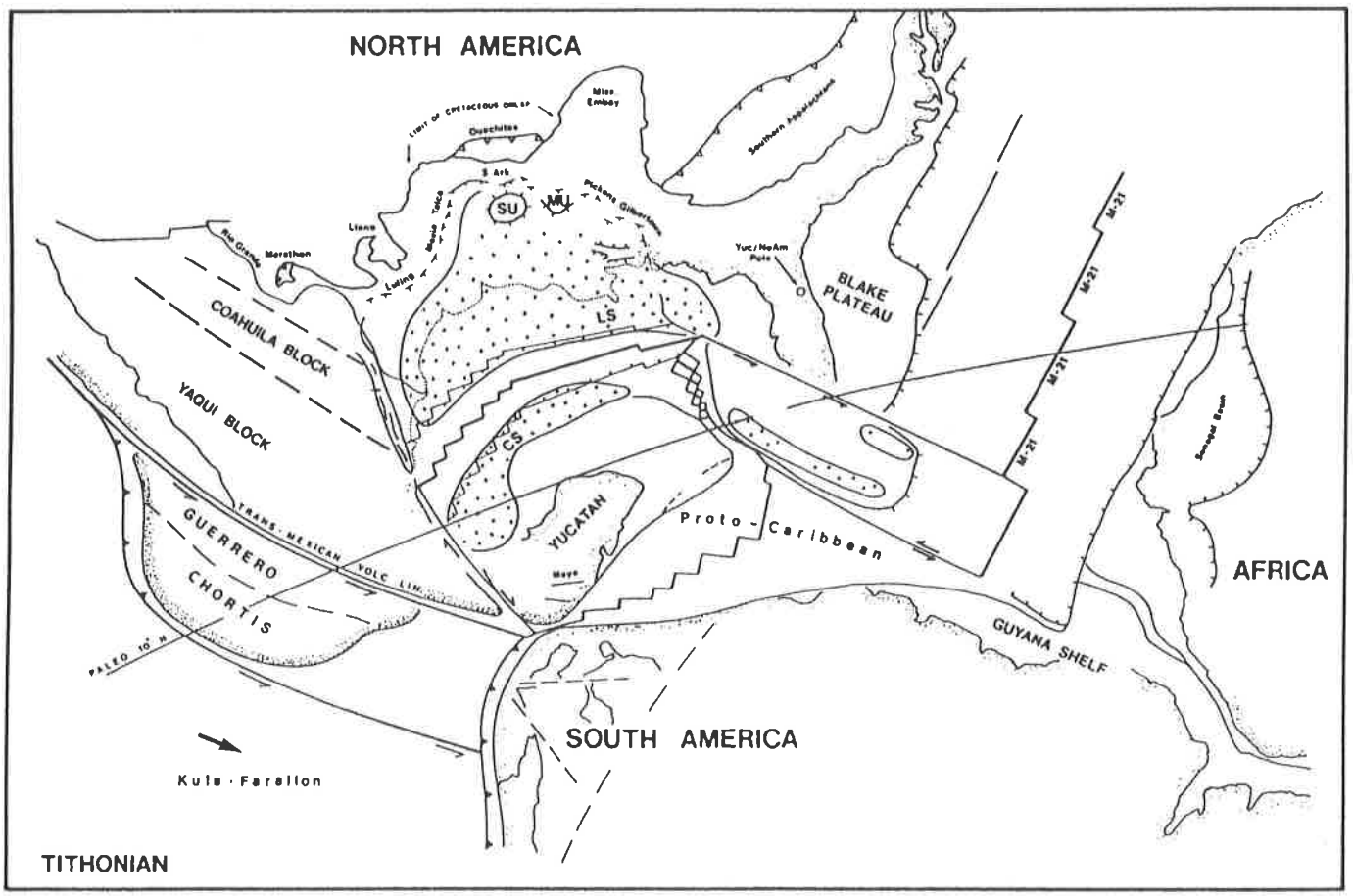

Fig. 1-3: Late Jurassic (Tithonian) sea floor spreading north of the Yucatan and Florida straits blocks separating the salt in two major provinces (LS, Louann salt to the north and CS, Campeche salt, modified from Pindell, 1985).

basin (east Texas) has been estimated between 1500 and 2100 m by Jackson and Seni (1983) . As demonstrated by Worral and Snelson (1989) and Wu (1990) the Louann salt is rooted in the late Middle Jurassic sediments (Callovian; Salvador, 1987) but most of it is now in allochtonous position serving as decollement level for faulting of the overlaying sediments. This is why exact reconstitution of initial salt thickness will always remain very difficult.

On top of the salt (early Late Jurassic), non marine red beds, aeolian sandstone and conglomerates of the Norphlet Formation were deposited (see fig. 1-4). Wedging out of these series up dip, under sediments of Early Cretaceous form good reservoir rocks.

By Late Jurassic (Oxfordian, Pindell 1985) sea-floor spreading between Yucatan and North America provoked the first major marine incursion in the Gulf. It is recorded as the Smackover carbonate

being of economic interest in the Gulf (both source and reservoir rocks, fig. 1-4). It is sealed at its base by organic rich mudstone and at the top by oolithic facies (Sassen & Moore, 1988) . It passes laterally and vertically to the Buckner evaporite red beds. The deep water equivalent of these deposits in the newly opened Gulf of Mexico consist of the Challenger carbonate unit. The top Jurassic Cotton Valley Formation (Mann & Thomas, 1964) is the first major detritic event recorded in the Gulf. There is evidence that the loading of Late Jurassic series started first lateral and vertical shifting of salt (McGowen & Harris 1984). By Early Cretaceous, the geographic, tectonic and stratigraphic framework of the Gulf is set, as relative plate motion stopped. A deep central trough surrounded by clastic or carbonated shelves was formed. Marine open connections with the Atlantic and eventually with the Pacific ocean are supposed to have functioned throughout the Cretaceous. Thermal contraction of the cooling oceanic crust controlled the

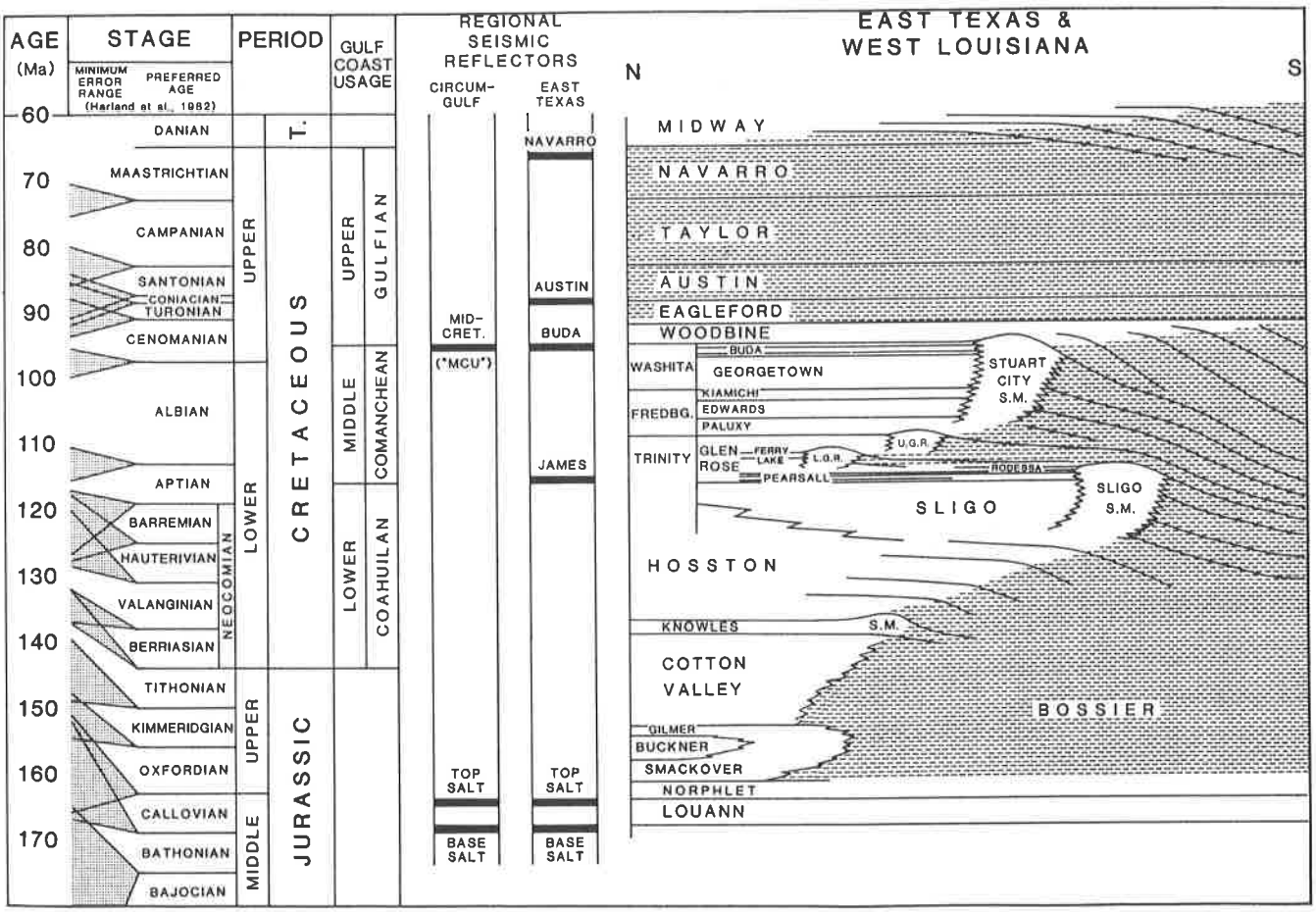

Fig. 1-4: Jurassic-Cretaceous stratigraphic chart, Texas and Louisiana (from Winker and Buffler, 1988).

subsidence rate. Carbonate shelves developed all around the Gulf at the tectonic hinge zones between normal and thinned transitional continental crust (Winker & Buffler, 1988 , fig 1-1). It is also during Early Cretaceous that several local uplifts occurred landward from the carbonate shelves. The Sabine uplift is presently located 250 Km north of the studied area and did separate the northern Gulf shelf in two salt provinces (East Texas and northern Louisiana, fig. 1-1). These local uplifts provoked two shelf sags that were able to keep enough Louann salt at their base to generate numerous oil productive structures during pre-Tertiary sediment loading (Jackson & Seni, 1983) . Since its deposition, the Louann salt migrated basinward to concentrate in large masses under the Early Cretaceous shelf areas. This ends the first major stage of salt movement as it seems to have stabilised during the starved sedimentation period of the Late Cretaceous-Early Oligocene (Wu et al. 1990).

Two major drowning of the Gulf of Mexico are recorded in early Aptian and early Cenomanian time. During the Cenomanian, an important Gulf-wide unconformity occurs (MCSB, Mid-Cretaceous sequence boundary, Buffler *et al.*, 1980 ; Schlager & Buffler, 1984) . A 30 Ma hiatus in the series is correlated with the mid-Cretaceous drop in sea level shown by Vail *et al.* (1977) showing important sub-aerial and submarine erosion. Strong contour currents related to the Tethys widening during Middle Cretaceous could be at the origin of submarine erosion. The Cenomanian disappearance of carbonate

shelves is primarily due to the rapid withdrawal of sea water occurring at the time of the MCSB. At the same time, the thrusting, uplift and erosion of the Sierra Madre Oriental and the Rocky mountains, re-initiated the drainage systems installed during Late Jurassic, bringing a voluminous amount of sediments on the north coast of the Gulf. This series is recorded as the Woodbine progradational sandstone which is the most prolific hydrocarbon producing interval in East Texas basin (Worral & Snelson, 1989) . Its lateral equivalent to the east, in Louisiana and Mississippi is the Tuscaloosa Formation in which deltaic progradation reached the shelf edge (Winker, 1982) .

Cenozoic

When the sea level began to drop at the beginning of Tertiary (Vail et al. 1977), increasing quantities of sediments started to prograde towards the basin. The Gulf of Mexico started to be filled from the north and north-west with laterally shifting depocentres (fig. 1-5 a and b). By mapping them, Winker (1982) noticed that most of the main large-scale changes in sedimentation are not synchronous at the basin scale. This indicates that eustasy might not be the only cause affecting the sandstone/shale ratio. He demonstrated that major Tertiary depocentres can be correlated with different phases of tectonic uplifts and erosions in the hinterland (fig.1-5 a).

The principal interaction between structure and sedimentation have occurred during relative low sea level episodes where main shifts in depocentres were likely to take place. During these periods, the depocentres follow the retreating shoreline and prograde over more distal silts and shale. The local overloading provoked by a major delta lobe is able to initiate growth fault systems by differential loading and compaction. These local depressions will in turn be filled by more sediments.

The estimated cumulative thickness of Cenozoic sediments reaches 16 Km (McGoockey, 1975) . It starts in the northern central Gulf with the Paleocene-Eocene "Midway, Wilcox, Clairbone, Jackson" depotrends and productive series, cropping out in south Texas and Louisiana (fig.1-5 b). They are composed at their base, of (1), a mud dominated stable progradational system (Midway, without growth faults), (2) unstable deeply faulted progradational sandy Wilcox deltaic systems intersected by major submarine canyons, (3) the Eocene Clairbone and Jackson regressive sequences (synthesis after Worral and Snelson, 1989).

Little sedimentation occurs in the central northern Gulf during Oligocene time, due to the long high sea level interval occurring during the Rupelian. With the late Oligocene fall of sea level, thick progradational deltaic systems of the Vicksburg, Frio and Anahuac develop offshore south Texas and Mexico reaching a total thickness of 5 to 6 Km . The Frio deltaic and inter-deltaic sequence is the most productive trend in south Texas and is characterised by important growth faulting. This renewed Paleogene voluminous sedimentation initiated important basinward salt movement in the eastern part of the Gulf. Figure 1-6 is a regional dip cross-section across the offshore Louisiana margin (modified from Winker & Edwards, 1983) . Its structure is dominated by large down to the basin growth faults affecting the Paleogene sediments under the present continental coastal plain. The salt morphology on this cross-section is not according to present knowledge. In the studied area, major growth faults flatten rapidly with depth and sole out allochtonous salt sheets (Louann salt), overlaid by offshore Neogene and Pliocene series.

The top Paleogene seismic sequence is characterised on seismic data by strong continuous high amplitude reflectors corresponding to the Late Oligocene world-wide transgression associated with thick silt and shale.

Miocene

By Early Miocene time, the ancient Mississippi was established as the largest source of terrigenous clastic material in the Northern Gulf region. Along the Corsair fault trend offshore Texas, the Miocene series varies from 1000 m up dip to a maximum of 4600 m in the down thrown blocks (Vogler & Robinson, 1987) . Neogene deposits form the main source of offshore hydrocarbons production in the northern Gulf.

Offshore Louisiana, Miocene deposits can reach up to 6000 m. From the coast down to the basin, these shaly and sandy units thicken and decrease in sand percentage (correlatively in hydrocarbons). The most prolific interval is between the Bigenerina humblei "Corsair Trend" zone (13-14 Ma) and the middle Early Miocene, "Siphonina davisi" benthic foraminifer zones (see fig.1-7). The "Big Hum" depocentre

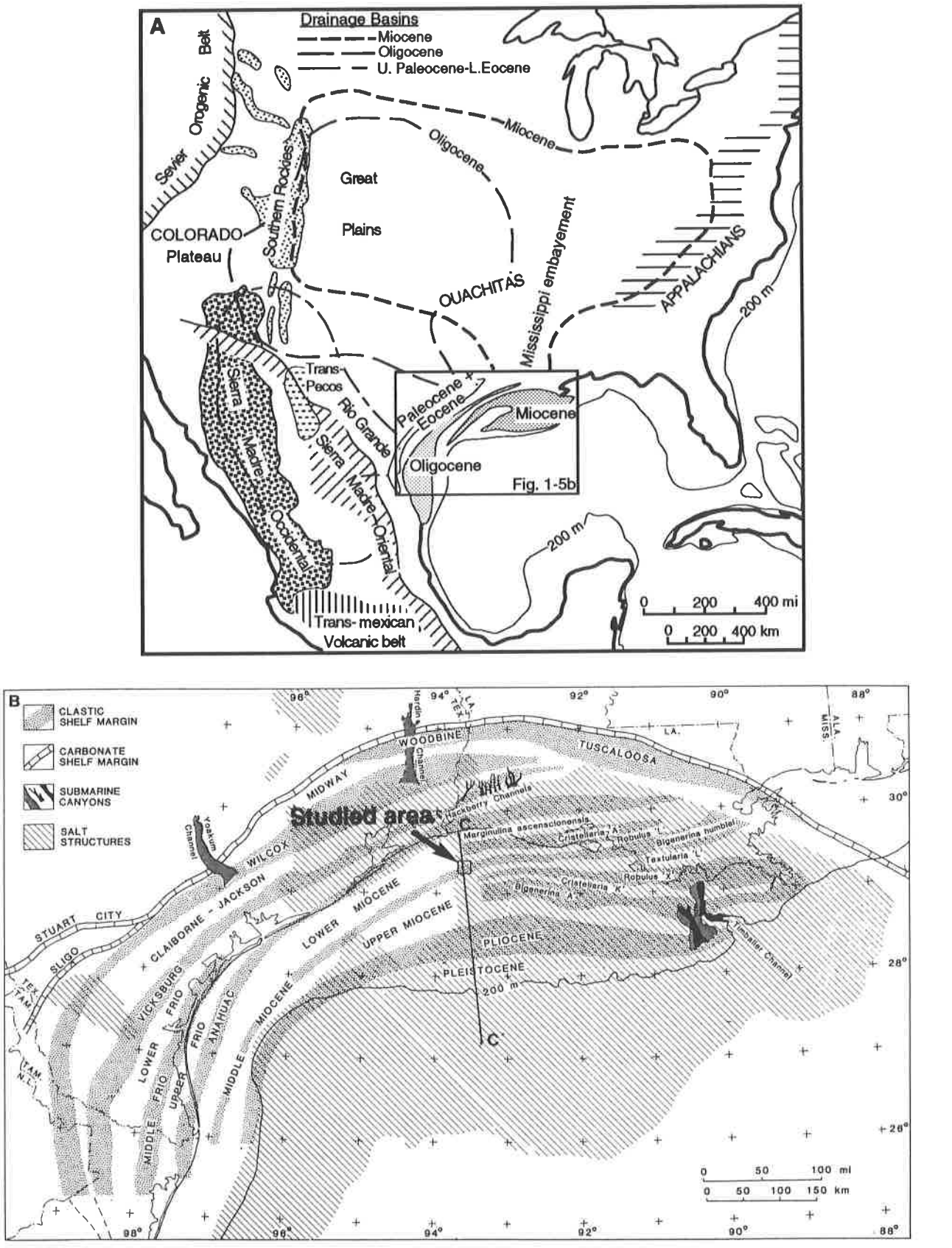

Fig. 1-5: ***a.*** *Postulated Tertiary drainage basins correlated with major tectonic uplifts, volcanism and deltaic sedimentation on the northern coast of the Gulf of Mexico (modified from Winker, 1982).* ***b.*** *Zoomed map showing main Cenozoic depotrends of principal stratigraphic units and submarine channels seaward of the mid-Cretaceous carbonate shelf margin in the northern Gulf of Mexico (modified from Winker, 1982). Profile C-C' is shown on figure 1-6.*

is located 50 Km offshore from the studied area (see fig. 1-5 b and Chap.6). During the Messinian erosive low sea level event, the complete Miocene shelf is exposed to sub-aerial erosion. This is recorded as a strong unconformity on the shelf break and slope, easily interpreted on seismic lines (further developed in Chapter 5.7). On the shelf, the unconformity can be difficult to identify on seismic lines but can be seen on logs by the transition from the Robulus E to the Textularia X benthic foraminifer zones (fig.1-7).

Based on the regional data from the OCS Report (Courtney Reed & Layendecker, 1987) , unpublished data provided by the oil industry and our data, ecological zone maps have been reconstructed on the base of seismic regional lines and fauna assemblages, in the central northern Gulf offshore Louisiana, for the productive interval of Early and Middle Miocene. They are given in Annexe 2 with a compiled synthetic chart of the reference faunas used for dating in the central northern Gulf of Mexico.

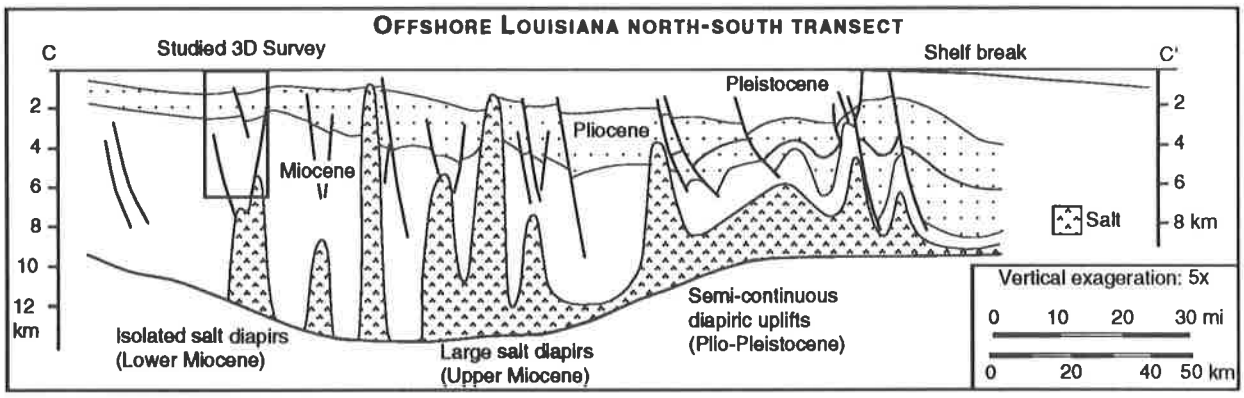

Fig. 1-6: Regional dip cross section running through the north central Gulf of Mexico, offshore Louisiana. Morphology of salt not according to present knowledge (modified from Winker 1983).

Pliocene

A thin uniform layer of Pliocene sediments covers the totality of the central northern shelf offshore Texas and Louisiana. The total thickness of Pliocene sediments increases from 1400 to 1700 m from east to west. In the same way, the sand content of these shaly sands and silts increases regularly from Texas to Louisiana as we get closer to the present Mississippi delta (Courtney Reed & Layendecker, 1987). The Pliocene can be subdivided in two units on the base of faunal assemblages (benthic forams, fig. 1-7) :

- Early Pliocene (Textularia X zone)
- Late Pliocene (Buliminella 1 zone)

Both top and base of the Pliocene are marked by major unconformities correlated to major sea level falls (fig. 1-7). The top Pliocene (in the Gulf coast sense) situated just above the 3.0 Ma sequence boundary is widespread on the entire surface of the shelf. It can have locally eroded the totality of Pliocene and top Miocene deposits (High Island Ridge area). The distal Pliocene equivalent is the Cinco de Mayo unit that has an average thickness of 200 m (Schaub *et al.*, 1984) . This unit thickens to nearly one kilometre offshore the Texas and Louisiana slopes. It is composed of abyssal fine grained clastic material acoustically transparent. On seismic data, the top Pliocene limit is often represented by strong amplitude continuous and homogeneous reflectors below a visible angular unconformity of lower Pleistocene sediments (see Chapter 5.5).

Plio-Pleistocene limit

According to different sources most ages estimated for the Plio-Pleistocene limit varies between 1.6 to 3.0 Ma (and even between 0.6 and 4.0 Ma ! Harland *et al.* 1989). The international time scales by (Harland *et al.*, 1989 ; Odin & Odin, 1990) propose an age of 1.65 Ma. Paleobathymetric, physic and faunal evidence show a systematic shallowing of facies in the very Late Pliocene and Early Pleistocene (1.65 Ma). The international Plio-Pleistocene limit is defined on the base of planktonic foraminifers in Sicily, correlated to the Gulf by Beard (1968). Globorotalia margaritae defines the Early Pliocene, and the appearance of G. truncatulinoides and Sphaeroidinella dehiscens define the very late Pliocene and Early

Pleistocene (annexe 2, Beard & Lamb, 1968). Thus, the base of the Pleistocene corresponds to an arrival of cooler water with invasion of cold-water species and extinction of warm water species like Globoquadrina altispira characteristic for the top Pliocene (Tab.A2-1, Annexe 2). This major shift in climate with the installation of periodic glacial cycles alternating hot and cold sea water conditions is likely to be what could define the Pleistocene. The base of the Gulf coast Pleistocene is generally taken at 2.8 Ma, corresponding to the transition from the "Valvulineria H" marine transgression to the major fall of sea level at 3.0 Ma. The lowstand unconformity sealed by transgressive shale is recorded on the major part of the shelf and is visible on seismic, logs and faunal data. On logs, in the Gulf of Mexico, the Lenticulina 1 presence (or Lenticulina 2, if 1 is absent) will definitely indicate Pleistocene age (see fig. 1-7). Wornardt and Vail (1991) in their revision of the Plio-Pleistocene cycles in the Gulf of Mexico, divide this period in seven 3rd order sequence with fourteen 4th order sequences (see fig.1-8). They propose that the 3.0 Ma limit corresponds to a major change in glacial rhythm affecting the sequences of deposition, justifying the attribution of the base of the Gulf coast Pleistocene at 2.8 Ma. From their curve (fig. 1-8), three major rhythms of 4th Order sequences are observed:

- from 0 to 0.8 Ma : the time-length for one sequence is 0.1 Ma (8 sequences)
- from 0.8 to 1.46 Ma : 2 sequences with each 0.3 Ma duration
- from 1.46 to 4.2 Ma : 1 sequence time-length ranges between 0.4 to 0.8 Ma
- below 4.2 Ma : 3rd Order sequences are registered (superior to 1 Ma).

What is actually observed below the 3.0 Ma limit is a hiatus in the sedimentation record making difficult the recognition of 4th order sequences, thereby suggesting a change in periodicity. But the presence of the short regional 4th order sequences at 3.1 Ma and between 3.8 and 4.2 Ma as well as the difference in range of coastal onlap above and below the 4.2 sequence boundary suggests a bigger shift in periodicity at 4.2 than at 3.0 Ma. Additional information on the type of lithologies and sedimentation processes enhanced by the 3D data presented in this study converge in that direction (see chapter 5) and indicate an eventual change in periodicity at 4.2 Ma. Furthermore, the 4.2-4.5 Ma time interval corresponds to the period when our first direct ancestor, "Australopithecus afarensis" definitely took a separated evolution trend from the Chimpanzees and Gorillas (Chaline, 1985) . This period also coincides with the replacement of large surfaces of forests by savannah (Caron *et al.* 1992). Was it related to a major global climatic change affecting the volume of the ice cap changing the periodicity of eustatic cycles ?

Pleistocene

Upper Pleistocene sediments are characterised by continental rapid and periodic glacial influences. Sea level variations induced drastic erosion of the shelf up to a maximum of 200 m. This brought up to 6 km of sediments on the shelf and a rapid migration of the shelf break towards the centre of the basin (Foote & Martin, 1981) . They were deposited in thick fan-shaped depocentres, concentrated in the area of the Mississippi fan. Offshore Texas, the Rio Grande, Colorado and Brazos rivers also build shelf edge deltas during Pleistocene time (Suter & Berryhill, 1985 ; Berryhill, 1987 ; Suter *et al.*, 1987) . The outer slope is characterised by a hummocky topography due to the alternation of structural salt cored highs surrounded by "mini-basins" or rim synclines filled with thick Plio-Pleistocene deformed sediments (fig. 1.1, Bouma & Coleman, 1986 ; Forrest, 1986). The overloading caused by the Plio-Pleistocene depocentres on the outer shelf of the north central Gulf contributed to further separate the downward flowing salt masses from their autochthonous positions (fig. 1-6). Very small amounts of sediments reached the abyssal plain during Plio-Pleistocene time, because of the active salt driven deformation trapping it all up dip from the main salt ridges. Based on these observations, Bally (1981) proposed for the first time, the complete allochtonous nature of the salt masses causing the Sigsbee escarpment (see Chapter 7 for salt tectonic development). The Sigsbee Pleistocene seismic unit (Gulf coast Pleistocene, see fig.1-1) has complex acoustic patterns showing channels, canyons, levees and mass transport down slope. On the shelf, the Pleistocene is characterised by repetitive emersions partially eroding the subjacent sequences in complex patterns.

The general view on figure 1-1 of the Gulf coast passive margin south from the Lower Cretaceous shelf edge shows two definite styles of growth faulting. To the east, onshore and offshore Texas, elongated, rectilinear down-to-the-basin fault systems predominate (Texas style, Worral and Snelson, 1989) and to the west, shorter arched-shaped fault systems dipping both basinward as well as landward (Louisiana style, Worral and Snelson, 1989). This change in faulting configuration can be related to the

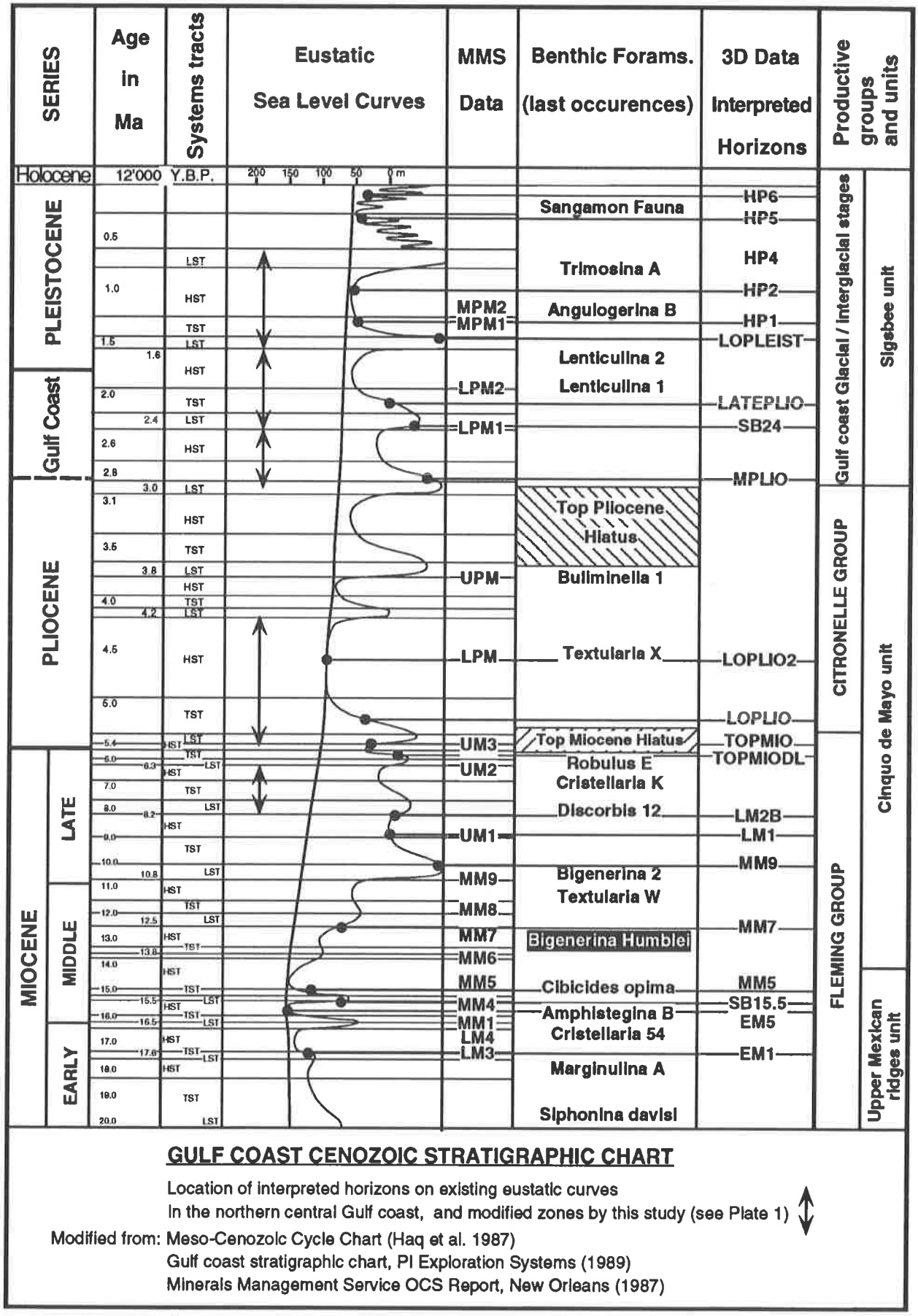

Fig. 1-7: Neogene-Pleistocene sequence stratigraphic correlation chart, north-central Gulf of Mexico. Black dots represent the 21 main 3D horizons interpreted in this study and alternative propositions will be proposed for the time intervals marked by an arrow.

more abundant surface salt positive features offshore Louisiana, probably connected to the Mississippi massive sediment input. This could also show the lack of information offshore Texas compared to the better prospected offshore Louisiana region.

1.5 Summary

Three-dimensional techniques of interpretation of seismic data is applied to a restricted portion of the continental shelf of the northern central Gulf of Mexico. The studied area is a cube of 225 sq. km. by 7 to 8 km in depth that intersects the complete Neogene and Pleistocene sediment offshore Louisiana, in the West- Cameron region. This research, directed by Professor G.M. Stampfli started in 1990 at the University of Lausanne on a CHARISMA VME™ interpretation software supported by a SUN Vicom station replaced in 1992 by the CHARISMA S™ system run on a Sparc 10 station.

The history of three-dimensional seismic is not very extended as the concept was presented for the first time by Walton in 1972 and the first real interactive system was produced only in 1984. In the 10 years between the realisation of the first horizontal display and the completion of this research an incredible development has taken place in hardware possibilities enabling amazing improvement of the software possibilities.

In the studied area, the Neogene and Pleistocene total thickness reaches approximately 6 to 7 km. The totality of the Cenozoic sediments of the northern Gulf of Mexico are dominated by clastic input coming from the broad drainage basins of central North America. They are arranged in offshore migrating depocentres as the Gulf coast gets saturated with sedimentation. The result of the massive sediment loading on the subjacent Louann salt enables large sheets of allochtonous salt to be driven basinward and to converge under the present foot of the continental slope (Sigsbee escarpment). Secondary loading of the allochtonous salt sheets induces salt positive features than can reach the sea bottom. Important mainly down-to-the-basin growth fault are connected to salt movements over the northern portion of the Gulf coast shelf. All Cenozoic sedimentation patterns on the shelf are directly related to mainly salt driven tectonic subsidence, rate of sedimentation input and eustasy. This research illustrates the Miocene, Pliocene and Pleistocene local sedimentation history and relation to deformation on the base of horizontal three-dimensional displays.

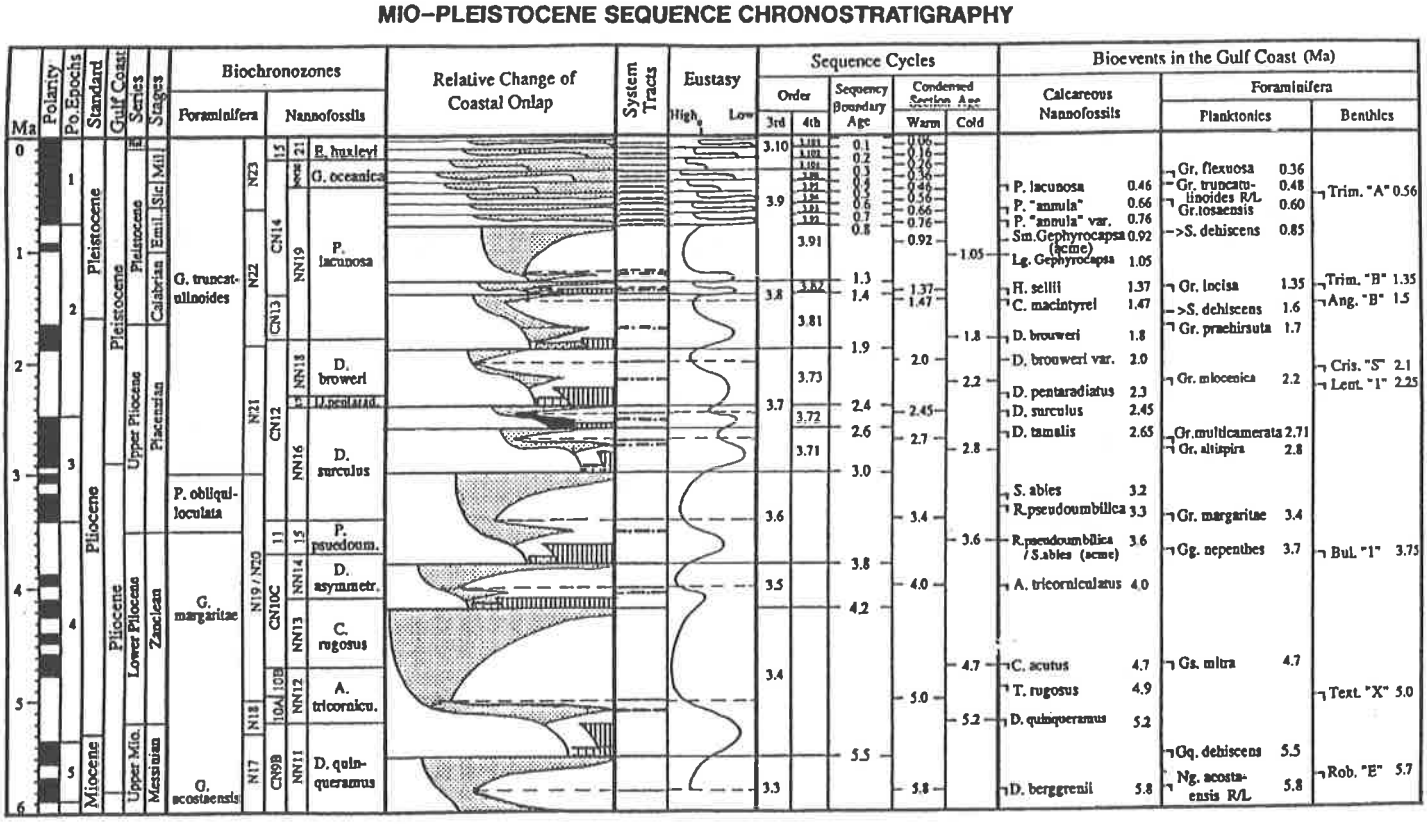

Fig. 1-8: Sequence stratigraphic zonations from Upper Miocene to present (Wornardt & Vail, 1991).

2. SEQUENCE STRATIGRAPHY

2.1 Introduction

Stratigraphy (the study of strata and their lateral correlation) is based on four different approaches. *Lithostratigraphy* is concerned with describing the physical composition and sedimentary features of sedimentary units. *Biostratigraphy* uses the fossil content of a rock unit to locate it in a relative time scale and to correlate it laterally. *Chronostratigraphy* defines the geologic time-span of both lithostratigraphic and biostratigraphic units in correlation with the absolute dating methods (this is not to be mistaken with the freshly born "*Chromo-stratigraphy*" using colour computer screens for correlation !).

When no fossils are available or when lithofacies cannot be directly assessed like on seismic data or non-cored well-logs, correlation from place to place becomes very difficult. Sequence stratigraphy proposes an eustatic chronostratigraphic correlation tool based on the assumption that sea level changes globally influence the development of sedimentary sequences.

What is sequence stratigraphy ?

This notion was still absent from the Glossary of Geology in 1987 (Bates & Jackson, 1987) . In the latter, a sequence is defined by Sloss (1963) as "a major informal lithostratigraphic unit greater than group or supergroup in rank, traceable over large areas of continent, and bounded by unconformities of interregional scope, such as in the cratonic interior of North America". The same glossary provides the definition for seismic stratigraphy stated as : "The study of stratigraphy and depositional facies as interpreted from seismic data " by (Mitchum, 1977) . But contrary to what one may think, the concept of sequence stratigraphy did not exist before 1987, when Van Wagoner *et al.*, (1987) defined it as: "the study of rock relationships within a chronostratigraphic framework of repetitive, genetically related strata bounded by surfaces of erosion or non deposition, or their correlative conformities". Therefore, sequence stratigraphy is an extension of the basic principle of seismic stratigraphy applied to vertical 2D seismic data, to well-log data and later, to outcrop stratigraphy. With the rapid expansion in acquisition, treatment and interpretation of 3D seismic data, providing additional information on the horizontal plane and images of surfaces limiting successive sequences and parasequences, the seismic stratigraphic concepts can be further extended to 3D sequence stratigraphy (Reymond & Stampfli, 1994a) .

But long time before seismic data existed, the concept of stratigraphy became the foundation for modern geology (Albritton 1980). Nicholas Steno enunciated for the first time in 1699 the principles of superposition and stratigraphic continuity and of successive sequences separated by unconformities. In 1799, William Smith achieved a stratigraphic table for England, characterising each strata by a faunal assemblage. Thus, two centuries of geology precede the recent major new step taken in stratigraphy by the "Vail school" in 1977 integrating seismic data as a rigorous tool to recognise and correlate sequences across a basin and even at the planetary scale.

The first time the glacio-eustatic lowering of sea level was demonstrated as a cause for incision of fluvial systems on the exposed continental shelf of the northern Gulf of Mexico was published in 1944 in a US Army report on the Lower Mississippian (Fisk, 1944). The concepts of cyclic sedimentation and climatic influences on sequences deposition leading to global correlation of stratigraphic events were first presented by Sloss (1963, 1972), then by Wheeler (1963), Merriam (1964), Duff et al. (1967) and Schwachrzacher (1975), before Vail et al (1977) proposed their first global eustatic cycle chart. The global validity of such a curve of sea level change cannot be tested within the scope of this study which limits itself to a very restricted portion of the Gulf of Mexico (although this region is the main reference for the construction of this chart). Present world-wide researches try to infirm or to solidify the bases for the existence of a global curve such as proposed by Haq et al (1988, fig. 2-1) . A discussion of the numerous factors affecting the local relative sea level and thereby making a global eustatic chart difficult to establish follows in the next chapter.

2.2 General concepts in sequence stratigraphy

Accommodation space and sediment flux are generally regarded as the two major controls on the development of depositional sequences, their stacking patterns and their component stratal units (Schlager, 1993; Leeder, 1994). Most existing sequence stratigraphic models show a very simplified tectonic component commonly represented by a uniform rate of subsidence superposed to a cyclic eustatic curve whose origins are primarily climatic.

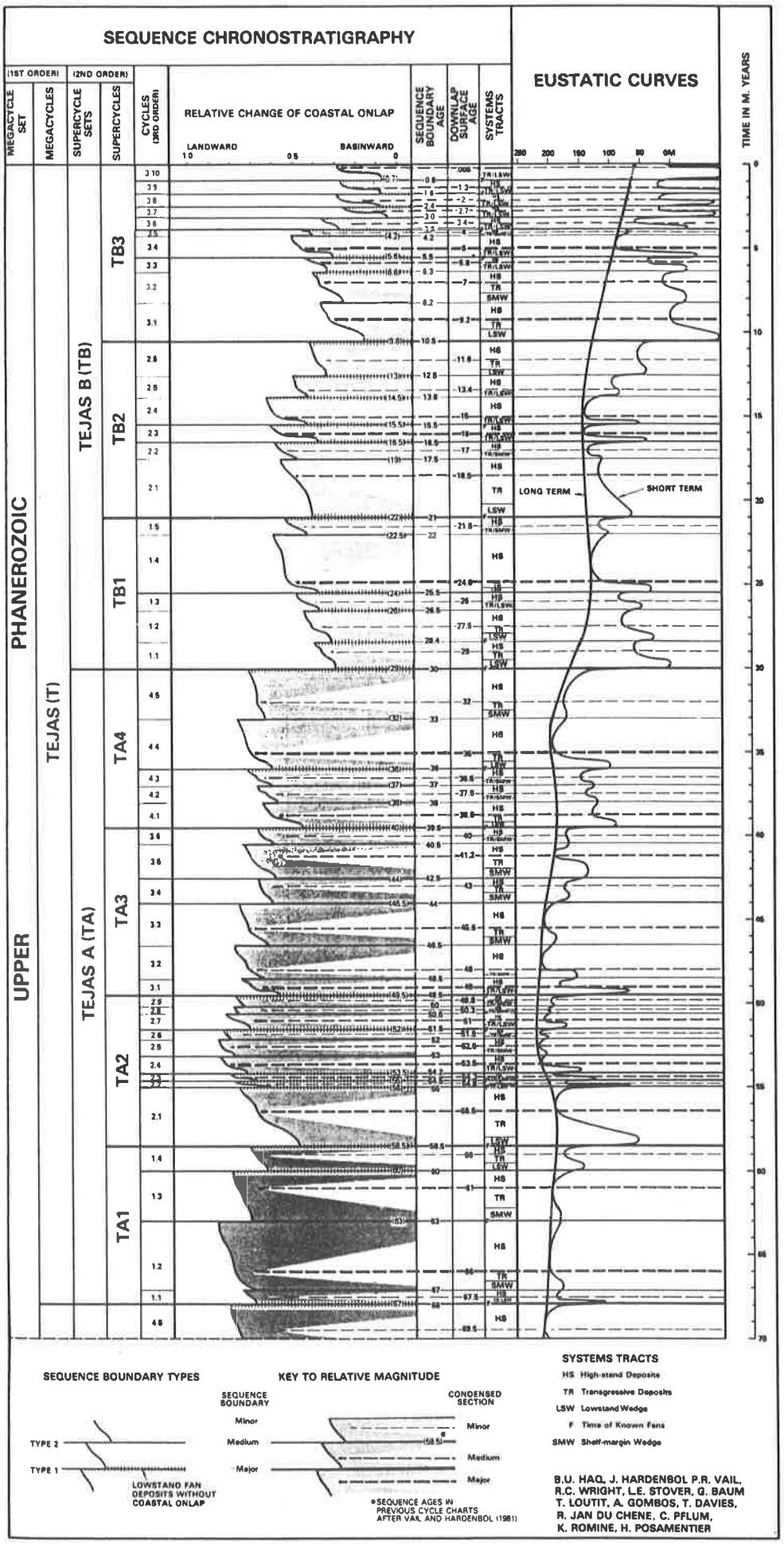

Fig. 2-1: Upper Cenozoic sequence stratigraphic correlation, northern Gulf of Mexico, (Haq et al., 1988).

The overall interaction of as many factors as tectonic, eustasy, climates, topography, biology, bathymetry, hydrodynamics and diagenesis can be represented on one schematic cross-section of a simplified passive continental margin (fig 2-2). The combination of tectonic, eustasy and sediment input produces local shifts in the shoreline registered as a three-dimensional assemblage of lithofacies (Depositional system, Fisher and McGowan, 1967) .

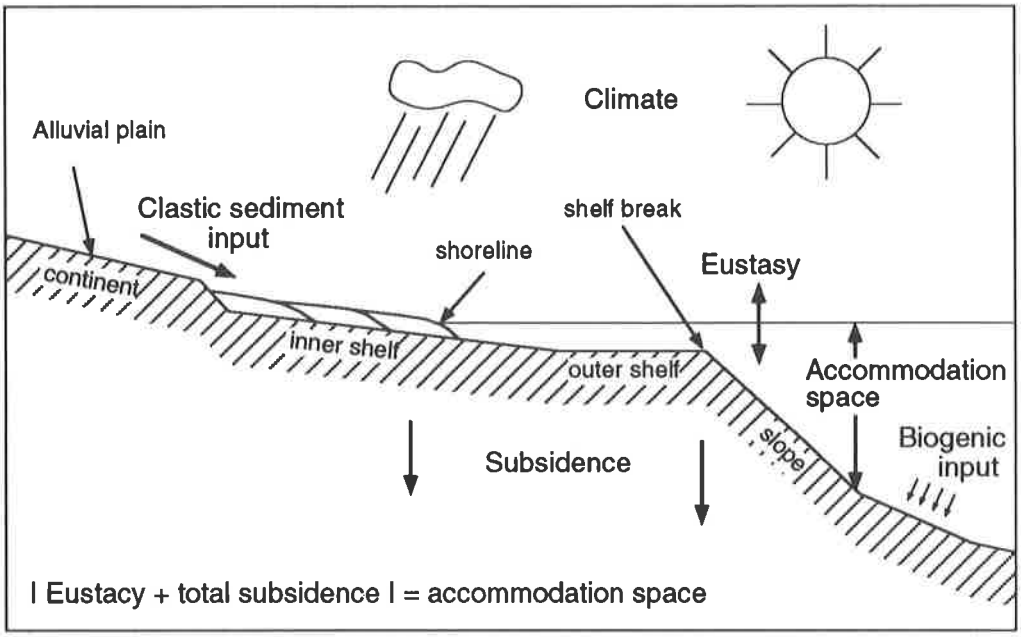

Fig. 2-2: Schematic cross-section across a continental margin. Interaction of 4 major factors regulating accommodation space (Clastic and biogenic sediment input, eustacy, subsidence and climate).

The classification and terminology of marine environments adopted in this research is summarised in figure 2-3. Assemblages of lithofacies characterise ecological zones and ranges of water-depth. Identification of sedimentary features on seismic data, well logs or on the outcrop scale and their correct attribution to paleoenvironments is the cornerstone of sequence stratigraphy.

Classification of marine environments, ecologic zones and depth range

modified after : OCS MMS Report 1987, PALEO-DATA Inc. 1988 New Orleans and Leeder M.R. 1985.

Note : in some classification the intertidal zone, the beach and brackish zone are included in the Ecologic zone I.
Fair weather wave base lies at about 5-15 m depth.

CONTINENTAL	BRACKISH ZONE	BEACH	INNER NERITIC	MIDDLE NERITIC	OUTER NERITIC	UPPER BATHYAL	LOWER BATHYAL	ABYSSAL
			0 -20 m	20 -100 m	100 -200 m	200 - 500 m	500-2000 m	> 2000 m
			I	II	III	IV	V	VI
Eolian dunes, fluvial stream, meanders and sand bars, flood plain and back swamp	Marshes, lagoons, estuarines, lakes, tidal channels, sheet sands	Sand bars, brackish and marine beaches, barriers, tidal deltas, and channels	Tidal deltas and channels,	Density current and storm deposits, debris flow, submarine canyon fill,			submarine canyons, density current and overbank deposits, turbidite fans, canyon fill	
DELTAIC DEPOSITS								
Distributary channels, main channel and levee deposits, cravasse splays			Delta fringe sands, delta mouth bars distributary channels, shoreface sands,		submarine channels and slumps			

Fig.2-3: Synthetic classification of marine environments, ecologic zones and depth range. Integration of OCS MMS Report (1987), Paleo-Data Inc. (1988) and M. R. Leeder (1985).

The morphology of depositional systems or sequences in a clastic environment is believed to be directly related to eustasy and can be further separated in systems tracts defined for the first time by Brown and Fisher in 1977 as: "a linkage of contemporaneous depositional systems". The interpretation of systems tracts on seismic lines is based on the assumption that seismic reflections, following former depositional or erosional stratal surfaces represent synchronous geologic time lines. Reflections occur on acoustic impedance contrasts caused by changes in lithofacies. A reflector can also indicate differences in diagenesis in a single homogeneous formation and therefore not correspond to a time consistent horizon. Furthermore, limits of systems tracts along one seismic reflector commonly cross several lithofacies boundaries from the shelf down to the basin.

The organisation of the sediment pile into sequences is done through the identification of sequence boundaries characterised by regional overlying regional onlap and truncation. There are two types of sequence boundaries.

Type-1 sequence boundaries are "regional" surfaces "characterised by sub aerial exposure and concurrent sub aerial erosion associated with stream rejuvenation, a basinward shift of facies, a downward shift in coastal onlap and onlap of overlying strata" (Van Wagoner et al. 1987, see fig. 2-4). Type 1 sequence boundaries occur when the rate of sea level fall is greater than the rate of basin total subsidence. Large surfaces of the shelf emerge and the depositional-shoreline closes on to the shelf break. The rivers will respond to this fall in base level by migration and incision, increasing the sediment flux on the shelf which in turn enables forced regression.

Type-2 sequence boundaries are "regional" surfaces "marked by sub aerial exposure and a downward shift in coastal onlap landward of the depositional-shoreline break"(Van Wagoner et al. 1987, see fig. 2-3). It is not accompanied by a major change in base level (no stream rejuvenation) and is therefore very difficult to identify on the shelf or on the outcrop. It occurs when the rate of eustatic fall is less than the total rate of basin subsidence.

A Type-1 sequence is bounded below by a Type-1 sequence boundary and above by either a Type-1 or a Type-2 sequence boundary. A Type-2 sequence is bounded below by a Type-2 sequence boundary and above by either a Type-1 or a Type-2 sequence boundary.

A sequence is commonly subdivided in three systems tracts as represented on the classical model for siliciclastic sediments illustrated on figure 2-4. A Type-1 sequence is composed of lowstand, transgressive and highstand systems tracts. A Type-2 sequence is composed of shelf-margin, transgressive and highstand systems tracts (see fig. 2-4).

The lowstand systems tract (Lst) is deposited as soon as the relative sea level starts to fall (fig. 2-4 c), when the eustatic fall of sea level "catches back" the total subsidence curve. The shelf starts to emerge and to be eroded with development of incised valleys (ivf). In deeper water (superior to 200 m) it consists of a basin floor fan (bf), a slope fan (sf) and a lowstand prograding wedge (lsw) or prograding complex. The base of a lowstand system tract is a Type-1 sequence boundary. A transgressive surface called "top lowstand surface" in this study (TS, on fig. 2-4) seals the gross sandy lowstand deposits with finer silt and shale when the rate of sea level rise reaches its maximum (first inflection point on the eustatic curve, fig. 2-4 c). Most hydrocarbon are found in siliciclastic rocks of the lowstand system tract due to the superposition of thick porous sands and continuous shaly seal on top (further developed in Chapters 5 and 6). It will be demonstrated in Chapter 5 that the lowstand interval is marked on the inner shelf by two distinct phases of erosion:

- when the relative sea level starts to fall shallow meandering channels develop perpendicularly to the shoreline.
- this first generation of channel is then partially removed by deeper incised valleys associated with the phase of maximum erosion (minimum relative sea level).

The equivalent lowstand systems tract in a Type-2 sequence is a shelf margin wedge (SMST, fig. 2-4) bounded below by a Type-2 sequence boundary and above by a transgressive surface. This sedimentary wedge usually deposited on the shelf break, is composed of very well sorted sands transported along the whole shelf and thereby constitutes a very good assemblage of potential reservoir rocks. As for the lowstand systems tract, the shelf margin wedge is sealed by a transgressive surface at least in the outer portion of the shelf.

Transgressive systems tracts (TST, fig. 2-4) have a transgressive surface at their base or a sequence boundary in a proximal position (inner shelf, 0-100 m) and a maximum flooding surface at their top.

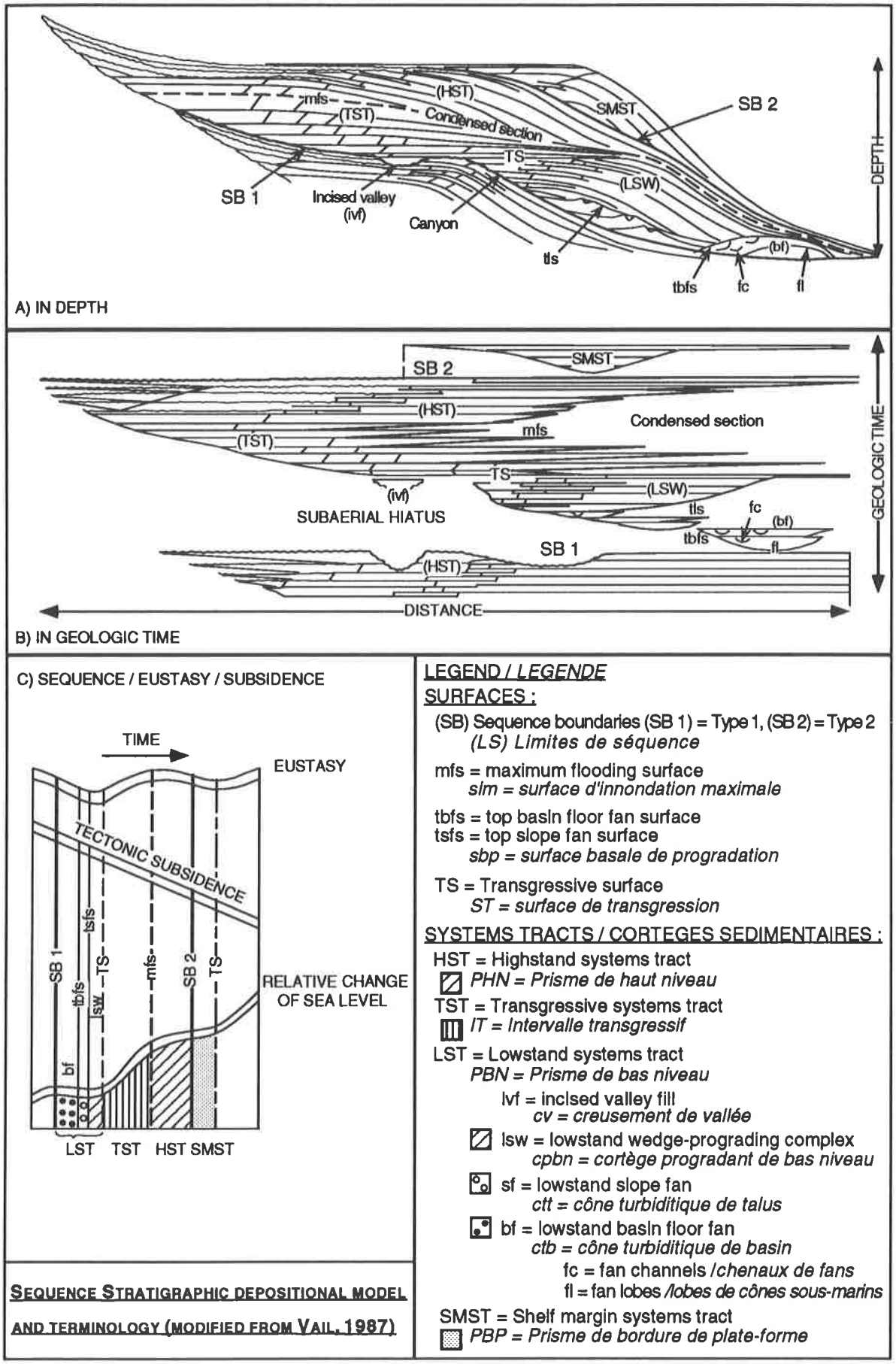

Fig. 2-4: Sequence stratigraphy diagrammatic section showing typical distribution of siliciclastic sediments within sequences and systems tracts presented in depth and geologic time (modified from Vail et al. 1987). Nomenclature in english and french.

They consist of a set of backstepping, retrogradational parasequences that thicken shelfward, deposited during the period of maximum rise of relative sea level. And this, even if a parasequence is defined by Van Wagoner et al. (1987) as "a relatively conformable succession of genetically related beds or bedsets bounded by marine-flooding surfaces and their correlative surfaces. Parasequences are *progradational* and therefore the beds shoal upward". In conditions of low sediment supply, the incised valley may be directly filled by transgressive fine or reworked sediments when the relative sea level is maximum and the shelf entirely flooded.

The maximum flooding surface (mfs, fig.2-4) is a basin wide conformable fine sediments interval deposited during the period where the relative sea level rise is maximum or starts to decline. Most detritic sources are flooded and the clastic sediment input is minimum. High abundance and diversity of faunas stored in these shale constitute an excellent tool to date and correlate sequences across a basin and even to a more global scale.

A highstand systems tract (HST, fig. 2-4) is bounded at its base by a downlapping surface on the maximum flooding surface or a sequence boundary in the very proximal zone and always has a sequence boundary on top (Type-1 or Type-2). The highstand systems tract is characterised by large prograding and slowly aggrading low angle sigmoidal patterns. The late sub aerial highstand complex is characterised by sediments deposited above sea-level.

Systems tracts succession and lithologic content will be presented with more details in the chapter on well-log sequence stratigraphic analysis, based on real data analysed in this research.

2.3 From the model back to reality

This simplified model (fig. 2-4) presents the successive sedimentation of systems tracts at a very unrealistic scale, in an area devoid of deformation (growth fault, diapiric piercement). Figure 2-5 schematically indicates the true proportions of systems tracts within a sequence in a siliciclastic environment on a continental passive margin. One of the major problem occurring in sequence stratigraphy is the correlation between the distal and the proximal offshore zones. In most cases a factor from 10 to 1000 exists in the thickness of a sequence between the inner shelf and the bathyal zone. Even more difficult is the correlation of continental fluvial behaviour in response to eustasy. Recent researches attempt to understand the impact of relative base level changes on rivers and flood plains as it has a direct control over the rate of sediment input on the shelf (Blum, 1994 ; Leeder, 1994) . In the studied area, the totality of the Plio-Pleistocene and the upper part of the Miocene series (Messinian, Tortonian) oscillate between continental and middle neritic conditions (0-100 m).

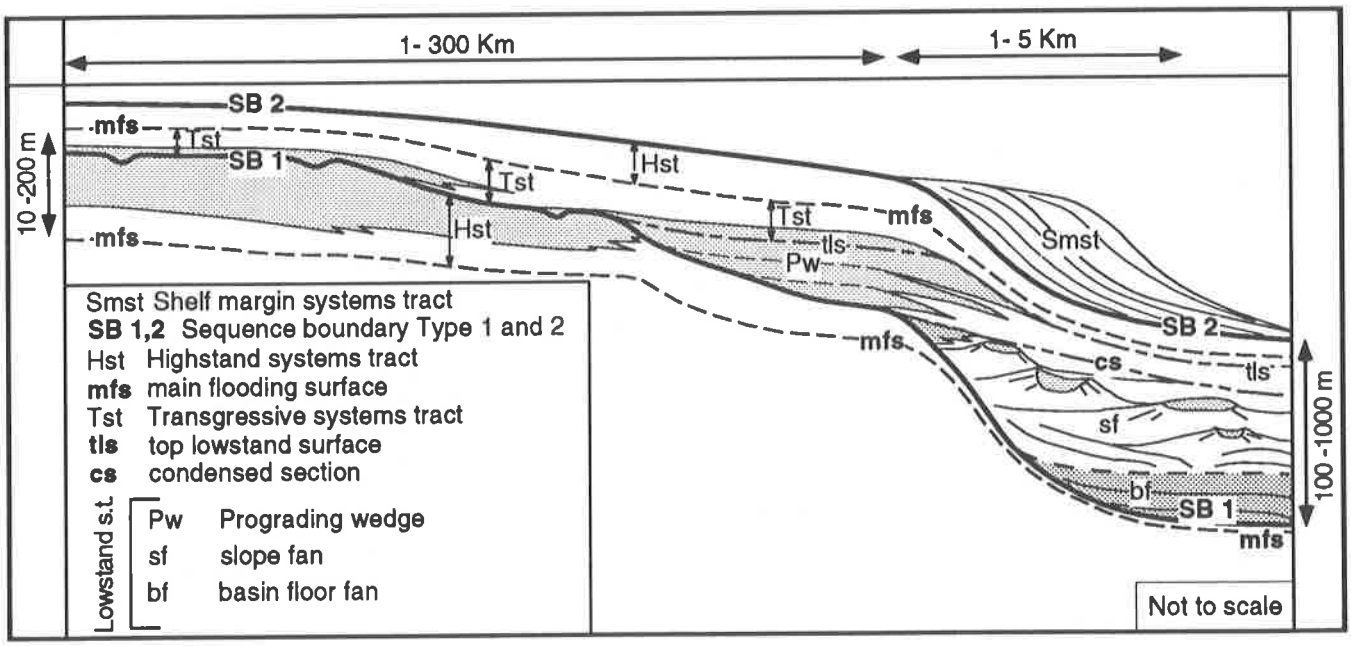

Fig. 2-5: Schematic representation of a sequence in a siliciclastic environment, bounded at its base by a Type-1 sequence boundary, with a Type-2 sequence boundary on top.

Only the lower portion of the studied sediments (middle to early Miocene) present sedimentary features belonging to the "down the shelf break" realm. Systems tracts arranged in the way depicted on figure 2-4 will not be found in this study. But rather, a succession of conformable sandy and shaly shelf facies will alternate regularly (fig.2-5).

In such conditions, sequence boundaries are difficult to recognise due to superimposition of the erosive effects. One of the objectives of this research is to show that where the classical 2D "truncation-onlap-downlap" seismic interpretation method is limited and even impossible to realise (inner shelf without correlation with the slope area), the recognition of succession of reduced systems tracts becomes possible on the horizontal images provided by 3D seismic data analysis of successive erosional features (see Chap.5)

The second complication occurring on most shelves of passive margins is caused by the development of down-to-the-basin and landward dipping numerous growth faults. Figure 2-5 shows a schematic cross-section across such a growth fault from an example of the Gulf of Mexico. One third order sequence is interpreted both from the seismic facies and well-log response, on both compartments of a growth fault. A thickness factor from 10 to 1000 can be observed between the footwall and the hanging wall. Rapid tectonic subsidence on the hanging wall accommodates enough space for thick and complete sedimentation of the 4 main systems tracts. On the footwall, very limited sedimentation is possible. This relatively elevated plateau is subject to deep erosion as soon as the water level falls, thus removing important portions of the sediment record. The product of this erosion is re-deposited down fault. The important differential loading on both sides of the fault still increases the subsidence of the hanging wall. It frequently becomes very difficult to correlate systems tracts and sequence boundaries across active growth fault on the base of seismic data only. Well-log analysis allow to recognise typical succession of lithologies that can be interpreted in term of systems tracts succession. But the only secure way to establish good correlation across growth faults is based on faunas recognition, being aware of the massive reworking and re-deposition occurring in such conditions.

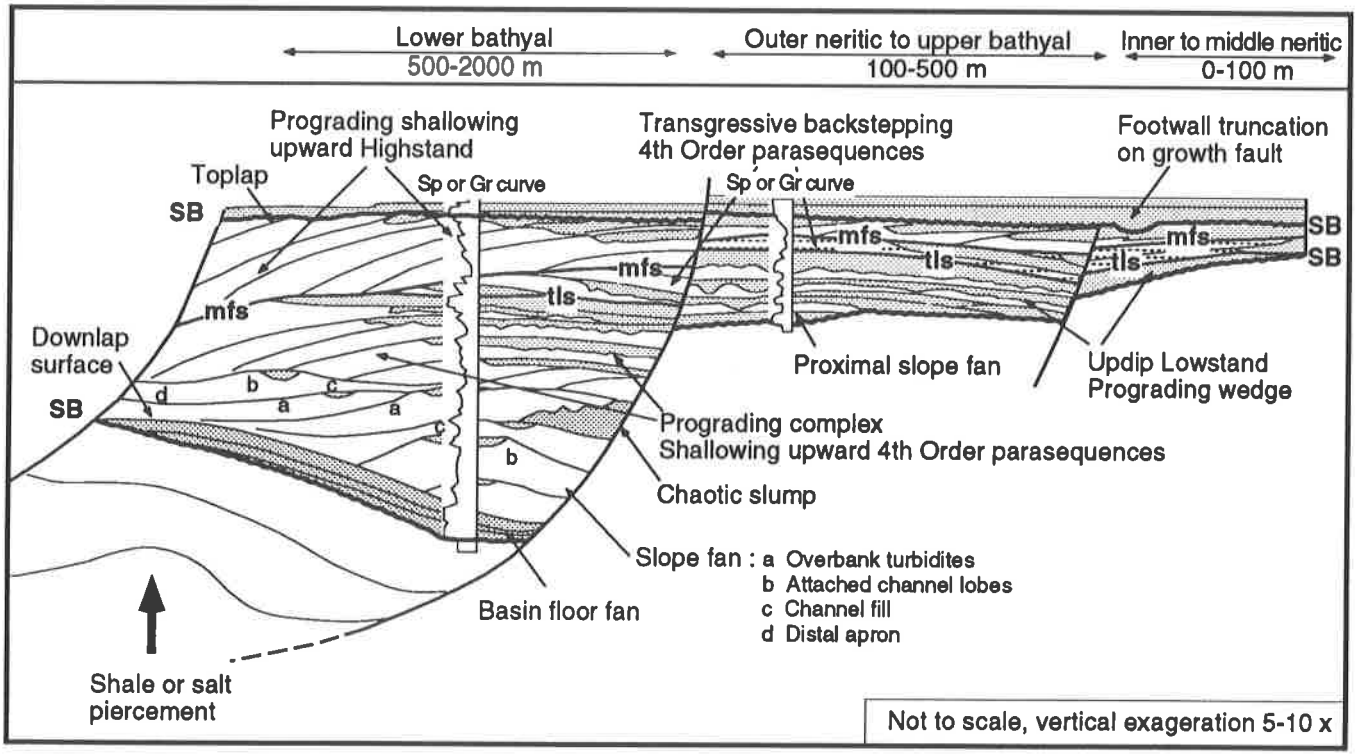

Fig.2-6: Systems tracts (with well-log response and lithology) for one 3rd order sequence across a schematic down-to-the-basin growth fault, representative for the Cenozoic series on the northern shelf of the Gulf of Mexico (modified from Vail et al. 1990).

2.4 What causes eustasy ?

Eustasy can be defined as world-wide sea level fluctuations caused by absolute changes in the quantity of free sea-water and is thereby closely related to climate and tectonic movements at the planetary scale.

Regular cyclic variations in sea level is a natural phenomenon that can be observed at many scales, from the daily tidal pulses to the global larger scale variations occurring over millennia. Therefore the true question would rather be: what causes eustasy, at what scale ?

Marine sediments work through geological time as an incomplete recorder of past conditions and are organised in stratal units ranging from millimetres to kilometres, from lamina to megasequences. Campbell (1967) described the hierarchy and characteristics of the finer units ranging from the smallest megascopic layer (lamina, deposited occasionally in a few minutes or hours) to the bed sets bounded by major facies changes, sedimented rapidly (minutes to year) in a episodic to periodic manner. Sequence stratigraphy applied to seismic data or at the outcrop scale does not consider stratal units smaller than the bed sets (always >1 m). The stratal units considered by sequence stratigraphy are listed below:

- parasequence
- parasequences set
- systems tracts
- sequences
- supersequences
- megasequences

Each of these stratal units have definite range of thicknesses, lateral extend and time span of deposition. Their reproducibility and observed periodicity suggest that they may represent the manifested effects of natural cyclic causes. By observing the global eustatic chart measured over Phanerozoic time (fig. 2-7), it is possible to attribute a range of periodicity to the four main stratal units and to propose mechanisms able to generate them.

Megasequences have a thickness superior to 1000 m and a time length superior to 50 Ma. They correspond to the 1st order cycles on the global eustatic chart and are called "smooth long term" cycles (fig.2-7). When continents are gathered in super-continents like 230 Ma and 560 Ma ago, slow rate of oceanic expansion is supposed to induce a planetary sea level fall. Super-continent fracturing initiates a transgressive phase reaching its peak when a maximum of mid-oceanic ridges activity is registered (maximum of continental break up, late Cretaceous and late Cambrian floods).

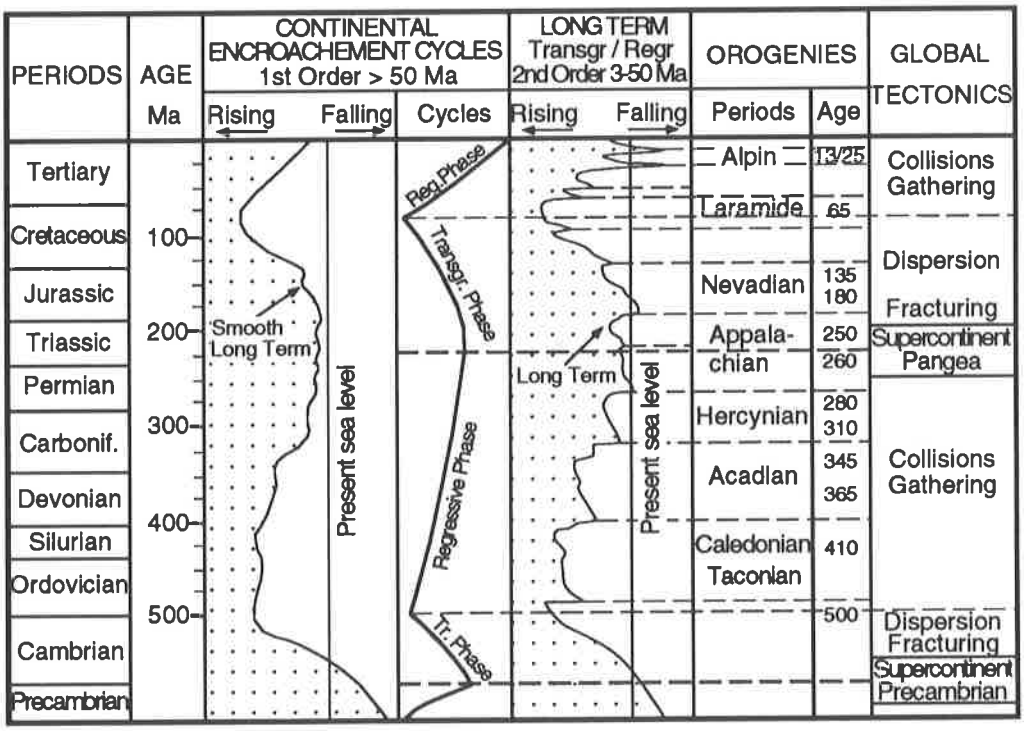

Fig. 2-7: Relation between eustacy and orogenies during the Phanerozoic. 1st and 2nd order cycles (smooth long term, long term) are correlated to global tectonic events. Gathering of continents induces sea level fall, continents break out overall marine transgression (modified from Duval & Cramez, 1990).

Supersequences have thicknesses superior to 400 m and a time span ranging from 3 to 50 Ma. They can be related to the 2nd order "Long term" cycles (fig.2-7). They seem to correlate to local changes in rate of tectonic subsidence caused by regional orogenies (Duval & Cramez, 1990) . This hypothesis is very doubtful but the supersequences could find an origin in the quicker pulses of back arc rapid opening followed by closing and obduction moving very large volume of sea water (Pillevuit, 1993) . As for the 1st order sequences, a high degree of symmetry is observed between the regressive and the transgressive phases.

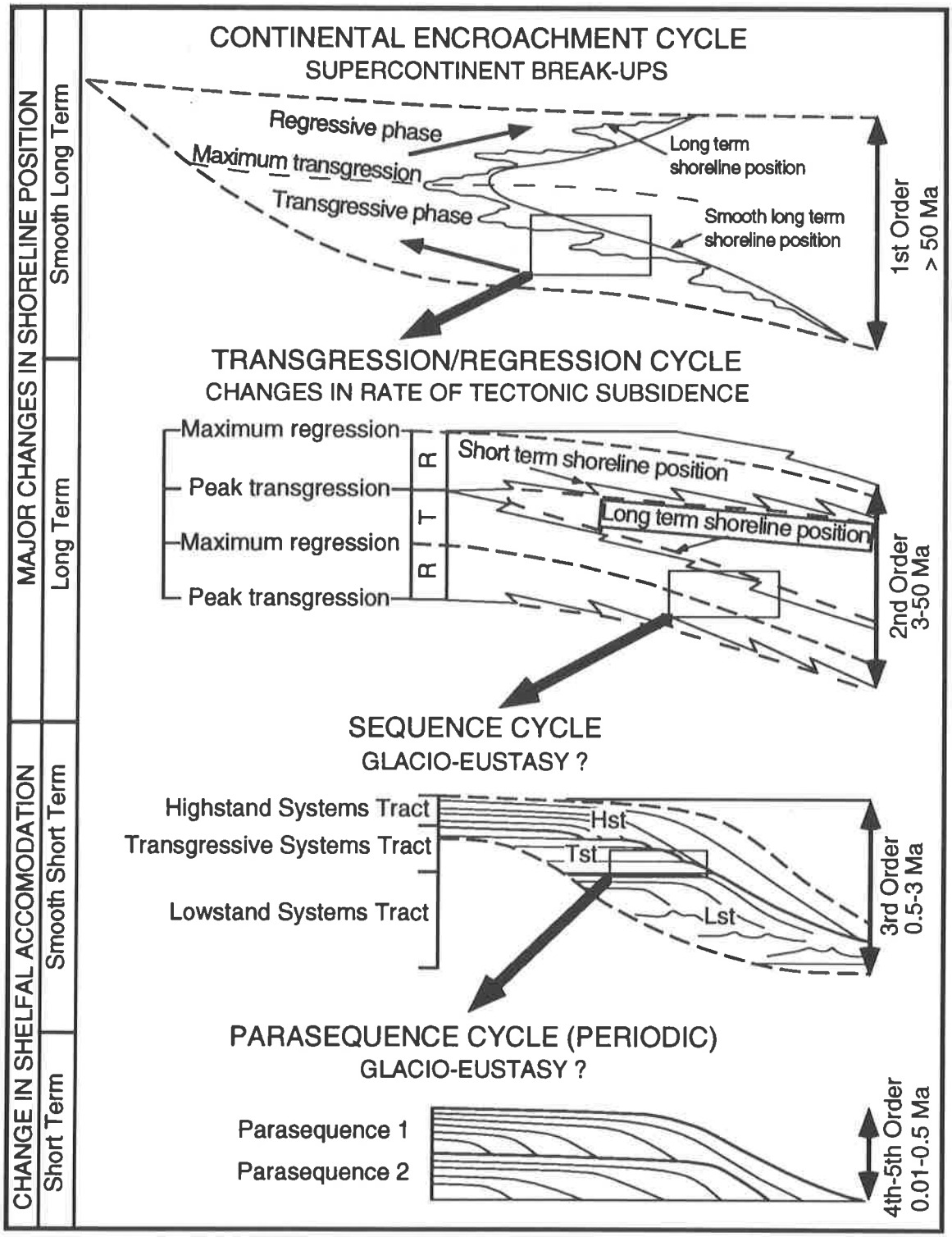

Fig. 2-8: Types and hierarchy of stratal units cycles for megasequences, supersequences, sequences and parasequences (modified from Duval and Cramez, 1990).

Sequences have an average thickness ranging from 10 to 400 m and a time span of the order of the million year (3-50 Ma).They correspond to the 3rd order cycles called "smooth short term" on figure 2-8. Even if no real astronomical factor seem to fit these well defined cycles, not showing an excellent periodicity, a glacio-eustatic explanation is believed to be at their origin. They can surely be explained by the complex interaction of the many factors locally affecting the relative sea level (see introduction above).
Parasequences whose thicknesses are typically within the 10th of meters can be deposited within a short time interval (between 0.01 and 0.5 Ma). They constitute the 4th order and higher cycles and are the building blocks of systems tracts and sequences. Many theories have been proposed to explain periodic glacial cycles controlling parasequences sedimentation. But orbital forcing definitively replaced other hypothesis based on volcanism, solar variability, interstellar dusts or magnetic field variations. Still, it will be mentioned in chapter 5 that very probable similar but may be not genetically related 0.8 Ma cycles are observed both on the eustatic and on the magnetic curves. The discovery of the Earth orbital characteristics and cycles published in 1941, by the Yugoslav astronomer M. Milankovitch (Milankovitch, 1941) was definitively adopted by Hays *et al.* (1976) as the main cause and explanation for cyclic quaternary climatic changes. 4th order parasequences (0.1-0.5 Ma) are responses to the changes in eccentricity of the orbit of the Earth around the Sun with a period of 96'000 yrs (fig. 2-9 a). 5th order parasequences are related to the tilt of the Earth's rotation axis (oscillating between 21° and 24°, with a periodicity of 41 kyrs, fig. 2-9 b) and to the precession of the equinoxes (the time when the Earth is nearest the Sun changes from January to July over a period of 21 kyrs, fig.2-9 c). Combinations of these three curves induce glacial cold periods with additive stadial and subtractive interstadial events with an approximate periodicity of 25'000 yrs (fig.2-9 d). These cycles are expressed in the succession in quaternary ice ages. At a larger scale, the seven glacial-interglacial periodic cycles over the 800'000 yrs before present, observed in this study (Chap. 5.2), confirm the fact of orbital forcing on cyclic sequences and parasequences.

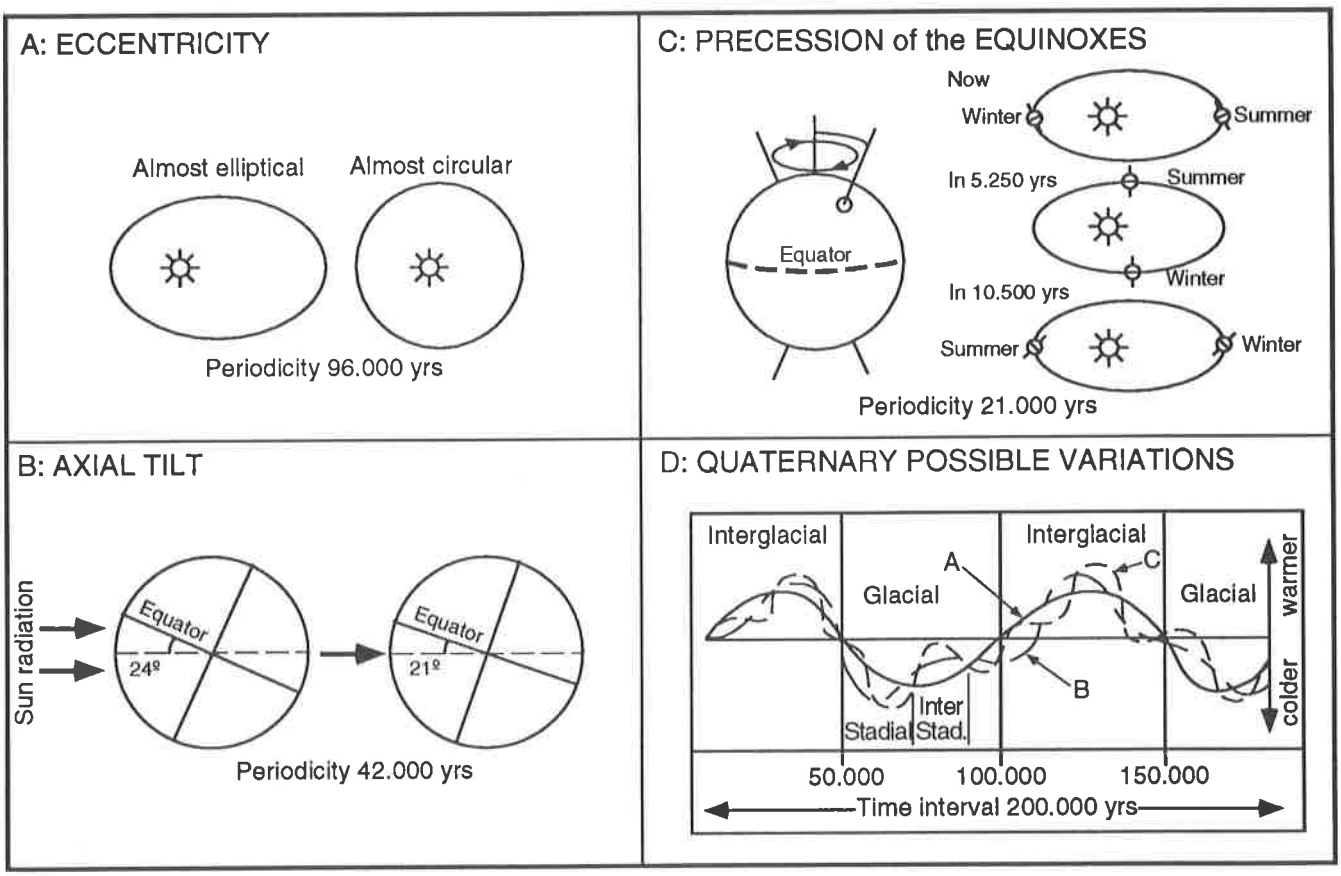

*Fig. 2-9 (**a**, **b**, **c** and **d**): Variations of the orbit of the Earth characteristics (**a**: orbital eccentricity, **b**: axial tilt, **c**: precession of the equinoxes and **d**: glacial and interglacial composite curve over 200.000 yrs.*

As a conclusion to this chapter on the causes of eustasy, two questions can be asked : On the sediment record, there is an apparent stronger asymmetry between the regressive and the transgressive phases observed on 3rd order and higher sequences than on the larger 1st and 2nd order sequences (fig.2-8). Do regressive and transgressive phases have the same extension through time at any scale of periodicity ? Does the sediment response to eustatic symmetric cycles produces asymmetric parasequences ? And secondly: Are the 0.1 Ma eccentricity related cycles absent from the sediment record below the 0.8 Ma limit because they do not exist or because they cannot be resolved as yet by sequence stratigraphy at the outcrop scale, on logs or on seismic data ? An attempt to answer these questions will be discussed in chapter 5.

2.5 Sea level changes: a key for future climate predictions ?

Eustatic records obtained from seismic data, well-logs and natural outcrops constitute merely one of the tools available to understand paleoclimates and predict large scale future climatic evolution on the planet Earth. Sea level is a direct indicator of climate and paleoclimate. But an important distinction has to be made between climatology and paleoclimatology. The main difference resides in the time factor. Paleoclimatic reconstruction from different analysis of sediment record (geochemistry, palaeontology, palynology, sequence stratigraphy, radiometric dating, etc....) have a time unit generally superior to 10 kyrs. Whereas historical climatic reconstruction are based on time units that are 100 to 1000 time smaller. Hence comes the difficulty in separating the subtle from the gross in climatic matters and in elaborating projections and even predictions for the near future.

Figure 2-9 presents 4 curves of sea level changes at different time scales and a projection of sea level rise for the next century as a result of complex modelling integrating as many factors as possible. The further we go back in time the worse the resolution and the more abundant the amount of hiatuses in the sediment record. Correlatively, the closer to the present, the higher is the frequency of recognised glacial events. Did high frequency glacial cycles exist in Plio-Pleistocene time, superposed to the observable 4th to 5th order parasequences ? What is the way to évaluate them ? And what is the way to try it further back in time ?

The sea level rise occurring since 15 kyrs is very well documented (fig.2-10 c Fairbridge, 1976) . A major rise of sea level (from -150 m to approximate present sea level) occurred from 15.000 to 6000 years BP. Since then, the sea level seems to be stable within the meter scale. On the historic scale (fig. 2-10 d) observations note an abnormal increase of a few centimetres since the beginning of the century. Can it be related to human industrial activity on the planet ?

Figure 2-10 e) proposes three curves of sea level rise for the next century. The lower one is close to the "normal" rate considered without abnormal human activity (green house effect limited). The middle curve, described as the most probable evolution (confirmed by several sources), proposes a sea level rise of about 50 cm for the next century. And finally the most extreme probabilities conclude to 120 cm of sea level rise caused mainly by an increase in green house effect (Warrick, 1993 ; Warrick *et al.*, 1993) . But after all, it is all merely in the range of one meter for a few hundred years which is definitively below geological resolution...

2.6 Summary

Sequence stratigraphy was defined for the first time in 1987 as: "the study of rock relationships within a chronostratigraphic framework of repetitive, genetically related strata bounded by surfaces of erosion or non deposition, or their correlative conformities"(Van Wagoner *et al.*, 1987). Based on the concepts of cyclic sedimentation and climatic influences on sequences deposition observed on seismic reflection data, Vail et al (1977) proposed their first global eustatic cycle chart leading to global correlation of stratigraphic events.

Depositional sequences are mainly controlled by accommodation space and sediment flux. The determination of lithofacies leading to the identification of paleoenvironments and to the identification of erosional surfaces interpreted as sequence boundaries allow to understand the organisation of the sediment record into sequences. Based on clastic shelf models, a sequence is organised in systems tracts related to changes in relative sea level. Most simplified models of sequences deposition lack the integration of the local tectonic component being a major controlling factor on the sequences morphology and development.

Eustasy is the world-wide sea level fluctuations caused by absolutes changes in the volume of free sea-water and is thereby directly related to climate and tectonic movements at the planetary scale. The various causes at the origin of eustasy are not clearly understood except for the shortest orbitally forced cycles (< 0.5 Ma).

Sea level changes at the historic scale (centuries) leading to predictions for the near future are difficult to relate to the time resolution of eustasy as observed from the resolution proposed by sequence stratigraphy on sediment records (100 to 1000 times larger cycles).

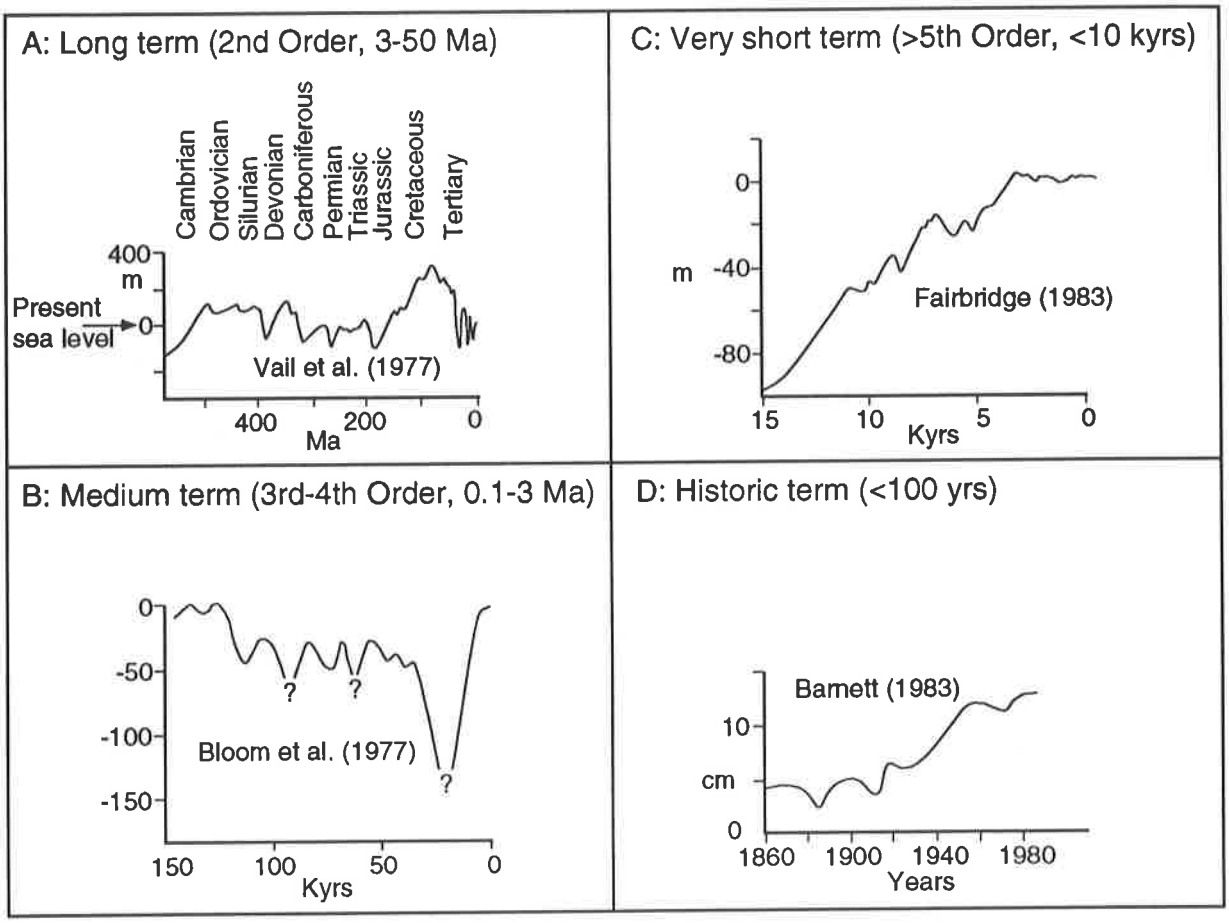

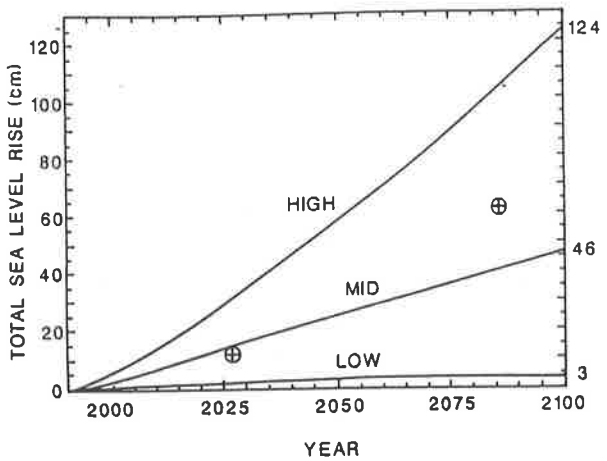

Fig. 2-10: Sea level changes on different geological time scales. ***a.*** *500 m range sea level changes over 600 Ma.* ***b.*** *Sequences in a range of 150 m sea level deviation from present.* ***c.*** *Detail of the present warming period (since 15 kyrs).* ***d.*** *Last century sea level rise in cm.* ***e.*** *Projection of sea level rise for the next century.*

3. WELL LOG INTERPRETATION (FORMATION EVALUATION AND SEQUENTIAL ANALYSIS)

3.1 Introduction

The first electric well-log analysis into a bore hole was realised by Marcel and Conrad Schlumberger in 1927 to determine down hole rock resistivity. Since that time, two types of well-log lithology determination were possible; direct information obtained from cuttings in the drilling mud during the process of drilling (geological sampling, fauna, formation resistance to drilling, presence of hydrocarbon traces, etc...) and indirect information measured in the hole (Wireline well logs analysis). The need to determine more accurately the amount of gas or oil contained in a formation caused rapid technological progresses and an explosion in new analytical methods. Rock porosity and water saturation measurement were needed to evaluate hydrocarbon content in a formation (fig. 3-1). Unfortunately, no tool could directly provide this information. Therefore, tool combinations were designed to meet that goal.

Basic interpretation principles of well-log evaluation used in this study are presented below. The main objectives in using well-log data are :

- to correlate lithologies obtained from well-logs curves to vertical and horizontal seismic facies (differentiate between shale, silt and sands).
- to elaborate a sequential analysis based on lithofacies succession on logs (identification of transgressive and regressive trends, main flooding surfaces, condensed sections and sequence boundaries on logs).
- to correlate and cross-check the sequential analysis realised on logs and the seismic stratigraphy interpretation done on the 3D data (based on seismic facies and unconformities identification).
- to be able to time correlate the 3D seismic data from the faunal content and the sequential analysis on logs through synthetics.
- to qualify lithologies of the potential traps discovered on 3D seismic data both in the productive zone (oil and gas window) and in the surface sediments.

The detailed well logs and seismic data analysis procedure used in this study is developed in Annexe 3.

Well log data was generously provided by Corpus Christi Oil and Gas thanks to Dave Scolman and Shell International oil companies in Houston, with the help of Professor A.W. Bally, from Rice University-Houston. The available data consist of 6 logs drilled within the 3D speculative survey. All of them were obtained on paper and consist of Spontaneous Potential (SP) or Gamma Ray (GR), a resistivity and a conductivity curve. Only one of them includes induction, caliper, sonic and neutron porosity curves. CHARISMA™ interpretation software is equipped with well-log treatment facilities but these printed data could not be entered into it. Four logs have incomplete faunal determination (mainly benthic foraminifers last occurrences in the productive zone) providing necessary information to establish a primary age calibration of the seismic data.

More precise determination of the age of the interpreted horizons have been obtained after integrating the sequential analysis of logs and seismic data. In the first place, well-log data have been interpreted in terms of lithology, then in terms of sequential interpretation according to the Well Log-Seismic Sequence Stratigraphy Analysis method defined by Vail and Wornardt (1990) .

3.2 Well log formation evaluation: main tools.

Spontaneous Potential (SP)

Major part of well log formation evaluation for sequential analysis purposes can be realised on spontaneous potential curves. The SP curve indicates differences between impermeable, electrically conductive beds such as shale, from the more permeable beds, and clearly marks their boundaries. It also indicates formation water resistivity and qualitative information on the degree of formation "shaliness". SP is measured as a function of depth between a single down hole electrode and an electrode in a mud pit on the surface. SP curves are relative measurements of deviation in millivolts from a reference taken as the shale line (to the right) and the clear sand line (to the left, fig. 3-6 and 3-7). The polarity of the SP curve is related to the contrast of salinity between the drilling mud and the formation water.

Natural Gamma Ray (GR)

Natural gamma ray curves are used as a secondary source of indication for the formation degree of "shaliness" and its curve is often superposed to the SP curve (same polarity if salinity of formation water is superior to the salinity of the drilling mud). The major source of radiation in sedimentary rocks is the ^{40}K presence in fine grained rocks such as shale and clays. As with the SP curve, a shale base line is established (high radioactivity, to the right) and deflections (to the left) towards clean lithology are registered (low percentage of radioactive material). This tool is finer than the SP curves for stratigraphic correlation as it provides a quantitative differentiation between shaly and non-shaly formation. GR curves can be used where SP are flat due to the lack of contrast between Rwf and Rw (fig. 3-1).

The major part of well-log interpretation done in this study for sequential analysis is based on SP and GR curves. The resistivity tools, caliper, sonic and density logs were used on one log to define porosity trend and a velocity law in order to calculate a synthetic log (see later in this chapter). A quick summary of the basic principle of these methods is given below together with their main field of application.

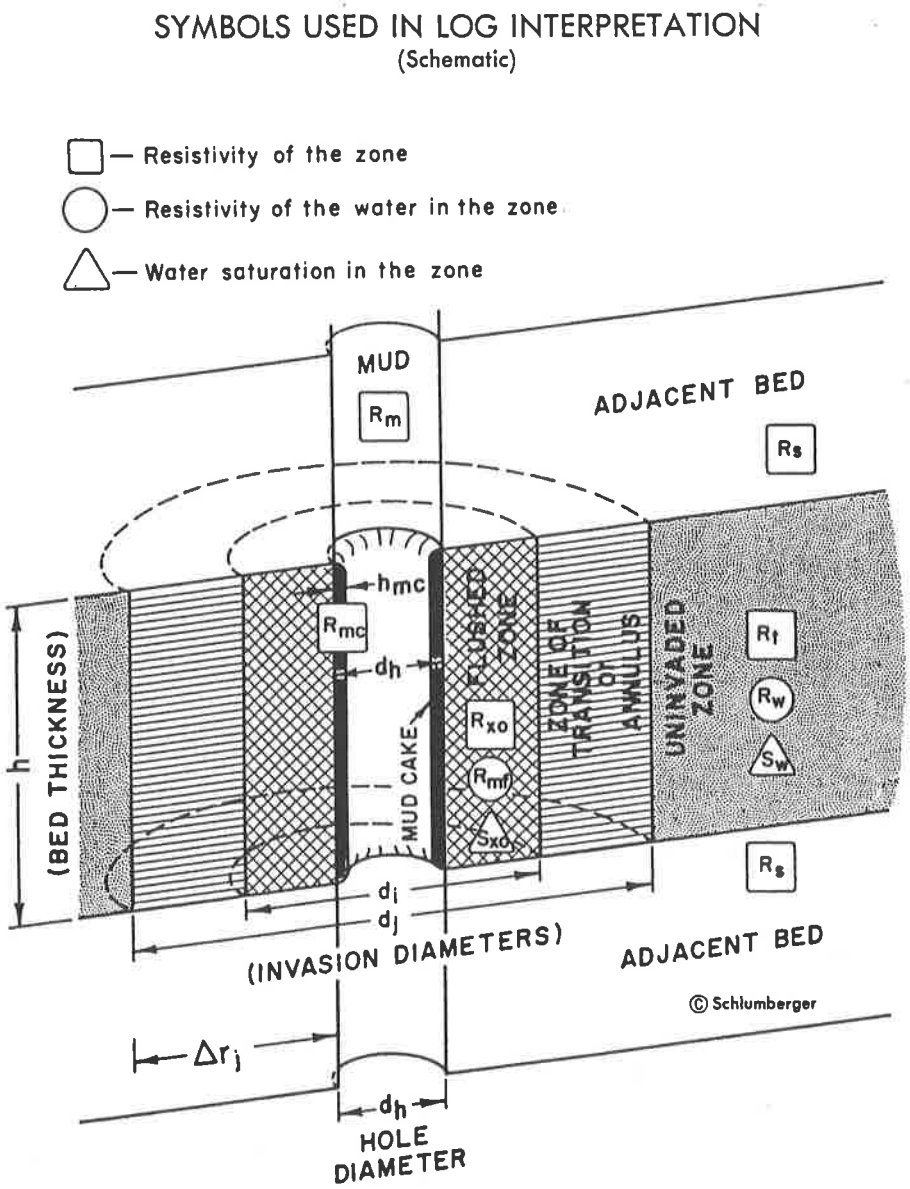

Fig. 3-1: Schematic representation of well-log interpretation parameters and symbols (m-mud; mc-mud cake; xo-flushed zone; mf-mud filtrate; s-surrounding formation; t-true value; w-formation water; from Schlumberger, 1955)

Electrode resistivity tools

Differences in spacing between the multiple electrodes of the different Laterolog devices (SFL, Spherically Focused Log) introduced in the hole give resistivity values for various depth of penetration. The numerous electrodes are arranged to focus the current into the formation to reduce bed boundary and borehole effects. These type of tools are used in combination with gamma ray measurement.

Induction tools provide resistivity values in dry holes or holes with an oil base mud. Induction tools have no exterior electrodes and measure conductivity through sets of coil combinations focusing the electric field into the formation. It is more effective in lower resistivity formations than in the higher ones and is a very successful tool in sand and shale sequences similar to the one observed in this study.

Resistivity logs or Microresistivity logs (MLL, PL, MSFL) provide resistivity measurement in a very small volume of formation. The tool is forced against the borehole wall as it is pulled up along the hole (most measurements are done from the bottom to the top to minimise depth evaluation problems). Microresistivity logs have a very predictable depth of penetration and can provide accurate resistivity values for the flushed zone (fig. 3-1). Excess in mud cake or borehole roughness can alter this measurement. The percentage of non-movable hydrocarbons can be estimated with these tools by measuring RXo and Rt as well as the saturations in residual hydrocarbons (Shr) in the flshed zone (fig. 3-1). They can also be used to determine degree of fracture and fluid permeability in the rock.

Total porosity logs (Sonic, Density, Neutron porosity logs)

Sonic log measures the time taken for an acoustic pulse to travel along the borehole between the source and the receiver (generally spaced of 60 cm). This travel time is proportional to the amount of fluid in the pore spaces and the amount of rock matrix, in comparison with the known travel time through the fluid and through the matrix. It is a porosity indicator when rocks are consolidated and compacted enough. It generally indicates values of minimum porosity.

Density log is one of the most effective logging tools used to determine porosity, bulk density and effective porosity in shaly sands. The sidewall pad device is composed of a gamma ray source and two receivers indicating the electron density in the rock. When the number of proton is not equal to the number of neutrons in presence, corrections must be made to determine bulk density. To convert density measurement into porosity, rock matrix and fluid density must be known. In combination with other logs, it can provide information on lithology, shale content, fluid saturation, gas presence mud cake thickness and under-compaction. The density log has good correlation to the caliper values (borehole diameter measurement).

Neutron porosity log commonly consists of two receivers measuring epithermal neutrons emitted from the source as a direct function of how much the formation is able to slow down the neutron flux. Elements having an atomic mass close to the neutrons (hydrogen) will slow the neutrons more than large atomic mass elements. Hydrogen ion content values can be interpreted in terms of porosity after calibration is done from the reference of the limestone sequence at the API pits in Houston. This tool seems specially adapted for limestone and non-shaly clastic sediments.

3.3 Well log formation evaluation: paleo-water-depth

Introduction

In 1989, the number of exploration and production wells drilled in the studied area (225 sq. km) by several oil companies (Odeco, Tenneco, Amoco, Shell, Mobil, Corpus Christi Oil and Gas) approached 40. We could obtain the logs on paper for six of them, numbered from Well 1 to Well 6 (see location on fig. 3-2). All drillings have been measured with SP or GR, SFL curves except for Well 4 for which we could also obtain the caliper, density log and neutron porosity curves. Well 3 is deviated but we could not get the deviation co-ordinates ! Well log analysis along most of the wells is not complete and parameters measurement starts at different depths for each of them. Two wells (Wells 3 and 4) start at the surface providing information for the top Pleistocene and the deepest well reaches 5200 m (Well 3, 17'000 ft). Three logs have biostratigraphic indications (benthic foraminifers last occurrences) mainly in the productive interval giving basic time indication for the interpreted sequences. The velocity law and synthetic log used for all correlation in this study have been obtained for Well 2 (porosity derived from the sonic log with Wylie's time-average equation (Wyllie, 1956).

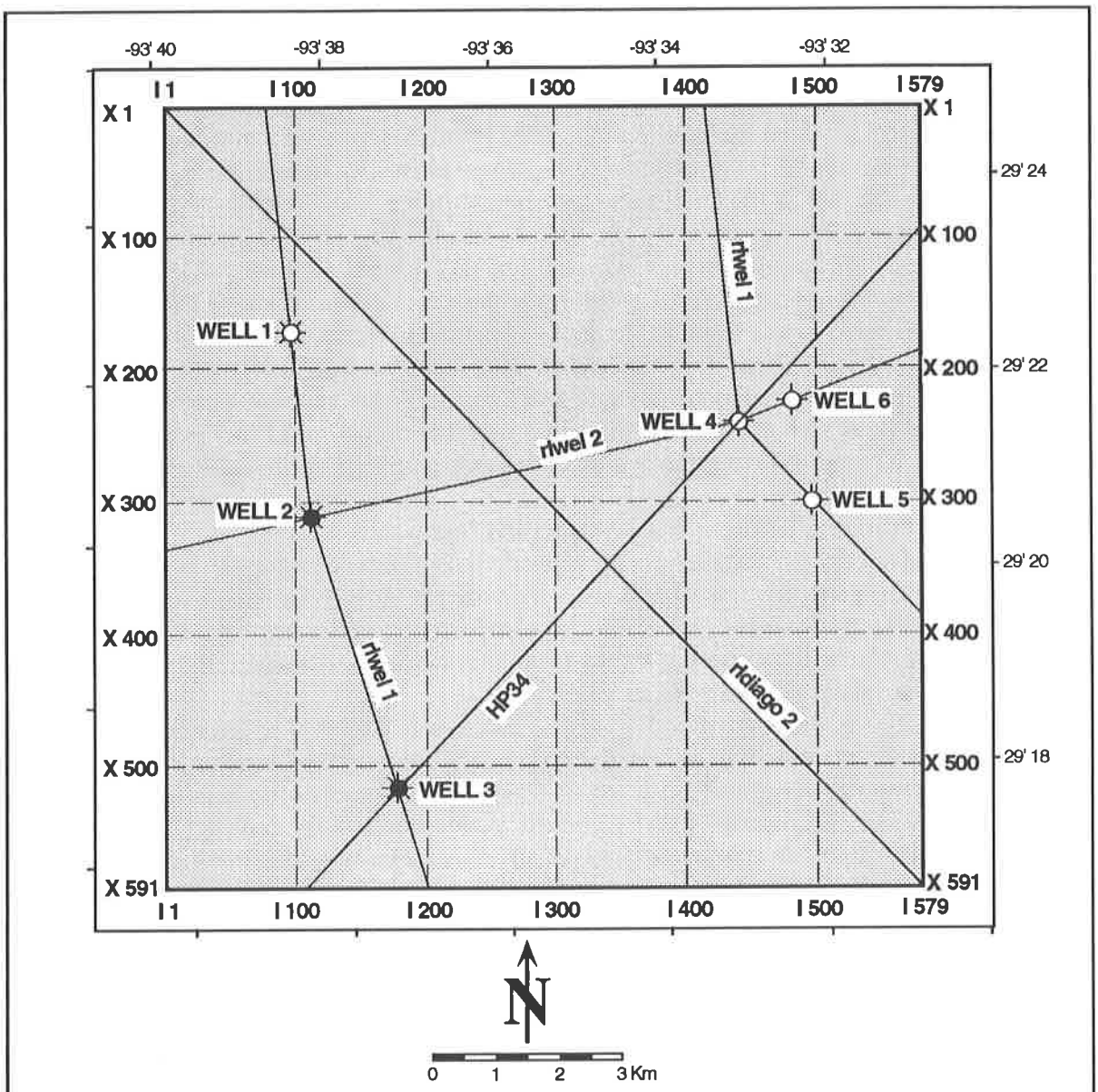

LEGEND :	**I 100**	**Inline 100**	**WELL 1**	**Surface location of Well 1**
	X 300	**Crossline 300**		**Oil and Gas**
	rlwel 2	**Random line joining wells**		**Gas**
	rldiago 2	**Diagonal randomline**		**Exploration, dry**
	29' 18	degrees in latitude		
	-93' 36	degrees in longitude		

Surface location of Wells :	**WELL 1**	**I 097 / X 173**	**WELL 4**	**I 442 / X 241**
	WELL 2	**I 112 / X 312**	**WELL 5**	**I 498 / X 300**
	WELL 3	**I 178 / X 512**	**WELL 6**	**I 482 / X 226**

Fig. 3-2: 3D Speculative survey geographical co-ordinates, bin centre location, well-log surface location and random lines connecting wells.

The basic principles of well log interpretation for the purpose of defining sequences of sedimentation on logs is described below. It consists of lithology identification, sequences and systems tracts recognition on logs, time correlation from the faunal assemblages and correlation to the seismic data with synthetic logs.

Lithofacies and paleo-water-depth

Basic lithofacies interpretation of SP and GR curves has been done on all the wells in order to differentiate the clean sands from the intermediary silt and shale (fig. 3-6). Typical shapes in the SP or GR curves sometimes allow to directly identify sedimentary features (prograding or backstepping shore face sands, channels, channels overbank, shingled turbidites, etc. ...).

In the studied area, there is a constant deepening trend in marine environments facies from the younger surface sediments to the deeply buried series of the Miocene, corresponding to the continuous offshore migration of depocentres from Early Miocene to present (fig. 1-5 b). Paleowater depths conditions obtained from fauna are important to determine because similar log patterns may be observed in shallow and deep water but interpreted differently. The biostratigraphic data available for this study consists of "Paleo tops" of benthic forams defined as the first down hole occurrence of a particular species in a well which may or may not be its true extinction point in time. In the Gulf of Mexico, the benthic forams tend to be good paleowater depths indicators on the shelf but are very imprecise correlation tools in the bathyal zones due to important reworking and redeposition. Calcareous nannofossils, planktonic foraminifers and benthic forams biostratigraphic checklists represent the ideal correlation tool between wells and enables good "Paleo tops" identification. When these data are present, high-resolution biostratigraphy based on abundance and diversity peaks along condensed sections provide a perfect dating agent for precise seismic sequence stratigraphy (Vail & Wornardt, 1991; Armentrout, 1994) . In the absence of such data, the determination of marine environments zones in the studied area was realised using a combination of a limited benthic forams information and evolution in the seismic facies observed on the 3D data set. On the inner shelf of the Gulf of Mexico, in the studied area, the transition from Zone 1 to Zone 2 (20 m) can be placed around 600 m below present sea level based on the sequential analysis of well log responses only as no faunal information is available in the first 2000 m. The Zone 2 / Zone 3 limit (middle to outer neritic transition, 100 m water depth) lies approximately 2500 m below the present sea level (see fig. 3-8 and fig. 2-4 for ecological zones classification). The shelf break transition from Zone 3 to Zone 4 (200 m) is found 3000 to 3500 m below sea level and corresponds to the main productive zone of the middle Miocene sediments (fig. 3-8). What is found below 3500 m on the seismic data was sedimented in the upper and lower bathyal ecological zones. Each of these marine environments will show characteristic sedimentary facies and typical sequences of well log signatures allowing to identify regressive and transgressive trends limited by cyclic unconformities and major flooding events. The coming chapter presents 4 typical sequences on logs from the inner shelf down to the bathyal zone in order to define the characteristic log patterns of each marine environment encountered in the studied area.

3.4 Well log formation sequential analysis

Introduction

Once lithology and depositional environments have been identified on well logs, the observation of their successions becomes significant in terms of sequence stratigraphy. In a clastic environment, each systems tract composing a sequence has typical log response that varies laterally from the inner shelf to the deeper bathyal zones. It is therefore important to determine the depositional environment before interpreting sequences in the sediment pile. An overview of log responses for systems tracts expected in a clastic environment has been given by Vail and Wornardt (1991) and is summarised below (fig. 3-3 and 3-4). The sedimentary block diagrams representing the systems tracts morphology are not to scale but will serve for basic comparison and references when describing the studied sequence on logs and on the horizontal maps provided by 3D data (Chap. 5).

Figure 3-3A is a reminder of the spacio-temporal organisation of systems tracts in response to eustasy and simplified tectonic subsidence as well as of basic terminology and symbols. (Note: to facilitate the lecture of the coming paragraphs, the systems tracts will be abbreviated in the text as: Hst, highstand systems tracts; Tst, transgressive systems tracts; Lst, lowstand systems tracts). These three main systems tracts and the surface separating them are presented below, from top to base.

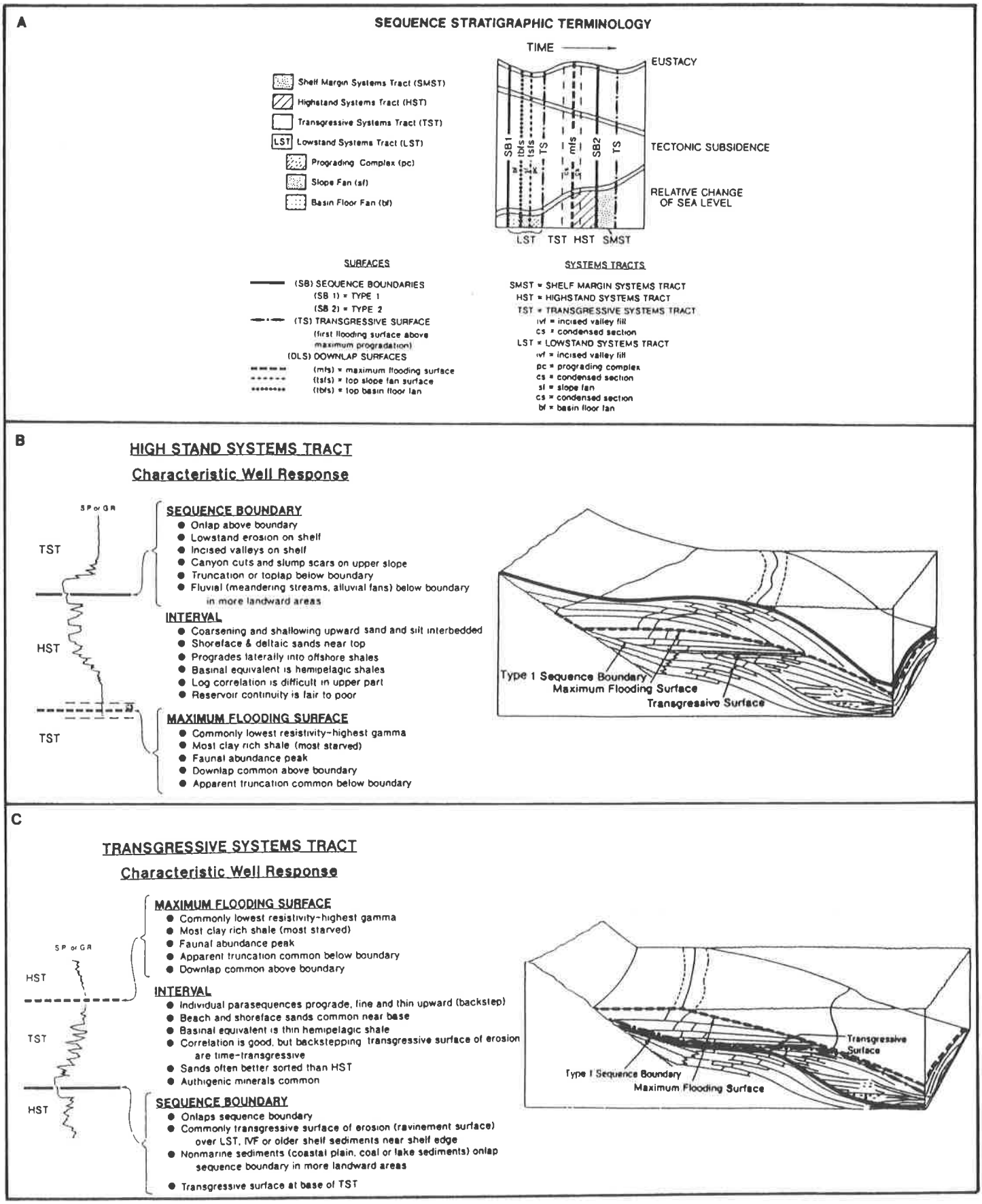

Fig. 3-3: Synthetic table of characteristic well log responses for systems tracts. ***a.*** *Curve of relative change of sea level and basic sequence stratigraphic nomenclature.* ***b.*** *Highstand systems tract well log response and model.* ***c.*** *Transgressive systems tract and main flooding surface well response.*

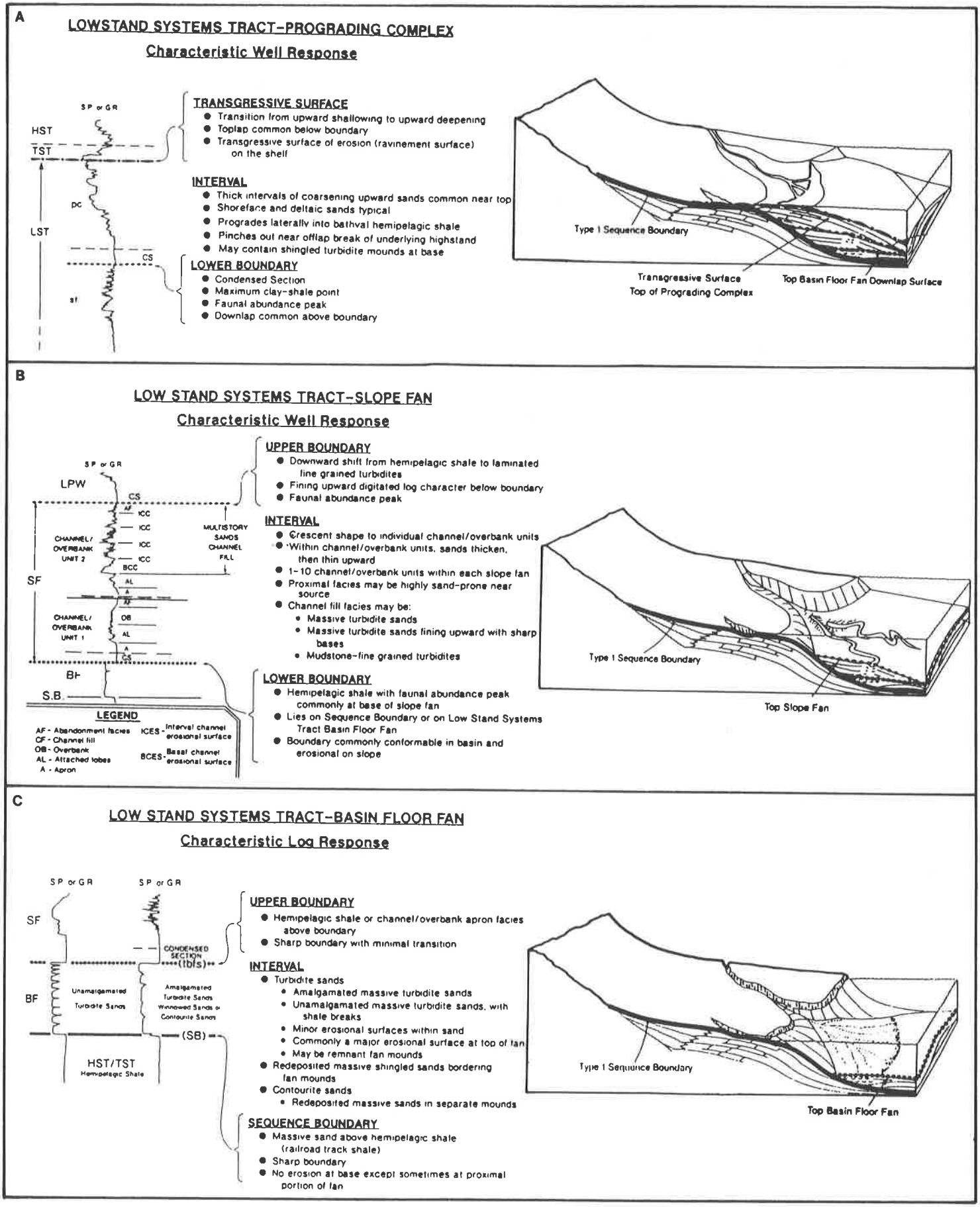

Fig. 3-4: Synthetic table of characteristic well log responses for systems tracts. ***a.*** *Lowstand systems tract-prograding complex well log response and model.* ***b.*** *Lst-slope fan well log response.* ***c.*** *Lst-basin floor fan well log response and sequence boundary.*

- Highstand systems tracts (Hst):

Most common Hst sedimentary features are low angle sigmoidal progradation patterns gently filling the accommodation space created by the maximum of relative sea level. On logs they are typically represented by coarsening and shallowing upwards alternations of sands and silts (fig. 3-3B). In deeper water, away from the reduced sediment input occurring at that time, Hst present reduced thicknesses of hemipelagic shale. The third characteristic of Hst is their partial incision and sometimes entire erosion induced by the following fall in sea level.

Between the Hst and the Transgressive systems tract below is the main flooding surface event composed of very clean and fine shale, indicating the "shale base line" for lithologic interpretation on logs. The mfs can be seen as a symmetry plane on logs between the overlaying prograding Hst and the backstepping Tst below (fig. 3-3B).

- Transgressive systems tracts (Tst):

The Tst characteristic well log responses are the fining and thinning upward of very clean, well sorted fine sands. In the basin, thinner silt and shale than during the Hst are accumulated. At the base of the Tst is the first transgressive surface, or ravinement surface which marks the transition between the upward deepening of the Tst and the upward shallowing of the top Lowstand systems tract below. This top lowstand surface often corresponds to a maximum in sand granulometry and bed thickness at the top of the Prograding wedge.

- Lowstand systems tracts (Lst):

The Prograding complex (fig. 3-4A) shows thick coarsening upwards shoreface and deltaic sands. It is absent on the inner shelf but can have a thin proximal equivalent on the middle and outer shelf. The log response is similar to the Hst interval but with much thicker and coarser sands. Dipmeter data can enhance the well marked high angle progradational patterns.

Below these thick sands is the first flooding surface (condensed section) occurring when the relative sea level starts to rise. A rapid sea water incursion floods the extended subaerial shelf and most of the fluvial erosive systems developed during the preceding sea level fall are sealed by a thin layer of silt and shale. This condensed section is indicated on logs by a very shaly interval (sometimes only fine silt). The GR or SP positive deviation is similar to the mfs but usually of lesser vertical extend. Similarly to the mfs, these shale show high faunal concentration and diversity.

The slope fan interval or outer shelf fan (Osf) on the offshore portion of the shelf (fig. 3-4 B) is characterised on logs by a succession of mounded features that can be interpreted as thick and coarse channel fills and channel overbank turbiditic sands. On the shelf, or on the footwall of major growth faults, the proximal sands can be very coarse and poorly sorted (fig. 3-5). Hemipelagic shale with minor faunal concentration but abundant reworking can be found at the base of the slope fan deposition in the distal regions. On the shelf, there is an increase in erosion of underlying sediments indicating the sequence boundary.

Basin floor fan are composed of thick turbidite sands with typical square blocky log responses. They are found in bathyal zones and on hanging wall of the major growth faults along the shelf break (figs. 3-4 D and 3-5). They clearly indicate the sequence boundary down the slope but this surface can be difficult to trace up dip.

In this mode of presentation the important lateral variations in facies for a single systems tract across the shelf are not taken into account. To fit one of the purposes of this research which is to characterise the systems tracts morphology from well logs and 3D seismic data taking into account the deposition environment, the well log characteristic morphology of 4 sequences registered from the shelf down to the basin is described within the limit of the studied 3D volume:

- Inner neritic to fluvial and middle neritic zones (0-100 m).

Sequences deposited in the inner portion of a clastic shelf (inner to middle neritic zones) are characterised by the absence of lowstand deposits except for the thick sands of the incised valley fill. Most eustatic falls in sea level are in the range of 40 to 100 m and therefore systematically affect the inner shelf sediments. The proximal zones and the topographic anomalies on the shelf (footwalls of major growth fault or salt related positive structures will be eroded and re-deposited further offshore down the shelf

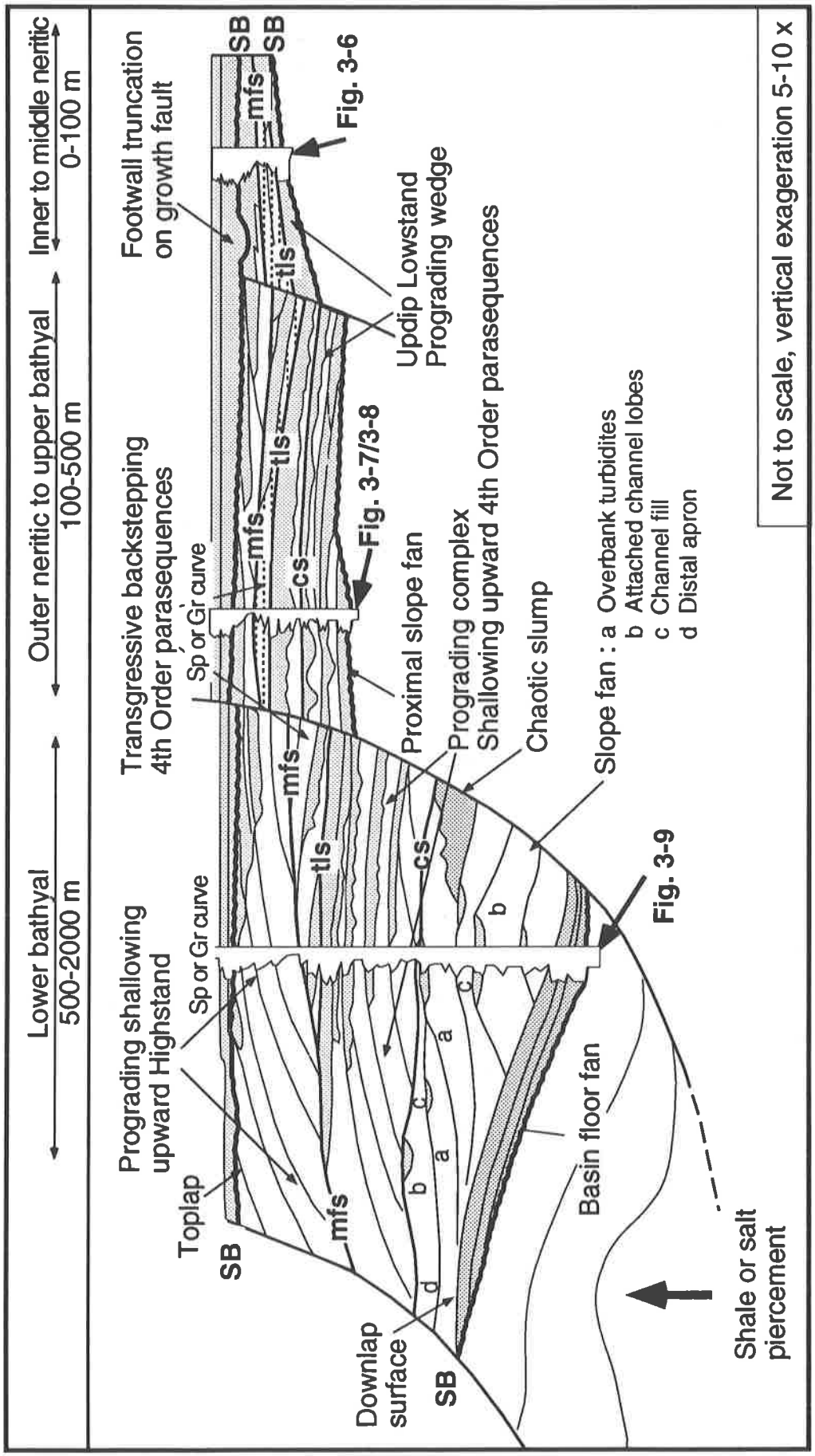

Fig. 3-5: Three characteristic well log sequences across a Late Cenozoic faulted clastic shelf: inner to middle neritic environment (see fig.3-6); outer neritic (fig. 3-7, 3-8); lower bathyal (fig. 3-9).

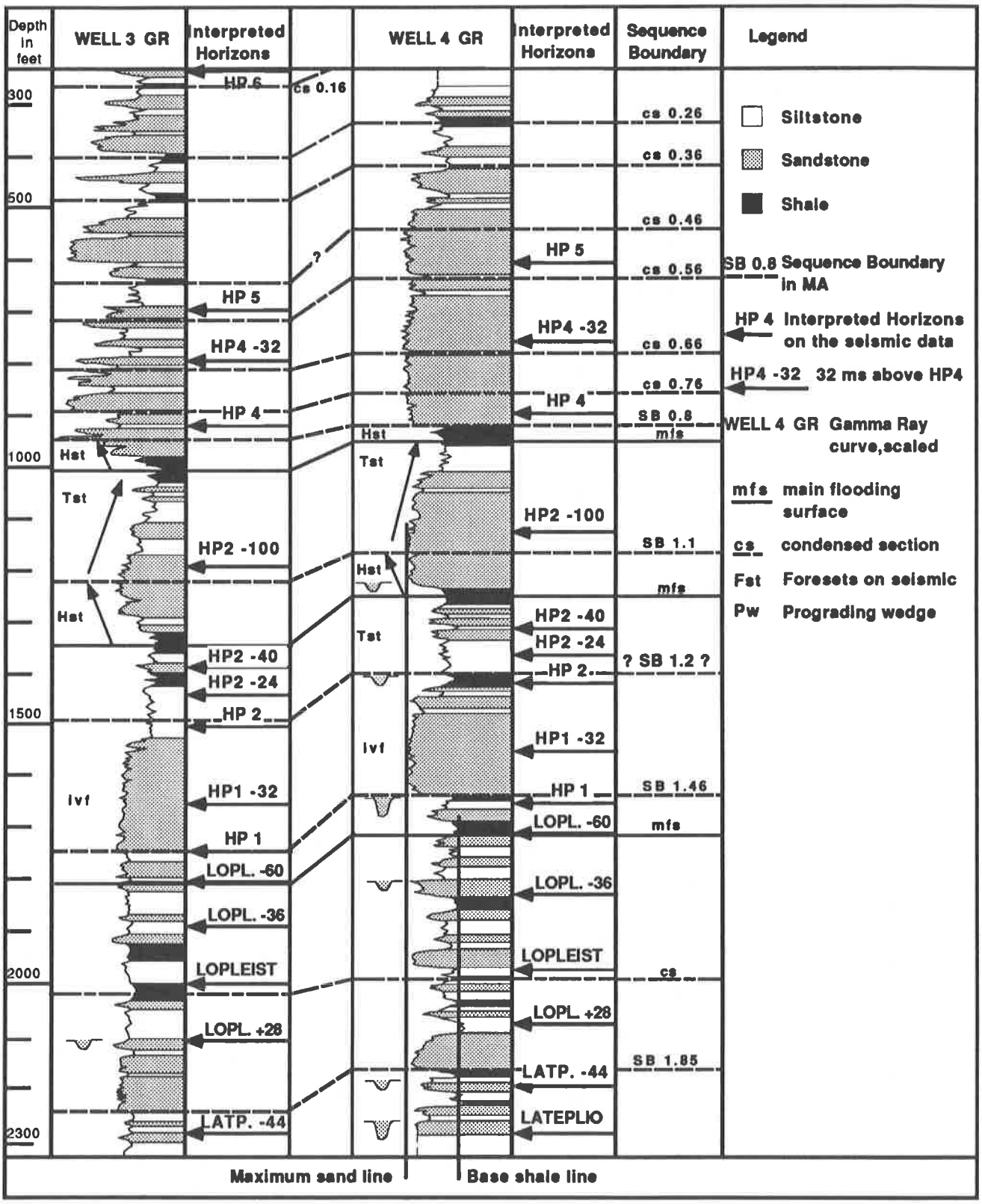

Fig. 3-6: Lithologic and sequential interpretation of gamma ray curves on Well 3 and 4 for the entire Pleistocene (inner neritic environment). Note the base shale and clean sand lines. Sequence boundaries can be interpreted at the base of incised valley sands (SB 1.46) or on top of Hst prograding coarsening up sands (SB 1.1).

break or be trapped in the growth fault hanging wall depressions. On well log data, sequence boundaries are located on top of the Hst prograding coarsening up sands and below the backstepping thinning up Tst sands or eventual incised valley coarse sands (fig. 3-6, SB 1.1). It can be problematic to differentiate between Hst and ivf sands on the base of well log only (fig. 3.6 SB 1.46). This is solved by looking at the sedimentary facies on vertical seismic lines and mainly on horizontal amplitude display of 3D data.

In the top Pleistocene (800 kyrs before present), erosive periods are so much intermingled that sequence boundaries cannot be determined on the base of basal unconformities but must be inferred from the less sandy periodic condensed sections corresponding to the Quaternary interglacial periods of warming up.

- Middle to outer neritic zones (100-200 m; fig. 3-7 and 3-8, located on fig. 3-5).

Sedimentary sequences adopt a more complete aspect as soon as the plainly inner and middle neritic zones are passed. The main difference resides in the possibility to develop a thin lowstand systems tract. The top lowstand interval (prograding wedge) corresponds to the beginning of the phase of relative sea level rise which can develop low angle shingle on the outer shelf that are the proximal equivalent of the thick prograding complex deposition down the shelf break. It can also develop larger progradations on the hanging wall depressions of major growth faults on the shelf (fig.3-5). The thickness of the proximal prograding wedge is entirely controlled by the accommodation space created on the shelf. The transgressive and highstand systems tracts separated by the main flooding surface show the same features as on the inner shelf except for a slight increase in thickness and changes in grain sorting (coarser Tst sands and finer Hst sands and silt). Only occasional drastic eustatic sea level falls (>100 m) can develop incised valley down to the outer shelf (i.e. SB 5.5 Messinian lowstand, fig. 5-47, 5-48).

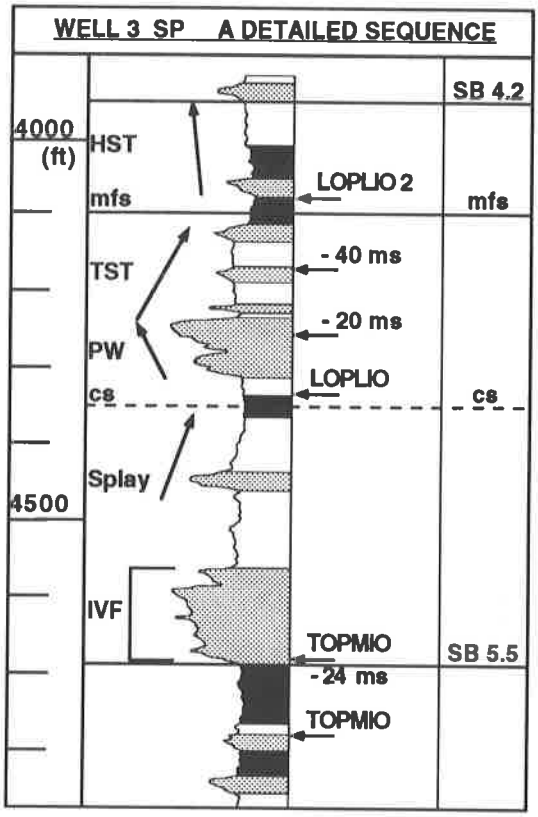

Fig. 3-7: Lithologic and sequential interpretation of spontaneous potential curve on Well 3. One 3rd order sequence in middle to outer neritic conditions.

Figure 3-8 presents a second example of a 3rd Order sequence definitely sedimented in the distal part of the outer neritic zone (near the shelf edge, water depth ≈ 200 m, see fig. 3-5 for location of fig. 3-8). The water depth is indicated by the faunal assemblages present in the logs in the studied area and confirmed by ecological zones maps established in the region for the productive interval (see Annexe 3, SB 13.8 and SB 15.5 maps). On figure 3-8 and all other well log tables, the wells positions are projected along a north-south profile to observe the lateral evolution of facies from the proximal to the distal. To show the lateral consistency of systems tracts observed on the sequence between SB 15.5 and SB 13.8, the image on figure 3-8 is flattened along the basal SB 15.5 sequence boundary interpreted at the base of the massive lowstand sands overlying the pure shale below. Thereby, the shaded surface traced above the 7000 feet limit represents the lateral variations in thicknesses for this interval.

A complete description of the successive systems tract characteristics is developed below as this sequence is the most productive interval of the studied area (further discussed in chapter 6).

The lower portion of the sequence shows thick blocky sands that could be interpreted as a basin floor fan when not taking the marine environment into account. But as proposed by the model on figure 3-5, it is rather interpreted as a coarse grained outer shelf proximal fan. On top of it is the first condensed section (cs1) composed of silt in the proximal portion (wells 1, 6, 4 and 2) that shows a progressive increase in shale basinward grading to pure shale (15-20 m, 60 ft). The SB15.5 interpreted horizon on

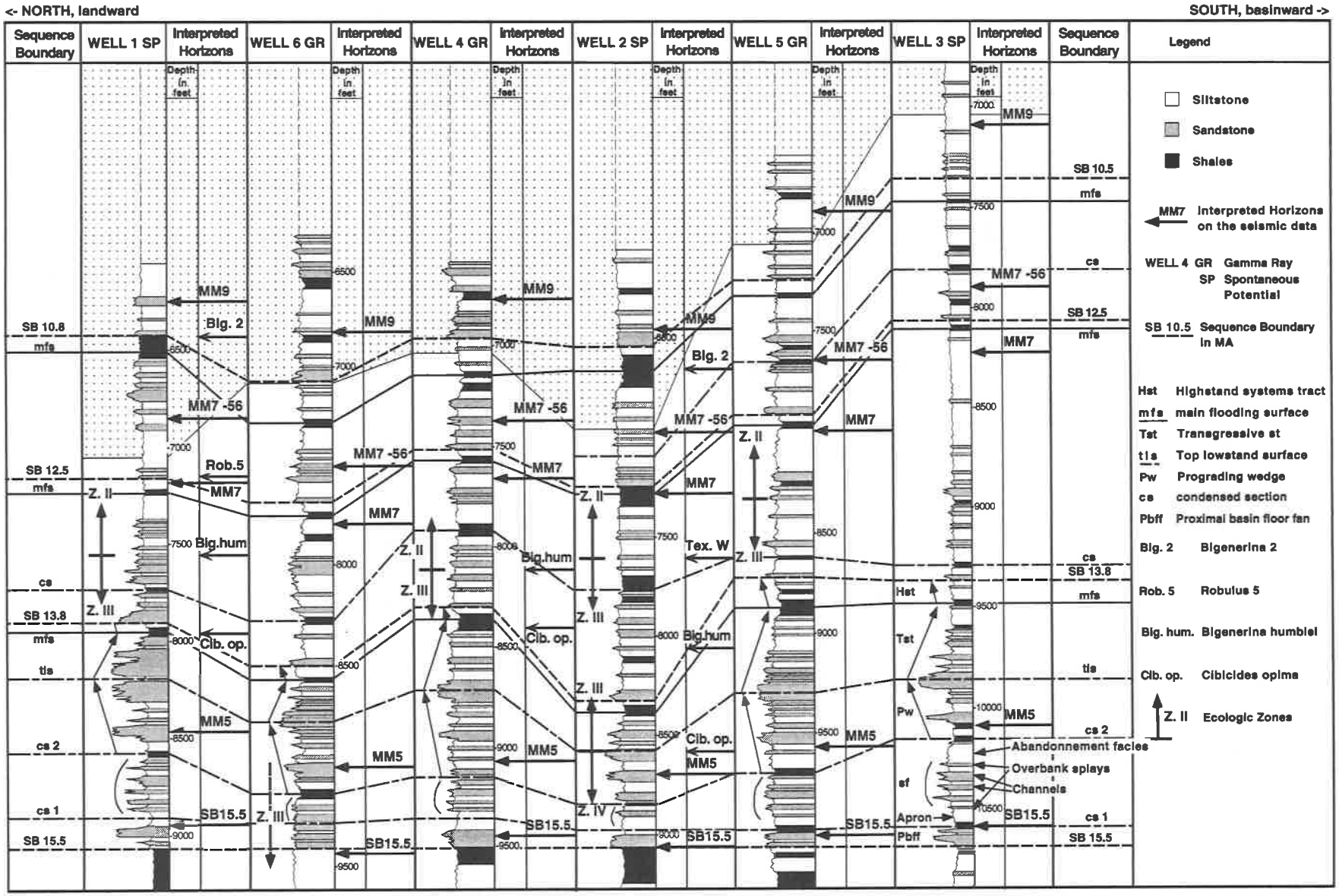

Fig. 3-8: Well log table flattened along the basal SB15.5 sequence boundary to represent the lateral consistency of interpreted systems tracts over the entire 3D survey for the SB 15.5 to SB 13.8 sequence. Outer neritic to upper bathyal transition, lowstand systems tract well developed.

seismic data (black arrow on fig. 3-8) is a high amplitude reflector caused by the strong contrast in lithology (acoustic impedance) between these two layers and between the basal sands and the Hst shale below (see fig.3-8, well 1, 4 and 2). The variable position of the interpreted horizons positions on logs is due to the fact that only for Well 2 a synthetic log was available for correlation of the entire survey. Resting on the first condensed section (cs1) is a perfect mounded slope fan complex feature (circular arc on fig. 3-8). The central blocky sands can be interpreted as channels and the finer sands above and below as overbank splays.

On Well 3, drilled down the main growth fault and presenting the larger sand thickness, these slope fan sands are bordered by two silty intervals (see fig.3-8, Well 3 between cs1 and cs2). The inferior one is interpreted as an apron (blanket like fine silty marine deposits or splays) and the one on top as an abandonment facies. The top slope fan surface is represented by the thicker shaly interval (cs2). Thick sands of the typical coarsening and thickening up prograding complex are sedimented above cs2. The strong lithologic contrast between the cs2 shale and the sands above are interpreted on the seismic data as the MM5 horizon (Middle Miocene marker 5) which are also gas productive sands. The top lowstand surface (tls, fig.3-8 or ravinement surface, fig. 3-4 A.) is placed at the transition between the upward shallowing and the upward deepening interval, in the middle of the thickest sand. It corresponds to the moment when the rate of relative sea level rise becomes maximum. It is followed by a characteristic backstepping fining and thinning upward transgressive interval up to the main flooding surface represented with 10 to 30 m shale on well 5 (fig. 3-8). A thin silty to sandy coarsening and shallowing Highstand systems tract on top of the mfs confirms the relatively proximal marine paleoenvironment. The upper limit of this sequence (SB 13.8 Ma) is placed at the base of the thick sand interpreted as an incised valley developed on the outer shelf.

In conclusion, sequential interpretation of well log data in clastic, middle to outer neritic environment is easier than for shallower facies because of the good vertical development of each systems tracts which show typical and laterally reproducible sedimentary signatures. Less ambiguity is present in the attribution of precise sedimentary facies to each sand bodies and therefore allows better predictions for exploration purposes. On the outer shelf environments, important growth faulting mainly affects the systems tracts thicknesses but not their well log signals organisation. Down slope, lateral correlation of systems tracts on logs is even easier.

- Upper to lower bathyal zones (200-500 and 500-2000 m; fig 3-9 located on fig. 3-5).

The further we go offshore, the thicker the lowstand systems tracts and the thinner and finer the transgressive and highstand systems tracts will be. The 3rd order sequence presented on figure 3-9 crosses a major growth fault between Well 2 and Well 3 (F6, ≈ 600 m of vertical throw). The basal sequence in Well 3 is the equivalent of the offshore portion of the schematic cross section on figure 3-5: Well 2 on the footwall and Well 3 on the hanging wall of the F6 growth fault. This sequence limited by two sequence boundaries (SB 21.0 and SB 17.5) is entirely represented on Well 3 and might be incomplete on Well 2. The lower bathyal marine environment of deposition is indicated by faunal assemblages. The base of the sequence (on Well 3) is characterised by two thick blocky sands interpreted as true basin floor fan deposits (see fig. 3-9 and fig. 3-4 C for theoretical comparison). They are absent on Well 2 (eventually present below the inferior limit of Well 2). If they are not, their absence on the footwall of the main growth fault would indicate that the shelf break was coincident with the growth fault at that period. This would be indicated on amplitude maps by a strong incision (visible channels) on the footwall and corresponding fans down the fault. Two mounded features found on both logs are interpreted as slope fan complex with channel fills and overbank sands (fig. 3-9 and fig. 3-4 C). The top slope fan surface is indicated by thick homogeneous silt. And as expected in the deeper and more offshore environment, the Prograding complex is present but reduced (see distal portion of fig. 3-4A). Similarly, the homogeneity of the transgressive and highstand systems tracts on Well 3 confirm a distal position where they are recorded as hemipelagic shale due to the increasing distance to the sediment source during the interval of relative sea level rise. Still, the Tst and Hst are represented by sands on Well 2 that could probably not make it down the growth fault to reach Well 3, five kilometres offshore (fig. 3-2). The next sequence boundary on top (SB17.5) is placed below the thick sands laying on top of the Hst shale. Again, there is a strong contrast in acoustic impedance along this interface that has been interpreted as the deepest productive horizon discussed in this study (EM1, Early Miocene marker 1, chapter 6).

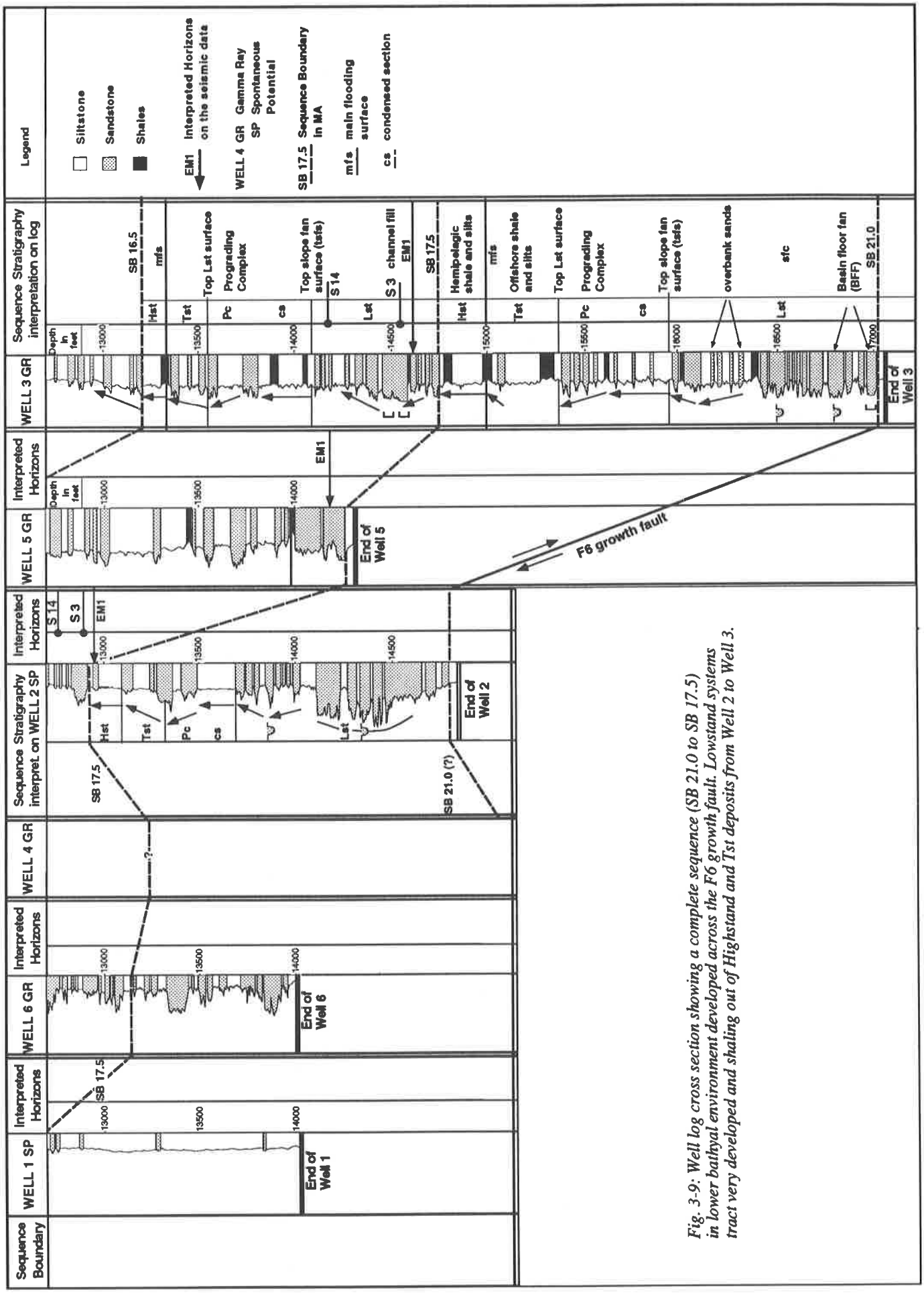

Fig. 3-9: Well log cross section showing a complete sequence (SB 21.0 to SB 17.5) in lower bathyal environment developed across the F6 growth fault. Lowstand systems tract very developed and shaling out of Highstand and Tst deposits from Well 2 to Well 3.

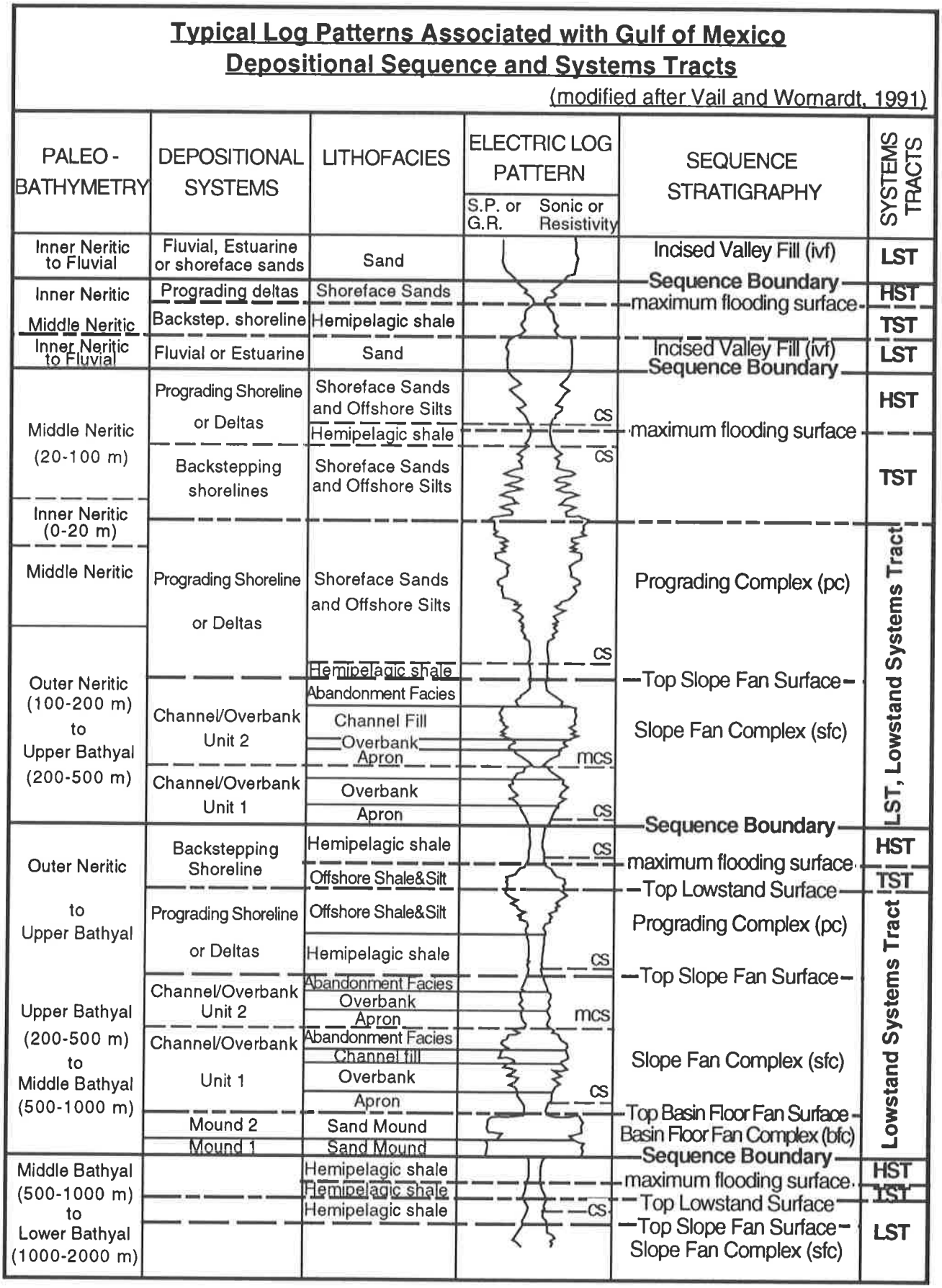

Fig: 3-10: Synthetic table of typical well log responses of clastic systems tracts as a function of depositional environments (modified from Vail and Wornardt 1991).

Conclusion to sequential analysis on well logs

Definite changes in well log response of stratigraphic sequences can be directly correlated to the paleowater depth condition. Therefore it is fundamental to take into account the marine environments of sedimentation to establish correct well log sequential analysis. Figure 3-10 (modified from Vail and Wornardt, 1991) summarises and integrates the differences of well log responses composing a sequence in relation to marine environment in a clastic sedimentary setting such as the Gulf coast shelf and slope.

Sequential analysis on well logs or vertical seismic sections can be uncertain in the inner to middle neritic marine environments due to complex superposition of erosional phases. It is therefore important to consider the sequential analysis made on the base of the 3D horizontal displays (presented in chapter 5) which shows the best resolution in the superficial areas corresponding to the inner and middle neritic zones to improve sequential analysis on well log and seismic data. And on the other hand, the power of horizontal resolution of 3D seismic data decreases in deeper marine environments where the accuracy in sequential analysis based on well logs or vertical seismic sections considerably improves. Interdisciplinary approaches integrating more and more complementary methods is the true way of solving complex problems.

3.5 Synthetic log, velocity law and porosity curves.

Synthetic log

The purpose of seismic inversion and of synthetic seismogram is to create a link between the well information and the direct imaging and interpretation provided by seismic reflection methods. Well logging can provide continuous measurement of velocity (m/sec) and density (g/cm^3) parameters of rock formations (chap. 3.2). From these data, a consistent model of the seismic response can be generated. The construction of a synthetic seismogram is based on the assumption that the earth is composed of a series of parallel planes with constant characteristics within one layer (density and velocity constant). The first attempt to construct such a seismogram based on this concept was made in 1955 by Peterson et al. (1955) (Waters, 1986) . The program used in this study to establish the synthetic seismogram (GMA™, Log M System by courtesy of Corpus Christi Oil and Gas-Houston) for Well 2 (fig. 3-11) supposes that the parameters within one layer are constant.

More complex programs take into account a linear evolution of the velocity and density parameters as a function of depth within one layer (Berryman *et al.*, 1958) . By entering the velocities and densities values at the corresponding time depth, the reflection coefficient (R) is calculated at each interface and then convoluted to the best fitting time variant wavelet to produce a synthetic trace. Normal and inverse polarity traces are generated (fig. 3-11) and compared with the original seismic data whose polarity is always to know with assurance. In this case, the synthetic trace in reverse polarity provides the best tie to the 3D data whose polarity convention attributes the compressional pulses (negative values (<0) to a decrease in velocity (negative white loops on seismic sections). Note that this convention is the same as the SEG Standard which uses:

- from slow to fast (>0) : compressional pulse, positive values.
- from fast to slow (<0) : compressional pulse, trough (in white).

The best way to nail down the synthetic log on the seismic data is to correlate the faults intersected on the bore hole to their position on a seismic line running through the Well. Once the best correlation is achieved, it is possible to transfer the faunal and lithological information from the well to the seismic data and cross check the sequential analysis realised independently on the 3D volume and on the well log data. The punctual chronostratigraphic information are then extended to the entire survey via the horizontal seismic maps interpreted along the critical levels (see chap. 5). Unavoidable minor mistie occur between the position of the interpreted reflectors (horizons) on the 3D data and their corresponding contrast in lithologies on logs (fig. 3-12).

Velocity law

A smoothed velocity law (fig. 3-13) generated on Well 2 shows the global t/z curve applied on the total volume of the 3D survey. But all time/depth conversions of interpreted horizons, sequence boundaries or main flooding surface (etc...) from the 3D data to the six logs available have been effectuated with the detailed velocity law table summarised in Annexe 3 (Plate 1 and 2).

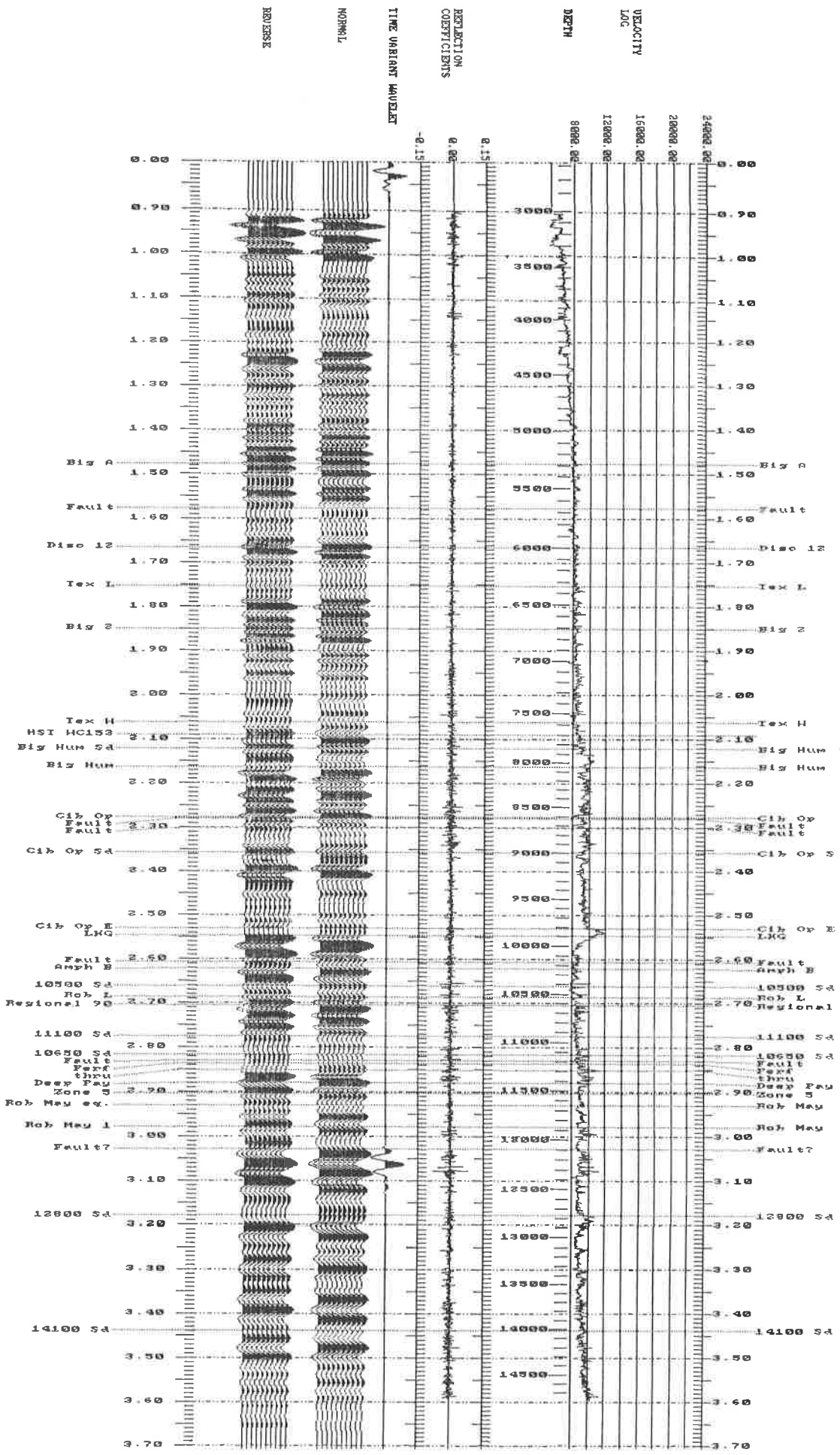

Fig. 3-11: Velocity log and synthetic seismogram in normal and reverse polarity for Well 2.

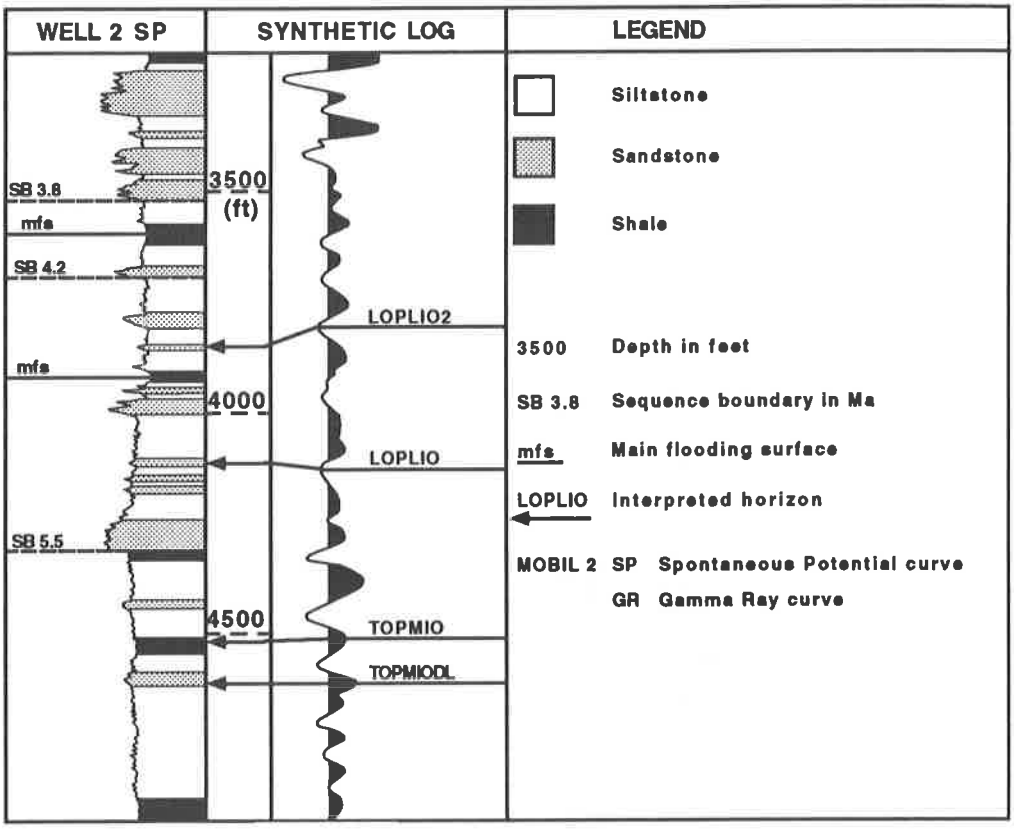

Fig. 3-12: Matching of interpreted horizons on the synthetic seismogram and on well log curve.

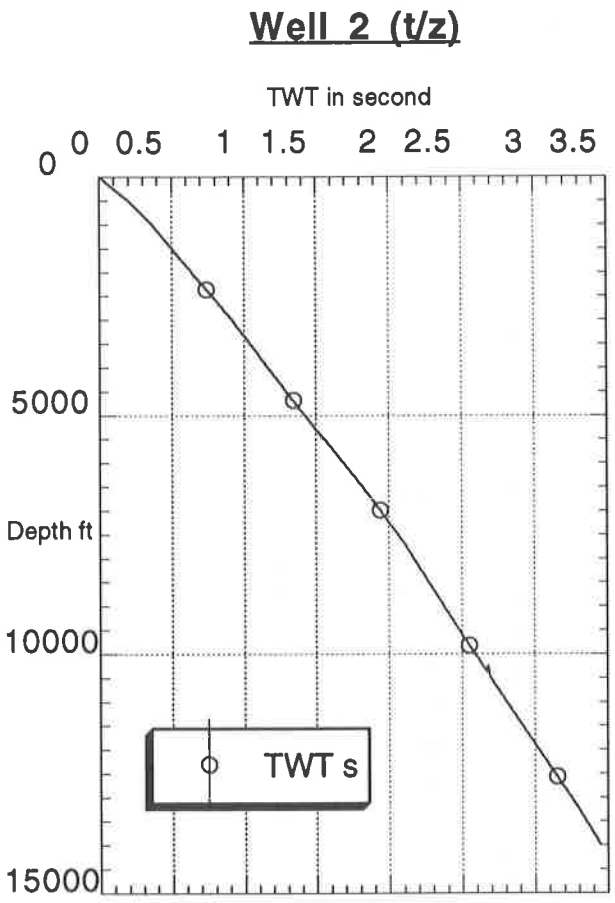

Fig. 3-13: Well 2 smoothed velocity law curve for time/depth transformation of the 5 five other wells available in the 3D survey.

Porosity curves

Lithology and porosity are the two main parameters to be known for hydrocarbon estimation on well logs. The porosity evaluation for a given formation is obtained from different tools (Sonic, density and neutron give a direct indication and microresistivity logs provides indirect porosity estimation, see chap. 3.2 for further details). The decrease of porosity and permeability with increasing depth is related to many factors (overburden pressure, increase in cement content, decrease in secondary porosity, etc...) and it varies from region to region. In this study, only 2 wells (Well 2 and 4) were provided with sonic logs and one with density (gamma-gamma) and compensated neutron curves were obtained for Well 4. A synthesis of the shale and sands porosity trends offshore Louisiana has been published by Gregory (1977) and has been adopted for the average porosity estimation for the decompaction calculation of the total subsidence trend (see chap. 7.3). The compensated neutron data on Well 4 are superposed to Gregory's data on figure 3-14 and show a good fit for the shale values and two distinct trends of sands. Some sands fit the average curve but most of them on Well 4 indicate lower porosity values. Definitive conclusions are difficult to draw from such a limited amount of data.

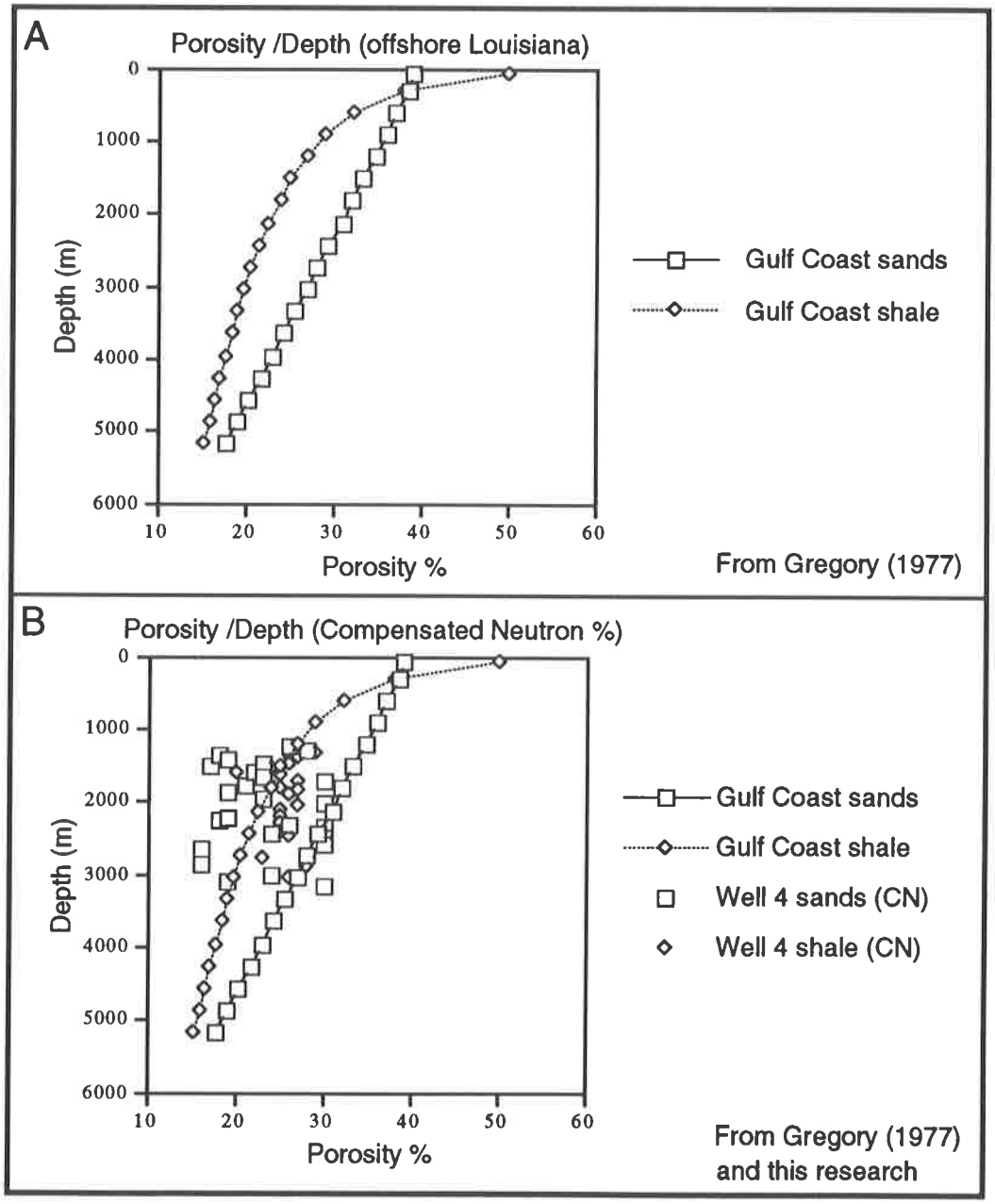

*Fig. 3-14: **a.** Average porosity curve of Gulf coast sands and shale from 17'000 wells. **b.** Compensated neutron porosity values (sands and shale) on Well 4, superposed to Gregory's average values.*

3.6 Summary

Well log data from combined tools are used in this study to correlate lithological, sequential and chronological information derived from well log data to the seismic 3D volume via synthetic logs. The biostratigraphic correlation are based on benthic foraminifers paleo-tops. 6 logs out of 40 drilled in the survey have been obtained for this study. The sequential interpretation on logs is realised on SP and GR curves after the depositional environments have been determined. On the inner shelf, a sequence of deposition is characterised by the absence of lowstand deposits (except for incised valley fill) and the sequence boundary is placed at the base of the transgressive s.t. or at the base on incised valley channels. A thin lowstand s.t. can develop in middle to outer neritic conditions and on hanging walls of active growth faults on the shelf. Transgressive and highstand sediments are still dominant. Down the shelf break, thick lowstand series are developed and the more basinward the section the more reduced the transgressive and highstand deposits.

A single velocity law is used for all time/depth transformations within the limited area of the 3D survey. Lithology and porosity are the two main parameters needed to identify the presence of hydrocarbons on logs. They are obtained from the sonic, density and neutron curves available for only one log in this research.

4. THREE-D SEISMIC ACQUISITION, INTERPRETATION METHODS AND APPLICATIONS.

"We are greatly mistaken in thinking that a three-dimensional body is something real. It is merely the projection of a four-dimensional body, its drawing, its image in our plane"
P.D. Ouspensky "Tertium Organum" (1920)

4.1 Introduction

Not many books, apart from the large user's manuals available with the various seismic interactive workstations have been written on the technique of three-dimensional seismic data interpretation. Up to today, the two only published references on the subject are rather theoretical and geophysical and do not enter in the detail of geological interpretation applied to exploration (Brown, 1986 ; Coffeen, 1990) . This relatively new science encroaching on the fields of geology and geophysics is born 10 years ago and will be subject to great development in the near future due to its great power to precisely visualise, delimit and analyse subtle buried geological objects (see 1, history of 3D seismic reflection). The purpose of the present overview of some applications of 3D seismic interpretation on screens is to define the necessary terms and theoretical concepts used in this study. The intention here is not to produce an exhaustive list of all options available on the CHARISMA™ 3.6 version (Schlumberger-Geoquest) used at the end of this research but rather to express some useful geophysical characteristics of 3D seismic interpretation options via particular and meaningful geological applications fitted in the general geological framework of this research.

4.2 Three-D seismic acquisition

Introduction

The main difference between 2D and 3D seismic data resides in the mode of acquisition. Contrary to the assumption made for 2D seismic acquisition, all reflections registered do not all come from the source-receiver plane, because of the sub-surface three-dimensional nature. 3D seismic does not record sub-surface reflections over a line but over as many portions of surfaces (bins) that the sound wave can reach in depth from the surface source/receiver disposition (Walton, 1972) . 3D data are gathered according to the bin centre location maps fitting the particular need of a survey. The surface of one bin is commonly 25 m x 25 m for offshore acquisition and can be smaller on onshore projects (higher resolution in the sub-surface; Selby, 1978) . This means that 3D acquisition is more than simply the juxtaposition of closely spaced 2D lines but that after a complex stacking procedures involving several hundreds of millions of traces, a coherent volume of seismic data is obtained. The second main improvement of 3D data versus 2D seismic methods comes from migration (Brown *et al.*, 1984) . 3D migration replaces the reflectors according to the way they were arranged in the sub-surface because of the gathering in common bins regrouping reflections coming from various azimuths and offsets (Mougenot, 1994) . This constitutes a complete volume of reflectivity values available for the interpreter to dissect in any chosen direction. Even transparent zones on 2D lines, below large salt pillows or allochtonous sheets can now be imaged via 3D specific migration of seismic turning waves reflections (turning waves are seismic waves travelling upward before and after reflection (Hale *et al.*, 1992)

3D marine seismic: this survey, acquisition and seismic data.

3D marine seismic necessitates a very sophisticated and expensive material to manage the huge amount of data registered during acquisition (one fully equipped boat, sources, streamers computers and radiopositionning is approximately 45 million $). 3D vessels have from 2 to 4 and even 8 parallel streamers (piezoelectric hydrophones) about a hundreds meters apart recording simultaneously the signals emitted by several sources (air gun or water gun). The complete configuration is precisely located every 10 seconds. The daily production of such a vessel reaches 10 to 20 km^2 and the cost of marine acquisition is around 10'000 $ / km^2 (4 to 7 times more for land 3D acquisition).

The West-Cameron speculative survey studied in this research is 225 km^2 and 6 seconds deep (only 5 s available in this study). It has been acquired at the end of 1987 by GECO™, 40 km offshore the Texas and Louisiana border. The acquisition configuration is composed of two 120 m long streamers (100 m

distance) with an airgun source (2000 psi pressure) located 7.5 m below sea level. The shotpoint and group intervals on the streamers are 25 m. The geometry assignment is 60 fold and the data is not in true amplitude as an automatic gain control has been applied. The polarity convention of the display shows the compressional pulses as troughs (negative white amplitude on the section). Figure 4.1 shows the transformation of a bipolar wiggle display to a raster density display. This enables to have greater vertical and lateral resolution making visible subtle lateral differences in seismic response occurring within half a loop. Any colour scale can be superposed to the raster display to facilitate the identification of small seismic objects (downlaps, shingles, shallow channels, shaling out of sand bodies, unconformities, etc...).

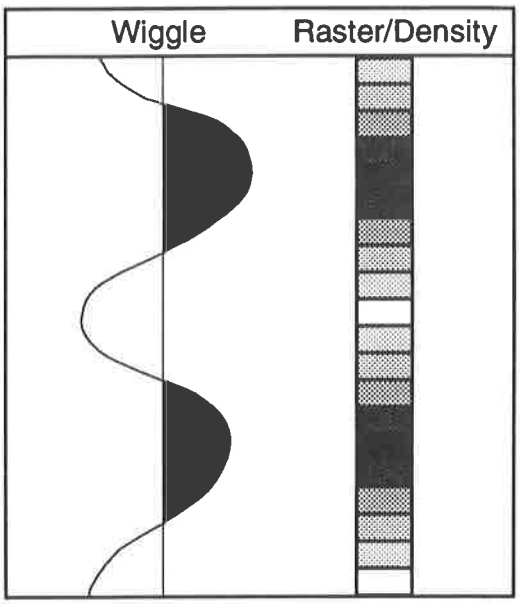

Fig. 4-1: Seismic trace displayed in wiggle trace and raster/density. A "gradational" colour scale can be superposed to the density scale.

A 3D volume of seismic data is composed of three different type of independent data (fig. 4-2): inlines, generally north-south vertical sections issued from acquisition, crosslines artificial lines generated on the computer perpendicularly to the inlines and the time slices (horizontal planes generated with an increment of 4 ms, fig 4-2). The studied 3D data volume is composed of 579 Inlines and 591 crosslines. When working with several surveys on one single machine, it can rapidly become impossible to store the entire cube of seismic data in the computer memory as a few Gigabits are used for one single survey of this dimension. Additional seismic data can be locally generated to facilitate the interpretation in complex zones. Random vertical lines can be generated in any direction, for instance to obtain true down dip cross sections or seismic profiles perpendicular to a complex fault system or to create a seismic line connecting two wells. In the coming versions of interpretation workstations it will even become possible to generate curved portions of seismic data connecting two deviated wells whose co-ordinates have been entered in the data base. Composite sections can be created to extend the interpretation from one direction to the other (compose the vertical with the horizontal plane to follow the lateral extension of a fault or a top lap etc..., see fig. 4-11). As the interpretation progresses, the necessary seismic data can be generated and erased at will. All interpretation is stored automatically and independently from the seismic data. So that what is called three-dimensional seismic is in fact the display of three quantities on a planar surface (x, y and t, t for time-depth or x-y-A, A=amplitude of seismic signal along that trace). But soon and before the end of 1994, true 3D interactive interpretation will become possible. The interpreter will not have a 2D plane with an attribute displayed in front of him to work with but rather a constantly present true three-dimensional volume of data to be interpreted (in any attribute desired). He will not pan (shift) any sections or time slices (independent seismic data) anymore but rotate or penetrate deeper within his single cube of data. This new extension is becoming possible because of the rapid expansion in computers performances.

Conclusions to 3D seismic acquisition

The nearly exponential expansion in 3D seismic acquisition since the early eighties (fig. 4.3 b, redrawn from (Nestvold, 1992) is caused by many different factors. The inversion of trend from 2D to 3D is due to the fact that technical advances made 3D acquisition and treatment possible at a lower cost. This, in turn helped to demonstrate that 3D seismic data was **the** tool to look for the oil that simply could not be found with 2D seismic data. Furthermore, the evolutionary trend from 2D to 3D goes hand in hand with the shift from the structural to the subtle stratigraphic traps. Three-dimensional surveys are now frequently shot on old productive fields to improve production and enhance recovery. Precise modelling of reservoir allow optimum fluid injections. Very large surfaces of continental shelves are getting rapidly covered with

offshore 3D data. When the studied survey was shot offshore Louisiana in 1987, only a few percent of the northern central Gulf coast shelf was covered with 3D data. Today, maps of available 3D surveys show that almost half of the Gulf coast shelf is covered by 3D seismic data. In 1987, 3500 sq. km of 3D data were shot in North America (both onshore and offshore, (French, 1992) , and 16'100 sq. km were acquired in 1990. And contrary to what the curve on figure 4-3 a) could suggest, the projected global geophysical expenditures should considerably increase in the near future (French, 1992) . When you are at the lowest point, the only thing you can do is to climb up again, just as a sea level would do !

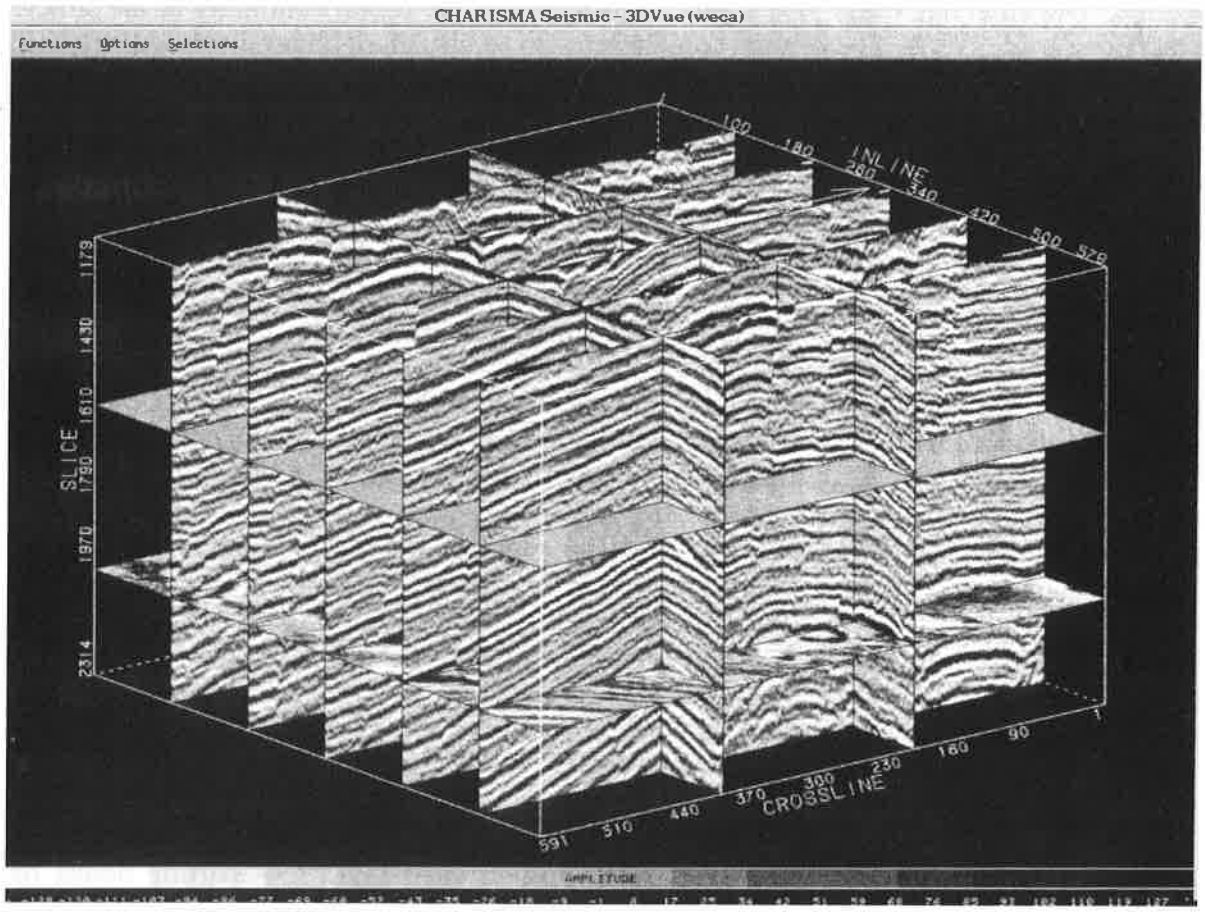

Fig. 4-2: 3DVue™ (CHARISMA S, Schlumberger-Geoquest) of a portion of the studied 3D seismic data set. North is to the upper right corner of the image, inlines are north-south oriented. Crosslines and horizontal time slices are generated to extrapolate seismic data from the inlines to the entire 3D volume.

4.3 3D seismic interpretation methods

4.3.1 Interpretation procedure and main tools

The present description of the interpretation procedure is limited to 3D seismic data but does not differ very much from the principles applied to 2D projects. The 3D seismic interpretation on workstation is organised on three complementary windows (Gerhardstein & Brown, 1984) . The first screen is where the seismic data is displayed and where all interpretation is done (mostly vertical displays, Seiscreen). The second screen (Interpretation) presents and updates, on a map view, the result of interpretation of the active or processed horizon. This is where the major editing and control of interpretation is done. A third window (Basemap) presents all the cultural data of the survey and gives information on the portion of the seismic data being displayed on the seismic window (inline or crossline number, active randomline, wells surface location and deviation trace projected on the surface, concession, blocks, etc...).

Before starting to interpret geological datum planes, it is important to use the various display possibilities provided by the workstation to get an overview of the general structure from different angles. Some of the main advantages of seismic on screens compared to classical 2D "paper work" is the possibility to instantaneously pan and zoom the seismic display at will and to squash a long line on one screen. The squashing and differential zooming options enable to distort the data (intense and reversible vertical exaggeration) in order to enhance low angle reflectors or subtle tectonic features invisible at the 1x1 scale. The multiframe options enable to have up to nine different seismic sections of different types simultaneously displayed on one screen (see fig. 4-7).

Lines in different directions combined to time slices (Seiscrop section, Trademark of Geophysical Service Inc.; Brown *et al.*, 1981) give a general overview of the lateral continuity of the structures to interpret (Bone *et al.*, 1983) . The seismic volume can also be visualised on perspective displays (3dVue CHARISMA S™, fig. 4.2) or using different shades of transparencies enabling to see through the entire 3D data set (Brown, 1992) . It is also possible to review the entire survey in animation where successive seismic planes (vertical, horizontal or combined) are displayed at a rhythm of two images per second. Once the structure is skimmed through, the oriented interpretation can take place. Similarly to the 2D seismic interpretation on paper, it is good to start by identifying and eventually marking (interpret) the fault traces against which the interpretation line will stop and be shifted to its equivalent loop on the next fault compartment. Then, the "closing loop" technique applied to regional 2D lines is still the best way to grid the 3D survey with a first set of consistent reference interpretation lines.

Before starting to systematically cover the entire survey with manual, automatic or semi-automatic interpretation, the main misties must be checked and corrected. Misties are mainly caused by loop skip due to subtle faults with low vertical throw or showing parallel intersection with the interpretation line. The best way to check them is to obtain consistent intersections of Inlines and Crosslines at any point on the survey. Once it is so, the entire horizon can be interpreted without to much problem using the three different semi-automatic interpretation modules. The simplest one (Draw-autotrack) proceeds to the automatic tracking of an amplitude window defined by the interpreter between two interpretation points (two faults) on one single section. This option applies particularly well to complex faulted zones where automatic procedures do more mistakes than correct interpretation. This is also the best way to have an optimum fit between the horizon and the fault planes. The Loop-Autotrack option does the same as the Draw-autotrack application but on a series of pre-defined inlines or crosslines. This option is optimum for large zones without discontinuities. The increment is fixed by the interpreter who quietly sits in front of the computer during execution ready to stop the process if it is going astray.

And finally the third fairly recent automatic 3D autotracker (ATRAK3D, CHARISMAS™-Schlumberger Geoquest) is a powerful tracking algorithm requiring a few starting points on each compartments to try to interpret the whole data set. In complex and abundantly faulted area and as soon as the amplitude contrast along the interpreted loop becomes too weak this procedure necessitates long manual corrections that can take as long as the semi-automatic interpretation with the Loop-autotrack option. To have greater vertical resolution, vertical seismic sections can be resampled to 1 millisecond sample data and the interpretation line will be stored to the nearest millisecond. This option is particularly used for precise reservoir delimitation.

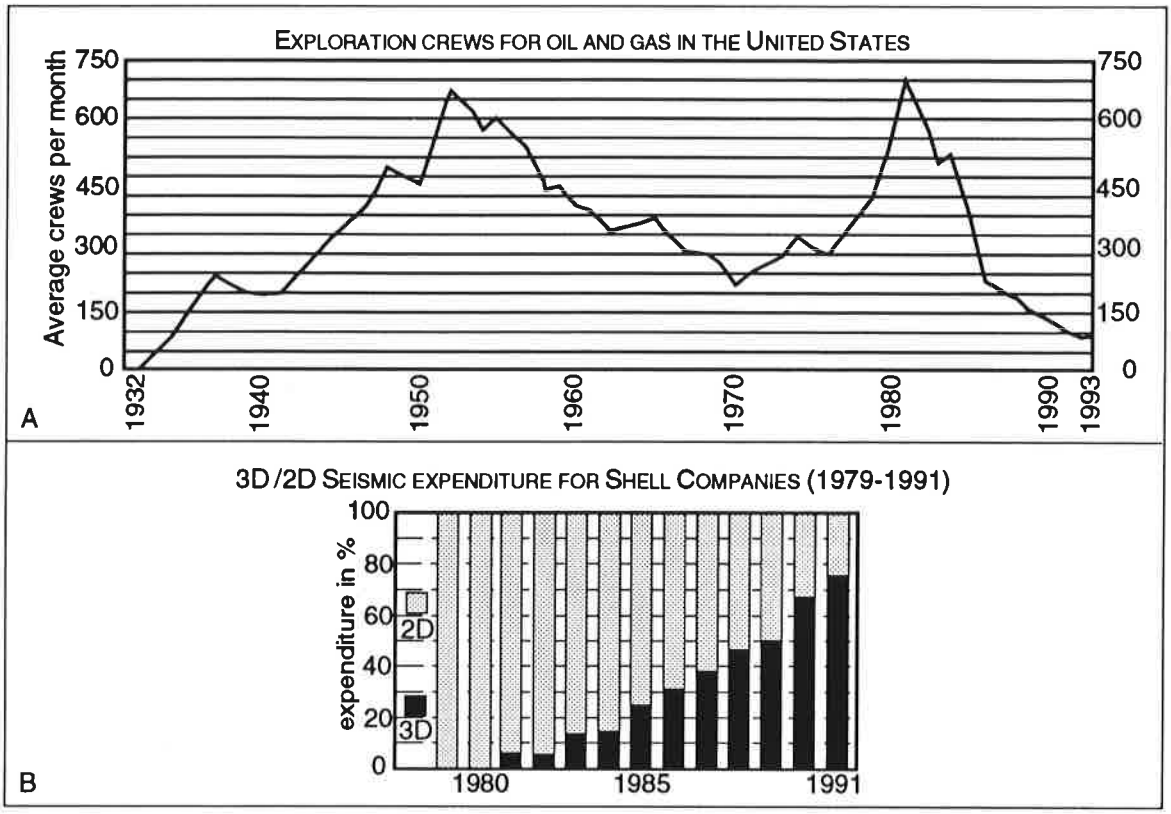

Fig. 4-3: ***a.*** *History of seismic exploration in the United States from 1932 to 1993 (The Leading Edge, Vol. 11, 1992).* ***b.*** *3D seismic acquisition expenditures exponential growth from 1980 to 1991 (Nestvold, 1992).*

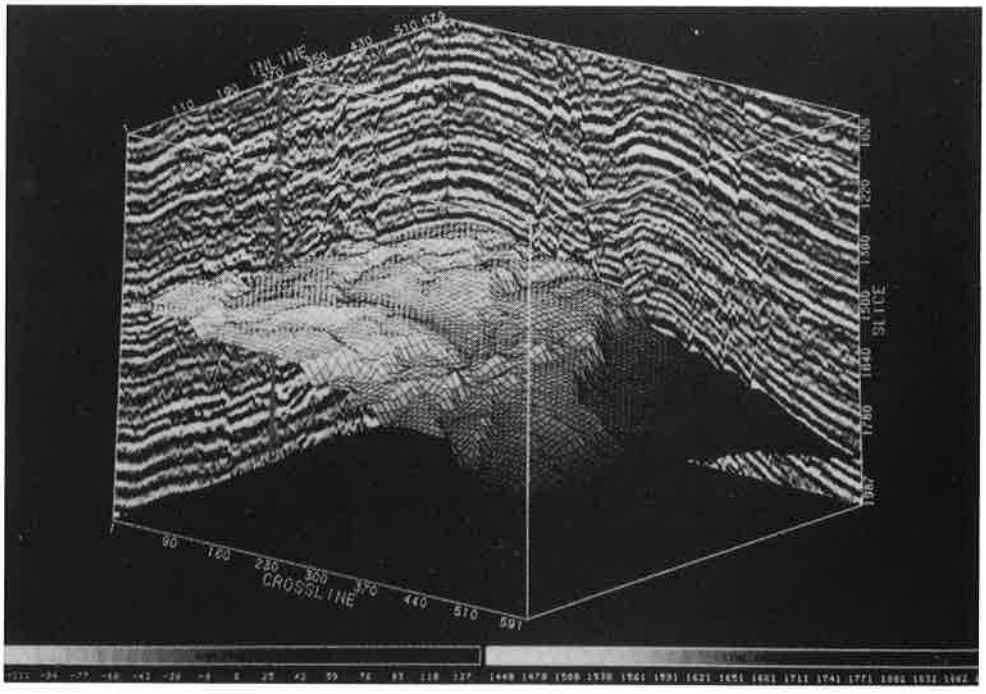

Fig. 4-4: LM2B interpreted horizon time structural map with Crossline 1 and Inline 579 displayed in three dimension. The flying carpet colour scale is gradational and topography like, the seismic colour scale is bimodal (negative loops in violet and the positive peaks in dark red).

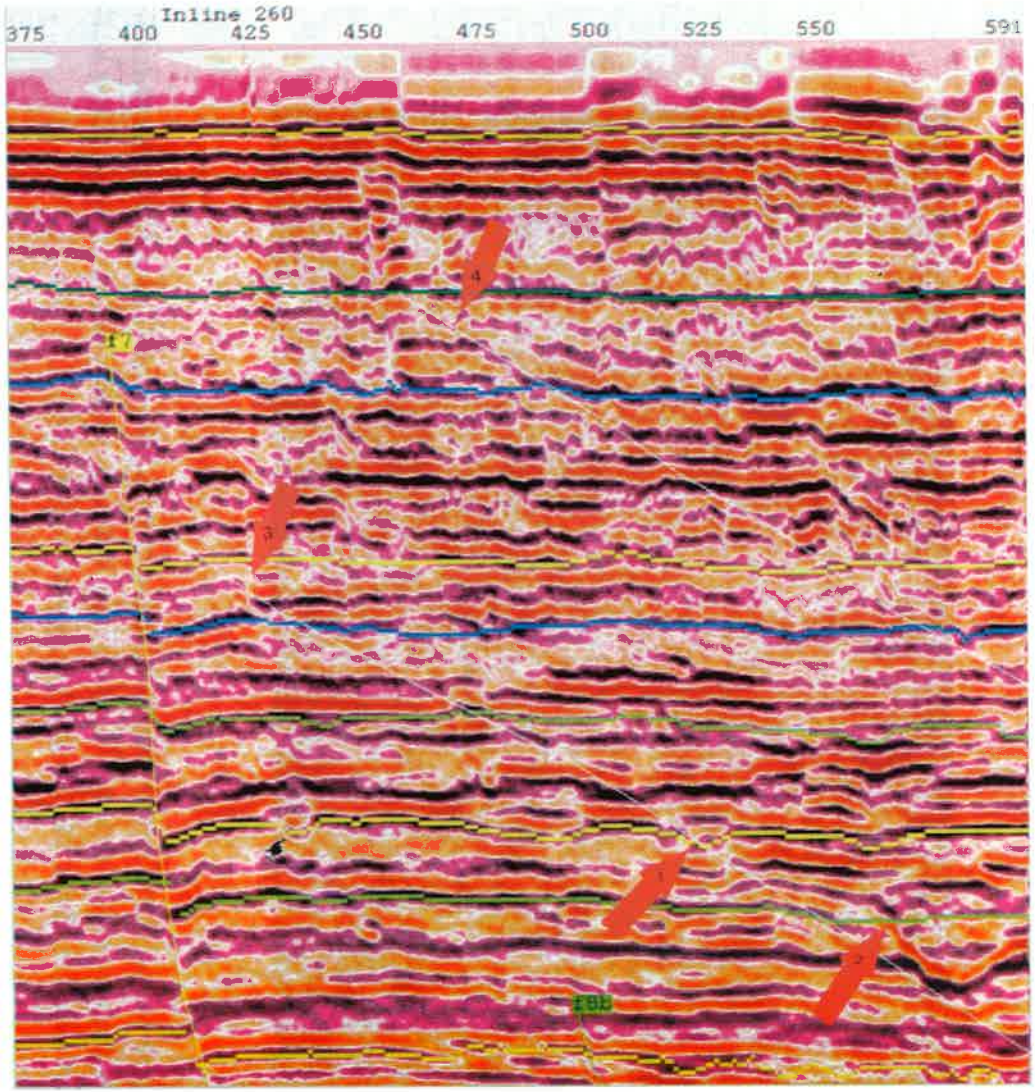

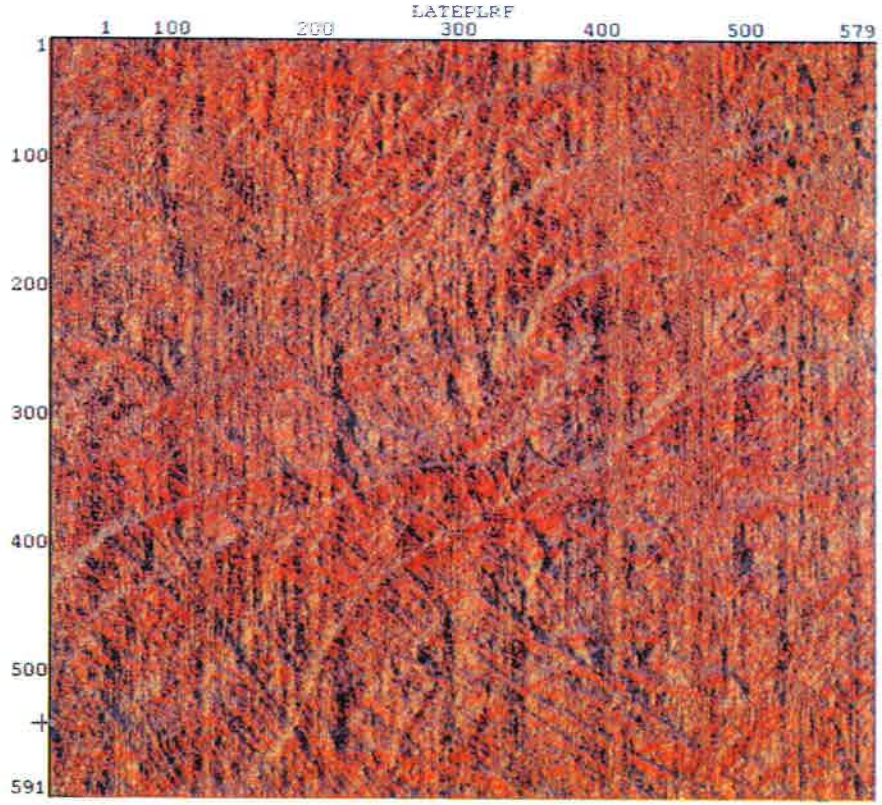

Fig. 4-5: ***a.*** *Southern portion of Inline 260 with oblique low angle minor fractures detected on the azimuth map of the LATEPLIO interpreted horizon (pointer 1).* ***1.*** *LATEPLIO horizon interpreted below all erosional features.* ***2.*** *SB24 horizon interpreted as planar datum cutting through erosional features for calculation of parallel consistent amplitude maps.* ***3.*** *and* ***4.*** *Subtle oblique faulting.* ***b.*** *Azimuth map (sun light from the east) to enhance subtle fractures almost perpendicular to general fault trend in the south-western portion of the image. The Inline on fig. 4-5 a intersects 3 times the meandering channel indicates by the azimuth map.*

There are two ways to map a seismic horizon over a 3D survey according to different purposes :

- 1) In order to obtain paleogeomorphic maps of erosional features, unconformities or definite sedimentary objects (reservoir delimitation), the interpretation line is drawn mostly manually along a time consistent surface (erosional or depositional event) mapping directly the surface topography on the time structure map on the Interpretation screen.

- 2) In order to be able to generate coherent maps for attributes analysis in the 3D volume above and below the interpretation line, the interpreter must create a smoothed datum plane coherent with the general structure by cutting through local discontinuities (channels, downlaps, etc...).

The combination of results provided by the two methods enable a complete reconstruction of the morphology and lateral seismic facies changes of complex erosional surfaces (Stampfli & Höcker, 1989; Reymond & Stampfli, 1994d) .

The figure 4-5a shows an example of two seismic horizons interpreted on Inline 260 (see also chap.5, fig. 5-23) in the two modes described above. The yellow horizon (LATEPLIO, pointer 1) has been interpreted along a negative trough (in violet) below all erosional features. The corresponding time structure map (fig. 4-5b) reveals that the three channels intersected on the hanging wall of the F7 main growth fault on figure 4-5a (see also black finger pointer) are in fact three intersections of the same meandering river (see also fig. 5-38, C41-C42-C43). This observation would have simply been impossible to guess from a single vertical section. Slicing the 3D volume parallel to this interpretation line would not produce the desired result reproducing by artefact the presence of the interpreted channels where they are not.

The green horizon below on figure 4-5 a, (SB24, fig. 5-33) has been interpreted with a higher filter (smoothed interpretation) as a consistent datum plane cutting through all discontinuities (see deep erosional channel associated with the lowstand period between 2.4 and 2.2 Ma, fig. 4-5a, pointer 2). This type of datum plane does not reveal the paleotopography of the erosional event at 2.3 Ma but enables for instance to cut through the channel with a regular 4ms interval to observe the vertical variation in the type and morphology of the sedimentary fill. For the purpose of this research which is to systematically describe the vertical evolution of sedimentary facies from horizontal images, most horizons were interpreted as conformable smoothed datum planes. The colour picture on figure 4.4 illustrates on a 3D display the time structure map of the LM2B horizon interpreted along a negative amplitude loop (in violet, see Crossline 1 and Inline 579). This horizon marks the transition or change in vertical seismic facies from three continuous high amplitude reflectors below the interpretation line to a more transparent interval on top (see on vertical sections, fig. 4-4). This "flying carpet" surface is coincident with the sequence boundary at 8.2 Ma attributed to the erosional surface exemplified by the seismic data (fig. 5-45 and Plate 3b). This geological aside demonstrates the important role of colour display in 3D seismic interpretation.

The art and psychology of colour applied to Earth Sciences would be in itself a great subject for a PhD research and all geologists and geophysicists make a more or less conscious usage of it. In seismic analysis, not many papers have been published on the usage of colour as it seems that the choice of colour scale is more a personal process than something following a precise law (Balch, 1971 ; Anstey, 1973 ; Taner & Sheriff, 1977 ; Lindseth, 1979 ; Neidell, 1985 ; Brown, 1986 ; Merriam & Allen, 1991 ; Brown, 1992 ; Russel, 1992)

Nevertheless four basic concepts of colour usage can be proposed:

- work with the colour range that you like to ease the interpretation's task and present the data in the preferred colour scale of the manager !
- reds and blues: the hot (red, orange, yellow and brown) colours are attractive, outstanding and can be aggressive. They also naturally refer to high topography or on land features). The cool (blue, blue-green, green) colours are soft, mellow colours referring to what is low and deep. Vio let is a dynamic neutral colour resulting of the mixing of equal proportions of red and blue.
- if you want to present precise points that need to be enhanced use contrasting (complementary) colours with a fitted legend.
- if trends or any expression of continuity need to be expressed then use gradational colour scales with appropriate scale.

Referring back to figure 4-4, the time structure map is displayed with a topographic like gradational colour scale and all vertical sections in this study are displayed with the same bipolar mode (negative loops in dark violet shading to orange and red-brown for the positive amplitude peaks). The difference in amount

of information between colour and black and white raster display is beyond words and simply needs to be observed (compare Inline 260 on figs. 4-5 a and 5-23). The human eye can distinguish up to 11 or 12 shades of grey. In particular, the difference in amplitude content between the transparent sandy intervals and the continuous high amplitude reflectors associated with the strong contrast in acoustic impedance between sands and shale is not directly noticed on black and white displays but is immediately visible with a bimodal colour scale. It shows the cyclic aspect of sedimentation on the proximal Gulf coast shelf alternating from sands to shale (fig. 4-4 vertical sections and fig. 4-5 a).

4.3.2 Attributes and Maps

Introduction

Once an interpretation grid is stored in the database, several mapping options are available to the interpreter to further the horizon analysis with additional attributes and to display his results in the most fitting way. In the CHARISMA S™ system (Schlumberger-Geoquest) these options are divided into four different parts:

- a. Seismic attributes applied to seismic data (reflection strength, instantaneous phase, response phase, instantaneous frequency, response frequency and apparent polarity).
- b. Attribute maps or horizontal display of seismic attributes along or in parallel to the interpretation line (amplitude, instantaneous phase and frequency, response phase and frequency, apparent polarity, 1st and 2nd derivative, amplitude deviation, dip and azimuth).
- c. Volume related attributes (reflection heterogeneity, reflection intensity and acoustic imped ance).
- d. Geomap™ display (posted value maps, contour maps, gridding and contour maps, coverage maps and isometric displays). They won't be described in this chapter as they consist mainly of display and plotting interfaces.

Geological applications taken from this 3D survey will be used to illustrate some of the more frequently used attributed listed above.

a. Seismic attributes

A wiggle seismic trace is the projection on one plane of a three dimensional reflectivity vector changing in direction (phase) and intensity (amplitude) along the time axis (see fig. 4-6, from Taner et al. 1979). Seismic attributes are the expressions of the same seismic signal in the time, real and imaginary dimensions to express complementary aspects of the seismic trace. Thereby additional specific information can be recognised on the seismic section such as lithology, sedimentary facies and structure. The three seismic attributes commonly used for interpretation and characterisation of lithology are reflection strength, instantaneous phase and instantaneous frequency. They are developed in the example below. Figure 4-7 presents a zoomed portion of a NE-SW randomline (HP34, see location on fig. 5-48 b) running through Well 4 (red vertical dotted line), perpendicularly to the main sediment input direction. The normal growth faults and 4 interpreted horizons are visible on the 4 windows multiframe display on figure 4-7.(from base to top: TOPMIODL, TOPMIO, LOPLIO, LOPLIO2, Plate 3-2).

- Amplitude and reflection strength

The first window (fig. 4-7 A) shows the seismic section in normal amplitude (violet as negative). The bimodal coloured amplitude display provides much more direct seismic information than black and white raster display(compare the same randomline on fig. 4-7a and fig. 5-22 or Plate 2-C). From correlation to the well log curve along Well 4 on figure 5-46, the transparent central low amplitude packages (1220 to 1300 ms along Well 4) represents thick sands and the strong amplitude anomaly below corresponds to the high contrast in acoustic impedance caused by sand/shale contacts in channels or along shaly condensed sections. Figure 4-7 b) shows the same section displayed in reflection strength. This attribute corresponds to the envelope or total energy of the seismic trace at a given instant (fig. 4-6 a and b, dashed lines). It is mostly significant for true amplitude data. Although fairly similar to the amplitude display this attribute is useful to highlight lateral and vertical lithological contacts. For instance, the abrupt change in reflection strength observed on pointer 1 (fig. 4-7 b). This drastic lateral transition is difficult to interpret on the unique basis of this display and is visibly not related to a fault.

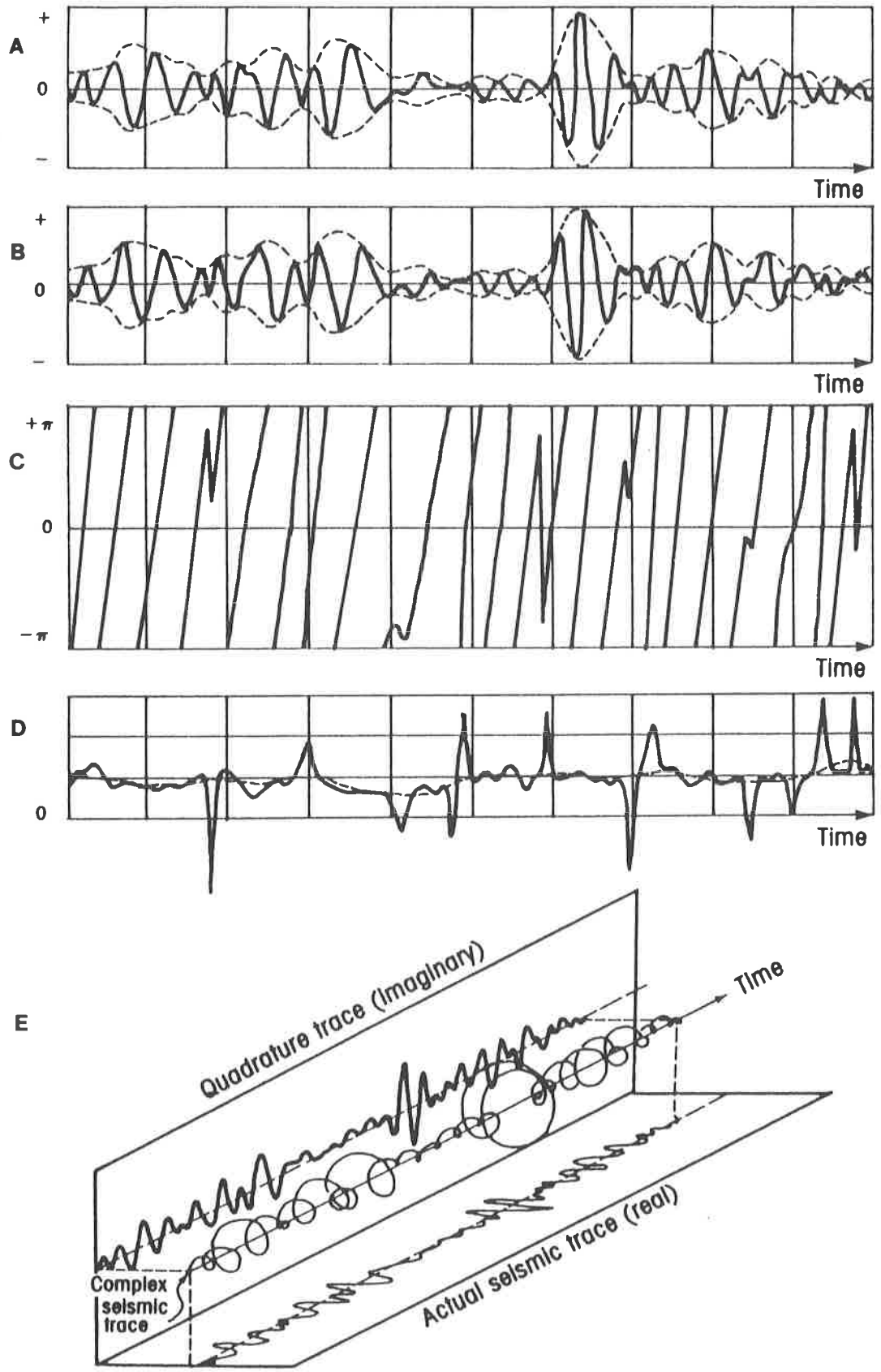

*Fig. 4-6: Seismic attribute complex trace analysis: real (**a**) and quadrature or imaginary traces on a portion of a seismic trace. The envelope or reflection strength attribute is shown as the dotted line in (A) and (B). **c.** Instantaneous phase (rotation angle). **d.** Instantaneous frequency (derivative of Instant. phase). **e.** Isometric display of a complex trace. Modified from Taner et al. (1979).*

- Instantaneous phase

Figure 4-7 c) presents the same section displayed in instantaneous phase which is an attribute indicating the rotation angle (phase) of the spiral like propagating seismic signal through time. This attribute presents the advantage of being totally independent from amplitude so that any reflection will have the same weight on the seismic display. The scale is from -180 to +180 degrees and both extreme values have the same colour. An automatic line drawing can be generated by compressing the instantaneous phase colour scale or by using a partial colour scale (only 2 stripes of colour on a white background). Instantaneous phase (fig. 4-6 c) helps for structural analysis and identification of subtle sedimentary and tectonic features (channels, downlaps, pinch-outs, subtle faulting, etc...). The pointer 2 on figure 4-6 c) indicates a U-shaped valley or trough that was not visible on the reflection strength display and not so easily identifiable on the amplitude section. The interpretation of this strong negative amplitude anomaly as an incised valley channel is confirmed by the horizontal amplitude map calculated along this level (see figs. 4-9 b and 5-56). Another example is illustrated in the transparent interval mentioned above in the centre of the image between 1250 and 1300 ms on top of the large negative amplitude anomaly. The instantaneous phase display reveals interesting details concerning the fill of the large incised valley demonstrated by the horizontal amplitude maps on figures 5-47 and 5-48 (Reymond & Stampfli, 1994a) . The two arrows (3 on fig. 4-7 c) point out at two oblique low amplitude reflections difficult to identify on the amplitude vertical display (fig. 4-7 a) that correspond to the intersection with point bar sands filling the outside portion of the meander intersected by the randomline on figure 4-7 (see fig. 5-48 b).
Without this tool it would not be so easy to interpret this transparent sandy fining upward (well log data, fig. 5-46) interval on a vertical section (wiggle or raster) as a major Messinian incised valley fill revealed by the instantaneous phase line drawing and the horizontal amplitude map.

- Instantaneous frequency

Instantaneous frequency is the time derivative of the phase which shows rapid and abrupt changes sometimes difficult to interpret (fig. 4-6 d and 4-7 d). It is a good indicator of the signal to noise ratio (seismic quality check) and is mainly used to identify reservoir filled with gas or condensate that can locally absorb the higher frequencies (in this case, red = dominance of low frequencies 0 Hz and the greens and blues correspond to the highest frequencies 125 Hz). Note that all attributes in this study except for the amplitude are displayed according to the international AAPG colour standard. The strong red (low frequency) anomaly indicated by the pointer (4 on fig. 4-7 d) indicates an abrupt lateral change in instantaneous frequency along a green line of higher frequencies below the TOPMIODL interpreted horizon (dark blue line). This indicates a lateral change in lithology or pore fill that can now be identified on the amplitude display once it has been enhanced by this attribute (fig. 4-7 a, pointer 4). When looking at an horizontal amplitude map across this polarity inversion centred on Well 4, the small depression marked by the two black arrows indicate an ovoid shape. From the structural point of view it is located right on top of the positive salt related structural high (see fig. 6-7 and 6-8). From the sequential analysis on logs it corresponds to a thick and sharp coarsening up sandy signal located at the base of the transgressive systems tract of the 6.3 to 5.5 Ma 3rd order sequence. All observation on complementary data converge in interpreting this initially meaningless instantaneous frequency anomaly as the sign of a local transgressive erosion on top of the zone of more active salt related uplift. This incision on top of this domed structure is at the origin of the coarse reworked sand body observed along the same level on Well 4 (fig. 5-46, TOPMIODL level). Other examples of productive transgressive reworked sand bodies showing the same characteristics will be discussed in chapters 5 and 6.

- Seismic attributes: conclusion

The amount of information provided by the simple display in four different attributes of one tiny portion of any line of a 3D seismic data is just astounding. That means that the fine sedimentary and structural information contained into one single 3D survey is almost inexhaustible. Seismic attributes analysis is limited to qualitative description of vertical seismic section unless the survey is displayed in true amplitude (not scaled, which is not case in this study). Other seismic attribute like the apparent polarity used specifically to detect gas related polarity inversion will be integrated into the hydrocarbon applications developed in chapter 6. Response phase and response frequency attributes are the averaged weighted display of the corresponding attribute. They display frequency and phase smoothed curves.

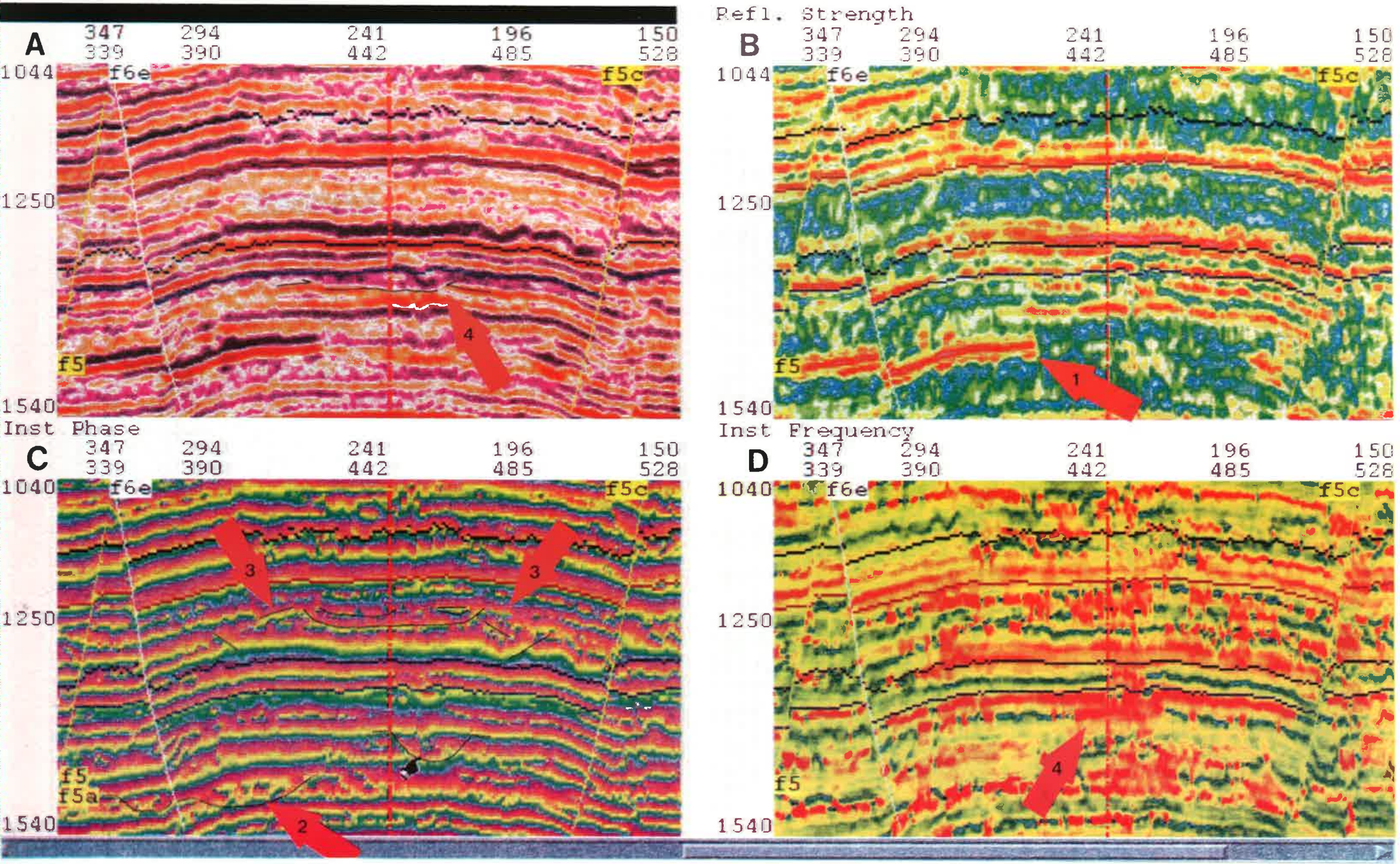

Fig. 4-7: Multiframe display of the most commonly used attributes on a zoomed portion of a NE-SW random line; vertical scale in milliseconds (HP34, see fig. 5-22 and 5-48 for location). ***a.*** *Coloured amplitude* ***b.*** *Reflection strength* ***c.*** *Instantaneous phase* ***d.*** *Instantaneous frequency.*

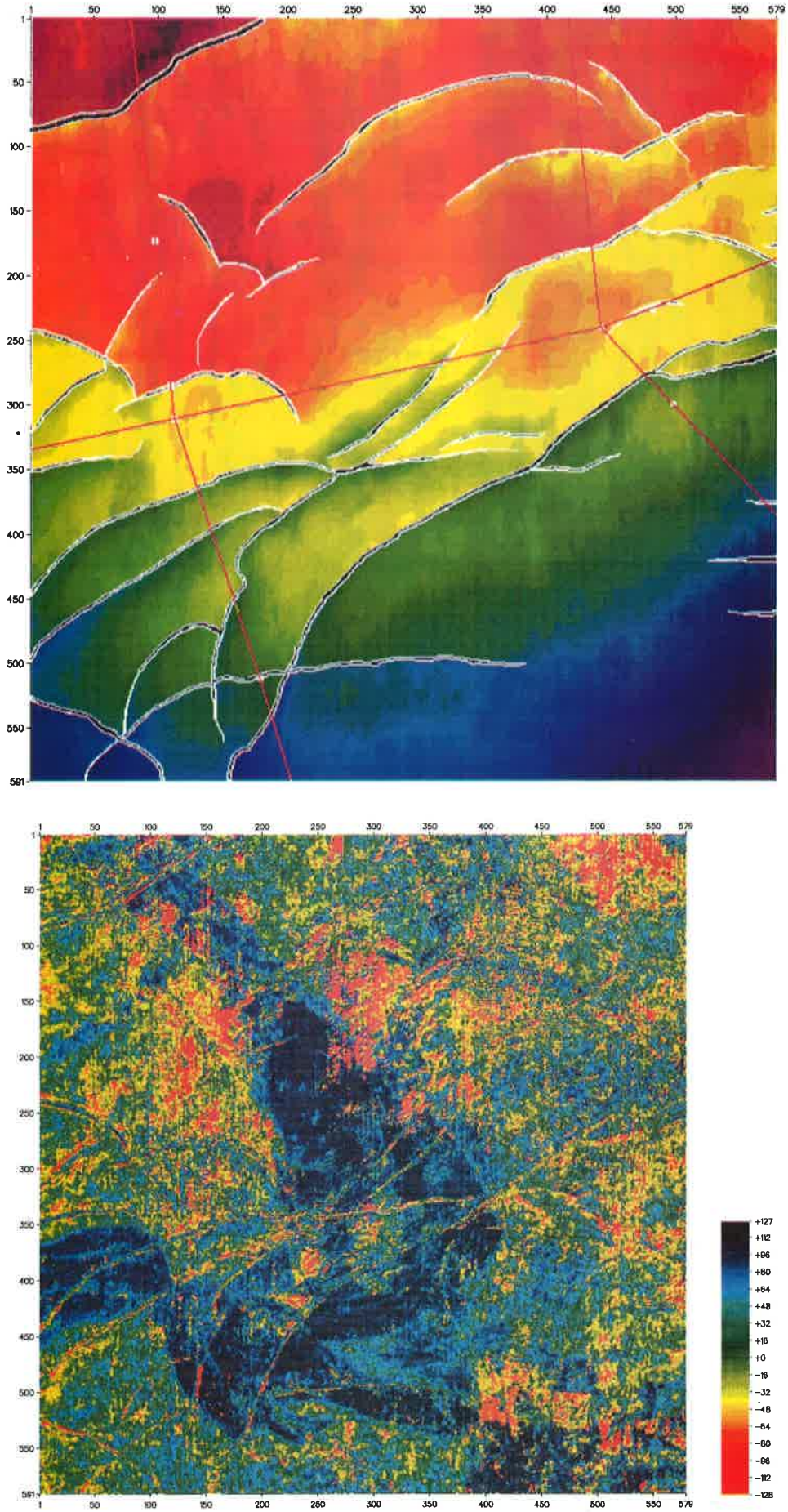

Fig. 4-9: ***a.*** *Refined and filtered time structure map of the LOPLIO2 horizon (≈ 4.4 Ma), coherent base (datum plane) for the amplitude map calculation.* ***b.*** *Amplitude map calculated 56 ms above and parallel to the LOPLIO2 datum showing a large incised valley (2 superposed meanders, SB 4.2 Ma).*

Their exact use is not yet exactly defined by lack of experience. For further information on seismic attributes, the following references can be consulted: (Bracewell, 1965 ; Balch, 1971 ; Harms & Tackenberg, 1972 ; Sheriff, 1976 ; Taner & Sheriff, 1977 ; Taner *et al.*, 1979 ; Sonneland *et al.*, 1990 ; Sonneland *et al.*, 1991 ; Brown, 1992 ; Hoetz & Watters, 1992 ; Keskes & Camy-Peyret, 1992 ; Nestvold, 1992 ; Sonneland, 1994) .

b. Attribute Maps

All attribute maps (sample level attributes) are based on time structure maps of an horizon interpreted on the total or partial portion of a 3D survey. An attribute map is obtained by extracting information from the seismic data at or near the interpretation line. For greater accuracy in the location of the interpretation line at a particular amplitude over the entire survey, it is possible to automatically refine the manual or semi-automatic interpretation. The input grid first needs to be interpolated to microsecond accuracy before the interpretation can be adjusted to the parameters entered by the interpreter. This option is of great help in the recognition of subtle sedimentary features registered as subtle lateral changes hidden within half a loop.

- Amplitude maps

Also called "Pick value at horizon" the amplitude map extracts amplitude information at the time value of the (refined) interpretation line. The result of this process applied to the entire surface of the survey is then displayed along an horizontal plane (x, y, A co-ordinates). This process is exemplified on figure 4-8 that shows a portion of a vertical seismic section displayed in wiggle trace (Inline 247A on which the TOPMIO horizon (≈ 5.6 Ma) is interpreted along a positive (black) peak across a normal fault. Figure 4-8B presents the result of the amplitude extraction along Inline 247 (white amplitude vector along the flattened TOPMIO interpretation line). An amplitude map is the display of the amplitude vector on all seismic traces intersected by a given horizon.

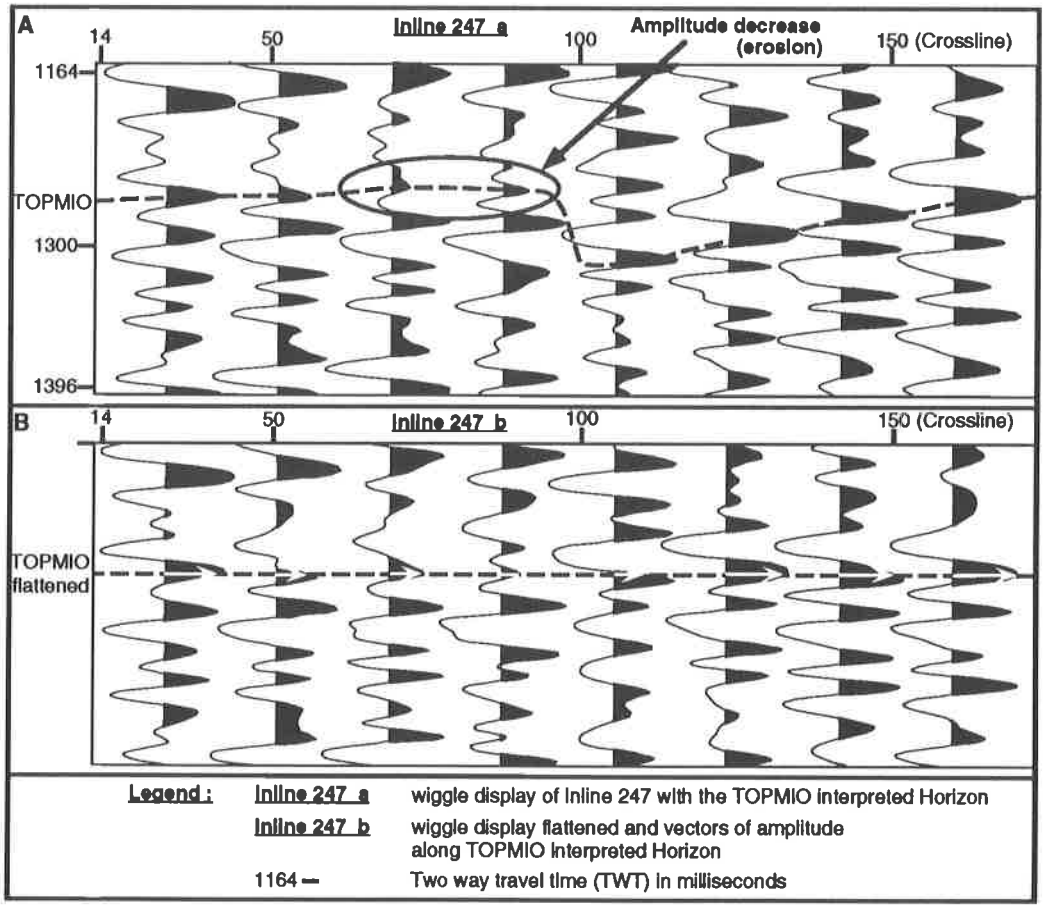

*Fig. 4-8: Inline 247 in wiggle trace and interpretation of the TOPMIO horizon (≈5.6 Ma). **a.** Interpretation line along a positive (black) peak across a normal fault **b.** Horizon flattened and amplitude vector indicated on each trace (principle of amplitude mapping).*

A spectacular example of the mapping of the amplitude vector on the totality of the 3D survey is presented on figure 4-9. Figure 4-9A is the refined and filtered time structure map for the LOPLIO2 horizon (≈ 4.9 Ma). The lateral consistency of the amplitude response at a given level (as an indicator of the lateral changes in seismic facies) is directly related to the quality and coherence of interpretation. Such a time structure map is the result of the semi-automatic interpretation of 300 lines amongst the 579 inlines composing this survey. These inlines are cross-checked with crossline before applying an interpolation filling the missing gaps in the interpretation. In zones of higher complexity, the systematic interpretation of every line might be needed to get the highest possible lateral resolution. Fault gap are indicated by white lines (fault marks) introduced in the data base during the interpretation. The amplitude map will not take into account the surfaces within the fault planes. The red straight lines indicate the location of randomlines generated to correlate the wells available in this study (surface location marked by white squares). The colour scale on figure 4-9A indicates the two way travel time depth of the interpreted horizon (1092 to 1404 ms). When the quality of interpretation is estimated as optimum, it is possible to extract the amplitude signal along the interpretation line or along datum planes parallel to it. Figure 4-9B presents the amplitude map calculated 56 ms above the interpretation represented on figure 4-9A. A spectacular large incised valley is marked by the negative amplitude in dark blue (thick sands) cutting in the more silty shelf sediments (green and red). The horizontal changes in seismic facies displayed by an amplitude map at any level are geologically interpreted as distinct sedimentary facies on the base of the shape, size and lithological information provided by the well log data at the corresponding level. It is interesting to note that the main river bed is located exactly in the depression between the two salt related positive structures mapped on figures 6-7 and 6-8. Many more examples of relationships between sedimentary facies and tectonic and eustatic influences will be developed in chapters 5 and 6 based on the systematic observation of successive amplitude maps. The vertical sampling on seismic traces is 4ms which enables the interpreter to calculate one horizontal seismic facies map approximately every 4 m. Deeper in the seismic data, the vertical and lateral seismic resolution starts to decline and amplitude maps get more and more difficult to interpret. A valid amplitude map obtained far away from the interpreted datum must still represent a time consistent line. For the upper 2 seconds below sea level and in the studied area amplitude maps calculated further than 100-120 ms away from the interpreted datum start to intersect inconsistent loops due to lateral thickness differences. Figure 4-10 shows a time slice (plane calculated parallel to the sea level) at a time depth of 860 ms. Its complex patterns exemplifies the time non-consistent intersections of such a seismic plane with the volume of 3D data. One interpreted negative loop is intersected in the lower right corner of the image (grey square lines, pointer 1). Pointer 4 and 5 show white amplitude zones parallel to the intersected loop (1). On the basis of this display they could eventually be interpreted in the same way. But time consistent amplitude maps calculated over this interval show that the white bands (4 and 5) are deep erosive channels. Pointer 2 and 3 indicate the apparent change in polarity of two channels across the main F7 fault (negative channels in positive loop on the hanging wall and the opposite on the footwall). This apparent switch of polarity in sedimentary events do not appear on amplitude maps flattened along the interpretation line which suppresses the effect of post-deposition deformation

- Attribute maps

The amplitude attribute mapping is the most direct of the "sample level" attribute maps. It is also possible to apply some pre-processing to the seismic data before displaying the intersected values along an interpretation line or along a datum shifted in parallel to the interpretation horizon. The pre-processors that can be applied to an horizon are similar to the ones applied to the vertical sections and will provide similar types of information but displayed along the horizontal plane (Instantaneous phase and frequency, response phase and frequency and apparent polarity, refer to the seismic attribute description in this chapter). These additional attributes are mainly used for local precise potential reservoir finer analysis and description. Three additional horizontal sample level attributes are used mainly for interpretation quality control (Amplitude deviation and first and second derivative). Amplitude deviation indicates the local difference between the position of the interpretation line and the actual maximum or minimum peak interpreted. The first and second derivative calculate the slope (and its variation) of the tangent of the zero-crossing (in wiggle) below the interpretation pick. It provides accurate additional information on the amplitude and frequency subtle lateral variations or trends.

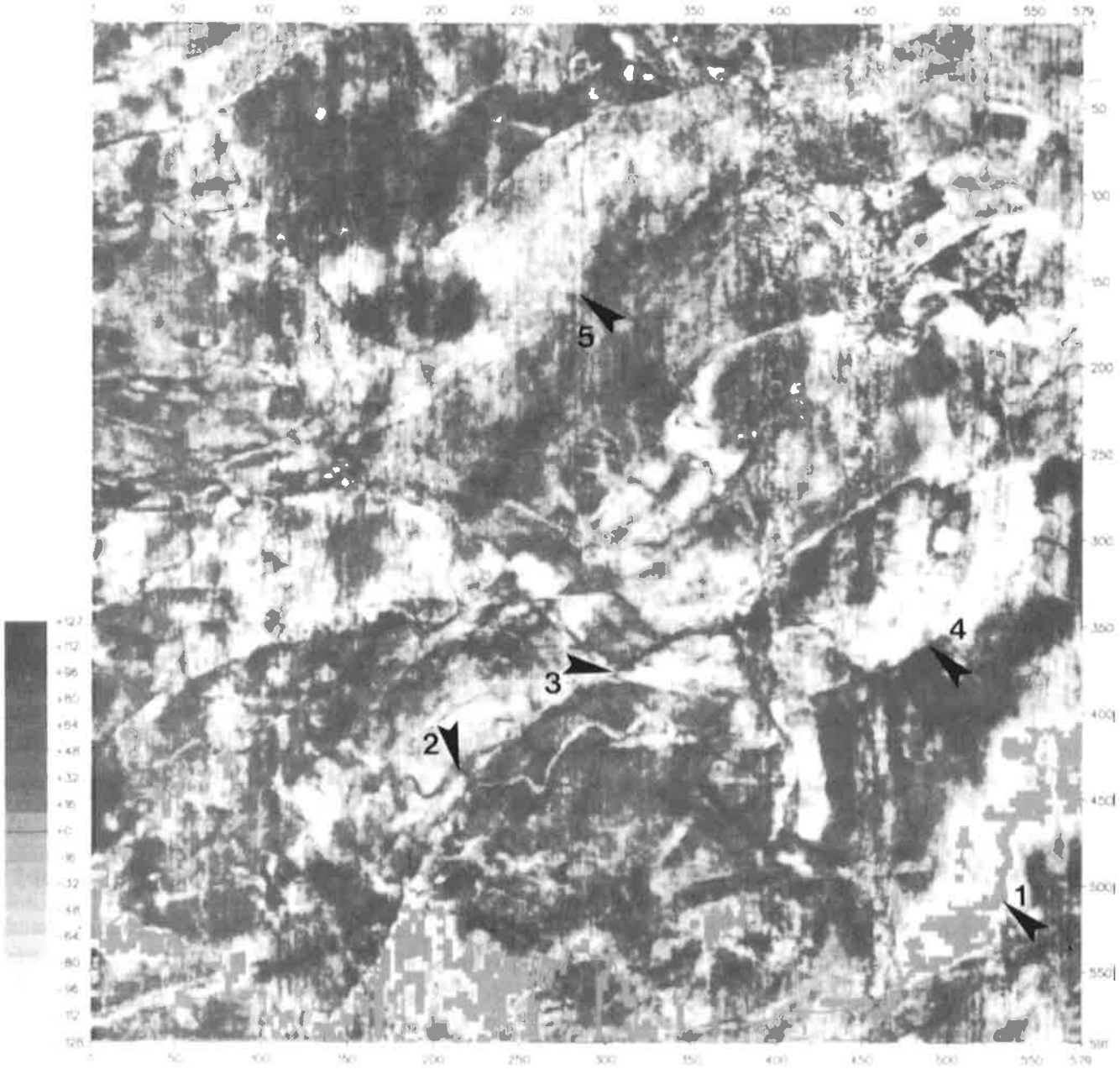

Fig. 4-10: Isotime (time slice) through the 3D data at 870 ms (TWT) below the surface showing the lateral inconsistency in seismic facies across the faults. ***1.*** *Intersection with an interpreted seismic loop.* ***2*** *and* ***3.*** *Polarity inversion artefact of two channels across a fault.* ***4*** *and* ***5.*** *Two distinct large channels to be distinguished from* ***1*** *(seismic loop).*

- Dip and azimuth

The dip and azimuth maps indicate respectively the dip changes from trace to trace by triangulation and the subtle changes in dip orientation (Dalley *et al.*, 1989). Both options can not be applied to the normal 4 ms sample rate data and necessitate a refined interpretation prior to calculation. This is done by using a spline function that transform the interpreted grid to an accuracy of 0.001 ms. The scale of dip and azimuth is in ms/m. Such maps enable very fine structural analysis and can easily differentiate the organised geological features from the organised or unorganised noises related to acquisition or treatment. An option to rotate the lighting direction on the map (rotate the colour scale) is always associated with these options. The example on figure 4-5B shows the azimuth map calculated along the LATEPLIO refined horizon (≈ 2.1 Ma) displayed in black and white with the sun from the east. The most striking feature with such a lighting is that the interpretation was realised on the Inlines (north-south stripes), perpendicular to

the lighting. Then the gentle rollovers associated with the major growth faults at that depth appear as smooth plane dipping towards the arched fault trace. The orientation of the general fault trend is NE-SW. Then the meandering channel intersected three times on the vertical section of Inline 260 (fig. 4-5 a) is also visible and highlighted with a black line. And on top of that, rectilinear marks are organised more or less perpendicularly to the main faults, in the lower left portion of the azimuth map (fig. 4-5b). By correlating these subtle features on the azimuth map and looking at the corresponding image on vertical sections (fig. 4-5a), we come to the conclusion that they are related to low angle zones of deformation registered as lateral changes in amplitude. Note that on figure 4-5a only two zones are interpreted (in white) but all the marks present on the azimuth map can be identified on the vertical section. Pointer 3 and 4 show evidence of normal movements along these lines and clear lateral changes in amplitude. Similar traces are seen on the azimuth maps calculated on the interpreted horizons above and below which should exclude the hypothesis of the seismic noise artefact. No definite explanation can be given concerning their origin. Their position and orientation could indicate that they are connected to the 2 salt related positive structures in the north-east portion of the image as these subtle faults seem to get round them (see fig. 6-8). The list of example of amazing discoveries done via dip and azimuth maps on a 3D data set is really as long as the amount of information displayed by vertical seismic attributes. They are powerful tools for fine structural and precise sedimentary studies and characterisation of subtle reservoir characteristics, simply not visible on more classical displays (Reymond & Stampfli, 1994d) .

c. Volume related attributes

The third class of seismic attributes involves volume calculation of attributes on the basis of one or two interpretation grids. Reflection heterogeneity, reflection intensity and acoustic impedance are the three most commonly used volume related attributes. They give the possibility to calculate an attribute between two interpreted grids (isopach seismic characterisation) or in a pre-defined slice above or below an interpreted horizon. Their main application field is for reservoir precise characterisation and also for subtle sedimentary description of fine objects not identified by one single amplitude or sample level attribute map. Practical examples are illustrated in chapter 6 (fig. 6-10 and 6-11) but their basic principles and applications are summarised below.

- *Reflection heterogeneity.*

The reflection heterogeneity sums up the amplitude changes from sample to sample along one single trace and maps these values representing the distribution of the wiggle trace variance. It enables to enhance subtle changes in homogeneous formation (shale lenses in thick sands). Zones of high heterogeneity are interpreted as possible more shaly zones and zone of very low heterogeneity can be seen as pure sands (eventually with good porosity).

- *Reflection intensity*

This attribute more directly sums up the absolute value of all amplitude encountered along one seismic trace for a given interval. This is closely related to lithology and can be of great help to unveil shallow channels or subtle faults missed along one single sample attribute map (see fig. 6-10). Chapter 6 will present an application of this attribute showing that it also enables to precise the lithology and fine texture of strong amplitude anomalies such as gas related bright spots or thick incised valley sands contrasting with fine silt and shale sands.

- *Acoustic Impedance contrast.*

The acoustic impedance contrast over a volume between two interpreted horizons is based on the measurement of the reflection coefficient of the seismic section as a function of acoustic impedance. It can be directly seen as an indicator for relative porosity values. A high porosity potential reservoir will show low acoustic impedance values.

Attributes and maps: conclusion

The constant need for more precise information of the underground characteristics led to the rapid development of numerous seismic attributes showing that a seismic trace contains much more information than expressed by a simple succession of wiggles. Seismic attributes calculated on seismic data,

interpreted surfaces or pre-defined volumes or slices help:

- to identify subtle sedimentary features.
- for reservoir delineation (structural or stratigraphic traps)
- to indicate the porosity distribution
- to identify and locate micro-fractures associated with major fault systems.

This large amount of additional data is becoming an ever more solid base for precise reservoir modelling (Hilterman, 1982 ; Neff, 1993 ; Wehr & Brasher, 1994)

The seismic attribute calculations and always more precise definition of distinct seismic facies based on quantifiable measurement of attributes open the door to automatic and even independent 3D seismic horizon tracking (Legget *et al.*, 1994) . It seems that it won't be long before most of the interpretation will be mostly effectuated by artificial neural network (ANN, Kohonen, 1984) that can very rapidly learn to distinguish and map different seismic facies. On the vertical plane, simple horizon tracking can be effectuated automatically and on the basis of an already interpreted grid or surface the same processes can "interpret" the seismic facies in terms of porosity, type of fluid content, etc... (Sonneland, 1994) . Computers seem almost ready to do the interpretation, interpret and test the interpretation and indicate the best place to drill !

4.3.3 Fault interpretation and annexes to 3D seismic interpretation.

Fault interpretation

Faults can sometimes be difficult to interpret on 2D vertical profiles that are almost parallel to the local major fault trends. The great advantage of 3D data sets is that any fault can be intersected in any direction and thereby be interpreted without any doubt. The second main problem on 2D survey is the correlation of faults from one line to the next when the 2D acquisition grid is too large. The main regional faults are usually correlated without hesitation but the secondary local faults rapidly changing laterally can be difficult to project from one line to the other. This "aliasing" problem is almost non-existent on 3D survey as the normal line spacing is in most cases inferior to 50 m (25 m in the present survey). Three types of fault intersections with the vertical plane can be defined as:

- U type: seismic line intersect parallel to the fault plane. Vertical throw progressively disappears (see continuous lower horizon on fig. 4-11 below the U shaped F2a fault). Such fault plane are easily missed during interpretation and provoke apparently incoherent structures. The double U shape (smaller U within the major fault) indicates subtle secondary faults parallel to the main fault plane. It indicates the micro-fracture along the major fault plane and is important for determining the type of contact between potential reservoir and the fault planes. This type of display can be assimilated to a fault slicing (Brown *et al.*, 1987) in the vertical portion of the fault plane.
- L or J type: seismic line oriented across the main structures. L intersections are the most common down-to-the-basin growth fault merging on deep lying glide planes. The slope of the fault diminishes with depth (curve accentuated by the vertical time scale). J type are mostly antithetic fault perpendicular intersections or oblique intersections of major growth faults (F2b on fig. 4-11)
- I type. Oblique intersection of the vertical portion of growth fault or antithetic fault. Also indicate "floating" almost vertical secondary faults whose vertical throw diminishes and becomes nil before joining any other faults (mainly related to differential compaction).

The interpretation of the fault traces on the horizontal plane is an easy task on the time slices or on the time structure maps resulting from an horizon interpretation (see fig. 4-10 and 4-9 a). Faults appear on time slices as rectilinear, softly curved limits showing possible apparent polarity inversion. Figure 4-11 shows extension of the vertical fault interpretation on the time slice (F2a).

For a few years the interpretation of faults on computer was entirely limited by the fact that only one point or one value could be assimilated to one (x-y) co-ordinate. In such conditions the number of different levels or horizons required to interpret only one major growth faults and associated minor parallel and antithetic fault was enormous as it is common to have up to 15 superposed faults along the same vertical trace. The same problem occurred for inversion tectonic or negative slopes associated with salt pillows or allochtonous salt sheets (Wu *et al.*, 1990b) . Today all workstations are equipped with fault interpretation systems able to have more than one z value for any (x-y) trace. Interpretation of fault planes on workstation is also facilitated by the lateral projection options enabling to project on the working plane

the interpretation of several sections in front or behind the active selection. The interpretation of any fault can also be automatically assigned to the corresponding fault plane. And finally the interpretation of a fault plane can be speeded up by the possibility to triangulate (interpolate) the fault plane from a small number of points. Each time a new point is added, the precision of the triangulation is improved by rapid re-calculation. Once a fault plane is generated it is possible on some systems to apply the "fault slicing" option in order to read the amplitude or any other attributes along the fault plane and along planes parallel and near to the fault. The fault slicing is fundamental for the observation and understanding of the reservoir / faults contacts (Brown *et al.*, 1987) . Up to today, the best way to do that on the CHARISMA S™ system (Schlumberger-Geoquest) was to interpret one fault plane as a normal horizon and extract amplitude or attributes maps above or below.

The interactive interpretation of horizon and fault planes is now greatly facilitated and the computers will soon be able to interpret the contacts entirely on their own and directly produce time structure maps with coherent fault gaps indicated. And again: what is the interpreter going to do ?

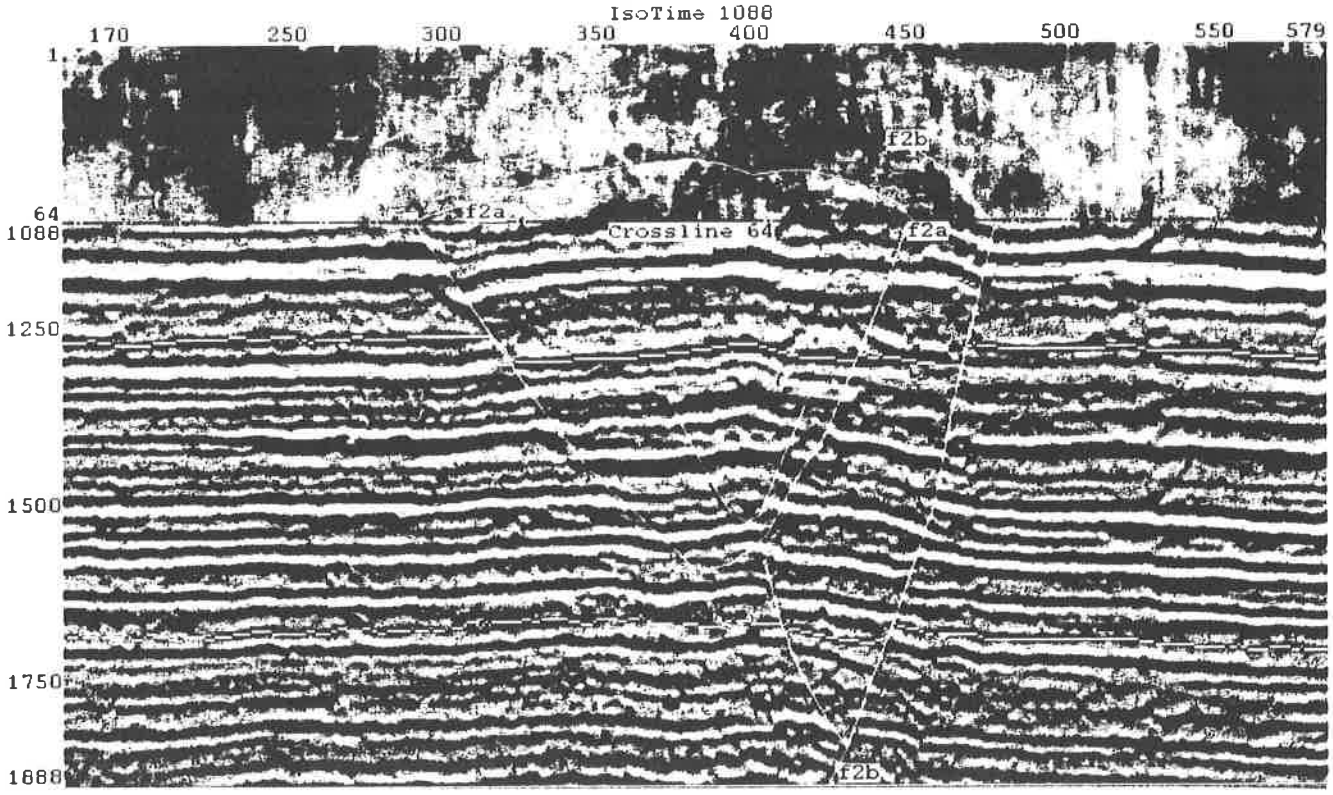

Fig. 4-11: Composite section (vertical crossline 64 and horizontal isotime 1088 ms). U type of fault intersection showing apparent disappearance of vertical throw (F2a growth fault plane parallel to Crossline 64). F2b normal and antithetic growth fault present L and J types intersections.

Annexes to 3D seismic interpretation

Seismic workstations evolve very rapidly and the number of possibilities for data integration, treatment and data management is growing in direct relation to the hardware expansion. Three recent major inputs to 2D and 3D seismic interactive interpretation are available on modern workstations:

- integration of well log data to the 2D or 3D projects and interactive programs for well log treatment and inversion.
- integration of 2D regional lines to 3D projects (expanded coherent regional data base).
- seismic reflection data interactive treatment on the workstation helping or forcing the geologist to do more geophysics and vice versa...

In this study we had no 2D regional lines on tape to be integrated on the workstation and similarly no digital well log data to interact directly with the 3D data set.

The seismic interpretation computer data base will more and more be directly interconnected to other programs used for basin analysis or modelling (decompaction, subsidence, fault analysis) and for reservoir modelling via inversion. Most of these programs will slowly be integrated to the ever larger and all-including seismic workstations.

4.4 Conclusions

That three-dimensional seismic data give better results was already demonstrated in 1979 in the paper from Alistair Brown introducing the seismic interpretation basic principles to the geophysical community (Brown, 1979) . Thirteen years later Woody Nestvold illustrates the main tools of 3D seismic interpretation and concludes that «3D seismic has become a cost effective tool for mapping subsurface structures and in many cases, hydrocarbon reservoirs themselves» (Nestvold, 1992) . To our knowledge this research constitutes the first published PhD research on 3D seismic interpretation methods applied to the systematic recognition of sedimentary facies to precise subtle clastic stratigraphic trap morphology and seismic characteristics. An unpublished precursory PhD work using 3D seismic data for the recognition of syn-rift sequences in the North-Sea was realised by Sarah Prosser in 1991 (Prosser, 1993) on a similar CHARISMA™ system (Schlumberger-Geoquest).

Some examples presented in this chapter amongst many hundreds of sedimentary features observed in this study show the amount of detail that can be read from the attribute analysis of 3D seismic data. 3D seismic data analysis is really becoming "four-dimensional" as computers are now able to display simultaneously the 3 co-ordinates of space with an attribute vector (Enachescu, 1992) . From this point of view, it can be considered that 3D seismic data is slowly becoming "five-dimensional" as more and more case-studies include the time factor as an additional dimension to the seismic data analysis (Nur, 1989) . Periodically re-shooting partial or entire 3D surveys enable to follow the evolution of the reservoir through time and provide optimum data for reservoir modelling and improved seismic inversion analysis (Hilterman, 1982 ; Neff, 1993 ; Wehr & Brasher, 1994)

The interpretation of the spatial distribution of amplitudes and other seismic attributes on 3D seismic data is the cornerstone of this research and the list below shows the multiple usage made of it in this study and in other published sources.

Interpretation of 3D seismic attribute can be used to:

- determine horizontal sedimentary facies from seismic facies interpretation (Reymond & Stampfli, 1992a) .
- follow the vertical evolution of sedimentary facies in relation to relative sea level changes (Reymond & Stampfli, 1992b ; Reymond & Stampfli, 1993 ; Reymond & Stampfli, 1994a ; Reymond & Stampfli, 1994b) .
- illustrate the relationship between sedimentation and deformation (Reymond & Stampfli, 1994c ; Reymond & Stampfli, 1994d) .
- describe and interpret subtle deformations (Dalley *et al.*, 1989 ; Enachescu, 1990a) .
- understand fault geometry and associated micro-fracture (Brown *et al.*, 1987)
- realise fine structural reservoir analysis (Dalley *et al.*, 1989 ; Nestvold, 1992)
- indicate distribution, size and continuity of reservoirs (Brown *et al.*, 1982 ; Brown *et al.*, 1984 ; Peterson & Reynish, 1989 ; Reymond & Stampfli,1995) .

- help in lithology estimation (sand/shale ratio) and describe the type and morphology of channel fills and seals.
- map unconformities and paleomorphologies (Stampfli & Höcker, 1989) .
- indicate porous intervals and fluid contacts (Enachescu, 1993) .
- point at gas filled reservoirs and indicate abnormal pressure zones (Reymond & Stampfli under press).
- precise the nature of the reservoir boundaries and thereby understand the origin of the reservoir (Reymond & Stampfli, in press).
- determine the depth of the permafrost in exploration zone and identify shallow gas sands (Berryhill, 1987 ; Mastoris, 1989) .
- study waste sites with high resolution 3D seismic data (Witka & Krummel, 1994)
- locate stable zones for sites of radioactive waste deposits (NAGRA, published report, 1994).

And so on...

The above list of possible application is far from being complete and the amount of geological information contained within a single 3D survey is almost inexhaustible. As ever larger surface of the Earth are rapidly covered with 3D data surveys and that the associated technologies are growing exponentially, the future of both theoretical and practical applications of 3D seismic data is very bright. It would be of great interest both for the hydrocarbon exploration and for the global understanding of the sedimentary processes on passive margins, to apply the same type of study as realised here on as many 3D surveys as possible with the collaboration of oil industries and the many universities starting now to get ever more involved with 3D seismic interpretation techniques.

Nevertheless, the very limited usage of onland 3D seismic reflection data is mainly controlled by its high cost (40'000 to 70'000 $/km^2) that require precise and highly productive objectives. If it can be forecasted that the price of offshore 3D seismic aquisition will decrease much rapider than for onland 3D seismic due to technology improvements (Nestvold, 1992).

5. THREE DIMENSIONAL SEQUENCE STRATIGRAPHY

«If the eye is assisted by lenses then even invisible things are seen to have form: if the mind be the eye then subtle forms are seen: thus the seeing eye and the objects seen are of the same nature»

Ramana Maharshi (1879-1950)

5.1 Introduction

The purpose of this fifth chapter is to show how to identify and map depositional environments on the base of horizontal amplitude maps provided by three dimensional seismic data interpretation on a restricted portion of the northern Gulf of Mexico shelf. Sedimentary facies are direct indicators of the conditions and processes of sedimentation that can be inferred by variation in seismic facies. A systematic observation of superposed seismic facies interpreted in terms of sedimentary features over a period of 17 Ma shows definite periodicity of sequences of deposition. This is observed on several type of geological and geophysical data: from the outcrop scale to the large vertical display of 2D seismic sections or well logs data. Cycles are separated by unconformities, dated by micro or macro faunas and absolute dating methods. Cycles of shorter periods are studied on the base of carbon and oxygen isotopes that provide a high resolution tool to determine short cycles sedimentary patterns related to climatic changes. In the same way, recent development in the observation of the inversion of the Earth magnetic field begins to unveil short and long period cycles.

Concerning the observation of sedimentary facies in the horizontal plane, subsurface observation was limited in offshore regions, to sea floor sampling (bottom grab sampler) and sea floor bathymetry maps via sonar methods. But since the sixties, marked by the birth of seismic reflection methods (deep penetration low resolution and shallow penetration high resolution data) ancient marine geological environments have started to become more visible. Until the early eighties only isolated 2D profiles and high density 2D information grids were acquired to construct contour maps of large sedimentary bodies with a high degree of uncertainty in lateral correlation. Since the middle eighties, numerous studies have been undertaken on several margins to observe recent depositional settings via high resolution shallow seismic (single channel reflections data) and correlate them to eustatic changes over the Pleistocene (Berryhill, 1987 ; Anderson *et al.*, 1990 ; Chiocci, 1994, etc...) . But the penetration depth of these methods is limited to a few hundreds meters with a vertical resolution close to the meter scale.

Through 3D seismic data, and in this study, surfaces bounding or intersecting sedimentary units (systems tracts) are described from the surface layers (observed by high resolution seismic data) down to about the three first kilometres below sea level. The vertical resolution of such data is between 10 and 20 metres and thereby allows to recognise definite sedimentary cyclic successions. There is an important step between the observation of cycles and the understanding of their causes. As mentioned in chapters 2.2 and 2.4, the factors controlling sedimentation are numerous and complex. The cyclic character of sedimentation is mainly related to eustasy, whatever the causes may be for the different scales of sea level changes. This study limits itself to the acknowledgement of periodic events recorded in continental, shallow and deeper marine condition.

More than 20 horizons have been interpreted in detail over the whole survey (225 sq. km) from late Early Miocene (Burdigalian) to the present (fig. 5-1). Hundreds of amplitude maps have been observed and about 80 of them have been interpreted in terms of sedimentary assemblages to qualify the changes in depositional conditions registered through time. Interpretations have been carried out on the base of colour displays on screen or on paper but for economical reasons they are presented here in black in white causing a real loss in legibility.

The high and constant rate of sediment influx and subsidence taking place throughout the Cenozoic on the central northern part of the Gulf of Mexico, allows for optimum preservation of erosions and deposition features on the inner shelf. During Pleistocene time, the main depocentre was located approximately 300 km offshore from the studied area. In the Pliocene, the depocentre was located 200 km to the south-east of the studied area (offshore Mississippi present delta). The Early and Middle Miocene depocentres correspond more or less to the present proximal shelf (fig. 5-2). This lateral shift of depocentres through time imply a corresponding adaptation of marine environments observed in the studied are.

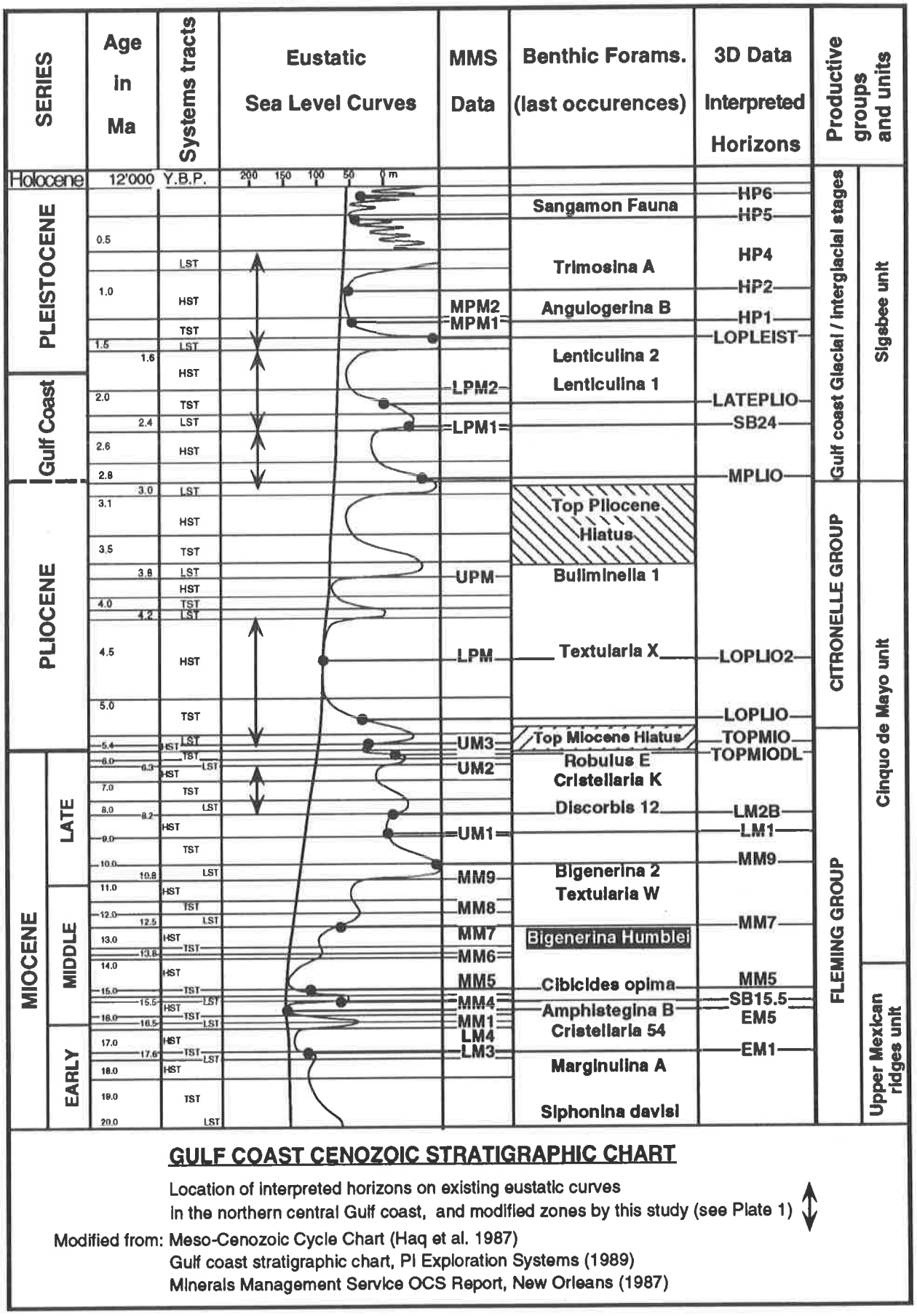

Fig. 5-1: Location of interpreted horizons, on existing eustatic curves and correlation benthic with the foraminifers biochronozones for the Gulf of Mexico.

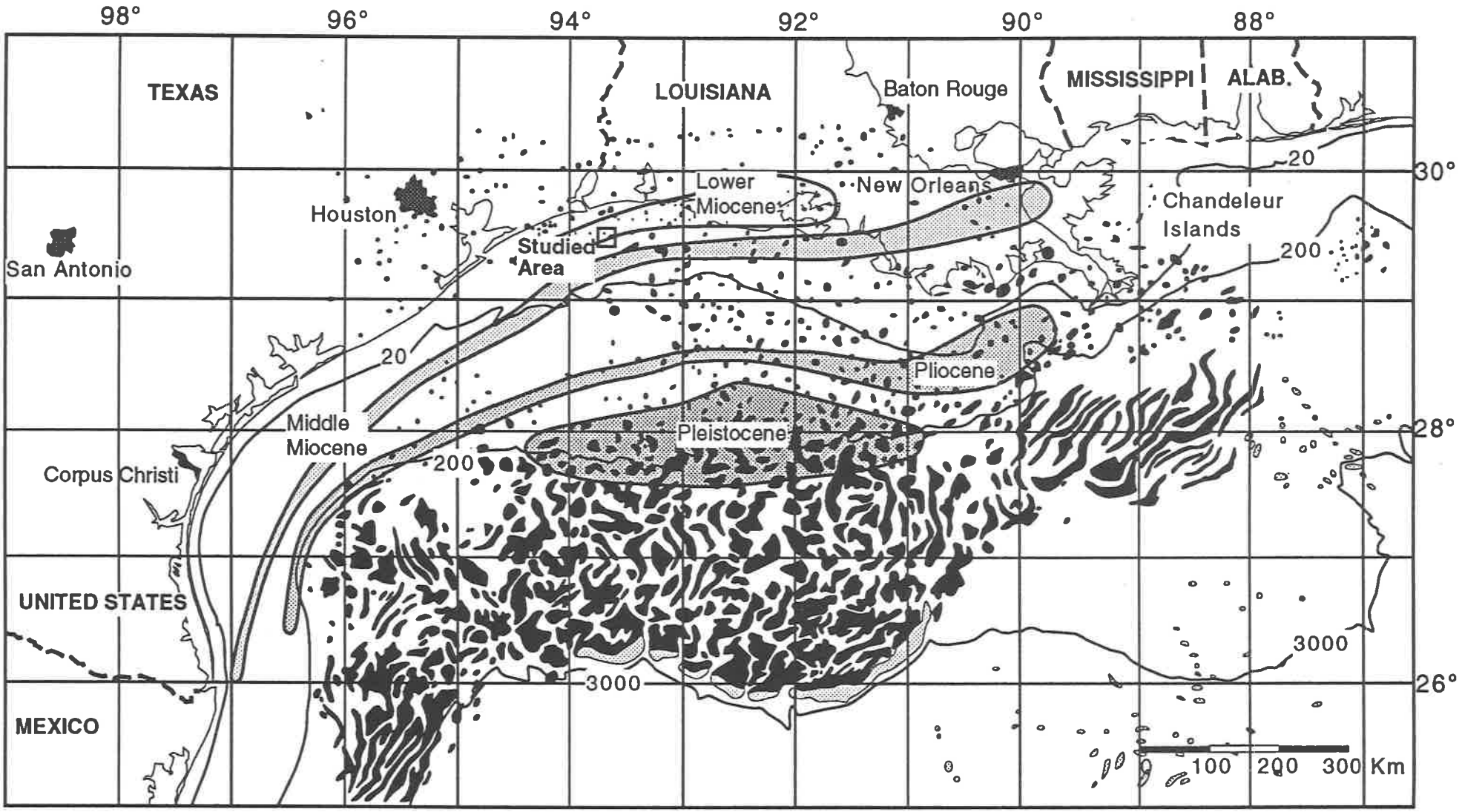

Fig. 5-2: Location of studied area and main depocentres for the studied interval (Early Miocene to present) superposed on main surface and deep lying salt features (modified from Winker 1982 and Worral and Snelson 1989).

Except for two major hiatuses (top Pliocene and top Miocene), the totality of the sedimentary history of this portion of the shelf can be retraced. In the inner shelf deposits, complex reworking of successive erosional events can fuse several unconformities that exist separately further offshore. A way to solve this problem would be to apply the same type of studies on a transect of 3D data sets across the shelf to follow the lateral evolution of unconformities and associated depositional systems on the horizontal plane. For the present research, only one 2D North-South 90 km long transect intersecting the studied area could be obtained from TGS-CALIBRE Geophysical Company with the help of Prof. Bally in Houston. The analysis of this seismic line will be presented in chapter 7 on deformation and salt related features.

This chapter is divided into seven parts discussing the typical sedimentation patterns associated with regionally, and in some cases globally, recognised eustatic events. Figure 5-3 is a zoomed portion of the regional transect with a factor 3 vertical exaggeration presenting the conformable aspect of the succession of sequences boundaries in the inner shelf condition (inner to middle neritic zone down to 2 s).

The studied sediments are shifted down by a succession of down-to-the-basin growth faults and a few minor antithetic faults. Major fans deposition on the platform are related to tectonic activity and will develop on the footwall of the main active faults during phases of progradation.

Figure 5-3 and 5-6 present the time intervals, sequence boundaries and interpreted horizons discussed in each chapter. 5.2 illustrates the eight glacially controlled 4th Order sequences recorded during the upper Pleistocene; 5.3 presents the lower Pleistocene change of 4th order sequences duration from 0.1 to 0.3 Ma; 5.4 illustrates one 4th order sequence marking the Plio-Pleistocene limit (1.65 Ma), 5.5 presents a global 3rd order sequence marking the top Pliocene hiatus, 5.6 discusses the Plio-Pleistocene limit in the Gulf coast sense (2,8 Ma), 5.7 (fig. 5-3) illustrates the Messinian lowstand and finally 5.8 (not shown on fig. 5-3) deals with the Miocene series and the limit of the method (loss of resolution of fine geological objects at about 2.5 s (TWT).

To facilitate the reading of this chapter three plates are provided at the end of the volume. They consist of the necessary vertical regional and local reference cross sections (Plate 1 and 2) and of the comparison of the pre-existing cycle charts with the one proposed by this study (Plate 3). Furthermore, special care has been given to provide conclusions at the end of each sub-chapter to allow a rapid and complete overview of the arguments presented in this research.

5.2 Upper Pleistocene (0 to SB 0.8 Ma)

Introduction

The 800 thousand years before present are characterised in geological time by the presence of 7 to 8 cyclic glacial events. The total thickness for the upper Pleistocene in the studied area reaches 300 m (≈1000 ft). The studied 3D data set has a frequency range around 30 Hz which provides good enough vertical resolution below 300 ms (Twt) for the purpose of 3rd to 4th Order sequences resolution. Above this limit, abundant noise on the seismic record make the recognition of sedimentary features difficult on the base of the horizontal amplitude maps.

High resolution shallow seismic data reaching a depth of 200 to 300 ms in optimum conditions is then the way to fill the missing gap on top of the studied 3D data set. Such high resolution data have been produced offshore Louisiana by Berryhill (1987) in the atlas of Late Quaternary facies and structure of a portion of the northern Gulf of Mexico that includes the area of the present research. This atlas describes the morphology and extension of the three major regressions before the present, registered on the Gulf shelf (Late and Early Wisconsinian and Sangamonian).

Figure 5-4 presents the correlation convention for the Pleistocene (sensus stricto) used in this study between the alpine continental glacial / interglacial stages and the North American stages used for the Gulf coast Pleistocene by most authors working in this area. The first continuous interpretable horizon below sea level on the West Cameron 3D data and on regional cross sections going down the shelf (HP6, SB 0.2 Ma) is assigned to the Early Wisconsinian regressive or cold period that can be correlated to the Riss alpine ice age. The latest Würm regression (Late Wisconsinian lowstand) is not identified on low resolution seismic data but the corresponding erosional unconformity is perfectly visible on high resolution data.

Figure 5-5 is a compiled map modified from Berryhill (1987), Worral and Snelson (1989) and this study that shows the structure and sedimentary facies for the Early Wisconsinian regression (Riss ice age). All main identified active faults and diapiric uplifts are indicated, as well as the Late Wisconsinian deltaic

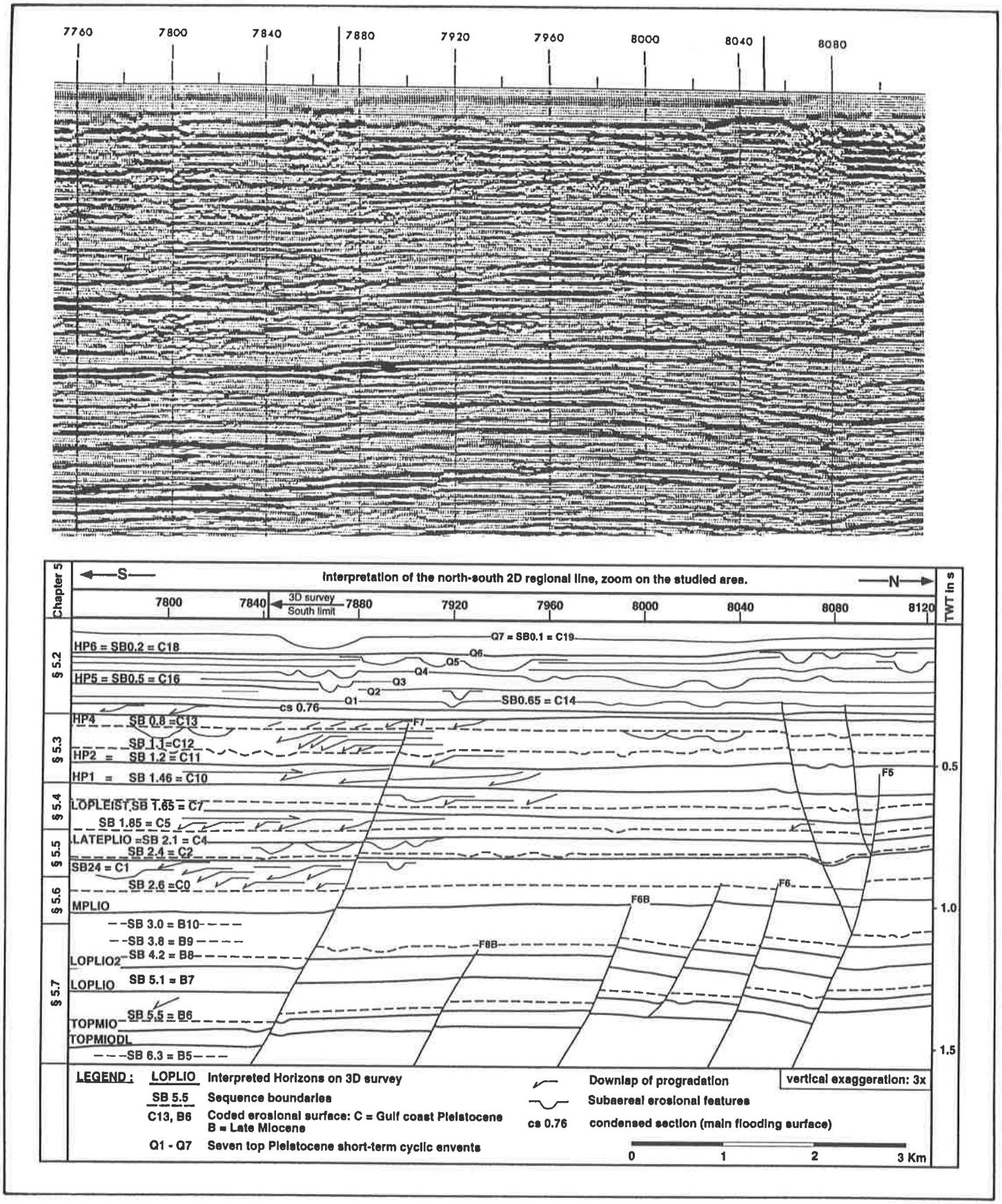

Fig. 5-3: ***a.*** *Zoomed portion of TGS-CALIBRE north-south transect across the studied area.*
b. *Interpretation of sequence boundaries in correlation with the 3D interpreted horizons. For discussion of each indicated intervals, see corresponding chapters (left margin of this figure).*

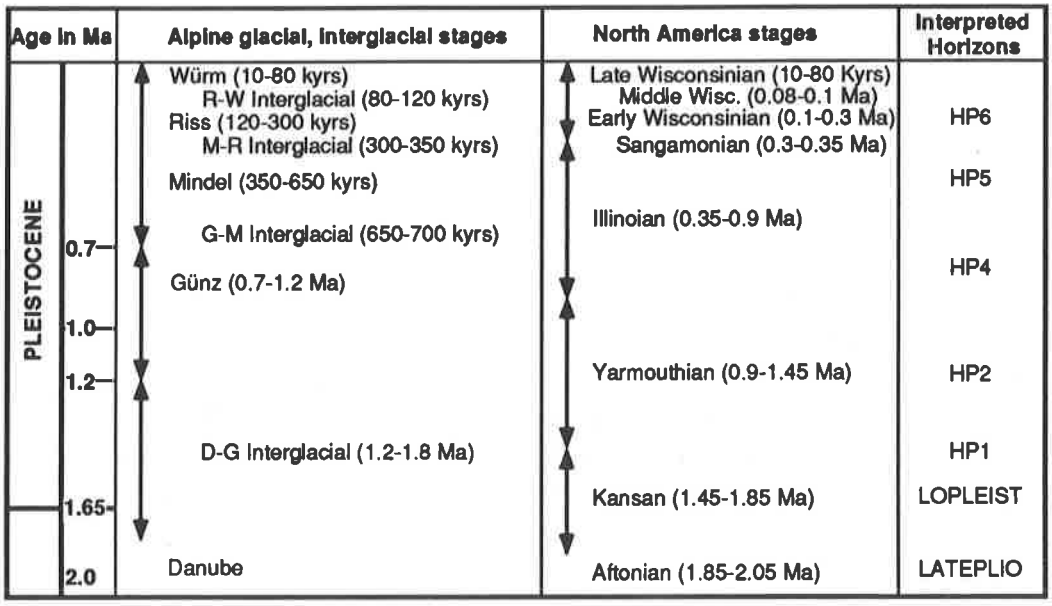

Fig. 5-4: Correlation table of the Pleistocene Alpine glacial/interglacial stages with equivalent names for the Gulf Coast and location of interpreted horizons.

deposits (Würm). The line of maximum late Wisconsinian transgression is represented by the dashed line and coastal onlap arrows. It is interesting to note that the curve adopted by the maximum of transgression has a shape influenced by sea floor topography locally affected by active diapiric uplifts (see arrows on fig. 5-5); similar features will be discussed on the base of several amplitudes maps encountered in the following chapters (5.6 and 5.8). This reconstruction of sedimentary facies has been realised by integrating high density 2D high resolution seismic data (line spacing 2 to 10 km). Such a large grid cannot prevent "aliasing" and eventual wrong correlation of channels or sand bodies from one line to the next. 3D data enables the interpreter to cut in any direction and any place through a cube of seismic data which limits the aliasing problem.

There is no data recorded or sedimentary features observed by Berryhill (1987) in the studied area for the level of the Early Wisconsinian lowstand that corresponds to the first interpreted horizon of the 3D data (HP6) thus preventing any comparison. Nevertheless, the map on figure 5-5 gives an idea of what facies reconstruction from seismic data looks like on the horizontal plane and also approximately indicates the size of the sedimentary features that can develop and be identified on the shelf during periods of major lowstands. This study proposes reconstruction of the same type on the limited surface of the studied area but with a higher resolution and on a larger time interval (from Early Wisconsinian to Early Miocene). The next step would be to obtain similar 3D amplitude maps over wider and continuous portions of continental shelves and on the same extended period in order to reconstruct maps similar to the one produced by Berryhill (1987) for the entire Neogene and Pleistocene. This might soon become possible as progressively larger portions of continental shelves get covered with 3D data. Only the interpretation remains to be done if the data becomes available ...

NB: At this stage, the reader might prefer to take out Plates 1 to 3 to which numerous references will be made in the development of the coming chapters.

Figure 5-6 (see also on Plate 3) is the reference chronostratigraphic chart used for further discussion of the Plio-Pleistocene interval. The Gulf coast Pleistocene succession of sedimentary facies is discussed in the four chapters below (5.2 to 5.5). When extending the inquiry out of the range of high resolution seismic data (2 or 3 cycles before the present), Late Pleistocene climatic changes and their influences on sedimentation are very well studied but still, no general agreement has been reached on precise dates of major Pleistocene regressions. Wornardt and Vail (1991) presented a revision of the Plio-Pleistocene cycles in the Gulf of Mexico and definitely confirm the eight 4th Order sequences registered between 0.8 Ma and present time (see fig. 1-10 and 5-1). On the studied seismic data, they are represented by eight hummocky noisy loops starting just below sea level down to the HP4 interpreted horizon (fig. 5-7 and fig. 5-22, Plate 2). The HP4 level corresponds to the first major regression above "Trimosina A" benthic

Fig. 5-5: Early and Late Wisconsinian erosional streams and deltaic systems and line of maximum of Late Wisc. transgression superposed on salt and fault related morphology of the offshore Louisiana portion of the Gulf coast shelf. True scale studied area is indicated.

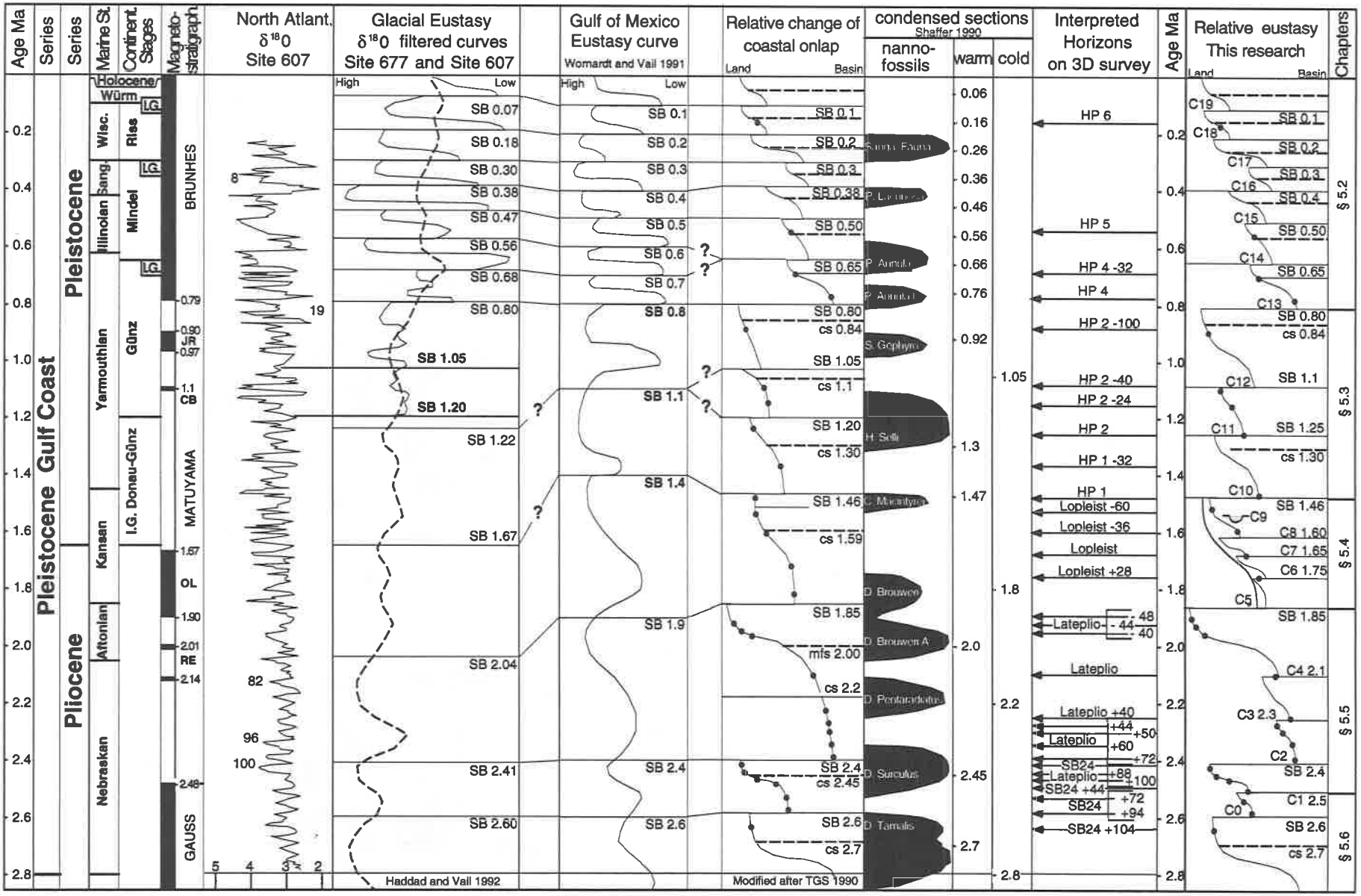

Fig. 5-6: Synthetic Pleistocene chart with series and continental stages, oxygen isotopes reference curve, eustatic and coastal onlap curves in the Gulf of Mexico, histogram of faunal abundance and presented amplitude maps(black dots). Note the four chapters: ***a.*** *§5.2 Upper Pleistocene 4th Order sequences discussion;* ***b.*** *§5.3 Lower Pleistocene, one or two 3rd Order sequence;* ***c.*** *§5.4 Plio-Pleistocene limit;* ***d.*** *§5.5 One large 3rd Order sequence.*

foraminifer first occurrence and is associated with the 0.8 Ma sequence boundary (fig. 5-1). Above HP5 horizon (≈ 300 ms, fig.5-7), major superposed erosional features can be recognised on vertical sections but the signal/noise ratio is too bad to identify them on amplitude maps.

Observation

(NB: In the following, sequence boundaries are age coded (SB 0.8) for conventional purposes but it does not mean that the absolute age of these events is correct. When true age is meant, the figures will be followed by the abbreviation "Ma" used for million years).

On the curve of coastal onlap proposed by TGS™ (1990), the interval between SB 0.5 and SB 0.8 is divided into two sequences where Wornardt and Vail (1991) place three sequences of 0.1 Ma each (fig. 5-6). This problem will be approached here from the angle of 2D seismic sections, well logs and amplitude maps obtained from 3D seismic data interpretation. The succession of sedimentary events is discussed from the oldest to the youngest.

On the vertical seismic section (Inline 539, fig. 5-7, Plate 2) the HP4 horizon is interpreted above the clear erosive unconformity assigned to the major sequence boundary at 0.8 Ma (SB 0.8). This surface is sealed in the proximal portion of Inline 539 by downlaps that prograde on the sequence boundary. Off the progradation front marked by the end of the strong amplitude foresets is a more transparent zone with "shingled" reflectors inclined both landward and basinward that could indicate transgressive erosion. On top of the foresets in the landward portion of Inline 539, two pyramidal sedimentary features are interpreted as transgressive reworked sand bars correlated to the incision registered down dip (t1 and t2; fig. 5-7). This type of juxtaposition of incision and deposition seismic facies is typical for landward reworking of sand bodies occurring during transgressive phases on the inner shelf (Saxena, 1990 ; Pattison & Walker, 1992) . This configuration is sealed by a strong amplitude reflector showing numerous deep channels; this surface is interpreted as SB 0.65. The same lateral arrangement in seismic facies is repeated just below HP5 horizon interpreted as SB 0.5.

Amongst the six wells available in this study only two of them have a gamma ray curve for the upper Pleistocene. In the absence of faunal calibration, sequential analysis based on gamma ray curves only is very tricky in the inner neritic zone (Vail & Wornardt, 1990) . On figure 5-8, the HP4 interpreted reflector corresponds to the transition from the underlying shale to the thick incised valley sands marking a sequence boundary (SB 0.8, Well 4). The curve on Well 4 above HP4 indicates a massive succession of sands that can be interpreted both as a succession of incised valley fills or as an alternation of incised valleys and highstand prograding sands. Objective interpretation of sequence boundaries in such a succession on the base of well log data only would be very difficult. On Well 3, SB 0.5 is located below the HP5 interpreted horizon at the base of the next thinning upwards sand package interpreted as a transgressive interval (fig. 3-3 b). The correlation of SB 0.5 on Well 4 is very hypothetical and mainly based on the positioning of the HP5 horizon on Well 4. Well log data is not sufficient in order to say if one or two sequence boundaries are present between SB 0.8 and SB 0.5. On Well 4, three backstepping thinning up series can be identified. These three transgressive phases can be assimilated to the three 0.1 Ma parasequences described by Wornardt and Vail (1991).

On the amplitude map obtained along HP4 (representing the horizontal facies morphology above SB 0.8), the lateral extension of the lowstand erosive channels (q amd m on fig. 5-7) intersected by Inline 539 can be visualised on figure 5-9 a and b. In the centre and upper left corner of the image, a NE-SW progradational fan can be traced indicating a NW-SE direction of local sedimentary influx. It corresponds to the base of the highstand progradational sands sedimented on the erosive surface (landward portion of Inline 539, fig. 5-7). This first map draws a perfect picture of the post maximum lowstand situation associated with SB 0.8 that shows the condensed transgressive and highstand sands filling the deep erosional topography and building low angle progradation, parallel to the shoreline.

To observe the changes in seismic facies occurring above SB 0.8 and to try to intersect the next sequence boundary, an amplitude map is calculated parallel to HP4, 32 ms above it (approximately 30 m higher in the sediments, fig 5-10; see fig. 5-7 on Plate 2 HP4-32, for location on seismic line). Three distinct sedimentary features appear on that map: North-south trending erosive channels, NE-SW foresets intersections and an oblique sand body in the central right portion of the image. The three of them are intersected by Inline 539 and can be correlated from the vertical section to the amplitude map. Along Inline 539 and from the proximal to the distal (fig. 5-7), the HP4 -32 horizon intersects very clear shingled

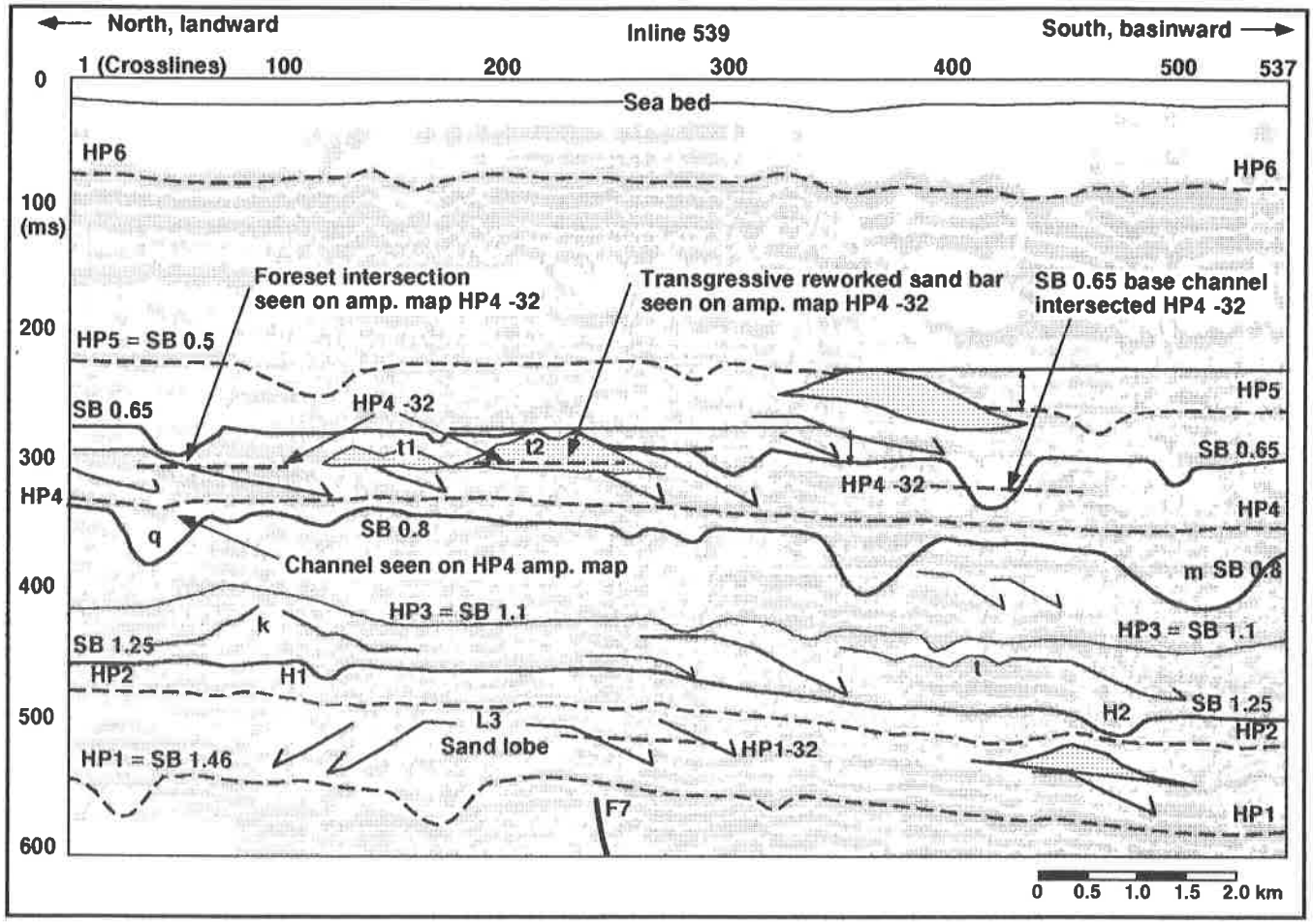

Fig. 5-7: North-south vertical seismic section (Inline 539, see fig. 5-5 for location) showing facies and sequence stratigraphic interpretation superposed on seismic data for the Upper Pleistocene.

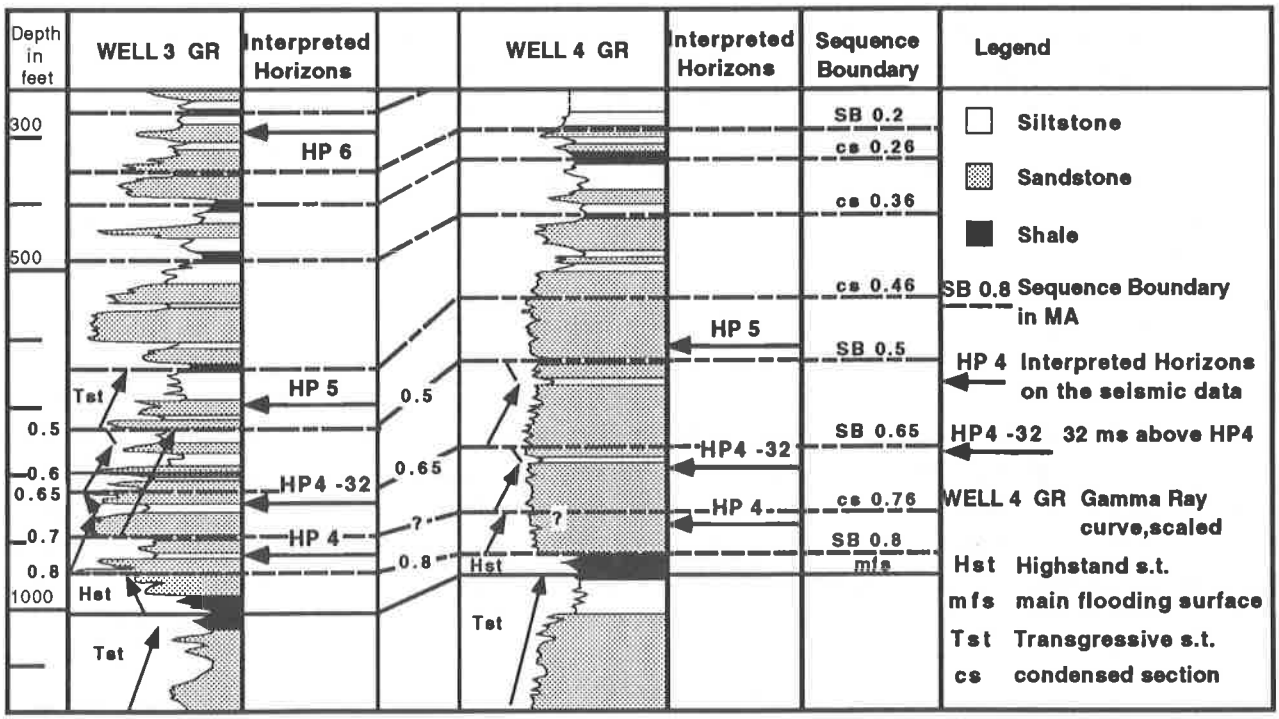

Fig. 5-8: Upper Pleistocene sequential analysis on well log (gamma ray curves on Wells 3 and 4 see fig 5-9 for location). Two alternatives: SB 0.5, 0.6, 0.7 and 0.8 proposed by Vail and Wornardt (1991) interpreted on Well 3 and SB 0.5, 0.65 and 0.8 this study, Wells 3 and 4.

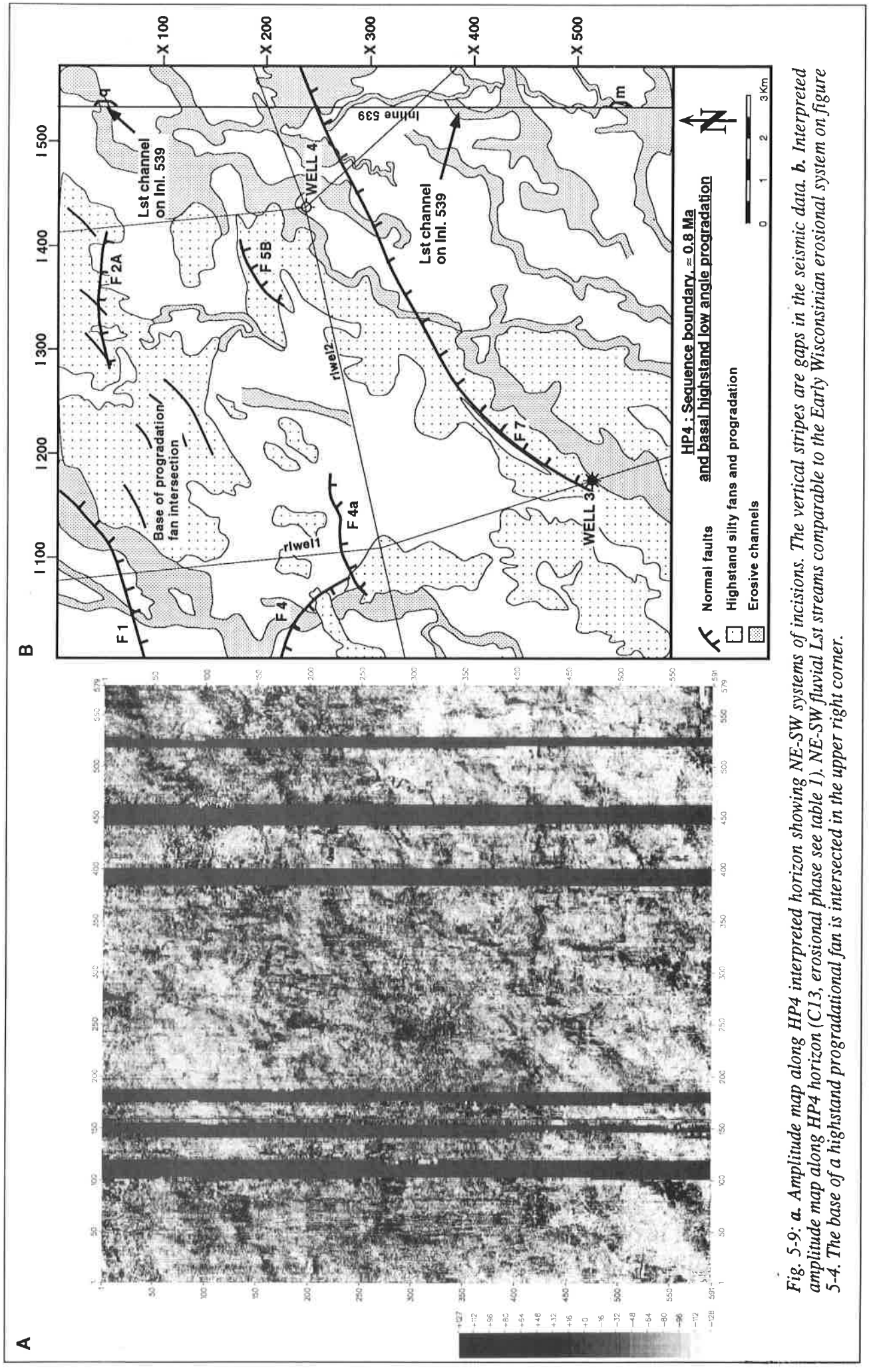

*Fig. 5-9: **a.** Amplitude map along HP4 interpreted horizon showing NE-SW systems of incisions. The vertical stripes are gaps in the seismic data. **b.** Interpreted amplitude map along HP4 horizon (C13, erosional phase see table 1). NE-SW fluvial Lst streams comparable to the Early Wisconsinian erosional system on figure 5-4. The base of a highstand progradational fan is intersected in the upper right corner.*

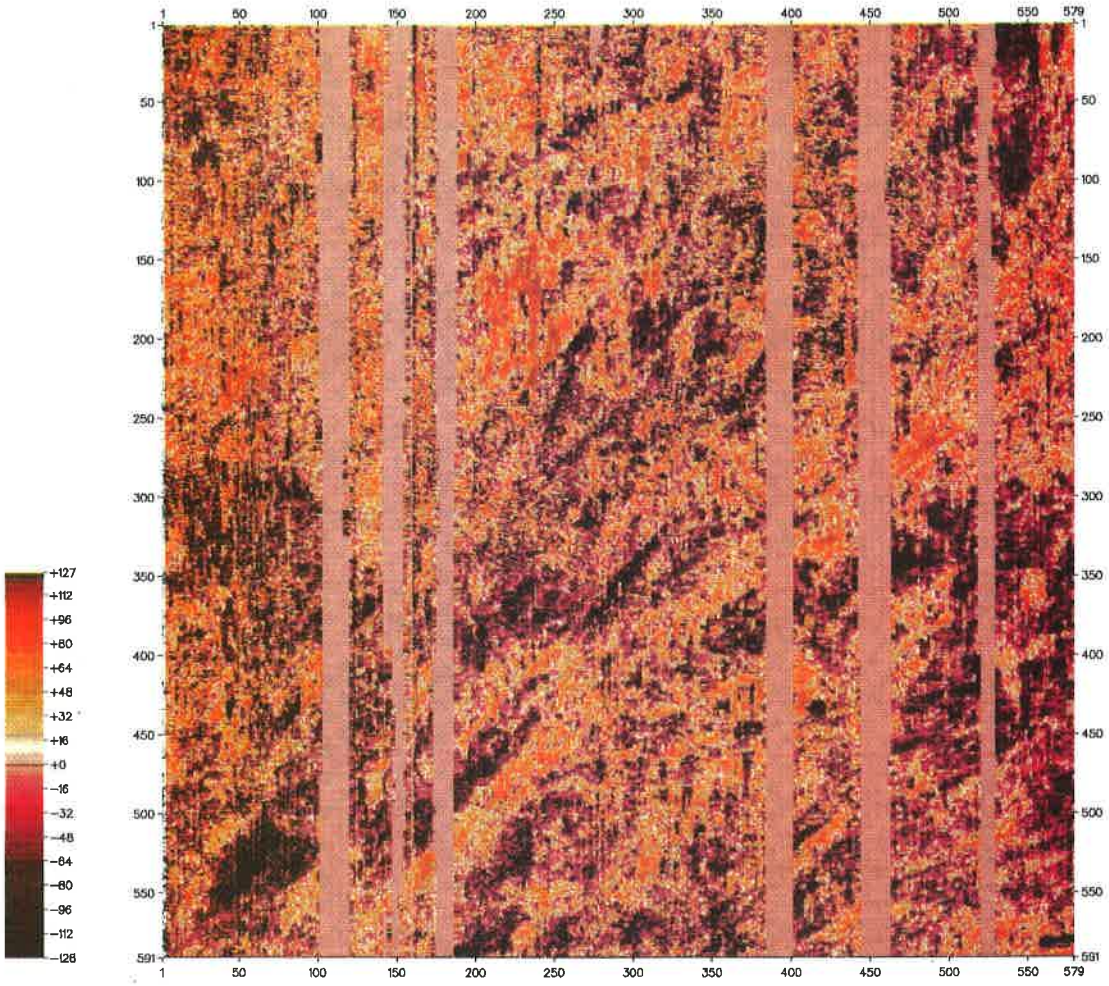

Fig. 5-10: Colour amplitude map obtained 32 ms above HP4 horizon. Positive (hard) loops are in orange and the negatives (soft) in violet. Vertical stripes are gaps in seismic data in the upper half second.

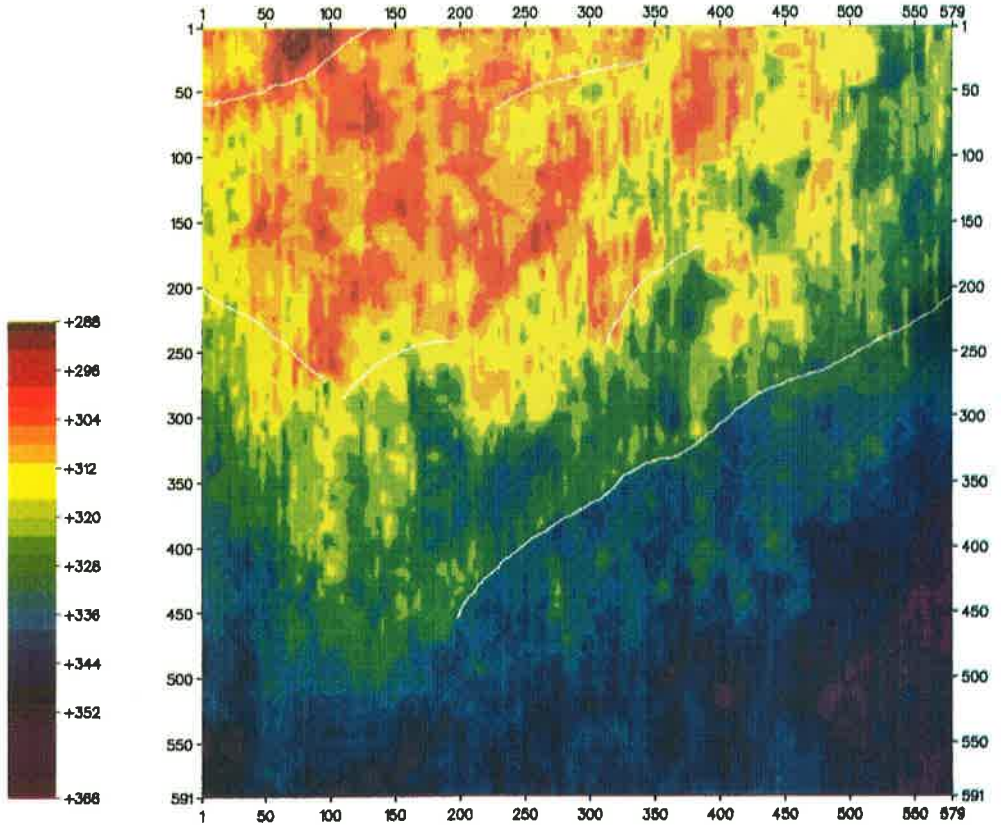

Fig. 5-12: Time structure map of HP4 interpreted horizon. Reds are high and blues are deep. Faults traces are indicated in white. Subjacent fan delta lobe with digit like features appears as a topographical high.

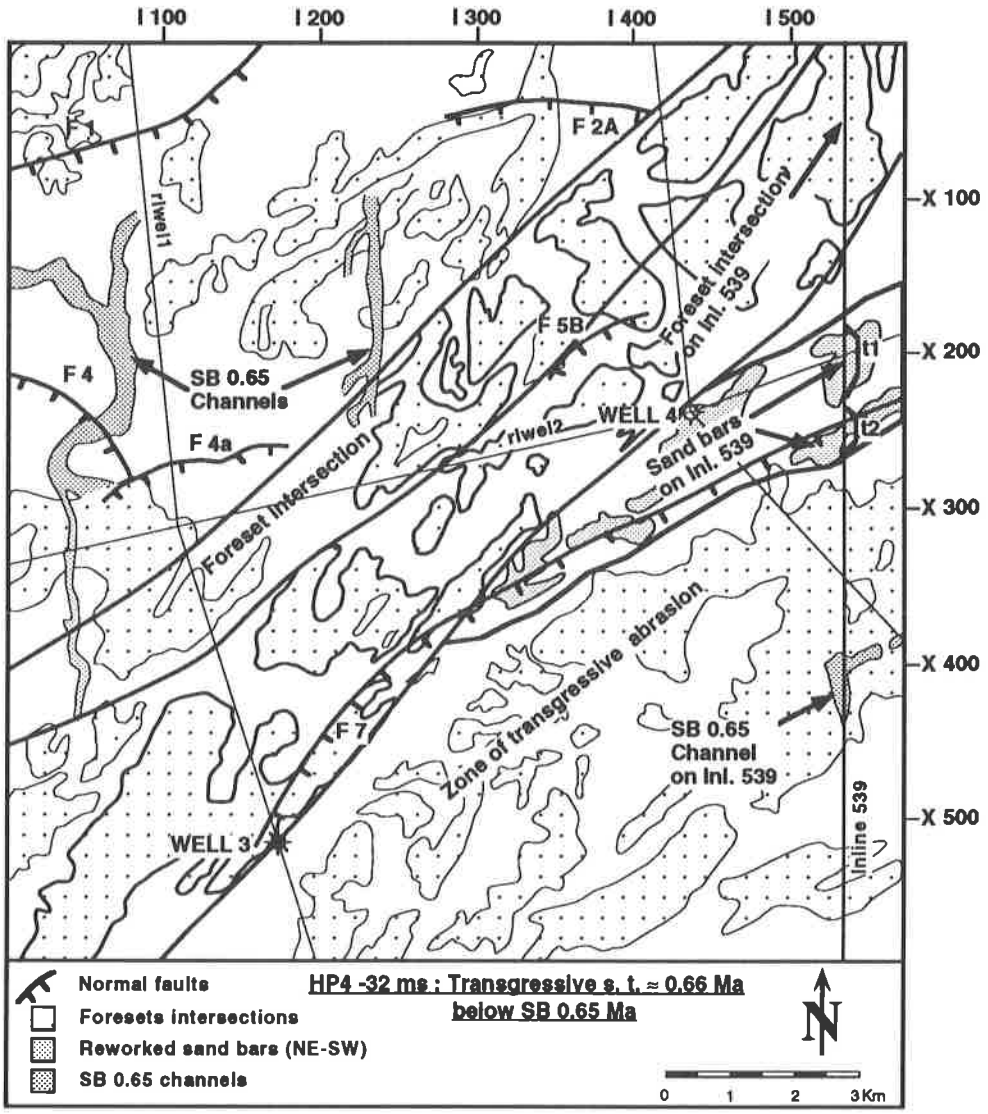

Fig. 5-11: Interpretation of fig.5-10. NE-SW amplitude anomalies are foresets intersections. The oblique high amplitude sand body (centre right) is assimilated to a reworked sand bar. NNW-SSE channels associated with SB 0.65 above cut through this level (C14, see table 1).

foresets corresponding to the prograding front of a large fan. Between Crosslines 150 and 240 both on fig. 5-7 and 5-10, the oblique sand body visible on the amplitude map is correlated on the vertical seismic section to the pyramidal sand bars (t1 and t2). They are interpreted as reworked transgressive sand bodies. Further offshore on the amplitude map, the contrast in amplitude decreases and the vertical section shows a more transparent seismic facies. This zone extending on the entire footwall of the F7 main growth fault can be interpreted as the base level of transgressive incision (abrasion) at the origin of the adjacent reworked sand bar. And on top of that the HP4-32 amplitude map is intersected in several places by north-south trending channels attributed to the base of the overlying SB 0.65 sequence boundary erosional level corresponding to the next major sea level fall registered above the SB 0.8 Ma. Above the SB 0.5 Ma sequence boundary the high proportion of seismic noise makes geological interpretation almost impossible. At this point, the limit of the method is reached and no coherent horizontal seismic facies can be interpreted in terms of sedimentary objects in the upper 200 ms of the 3D data set.

Conclusion

The interval between SB 0.8 and SB 0.5 sequence boundaries shows the superposition of two similar sequences of 4 events: (1) an erosional basal unconformity filled by (2) transgressive thinning up sands on which (3) highstand sands start to prograde. The offshore portion of the low angle progradational front lobe can be partially abraded and reworked up hill to form (4) elongated pyramidal sand bodies during

phases of still stands at the end of the phase of relative sea level rise. This juxtaposition of Tst and Hst facies will then be locally eroded by the next erosional base level (1). The origin and distribution of elongated sand bodies reworked during relative transgressive and highstand periods have been described by many authors as they represent new type of subtle stratigraphic traps (Anderson *et al.*, 1990; Saxena, 1990; Pattison & Walker, 1992; Reymond & Stampfli, 1994a).

The reworking of inner shelf low angle prograding sands or distributary mouth bars and associated deltaic lobes near the shelf break into well sorted elongated sand bodies can be beautifully and precisely illustrated by 3D horizontal facies reconstruction and are generally missed on vertical profiles due to their limited thickness and width. Incised shorefaces are backstepping according to pulses in sea level rise and might form these long straight and narrow sand bodies that are good indicators of the approximate paleoshoreline orientation. The depth of late transgressive incision (≈ 10-15 m.) can be measured on vertical sections offshore from the sand bars (indicated by vertical arrows on fig 5-7), below SB 0.65 and SB 0.5. On the base of the present observation showing the presence of two sand bars, two phases of partially reworked low angle progradations and only one major unconformity between HP4 and HP5, it is likely that only one major sequence boundary (SB 0.65) is recorded between the two main sequence boundaries (SB 0.8 and SB 0.5) at the base of the Upper Pleistocene in the studied area. Nevertheless, it is probable that 8 global eustatic cycles connected to the eccentricity period of the earth orbit of 96 kyrs observed by Milankovitch (1941, fig 2-10) are present over the 800 kyrs before the present but can locally be eroded or not recorded. The eventual additional sequence boundary could be located between the HP5 horizon and the very clear SB 0.65 erosive surface (fig. 5-7, Plate 2). Local (mini-basin, salt related) and more global (Gulf coast shelf, basin scale) changes in subsidence rates are important factors able to mask locally short duration and relatively low amplitude eustatic cycles.

On the pre-existing local eustatic curves valid for the Gulf of Mexico, a change in sequence duration is recorded at the regional well marked 0.8 Ma sequence boundary. The origin and the validity of this limit are described in the next chapter.

An additional tool

The time structure map of interpreted horizons can be an additional tool to define sediment packages morphology. Figure 5-12 is the filtered (smoothed) time structure map of HP4 horizon. There is a difference of about 80 ms (80 m) between the highest and the deepest portion of the HP4 interpreted level. In the upper left corner, the morphology of a distributary birds foot delta is observed. It covers a surface of approximately 6 by 6 km which makes it similar to one of the present Mississippi distributary lobe. Five sub-lobes spread out in radiating directions and a crevasse channel can be seen on the central lobe. The front of the delta lobe is marked by 2 elongated high (red) NE-SW trending bars. This lobe could eventually be the Upper Pleistocene extension of the Sabine river (Sabine Lake and the Sabine river are situated just to the north of the studied area). The cause of such an organised topographical high along a sequence boundary can be found either in the presence of a delta lobe on top of it affecting the position of the interpreted line by a pull-up artefact or in the presence of a thick delta lobe below HP4 whose surface drapes the subjacent delta. A delta lobe below an interpreted horizon would equally affect its position by differential compaction. The morphology seen on HP4 could also be the sum of three components (Pull up, topography, differential compaction).

On a seismic section taken across the lobe in the down dip direction, two lobes are indicated above and below HP4 by visible progradations and a transparent seismic facies. The outer most portion of the wide spread fan above HP4 is intersected by Inline 539 (fig. 5-7) and is approximately 25 m thick. It is associated with the highstand progradation on top of the HP4 interpreted horizon. The lobe below HP4 is thicker and extends further south and will be discussed in the next chapter. The deltaic morphology unveiled by HP4 time structure map is therefore mainly influenced by the thick underlying delta lobe. The lobe below the HP4 horizon was deposited down the main active growth fault (F1) possibly during a period of relative low sea level. A slight difference in topography on the emerging shelf accommodated by the differential compaction induced fault movement enables progradation on the down thrown side of the growth fault. The outer parts of the delta lobe are shifted down by post-deposition down-to-the-basin secondary growth faults.

The next example discusses a similar problem on the interval below, between the HP1 and HP4 interpreted horizons.

5.3 Lower Pleistocene (SB 0.8 to SB 1.46 Ma)

Introduction

This interval corresponds to the Yarmouthian American marine stage and to the base of the Emilian and Calabrian European stages (fig. 5-6). Different sources in the Gulf Coast recent literature present contradictory interpretations for this time interval. The table below lists the chronology of 4th Order sequence boundaries and warm condensed section intervals observed between 0.8 and 1.45 Ma taken from three recent published sources as well as the solution adopted by this study.

Vail&Wornardt 1991		Wornardt&Vail 1991		TGS™1990		Horizons	This study	
SB	cs	SB	cs	SB	cs		SB	cs
0.8	-	0.8	-	0.8	-	HP4	0.8	-
-	0.92	-	0.92	-	0.95		-	0.95
-	-	1.1	-	1.1	1.15		1.1	1.15
1.3	-	-	-	1.25	-	HP2	1.25	-
-	1.37	-	1.3		1.3		-	1.3
1.4	-	1.4	-	1.46		HP1	1.46	-

The first two columns are data found in the same volume of the Transactions - Gulf coast associations of geological societies (Vol. XLI). In the first publication, only one sequence boundary (SB 1.3) is placed between SB 1.4 and SB 0.8 (see fig. 1-8, Vail & Wornardt, 1991) . The same authors published a different version of the same figure in the same book and indicate a single sequence boundary placed at 1.1 Ma (Wornardt & Vail, 1991; fig. 5-13). A third reference curve used by most Gulf coast exploration geologists (TGS™, 1990) proposes two 4th order sequences boundaries in that interval. The first one (SB 1.1) matches the SB 1.1 from Wornardt & Vail (1991) and the second (SB 1.25) can be seen as an equivalent of SB 1.3 from Vail & Wornardt, (1991). Is there two or three 4th order sequences registered in the northern central Gulf coast during that time interval ?

Observation

The SB 0.8 to SB 1.46 interval is shown on two north-south seismic lines (figs. 5-7 and 5-14, Plate 2). The second one (Inline 42) is displayed with a vertical exaggeration of 10 and the data is flattened along the HP4 horizon (on top of fig.5-14) to restore the paleomorphology of the underlying sediments. The HP1 horizon can be interpreted as a sequence boundary on the base of the clear unconformity present just below it on any vertical seismic section in the 3D survey. The HP1 surface shows 30 to 40 meters deep erosive channels sealed by obvious downlaps. The morphology of this erosive system developed during the 1.46 Ma fall of sea level is beautifully illustrated on the amplitude map of figure 5-16 (a and b) presenting both the raw data (seismic horizontal facies) and the interpretation in terms of sedimentary features. Similarly to the preceding chapter, sedimentary objects and faults are consistently labelled on amplitude maps and on vertical sections to bridge the vertical seismic facies to the horizontal amplitude information.

Many unsuspected features on vertical sections like subtle secondary channels or fan conformable splays are unveiled by horizontal amplitude maps. For instance, the broad and thin fan lobe (C9) developed down the F7 growth fault along the HP1 level corresponding to the beginning of relative sea level fall would be impossible to detect on Inline 539 (fig. 5.7) for lack of definite prograding foresets or shingles. But it clearly appears on figure 5-16 due to organised subtle lateral changes in amplitude. This fan accumulates thin layers of silt and sands in the depression created by the active growth fault at the beginning of the lowstand period. These sands can later on be partially removed and transported further offshore if the relative sea level keeps on falling. Another example of the resolution provided by horizontal amplitude maps is the possibility to distinguish between two superposed generations of channels apparently associated to one single erosional phase on the basis of 2D lines (fig. 5-16 a and b, C10 and C10 b). In the upper left corner is a large, NE-SW trending, straight channel (F, on Inline 42, C10). It is marked channels related to the silty fan splay down the F7 fault. The NE-SW channels (C10 b) correspond to the by a strong negative amplitude (black) and are deeper than the other more sinuous and fine E-W oriented

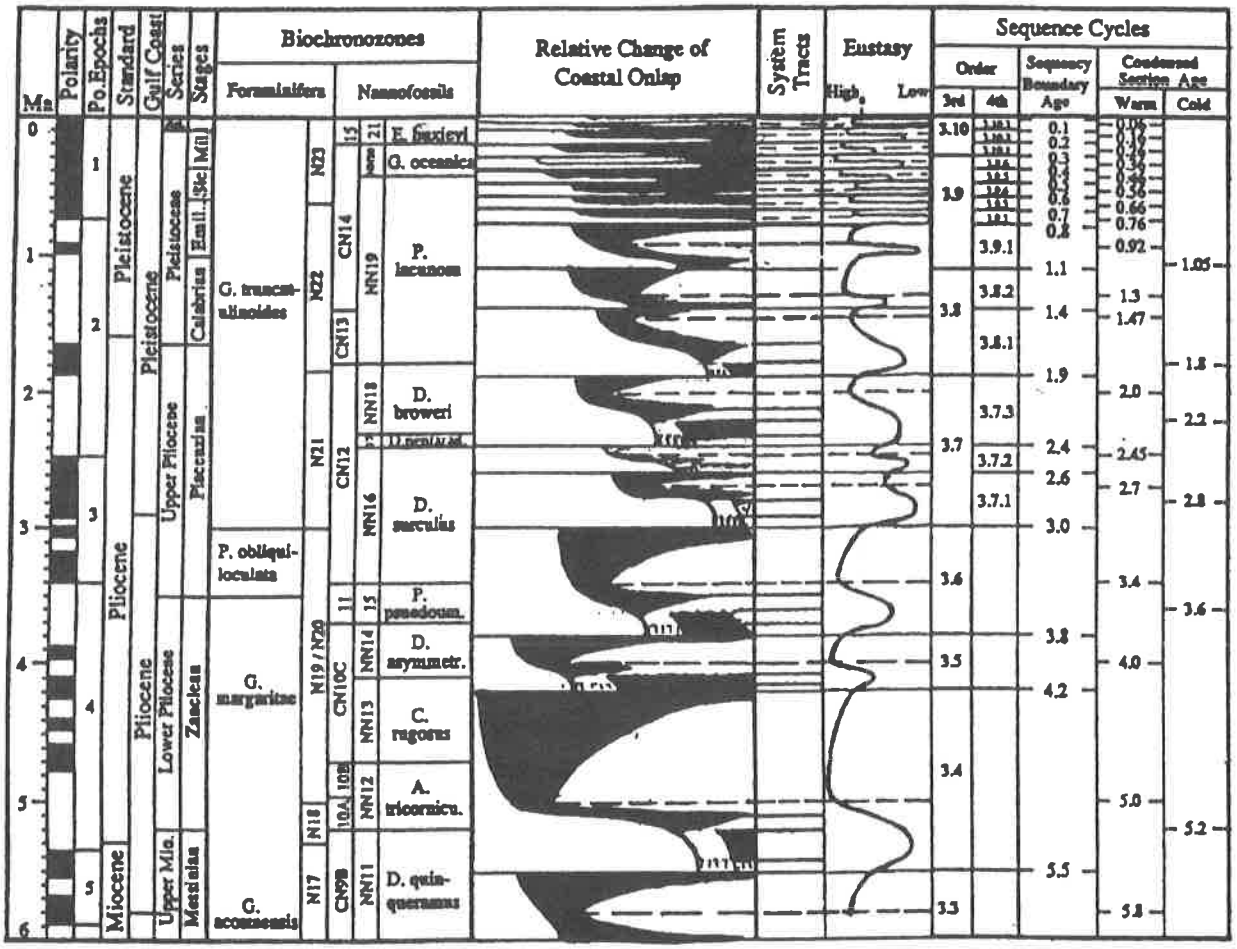

Fig. 5-13: Mio-Pleistocene sequence chronostratigraphic chart for the Gulf of Mexico. (from Wornardt and Vail, 1991).

main lowstand erosive event showing a greater depth of incision subsequent to the E-W shallower channels (C10) which developed towards the end of the highstand period when the relative sea level started to drop.

To observe the spatial arrangement of the large and low angle foresets and wide sand lobes downlapping on HP1, an amplitude map is calculated 32 ms above the HP1 horizon. This map (fig. 5-17 a and b) shows two main sand lobes: Lobe 1, in the upper left corner indicates a NW-SE direction of deposition and the horizontal intersection traces of the foresets with Inline 42 are indicated on figure 5-14 (d and e). A second lobe, subdivided in three secondary lobes (lobes 2,3 and 4) on the amplitude map shows a slight difference in orientation from lobe 1. These lobes have approximately the same size as the one observed along HP4-32 horizon and must have a fan width of about 10 km. Inline 539 (fig. 5-7) intersects the proximal lobe 3 and the more distal foresets offshore of the main fault F7. The oblique intersection of lobe 3 on the vertical section presents clear landward and basinward oriented foresets.

The location of the HP1 horizon on the well log data correlated through synthetic log (fig. 5-15, HP1) corresponds to the abrupt change in lithology from shale to thick sands creating a good contrast in acoustic impedance at the origin of the continuous HP1 reflector. The sands above HP1 do not show any typical features of incised valley fill or progradation on logs. A randomline running through Well 3 and 4 is generated to look at the corresponding vertical seismic facies (HP34, fig. 5-22 and fig. 5-16b for location). The overall vertical seismic facies between HP1 and HP2 has a chaotic low amplitude signal typical for thick homogeneous silt and sand signature. This line indicates that Well 3 intersects a channel between the HP1 and HP2 horizons but that for the same interval on Well 4, the sands are most likely thin and conformable. The succession of fan lobe like sand bodies intersected by the HP1-32 ms amplitude map (fig.5-17) and illustrated by a typical sand facies on logs are interpreted as transgressive backstepping sands followed by low angle highstand progradation on the interval between SB 1.46 and SB 1.25. The 1.46 Ma sequence boundary is placed below the incised valley sands on Well 3 and on top of the highstand progradation on Well 4. No progradation is observed on this randomline which is normal to the direction of main sediment input.

HP2 interpreted horizon: a minor sequence boundary (SB 1.25) or a condensed section between SB 1.46 and SB 1.1 ?

On top of the sandy interval sedimented above HP1 (SB 1.46) is a negative continuous loop interpreted as HP2 horizon. This reflector corresponds to the contrast in lithology between sands and the shale on top (HP2, fig. 5-15). This surface contains a few shallow and narrow channels seen both on the amplitude map (fig. 5-18) and the vertical sections (fig. 5-7, H1 and H2 channels). In the absence of faunal data but based on the sequential interpretation on logs of the SB 0.8 Ma above and the SB 1.46 Ma below HP2, this surface of erosion can be assigned to the SB 1.3 proposed by Vail and Wornardt (1991) equivalent to the SB 1.25 of the TGS™(1990) curve. Clear examples of incision at the level of HP2 are seen on figure 5-22 g (hp34 oblique random line) to the north-west of Well 4. The lateral extension and orientation of this channel are indicated on HP2 amplitude map (fig. 5-18 g). The general direction of erosion along HP2 is north-south but in the upper left corner of the image, two parallel narrow ENE-WSW trending channels are observed and must be related to a different erosional event.

On Inline 42 section (fig. 5-14, 1 and 3), these two deep erosional features (50 to 60 m) are identified as the base of the overlaying erosive level (SB 1.1) reaching down and intersecting HP2 horizon. Therefore they do not primarily belong to the HP2 paleomorphology but are the indication of the superposition of 2 distinct successive sequence boundaries along one single level. Progradation downlaps are rarely observed on HP2 and the well log response along this surface (fig.5-15) indicates a silty and shaly interval reposing on top of the thinning up sands mentioned above. The HP2 horizon is attributed to the SB 1.25 sequence boundary locally interpreted below erosional channels and laterally at the base of the thinning upward transgressive sands.

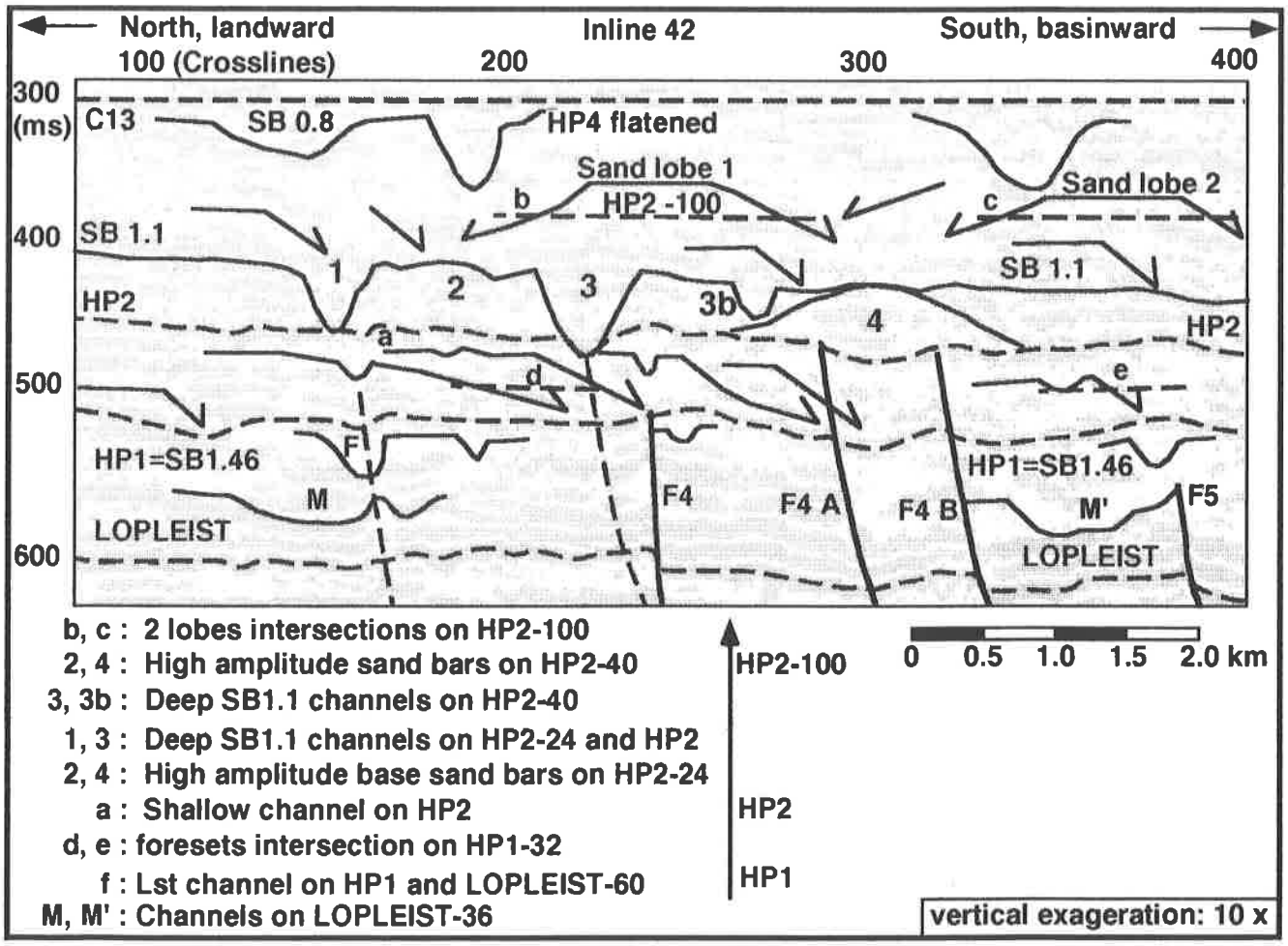

Fig. 5-14: North-south seismic section in the western part of the 3D survey (Inline 42). Interpreted horizons are dashed lines. HP4 horizon is flattened to restore the subjacent sediment morphology.

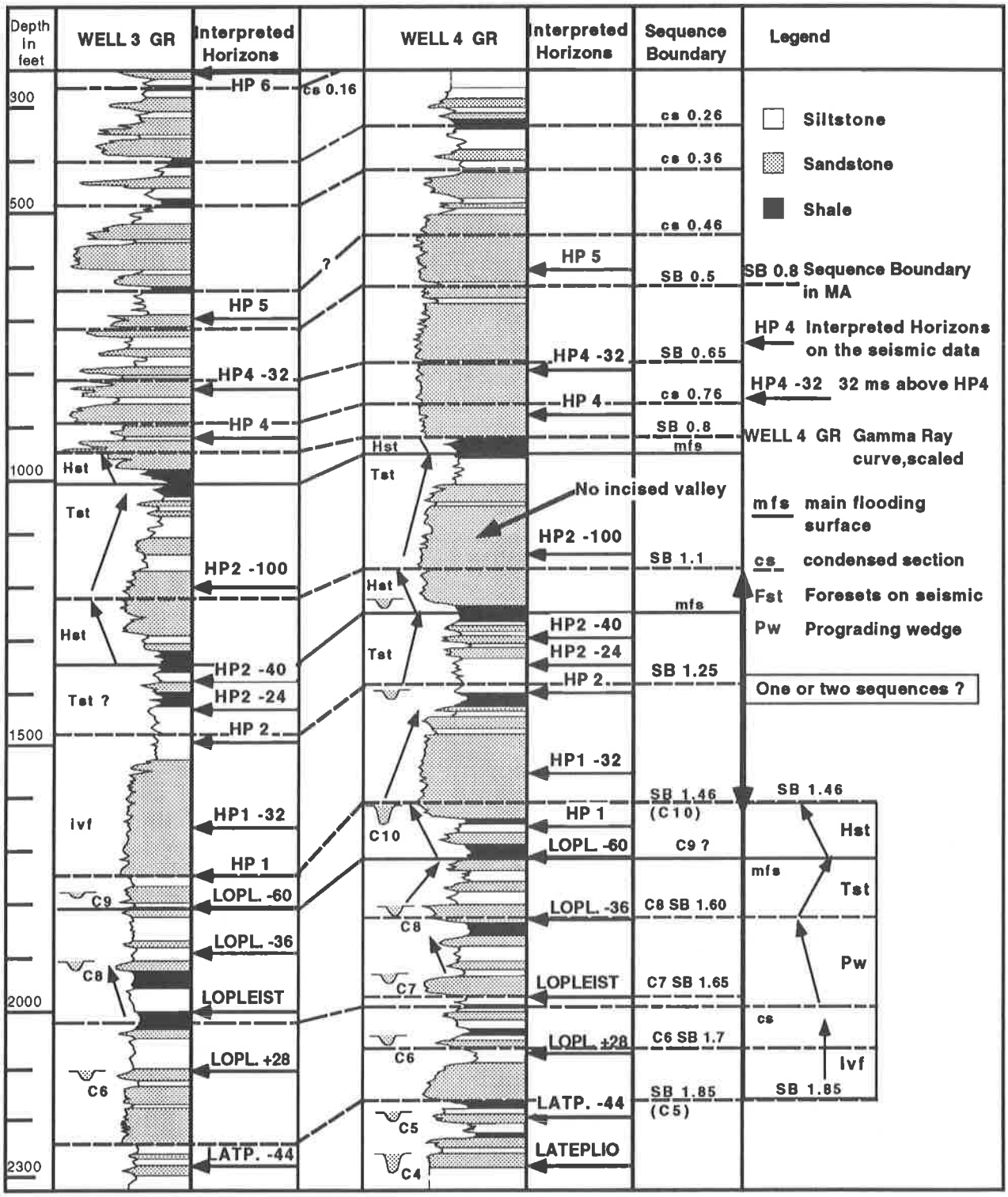

Fig. 5-15: Well log data sequence stratigraphic interpretation for the Lower Pleistocene (SB 1.85 to SB 1.1 interval). SB 1.85, 1.46 and 1.1 (Wornardt and Vail , 1991) or SB 1.85, 1.7, 1.65, 1.60, 1.46, 1.25 and SB 1.1, this study.

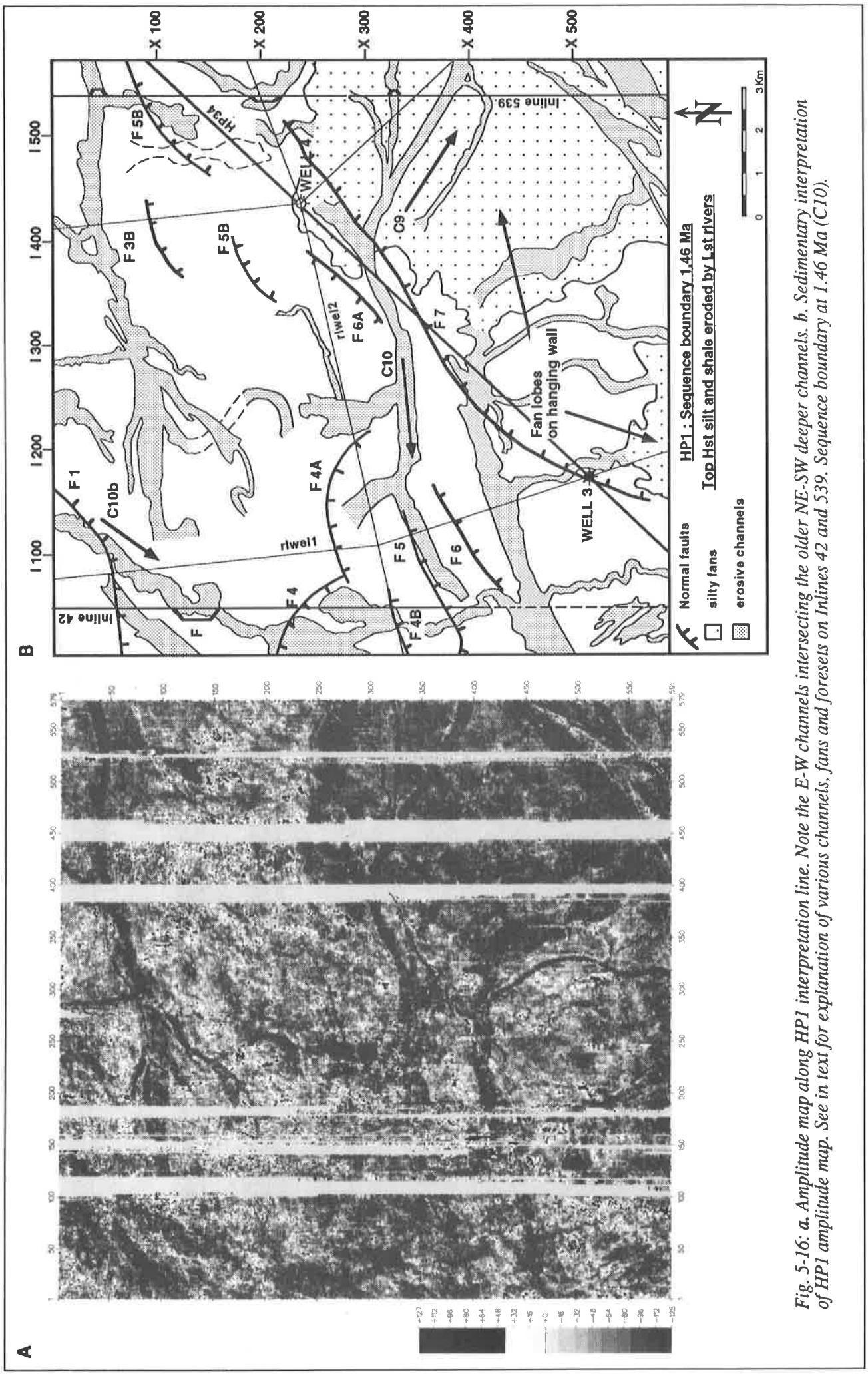

Fig. 5-16: a. Amplitude map along HP1 interpretation line. Note the E-W channels intersecting the older NE-SW deeper channels. b. Sedimentary interpretation of HP1 amplitude map. See in text for explanation of various channels, fans and foresets on Inlines 42 and 539. Sequence boundary at 1.46 Ma (C10).

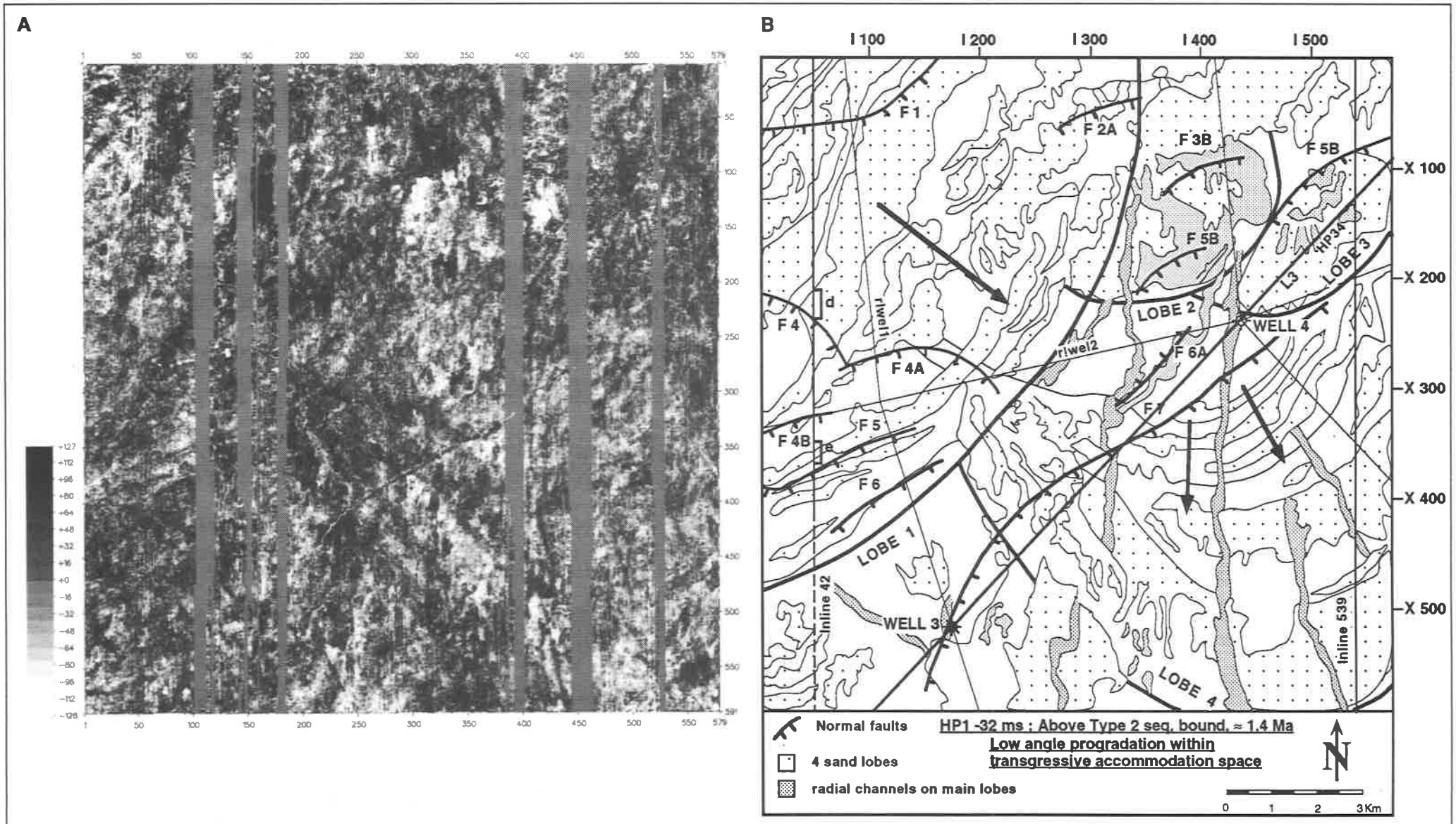

Fig. 5-17: ***a.*** *Amplitude map calculated 32 ms above and the HP1 interpretation line.* ***b.*** *Sedimentary interpretation of HP1-32 map showing the juxtaposition of two major sand lobes. Lobe 1 is more proximal than lobe 4 and downlaps on lobe 4 implying a possible retreat of shoreline (relative sea level rise).*

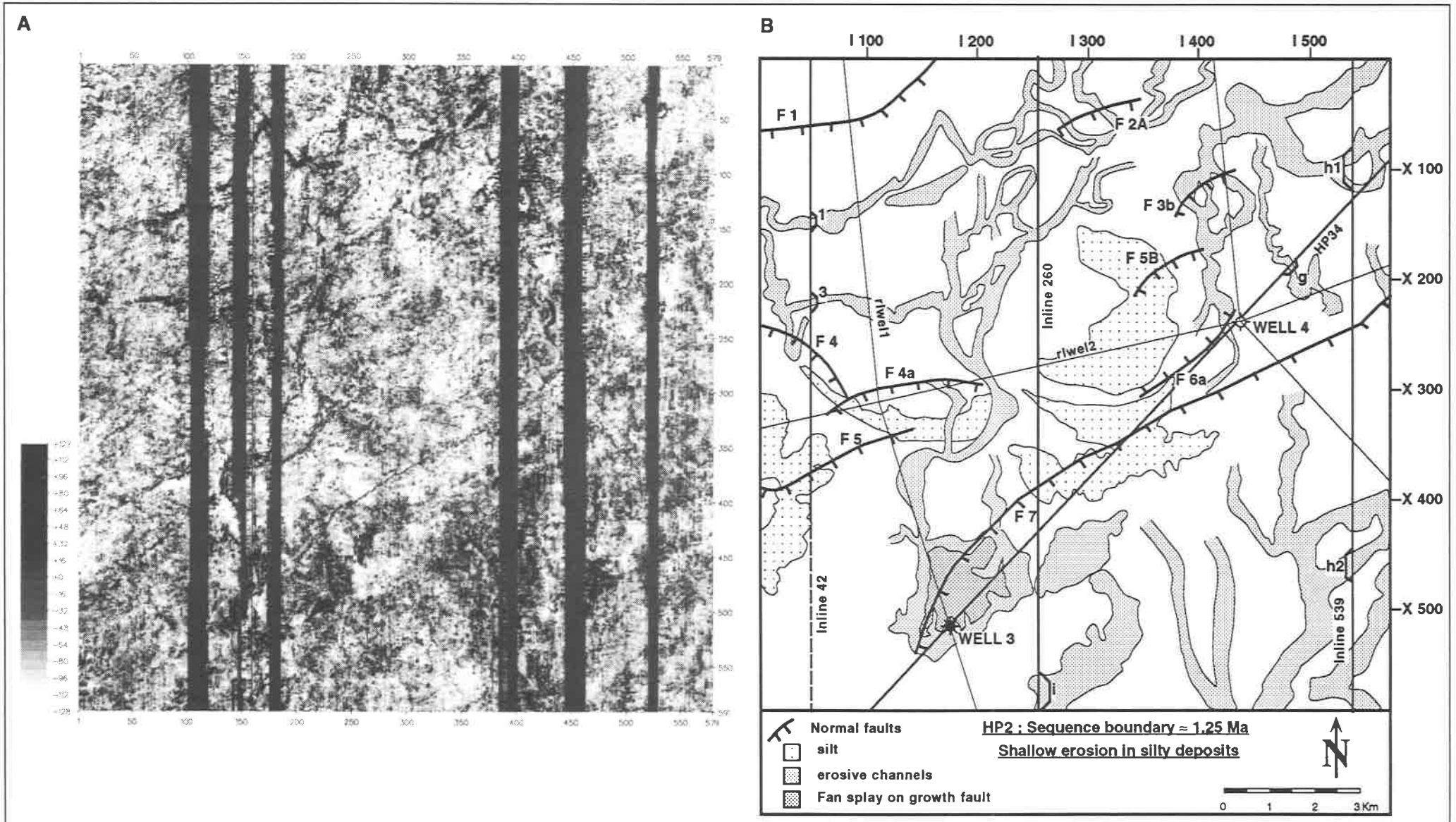

*Fig. 5-18: **a.** Amplitude map calculated along the HP2 interpreted horizon. **b.** Interpretation of amplitude map along HP2. Two generations of channels intersect this level. The shallow north-south channels belonging to HP2 (SB 1.25, C11) sequence boundary and the ENE-WSW channels in the upper left corner representing the base erosive level of the overlaying sequence boundary (SB1.1, C12).*

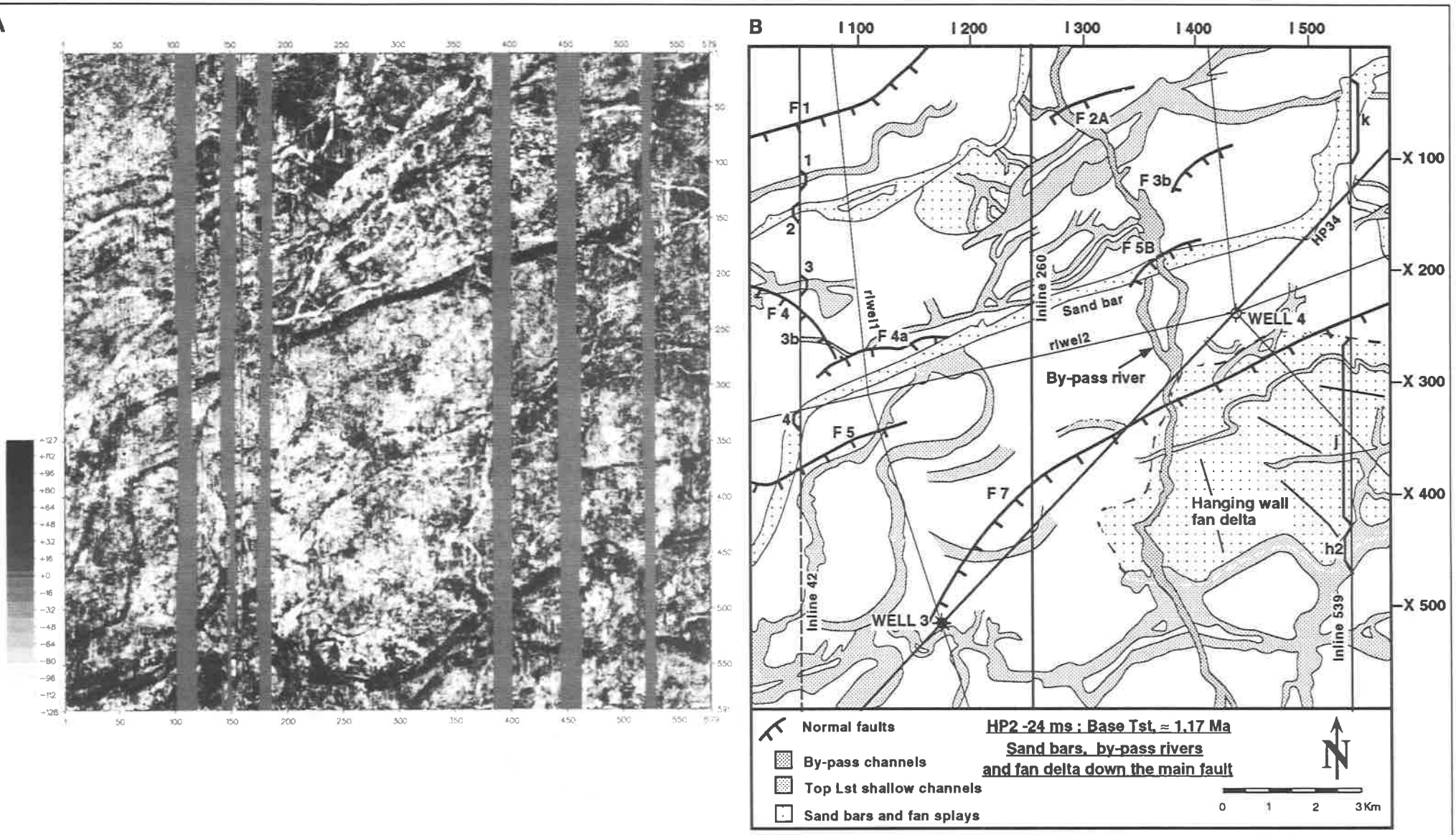

*Fig. 5-19: **a.** Amplitude map calculated 24 ms above the HP2 interpreted horizon. **b.** Sedimentary interpretation of HP2-24 map. See corresponding geological objects on vertical lines: - Inline 539 (fig. 5-7): i=progradation of fan delta related to the F7 growth fault; h=early lowstand channel below fan progradation; k=sand bar. On Inline 42 (fig.5-14): 1 and 3 = SB 1.1 lowstand channels intersecting HP2-24; 2 and 4=transgressive sand bars.*

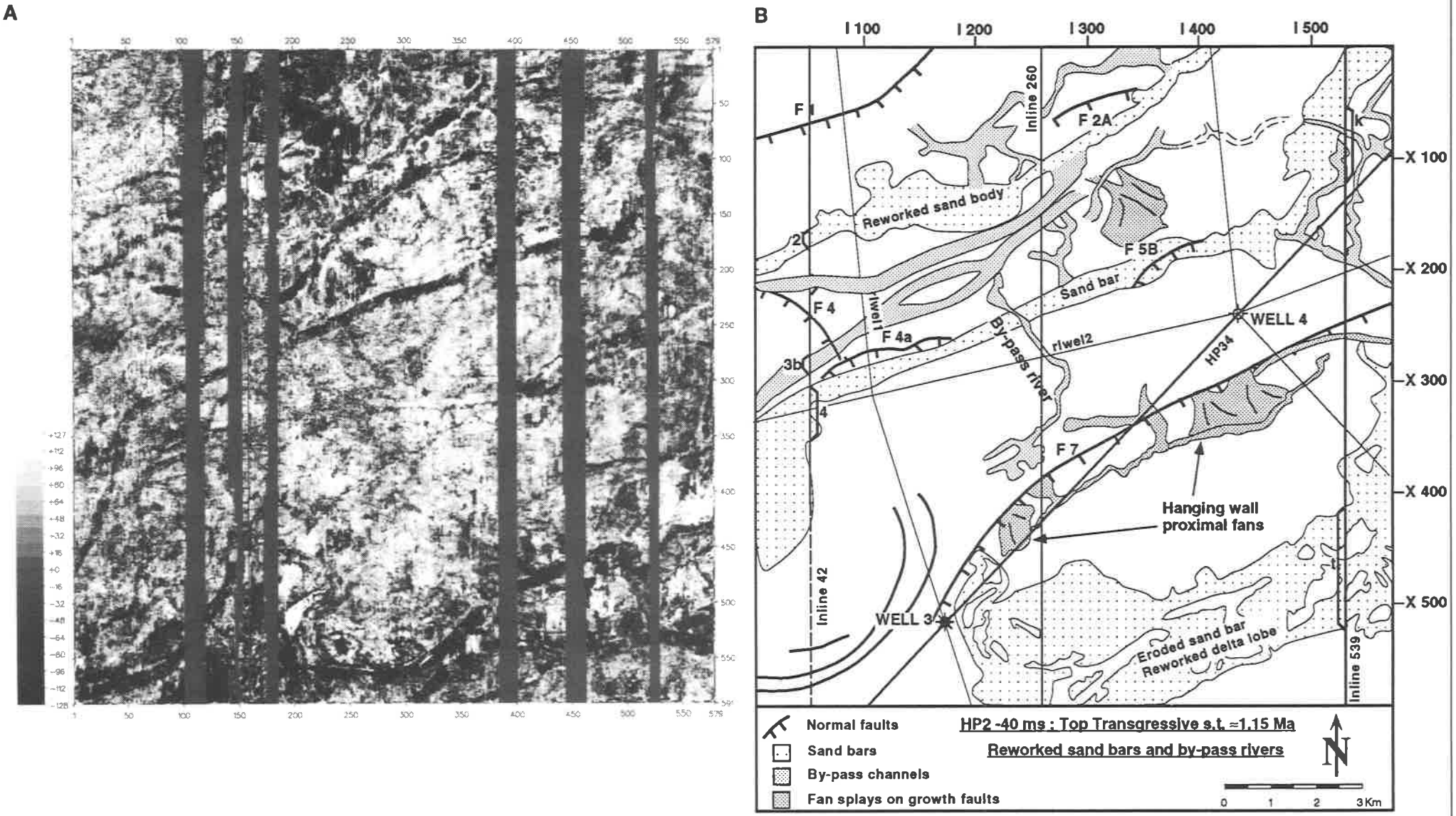

Fig. 5-20: ***a.*** *Amplitude map obtained 40 ms above HP2 seismic horizon.* ***b.*** *Interpretation of HP2-40 map. On Inline 539 (fig. 5-7): k=sand bar; t=toplaps, reworked top fan delta transgressive incision. On Inline 42 (fig.5-14): 1,3 and 3b = SB 1.1 lowstand channels; 2 and 4=transgressive sand bars.*

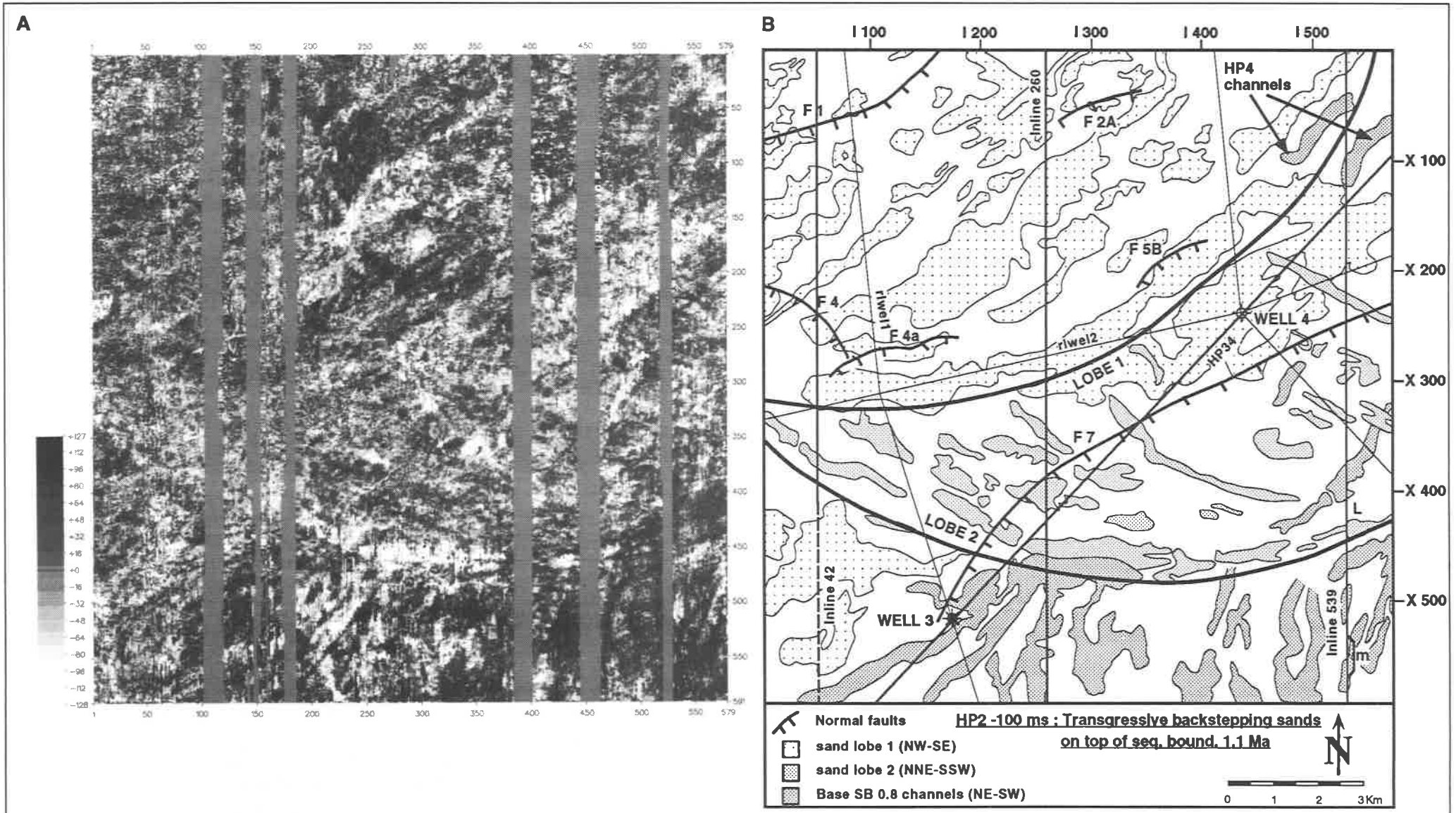

*Fig. 5-21: **a.** Amplitude map along HP2-100 ms. **b.** Sedimentary interpretation of HP2-100. On Inl.539 (fig. 5-7): l=frontal progradation intersection; m=HP4 (SB 0.8) deep lowstand channels. On Inl. 42 (fig.5-14): b and c=lobe 1 and lobe 2 intersections. Lobe 1 is slightly higher and in more proximal position indicating a retreating shoreline during the transgressive phase (see fig. 5-6 at HP2-100).*

An alternative solution would be to interpret HP2 as a condensed section period on top of thick incised valley sands deposited above the HP1 horizon and preceding the transgressive interval illustrated on the well log data and on the following amplitude maps. This supposition would imply a major sequence (from SB1.46 to SB 1.1) similar in time length and in facies succession to the following SB1.85 to SB 1.46 4th order sequence recorded below and discussed in the next chapter. But if HP2 is considered as a sequence boundary then the interval between SB 1.46 and SB 1.1 is subdivided into two equivalent shorter 4th order sequences (0.15 Ma). A major change in sequences rhythm could then be located below the SB 1.46 and not below SB 0.8 as proposed by Vail & Wornardt (1991) .

To understand the sedimentary evolution above HP2, more than thirty amplitude maps have been observed in the interval between HP2 and HP4. This interval is about 150 to 160 ms (TWT, ≈ 160 m) thick and is represented by nine to ten distinct seismic loops on the vertical seismic data (fig. 5-22). This means that the vertical resolution provided by the horizontal seismic facies identification on amplitude maps is at least 4 times superior to what the classical vertical seismic sections can provide. The three most representative interpreted maps are discussed below and summarise this interval composed of 2 complete 4th order sequences recorded in inner neritic condition (SB 1.25 to SB 1.1 and SB 1.1 to Sb 0.8).

The amplitude map on figure 5-19 shows a complex juxtaposition and superposition of 3 successive events intersected 24 ms above the HP2 reflector. From the sequential analysis on logs, this level corresponds to the transgressive systems tract on top of the condensed interval just above the HP2 horizon on well logs (fig. 5-15). The inferior sedimentary features intersected by HP2-24 are the broad meandering rivers having a NNE-SSW orientation. An example of these streams can be seen on Inl.539 (fig. 5-7, h). They show similar characteristics (depth-width-degree of meandering-orientation) with the channels related to the beginning of relative sea level fall along the HP1 horizon (SB 1.46 sequence boundary below). They suggest that the maximum of fall of relative sea level occurred just above the HP2 interpreted horizon, hence precisely locating the SB 1.25 sequence boundary. On top of these channels and corresponding to the maximum of sea level fall and to the beginning of sea level rise lays a fan delta taking advantage of some extra space accommodated down the active growth fault to prograde offshore (F7, foreset i on fig. 5-7; note the difference in thickness between HP2 and HP3 across the fault).

This facies succession along the SB 1.25 sequence boundary is the exact reproduction of the one observed in the cycle above and is characteristic for the basal part of a sequence in inner neritic conditions. The next sedimentary facies visible on the HP2-24 amplitude map (fig. 5-19 a) is represented by a straight black line that seems to cut in an oblique way all other seismic facies. This is interpreted as the base of a transgressive sand bar. Its very sharp limit, rectilinear aspect and lateral seismic facies homogeneity constitute the main arguments for not mistaking this signal with an erosional feature. This interpretation is confirmed by Inline 539 (fig. 5-7, k) that shows the positive mounded aspect of this sand bar. This sand body lays parallel to the major trend of growth faults (F1 and F7) which is also coincident with the local paleoshoreline orientation. The same sand bar is also intersected by Inline 42 (fig. 5-14, 4). It shows the typical lateral "square" amplitude anomaly not related to any incision in the sediments but rather indicative of an entirely depositional sedimentary body. The amplitude anomaly related to transgressive sand bars can be caused by the high porosity of a clean reworked sand frequently with methane in the recent sediments or more condensed fluids in the deeper buried portions of the shelf. Landward of this sand bar, the two SB1.1 deep channels already intersected 24 ms below appear again but in addition to the HP2 level, a second sand bar is intersected on the HP2 -24 level along Inline 42 (fig.5-14, 2). This second sand bar shows the same amplitude anomaly as the one present 2 km offshore (fig. 5-14, 4).

Thus, the sedimentary facies disposition on HP2-24 map suggests that a short lowstand event caused a shallow erosion on the shelf (NNE- SSW channels) followed by the deposition of local thin fans down the growth faults as relative sea level started to rise again (see also small lobe down F1 fault on fig. 5-19). These two "lowstand" related facies were followed by a stage of transgressive reworking of shelf deposits into elongated sand bodies parallel to the present shoreline, indicating the paleoshoreline orientation. It is important to realise that this three stages history is explicitly contained into one single amplitude map but that its detailed chronology is the result of the observation and interpretation of the maps above and below.

The next amplitude map calculated 40 ms above the HP2 horizon confirms the phase of relative sea level rise deduced from the preceding map. Less erosive north-south channels are observed and only the channels belonging to the SB 1.1 above intersect this level. The transgressive character of this interval is

confirmed by the visible reworking of the sand lobe developed down the F7 growth fault as illustrated by the preceding map (5-19) and by the intersection of the upper portion of the two previously described parallel sand bars. In the lower right corner of figure 5-20, the HP2-40 amplitude map intersects the eroded top of the subjacent low angle fan associated with the F7 synsedimentary activity. This crescent shaped sand body shows the probable transgressive incision of the underlying proximal deltaic sands. This transgressive abrasion surface can be seen on the vertical seismic section on figure 5-7 (Inline 539, t). On the same line, the sand bar already intersected by the previous amplitude map is intersected at a higher level (fig. 5-7, k). Similarly, in the western portion of the studied area on Inline 42, the lateral extension of the same sand bars are visible and present wider intersections compared to HP2-24 level (2 on fig. 5-7, 5-19 and 5-20). This can be interpreted as the vertical sedimentary facies evolution correlated to the ongoing relative marine transgression. This is confirmed by the shale layers deposited on top of these transgressive sands that can be seen on well logs data (fig. 5-15, mfs shale above HP2-40). These shale are interpreted as the main flooding surface deposits preceding the overlying highstand and transgressive systems tracts thick progradational sands marking the transition to the next sequence. This shaly interval is indicated on all seismic lines by a continuous strong amplitude reflector interpreted as HP3 (fig.5.7).

An amplitude map calculated along the HP3 level shows the almost total absence in lateral variation of seismic facies except for the overlaying channels intersecting it. This constitutes the typical aspect of main flooding surfaces amplitude maps (see fig. 5-52). This reflector marks the transition to the overlying thick sands represented on the seismic sections as low contrast in amplitude, hummocky seismic facies. It is above this transition and within the sand package that the SB1.1 sequence boundary is placed. On the well log data (fig.5-15 below HP2-100), this surface is placed within the sands where the coarsening up tendency switches to thinning up indicating the direct transition from the highstand progradation to the transgressive backstepping(see fig. 3-3 b). This transition associated with a sequence boundary in inner neritic condition can be observed on Well 3 and 4 because they do not intersect any lowstand incised valley channels. But laterally on Inline 42 (fig. 5-14), 40 to 60 m deep channels indicate the SB 1.1 erosive base level.

The horizontal morphology of the 40 to 50 m high transgressive foresets sedimented above the SB 1.1 channels in the northern portion of the studied area can be seen on an amplitude map calculated 100 ms above the HP2 horizon. Figure 5-21 a can be divided into two distinct zones according to amplitude content and orientation of seismic facies. The upper left corner shows a dominance of negative amplitude objects (in black) oriented along a NE-SW trend that can be interpreted as a first large sand lobe (fig. 5-21 b, lobe 1). A second sandy lobe dominated by positive (white) amplitudes with foresets intersections indicating a NW-SE orientation occupies the centre of the image. These two lobes can be distinguished on vertical sections intersecting both of them (see letters b and c on fig. 5-14 and fig.5-21 b). The clear frontal foreset of lobe 2 (white sand body on fig. 5-21 b) is intersected by the seismic section on figure 5-7 (l). This level (HP2-100) intersects the base of the channels belonging to the overlying SB 0.8 sequence boundary (see fig. 5-7 and 5-21 m and q). They show a NE-SW orientation characteristic in the area of the drastic fall in relative sea level associated with major sequence boundaries. The thickness of these two sand lobes (50 to 60 m of sands) is the direct expression of the accommodation space created on the shelf during the transgressive phase of sea level following the SB 1.1 maximum of erosion. These transgressive thinning upwards sands are sealed by the main flooding surface registered on well log data as finer silts and shale and on the vertical sections by one or two continuous high amplitude reflectors corresponding to the lithological contrast between the mfs shale and the overlaying sands below the SB 0.8 erosional surface described in chapter 5.2 (see fig. 5-14 and 5-15)

Conclusion

The succession of superposed sedimentary facies between SB 1.46 (HP1, C10 erosional phase, see fig. 5-65) and SB 0.8 (HP4, C13) observed on complementary type of data enable to discuss the relative sea level cycles registered on the Gulf coast during this interval. Yet, only qualitative proposition can be made as the coastal onlaps for each cycles cannot be found on the limited portion of the Gulf coast shelf. There is definitely one major 4th order sequence boundary in this interval as proposed by Vail & Wornardt (1991) and Wornardt & Vail (1991). This major sequence boundary is attributed to SB 1.1 (C12) and not to SB 1.3 (deep erosion along the sequence boundary, transgressive reworked sand bars in the fine silt below and progradation on top). The erosional surface (SB 1.25, C11) found above the HP2 horizon is

attributed to a lower order relative sea level pulse occurring during the beginning of the transgressive phase of the major SB 1.46-SB 1.1 fourth order sequence. It corresponds to the SB 1.25 proposed by the TGS™(1990) coastal onlap curve and also to the Vail and Wornardt (1991) SB 1.3 sequence boundary.

This lesser fall in relative sea level occurring during the H.Selli nanno-fossils condensed interval (Schaffer, 1990) can be correlated to a cold peak on several oxygen isotope curves in and around the Gulf of Mexico (fig. 5-6). The oxygen isotope curves presented on figure 5-5 is from the North Atlantic Ocean (DSDP Site 607) and the filtered curve of DSDP Sites 677 (equatorial Pacific Ocean) and 607 as produced by Haddad & Vail, (1992). The above-mentioned authors have suppressed by filtering the high frequency Milankovitch type eustatic cycle to compare the high frequency oxygen isotopes curves with the low frequency eustatic curves obtained from seismic and well log data in the Gulf. They have interpreted the filtered curve in term of 3rd and 4th Orders cycles and compared it with the Haq et al. curve (1988) and the Wornardt and Vail (1991) synthesis for the Plio-Pleistocene in the Gulf. In the interval discussed here they indicate two very clear cold periods starting at 1.20 and 1.05 Ma (age are constrained by biostratigraphy, magnetostratigraphy and orbital stratigraphy) This confirms the presence of a glacio-eustatic SB 1.25 sequence boundary (4th Order) registered in the Gulf of Mexico between SB 1.1 and SB 1.46.

Thus, the interval between SB 1.46 and SB 0.8 is divided into at least 3 sequences between 0.1 and 0.15 Ma long. A first change in rhythm of 4th order sequences was clearly defined along the SB 0.8 Ma limit when 0.1 Ma sequences where found only above that limit marking a clear transition with the two 0.3 Ma sequences in the lower part of the Pleistocene. Now that the early Pleistocene can also be subdivided into three shorter sequences the question can be asked whether there are 0.1 Ma sequence registered on the entire Pleistocene ? The next chapter deals with the first 4th Order sequence longer than 0.3 Ma, between SB 1.46 and SB 1.85. It is characterised by a prolonged lowstand whose maximum coincides with the Plio-Pleistocene limit (1.65 Ma). It will be shown that the same interdisciplinary approach can lead to the subdivision of this 0.4 Ma long sequence into three to four 0.1 to 0.15 Ma 4th order sequence confirming the identification of possible 0.1 Ma sequences down to the base of the Pleistocene.

5.4 Plio-Pleistocene limit (a 4th order sequence from SB1.46 to SB 1.85)

Introduction

The purpose of this short chapter is to illustrate on the base of amplitude maps the characteristic sedimentary features associated with the first prolonged lowstand interval corresponding to the Kansan marine stage in the Gulf of Mexico that can be correlated to the second half of the Donau continental glacial age (fig. 5-4). There is a convergence of data indicating a global climatic change around 1.7 Ma before the present to which the international limit for the Plio-Pleistocene is presently attributed (Harland *et al.*, 1989 ; Odin & Odin, 1990) . At 1.67 Ma, the magneto-stratigraphic curves is "black" to normal for the Olduvai stage after a long reversed polarity interval between 0.79 and 1.67 Ma (Brunhes, see fig. 5-6). Most oxygen isotopic curves in the Atlantic and Pacific oceans as well as in the Gulf of Mexico indicate longer and colder peaks between 1.7 and 1.5 Ma. The same time interval is also the first long period since present time without any major condensed section registered in the Gulf coast region indicated by the lack of high abundance and diversity peak of nanno-fossils (Shaffer, 1990; fig. 5-6).

The Plio-Pleistocene limit, defined in southern Italy in on land marine sections is marked by the extinction of most warm water foraminifers species and the apparition of cold water species like Arctica islandica and Hyalinea baltica (Harland *et al.*, 1989) and can be correlated to the important local eustatic fall of sea level registered at that time in the Gulf of Mexico. The next paragraph discusses the aspect of this climatic change as recorded on well logs, vertical and horizontal seismic data in the studied area.

Observation

The description of the complex lowstand interval below SB 1.46 (HP1) horizon is realised from the LOPLEIST horizon. On most regional and local vertical seismic sections studied in the Gulf coast, this level is represented by one or two very strong positive amplitude reflectors marking a first drastic change from the more chaotic variable amplitude above (Upper Pleistocene) to the more layered and conformable reflectors below (base Pleistocene-Pliocene). LOPLEIST, like most other horizons in this study, is interpreted along the negative trough below the main positive signal (see seismic sections on fig. 5-22 and

5-23, Plate 2). This strong amplitude signal is correlated on logs with the gradual change from the basal lowstand thick sands (incised valley) to a condensed shaly and silty interval at the level of LOPLEIST which can locally be quite thick (up to 30 m, Well 3, fig. 5-15). These shale are not present on the entire surface of LOPLEIST and are almost entirely intersected and eroded laterally by a second generation of channels (fig. 5-15, C7 thick "blocky" sands on Well 4). The sequence boundary (C5) at the base of the interval (SB 1.85) is placed at the base of the 40 to 60 m thick sands associated with lowstand channels on the shelf (see sequential analysis on logs, fig. 5-15 and 5-30, wells 1, 3 and 4).

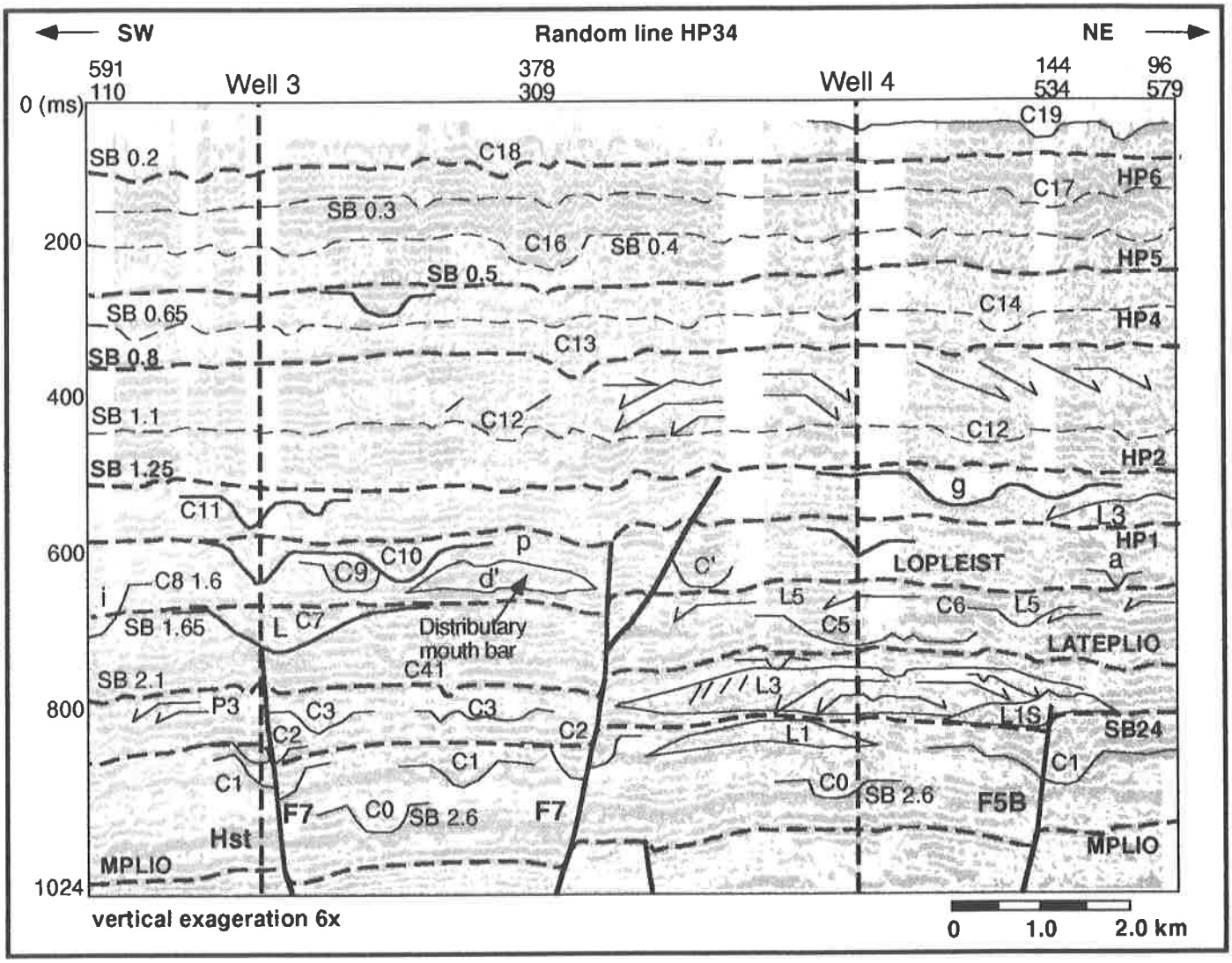

Fig. 5-22: NE-SW random seismic section (HP34), connecting Well 3 to Well 4 (shaded seismic data with superposed interpretation , see fig. 5-25 for location). This line is perpendicular to the main direction of sediment input and intersects most main channels.

The interval between SB 1.85 and SB 1.46 is approximately 100 m thick and presents a complex superposition of at least 4 successive erosive and sedimentary events within one single 4th Order sequence. In order to apprehend and sort out the intricate successive generations of channels partially removing and reworking what is below, 4 amplitude maps are interpreted and displayed in this chapter to sum up this complex story. These maps (LOPL. +28 to LOPL. -60) are located on the well logs data through synthetic logs before being correlated on the chronostratigraphic chart of Figure 5-6. More than 20 amplitude maps were necessary to follow the rapid changes in river beds occurring at that time and to understand the variations in sedimentary environments. This succession is presented from base to top.

Amplitude map LOPLEIST+28, calculated about 30 m below the interpretation line (fig. 5-24 a and b) intersects the data volume above the SB 1.85 and present the juxtaposition of two different seismic facies. On the left, it cuts through arched reflectors interpreted as the top part of a fan lobe progradation developing during the period of maximum relative sea level. These prograding sands are intersected by Well 1 on figure 5-30 and do not show the characteristic signals of incised valley sands. Laterally, parallel north-south oriented, deep erosive channels cuts through the underlying sediments. These straight incisions are indicators of the maximum phase of relative sea level fall (C6, ≈1.75 Ma) forcing the streams to take the shortest way to the sea eroding the underlying top highstand coarsening up progradation.

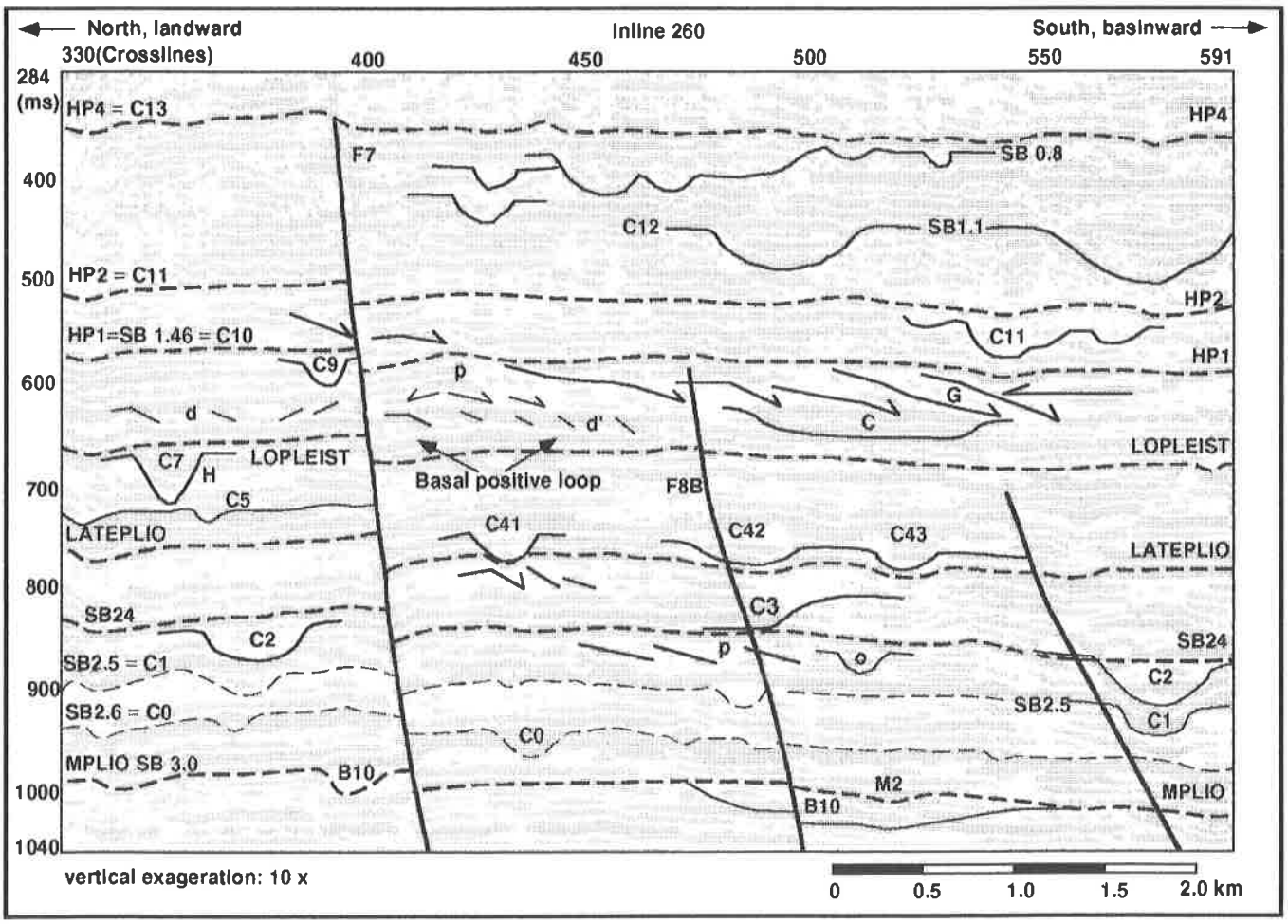

Fig. 5-23: Offshore portion of the North-south Inline 260, across the F7 main growth fault (see fig. 5-25 for location). Raster density seismic data with superposed interpretation and location of erosional surfaces (C = Gulf coast Pleistocene, B = Middle and Late Miocene).

The initial phase of erosion associated with the beginning of the lowstand period (SB 1.85, C5) will be discussed in the next chapter. Similarly to the important fall in relative sea level occurring at the SB 1.46 limit (HP1, C10), two distinct phases of erosion with characteristic facies can be recognised along the SB 1.85 major fall in sea level:

1) As soon as the inner portion of the shelf starts to be emerged, meandering streams develop on the shelf and show mainly oblique ENE-WSW orientation (C5 erosional surface, more or less parallel to the present shoreline, fig. 5-16 and 5-39a). Frequent low angle fine sand lobe associated with shallow meandering streams develop in the depressions caused by active growth faults. These tectonically related local fans on the inner shelf in the top highstand / lower lowstand interval can be mistaken for true highstand progradation covering larger portion of the outer shelf.

2) When the rate of relative sea level fall is maximum, these meandering streams and fans are partially eroded by deeper, rectilinear frequently almost north-south oriented incised valleys (C6 erosional surface, see table 1) marking the second phase of erosion associated with major eustatic changes (see LOPLEIST+28, fig. 5-24 or fig. 5-16 NE-SW channels).

The same lateral difference in seismic facies is observed on the amplitude map calculated along the LOPLEIST horizon (fig. 5-25 a and b). On this image, the colour scale had to be compressed in order to see the subtle changes in amplitude. The western part of this map presents an homogeneous negative amplitude (white) corresponding to the shale deposits indicated by Well 3 (fig. 5-15). They are intersected by shallow meandering channels. On the eastern part of the image, wider negative amplitude channels cuts through an area dominated by positive amplitudes (black) explained by the absence of shale lowering the contrast in acoustic impedance. These broad meandering channels can develop at the end of relative sea level fall and when the shelf reaches equilibrium before starting to be flooded again (see position of LOPLEIST on chart fig. 5-6). The wide and shallow channels filled with fine sand and silt show a NNW-SSE trend and are different from the deep straight N-S channels intersected 30 m below. They represent a distinct shallow erosive phase (C7, ≈ 1.65 Ma on figures 5-15 and 5-30).

Amplitude maps calculated with a vertical increment of 4 ms gradually cut through the thick positive loop overlaying the LOPLEIST horizon and reveal sedimentary features marking the end of the relative sea level fall and the first signs of the onset of the shelf flooding. On figure 5-23 (d, Inline 260, Plate 2) between Crosslines 350 and 460, a very subtle depression is observed on top of the positive loop marked by a series of very fine shingled reflectors dipping both landward and basinward. On top of that, a positive feature (p) is observed passing laterally and basinward to very clear foresets progradations (G).

An amplitude map obtained 36 ms above LOPLEIST (fig. 5-26 a and b) shows that this invisible, unnoticeable depression on top of the basal positive loop (d) reveals itself to be a perfectly shaped distributary mouth bar. This sand body is intersected on 5 successive maps indicating a total thickness of about 20 m. Furthermore, the superior intersection of this sand body shows a substantial decrease in size indicating its lunar shape. It is about 2 km wide and 5 to 6 km long corresponding to the mean values of such paralic sandstone bodies as described by Bryant and Flint (1993) and Reynolds (1994). This mouth bar is bordered on both sides by two relatively broad channels (500-700 m) flowing towards the south-east.

On Inline 260 (fig.5-23 c), the southern channel is intersected along strike and is registered as an elongated high amplitude positive anomaly (red on amplitude map and black on vertical section). The base erosional level of these channels is situated above the base of the distributary mouth bar. It is interesting to note that they pass around the positive mounded pre-existing mouth bar. Their associated distributary mouth bar, if existent, must lay a few kilometres basinward, out of the studied area. Figure 5-28 shows two models modified from Wright (1977) and Reynolds (1994) to illustrate the situation represented on LOPLEIST -36 amplitude map. Figure 5-28a is a representation of a synthetic fan lobe comparing the statistical size of sand bodies to well known oil fields. The second part of this figure (fig. 5-28 b and c) is a close up in plan view and cross section of a distributary mouth bar (modified from Wright, (1977) . The plan view shows an image exactly similar to the one observed on the 3D data set. The vertical cross section (fig. 5-28 c, with a strong vertical exaggeration) indicates that the bar crest can lay a few meters (5 to 20 m) above the channel bed. The low angle equally spaced progradation foresets fit the observation of the subtle "shingles" on Inline 260 (fig.5-23 a and b). Based on this comparison, the distributary channel associated with the observed lobate sand bar must have an approximate width of 500 m and lay below the bar crest. This channel is hardly observed on figure 5-26 (a and b) at the back of the distributary mouth bar and has probably been eroded by the two channels flowing on each side of the mouth bar.

On the western portion of the image, a shallow broad meandering channel (≈ 2 km wide) is indicated by a strong negative amplitude (violet on fig. 5-26 a). It is intersected by Inline 42 and can be seen on the vertical section on figure 5-14 (M and M', Plate 2). This soft signal is interpreted as the top of a lowstand channel that extends further down for about 25 m and that is filled with shale or silt at the end of the lowstand period. The sedimentary facies depicted on LOPLEIST-36 is typical for the inner portion of a fan delta developed on the inner shelf during the beginning of relative sea level rise. The 40 m of sediments deposited above the conformable shale from the LOPLEIST horizon are extremely rich in information and show at least three successive phases of deposition that would have been missed on the base of vertical sections and well logs data. This interval on the vertical section (fig. 5-23, between LOPLEIST and HP1) showing low angle shingled reflections is typical for the transgressive and highstand systems tracts

developed over an erosional surface (LOPLEIST, C7).

On logs, the interval between LOPLEIST-36 and LOPLEIST-60 (fig.5-15) could be interpreted as a "normal" thinning upwards transgressive package below the mfs interpreted along the LOPLEIST-60 horizon. But the amplitude maps along LOPLEIST-36 (fig. 5-26) reveals that the thick sands intersected on Well 3 and 4 at that level correspond to thin channels flowing from NE to SW (C8a, fig. 5-26). These channels are themselves intersected by the NW-SE oriented prograding delta system (C8b, distributary mouth bar, and two superposed channels, C8c indicating a possible basinward shift of facies. And finally, in the western portion of the studied area this complex configuration is partially eroded again by a north-south meandering deep channel filled with fine silt (C8d, LOPLEIST-36). This complex erosional surface (C8) can be subdivided into 4 phases that can be interpreted in terms of systems tracts progressively shifting basinward as the relative sea level fall reaches its peak:

- C8a: NE-SW shallow channels => relative lowstand
- C8b: proximal fan down the F7 growth fault
- C8c: basinward shift of facies (meandering NW-SE channels
- C8d: late erosion phase, north-south large meandering channels, incised valley corresponding to the maximum of basinward shift of facies.

These four successive erosional phases can be interpreted as one large lowstand interval (C8) but can also indicate four 5th order parasequences. The offshore equivalent of these 4 erosional phases could be aggrading and prograding parasequences accumulated near the shelf break or in local depressions on the shelf (salt related mini-basins, see fig. 7-1).

The vertical evolution in sedimentary facies on top of this level is presented on two amplitude maps "LOPLEIST -60 and -64" (fig. 5-27 a and b). They intersect the 3D data volume about 25 m above the preceding map and are located some 15 to 20 m below the HP1 interpreted horizon (SB 1.46, C10). The LOPLEIST-60 amplitude map intersects the SB 1.46 incised valley channels eroding the highstand fine silt and shale as deep as the main flooding surface (well log data on fig. 5-15 and fig. 5-27, E-W trending channels). These channels cut into a highstand prograding fan lobe developed on the F7 main growth fault (Inline 260 fig. 5-23 g). This local distributary highstand sand lobe is entirely controlled by the F7 growth fault activity and marks the culmination of relative sea level rise before it starts to fall again and develops the SB 1.46 erosional surface (C10).

Conclusion

Precise identification of sedimentary facies from seismic horizontal facies, well log data and vertical seismic sections enable to follow relative movement of sea level in the inner portion of a clastic shelf. Complex superposition of successive erosive phases can be sorted out by precise interpretation of differences in morphology and orientation. In the example of this long-lasting lowstand interval, 4 to 5 generations of channels are recorded within 100 m of vertical section. Depth of incision, width and degree of meandering of channels are direct indicators of depositional environments. One 4th order sequence limited by two type 1 sequence boundaries is identified on 3D horizontal images by the succession of (from base to top) :

- Oblique (NE-SW) meandering channels (40 to 50 m deep) marking the beginning of relative sea level fall cutting into the top highstand low angle progradational lobes (SB 1.85, C5 fig. 5-39 a and b, LATEPLIO-44).
- Rectilinear deep (similar to braided, 50 to 70 m deep) channels cutting in the subjacent top highstand progradation. They are developed at the maximum of relative sea level fall (SB 1.75, C6 N-S oriented, fig. 5-24, LOPLEIST+28).
- Wider, shallower, meandering streams with finer granulometry are associated to the starved period following the maximum in relative sea level fall. Proximal estuarine type shale can be laterally accumulated (SB 1.65, C7 NW-SE, fig. 5-25, LOPLEIST).
- As the shoreline starts to transgress, the general backstepping and local progradation of deltaic sand bodies and associated fluvial channels can be identified. (SB 1.8, C8 subdivided into 4 complex channels generations, fig. 5-26, LOPLEIST-36). NB: 5th order cycles superposed to the 4th order sequences are visible because preserved at the base of the transgressive systems tracts in the inner portion of the shelf. They represent the inner shelf equivalent of aggrading and prograding 5th order parasequences.
- The distal deltaic progradation coming after the period of relative maximum in sea level rise (SB

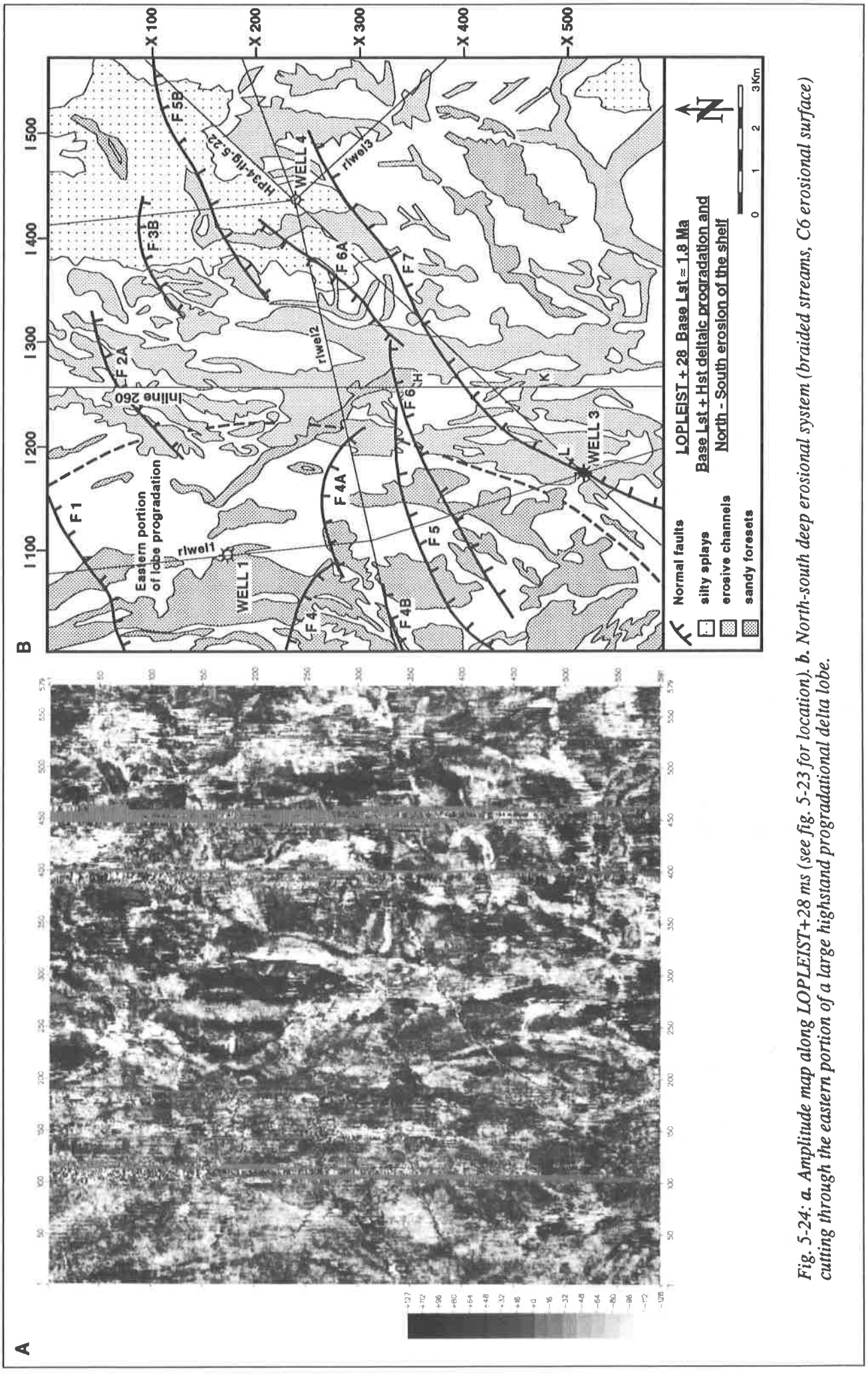

*Fig. 5-24: **a.** Amplitude map along LOPLEIST+28 ms (see fig. 5-23 for location). **b.** North-south deep erosional system (braided streams, C6 erosional surface) cutting through the eastern portion of a large highstand progradational delta lobe.*

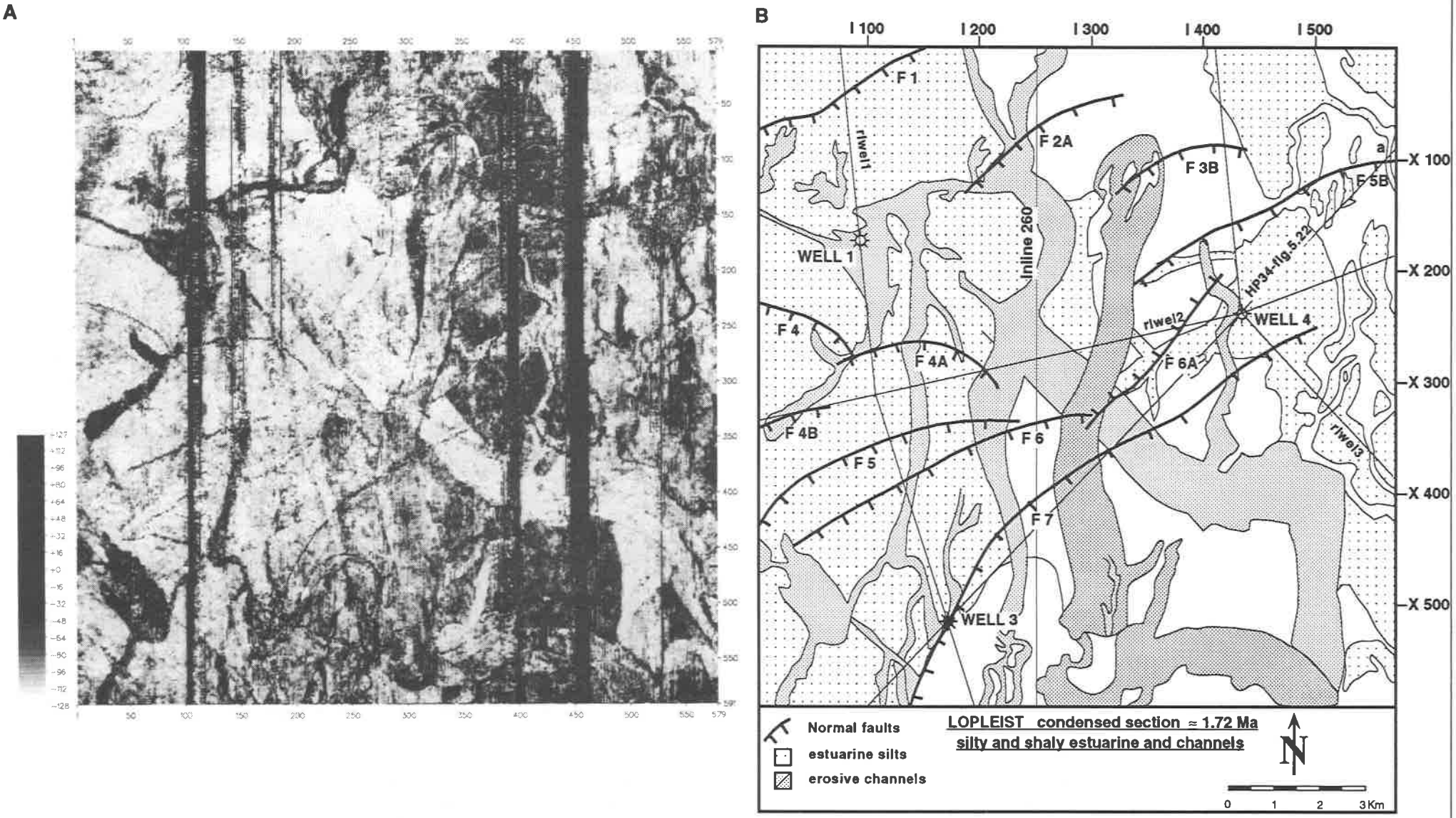

Fig. 5-25: ***a.*** *Amplitude map along LOPLEIST interpreted horizon (displayed with compressed colour scale to enhance subtle lateral differences in amplitude.* ***b.*** *Wide and relatively shallow NNW-SSE channels (≈ 40 m, C7 erosional surface) in a silty interval.*

*Fig. 5-26: **a.** Amplitude map 36 ms above LOPLEIST horizon. Complex superposition of four generations of channels associated with an erosional phase at 1.6 Ma. Violet (negative amplitude) large meandering incised valley in the left portion of the image and perfectly shaped distributary mouth bar below the centre.*

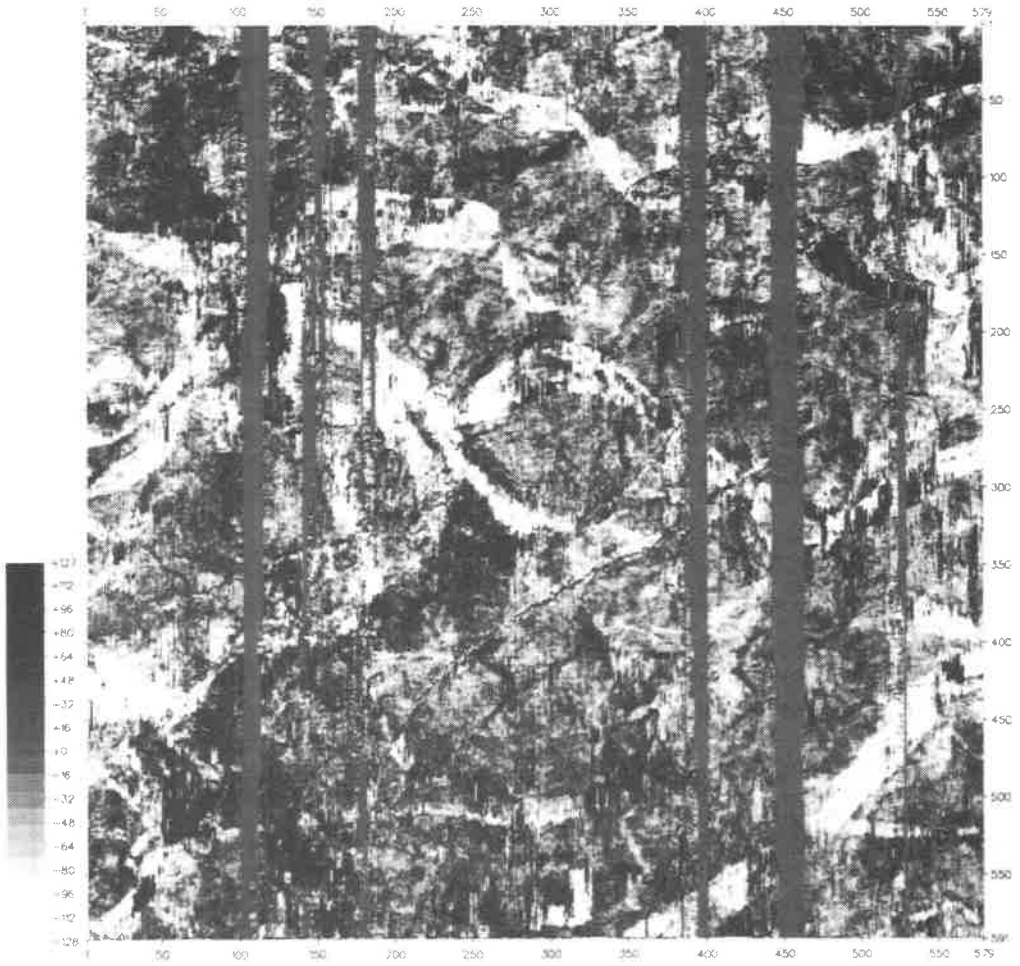

*Fig. 5-27: **a.** Amplitude map calculated 60 ms above the LOPLEIST horizon. Large (15 km wide) proximal delta lobe and distributary channel intersected by a second oblique generation of incision (brown-orange positive amplitude).*

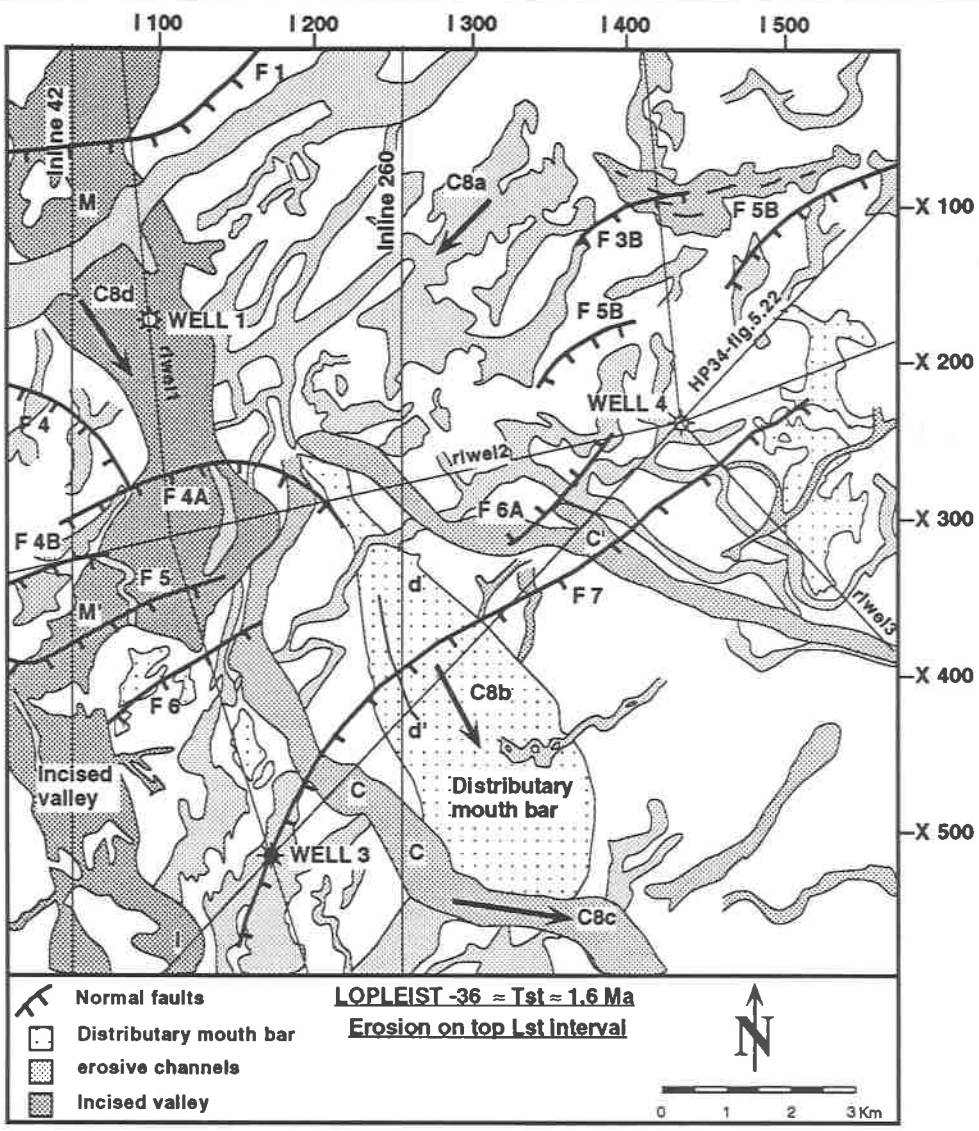

Fig. 5-26: ***b.*** *Interpretation of four distinct and superposed erosional events associated with the fall in relative sea level near 1.6 Ma (C8 erosional phase). C8a: shallow channels. C8b: proximal fan (distributary mouth bar) down the F7 growth fault. C8c: basinward migration of delta lobe. C8d: incised valley (further basinward migration).*

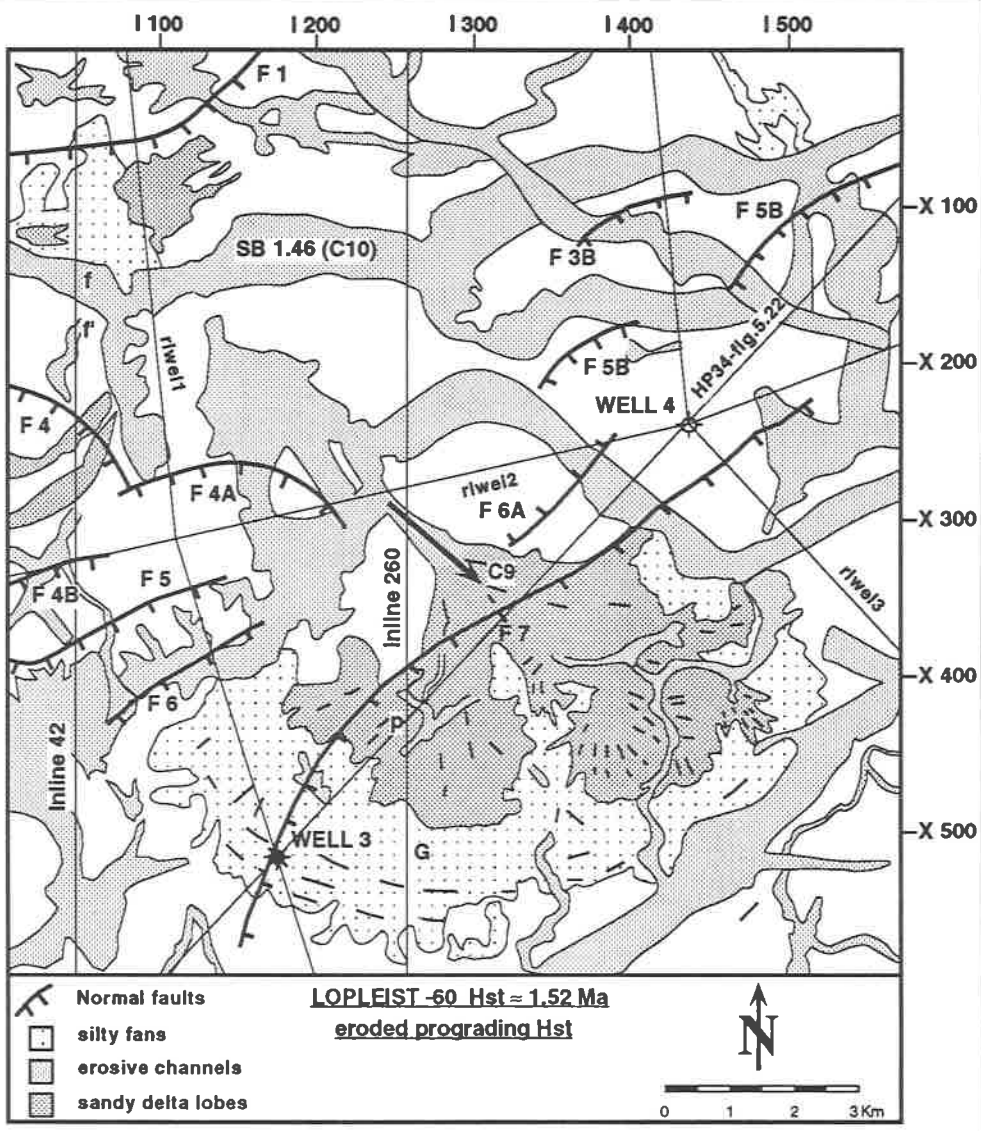

Fig. 5-27: ***b.*** *Interpretation of figure 5-27 a. Top highstand and initial lowstand shallow NW-SE channels (C9) and associated fan connected to the F7 growth fault. Superposition of oblique (ENE-WSW) deeper channels associated with the following maximum of lowstand at 1.46 Ma (C10).*

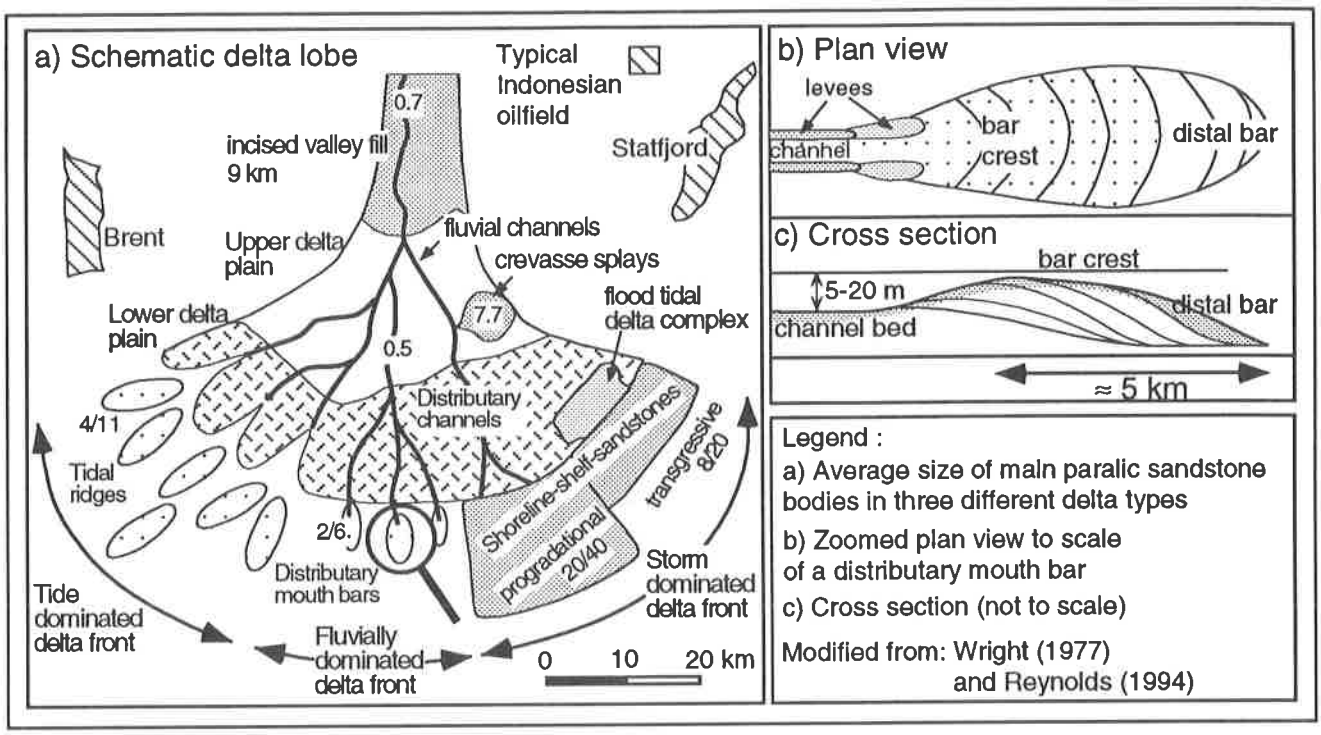

Fig. 5-28: ***a.*** *Schematic representation and size indication of the main sand bodies associated with deltaic sedimentation. Comparison with Brent and Statfjord giant fields Reynolds (1994).* ***b*** *and* ***c.*** *Detailed morphology of a distributary mouth bar (Wright, 1977). Note the exact resemblance in size and shape with the one observed on figure 5-26.*

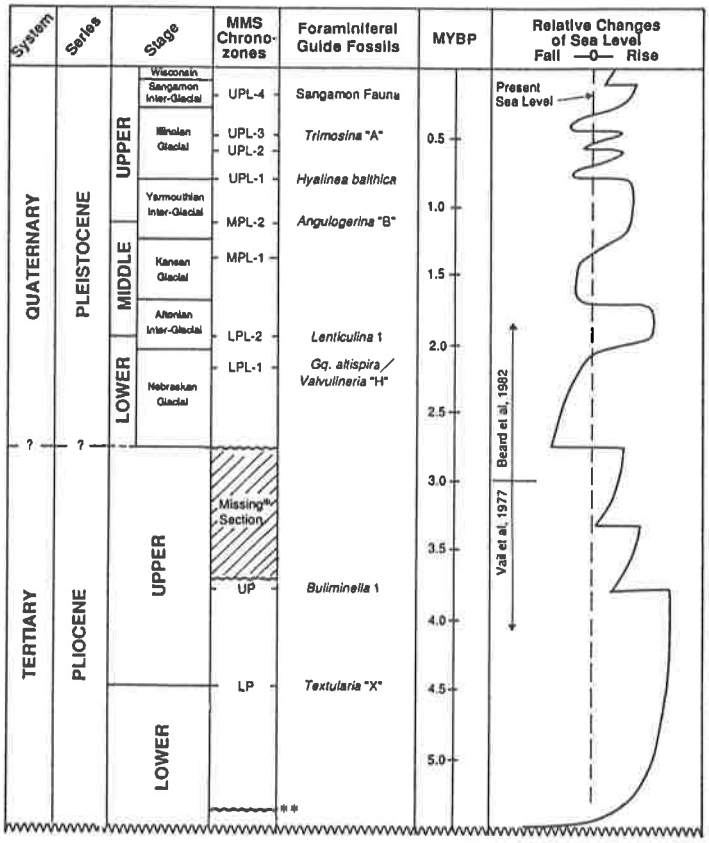

Fig. 5-29: Eustatic curve, benthic foraminifers zones and reference seismic horizons interpreted on the entire offshore Louisiana shelf used for correlation at the beginning of this research (Courtney Reed and Layendecker, 1987 and Beard 1982).

1.52, C9 end of highstand, low angle fans related to growth faults, fig. 5-27) are sharply eroded by the channels developing as soon as relative sea level starts to fall again (SB 1.46, C10 HP1, fig. 5-16, LOPLEIST-60).

This complex chronology would be impossible to sort out on the basis of vertical sections only presenting this interval as 3 to 4 parallel loops showing subtle lateral changes in amplitude. And it is only on the base of horizontal attribute maps that such resolution is possible in a similar setting. In the search for subtle traps it is fundamental to define the exact size of each sand body and to be able to correlate it to a particular systems tract. Chapter 6.2.5 will provide a synthetic table summing up the enormous amount of sedimentary information contained into this 3D survey for exploration purposes. In this example, it is possible to qualify the type of facies succession encountered during the lowstand event (maximum at about 1.6 Ma). It is interesting to note that similar sedimentary facies successions are observed along the 0.8, 2.4 and 3.0 to 3.2 major erosive phases (see fig.5-6, Table 1 and 5-40 Table 2). It suggests a possible 0.8 Ma periodicity marked by stronger falls of relative sea level registered in the northern Gulf of Mexico. Do each of this 0.8 Ma cycles contain eight 0.1 Ma 4th order sequences similarly to the top Pleistocene ? Were they present but not recorded or present and non-identified ? The answer might be available when we will be able to have true high resolution seismic data down to the first one or two seconds of seismic records, or 3D data sets extending from the inner shelf to the slope...

Based on 3D data presented in this chapter, it is likely that the imprint of four 0.1 Ma eustatic events (eccentricity 96 kyrs cycles, Milankovitch (1941) can be found in this part of the Gulf coast shelf between SB 1.85 and SB 1.46 Ma. Then, the entire Pleistocene (sensus stricto) would be marked by short terms orbitally forced cycles superposed on the gross 4th and 3rd order trends interpreted by classical sequential analysis such as proposed by Vail and Wornardt (1990) . A synthetic table summarising all new information on this complex superposition of organised erosional surfaces is presented in the conclusion at the end of chapter 5 (fig. 5-65).

Introduction to 5.5 and 5.6

The two following chapters discuss the complex interval at the top of the Pliocene corresponding to the base of the Gulf coast Pleistocene (1.85 to 3.2 Ma). This interval is recognised on most regional seismic sections across the shelf of the northern Gulf of Mexico as a 200 to 300 m thick, discontinuous, irregular and low amplitude interval comprising numerous unconformities (fig. 5-22, MPLIO-LOPLEIST, Plate 2). This thick sand package is limited above and below by continuous high amplitude reflectors corresponding to the two major shaly transgressive events registered at 1.6 and 3.2 Ma (see respectively: LOPLEIST and MPLIO+32 horizons on fig. 5-30). The Minerals Management Service (MMS) report of the U.S. Department of the Interior (1987) presents lateral correlation across the entire Louisiana and Texas shelf and concludes to the presence of one major phase of sea level fall between 2.7 and 2.4 Ma within one large 3rd order sequence ranging from 1.7 to 2.7 Ma (fig. 5-29, Beard 1982). They see this important fall in relative sea level as the main cause for the important hiatus indicating the top Pliocene in the Gulf coast region. Recent studies in the same area (TGS™, 1990 ; Wornardt & Vail, 1991) agreed in subdividing the same interval into three 4th order sequences (sequence boundaries at 1.85, 2.4, 2.7 and 3.0 Ma). We propose that the period between SB 1.85 and SB 2.4 can be further subdivided into at least three 4th order shorter sequences based on the observed succession of distinct erosive phases identified on 3D horizontal data.

Furthermore, the existence of an additional erosive phase registered between SB 2.4 and SB 2.6 is demonstrated by the same method. The 4th order sequence between SB 2.6 and SB 3.0 will be discussed in chapter 5.6 and will illustrate the deep incision related to the 3.0 Ma sequence boundary marking the inferior portion of the complex hiatus, recorded at the base of the Gulf coast Pleistocene. Thus, the major unconformity present at the top of the Pliocene is the result of two superposed major fall in relative sea level (2.4 and 3.0 Ma) which partially eroded lesser amplitude eustatic oscillations identified in this study as distinct erosional phases. A synthetic table for the entire Gulf coast Pleistocene will be displayed at the end of chapter 5 to compare the fourteen 4th order sequences described by Wornardt and Vail (1991) to the twenty successive erosional surfaces described in this study. This research tends to demonstrate that the periodic 0.1 Ma 4th order sequences, similar to the ones recognised in the eight cycles of the upper Pleistocene can be identified (when preserved) over the entire Gulf coast Pleistocene (0 to 2.8 Ma).

5.5 SB 1.85 to SB 2.4: a large 4th order sequence.

Introduction

This interval represents the longest and the more contrasted 4th order sequence registered during the Gulf coast Pleistocene. It is characterised by a deep erosional lowstand corresponding to a major fall in sea level related to the Nebraskan cold period correlated to the Danube continental glacial stage. The rapid warming occurring during the next interglacial (top Nebraskan) is marked by a prolonged condensed section (fig. 5-6, D. Pentaradiatus) and by the high amplitude flooding event known in the Gulf as the "Discoaster Brouweri" main flooding surface (fig. 5-6 and Annexe 2). On the magneto-stratigraphic curve (fig. 5-6), it is also striking that this 0.65 Ma long sequence exactly matches the inferior portion of the reversed Matuyama epoch, below the Olduvai normal event 1.9 to 2.48 Ma. This cold period followed by a phase of global high sea level is registered as thick progradations and large deltas on most passive margin in the world (Niger Delta, Offshore Brunei, both Atlantic margins, G. Stampfli oral communication; Barber, 1981 ; Bally *et al.*, 1985 ; Bally, 1989) .

Rapid sea level movement can be identified on the base of 2D and 3D seismic data by picking out the horizontal shifts in sedimentary facies registered on the shelf. Similarly their responses on well logs (massive lowstand progradational sands and homogeneous draping highstand shale on top) make them very easy to recognise, interpret and correlate laterally. The cyclic superposition of thick and coarse deltaic sands with continuous strata of shale sealing them at their base and top constitute ideal condition for hydrocarbons stratigraphic traps. Exact location and orientation of incised valleys, distributary channels and mouth bars, as well as delta lobe progradation direction and exact delimitation as identified by 3D horizontal images are precious information enabling to precise lithology content and to avoid drilling dry holes.

Observation

Three seismic horizons have been interpreted in the interval between the SB 2.4 to SB 1.85 sequence boundaries and each correspond to a distinct sedimentary event recorded on well logs, vertical sections and horizontal facies reconstruction:

- 1.The basal 2.4 Ma type 1 major sequence boundary
- 2.The thick sand progradation and rapid shoreline retreat connected to the rapid rise in sea level ("catch up cycle" in which sedimentation initially lags behind creation of accommodation space and then accelerates to fill the accommodation space created (Soreghan & Dickinson1994).
- 3.The highstand silt and shale partially eroded by the overlying SB 1.85 erosional surface.

Well log data

On the base of well log patterns (fig. 5-30), the three distinct assemblages defined above can be recognised and interpreted as:

- 1) a shaly and silty interval located below the massive sands (below SB24 interpreted horizon) showing transgressive backstepping trends intersected by sandy peaks attributed to SB 2.4 lowstand channels from correlation with amplitude maps.

- 2) the massive thick sandy interval between interpreted horizon SB24 and LATEPLIO in which it is difficult to distinguish, on the base of well logs only, between progradational sands and incised valley fill. This subtle distinction in well log pattern can be made on Well 3 at the level of LATEPLIO +40 (fig. 5-30, well 3). The inferior half of the thick sand signal has a blocky aspect interpreted as an incised valley fill whereas the upper half shows a prickly signal corresponding to progradational sands. This log interpretation is confirmed by the seismic facies encountered on amplitude maps at the corresponding levels (see Well 3 location on fig. 5-35 and 5-36).

- 3) a shaly and silty interval resting on the top of the basal sands, very resembling to the one described above, intersected by lowstand sandy channels attributed to SB 1.85 (Well 4, LATEPLIO -44, fig. 5-39).

Such a gross subdivision is the result of sequential analysis realised on the base of well log data and vertical seismic sections following the sequential interpretation procedure in 3.4 without taking into account the fine resolution tool provided by 3D seismic data. When interpreting the well log patterns together with amplitude maps it becomes possible to define at least 5 distinct superposed levels of erosion within this one sequence (numbered from C1 to C5 on fig. 5-30 and on amplitude maps, fig. 5-65).

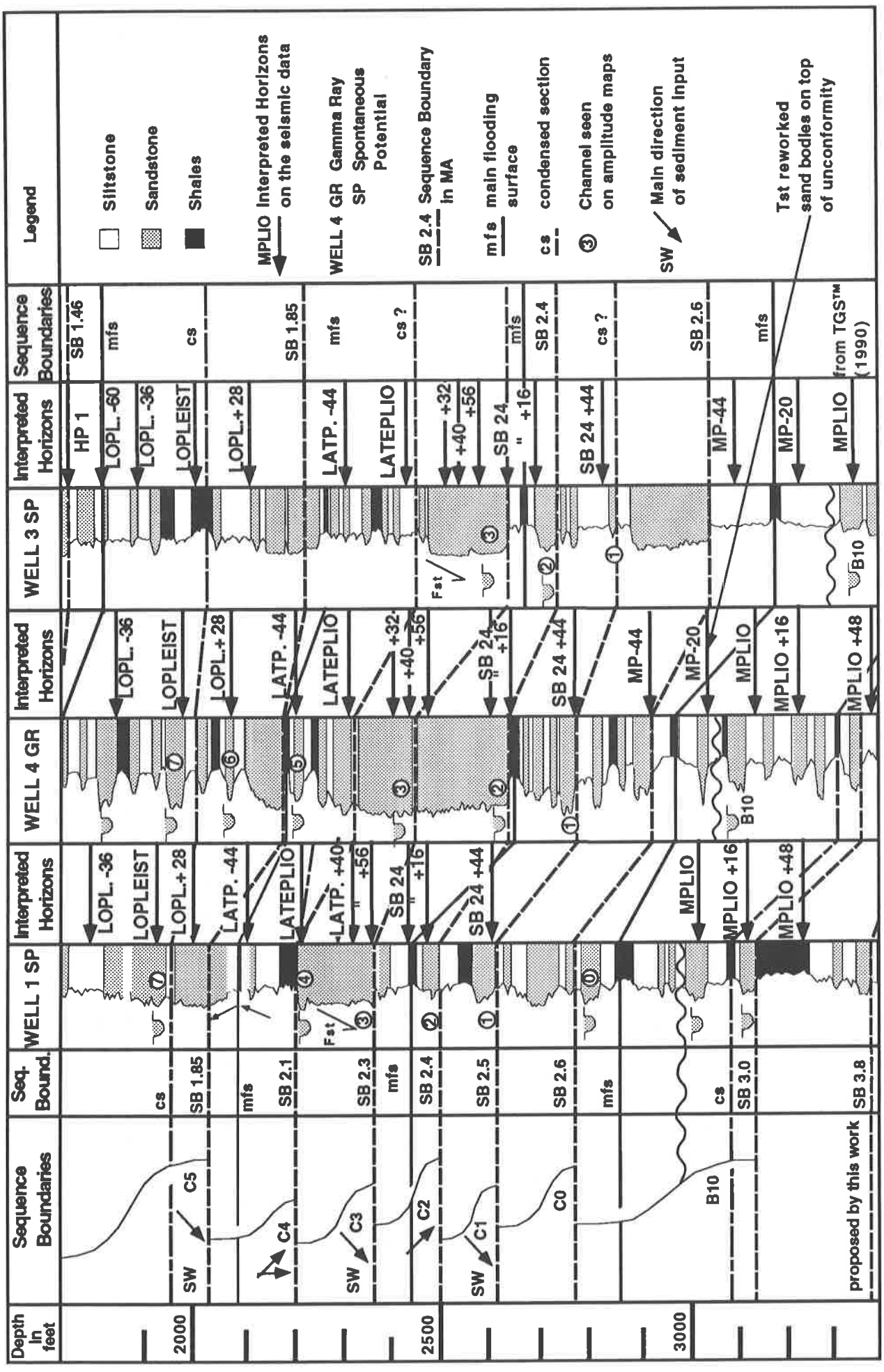

Fig. 5-30: Well log data sequential analysis for the lower half of the Gulf coast Pleistocene (SB 1.46 to SB 3.0). Sequence boundaries on the right from TGS ™ (1990) and the proposition of this study to the left based on observations of successive distinct erosional phases (B10 to C5, see table 1).

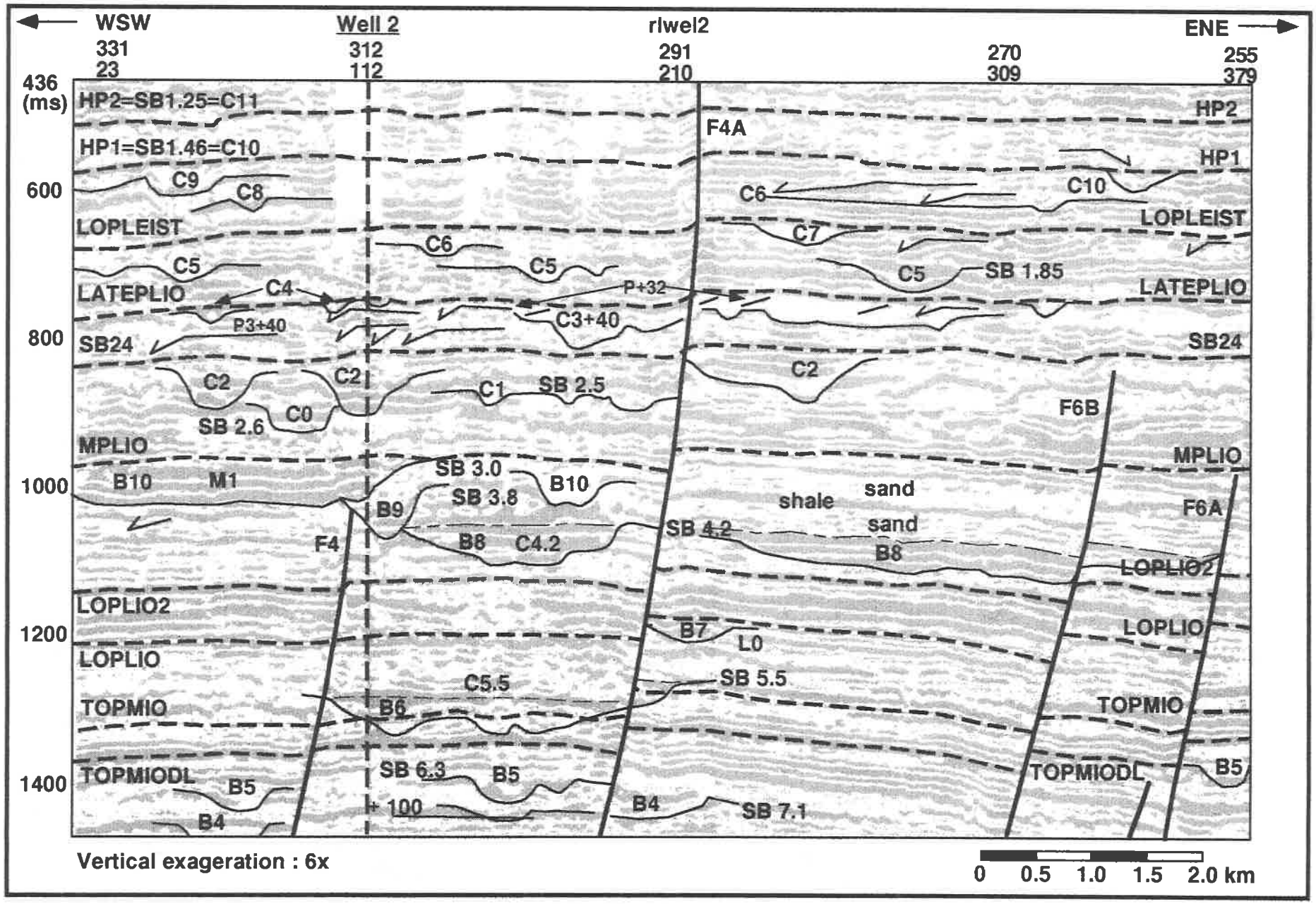

Fig. 5-31: ENE-WSW randomline running through Well 2, perpendicular to the main direction of sediment input intersecting all major erosional features (see fig. 3-2 for location). Raster density seismic data with superposed interpretation and location of erosional surfaces (C = Gulf coast Pleistocene, B = Middle and Late Miocene).

The distinction and correlation of channels from well to well would be totally impossible on the only basis of logs and vertical seismic data. The most convincing argument provided by 3D horizontal images in sorting out superimposed phases of deep erosion in periods of long-lasting lowstand is the possibility to distinguish the different channels according to their base level depth , orientation, size and degree of sinuosity.

Vertical seismic section and amplitude maps

On an oblique ENE-WSW randomline running in parallel to the present shoreline through Well 2 (fig. 5-31), the two above mentioned horizons (SB24 and LATEPLIO) delimit a sandy interval showing progradations and are intersected by several channels. It is characterised on the seismic section by a transparent and hummocky seismic facies. Fifty amplitude maps and volume attributes maps have been calculated from these two horizons over an interval of 200 m. Volume related attributes and in particular reflection intensity maps allow to unveil subtle buried channels not identified on amplitude maps and to bring several superposed events into one single plane. Attribute mapping constitute an important additional tool for the observation of the succession of sedimentary facies (see Chap. 4). To illustrate and summarise this complex succession, height amplitude maps are presented below, starting from the deepest portion of this sequence.

The map displayed on figure 5-32 represents the superposed results of the interpretation of several amplitude maps and volume related amplitude maps over an interval of 20 ms centred around the SB24+44 level (see fig. 5-30 for location on logs). SB24+44 is an horizon seiscrop calculated 44 ms below and parallel to SB24 horizon. On this map, two distinct generations of deep erosive channels can be identified.
C1: The deepest channel system (C1) shows profound and broad incised valleys (up to 100 m deep and 1.5 to 2 km wide) flowing from the north-west to the south-east. Two C1 channels can be identified on the HP34 line to the NE of Well 3 (fig. 5-22, C1). The inner portion of Inline 260 (not presented here) intersects the broad erosive feature appearing in the upper right corner of the combined interpretation map (fig. 5-32). It shows a 2 to 3 km wide and 80 to 100 m deep incised valley fill. This system of incised valleys is associated to an erosive level situated 10 to 20 m below the level of erosion corresponding to SB 2.4 and is entirely distinct from it. It is interpreted as a SB 2.5 erosional phase.
C2: The same map intersects also the base of a second system of more sinuous channels (C2) running perpendicularly to the C1 broader incised valley. The more we go up in the sediment pile towards SB2.4 interpreted horizon, the clearer the C2 NW-SE trending erosive system becomes visible. Along the SB24+44 level (fig.5.32), one meandering channel (C2) is intersected by the HP34 and rlwel2 randomlines in the centre of the amplitude map (cross sections 5-22 C2 and 5-31 C2). The channel morphology on the vertical section (C2, fig. 5-31) shows a strong asymmetry consistent with its meandering aspect seen on the horizontal plane (outer bank erosion and point bar filling in the inner bank).

The next level considered is located some 30 m above the preceding composite interpreted map and 16 ms (about 17 m) below the SB24 interpreted horizon. On this amplitude map, the C1 channel generation is no more apparent and the image is dominated by NW-SE trending C2 channels (fig. 5-33 a and b). This observation confirms the affiliation of C1 to an erosional event distinct and anterior to the SB 2.4 phase of erosion. The two main NW-SE channels are intersected perpendicularly by HP34 randomline (fig. 5-22, C2) and show two 50 m deep channels (C2 and C2') rooted on the level of SB24 interpretation line. The C2' incised valley is intersected by Well 3 and the base of its sandy signal on logs defines the SB 2.4 Ma sequence boundary. The SB 2.4 sequence boundary on Well 4 which does not intersect any C2 incised valley is located higher, at the base of the thick prograding sands sealing the SB 2.4 erosional surface (fig. 5-30, and fig. 5-33b). Sequence boundaries on well log data in inner shelf conditions can therefore be placed differently depending if the wells intersect incised valleys or not. In most cases the sequence boundary is placed at the bottom of the incised valley sand but can also be located laterally along the downlap surfaces corresponding to the top of the incised valley.

The C2 channels develop proximal delta lobes in the local depression created by the F7 active growth fault. Two delta lobes and their associated distributary channels are intersected by the SB24+16 amplitude map (Lobe 1 and 2 on fig. 5-33). Lobe 1 lays below the SB24 interpretation line and would have been very difficult to identify on the base of vertical seismic section only (see L1, fig. 5-22). Once identified by its horizontal morphology on the amplitude map it can be located on the vertical line. Lobe 2 is partially visible along SB24+16 map intersecting only the basal portion of the delta lobe. The top of this progradational

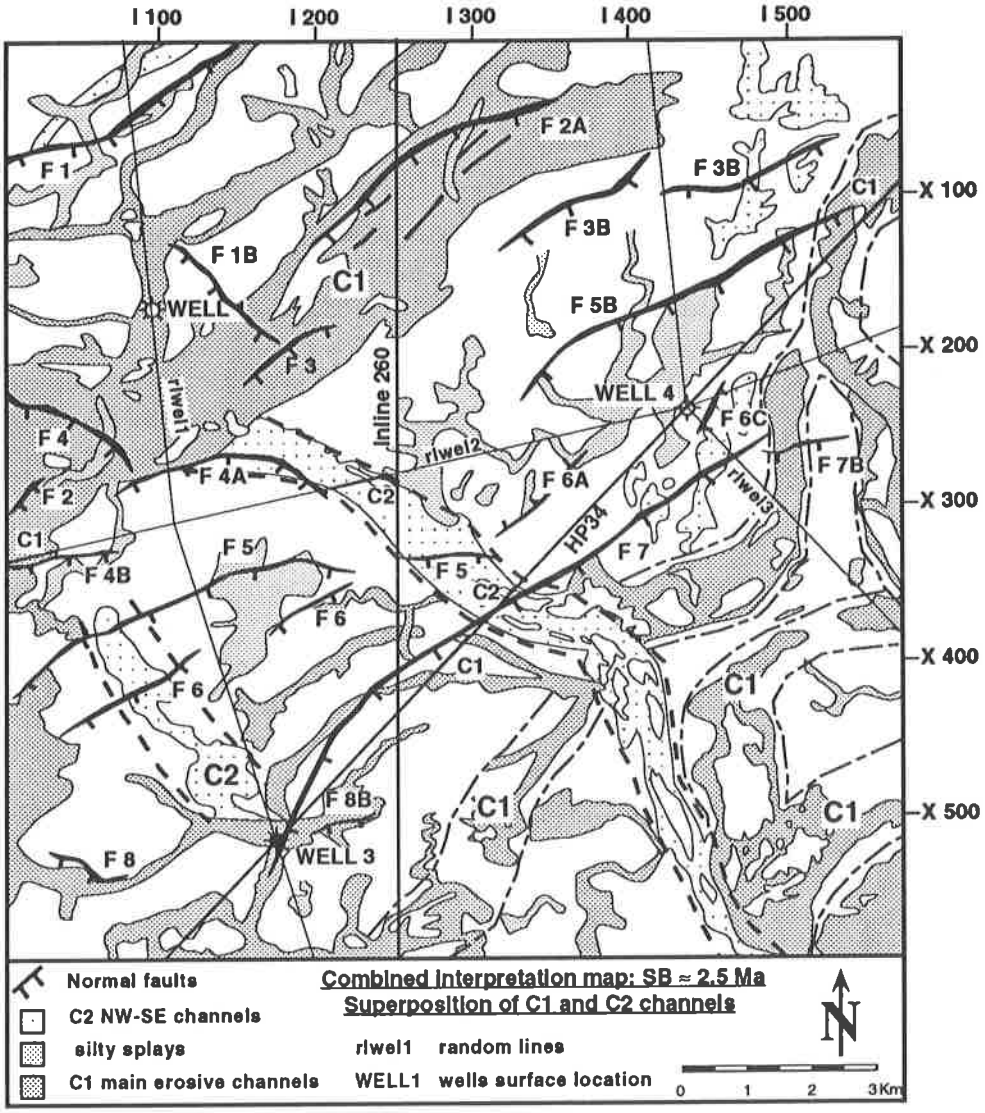

Fig. 5-32: Combined map based on the interpretation of the SB24+44 ms amplitude map and of the reflection intensity volume attribute map calculated 15 ms above and below SB24+44 ms. TWo superposed generations of erosional features: C1 NE-SW incised valleys (SB 2.5) and C2 NW-SE shallower channels (SB 2.4).

delta lobe (L2) is intersected on the next amplitude map obtained along the SB24 interpreted horizon (fig. 5-34). The progradation of the L2 lobe is illustrated on Inline 260 (fig.5-23 p) just below the SB24 interpretation line.

Figure 5-34 shows that the L2 delta lobe has stepped back with time of a few kilometres to a more proximal position, laterally shifting the secondary L1 lobe to its new position (Lobe 1S, fig. 5-34b). The displacement towards the NE of the small L1 lobe can be seen on randomline HP34 (fig 5-22). L1 S is juxtaposed to the larger L2 lobe. The vertical section on figure 5-22 indicates a third larger fan lobe intersection (L3) draping the three piled up delta lobes below. The best amplitude map to visualise the horizontal morphology of L3 lobe is obtained by cutting 56 ms below the LATEPLIO interpreted horizon (fig. 5-35). This slice intersects the data set some 25 m above the SB24 horizon and presents a new generation of erosional and associated depositional features (C3). The L3 lobe can be interpreted as a phase of still-stand progradation marking a third shift in position of the L1 and L1 S lobes associated with the C2 generation of NW-SE sediment input on the shelf. Its flat top could be the result of the following C3 erosional phase (L3, fig, 5-22).

C3: The most striking feature corresponding to the C3 erosional phase is a 2 to 3 km wide and 60 to 80 m deep incised valley flowing from NE to SW indicated in black (positive amplitude) on figure 5-35 a.

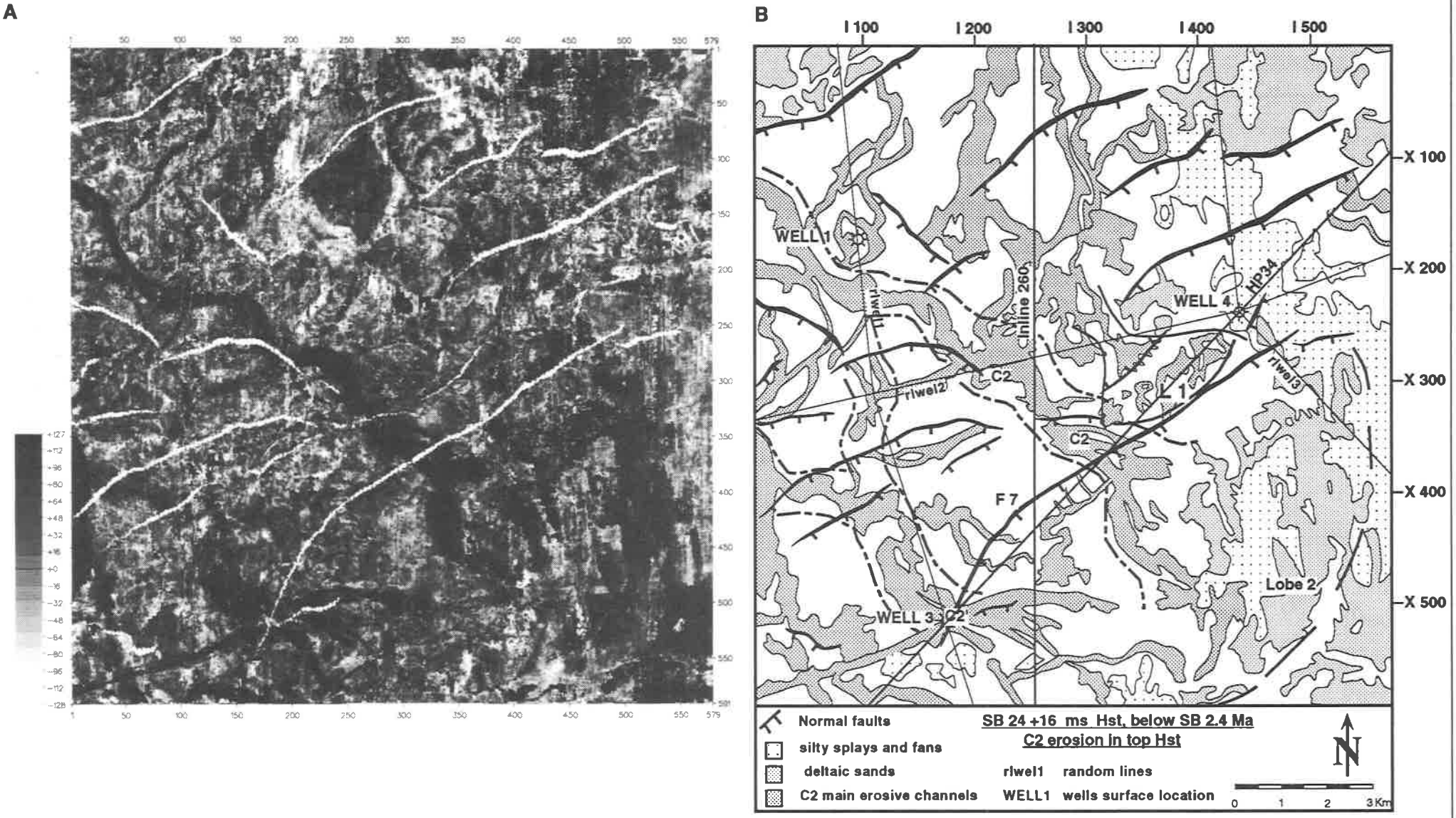

Fig. 5-33: ***a.*** *Amplitude map 16 ms below SB24 interpreted horizon (black are positive amplitudes, fault traces in white).* ***b.*** *Interpretation of a distributary channel (C2) and proximal delta lobe sedimented down the main growth fault (F7). Note the presence of a secondary lobe (L1) and associated channel at the back of the main lobe (Lobe 2).*

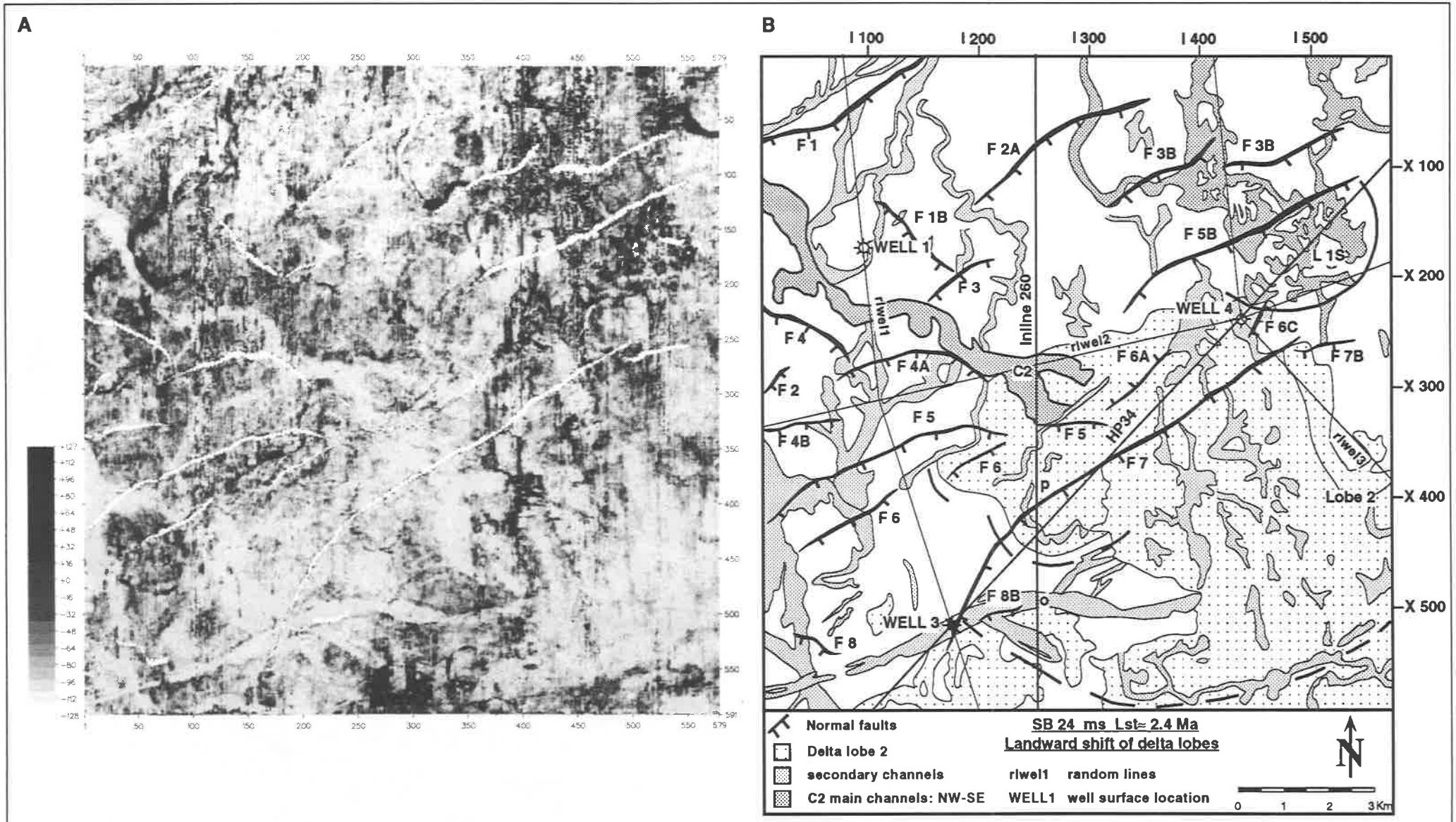

*Fig. 5-34: **a.** Amplitude map calculated along SB 24 interpreted horizon (negative amplitude in white). **b.** Backstepping or landward migration of the delta lobe seen on fig. 5-33 (Lobe 2, C2). L1S corresponds to the shifted L1 lobe seen on fig. 5-33. It implies a short phase of rapid sea level rise taking place before the next erosion (C3, fig. 5-35).*

This incised valley is similar in size and orientation to the one observed along the C1 erosional surface (fig. 5-32). Besides the incised valley and the L3 fan lobe, the amplitude map on figure 5-35 intersects parallel sand bodies (oriented NW-SE) in the upper left corner of the image. Their interpretation as foresets belonging to a large delta fan associated with the C3 incised valley is confirmed by the two following amplitude maps calculated above this level.

Figure 5-36 (LATEPLIO+40), amplitude map 16 ms above figure 5-35 shows the same C3 incised valley but in a more proximal position. This image is interpreted as the large distributary mouth and proximal deltaic progradation of the C3 main channel. This interpretation is confirmed on the rlwel2 vertical randomline (fig. 5-31 and fig. 5-36b for location of rlwel2). On this seismic section, the broad incised valley is indicated as a transparent channel (C3+40) and the corresponding proximal progradation is seen at the same level further offshore (P3+40). To follow the lateral and vertical migration of these facies identified on amplitude maps and vertical sections, an amplitude map is calculated 8 ms (about 9 m) above the LATEPLIO+40 level.

Figure 5-37 (LATEPLIO+32) shows a map with homogeneous amplitude distribution intersecting arched reflectors interpreted as delta lobe foresets. On an oblique vertical section (fig.5-31, P+32) this phase of distal progradation is represented by shallow shingles above the distributary mouth bar and by bigger downlaps further offshore on the footwall block of fault F4a. The top level of progradation lays just below the continuous strong amplitude reflector interpreted as the LATEPLIO horizon.

The succession and landward migration of the sedimentary facies observed on the 3 preceding maps implies a rapid rate of relative sea level rise greater than the volume of sediment input on the shelf. This vertical transition from an incised valley bed to the distributary mouth bar, to the more distal part of the delta lobe associated with the C3 erosional phase is characteristic of a "catch up" cycle on the inner shelf where the rate of sediment input cannot keep pace with the rapid creation of accommodation space (Soreghan & Dickinson, 1994). It expresses the extremely rapid period of sea level rise following the main lowstand event between 2.4 and 2.2 Ma.

C4: This large delta lobe progradation is sealed by a silty and shaly interval corresponding to the continuous LATEPLIO interpreted horizon. An amplitude map along that horizon (fig.5-38) shows a myriad of shallow and narrow channels represented by positive signals (red-orange) within a negative loop (violet). Some of the small channels can be recognised on vertical sections (in raster display but not in normal wiggle traces) and some of the smallest ones are only appearing on the amplitude map because of their lateral continuity. Two examples of these shallow channels are shown on the oblique randomline (fig. 5-31, C4) and on the north-south Inline 260 intersecting three time the same meandering channel (C41, C42, C43 on figs. 5-23 and 5-38 a).

The sequential analysis on well logs indicates that the LATEPLIO horizon corresponds to the base of the silt and sands at the top of the thick prograding sands below (fig. 5-36). This could be interpreted as the top Lowstand condensed section preceding the regular transgressive phase of the large 4th Order sequence (SB 2.4 to SB 1.85) as indicated by the TGS™, (1990) coastal onlap curve. But the presence of erosional channels as deep as 30 to 40 m rooted right on top of this shaly surface (C4) has to correspond to an additional short term relative fall in sea level occurring during a still stand period of the SB 2.4 to SB1.85 transgressive phase.

Figure 5-38 c displays in colour the delta time or isopach map for the interval between SB24 and LATEPLIO interpreted horizons respectively C2 and C4 erosive phases. The minimum values are indicated as hot colours and the thickest intervals are indicated by cold shades. The colour scale is compressed to obtain an optimum contrast in the lower right corner of the image where the two delta lobes (Lobe 1 and Lobe 2) interpreted on figure 5-33 b are recognised. On the vertical seismic section on figure 5-22 it was possible to identify three different delta lobes (L1, L1S and L3) but the large and flat L2 lobe was not clearly visible on vertical profile (fig. 5-22 small shingles above C1 channel to the right of Well 3). The SB24 horizon was interpreted on top of the L2 gently domed lobe and its morphology is made visible by an isopach map calculated between the continuous LATEPLIO datum and the SB24 horizon (slightly shifted upward by the underlying L2 lobe). This lobe shows a very clear birds-foot morphology with 4 to 5 radial branches (in red). On the left hand side of the lobe, the meandering channel identified on LATEPLIO amplitude map (fig.5-38 b) is indicated in red expressing the subtle diminution in thickness between LATEPLIO and SB24 caused by the interpretation of LATEPLIO at the base of the channel. Furthermore, the secondary deltaic lobe L1 recognised on the vertical section (fig. 5-22) as laying below

the SB24 horizon (doming it up) or on the amplitude map (5-33 b) is marked by a red arch at the back of the F7 fault, on the left of the distributary mouth of the main L2 lobe. Thus, isopach maps constitute a valuable tool to precise thicknesses and morphologies of visible sand bodies but also contributes in unveiling subtle sedimentary features that can be missed by vertical sections and amplitude maps.
Above the LATEPLIO horizon and the C4 erosive phase are two to three continuous reflectors corresponding to the transgressive systems tract and to the main flooding surface containing the "Discoaster Brouweri A" condensed fauna assemblage. They are visible on the vertical seismic section of figure 5-31. This interval of sedimentation is related to the strong incursion on land of coastal onlap, registered on the totality of the Gulf shelf.
C5: These continuous loops are intersected by deep erosive channels (60 to 80 m) attributed to the SB 1.85 fall in relative sea level (see for instance, fig. 5-31, C5). The horizontal morphology of the corresponding channels can be seen on an amplitude map calculated 44 ms (about 50 m) above the LATEPLIO horizon (fig. 5-39 a and b). These two maps show a system of incised valleys running ENE/WSW similar to the C1 and C3 major erosive phases. The probable delta lobe progradation associated with these incised valleys must be found further offshore to the south-west.

The amplitude map on figure 5-39 a (LATEPLIO -40) is located 4 ms below the map on figure 5-39 b (LATEPLIO-44 ms). Very little changes in seismic facies are observed between the two. But the amplitude map calculated 4 ms higher in the 3D volume presents a totally different sedimentary setting (fig. 5-39 c, LATEPIO-48 ms). The deltaic lobe progradation towards the south-east seen in the upper left corner of the image is confirmed by vertical seismic sections (fig. 5-22, L5) and is also intersected on figure 5-24 (LOPLEIST+28). It indicates a succession of sedimentary facies similar to the C3 phase (NE-SW progradation associated with rapid relative sea level, over large incised valleys, fig. 5-35 to 5-37).
The systematic observation of the vertical evolution in reconstructed sedimentary facies interpreted from horizontal seismic facies maps over the three initial subdivision of the SB2.4 to SB 1.85 sequence (lowstand incised valleys-massive sandy progradation-transgressive and highstand silt and shale) enables to propose further subdivisions based on the recognition of distinct erosional phases.

Conclusion

As no faunal data is available in this study for the Pleistocene, the ages attributed to each of the proposed subdivisions are purely conjectural and based on the "forcing" of pre-established local eustatic curves on the well log data. By doing so we assume that the existing correlation and dating are correct and can be used as chronostratigraphic correlation tools within the Gulf of Mexico basin. This provides a qualitative framework in which cycles and successive phases of erosion can be put in perspective but surely not dated nor correlated outside the basin. Similarly, no true scale curve of coastal onlap can be established as the portion of the Gulf of Mexico shelf studied here is limited to a square of 15 by 15 km through which sedimentary facies simply come and go ! The input of 3D seismic stratigraphy enables to further the vertical resolution proposed by sequential analysis done on the base of vertical seismic sections and well log data. The pre-existing 4th Order sequence between SB 2.4 and SB 1.85 can be subdivided at least into three shorter 4th Order sequences by integrating the information given above on figure 5-30. They are listed and summarised below, from top to base:

- the **C5** ENE-WSW deep erosion phase (LATEPLIO-44, fig.5-39 a, b and c) corresponds to the SB1.85 sequence boundary indicated as channels number 5 on the well log table (fig. 5-30).

- The **C4** (LATEPLIO, fig. 5-38) shallow meandering channels mainly oriented towards the south to south-east and developed on top of the massive sands is attributed to a 2.1 Ma minor sequence boundary (channels number 4 on fig. 5-30). This hypothesis is supported by the nanno-fossils condensed intervals curve presented by Shaffer (1990) , which shows a gap or "non-condensed" interval between the Discoaster Pentaradiatus and the Discoaster Brouweri condensed sections thus confirming the presence of an erosional phase (fig. 5-6, Plate 3).

- The **C3** erosive phase (LATEPLIO+32, +40, +56; fig. 5-35, 36, 37) and well developed deltaic progradation towards the SW corresponds to the maximum of Lowstand around 2.3 Ma immediately followed by the drastic rise of relative sea level flooding the entire shelf (catch up cycle). This corresponds on logs to the base of the incised valley thick sands and laterally to the small silty interval on Well 4 intercalated within the massive sands (fig. 5-30, channels number 3).

- The **C2** erosive phase (SB2.4, fig. 5-33 and 5-34) and associated progradation towards the SE

corresponds to the SB 2.4 sequence boundary or to the primary pulse in fall of relative sea level after the Highstand phase corresponding to the Discoaster Surculus condensed section. The main reasons for splitting the major lowstand phase into C3 and C2 is the difference in types of channels, orientation and sinuosity as well as the difference in the base level of channels. The C3 channels are definitively posterior and higher in the sediment record than the C2 channels which cut into the underlying shale of the preceding relative high sea level (see channels 2 and 3 on logs, fig. 5-30).

- And finally, the **C1** deep erosive phase (SB24+44, fig. 5-32) oriented towards the SW, below the SB 24 base level is definitively distinct from the C2 phase as demonstrated by the difference in channel size, orientation and base level. The condensed interval seen on logs below the C1 channels was primarily interpreted as a condensed section or top lowstand surface within the 2.4 to 2.6 Ma subjacent 4th Order sequence. It is proposed that the C1 erosive phase corresponds to a 2.5 Ma sequence boundary distinct from the SB 2.6 Ma found further down in the seismic data. The shaly interval below SB 2.5 is interpreted as a reduced highstand systems tract belonging to the SB 2.5 to SB 2.6 Ma short duration 4th Order sequence.

The 3D sequential analysis of this complex interval shows that:

- In a given faulted sedimentary setting, erosive phases can be distinguished on the base of the orientation of erosive channels. In the studied area, drastic sea level falls tend to be marked by channels parallel to the local fault trend (C1-SB 2.5, C3-SB 2.3, C5-SB 1.85, see synthesis on fig. 5-30 and chap. 7) whereas gentle relative sea level fall (shallower meandering channels, C2 and C4) tend to be oriented perpendicular to the growth faults.
- Major lowstands can be subdivided into 2 distinct erosional phases:
  1) beginning of sea level fall is recorded on the shelf as shallow meanders developing fan lobes on the hangingwall of major growth faults.
  2) the maximum of lowstand is recorded as deep rectilinear thin channels and wide incised valleys.

This succession or gradation in erosional phases associated with major lowstand periods on the inner shelf is observed on four distinct sequences during Pleistocene:

- C9 and C10 erosional phases during the SB 1.46 Ma lowstand (fig. 5-65)
- C8 a, b and c (shallow channels and fans) followed by the deep incised valley attributed to the C8d phase.
- C2 and C3 erosional phases along the SB 2.4 lowstand
- C0 and C1 incised valleys at the SB 2.6 lowstand.

The observed reproducibility in sedimentary facies succession confirms that two distinct erosional phases can be recorded on the inner shelf in response to large lowstand events recorded as a single event on the outer shelf.

- Volume related attributes and in particular reflection intensity maps can help to distinguish successive closely spaced erosive phases by superposing several channels generation that can be identified by their differences in orientation, width, depth and degree of sinuosity.
- Isopach maps calculated between closely spaced interpreted datum indicate sand bodies thicknesses but can also reveal detailed morphologies of subtle objects unnoticed on vertical sections or on amplitude maps.

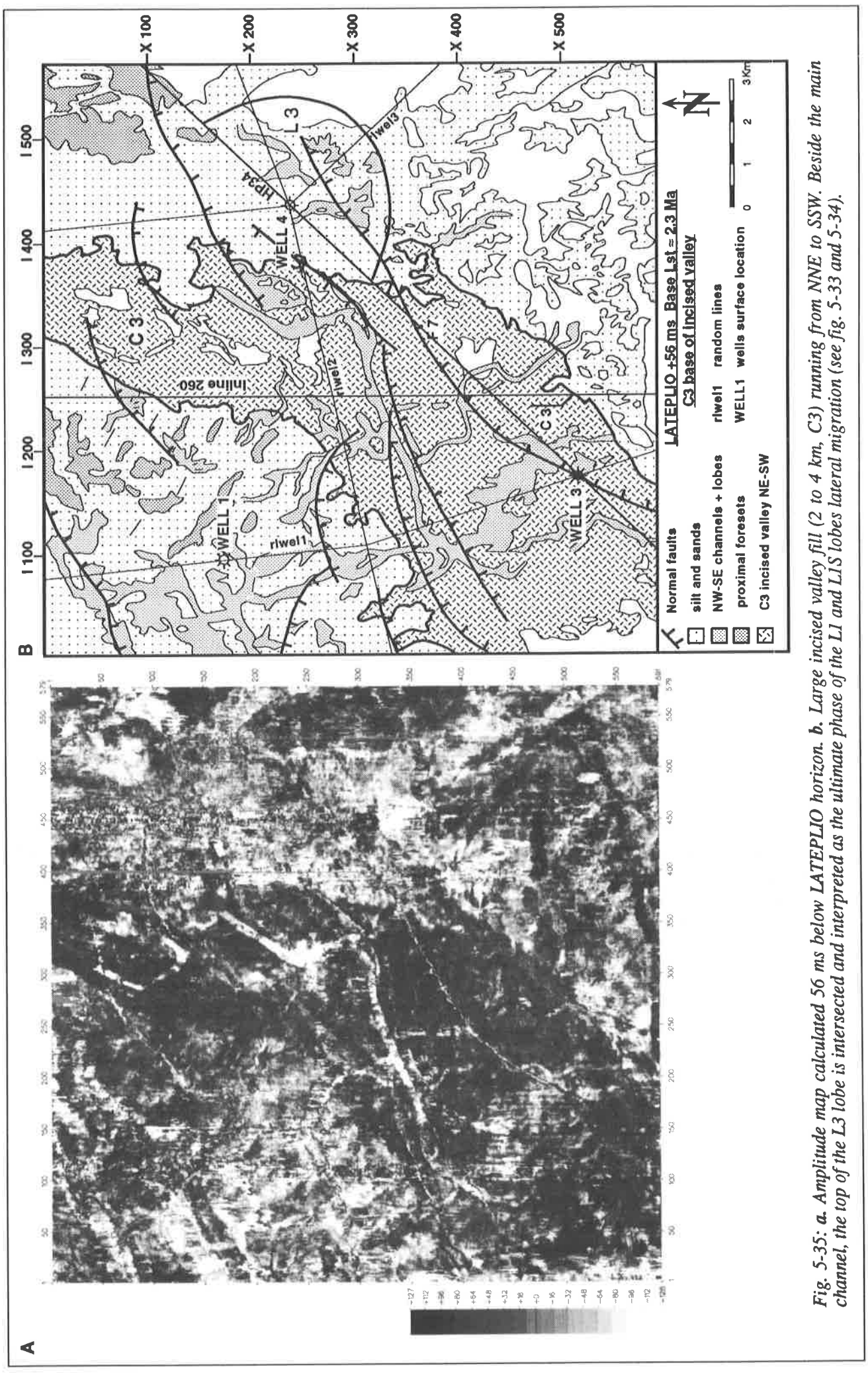

*Fig. 5-35: **a.** Amplitude map calculated 56 ms below LATEPLIO horizon. **b.** Large incised valley fill (2 to 4 km, C3) running from NNE to SSW. Beside the main channel, the top of the L3 lobe is intersected and interpreted as the ultimate phase of the L1 and L1S lobes lateral migration (see fig. 5-33 and 5-34).*

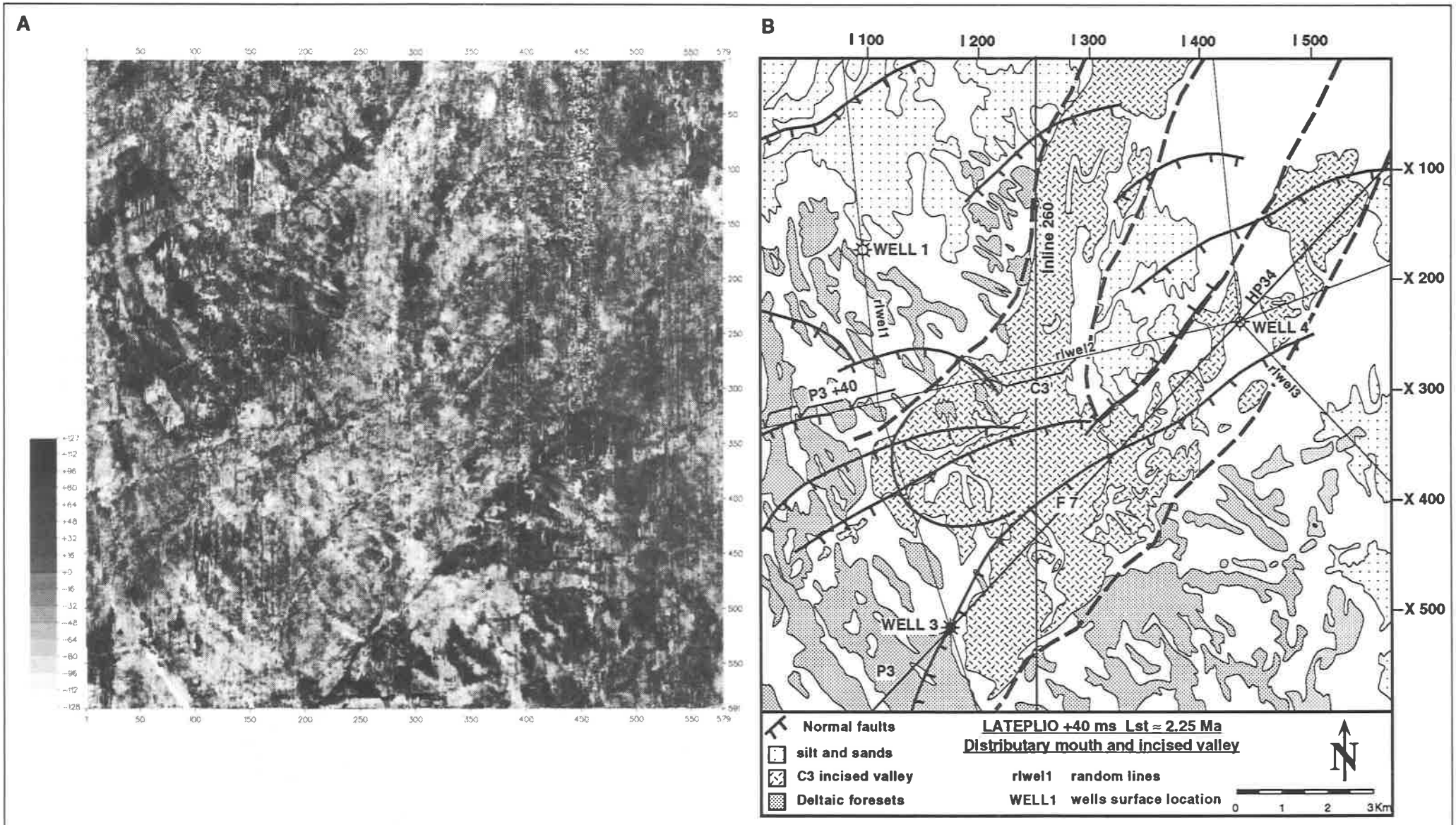

Fig. 5-36: ***a.*** *Amplitude map obtained 40 ms below LATEPLIO horizon.* ***b.*** *Interpretation of seismic facies shows very clear proximal foresets intersections and distributary mouth of the incised valley intersected on fig. 5-35.*

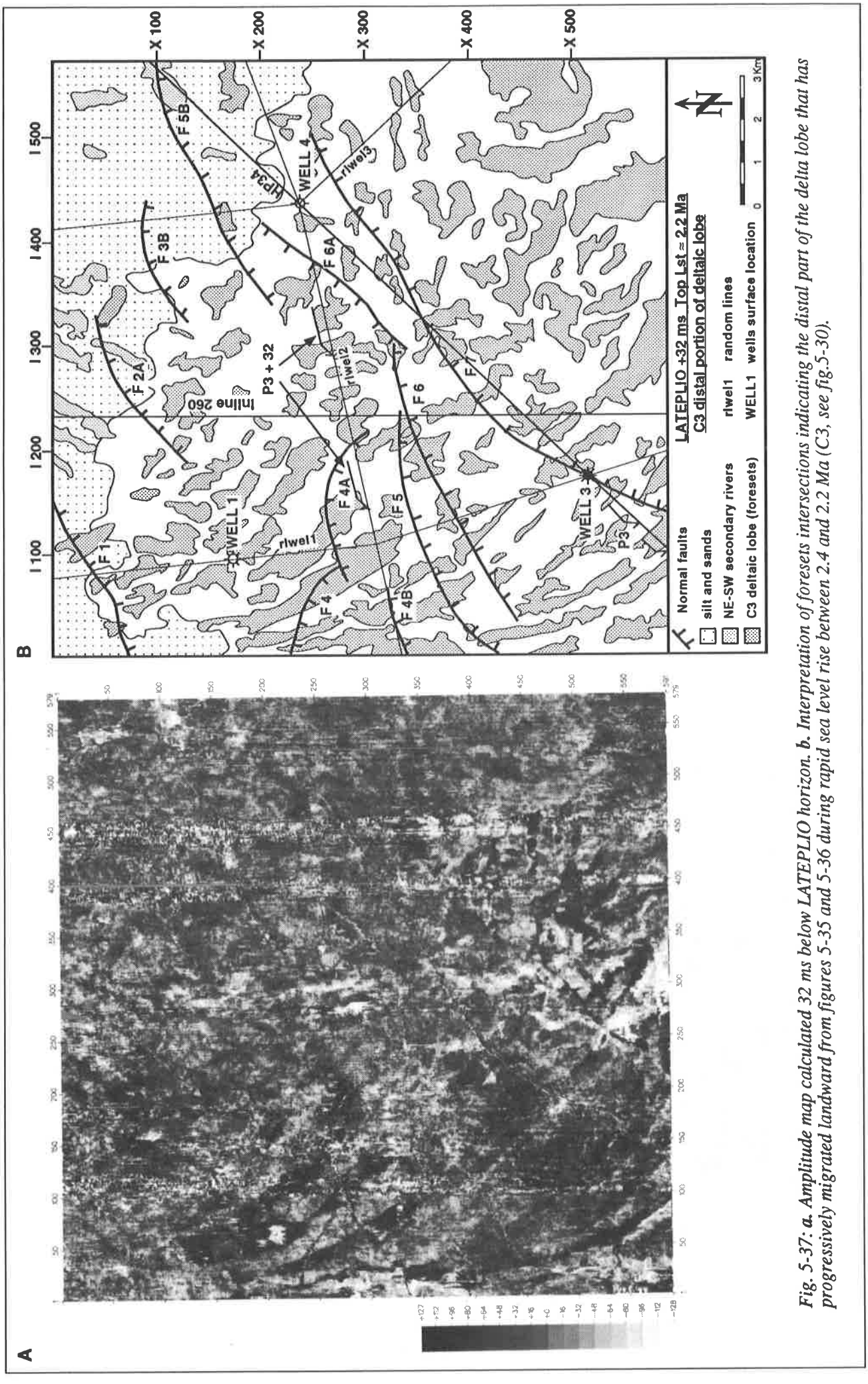

*Fig. 5-37: **a.** Amplitude map calculated 32 ms below LATEPLIO horizon. **b.** Interpretation of foresets intersections indicating the distal part of the delta lobe that has progressively migrated landward from figures 5-35 and 5-36 during rapid sea level rise between 2.4 and 2.2 Ma (C3, see fig.5-30).*

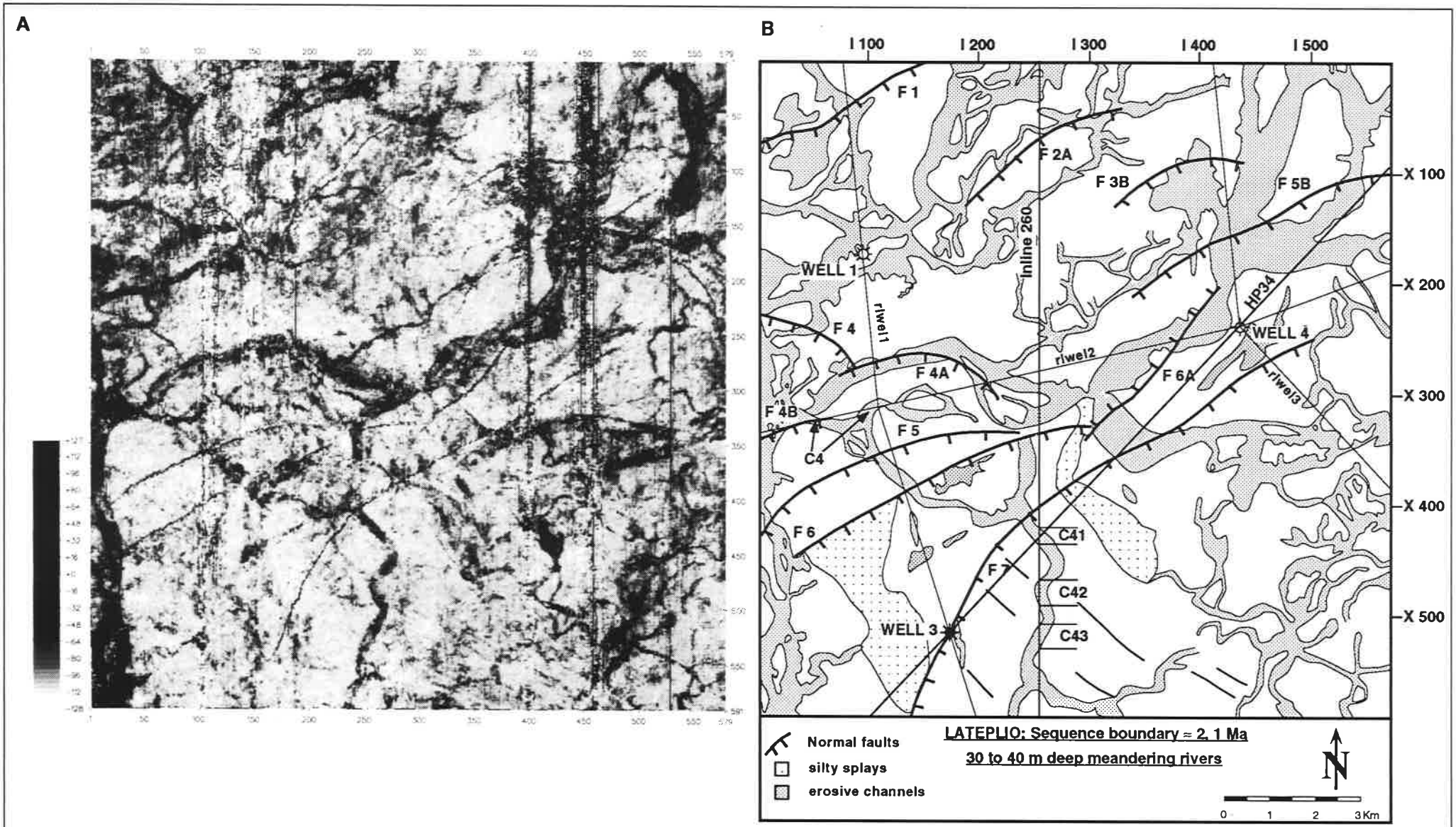

Fig. 5-38: ***a.*** *Coloured original amplitude map along LATEPLIO horizon. Violet corresponds to the negative amplitudes and orange to the positives.*
b. *Interpretation of complex system of shallow meandering channels (C4, positive orange amplitudes).*

Fig. 5-39: c. Drastic change in seismic facies 4 ms above LATEPLIO-44 showing the base of highstand delta lobe progradation towards the SW.

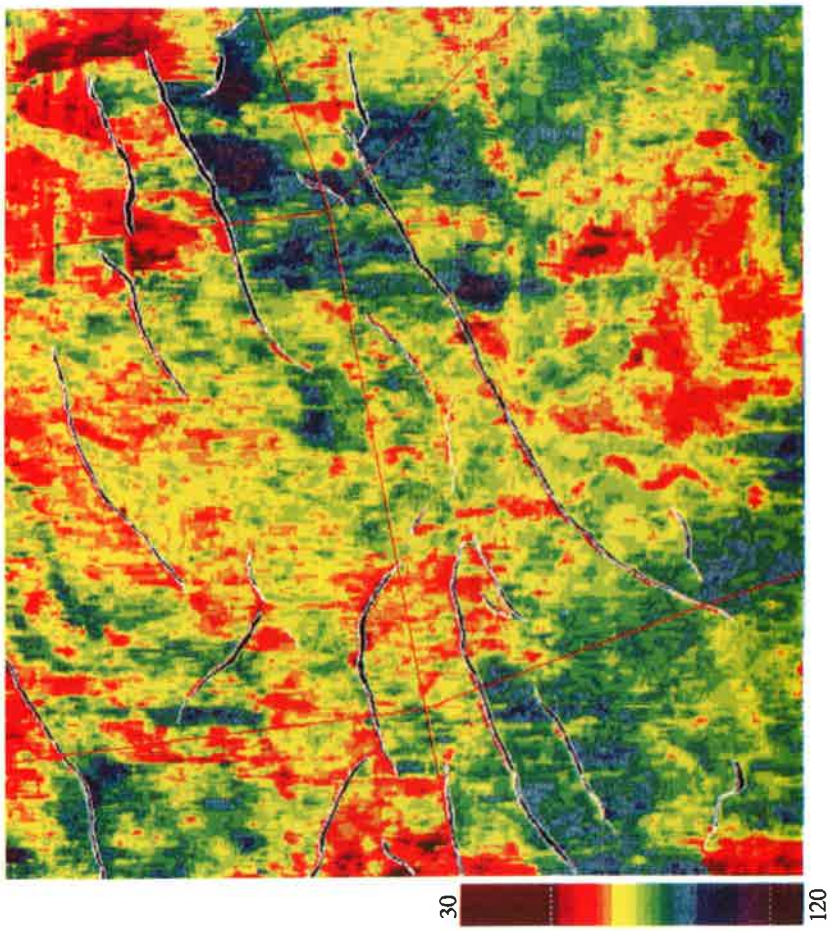

Fig. 5-38: c. Isopach map between LATEPLIO and SB24 interpreted horizon revealing the morphology of two delta lobes (L1 and L2, see fig. 5-33 b for location).

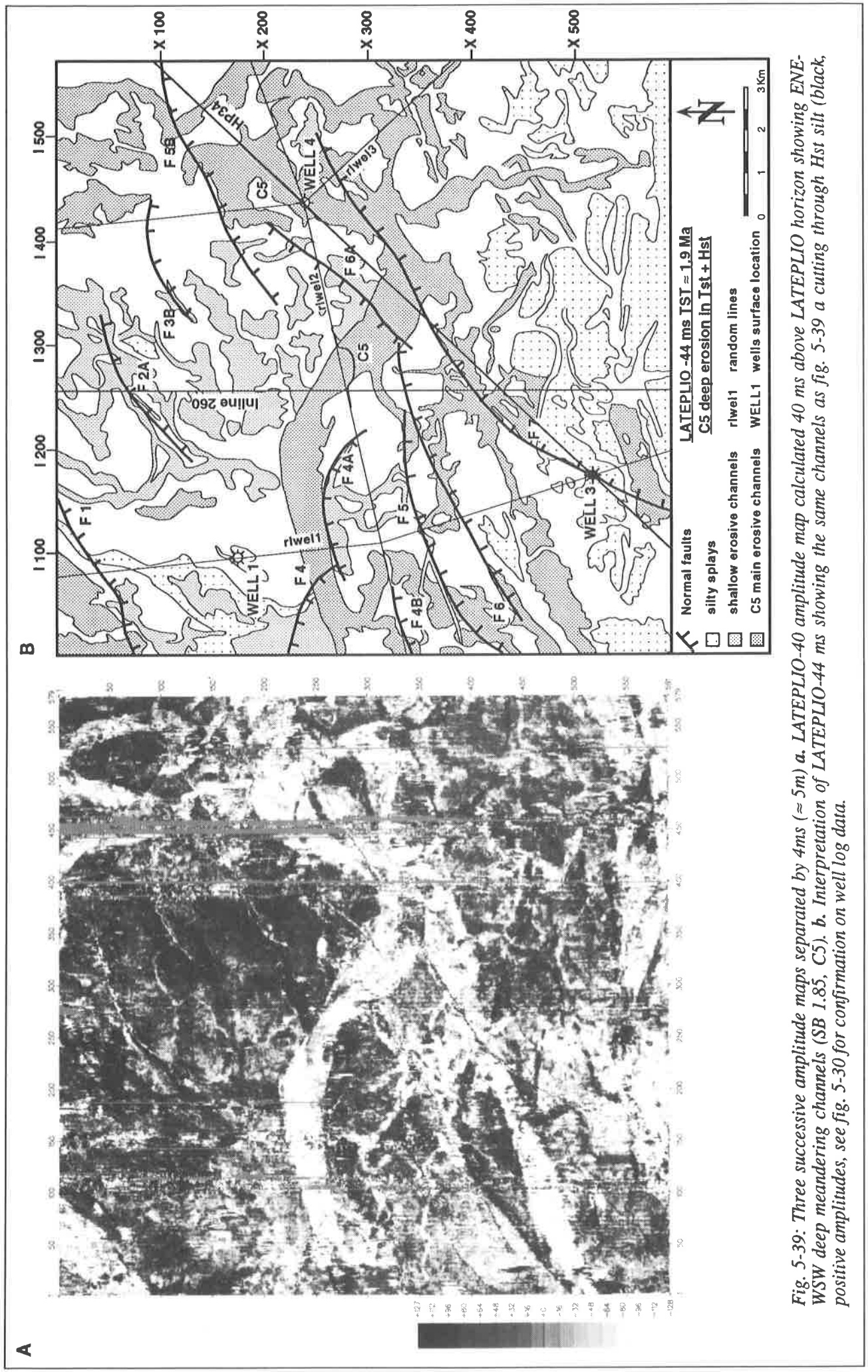

*Fig. 5-39: Three successive amplitude maps separated by 4ms (≈ 5m) **a.** LATEPLIO-40 amplitude map calculated 40 ms above LATEPLIO horizon showing ENE-WSW deep meandering channels (SB 1.85, C5). **b.** Interpretation of LATEPLIO-44 ms showing the same channels as fig. 5-39 a cutting through Hst silt (black, positive amplitudes, see fig. 5-30 for confirmation on well log data.*

5.6 Top Gulf coast Pliocene hiatus (2.6 to 3.0 Ma).

Introduction

This chapter discusses the Top Pliocene hiatus as observed in the 4th order sequence between 2.6 and 3.0 Ma. The important fall of relative sea level registered during the lowstand episode between 2.7 and 3.0 Ma is at the origin of most of the missing sections observed in the top Pliocene sediments on the Gulf coast shelf (Beard *et al.*, 1982; Wornardt & Vail, 1991) . This event is correlated to the beginning of the Nebraskan marine cold period (Danube European continental ice age). The lowstand event centred around 2.8 Ma is correlated to a minor cold period observed on the oxygen isotopic curves on a trend reaching a cooling maximum around 2.3 Ma (fig. 5-40, Plate 2). It corresponds to a strong fall in relative sea level on the eustatic curve from Haq et al. (1988) and to the strongest basinward shift on the coastal onlap curve produced by TGS™ (1990).

The limited portion of the Louisiana shelf studied here and the absence of fauna for the Plio-Pleistocene in the available wells make any quantitative discussion on the age of the Gulf coast Plio-Pleistocene boundary impossible. But observation of vertical seismic sections, well logs, horizontal amplitude maps and volume related attribute maps in that interval allow to identify and characterise two distinct erosive phases assigned to the 2.6 and 3.0 Ma main sequence boundaries (synthetic Neogene chart, fig. 5-40 a). A summary of the main features of all the sequences observed on the Gulf Coast Pleistocene is proposed as a conclusion to this chapter.

Observation

The base of the top Pliocene hiatus on the northern Gulf coast shelf is marked on most seismic lines by a continuous and homogenous amplitude reflector lying just below the major unconformity pictured on figure 5-41 (MPLIO, a and b). On the studied 3D data set, this positive amplitude reflector (red-orange) has been interpreted as the MPLIO horizon and is referred to as the "UP, Upper Pliocene marker" in the OCS Report on correlation of Cenozoic sediments for the Gulf of Mexico continental shelf (Courtney Reed & Layendecker, 1987) . It corresponds to the top Buliminella 1 zone that extends between 4.1 and 3.6 Ma (see Annexe 2). On the vertical section (fig. 5-41), a strong lateral increase in amplitude is observed along this horizon at the 312/112 co-ordinate (M1 on fig. 5-41 a and pointer on fig. 5-41 b). On the basis of the vertical section it is difficult to attribute this amplitude swell to any particular sedimentary feature.

On the well log data inserted in figure 5.41b the amplitude swell corresponds to the local increase of contrast in acoustic impedance between the thick sands and the silt and shale above and below. On Well 2, the sandy signal along the MPLIO horizon can be divided into an inferior part showing the typical square signal attributed to coarse sands found at the bottom of an incised valley fill and an upper portion showing a less sandy signal suggesting that the top of the channel is filled with finer material. On Well 2, the SB 3.0 sequence boundary is placed at the base of the incised valley sand. This interpretation is confirmed by the horizontal amplitude maps intersecting the M1 channel (fig.5-45 b, M1). A similar amplitude swell is observed down the F7 growth fault on the same seismic line and along the same horizon. It is correlated to the broad and shallow NW-SE trending M2 channel seen on figure 5-44 b) associated with the SB 3.0 erosional surface.

Five amplitude maps extracted parallel to the MPLIO horizon between SB 2.6 and the bottom of the highstand shale registered 50 m below SB 3.0 summarise the sedimentary facies succession registered above and below the Top Pliocene unconformity (see emplacements of maps along Well 1, fig. 5-30) :

- a: MPLIO-44 (fig.5-42 a) intersects the SB 2.6 sandy channels that cuts in the highstand silt below SB 2.6 (C0, fig. 5-65).
- b: The base of unconformity oblique truncation and transgressive onlaps are intersected by the MPLIO-20 map (fig. 5-42 b).
- c: MPLIO horizon (fig. 5-43) intersects the top of the SB 3.0 channels (B10, fig. 5-30,well 1 and 3) sealed by silty deposits (fig.5-30, Well 4).
- d: MPLIO+16 (fig. 5-44) cuts in the main sand bodies of the deep erosive channels associated with the SB 3.0 erosion and shows two superposed generations of incised valleys
- e: MPLIO+48 (fig. 5-45) intersects the top of the transgressive interval preceding the shaly main flooding surface recorded below SB 3.0.

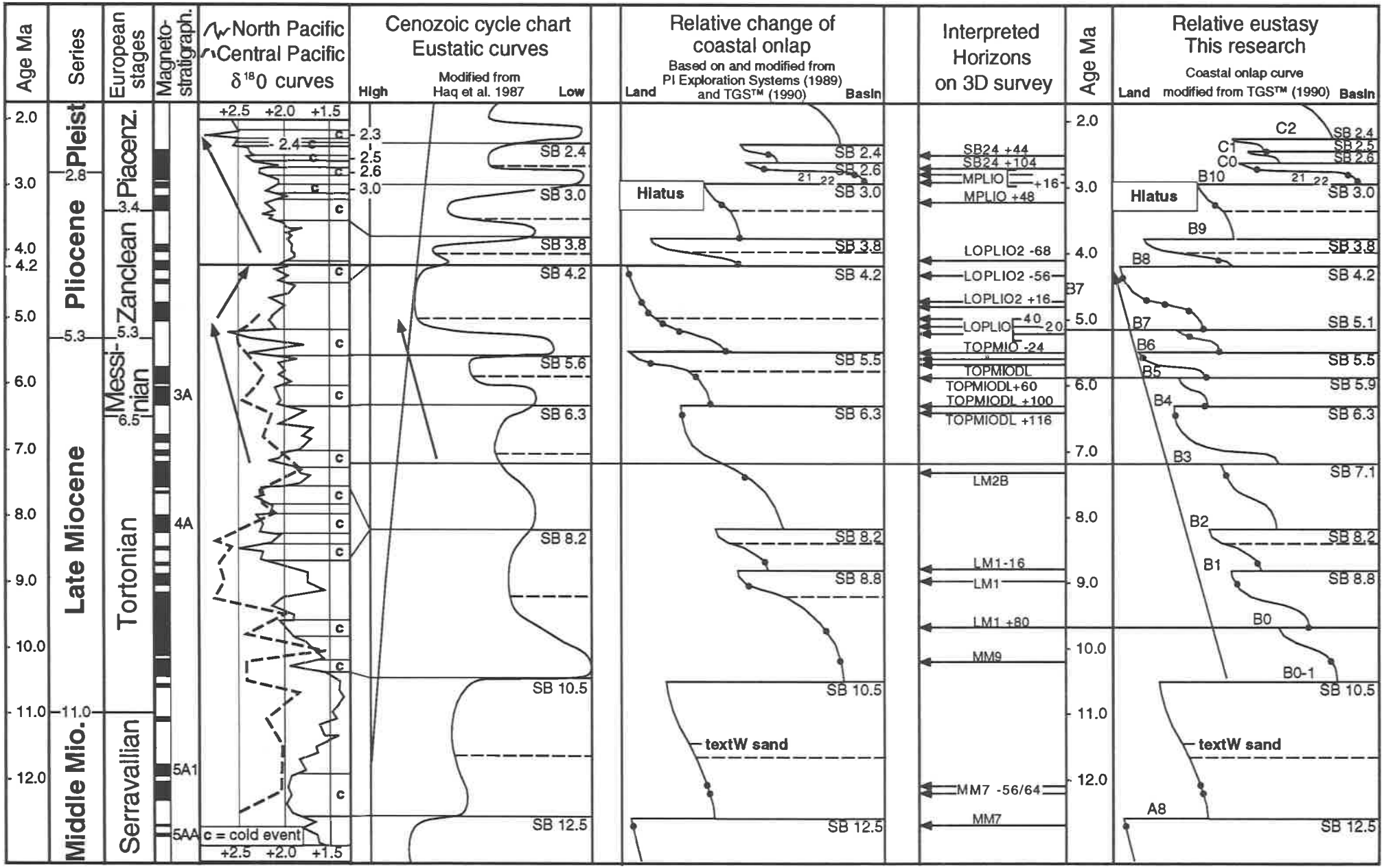

Fig. 5-40: Neogene synthetic chart with comparison of oxygen isotopes curves in the Pacific, global eustatic curves (Haq et al. 1987), a curve of relative coastal onlap for the Gulf of Mexico from PI Exploration Systems, (1989) and TGS™ (1990) and the curve of relative coastal onlap proposed by this study. Interpreted horizon on the 3D seismic data are indicated by black dots on the coastal onlap curve.

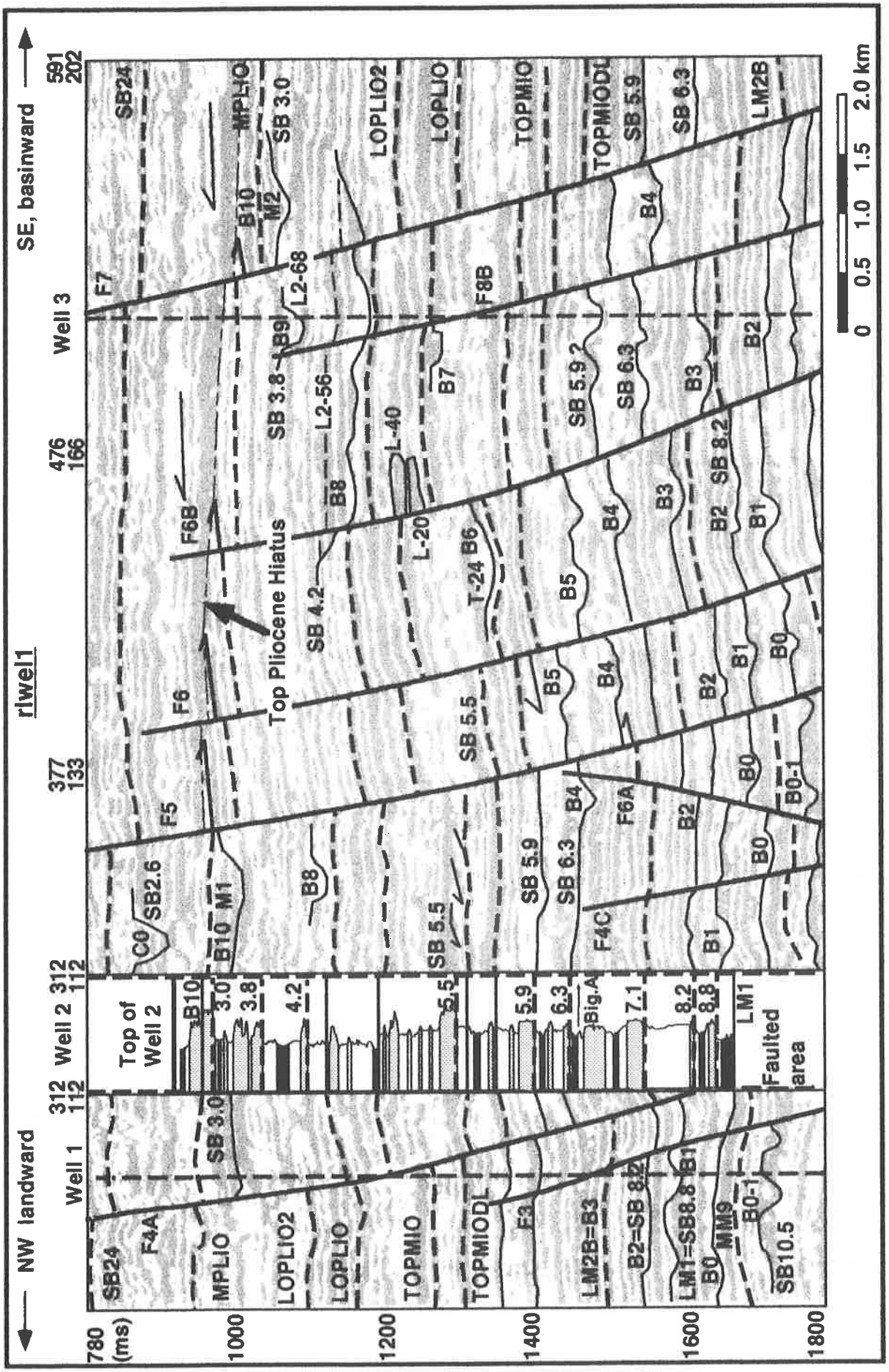

Fig. 5-41 : b. Interpretation superposed to the seismic data with interpreted horizons, sequence boundaries and the correlation with the Spontaneous Potential curve on Well 2. Note the angular unconformity above MPLIO horizon.

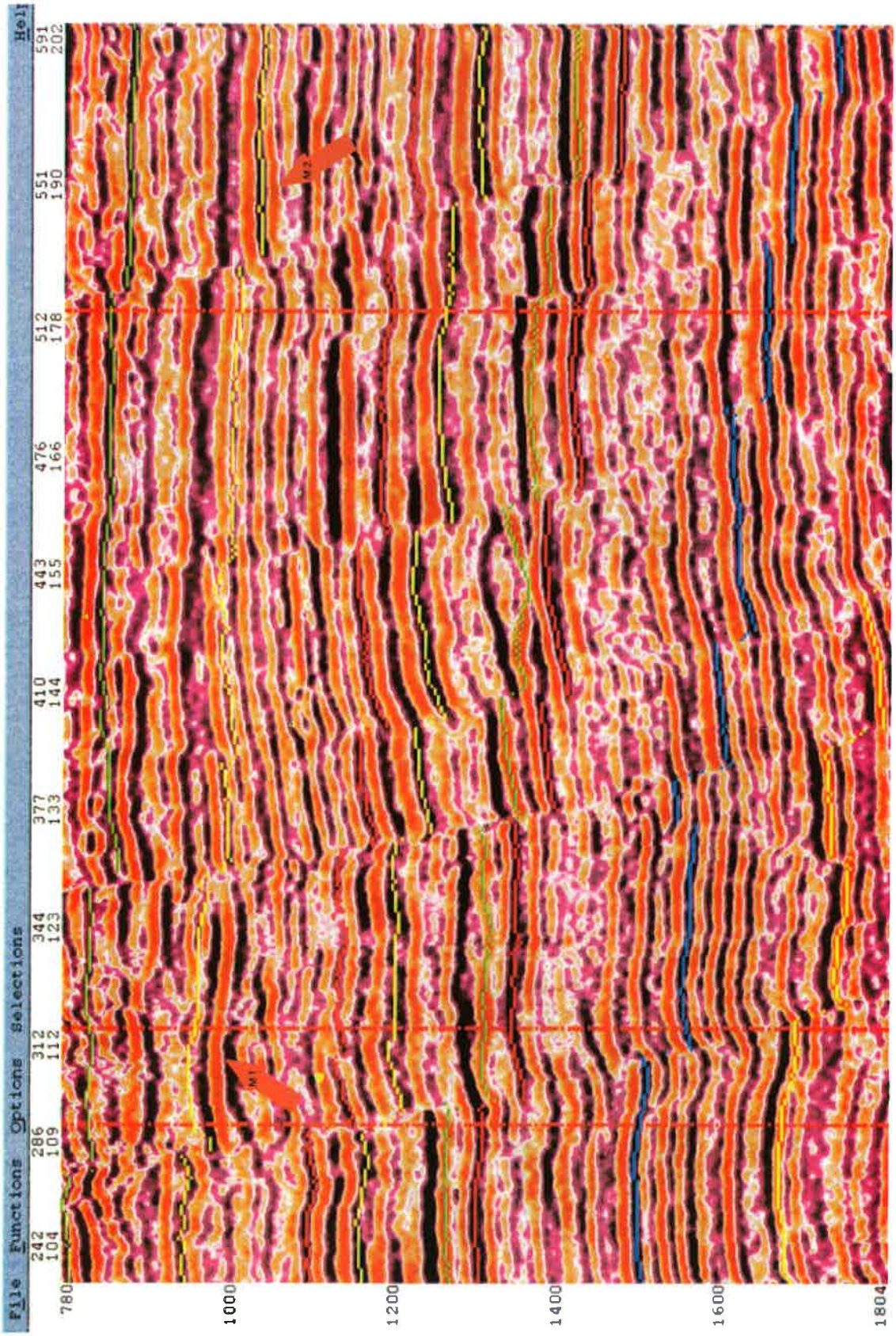

Fig. 5-41: a. NNW-SSE randomline profile running through well 2 and well 3 showing the Top Pliocene and Top Miocene hiatuses.

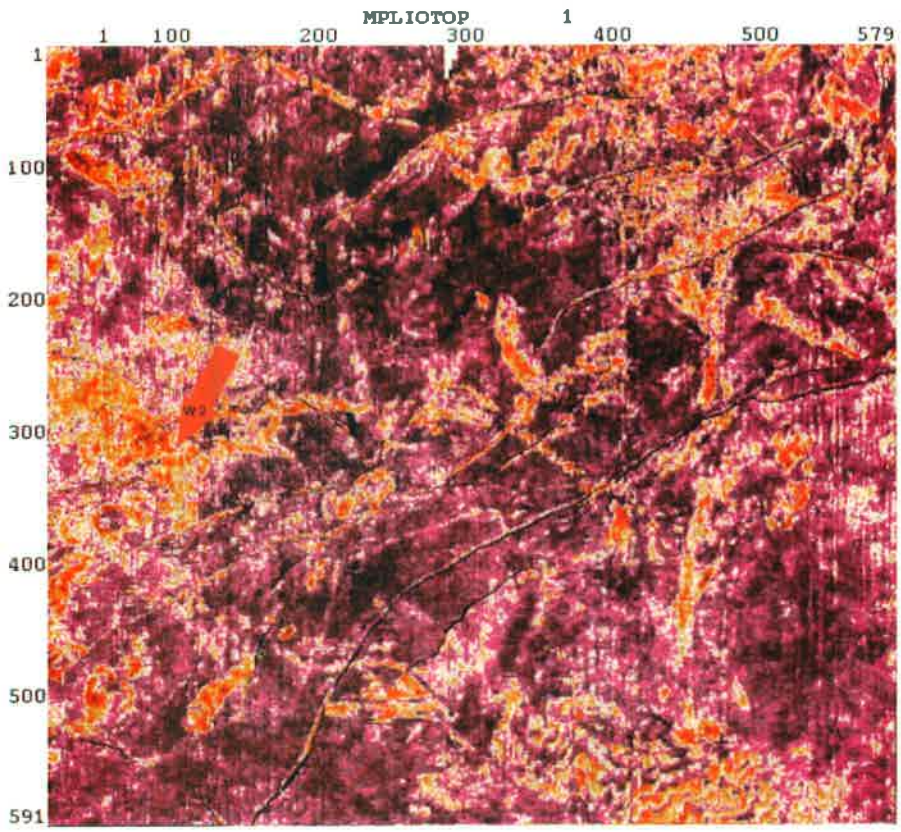

*Fig. 5-42: **a.** Amplitude map 44 ms above MPLIO horizon to intersect the base of the 2.6 Ma erosion (C0, violet negative loop are the Hst silt and shale, orange channels indicate the base of the SB2.6 erosion).*

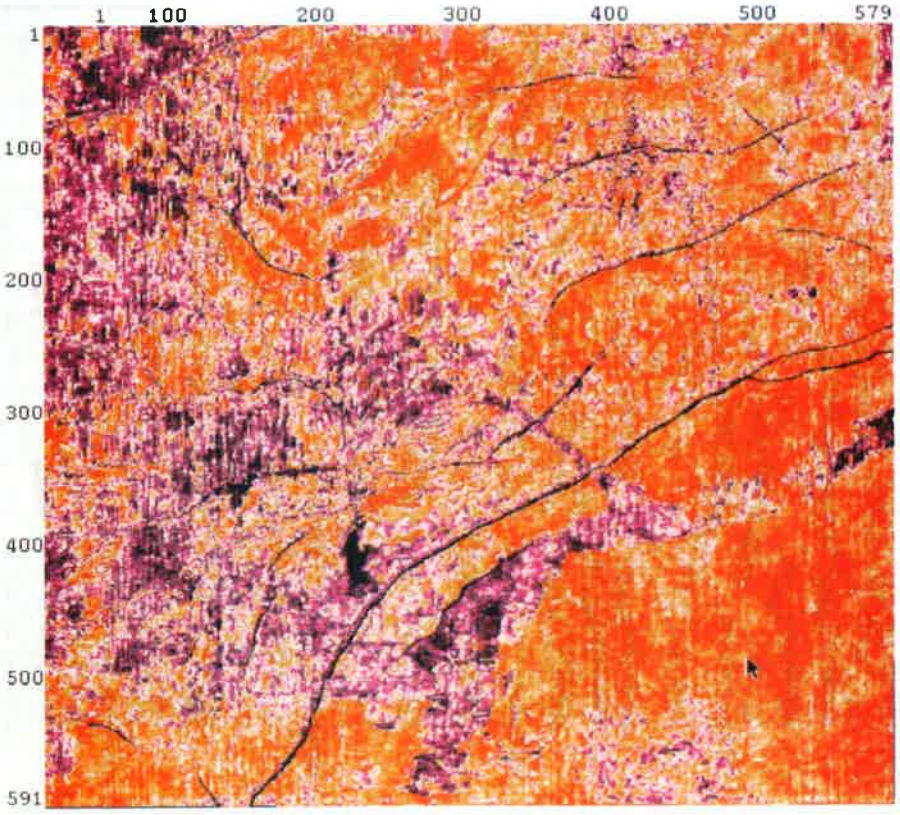

*Fig. 5-42: **b.** Amplitude map calculated 20 ms above the MPLIO horizon. Intersection with the base of the unconformity and signs of transgressive reworking shown as oblique (NE-SW) sand bodies.*

- a: Figure 5-42 a) (MPLIO-44) intersects the top of the first continuous negative loop (violet) on top of the unconformity. This level, parallel to the MPLIO datum cuts through the base of the deep channels related to the SB 2.6 erosional phase. One SB 2.6 channel is seen on the vertical seismic section (C0, fig. 5-41 a) just to the south-east of Well 2. It is hardly visible on the amplitude map (fig.5-42 a) displaying discontinuous meandering north-south oriented shallow channels.
- b: An amplitude map calculated 20 ms above MPLIO (fig. 5-42 b) shows a juxtaposition of amplitude lateral changes parallel to the general fault trend. They correspond to the intersections of the thin coastal onlaps seen on the vertical section (fig. 5-41 a) with the horizontal datum parallel to MPLIO. On the well log curves, these coastal onlaps on top of the unconformity are marked by sharp sandy signals (fig.5-30, Well 4, MPLIO-20). Such Gamma Ray response are typical for transgressive clean and porous fine sands interpreted as reworked lowstand sand bodies during periods of rapid shelf flooding (see chapter 5.7 and 6). These high porosity sands are commonly sealed on top by the main flooding surface draping shale and are limited below, in the present situation, by the erosional unconformity. This configuration is an example for an ideal paleogeomorphic subtle potential trap such as described by Halbouty (1982) .
- c: Figure 5-43 (a and b) show the seismic facies and interpreted sedimentary facies along the MPLIO horizon. On figure 5-43 b, a few hundreds meters south of Well 2 the deepest portion of a SB 2.6 channel is still intersected. It shows an orientation perpendicular to the rest of the erosional features present along that level confirming its attribution to a distinct erosional surface. In the lower right corner of the image, an homogeneous negative amplitude anomaly (white) is interpreted as the contrast in acoustic impedance between the SB 3.0 Ma incised valleys gross sands and their overlying silt (MPLIO on Well 4, fig. 5-30).
- d: MPLIO+16 amplitude map on figure 5-44 (a and b) cuts right through the incised valley thick sands indicated on logs below the MPLIO horizon (fig. 5-30) and enables to distinguish several additional erosive features not visible on the preceding map. The most striking feature on this map is the white (negative amplitude) channel running north-south in the left portion of the image. It expresses the horizontal morphology of the wide and deep (2 km / 70 m) amplitude anomaly intersected by the WSW-ENE randomline of figures 5-31 and 5-41 (M1). It is interpreted as a major incised valley associated with the SB 3.0 Ma erosive surface. In the lower right portion of figure 5-44, it is possible to distinguish between two superposed meandering channels under the silty white lobe observed on the preceding map (see M2 wide and shallow channels on Inline 260, fig. 5-23 and on rlwell fig. 5-41 a). The M1 and M2 are probably two distinct generations of incision because they show a difference in orientation and style of erosion (the base level of erosion or bottom of the incised valley cannot be used as a chronostratigraphic argument to distinguish between erosive phases that can have variable depth of incision unless we know the amplitude of sea level fall). Several finer and shallower channels oriented NW-SE and NE-SW are clearly distinct from the deep incised valley. They are influenced by the faults geometry and are interpreted as reflecting the onset of the lowstand associated with the main SB 3.0 unconformity.
- e: The SB 3.0 channels are cutting down to 80 m in the underlying fine silt and shale below the MPLIO horizon. They are still visible along the MPLIO+48 level (M1 on fig. 5-45 b). But apart from these channels, the amplitude map on figure 5-45 a) can be subdivided into two zones dominated by amplitudes of opposite value. The south-west portion of the image is dominated by white, negative amplitudes corresponding to pure shale confirmed by the three wells intersecting them along that level. The north-east area is dominated by black positive amplitudes. Well 4 along that level (fig. 5-30) presents fine silts confirming the lateral difference in sedimentary facies. This lateral contrast along one horizon is interpreted as the intersection with a transgressive shaly coastal onlap. This is confirmed by the sequential and lithological interpretation on logs that attributes these silt and shale to the highstand deposits below the SB 3.0 sequence boundary. Such lateral differences in seismic facies along an amplitude maps calculated above or below the datum plane could also be the result of the difference in thickness of sediments between the onshore and the offshore regions. Nevertheless, in this area and at this depth, amplitude maps calculated parallel to the datum plane are consistent (stay within half a loop) for as much as 60 to 80 ms.

It has been mentioned in the introduction of chapter 5.2 when discussing the Late Pleistocene facies reconstruction made by Berryhill (1987) that the line of coastal onlap can be influenced by deep lying positive features. The line of coastal onlap interpreted on figure 5-45 is actually deflected by the two underlying salt related positive features present in the north-eastern portion of the studied surface (see fig. 6-8 for location of salt domes). This demonstrates that these positive structures were still active at that time.

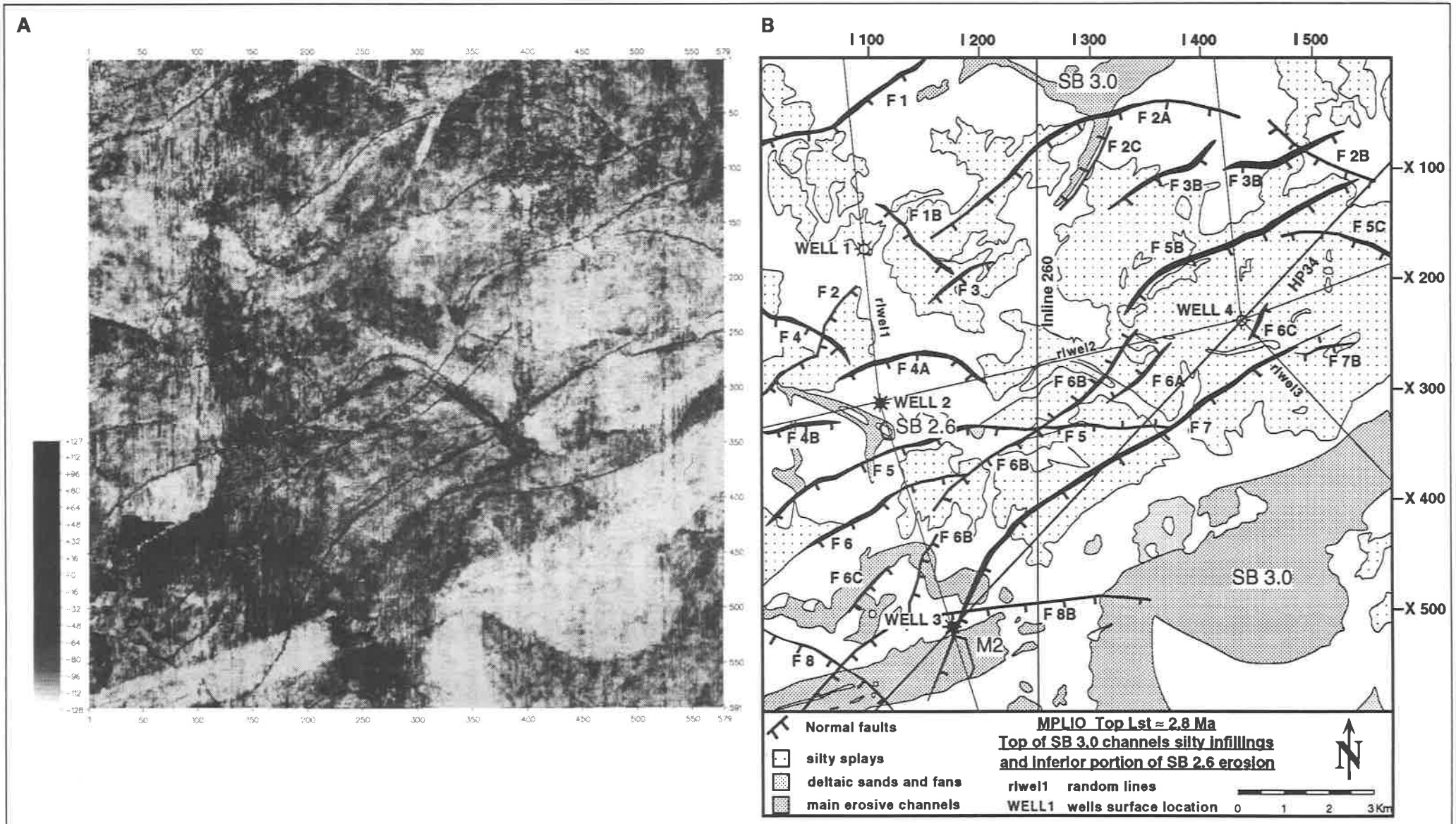

Fig. 5-43: ***a.*** *Amplitude map along the MPLIO horizon about 20 ms below the top Pliocene unconformity (see fig. 5-41).* ***b.*** *Two distinct perpendicular erosional phases are identified on the interpretation: the inferior portion of SB 2.6 channels (C0) and the top of the deep SB 3.0 channels (B10). (C = Gulf coast Pleistocene, B = Middle and Late Miocene).*

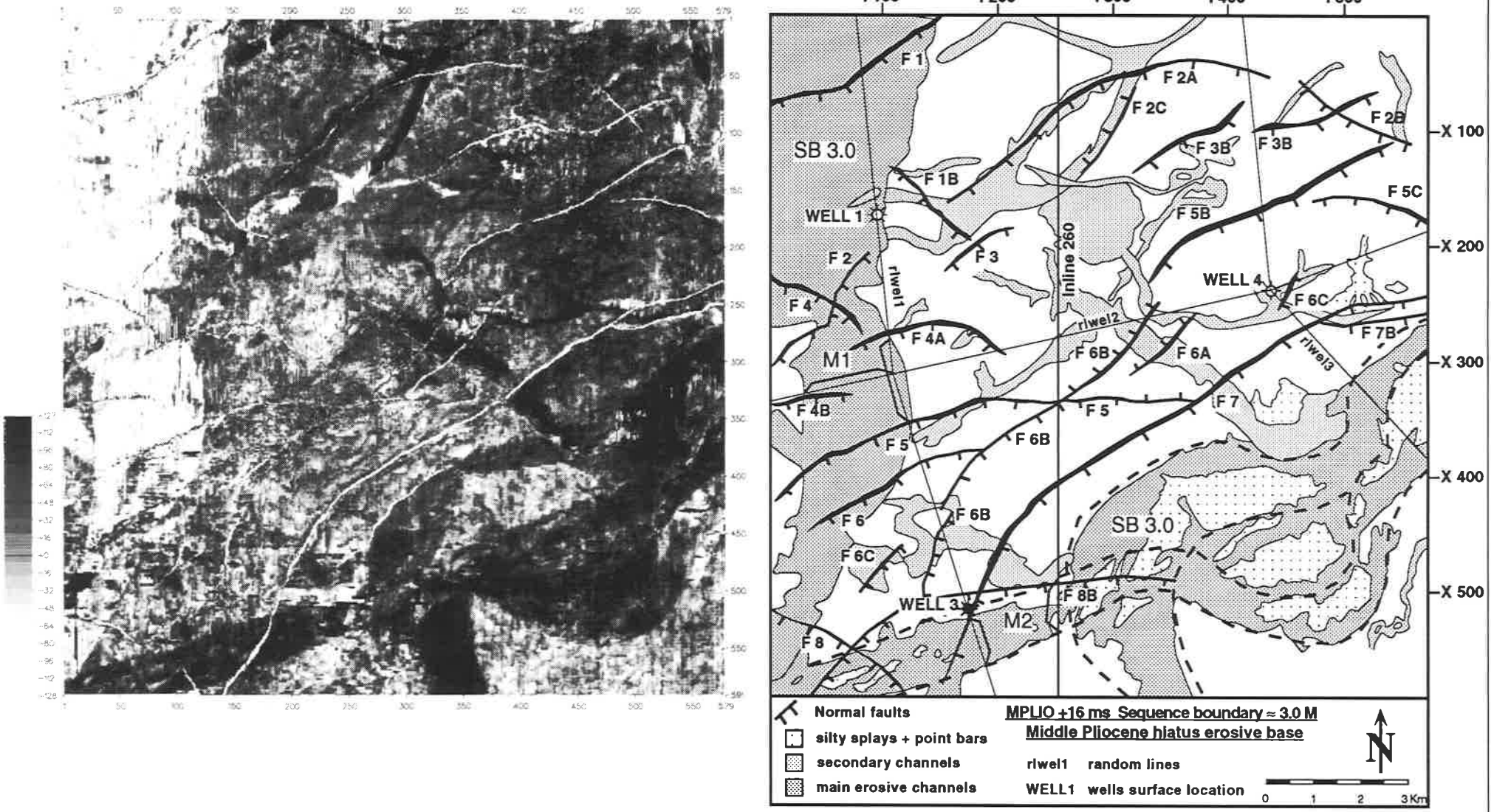

Fig. 5-44: ***a.*** *Amplitude map obtained 16 ms below the MPLIO datum that cuts through all the main channels associated with the SB 3.0 erosion (B10, see table 1).* ***b.*** *Interpretation showing one north-south major channel and two superposed meandering channels in the south-eastern portion of the map (SB 3.0 B10). Note the inversion in amplitude polarity between the two channels along this level explained by a difference in depth and type of filling material (finer material for the black meandering channels, see vertical section on fig.5-41 a.*

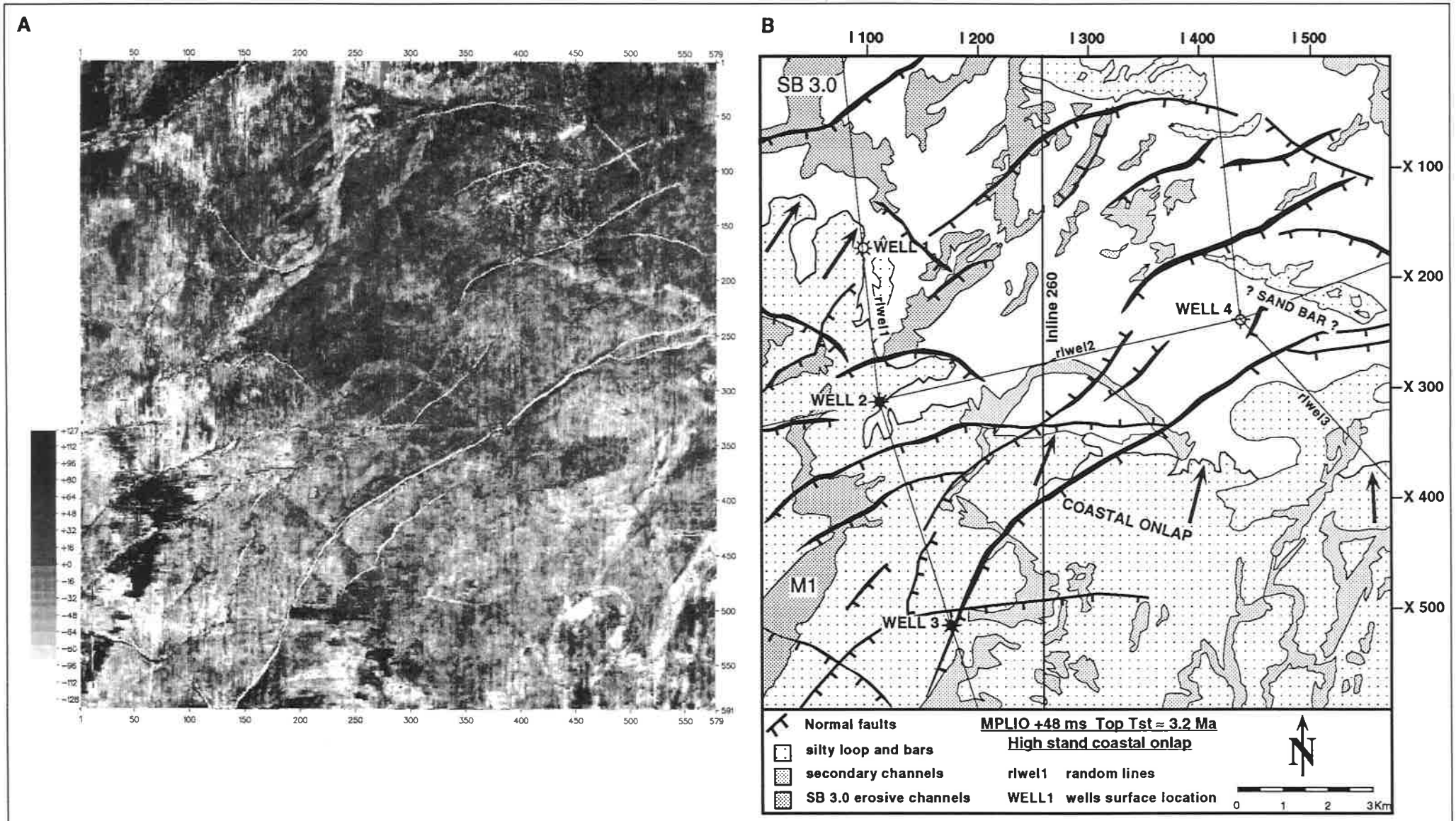

*Fig. 5-45: **a.** Amplitude map calculated 48 ms below the MPLIO datum. **b.** Deepest part of SB 3.0 channels intersected and lateral contrast in amplitude interpreted as the intersection with a silty coastal onlap in the transgressive phase recorded below SB 3.0 (B10, see well log data, fig. 5-30)*

Conclusion

This short chapter discussing the Gulf coast Pleistocene basal unconformity is rich in sedimentary conclusions and completes the systematic sequential analysis of 2D, 3D seismic and well log data leading to the distinction of subtle successive erosional phases.

- Unconformities and associated hiatuses are easily missed on well log data in the absence of accurate enough faunal data. They are mostly identifiable on vertical profiles and their surfaces can be mapped on 3D seismic displays to delimit paleogeomorphic subtle traps associated with erosional surfaces.
- Once an unconformity is identified on 2D lines, successive horizontal amplitude and volume related attributes maps can precise the type of sediments filling an incised valley (fig. 5-43, 5-44). The presence and lateral extension of shaly seals is directly determined from 3D data sets if consistent well log information and correlation are available.
- Condensed superposed erosional phases above and below important hiatuses can be distinguished on 3D data sets on the base of the youngest (highest) intersection of incised valleys in the seismic record and not the base level of erosion which is related to the rate of relative sea level fall.
- Above and below unconformities, oblique truncations, coastal onlaps and transgressive reworking or incisions can be identified on 2D sections having a sufficient vertical resolution. A display in coloured raster density helps in unveiling subtle shingles present within half a loop that would not be seen on normal wiggle traces (Reymond and Stampfli, 1992a) . The same sedimentary objects can be visualised on horizontal maps parallel to chronostratigraphic interpreted horizons. They appear as successive parallel bars of consistent amplitudes indicating the main paleo-orientation of transgression or erosion and abrasion.
- And finally, transgressive reworking on top of unconformities can also be identified on well log data based on their typical sharp clean porous sandy signals located as a result of sequential analysis on logs.

The top of the Gulf coast Pliocene hiatus is associated with the complex SB 3.0 Ma (B10/B11) major fall in sea level. This major erosional phase distinct from the base Pleistocene SB 2.6 Ma erosion (C0) bears the traces of two distinct erosional phases at the origin of the unconformity:

- a first phase (B10 a) of erosion marked by shallow meandering channels corresponding to the earliest phase of erosion (fig. 5-44 b).
- and the major erosion (B10 b) corresponding to the maximum of relative sea level fall indicated by the large and deep NNE-SSW incised valley partially eroding the older shallowmeanders below.

It is probable that shorter 0.1 Ma cycles recorded on the Gulf coast inner shelf at the base Pleistocene limit were entirely removed by the strong SB 2.6 and SB 3.0 Ma erosions (unconformity above MPLIO horizon on fig. 5-41 b).

Gulf coast Pleistocene (0 to 2.8 Ma) synthesis and conclusions.

The characteristics (orientation, type and depth, simplified labels, names of corresponding interpreted horizons and hypothetical ages) of every erosional surfaces discussed above are summarised on figure 5-65. The erosional surfaces observed in this research that are not described on the Plio-Pleistocene revision by Wornardt & Vail (1991) are indicated in bold. Their attribution to global sequences boundaries is not the purpose of this study. But the ideal sedimentary and tectonic setting of the Gulf of Mexico continental shelf and the proximal situation of the studied 3D seismic data enables to describe at least 23 distinct erosional surfaces down to 3.1 Ma before present. Based on the results presented above, short 4th order sequences of 0.1 Ma are likely to be found over the entire Gulf coast Pleistocene period. Considering that every 0.1 Ma orbitally forced eustatic cycle can potentially have a sea level fall superior to 40 m which is enough to develop a system of erosional channels on the inner portion of the Gulf coast shelf, 30 to 31 distinct erosional phases should be recorded in the Pleistocene sediments. Seven are not observed and this is related to the periodic stronger falls in relative sea level that have partially erased the traces of the missing shorter cycles. A time interval of 0.8 Ma corresponds to the recurrence of stronger fall in relative sea level (0.8, 1.65 to 1.85, 2.4 to 2.5, 3.0 to 3.1 Ma). All these major erosional phases are marked by deeper erosions mainly north-south oriented (fig. 5-65) confirming the drastic fall in sea level (shoreline far away offshore, higher erosional angle on the inner shelf). A systematic gap of 0.2 to 0.3 Ma is observed below each of the major cycles that could explain the missing sections or secondary hiatuses correlated to these stronger erosions. The missing 0.1 Ma cycles are simply reworked offshore !

All these considerations are only relative and qualitative in the absence of confirmation by precise faunal data. Nevertheless, there is a good degree of confidence in the correlation of our data to the pre-existing well documented and dated local reports and regional seismic sections.

The uniformity of cyclic events on the entire Gulf Coast Pleistocene proposed by this study based on the repetition of four 0.8 Ma cycles is also illustrated by the magnetostratigraphic cycles showing major inversions at 0.79, 1.67, 2.48 and 3.2 Ma ! This eustatic and magnetostratigraphic 0.8 Ma periodicity was not expressed in the litterature before this research. A possible solution to this could be found in the periodic changes in the distance between the Earth and the Sun influencing simultaneously both the eustatic, climatic cycles and the magnetic inversions of the Earth magnet. The 0.8 Ma periodicity could correspond to the double wave-length of the 400'000 years orbital cycles described by Milankovitch (1941).

Everything is interconnected and works in cycles.
We are simply slowly re-discovering it.

5.7 Top Messinian lowstand and base Pliocene series.

Introduction

The top Messinian Mio-Pliocene limit is defined according to different sources between 5.3 and 4.9 Ma. Odin and Odin, (1990) and Berggren et al. (1985) agree in placing this limit at the base of the Gilbert normal magnetic epoch (5.3 Ma). Cita (1975) defines the base Pliocene at the top of the first inverse event registered in the Gilbert epoch (4.9 Ma) on the base of studies on the Messinian stratotype in Sicily . From biostratigraphy, the Mio-Pliocene transition is defined by the Globoquadrina dehiscens LAD and the Globorotalia tumida and G. margaritae FAD at about 5.3 Ma (Annexe 2).

The top Late Miocene series corresponds to the Messinian Mediterranean salinity crisis which has been the subject of many publications concluding to a tectonically related local sea level drop of at least 2000 m (Ryan, 1976 ; Cita & Ryan, 1978 ; Stampfli & Höcker, 1989) . It is interesting to compare the chronology of events observed on the base of studies in micropaleontology in the tectonically affected southern Rif region in Morocco as described by Wernli (1987) with the succession of erosive phases during the top Miocene as described in the Gulf of Mexico by previous studies and by this research (Haq *et al.*, 1988 ; TGS, 1990 ; Reymond & Stampfli, 1994a) . The Mediterranean closure is strongly influenced by local tectonic (Alboran / North Morocco late Miocene collision; Favre, 1992) but may also coincide with major and global eustatic sea level falls identified in the Mediterranean offshore Spain, (Stampfli & Höcker, 1989) , in the Niger delta (Barber, 1981 ; Bentz & Hudges, 1981) and in the Gulf of Mexico (this research). In north Morocco, Wernli (1987) describes two successive phases of transgression at the Plio-Miocene limit separated by one major phase of regression indicated by planktonic foraminifers faunas. This first transgressive event is marked by the Globorotalia primitiva fauna which is the palingenetic ancestor of the Globorotalia margaritae marking the low Pliocene transgression. This two faunas are separated by the first Early Messinian regressive phase that can be compared with the SB 6.3 Ma found in the Gulf of Mexico. The same author notes that this first regressive phase is synchronous with the local salinity crisis but is difficult to identify or date because it is re-eroded by an important posterior regressive phase preceding the Moghrébien transgression (Early Pliocene, G. margaritae yellow marls, Wernli, 1987). This second erosive phase could be related to what is identified as the SB 5.5 Ma sequence boundary recorded in the Gulf of Mexico that shows deeper erosion features than the SB 6.3 regressive event and that partially erodes the sequence boundary below. This comparison proposes that even if the Mediterranean Messinian events are mostly influenced by local tectonic the eustatic phases recorded in the Gulf of Mexico or in the Nile delta can also be identified in the Rif geology of north-west Morocco.
This chapter is divided into three part:

- 5.7.1: Base Pliocene; a 3rd order sequence between SB 5.5 and SB 4.2 Ma.
- 5.7.2: An alternative interpretation for the SB 5.5 to SB 4.2 interval.
- 5.7.3: Middle and top Pliocene depositional gap (SB 4.2 to SB 3.0 Ma).

5.7.1: Base Pliocene; a 3rd order sequence (SB 5.5 to SB 4.2).

Introduction

The marine environment of sedimentation for this interval corresponds to the transition between the middle and the outer neritic zones. The sequence between SB 5.5 and SB 4.2 on Well 3 (fig. 5-46) was illustrated in chapter 3 (fig. 3-7) to illustrate the typical aspects of systems tracts on logs on the middle to outer portion of a clastic shelf. On vertical seismic sections, systems tracts in the middle neritic zone in clastic environments do not show characteristic features and are not developed enough to enable good sequential analysis. In this kind of environment, the best sequential analysis are realised on well log and 3D horizontal images provided the depositional environment is precisely defined by faunal assemblages.

Observation

The well log sequential analysis applied on the four available wells for the base Pliocene interval in the studied area identifies two 3rd order sequences with typical lithological signatures of the middle neritic zone (fig. 5-46, SB 3.8, SB 4.2 and SB 5.5). The SB 5.5 Ma sequence boundary is placed at the base of the thick sands present on all logs corresponding on vertical seismic sections to a chaotic, low positive amplitude interval (fig. 5-31 and fig. 5-41, above TOPMIO horizon).

To observe the vertical evolution in horizontal seismic facies morphology in the base Pliocene, above the top Miocene hiatus, three horizons have been interpreted over an interval of 200 m (TOPMIO, LOPLIO and LOPLIO2, see fig.5-46). Nine amplitude maps obtained in this interval summarise the changes in seismic facies (sedimentary features) in response to cyclic changes in marine environment. This interval on a vertical seismic section (fig. 5-41, between TOPMIO and LOPLIO2 horizons) is indicated by alternating of high amplitude continuous reflectors and more transparent zones. Several erosional features can be identified. They are presented below from base to top.

The amplitude map on figure 5-47 shows the subtle variations in amplitude registered along the TOPMIO horizon interpreted along a positive loop (compressed colour scale, channel in the positive amplitudes range). The fault traces along this horizon are indicated in white. This large and deep channel (2.5 km / 100 m) corresponding to the base of the SB 5.5 Ma erosion phase is not influenced by the fault activity present at that time and cuts right through all of them contrary to the lowstand channels mentioned in the preceding chapters (fig. 5-33 a and b, SB 2.4 channels and fans developed down the main growth fault). This indicates that the major erosional phase recorded at the base of the Pliocene was important enough to level the pre-existing fault related topography.

The next amplitude map and sedimentary facies interpretation is obtained 24 ms (25 m) above the TOPMIO horizon (fig. 5-48 a and b). It shows the same meandering channel but indicated as a negative anomaly (white) in the thick negative loop above the TOPMIO level. This reflector corresponds to the strong contrast in acoustic impedance between the top incised valley sands and the silt above and below (fig. 5-41, Well 2). This map intersects the central portion of the incised valley fill which allows to see greater details in the channel sedimentary fill. Point bar sands are visible in the inner part of both meanders and sub-canyons can be identified within the major incised valley that reaches 2.5 km width in the rectilinear portions. Three parallel canyons visible in the south-western part of the image within the incised valley are intersected by the east-west trending rlwel2 randomline (fig. 5-31, C5.5). If Well 2 location is accurate enough at that depth, it intersects the deepest canyon and shows that the thick sands above TOPMIO-24 correspond to the upper part of the canyon fill. On the base of this observation, the true position of the sequence boundary on logs (bottom of the incised valley) would not be the base of the thick sands but rather above the pure shale seen on Well 2 below the TM-24 level, within the silt (see fig. 5-46, Well 2).

The north-south rlwel1 randomline (fig 5-41) presents a longitudinal transect through the main channel seen on figure 5-48 b. An erosive feature (T-24 on vertical section fig. 5-41 and amplitude map, fig.5-48 b) show longitudinal intersections with the deepest canyon within the western part of the incised valley. Without the amplitude map it would have been impossible to tell that the totality of the seismic line on figure 5-41 along the TOPMIO horizon was within a major incised valley and the channel location would have been limited to the T-24 depression. These two amplitude maps illustrate the horizontal morphology of a typical basal lowstand systems tract related to a major fall in relative sea level. The quantification of the sea level fall is difficult to establish because the amount of missing section between

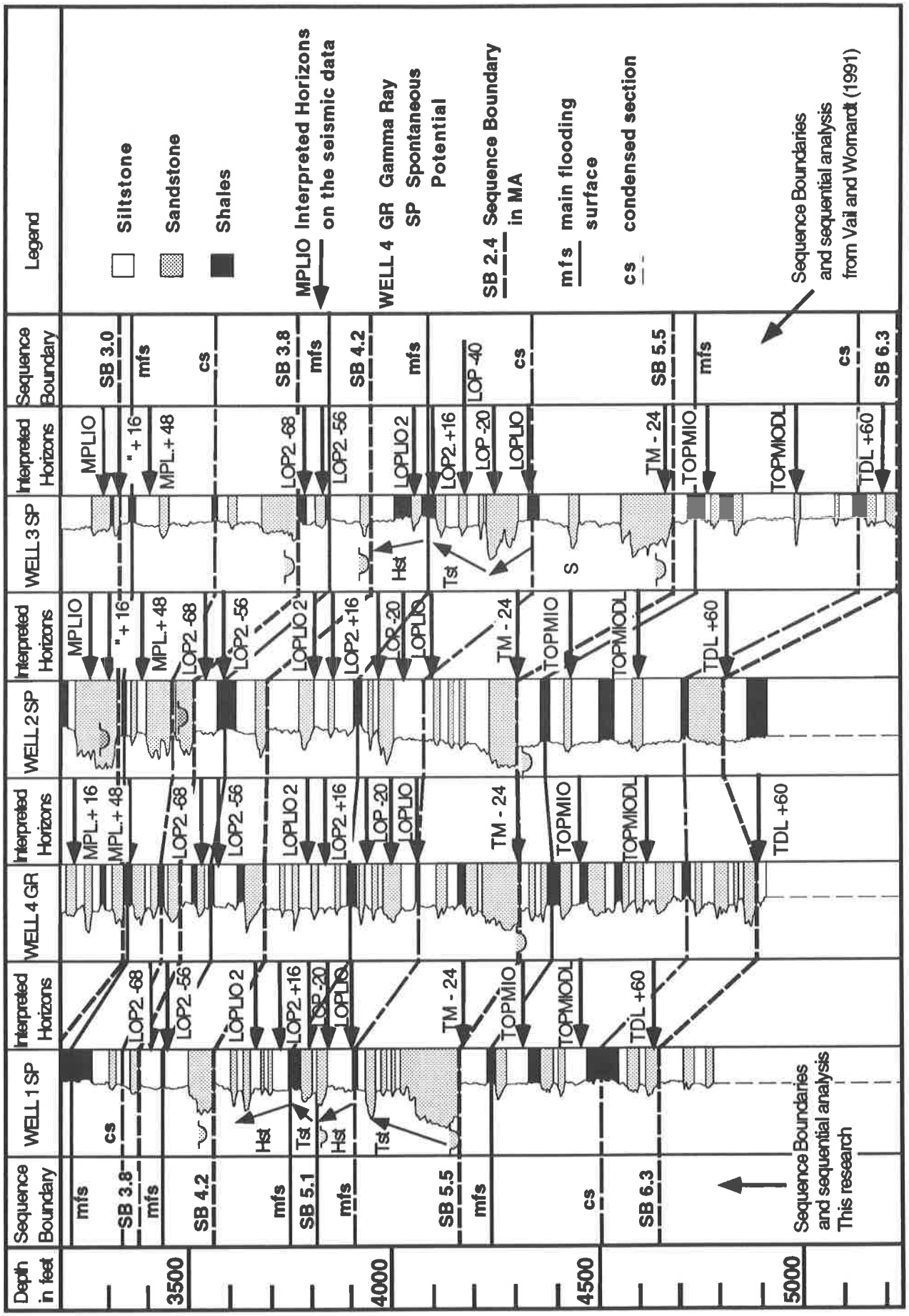

Fig. 5-46: Well log data sequential analysis for the Pliocene and top Miocene unconformity (SB 3.0 to 6.3, B5 to B9, see table 1).

the transparent transgressive sands sealing the incised valley and the top of the incised valley fill is impossible to determine. The minimum of sea level fall is indicated by the maximum depth of the incised valley which locally reaches 100 m.

Right on top of the transparent zone on the vertical profile (fig. 5-41) is a continuous and high amplitude reflector interpreted as the LOPLIO horizon. This reflector coincides on the well log data with the shaly condensed section present at the base of the Prograding wedge (fig.5-46, Well 3). No lateral amplitude variations are seen along this horizon on the 2D sections but a channel system is unveiled by the corresponding amplitude map displayed with an extremely compressed colour scale (fig. 5-49 a and b). The channels dimensions are much smaller than the one on figure 5-48 (500 to 600 m wide and 20 to 30 m deep). Once their location has been identified on the horizontal display it becomes possible to go back to the vertical sections and identify the subtle lateral changes in amplitude corresponding to these channels (L0 on figures 5-31 and 5-41 along LOPLIO horizon). They correspond in size and morphology to the present estuarine and tidal by-pass channels of the northern Gulf of Mexico proximal shelf (Anderson *et al.*, 1990 ; Saxena, 1990 ; Abdulah & Anderson, 1991 ; Anderson *et al.*, 1991) . They can also be compared to the present sandy estuarine facies of the eastern coast of the North Sea (Leeder, 1985) . This system of tidal channels and estuarine shaly and silty sediments can develops when the first sign of relative sea level elevation creates a short period starvation episode when shallow sea water floods the shelf before the prograding wedge start to prograde out towards the basin again (Reymond & Stampfli, 1993).

All logs show clear prograding thickening and coarsening upwards sands sedimented on top of this first condensed section (see fig.5-46 Well 3). An amplitude map calculated 20 ms above the LOPLIO horizon intersects the thicker and upper sandy signal of the prograding wedge (fig. 5-50 a and b). The subtle lateral variations in amplitude within the first positive loop above the LOPLIO horizon show an elongated sand body parallel to the present shoreline and two by-pass channels disappearing offshore from the sand bar (distal portion of the by-pass river seen on the previous map partly flooded).

The signal on 2D lines corresponding to this sand bar is seen on figure 5-41 to the north of Well 3 (L-20). Such a subtle amplitude anomaly would have remained unnoticed without the horizontal visualisation provided by 3D data as it resides within half a seismic loop. The dimensions of this offshore sand bar is more than 15 km long, 500 to 900 m wide and 10 to 25 m thick. This morphology is very similar in shape and size to the present Galveston area south of Houston where similar sand bars are intersected by by-pass rivers such as the Brazos, Sabine or Texan Colorado. This indicates that the sand bar coincident with the F7 growth fault on figure 5-50 b) was close to the paleoshoreline at that period (Base Pliocene fish and chips shops could be in the range of resolution of such seismic data but could not be identified in the studied area !).

All logs show a thinning and deepening upwards interval between the top of the prograding wedge and the shaly main flooding surface. An amplitude map taken 40 ms above the LOPLIO horizon intersects the middle portion of the transgressive systems tract of this 3rd order sequence (fig. 5-46, Well 3). Figure 5-51 a and b) shows the disappearance by flooding of the by-pass rivers and the apparition of a succession of sand bodies at the back of the above described sand bar . The main sand bar along this level can also be identified as a subtle increase in amplitude on the vertical section of figure 5-41(L-40). The secondary sand bodies developed at the back of the main sand barrier are interpreted as reworked sand bars transported a few kilometres landward during the phase of maximum relative sea level rise preceding the main flooding surface.

Up to date three different theoretical explanations exist for the formation of elongated thin sand bodies developed close to the shoreline. The first idea defended for instance by Berven in 1966 to explain the formation of elongated sand bars sedimented on the Cretaceous proximal clastic shelf of the eastern Rockies (Alberta, Canada) was that they are the result of lowstand offshore bars deposition (Berven, 1966) . The same sand bodies have been reinterpreted by (Pattison & Walker, 1992) as shoreface deposits accumulated during pauses in transgression (still stands). And the third possible origin for elongated sand bodies would be to consider them as top lowstand material reworked landward during the transgressive phase or period of rapid relative sea level rise. Such examples are known today in the example of the Chandeleur Islands in the eastern Gulf of Mexico (Saxena, 1990). Such reworked transgressive sand bodies show similar features on well logs with the one observed in this study and are composed of well sorted coarse and clean sands that make them ideal reservoir rocks.

The contact between the shaly main flooding surface and the silty and sandy thickening and

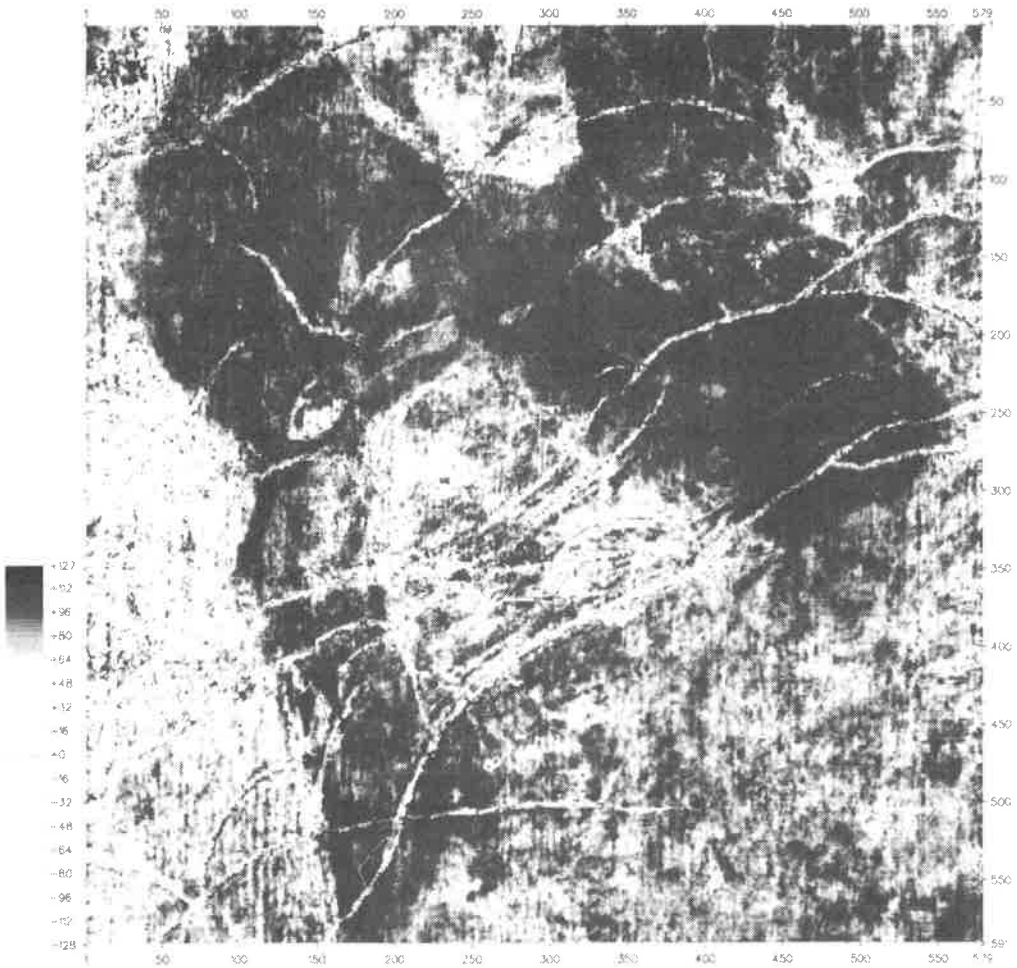

Fig. 5-47: Amplitude map along the TOPMIO interpreted horizon displayed with an extremely compressed colour scale to enhance the lateral changes in amplitude showing the beautiful meandering deep incision associated with the top Messinian erosion (B6).

coarsening up highstand systems tract on top creates a strong contrast in acoustic impedance at the origin of the negative loop interpreted as the LOPLIO2 horizon (fig. 5-41). The amplitude map along this datum shows homogeneous values except for the fault traces. An amplitude map calculated 16 ms below the LOPLIO2 horizon intersects the top of the shaly main flooding surface interval and shows a juxtaposition of two zones dominated by different amplitudes (fig. 5-52 a and b). The lower left corner is dominated by positive amplitudes (black) and the upper right corner of the image is mainly intersecting negative amplitudes (white). This lateral changes in amplitude usually occurs when cutting through the data set too far away from the interpreted datum thereby intersecting different seismic loops shifted by lateral differences in sediment thickness. But in that case the amplitude map on figure 5-52 a) is calculated 16 ms below a conformable datum surrounded by conformable reflections above and below. The signal observed can be explained by a subtle lateral difference in amplitude occurring in the positive loop below LOPLIO2 horizon that would remain unnoticed on vertical displays. The upper right portion of the map is therefore interpreted as the intersection with the first highstand prograding fine sands downlapping with a very low angle on the conformable silt below.

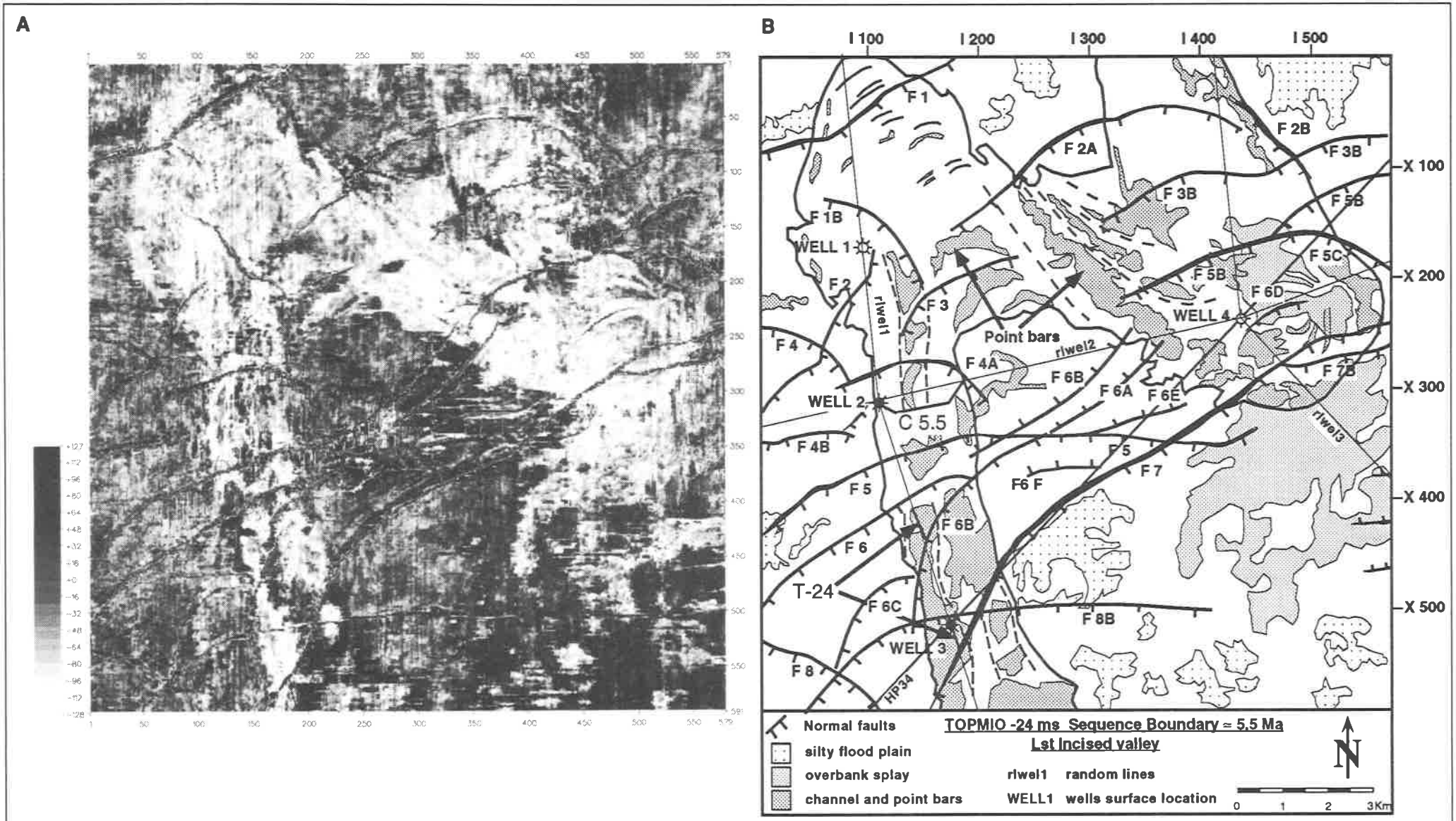

*Fig. 5-48: **a.** Amplitude map calculated 24 ms above the TOPMIO horizon showing the same incised valley one loop above fig. 5-47. Note the polarity inversion and the greater details in the valley fill. **b.** Sedimentary facies interpretation of fig. 5-48 a. Arched point bars are identified in both meanders and three parallel canyons can be distinguished in the straight portion of the incised valley (C5.5, B6) to the right of Well 2, see vertical section on fig. 5-31.*

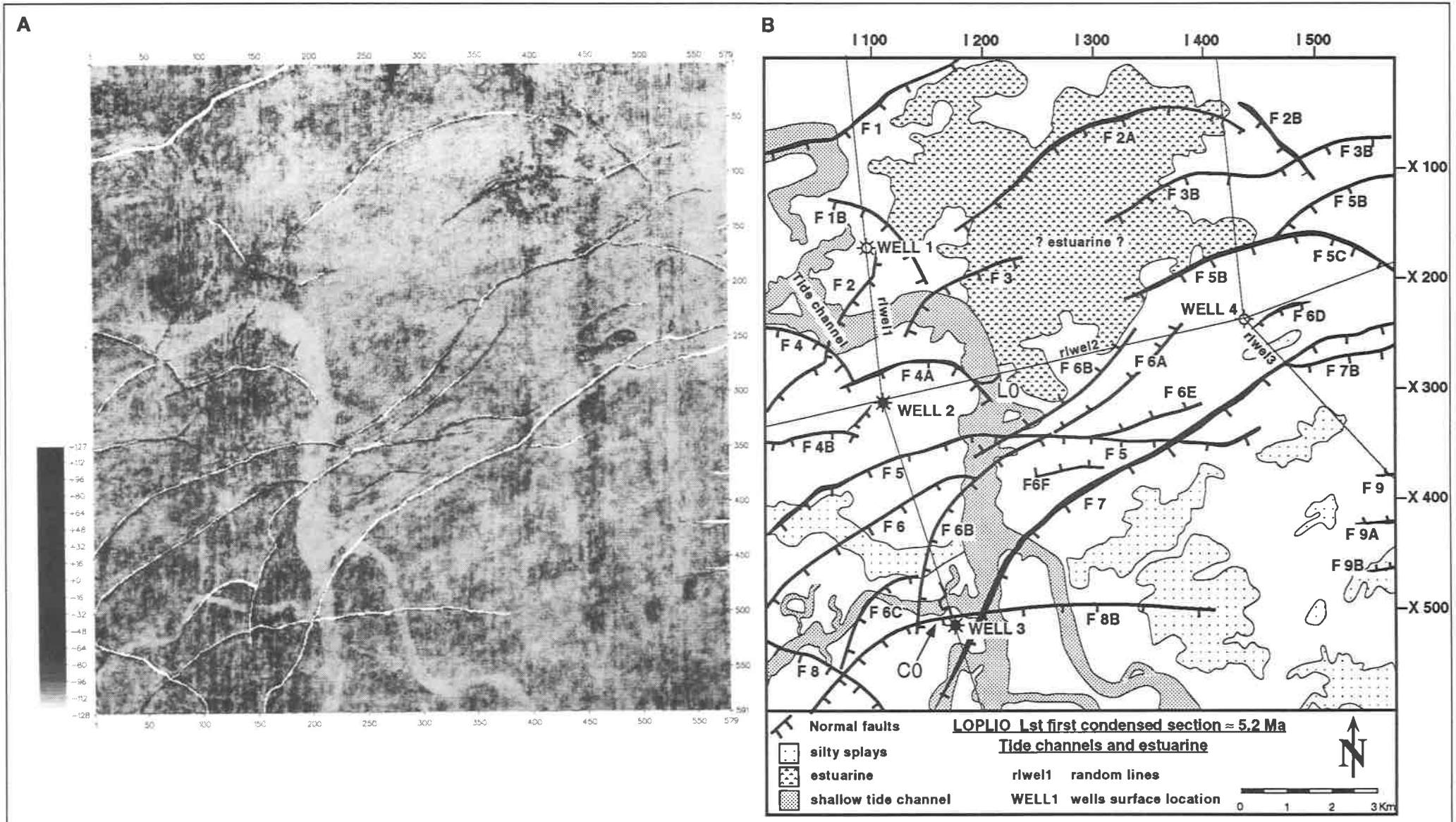

Fig. 5-49: ***a.*** *Amplitude map calculated along the LOPLIO horizon interpreted in the first thick and homogeneous negative amplitude loop on top of the transparent seismic facies above TOPMIO (see fig. 5-31 and fig. 5-41). Extremely compressed colour scale to identify the meanders.* ***b.*** *Interpretation of the B7 erosional phase (see table 1). The meandering shallow silty channels can be interpreted as a condensed section tidal erosion or as the base of the SB 5.1 erosional phase (see fig. 5-55 for discussion on well log data).*

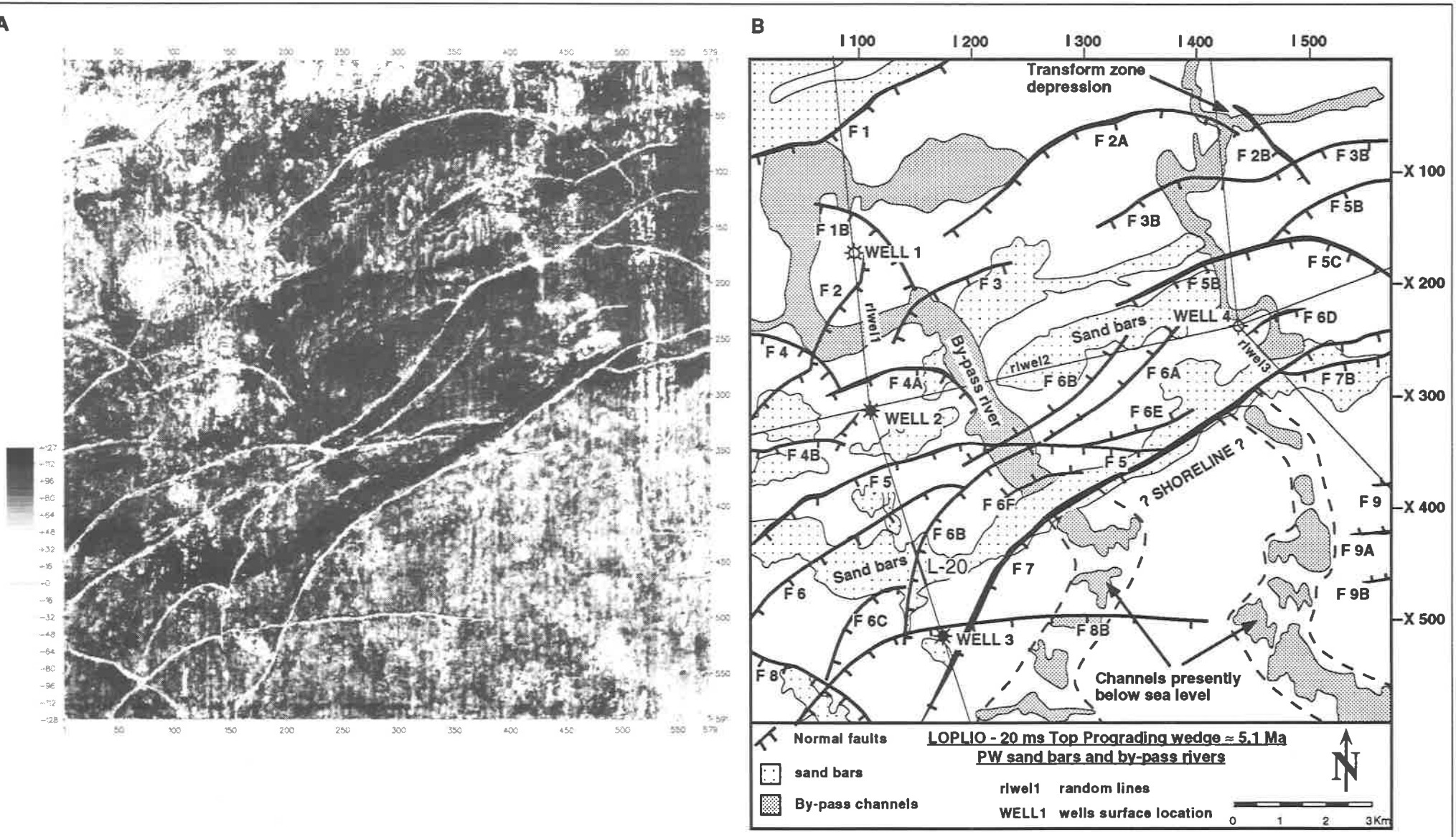

Fig. 5-50: ***a.*** *Amplitude map calculated 20 ms above the LOPLIO horizon showing the upper portion of the same shallow channel intersected on fig. 5-49 (B7). Compressed colour scale.* ***b.*** *Sand line parallel to the present shoreline and perpendicular channels. This can be interpreted as highstand or top lowstand progradation (see fig. 5-55 for discussion).*

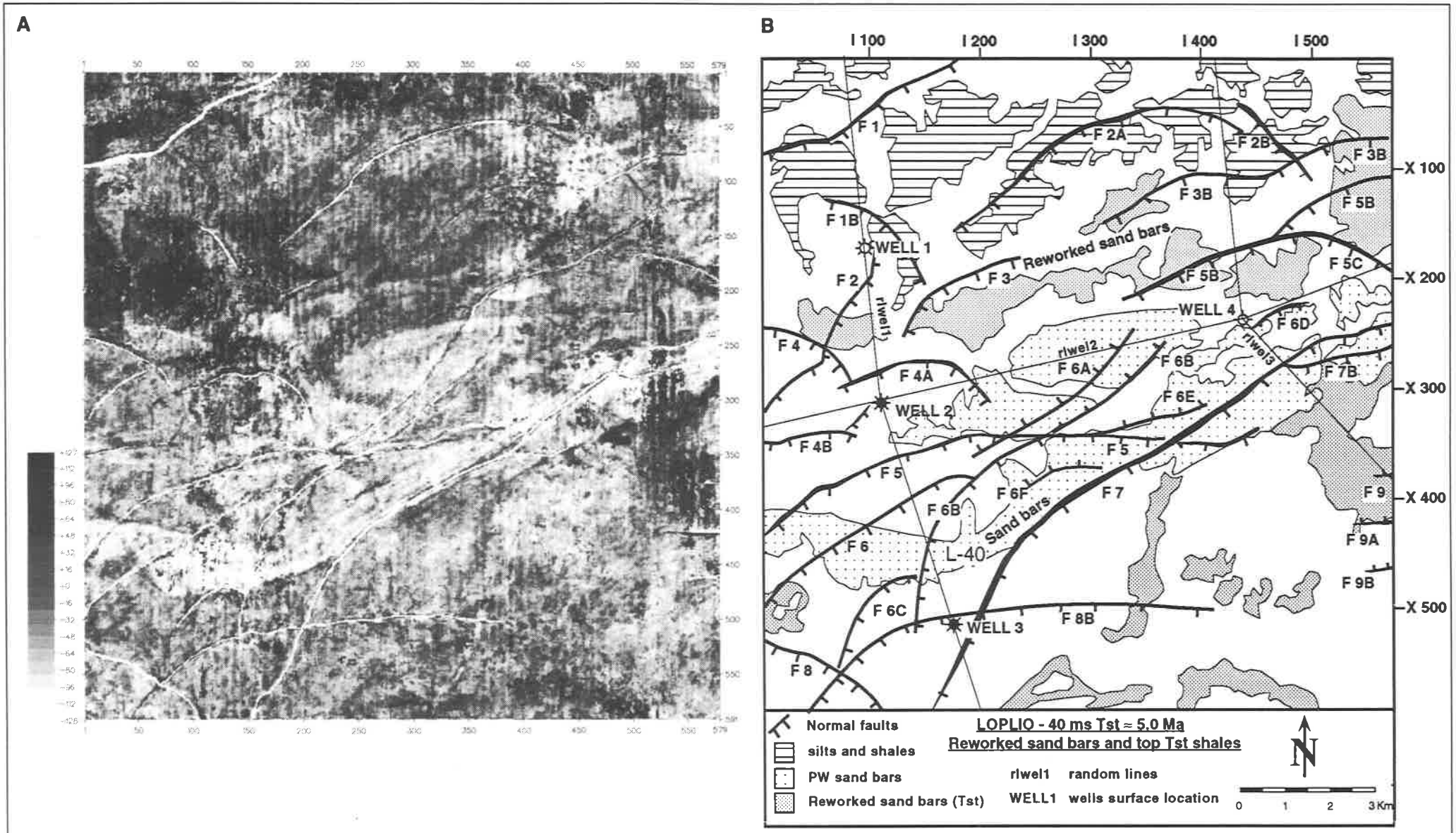

Fig. 5-51: ***a.*** *Amplitude map calculated 40 ms above the LOPLIO horizon.* ***b.*** *Transgressive reworking of the progradational sands below and entire flooding of the channels intersected on figures 5-49 and 5-50.*

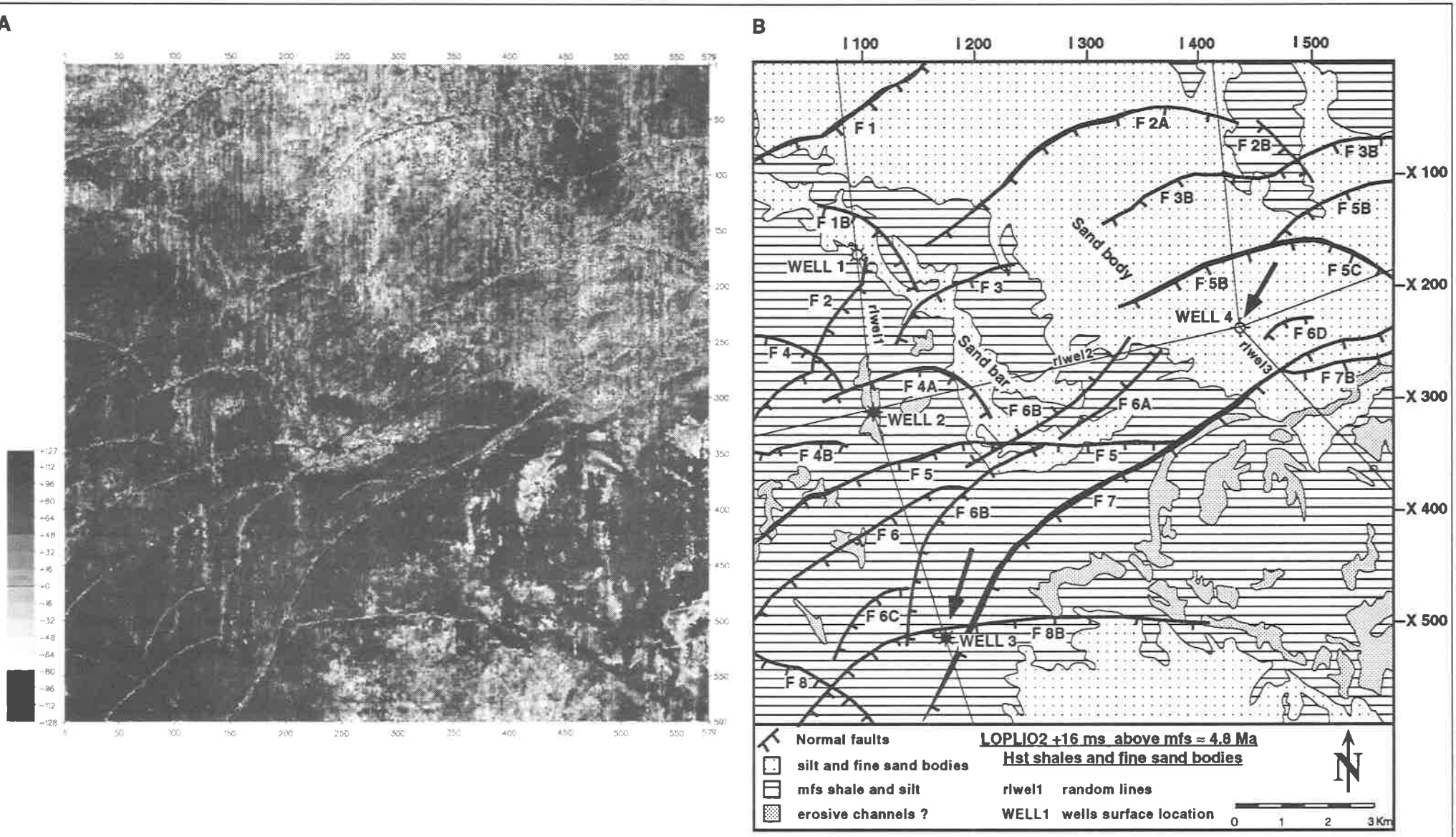

*Fig. 5-52: **a.** Amplitude map calculated 16 ms below the LOPLIO2 interpreted horizon. **b.** Interpretation of an amplitude map running through a maximum flooding surface (see fig. 5-46 and 5-55). The white negative amplitudes in the upper right corner are interpreted as highstand low angle prograding sands on the mfs shale (confirmed by well log data, fig. 5-46).*

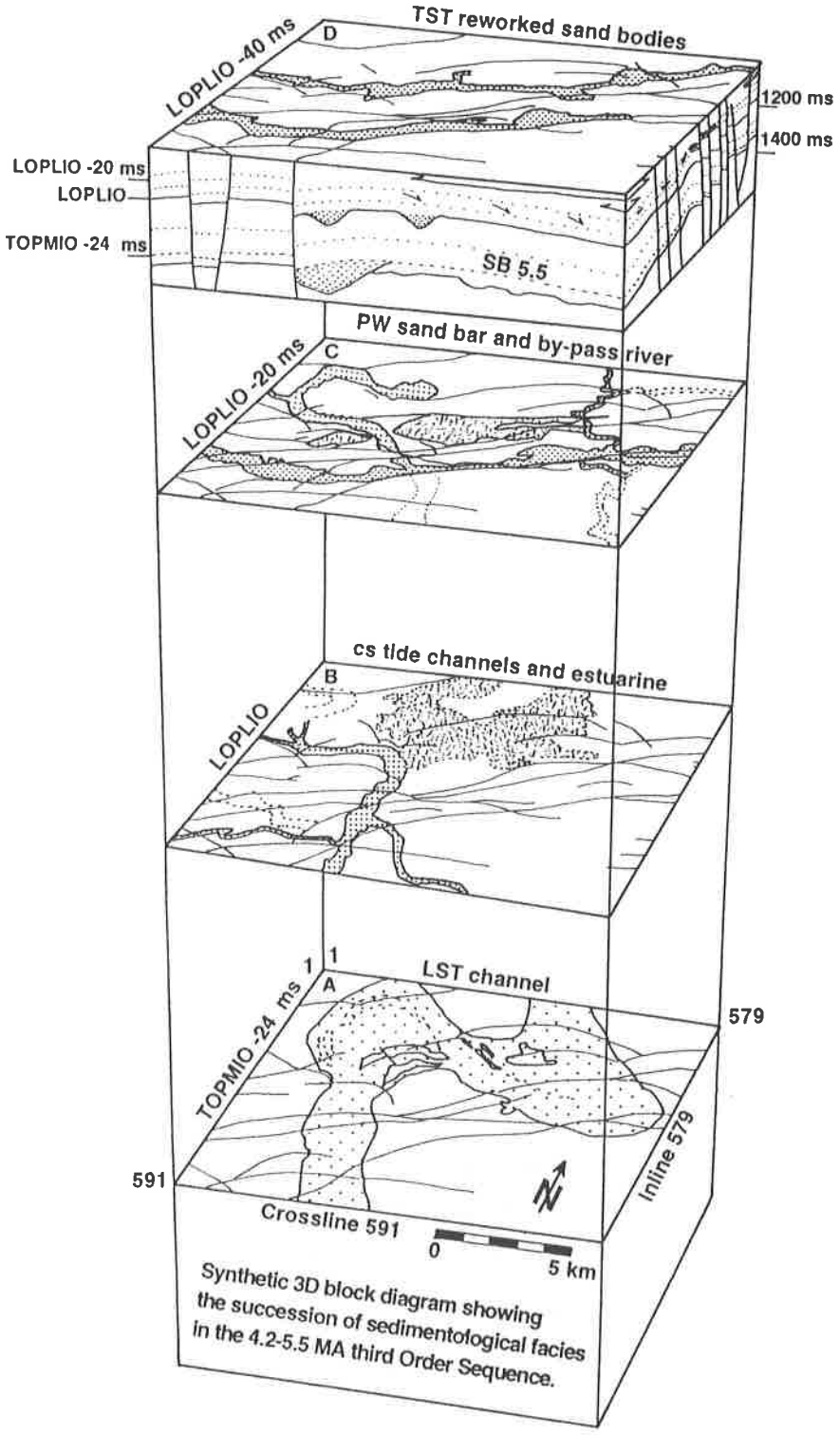

Fig. 5-53: Synthetic 3D block diagram showing the vertical succession of sedimentary facies in the 5.5 to 4.2 Ma interval. Two different interpretation proposed on figure 5-55. ***A.*** *TOPMIO-24 incised valley.* ***B.*** *LOPLIO base of shallow silty channels.* ***C.*** *LOPLIO-20, channels and prograding sand bars.* ***D.*** *LOPLIO-40 transgressive reworked sand bars.*

Conclusion

The five successive sedimentary facies exposed above on amplitude maps illustrate the four systems tracts composing a third order sequence and the main condensed surfaces separating them as deposited in middle neritic environment. They are gathered on a synoptic figure comparing the aspect of systems tracts on vertical line drawings (Crossline 591 and Inline 579, fig. 5-53) and on the corresponding horizontal displays. The same succession of sedimentary facies interpreted in terms of systems tracts is summed up in figure 5-54 inspired by the schematic representation of clastic environments subjects to eustatic changes proposed by Posamentier *et al.*, (1988) and Posamentier & Vail, (1988) . On this figure the zone to take into consideration for comparison with the studied area is limited to the proximal portion of the shelf, not to scale on figure 5-54.

During the lowstand event (fig.5-54 b and TOPMIO-24 map in fig. 5-53) deep erosion of the underlying sequence (incised valley) leads to abundant re-deposition seaward, both on the shelf in the pre-existing growth fault related depressions and down the shelf break. With the first signs of relative sea level rise, the entire shelf is rapidly flooded and a condensed section starvation episode develops shallow water thin and fine estuarine sediments (LOPLIO map, fig. 5-53). Thin layers (20 to 30 m) of proximal prograding sands fill the increasing amount of accommodation space created on the shelf as the rate of relative sea level rise increases. By-pass rivers are progressively backstepping then entirely flooded with the ongoing marine transgression of the shelf that can partially abrade and rework landward the top lowstand and basal transgressive sands (third and fourth maps on fig. 5-53).

At the back of the reworked sand bars large surfaces of proximal shelf are in very shallow water conditions where large swamps or lagoonal facies can develop as in the present Chandeleur Islands, offshore Louisiana. As sea level keeps on rising the complete shelf gets flooded and an homogeneous layer of fine silt and shale belonging to the main flooding surface interval seals the underlying juxtaposition of large surfaces of rich organic matter rocks and porous clean reworked elongated sand bodies. This describes the morphology of a perfect subtle stratigraphic trap.

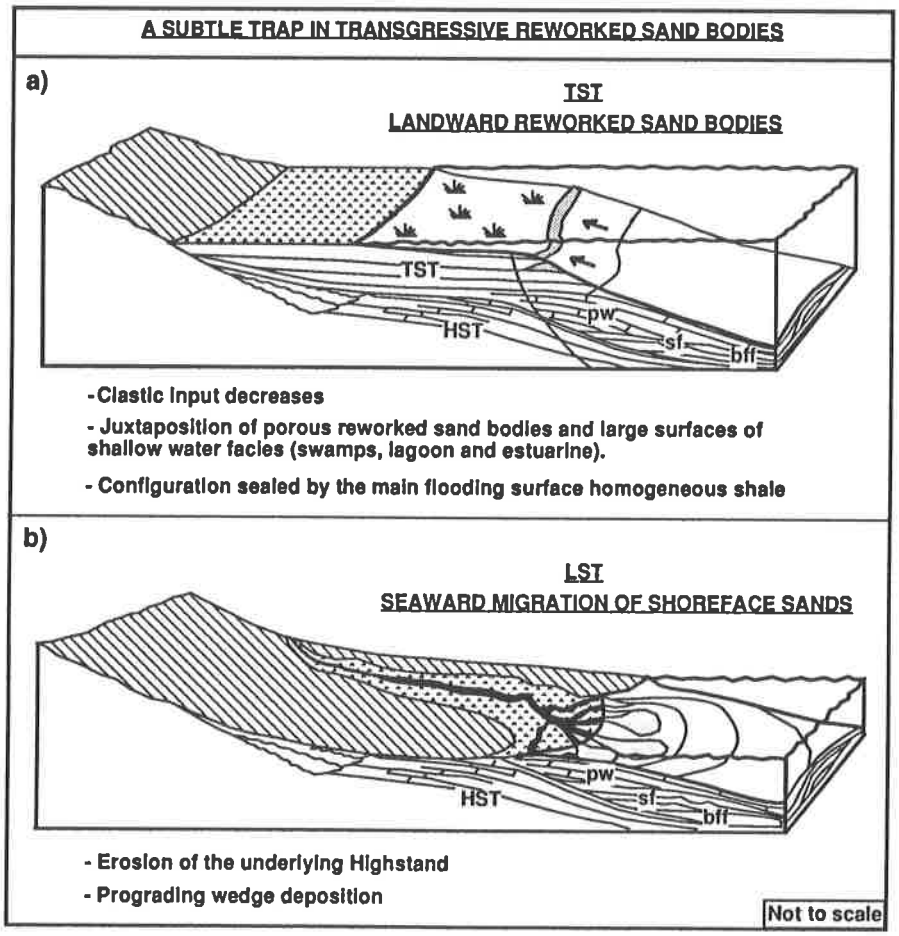

Fig. 5-54: Schematic integration of the four sedimentary facies presented on fig. 5-54 to describe a potential subtle stratigraphic trap in the transgressive reworked sand bodies of prograding sands below.

5.7 2: An alternative interpretation to the SB 5.5 to SB 4.2 interval.

Introduction

The preceding interpretation of the six amplitude maps showing a vertical evolution in sedimentary facies interpreted as the successive systems tracts of one 3rd order sequence (SB 5.5 to 4.2) is based on the sequential analysis on logs considering that this interval was deposited in middle to outer neritic conditions enabling partial lowstand sedimentation on the shelf. As described in chapter 3 (fig. 3-5), a 3rd order sequence in a similar setting can be composed of (see corresponding facies on fig. 5-55, Middle neritic zone):

- (IVF) an incised valley thick sand at its base (dry deltaic zone)
- (Osf) continental to marine deltaic low angle prograding fine sands and silts withoccasional lat eral sandy splays (Osf, outer shelf fan, wet deltaic zone)
- (cs) a condensed section at the beginning of the more rapid sea level rise indicated by silty tide and estuarine like shallow meandering channels.
- (PW) a thin proximal low angle prograding wedge (middle to outer shelf). Its presence on the shelf is dependent on the rate of accommodation space creation.
- (tls) top lowstand surface marking the beginning of the ...
- (TST) transgressive backstepping due to rapid relative sea level rise ...
- (mfs) leading to the maximum of transgression followed by ...
- (HST) low angle highstand fine material progradation.

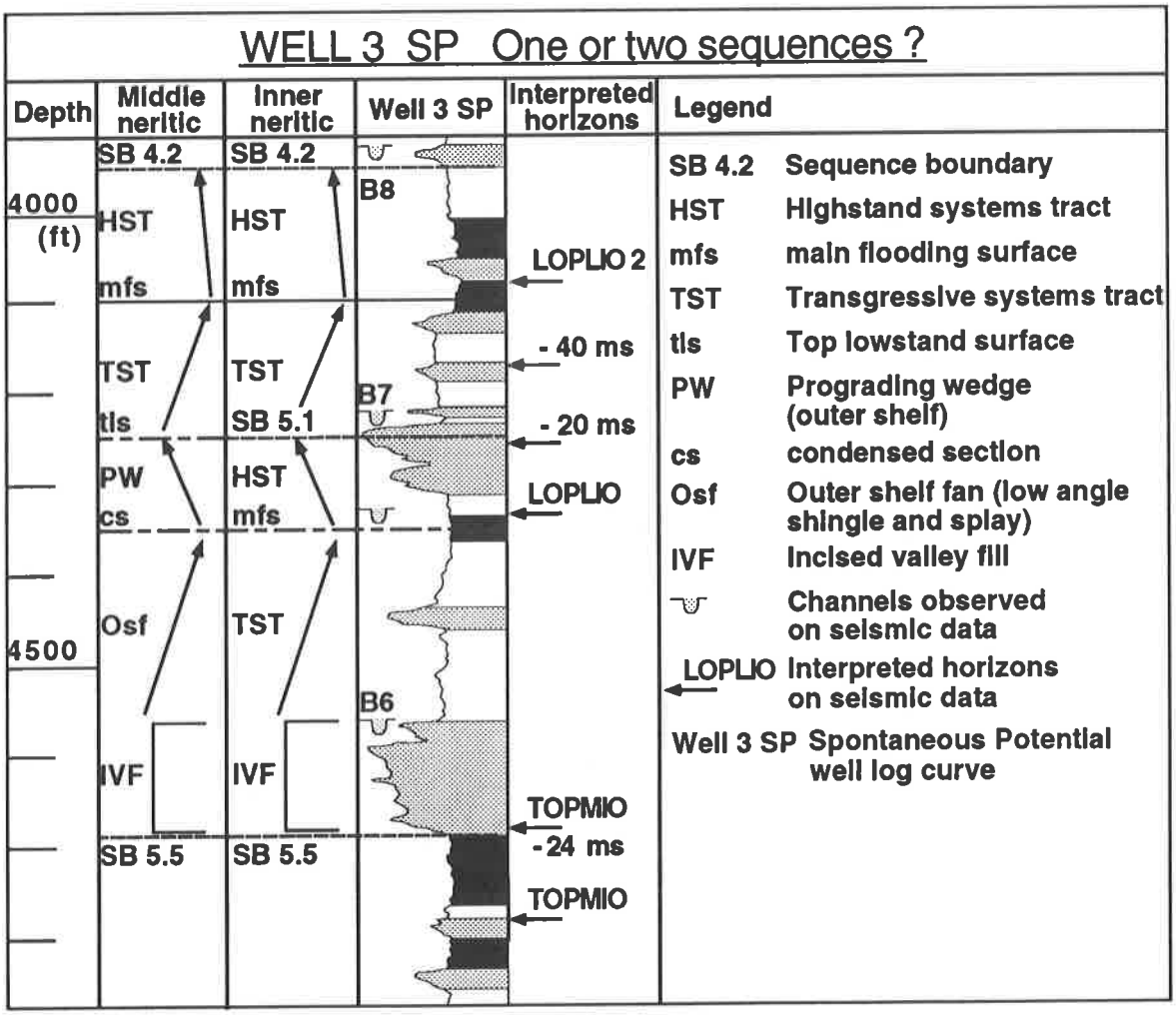

Fig. 5-55: Discussion of sequential analysis on the interval between SB 5.5 and SB 4.2 for inner and middle neritic conditions. How can the erosional surface along LOPLIO-20 horizon be explained ?

This interpretation of the successive lithological patterns of this sequence on Well 3 spontaneous potential curve is consistent with the eustatic and coastal onlap curves from Haq et al. (1988) and TGS (1990) for that interval. As no faunal data is available to specify the exact depositional environment, it is difficult to affirm if no lowstand sediments were deposited on the inner shelf. Considering this interval as sedimented in proximal middle neritic zones related to this important lowstand event implies that no lowstand deposits apart from the incised valley fill can be found on the shelf. The same interval on logs and on the six amplitude maps discussed above must then be interpreted differently.

Observation

In the inner to middle neritic domain (fig. 3-10), a sequence is composed of (fig. 5-55):

- (IVF) possible incised valley if intersected by the well.
- (TST) backstepping silt and shale.
- (mfs) main flooding surface (shallow silty channels on the inner shelf).
- (HST) thin Hst low angle progradation of silt and fine sands
- (SB) partial erosion of underlying sediments by type 1 sequence boundary.

This second sequential interpretation leads to the subdivision of the 3rd order SB 5.5 to SB 4.2 sequence in two shorter 4th order sequences recorded and identified on the base of the inner shelf well log patterns. Such a subdivision in two distinct cycles is supported by the paleo-temperature oxygen isotopic curve of the North Pacific (fig. 5-40) showing that the major cold period between 5.6 and 5.0 Ma has two distinct peaks at 5.5 and 5.1 Ma. Based on this observation, an hypothetical age of 5.1 Ma is attributed to the additional 4th order sequence boundary interpreted on the well log data (fig. 5-55). No deep incised valley similar to the SB 5.5 event are present along the LOPLIO-20 and LOPLIO-40 horizon in the studied area.

But the NNW-SSE channels seen on figures 5-49 and 5-50 interpreted as shallow (30 to 40 m) tidal streams passing vertically to by-pass rivers developed during the beginning of the phase of relative sea level rise of the 3rd order sequence are now interpreted as shallow lowstand channels cutting in the low angle highstand progradation marked by sand bodies parallel to the present shoreline previously interpreted as a thin prograding wedge !

No differences in interpretation are needed on amplitude maps or on well log data for the upper part (TST and HST) of the 3rd order sequence now interpreted as an additional 4th order sequence between SB 5.1 and SB 4.2.

Conclusion

In conclusion, this example shows one more example where a subtle erosional phase occurring during the period of general transgression of large sequence can be missed by the coastal onlap curves constructed on the outer shelf and further offshore but can be enhanced by the observation of the superposition of distinct erosional phases on the inner shelf through 3D seismic data and well log sequential analysis.

The subdivision of the longer 4th order and 3rd order sequence into shorter cycles (0.8, 0.4 and 0.1 Ma) based on this method must absolutely be confirmed by detailed biochronostratigraphic or isotopic data (range of benthic and even planktonic forams about the same resolution as these cycles !). The Pliocene interval in the Gulf coast sense (SB 5.5 to SB 3.0) can be subdivided into four 3rd and 4th order sequences ranging from 0.3 to 0.9 Ma and are summarised on table 1 (SB 3.0, 3.8, 4.2, 5.1, 5.5). Based on the observed succession of sedimentary facies on that interval it seems difficult to find any 0.1 Ma cycles in the Gulf coast Pliocene. This might be related to the important hiatuses caused by the strong and deep incision at the SB 3.0, 4.2 and 5.5 that can have removed most traces of more subtle erosions.

We could conclude that no 0.1 Ma cycles were recorded during the Pliocene but a recent paper from Aharon et al. (1993) demonstrates the presence of eight 0.1 Ma cycles recorded at the Mio-Pliocene boundary between 6.14 and 5.26 Ma The cycles are identified by O^{18} and C^{13} anomalies found in a drilled mid-oceanic carbonate plate-form in the south Pacific converted to apparent ages based on measured $^{87}Sr / ^{86}Sr$ ratio. The amplitude of these eustatic pulses are estimated between 10 and 30 m. Once tested, this hypothesis of 0.1 Ma cycles identified down to the top Miocene could confirm the interpretation presented in this study. The same author explains the disappearance of shorter purely glacio-eustatic cycles below this limit by the major change in ice cap volume estimated in the Late Miocene (Aharon *et al.*, 1993) .

5.7.3: Middle and top Pliocene hiatuses (SB 4.2 to SB 3.0 Ma).

If the sequential interpretation done on logs and seismic data is valid and if a periodicity in eustatic events is superimposed to the regular subsidence of the studied area, the highstand deposits on top of the SB 5.5 to 4.2 Ma 3rd order sequence should contain the erosive traces of the next relative fall in sea level. To check that, two additional amplitude maps are calculated above the LOPLIO2 horizon. They show two distinct erosive features that can be associated to two successive relative falls of sea level. But the interval between the 4.3 Ma highstand mapped along the LOPLIO2 horizon and the deep erosion associated with the sequence boundary at 3.0 Ma (fig. 5-44) is very complex and probably shows a depositional gap.

This complicated interval is discussed below on the base of seismic sections, amplitude and volume attribute maps, well log data and the pre-established eustatic curves constructed for the Gulf of Mexico (Haq *et al.*, 1988; TGS, 1990) .

On the seismic sections (figs. 5-31 and 5-41) the interval between the LOPLIO2 and the MPLIO horizons show two superposed generations of channels. The inferior one (labelled as C4.2, B8) shows deep (50 to 70 m) broad open channels filled with characteristic high amplitudes. They correspond to large meandering incised valleys showing several generations of channels contained within the main valley bed (fig. 5-56 a and b). On top of them is a transparent interval which is partially eroded by shallower and narrower channels (labelled as SB 3.8, B9 on fig. 5-31 and 5-41).

Figure 5-56 a and b presents the amplitude map calculated 56 ms above the LOPLIO2 horizon that intersects the upper portion of the large C4.2 channels seen on vertical sections (rlwel1 and rlwel2). This broad meandering incised valley is marked by a strong amplitude anomaly comparable to the one associated with the preceding important fall in sea level that occurred in relation to the 5.5 Ma top Messinian lowstand (see fig. 5-47 and 5-48). The shallow meandering channels located on top of this major erosive event intersected by an amplitude map calculated 68 ms above the LOPLIO2 horizon are visible on figure 5-57. The channels are not easy to identify on such a black and white amplitude display. But a myriad of very shallow and narrow meandering channels flowing mainly from NW to SE can be seen on volume attributes maps calculated over the same interval.

Conclusion

These two types of seismic data suggest that at least two distinct erosive phases are present in this interval and that the lower (older) one must be related to a fall of relative sea level more important than the one on top.

The eustatic curve from Haq et al. (1988) and the TGS™ (1990) coastal onlap curves both indicate first a minor sequence boundary at 4.2 Ma and then a second sequence boundary at 3.8 Ma related to an important fall in relative sea level similar in amplitude to the one observed at 5.5 Ma. As the data available for this study lack microfauna information for the Plio-Pleistocene it is impossible to propose a sure correlation of the observed event to the pre-existing local eustatic curves. If the important phase of erosion seen on amplitude map LOPLIO2 -56 ms corresponds to the drastic fall in sea level registered at 3.8 Ma as proposed by Haq et al. (1988) then the erosive phase determined on top of the 3.8 Ma event represents a 4th order pulse between SB 3.8 and SB 3.0 not indicated on the Haq et al. curve.

When looking at the oxygen isotopic curve of the North Pacific (fig. 5-40) which shows an excellent correlation for the entire Miocene with the eustatic curve present on the same figure, it can be observed that no cold period is registered in relation to the 3.8 sequence boundary.

Is the SB 3.8associated relative fall in sea level not directly connected to climatic changes or is it wrongly dated ? This study shows that two erosive phases are observed in this interval and that the oldest is related to the stronger erosion. On the basis of the correlation with the oxygen isotopic curve for the north Pacific (fig. 5-40) we are inclined to attribute the major erosion observed on figure 5-55 to the cold period occurring between 4.1 and 4.2 Ma (B8, fig. 5-65). but this needs to be checked by additional biochronostratigraphic data. An alternative solution would be to attribute the deep lower erosion to the SB 3.8 Ma sequence boundary that would have eroded the totality of the SB 4.2 to SB 3.8 interval in the studied region.

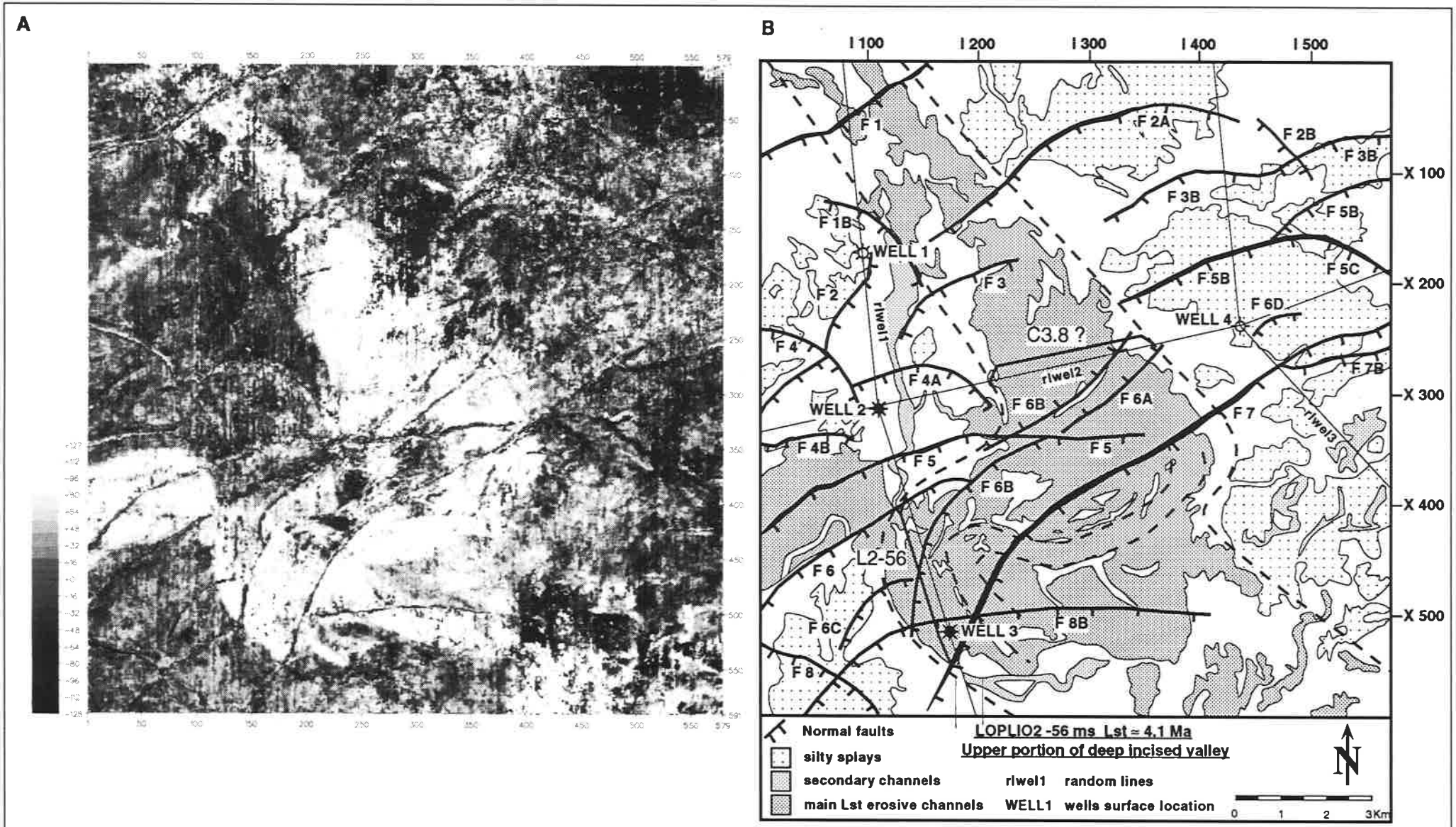

Fig. 5-56: ***a.*** *Amplitude map calculated 40 ms above the LOPLIO2 horizon showing the incised valley 16 ms (≈ 18 m) below the interpreted map on figure 5-56 b. The migration of the main canyon in the meanders can be distinguished. On this map, positive amplitude are in white.* ***b.*** *Interpretation of an amplitude map 16 ms above figure 5-56 a (56 ms above LOPLIO2 horizon) to show the slightly wider upper portion of same incised valley (B8, see table 1).*

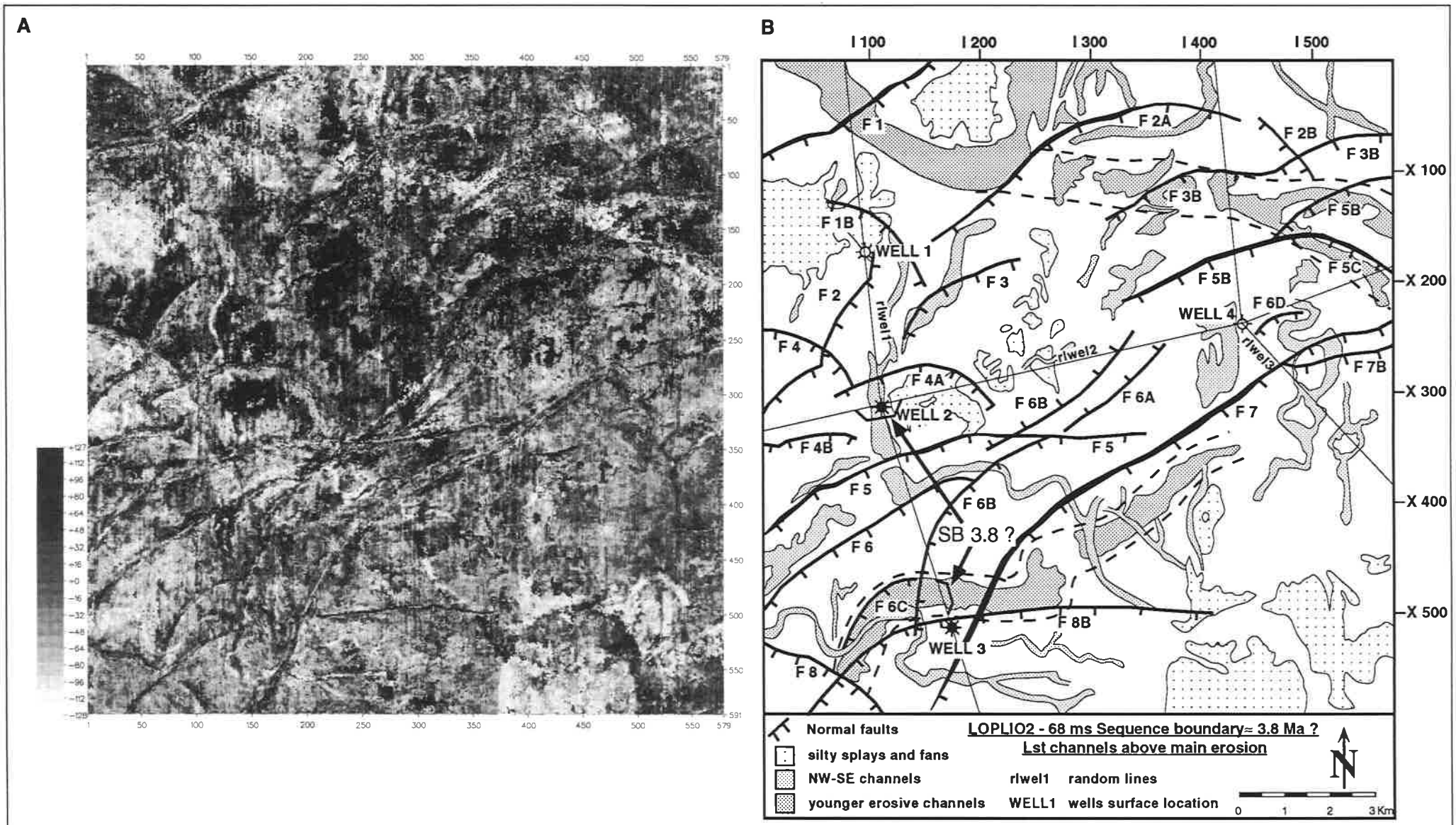

*Fig. 5-57: **a.** Amplitude map calculated 68 ms above the LOPLIO2 horizon. The chaotic aspect of this map can indicate the strong gap in sedimentation related to the SB 3.8 Ma strong erosion (no incised valley in the studied area for that level). **b.** Interpretation of a complex superposition of channels associated with the erosional phase (SB 3.8, B9) on top of the incised valley on fig. 5-56.*

5.8 Middle and Late Miocene 3rd order sequences

Introduction

This final chapter discusses the Late Miocene Tortonian stage (6.5 to 11 Ma; Odin and Odin, 1990) marked by an extended peak of cold paleotemperature as indicated by the oxygen isotope curves on figure 5-40. The Tortonian stage is dominated by reverse Earth magnetic field polarity. In the studied area, the base of the Late Miocene constitutes the superior limit of the productive interval. Some of the sequence boundaries identified below this limit are discussed in chapter 6, in association with stratigraphic traps descriptions. This time limit also coincides with the transition from the middle to the outer neritic condition in the region indicating that all productive sands (Text W, Big. Hum. and Cib. op.) correspond to outer shelf and upper slope environments (Zone 3, 2500 m below present sea level, at SB 10.5 Ma).

The Haq et al. curve (1988) divides the Tortonian into two large 3rd order sequences (SB 10.5, SB 8.2 and SB 6.3). The TGS™ coastal onlap curve (1990) indicates one more sequence boundary at SB 8.8 Ma. On the studied 3D survey and based on the available well log data, 2 additional erosional surfaces are interpreted as regional sequence boundaries and correspond to cold peaks registered on the Pacific oxygen isotopes curves at 7.1 and 9.7 Ma. These erosional surfaces are preserved in the studied area due to their position in the transgressive period of the larger sequences indicated on the TGS™ (1990) curve (SB 6.3 to 8.2 and 8.8 to 10.5).

Observation

On well log data this interval is perfectly time constrained by the benthic foraminifers paleo-tops. One homogenous and regional layer of 25 to 30 m of shale systematically showing the first down hole apparition of Bigenerina A. (LAD at 6.2, see Annexe 2) is found on all logs and is associated with the main flooding surface event recorded below the clear erosional surface marking the 6.3 Ma sequence boundary (see fig. 5-58). A thicker layer of shale (30 to 40 m) bearing the Bigenerina 2 LAD dated at 10.5 Ma (Annexe 2) is found below the SB 10.5 erosional surface (fig. 5-58). In between, the Discorbis 12 (8.2 Ma) and Textularia L (8.8 Ma, see Annexe 2) shale levels respectively help in dating the SB 8.2 and SB 8.8 sequence boundaries and associated erosional surfaces. The north-south well log profile on figure 5-58 indicates that Well 2 and 3 (south-west portion of the studied area, see fig. 5-59) present an inferior concentration of sands on the totality of the Tortonian. Lateral abnormal reduction of sequences thickness can be related to intersections with normal growth faults (SB 8.2 to 8.8 on Well 2).

The seismic section on figure 5-41 presents a NNW-SSE randomline profile across Well 2 and Well 3 (rlwell, see fig. 5-59). 8 superposed generations of erosional features are identified between the SB 5.5 top Messinian erosion and the base Tortonian at SB 10.5 (B0 to B6, see fig. 5-64). This interval is recognised on vertical seismic sections on the 3D data and on regional seismic lines across the northern Gulf coast shelf by 8 to 10 continuous reflectors bordered at the base and top by two transparent seismic facies corresponding to the thick transgressive and highstand shelf sands found below SB 10.5 and above SB 6.3 (see fig. 5-41).

6 amplitude maps and/or their geological interpretations are presented below to illustrate the vertical succession in horizontal sedimentary facies during that period. The base of the transgressive thinning up sandy interval identified on logs in the upper half of the sequence between SB 5.5 and SB 6.3 is intersected by the amplitude map calculated 56 and 60 ms below the TOPMIODL horizon (fig. 5-58, TDL+60). This map shows a NW-SE systems of shallow channels and the development of two fans down the major F1 and F7 growth faults (see Fst and B5 intersected along Well 1 and 4 on logs, fig.5-58 and on the map). Again, erosional features recorded at the base of the transgressive systems tract of a larger sequence implies the presence of a lower order eustatic pulse attributed in this case to an additional regional sequence boundary at 5.9 Ma (B5, see fig. 5-65).

The global, world-wide recorded basal Messinian 6.3 Ma sequence boundary dated on logs by the "Big. A" shale shows very deep erosional features illustrated on figures 5-60 a, b and c. The B4 sandy channels identified on logs (fig. 5-58) are intersected by the TOPMIODL +100 and + 116 amplitude maps. On these images, a lateral difference in thickness of the sediment pile produces the apparent inversion of polarity of the main SB 6.3 channel. Like on figure 5-59, the channels mainly flowing form NW to SE are clearly deviated in the centre of the image by the depression related to the antithetic faults (F6 A, B and E) associated with the F1 growth fault system before crossing down the next major F7 growth fault. Figure

5-60 a is the combined interpretation of the two aforementioned amplitude maps.

Figure 5-61 presents a high degree of similitude with the map seen on figure 5-59 and represents a shallow erosional surface recorded during the transgressive interval of a larger sequence (shallow channel and fan development down the growth faults). In correlation with the oxygen isotopic curve on figure 5-40, this cold erosive event dated at 7.1 Ma is attributed to an additional lower order sequence boundary (SB 7.1, B3 on fig. 5-65). B3 sandy shallow and narrow channels are intersected by Well 2, 4 and 6 (see fig. 5-58 and 5-61).

The last map on figure 5-62 b results from the combined interpretation of two amplitude maps calculated along the LM1 horizon and a map 16 ms above it. The amplitude map obtained along the LM1 horizon is displayed on figure 5-62 a with a compressed colour scale. Figure 5-62 b shows three distinct sedimentary facies (from base to top):

- an oblique lateral difference in seismic facies recorded along the LM1 horizon interpreted along a positive loop indicates shale (in white, positive loop from slow sands to fast shale) in the south-west corner and silt or fine sands (to the north-east). This level represents the period of relative high sea level recorded below the SB 8.8 Ma erosional surface and can be interpreted as the landward transgression of shale on silt or rather as the highstand progradation of silt on the mfs shale.

- the same map presents also narrow north-south meandering (B1) channels also identified on the vertical seismic section (fig. 5-41). They mark the shallow incision associated with the SB 8.8 Ma erosional surface dated by the shale below.

- The inferior traces of the deep SB 8.2 NW-SE large channels are still visible on this map and better expressed on amplitude maps calculated above the LM1 horizon. North of Well 1, the seismic section on figure 5-41 intersects longitudinally a portion of the main B2 channel running through the studied area. These observations confirm the presence of two closely spaced sequence boundaries at 8.8 and 8.2 Ma partially cutting through the thick shale below, sedimented during the pronounced hot transgressive interval registered around 9.0 Ma (see fig. 5-40, oxygen isotopes curves). The difference in amplitude between these two sequence boundaries is expressed on regional lines across the shelf by coastal onlaps and on 3D horizontal local images by differences in depth, size and degree of sinuosity of the two channels generations.

At the base of the Tortonian, two distinct erosional surfaces are identified above and below the MM9 interpreted horizon (B0 and B0-1, seismic section on fig. 5-41). The amplitude map on figure 5-63 calculated 80 ms below the LM1 horizon intersects rectilinear NW-SE shallow channels and a fan down the F7 growth fault. This erosional surface recorded during the transgressive interval of the SB 10.5 to SB 8.8 Ma sequence corresponds to sharp cold peak recorded on the oxygen isotopes curves that culminates at 9.7 Ma. This additional sequence boundary is placed at the culmination of the Hst progradation and at the base of the following thinning up Tst (see fig. 5-58, B0 on Well 5). This sequence boundary splits in two equal halves the 1.6 Ma year long 3rd order sequence into two 0.8 Ma sequences.

Due to the poor lateral homogeneity of the reflector interpreted along the MM9 horizon and of the relative transparency of the seismic facies below it, the erosional features associated with the SB 10.5 sequence boundary are better illustrated on vertical sections and on logs than on amplitude maps (figs. 5-58 and 5-41). It is therefore not worth being illustrated here.

Conclusion

The curve of coastal onlap that cannot be directly checked by this study shows a constant increase in relative marine transgression rate over the entire Tortonian and Messinian stages. In this interval (SB 5.5 to SB 10.5), where 4 distinct erosional surfaces are recognised on the Haq et al. curve (1988), 8 are now identified on the vertical seismic sections, the well log data sequential analysis and the horizontal facies reconstruction of this 3D data. They all fit colder paleo-climates intervals as indicated by oxygen isotopic curves. The 0.8 Ma periodicity in stronger erosions can also be observed on the almost totality of this interval (SB 5.5, (5.9), 6.3, 7.1, 8.2, 8.8, 9.7, 10.5).

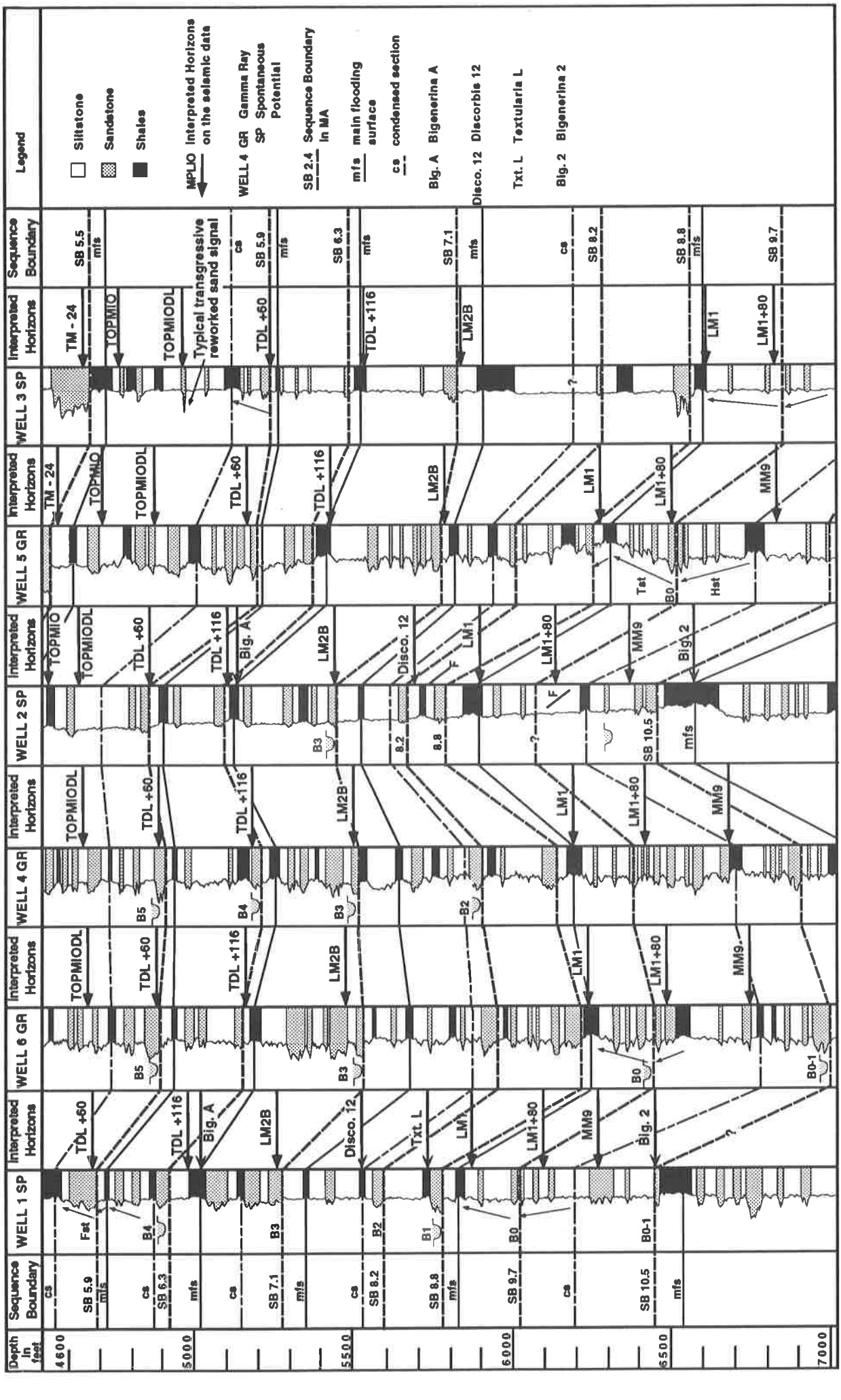

Fig. 5-58: North-south well log cross section for the Messinian and Tortonian stages (6.3 to 10.5 Ma). 8 sequence boundaries are recognised on this interval. The 10.5 Ma limit corresponds in the studied area to the transition from the middle to the outer shelf environment (100 m limit).

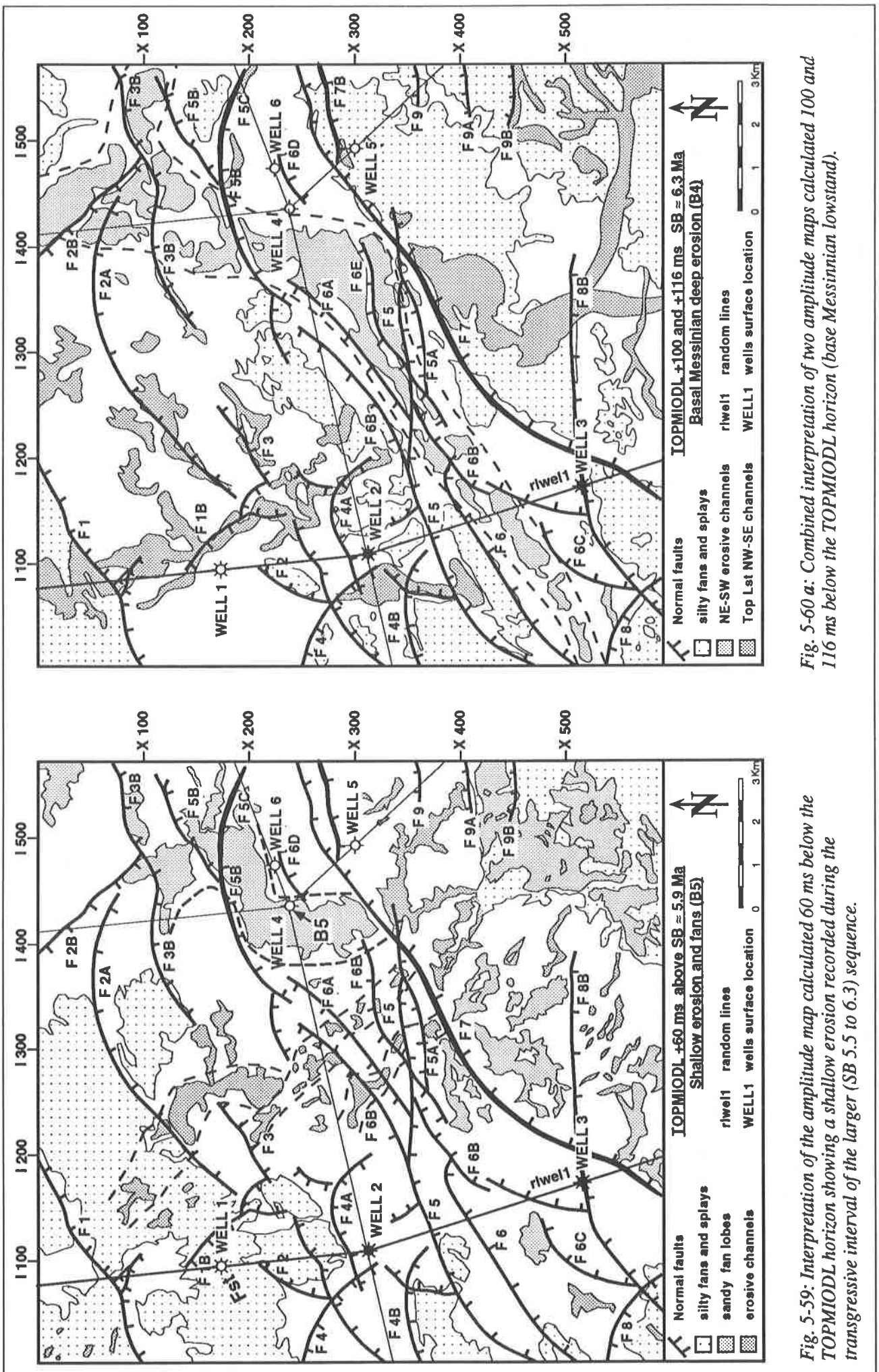

Fig. 5-59: Interpretation of the amplitude map calculated 60 ms below the TOPMIODL horizon showing a shallow erosion recorded during the transgressive interval of the larger (SB 5.5 to 6.3) sequence.

Fig. 5-60 a: Combined interpretation of two amplitude maps calculated 100 and 116 ms below the TOPMIODL horizon (base Messinnian lowstand).

*Fig. 5-60: **b.** Amplitude map claculated 100 ms below the TOPMIODL horizon. Deep NE-SW channels parallel to the growth fault trend.*

*Fig. 5-60: **c.** Amplitude map calculated 116 ms below the TOPMIODL horizon. Shallower NW-SE channels and southern portion of the main incised valley (see fig. 5-60 a. for interpretation).*

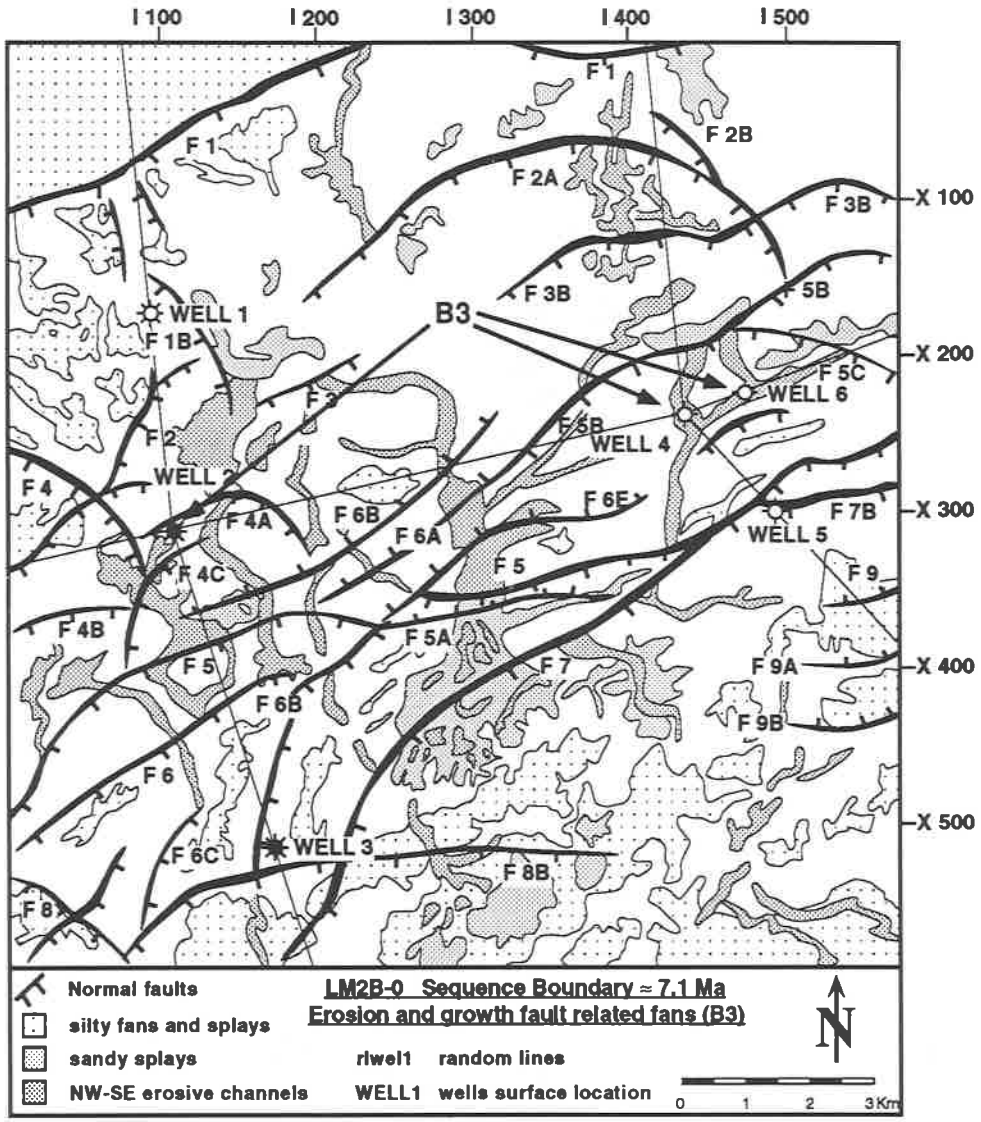

Fig. 5-61: Shallow NW-SE channels recorded during the transgressive interval of the SB 6.3 to SB 8.2 larger sequence and thin fans deposition down the faults.

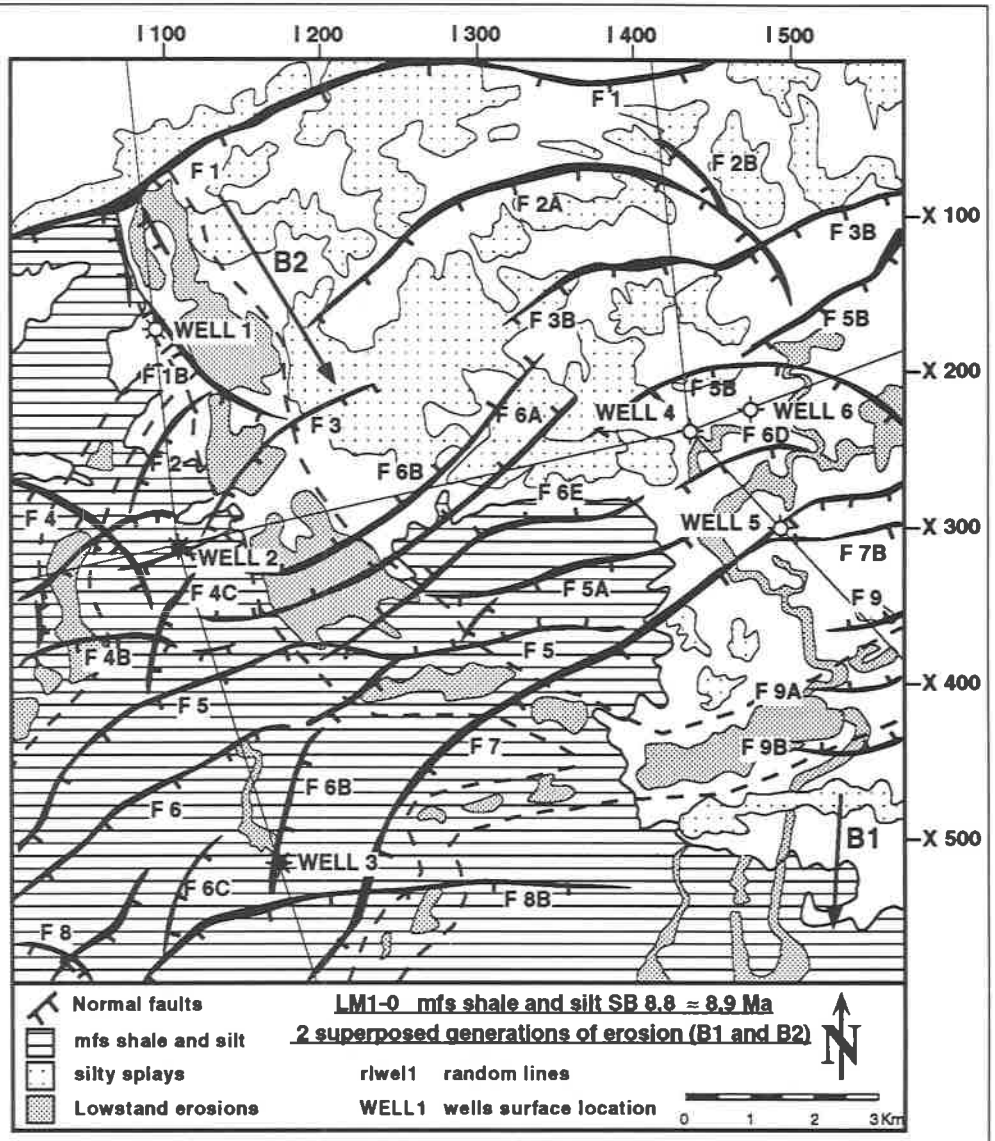

Fig. 5-62 b: Combined interpretation of two amplitude maps along the LM1 horizon and 16 ms above it. Three superposed sedimentary facies are recognised: 1) silty coastal onlap along the 8.9 Ma mfs; 2) shallow north-.south meandering channels (SB 8.8, B1); 3) large NW-SE incised valley (SB 8.2, B2).

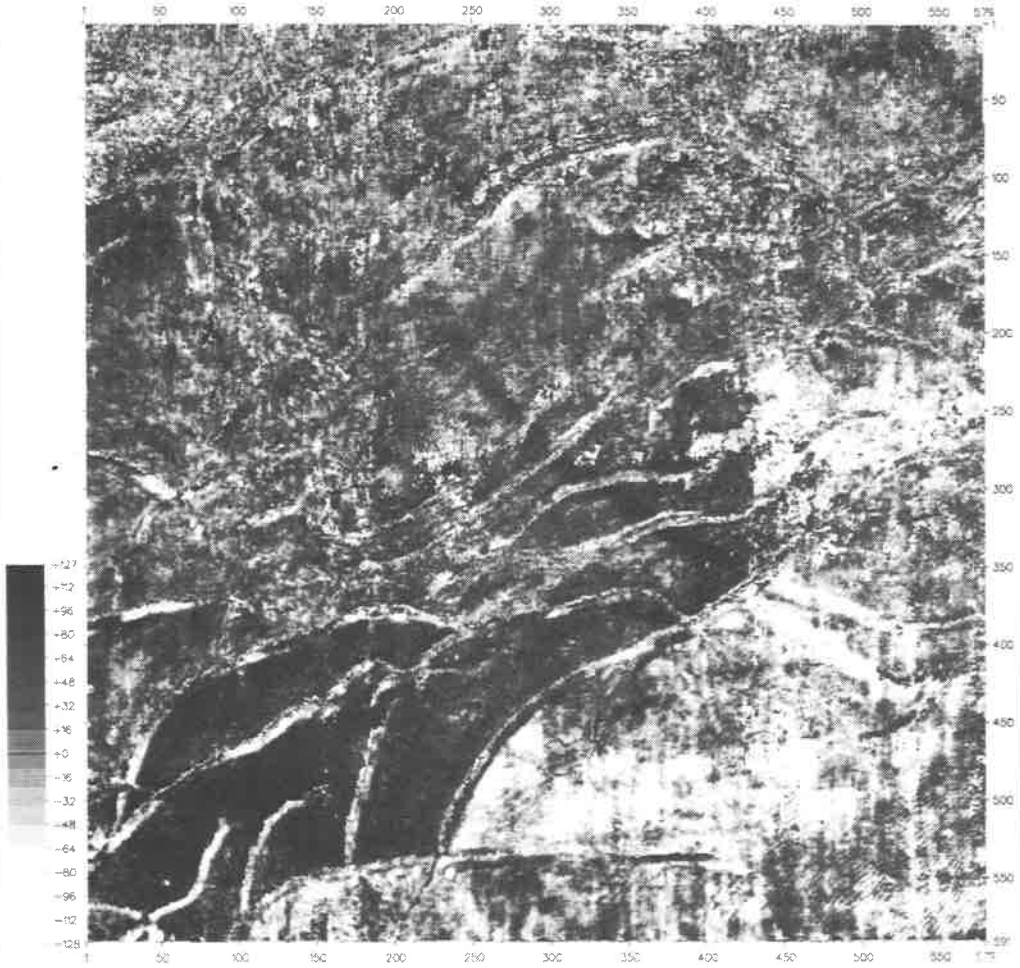

Fig. 5-63: Amplitude map calculated 80 ms below the LM1 horizon to intersect the erosional surface at 9.7 Ma (SB 9.7, B0).

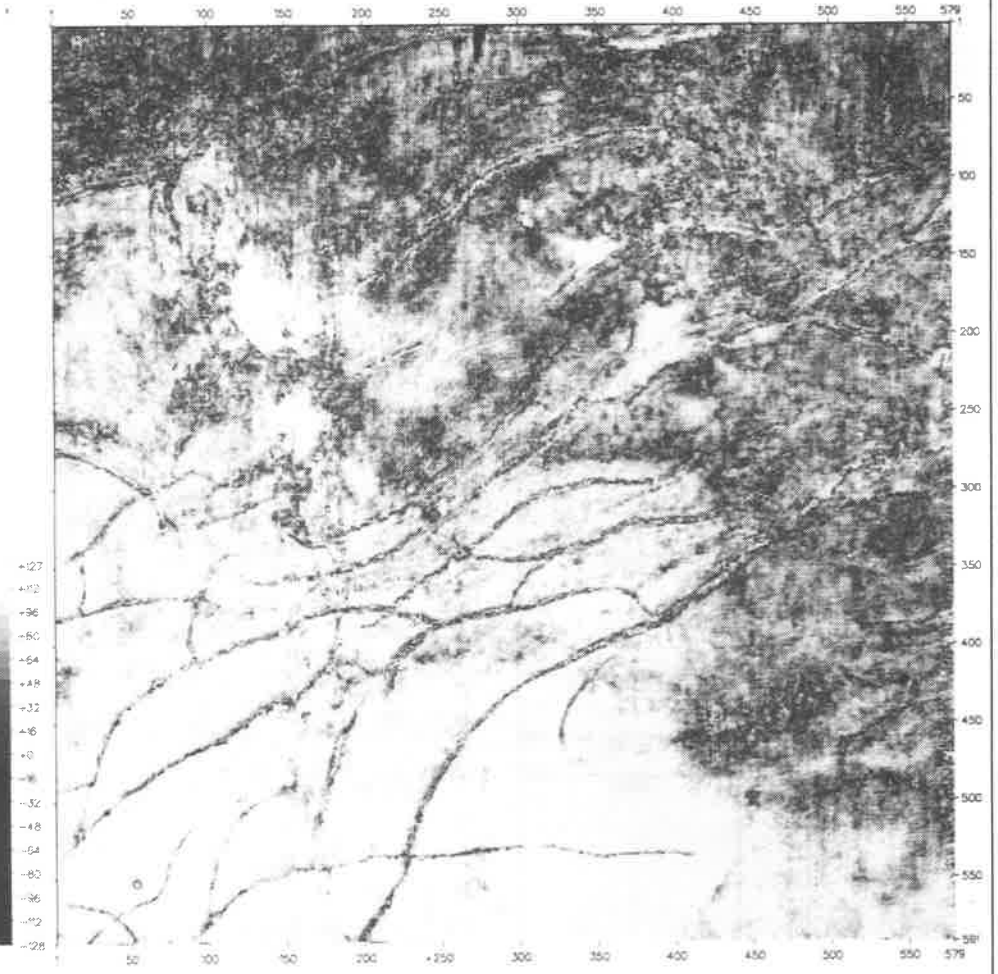

*Fig. 5-62: **a.** Amplitude map calculated along the LM1 interpreted horizon. Note the reversed and compressed colour scale (see fig. 5-62 b for interpretation). Fault traces appear clearly in black.*

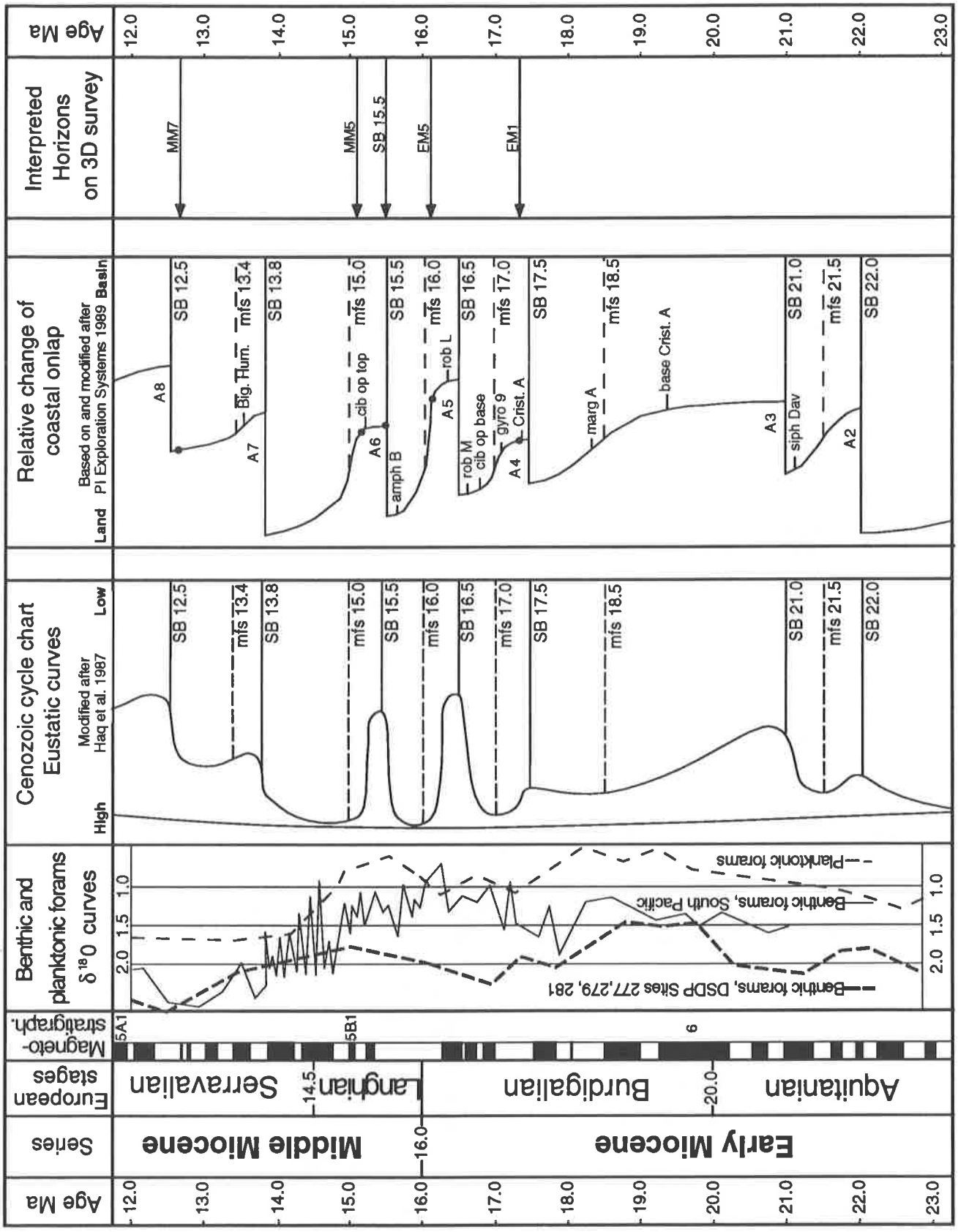

Fig. 5-64: Synthetic Early and Middle Miocene chart with series and continental stages, oxygen isotopes reference curve, eustatic and coastal onlap curves in the Gulf of Mexico, and interpreted horizons (black dots).

5.9 Synthesis

3D sequence stratigraphy defined as the sequential analysis of interpreted chronostratigraphic maps (3D seismic data horizontal attribute maps), of well log data and of the high density of vertical seismic data provided by 3D data sets (Reymond & Stampfli, 1994a) is presented here as a potent new tool for the description of depositional processes. The size, morphology, lithologic content and genesis of clastic sedimentary bodies in inner shelf condition can be systematically investigated over the entire surface of the available 3D data set . The recognition of subtle superposed erosional phases recorded on a small portion of the inner shelf of the northern Gulf of Mexico shows that 0.1 Ma eustasy related cycles can be recognised over the entire Gulf coast Pleistocene (0-3.0 Ma).

A 0.8 Ma periodicity is indicated in the studied area by a recurrence of stronger erosions recognised by deep incised valleys and a hiatus in the sediment record partially removing the traces of the shorter cycles below. A similar 0.8 Ma periodicity is also observed on the magnetostratigraphic scale. The 0.8 Ma periodicity is recognised over the Middle and Late Miocene (SB 5.5, 6.3, 7.1, 8.2, 8.8, 9.7 and 10.5. A possible explanation could be found in the periodic changes in the distance between the Earth and the Sun influencing simultaneously the eustatic, climatic cycles and the magnetic inversions of the Earth magnet. The 0.8 Ma periodicity could correspond to the double wave-length of the 400'000 years orbital cycles described by Milankovitch (1941).

The extensive conclusions provided at the end of each sub-chapter in chapter 5 are summarised on Table 1 (fig. 5-65) where the distinct successive erosional phases not present in the literature are indicated in bold. The Gulf coast Pleistocene is characterised by systems of erosion on the shelf developed during period of relative lowstand oriented from NE to SW (or ENE-WSW) indicating a general sediment input from the Mississippi drainage basin. Below the top Pliocene hiatus (Gulf sense, 2.8-3.0 Ma, C0 phase) and over the entire studied portion of the Neogene, incised valleys and associated erosion are oriented almost perpendicularly (NW-SE) to the river systems developed during the Pleistocene. They show deeper and wider incision and the shorter cycles (4th order 0.1 Ma cannot be identified). They correspond to a sediment input dominated by the Texan drainage basin (Brazos, Colorado and Sabine rivers).

Major phases of relative lowstand described in the literature (SB 0.8, 1.46, 2.4, 2.6, 3.0, 4.2, 5.5, 6.3, 8.8, 10.5 and 15.5) are marked by deep erosions recognised by incised valleys. This study shows that they are all preceded by shallower and distinct phase of erosion affecting the footwall of active growth faults and systematically developing proximal lowstand fans on the hanging wall of active growth faults (see figs. 5-65 and 7-2). This characteristic alternation of erosional features is observed in the studied area from the Late Miocene to the Middle Pleistocene.

The interpretation of seismic features displayed in various attributes and enhanced by sometimes extensive colour scale manipulation into sedimentary bodies is based on their lateral continuity and coherence recognised on reconstituted horizontal surfaces of deposition or erosion. This study provides a vast number of different typical stratigraphic and morphologic templates of horizontal seismic responses to sedimentary facies in an inner to outer shelf clastic environment.

The application of 3D sequence stratigraphy for an oriented search for subtle stratigraphic traps on the inner portion of a clastic shelf (Gulf coast, Nigeria delta, offshore Brunei) is developed in the next chapter.

Figures	Interpreted Horizons	Erosional surfaces	Label	Channels Orientations		Type of Channels	Depth of Channels (m)
		0.1 Ma	C19				
5-22	HP6	0.2	C18	NE-SW	↙	Incised valleys	40-60
		0.3	C17	NE-SW	↙	Incised valleys	40-60
		0.4	C16	NNE-SSW	↙	Meandering	20-50
5-22	HP5	0.5	C15	N-S	↓	Meandering	20-50
5-11		***0.65***	C14	NNW-SSE	↘	Meandering	40-60
5-9	HP4	0.8	C13	NNE-SSW	↙	Incised valleys	70-80
5-19 / 5-21		***1.1***	C12	NE-SW	↙	Meandering	40-60
5-10	HP2	1.25	C11	NNW-SSE	↘	Shallow	20-40
5-16	HP1	1.46	C10+b	NE-SW	↙	Incised valleys	50-70
5-27	LOPLEIST-60	***1.52***	C9	NW-SE	↘	Shallow+fans	10-30
5-26	LOPLEIST-36	***1.6***	C8	NW-SE	↘	Shallow+fans	20-40
5-25	LOPLEIST	***1.65***	C7	NNW-SSE	↘	Wide meanders	40-60
5-24	LOPLEIST+28	***1.75***	C6	N-S	↓	Braided type	50-70
5-39	LATEPLIO-44	1.85	C5	ENE-WSW	↙	Meandering	40-60
5-38	LATEPLIO	***2.1***	C4	NW-SE	↘	Shallow	20-40
5-35-36-37	LATEPLIO+40	***2.3***	C3	NE-SW	↙	Incised valleys	60-80
5-33-34	SB24	2.4	C2	NW-SE	↘	Shallow+fans	40-60
5-32	SB24+44	***2.5***	C1	NE-SW	↙	Incised valleys	60-80
5-42	MPLIO-44	2.6	C0	N-S	↓	Shallow	20-40
5-44	MPLIO+16	3.0	B11	NNE-SSW	↙	Incised valleys	80-100
5-44	MPLIO+16	3.1	B10	NW-SE	↘	Shallow+fans	40-60
5-57	LOPLIO2-68	3.8	B9	NE-SW	↙	Meandering	
5-56	LOPLIO2-56	4.2	B8	NW-SE	↘	Incised valleys	80-100
5-49-50	LOPLIO-20	***5.1***	B7	NW-SE	↘	Shallow+fans	
5-47-48	TOPMIO-24	5.5	B6	NNW-SSE	↘	Incised valleys	90-110
5-59	TOPMIODL+60	***5.9***	B5	NW-SE	↘	Shallow+fans	40-60
5-60a, b, c	TDL+100/+116	6.3	B4	NNW-SSE	↘	Incised valleys	70-90
5-61	LM2B	***7.1***	B3	NW-SE	↘	Shallow+fans	20-40
-	LM1-16	8.2	B2	NW-SE	↘	Shallow+fans	10-30
5-62 a, b	LM1	8.8	B1	NW-SE	↘	Incised valleys	40-60
	LM1+80	***9.7***	B0	NW-SE	↘	Shallow+fans	20-40
	MM9+24	10.5	B0-1	NW-SE	↘	Incised valleys	40-60
6-15	MM7	12.5	A8	NW-SE	↘	Incised valleys	40-60
-	-	13.8	A7				
6-11	MM5	-	A6+b	NNE-SSW	↙	Shallow+fans	20-40
6-16	SB15.5	15.5	A6	N-S	↓	Incised valleys	40-60
6-16	EM5	16.5	A5				
6-16	EM1	17.5	A4				

Fig. 5-65: Synthetic chart of Neogene and Pleistocene successive erosiona phases and characteristics observed in this study (Table 1). A, Early and Middle Miocene; B, Late Miocene and Pliocene; C, Gulf coast Pleistocene (0 - 2.8Ma).

6. THREE-D SEQUENCE STRATIGRAPHY AND THE SEARCH FOR HYDROCARBONS

6.1 Introduction

3D Sequence Stratigraphy is a potent exploration and development tool for subtle stratigraphic traps discovery. Reservoir morphology, heterogeneity and subtle stratigraphic trapping mechanisms can be better understood through systematic horizontal identification of sedimentary facies of systems tracts provided by 3D attribute maps (sample level and volume related attributes). On new prospects as well as on already producing fields the additional input of sequential analysis on logs and on 3D data enables to locate and identify new productive zones (Reymond & Stampfli, under press).

The first part of this chapter (6.2.2) presents six typical horizontal seismic facies assigned to the successive systems tracts of a 3rd or 4th order sequence recorded in inner to outer neritic condition on a clastic shelf. The construction of this composite sequence is based on the observed reproducibility of horizontal seismic facies response to cyclic eustatic events on more than 20 sequences registered in the Gulf coast Plio-Pleistocene and Late Miocene. The second part (6.2.3) shows how 3D sequence stratigraphy (Reymond & Stampfli, 1994c) can contribute in localising and understanding sedimentary facies associated with productive zones. A case study in the early Middle Miocene Cibicides opima sands shows multiple stacked gas accumulation in the top slope fan, prograding wedge and basal transgressive systems tract of the 3rd Order sequence between SB 15.5 and SB 13.8 Ma.

So far, hydrocarbon exploration was mainly based on structural analysis, either from surface outcrop data or from 2D seismic lines. The lack of lithologic information outside the drilled wells made it difficult to reconstruct paleosedimentary facies in the sub-surface. The rapid improvement of reflection seismic data allowed to determine seismic velocity which is a direct function of porosity and type of fluid content. It then became possible to represent subtle lateral variations of seismic velocity on 2D vertical seismic sections amongst conformable and non-deformed strata and visualise non structural traps that could be related to hydrocarbon accumulation (Savit & Wu, 1982) . Subtle traps and subtle deformation patterns hardly visible on 2D wiggle display but identified by semi-automatic programs defining the lateral extension of gas or oil anomalies are now made directly visible by raster density coloured vertical and horizontal display of scaled or true amplitudes seismic data. The further development of seismic reflection data into almost systematic acquisition of 3D surveys for exploration purposes on new regions and on old fields brought into existence the possibility to visualise lateral changes in physical properties on the horizontal plane. The existence of subtle stratigraphic traps was demonstrated when it became possible to show that productive stratigraphic features were extending across structures partially overprinting original sedimentary morphology.

The geological interpretation of seismic facies horizontal maps now enables to reconstruct and to represent paleosedimentary facies in a way that can convince management to drill subtle stratigraphic traps. Up to recently, finding oil as cheaply as possible was realised by drilling large structures in unexplored regions. Nowadays, all major productive basins in the world are known and the required reserves for the future are hidden in subtle features hidden in the already "well-known" basins (Halbouty, 1982) . To match this change in objectives new tools are required which explains the constant expansion in 3D seismic acquisition and interpretation techniques. Additional attributes of the seismic signal are continually invented to fit the interpreter's requirements who needs as many different information as possible to guaranty the presence of hydrocarbon on the base of seismic and well log data (dip and azimuth, sample and volume related attributes like amplitude maps, reflection heterogeneity, reflection intensity, acoustic impedance, improved visualisation facilities such as true 3D views or transparencies, etc... (Brown, 1986 ; Brown, 1992 ; Nestvold, 1992)

In parallel to the geophysical expansion in seismic methods, the seismic stratigraphy concepts proposed by the Exxon team in the late seventies (Vail *et al.*, 1977) further extended to sequence stratigraphy in 1987 (Van Wagoner *et al.*, 1987) followed a rapid evolution both in clastic sediments and in carbonates (Schlager, 1994) . The incredible amount of work, additional data and criticism developed around sequence stratigraphy have made it a reliable tool for lateral correlation of time-stratigraphic units or stratal geometry developed in response to relative changes in sea level within the limit of one basin. The purpose of this chapter is to show that in a fitting environment such as the northern central Gulf of Mexico Neogene clastic shelf, the input of 3D sequence stratigraphy (Reymond & Stampfli, 1994a) in the finding and understanding of subtle stratigraphic trap can be significant.

6.2 Three-D sequence stratigraphy in clastic rocks: a composite sequence

3D sequence stratigraphy integrates sequential analysis of regional 2D lines, well log data, 3D horizontal sample and volume related attributes maps to locate, define and understand sedimentary facies of subtle stratigraphic traps.

The studied West-Cameron 3D Spec. Survey (GECO™) is located 40 km offshore from the Texas and Louisiana border (Gulf of Mexico) and covers a total surface of 225 sq. km. Present water depth is 15 m and the Holocene depocentre is located about 250 km basinward (fig. 6-1). Offshore western Louisiana, the Pleistocene reaches 700 m, the Pliocene 500 m and the Middle and Upper Miocene about 1300 m all deposited in shelf condition. The early Middle Miocene depocentre is located a few kilometres offshore from the studied area (Winker, 1982) and the transition to deeper depositional environments occurs just below the 15.5 Ma sequence boundary (figs. 6-1, 6-9 and Plate 1).

Taking into account the variation of sediment input through time and the local tectonic subsidence (salt driven growth faults) added to the general subsiding trend of the northern central Gulf coast, it can be seen that the eustatic component is still dominant enough on the shelf to give a cyclic character to sedimentation. Systematic observation of horizontal morphology of systems tracts on more than 150 amplitude maps and volume related attributes maps calculated from 25 interpreted horizon in the 3D data enabled the author to describe typical cyclic and reproducible horizontal sedimentary facies associated with each systems tracts. They are related to local changes in relative sea level.

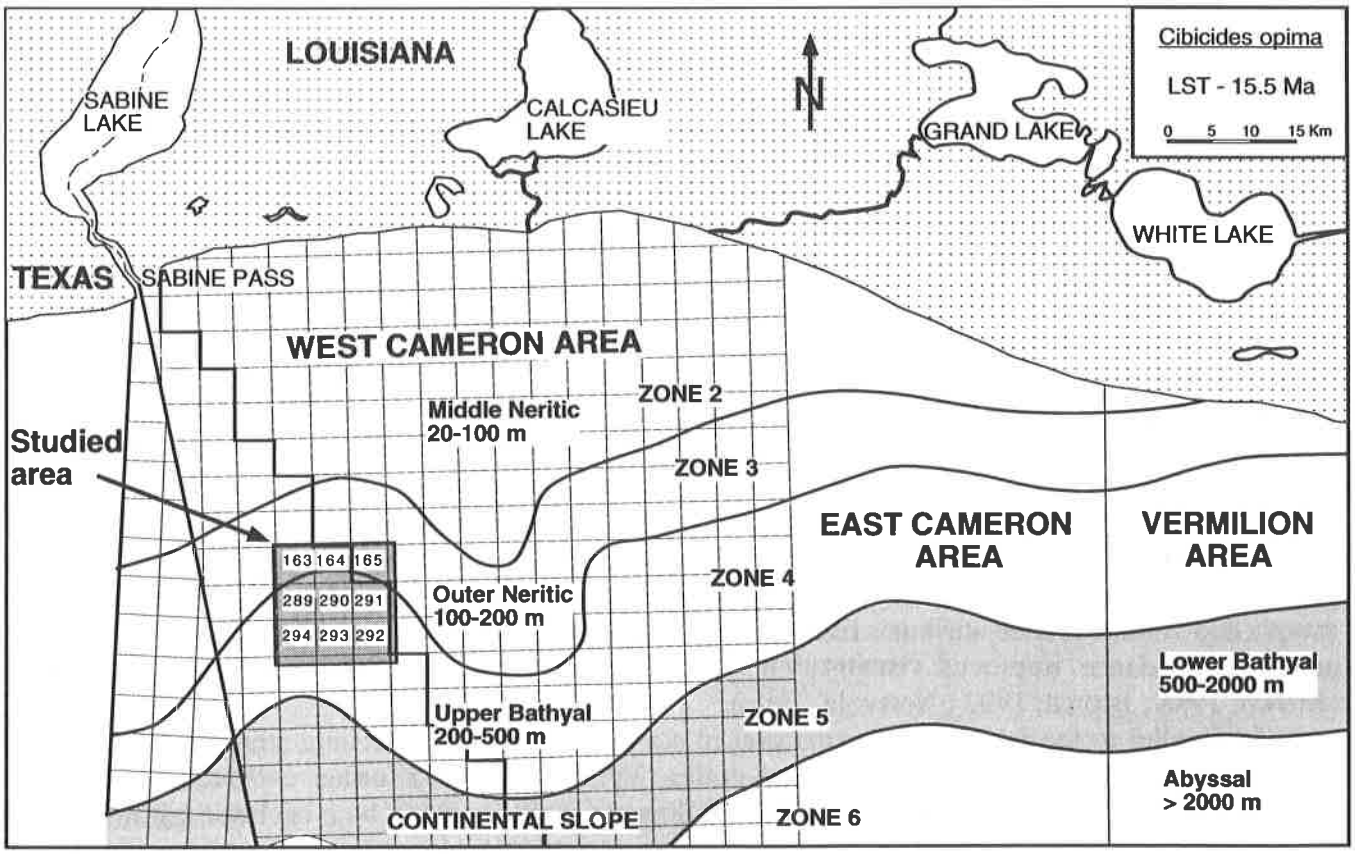

Fig. 6-1: Geographical location of studied 3D Spec. survey and reconstruction of the paleoenvironment zones for the Cibicides opima benthic foraminifers zone (Early Middle Miocene sequence boundary at 15.5 Ma).

The six amplitude maps presented below (seismic data and sedimentary interpretation, figs 6-2 to 6-7) are chosen examples of typical systems tracts horizontal morphologies as recorded in a representative composite sequence for the studied area. The vertical aspects of successive systems tracts are well-known from the Vail *et al.*, (1977) models but their true scale horizontal morphology and associated subtle traps are summarised below. The six successive sedimentary facies described here are expressed as a function of the simplified curve of relative change in sea level (location of discussed interval on each figure, see fig. 6-2).

- Maximum sea level fall (base lowstand):

Figure 6-2 shows a deep incised valley (60 to 100 m) cutting through the highstand silt below occurring during the phase of maximum relative sea level fall. Secondary braided streams (300 to 400 m wide) can be recognised within the main incised valley bed (2 to 3 km wide, see fig. 5-35 for original amplitude map). Below Well 4 location in the centre right portion of the image, a delta lobe is seen and confirmed by vertical seismic sections. It is interpreted as the top of a NW-SE highstand progradation developed on the shelf before the incised valley erosion.

Coarse grain porous sands of the incised valley bed constitute the main type of reservoir in the lowstand systems tract on the inner portion of the shelf. Many published case study present gas and oil accumulations in similar settings (Brown *et al.*, 1981 ; Gordon, 1982) . Eventual lateral crevasse splay sands are also good potential lowstand reservoirs sealed above and below by fine silt and shale.

- Beginning of relative sea level rise (top lowstand prograding complex).

The prograding interval is generally absent on the inner portion of the shelf. It corresponds on the inner shelf to a gap in sedimentation below the fine transgressive sediments progressively filling and sealing the incised valley sandy channels. Still, in case of rapid relative sea level rise the fans developed on the shelf edge can step back together with the shoreline rapid landward movement. This situation is represented on figure 6-3 presenting an amplitude map calculated 16 m above the preceding image showing the distributary mouth bar and proximal fan sands associated with the main incised valley channel seen on figure 6-2 (fig. 5-36 for amp. map).

Most reservoir associated with the upper lowstand systems tract on the outer shelf are found in distributary mouth bar and proximal deltaic lobes showing similar dimensions as the one represented on figure 6-3 (Reynolds, 1994) . Local lowstand thin fans on the inner shelf are almost systematically observed in the depressions caused by active growth faults (deep erosion on the up thrown block and proximal fan lobe on the footwall, fig. 7-2). The case study discussed in chapter 6.2.3 presents a practical illustration of gas condensate stored in a similar sedimentary setting.

- Top lowstand and early transgressive systems tract.

Figure 6-4 shows the intersection of an amplitude map calculated 8 m above the distributary mouth bar on figure 6-3 with large and arched foresets of a more distal portion of the same deltaic lobe. The corresponding distributary channel at that level should be found a few kilometres landward and to the NE of the studied area.

The thickness of these backstepping deltaic sands and associated potential reservoir is directly function of the accommodation space created by the difference between the rapid rate of relative sea level rise and the total sediment input. These top lowstand fans in middle shelf environment are rarely thick enough and generally difficult to identify on vertical sections (low angle 10 to 20 m thick shingled loops). They do not represent good reservoir on the inner shelf but their lateral equivalent down the shelf break represent the major reservoirs associated with lowstand systems tracts.

The three initial images (figs. 6-2, 6-3 and 6-4) used to illustrate a type 1 sequence boundary and associated lowstand sedimentary facies on the shelf are taken from one single sequence that characterise a "catch-up cycle" (Soreghan & Dickinson, 1994) where the initial rate of relative sea level is greater than the sediment input. The following maps used to illustrate the systems tracts above the top lowstand surface in this composite sequence are taken from other sequences.

- Maximum rate of relative sea level rise.

Amplitude maps and volume related attribute maps on the shelf at the time of maximum relative

sea level rise often present subtle lateral differences in seismic facies that are impossible to detect on vertical sections as they occur within half a loop. Well log data allow to differentiate the shale and fine silt from the coarser conformable sands deposited laterally and generally in more proximal position (interpreted amplitude map on fig. 6-5, raw data on fig. 5-52). Such a typical juxtaposition can be interpreted in two different ways according to its position relatively to the main flooding surface:

- When observed below the mfs, the shale is interpreted as fine top transgressive deposits reposing as coastal onlaps on the partially flooded shelf. The sand bodies in the more proximal position are interpreted as reworked deltaic sand bars. They form elongated, thin, well sorted and porous potential reservoir almost entirely surrounded by shale seals (Saxena, 1990 ; Pattison & Walker, 1992 ; Reymond & Stampfli, 1994a) .

- When observed above the mfs, at the base of the prograding highstand systems tract, the shale are interpreted as conformable fine sediments deposited on the entire shelf. The sands in more proximal position are interpreted as low angle shingled highstand progradation slowly filling the accommodation space created at the end of the relative transgression. These sands on top of the mfs are not as good reservoir as the reworked sands below because they are less confined and spread over larger surfaces. On the shelf such sands are commonly partially eroded by the following relative fall in sea level associated to the next sequence boundary. The presence of highstand clean sands below well marked unconformity surfaces constitutes a common example of paleogeomorphic subtle stratigraphic traps (Halbouty, 1982) .

- Decrease in rate of relative sea level rise and inversion of trend.

The interpreted amplitude map on figure 6-6 (raw data on fig. 5-21) shows two front lobe progradation associated with inner shelf highstand progradation. On vertical sections it would have been impossible to distinguish the two different lobes that are identified on horizontal display by their differences in orientation. These fine and wide spread sands rarely constitutes good reservoirs. But the more confined top highstand or basal lowstand sand lobes associated with growth fault depression can be good potential reservoir rocks.

- Sequence boundary "type 2".

«A type 2 sequence boundary is marked by sub-aerial exposure and a downward shift in coastal onlap landward of the depositional-shoreline break; however, it lacks both sub aerial erosion associated with stream rejuvenation and a basinward shift in facies» (Van Wagoner *et al.*, 1987). The existence of type 2 sequence boundary is often contested and the example on figure 6-7 shows the typical signature on the inner shelf (inner neritic ecological zone) of what could be interpreted further offshore on the shelf as a type 2 sequence boundary according to the above somehow confusing definition. Depending on the position on the shelf, a lowstand fall in relative sea level almost equivalent to the rate of total subsidence can cause shallow meandering incision on the inner shelf. Such sedimentary features are often observed in the Pleistocene series of the studied area.

The channels are never deeper than 40 m and are filled with fine silty material. They are commonly re-eroded and sometimes entirely removed by more important ulterior erosion phases. No subtle traps are usually associated with these shallow channels but a constant gradation exists between this type of erosion and the deeper large incised valley presented on figure 6-2.

Conclusions

Based on the observed reproducibility of 3D horizontal sedimentary facies of successive systems tracts related to eustatic cyclic changes as recorded on a clastic continental shelf, it is possible to define characteristic sedimentary morphologies and associated subtle stratigraphic traps. The observed periodicity in sedimentary facies derived from sequential analysis in clastic rocks enables to look directly at the right place through time and space for the hidden potential stratigraphic traps similar to the one discovered in drilling structures !

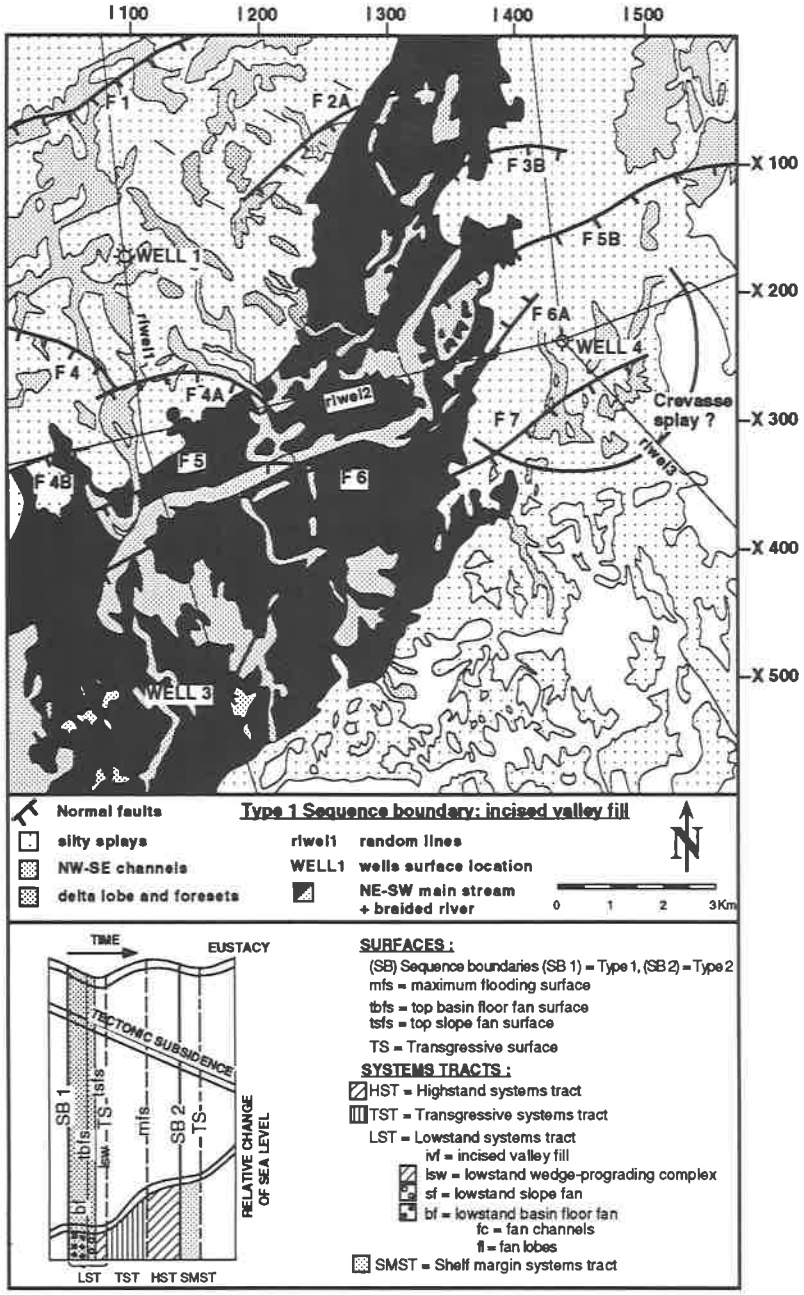

Fig. 6-2: Interpretation of an amplitude map (fig. 5-35) in terms of sedimentary facies showing a characteristic incised valley developed along a type 1 sequence boundary.

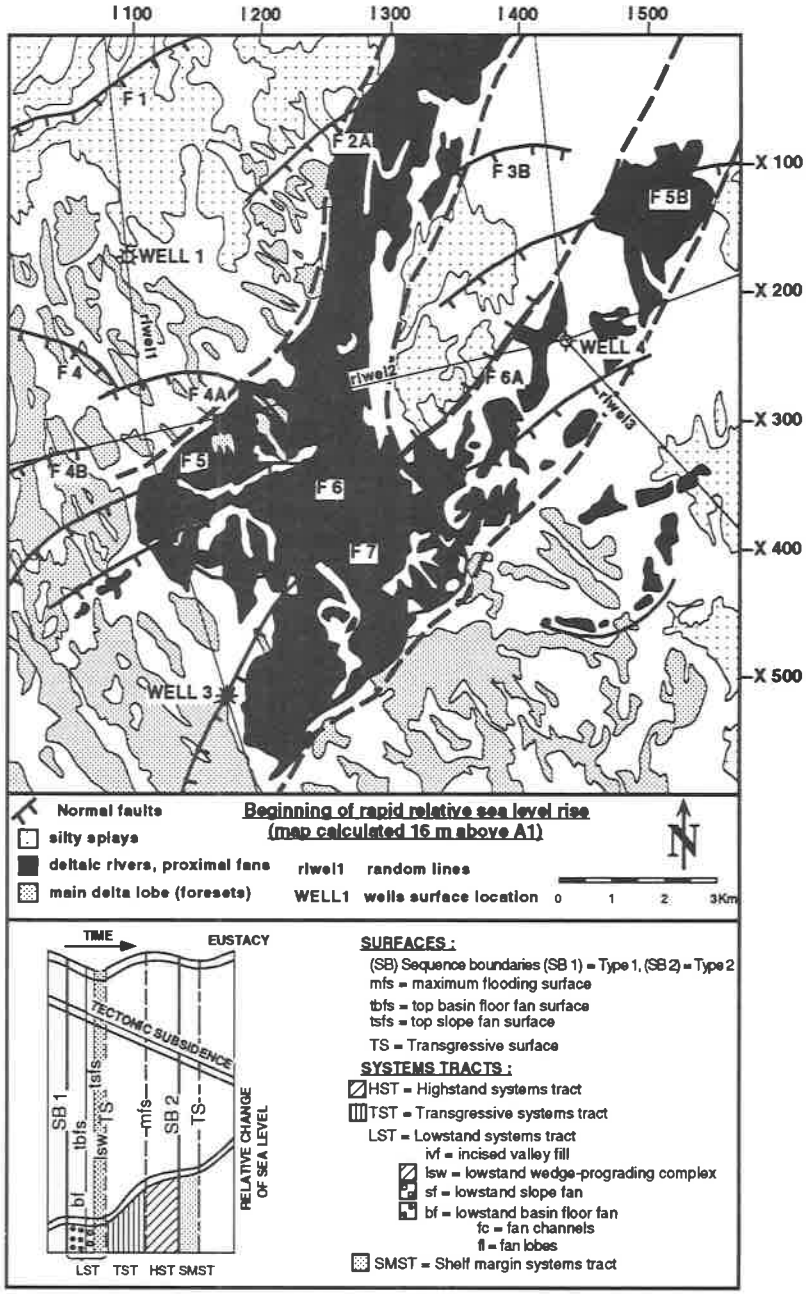

Fig. 6-3: Interpretation an amplitude map (fig. 5-36) showing the backstepping of the distal facies on the platform during the beginning of the rapid relative sea level rise (top lowstand systems tract).

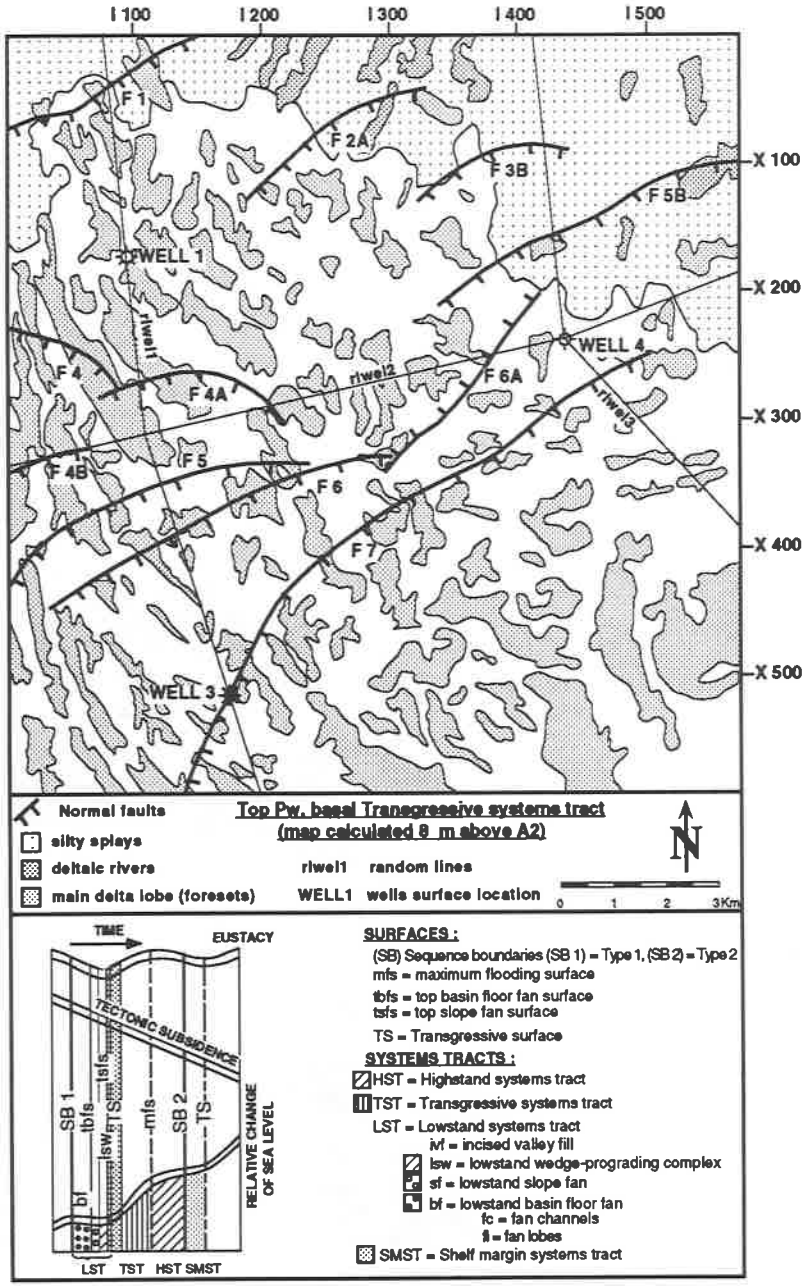

Fig. 6-4: Interpretation of the further backstepping of the distributary mouth bar and associated facies (fig. 5-37). Increase in rate of relative sea level rise (top lowstand and base transgressive systems tracts).

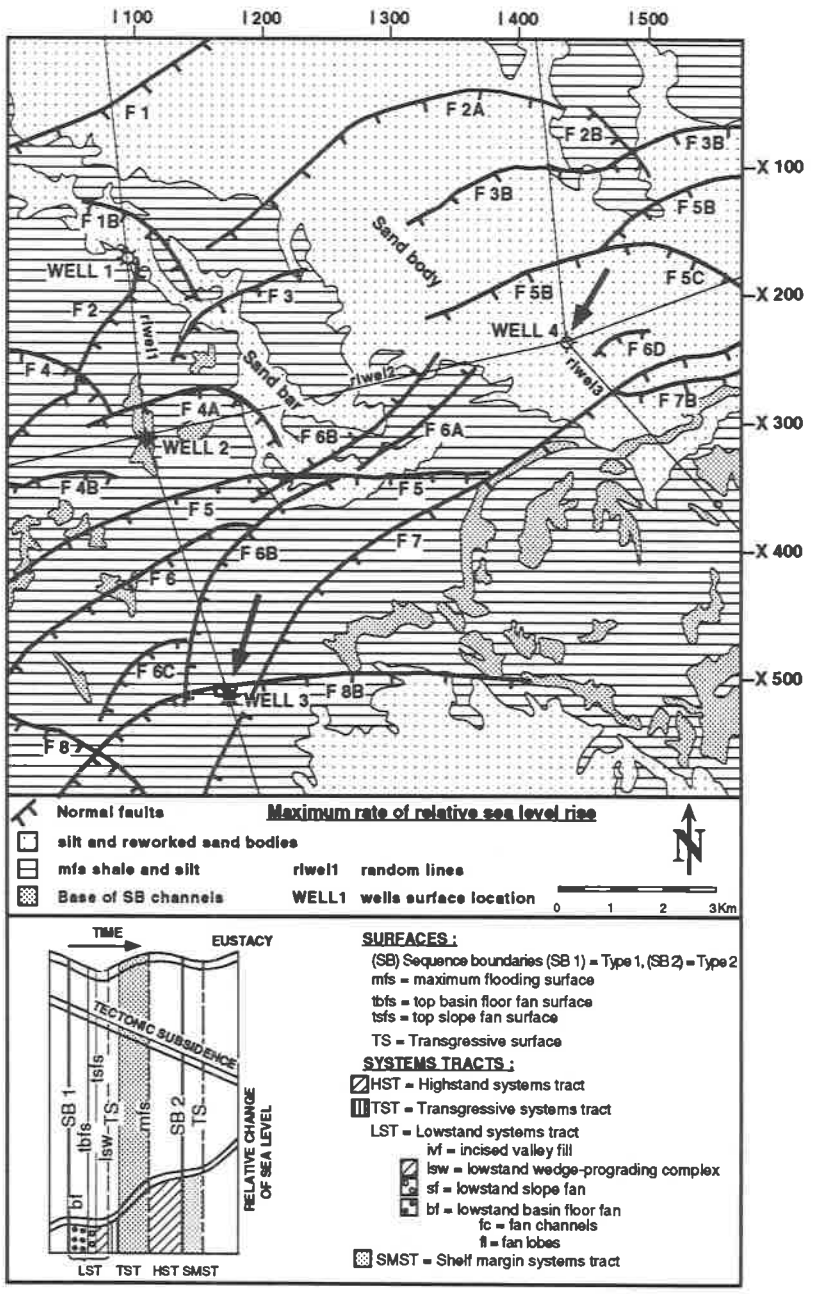

Fig. 6-5: Top transgressive interval (fig. 5-46). Low angle shaly coastal onlaps to the south-west, proximal reworked sand bodies and first signs of low angle highstand fine sands progradation from the inner shelf (from the north-east, lithology lateral changes confirmed by well logs).

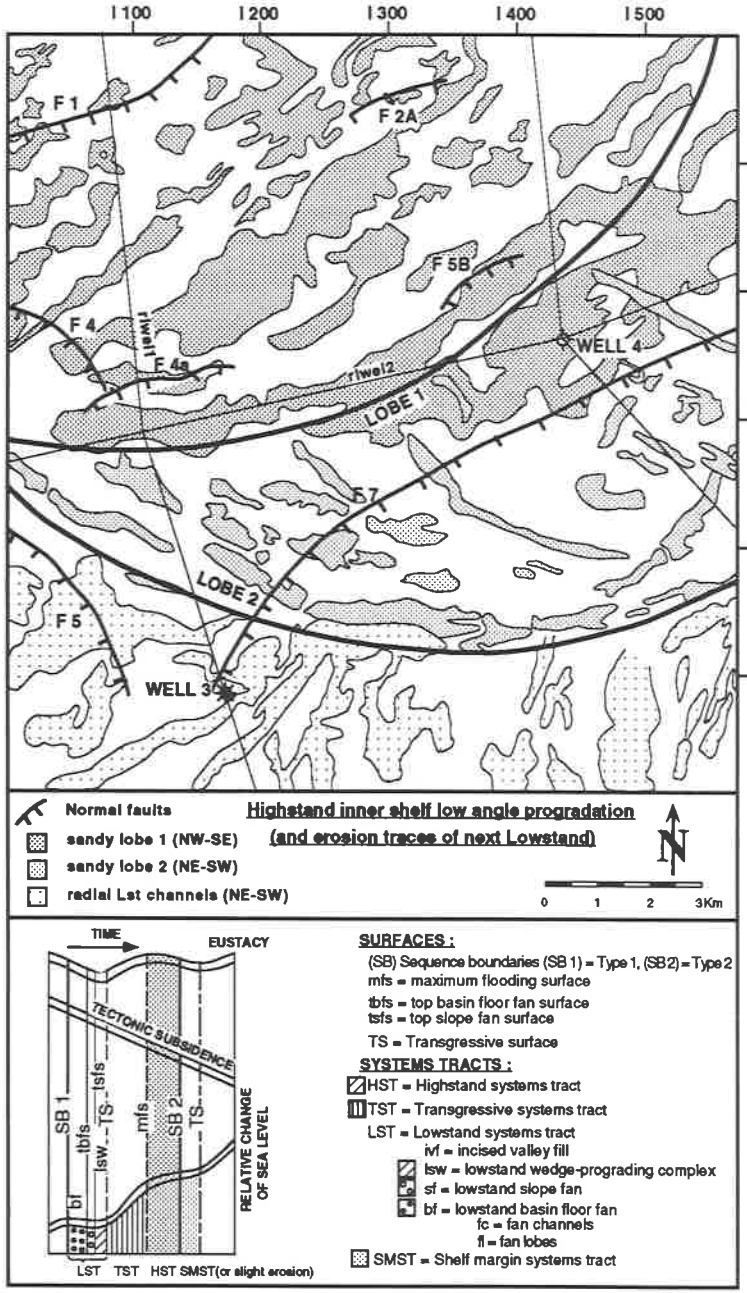

Fig. 6-6: Interpretation of highstand low angle prograding fine sands (fig. 5-21) filling the maximum of accommodation space created on the inner shelf.

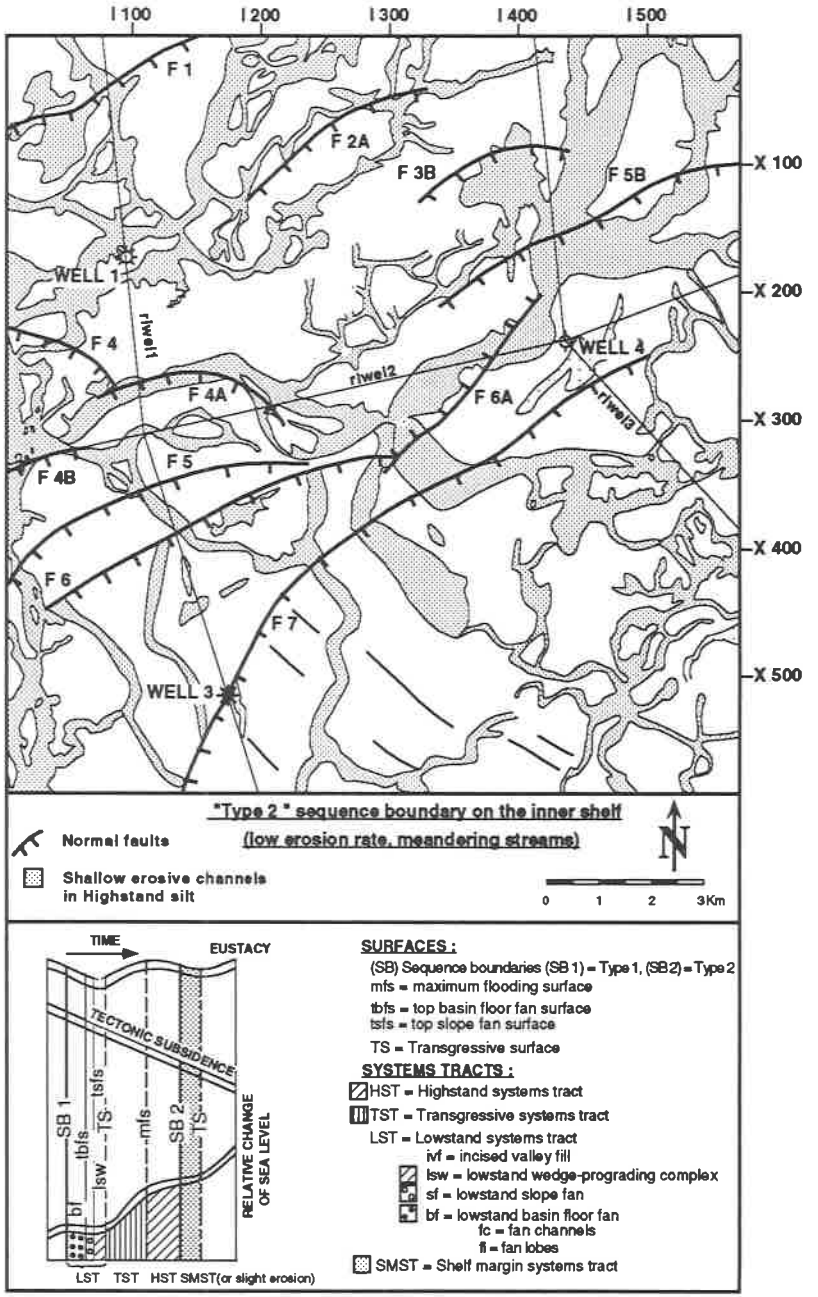

Fig. 6-7: Interpretation of shallow incision of the underlying highstand sands along a "type 2" sequence boundary on the inner portion of the shelf. First phase of erosion indicating initial signs of relative sea level fall.

6.3 Application of 3D sequence stratigraphy to early Middle Miocene productive Cibicides opima sands.

Introduction

The most productive Cenozoic interval offshore Texas and Louisiana is found in the late Early Miocene and Middle Miocene depocentres located a few kilometres offshore from the present shoreline of the northern Gulf of Mexico (Bigenerina Humblei to Siphonina Davisi benthic foraminifers zones, Corsair trend; Winker, 1982 and Worral & Snelson, 1989) . The gas field presented here was discovered on the base of 2D regional lines before the studied 3D data set was shot. Well 3 on figure 6-8 was drilled on the crest of the F5 / F6 anticline and intersected a multiple stacked accumulation of gas productive sands within the Bigenerina H., Cristellaria I and Cibicides op. benthic foraminifer zone (MM7 and MM5 interpreted horizons on figure 6-8). The pay sands were interpreted as fault related structural traps associated with the anticline and the growth fault closures. The field was temporally abandoned in 1980 after a few dry wells were drilled on lateral extensions of the same anticline. Between 1985 and 1987 the production started again on that field producing up to 1000 bbl per day from the deeper Crist.I and Robulus Mayeri sands at the base of the Middle Miocene trend (EM5 and EM1 horizons, fig. 6-8). The reservoir morphology was still described as structural traps related to growth fault anticlines (Strahan, 1987) . The 3D speculative survey data interpreted in this study was shot in December 1986 and January 1987. The data set is not mentioned by the author of the report quoted above and we do not know if they used it or not. The sequential analysis realised in this study on well log data, 2D regional lines and the 3D vertical and horizontal images on the upper productive interval enables to precise the sedimentary facies of the pay sands associated with the F5 / F6 anticline. We can demonstrate that these traps are deformed subtle stratigraphic features extending across the faults and that they can be correlated to definite systems tracts characteristic horizontal sedimentary morphologies.

Observation.

The sequential interpretation of the available logs in the productive interval is summarised on a north-south well log transect (fig. 6-9). To show the lateral variations in thickness of the productive sands and associated systems tracts, the well log data are flattened along the interpreted 15.5 Ma sequence boundary placed at the base of the thick and massive "blocky" sands (proximal basin floor fan). This sequence was sedimented at the transition between the outer neritic and the upper bathyal zone (zones III to IV, 200 m limit, see map on fig. 6-1). It shows a characteristic succession of lithofacies that can be interpreted in terms of systems tracts according to the model presented by Vail & Wornardt (1990) for a similar setting. The main productive sands discussed here are located in the thick coarsening up sands belonging to the prograding wedge and to the inferior portion of the transgressive systems tracts thinning up sands (see location of interpreted horizon, MM5 and MM5 -44 on Well 3, fig.9). The interpreted horizon on the 3D data are transferred on the well log data via a synthetic log.

Figure 6-10 shows the azimuth map calculated along the MM5 horizon that coincides with the top "Cib. op" zone. In the upper part of the image two positive domes show a NW-SE orientation. On the most recent compiled maps of salt distribution (Martin & Bouma, 1982 ; Berryhill, 1987 ; Worral & Snelson, 1989) two deep lying active salt domes are indicated in correspondence with the observed positive features on figure 10. Nevertheless, we interpret the visible dome below the F1 main fault on figure 6-8 as a mass of high pressure shale on top of the underlying salt dome not seen on Inline 204 (the strong amplitude top salt reflectors are found below, around 6 seconds TWT on a regional line running across the studied area, Plate 1). The topography on figure 6-10 indicates the present morphology of the MM5 level with an artificial vertical scale in milliseconds. But isopach maps and fault throw measurements indicate that the domes were already active at the time of deposition of the MM5 level.

The seismic facies lateral changes, 20 ms below a surface parallel to the MM5 interpretation line is represented on figure 6-11A. The interpretation of this amplitude map (fig. 6-11B) shows a main lowstand channel flowing from north-east to south-west (strong diagonal positive amplitude anomaly in red-orange). This amplitude anomaly is clearly appearing on the horizontal display because of the natural lateral continuity of the channel but would be completely missed on a classical wiggle display or even on a raster coloured section. The main contour of the positive domes are transferred from a MM5 contour map onto the interpretation of the amplitude map (fig. 6-11B). It is striking to see how the channel course was

influenced by the two domes and made his way in the depression between them. The same channel developed a distributary mouth bar and a proximal fan lobe down the F5 and F6 growth faults.

From the sequential analysis on logs (MM5+20, see fig.9, well 3), it can be proposed that the sedimentary facies seen on figure 6-11A is coincident with the base of the prograding wedge in the lowstand systems tract. The same sedimentary facies is represented on figure 6-3 corresponding to the beginning of relative sea level rise in our composite sequence. A strong positive anomaly at that level (but negative at the level of the MM5 sand 25 m above) is superposed to the outer eastern portion of the fan lobe (chequered pattern on the interpretation). It is interpreted as a gas bright spot trapped in the distributary mouth bar sands. It is important to note that the gas anomaly crosses the F6 fault but stops against the F5 main growth fault. This could indicate that the F6 fault is younger than F5 and developed after the delta lobe deposition as a consequence of the concentrated sedimentation down the F5 fault (Galloway, 1986 ; Lowrie, 1986) .

A second locally stronger amplitude anomaly is registered to the north of the F5 fault and is interpreted as the proximal distributary mouth bar and transition to the main channel (deep erosion on the footwall of the F5 fault). This anomaly is not so clearly confirmed on volume attribute displays (figs. 6-13 and 6-14) as the one down the F5 growth fault and therefore might not correspond to a gas related bright spot.

The 3D data set was shot after the production on Well 3 had started which could explain the zone devoid of amplitude anomaly present below the Well 3 surface location (fig. 6-11B). This could be an indication of gas depletion around the well as a result of production (it is now becoming a current practice to re-shoot part or entire 3D data sets during production to follow the evolution of major productive traps and to realise exact modelling of fluid movement within the reservoirs (Wehr & Brasher, 1994) .

The amount of structural and sedimentary data obtained from a single amplitude map is simply astonishing. Although all amplitude anomalies do not always correspond to gas accumulations. Gas bright spots generally correspond to negative reflection coefficient marked by a lowered acoustic impedance because of the lower velocity and density of the gas sandstone. But similar high amplitude anomalies can be related to high-pressured shale or to wavelet interferences (constructive interferences or tuning effect, Widess, 1973) occurring for instance in zones of superposition of shaling out outer portions of juxtaposed lowstand fans. Several ways exist today to precise the origin of amplitude anomalies. The best way is to work with true amplitude 3D data and to apply volume related attributes now available on most interactive interpretation systems. acoustic impedance, reflection heterogeneity and Intensity attributes provide additional tools to establish further distinctions between amplitude anomalies at a given level.

Figure 6-13 shows the reflection intensity map calculated between the MM5 and the SB 15.5 interpreted horizon on the entire surface of the 3D survey (see fig. 6-9 for location of horizons, approximately 100 ms interval corresponding to the basal lowstand). The reflection intensity represents the sum of the absolute value of amplitudes along a given trace within a pre-defined volume. It is useful for the detection of subtle faults and buried channels. A strong positive anomaly is present in the depression between the two domes and shows several fine streams not identified on the amplitude map. They correspond to several successive stream generations registered during the lowstand interval. In the zone of amplitude anomaly corresponding to the gas accumulation (see pointer on figure 6-13), the fan shape of the distributary mouth bar is more evident and some radial features can be interpreted as secondary distributary channels. As this map takes into account more than 100 m of sediments below the MM5 horizon, the anterior prolongation of the main channel corresponding to the early lowstand erosion can be seen below the distributary mouth bar flowing down to the major F7 growth fault (see fig. 6-11B for location).

Another useful tool for reservoir characterisation is the acoustic impedance volume attribute. Acoustic impedance is related to the reflection coefficient whose lateral variation can indicate changes in porosity. Figure 6-14 shows this attribute calculated over the same interval as before on the entire thickness of the inferior portion of the lowstand systems tract. Zones of low acoustic impedance may correspond to pure sands with high porosity (in dark blue on figure 13). It is interesting to note that the productive area shows high porosity and that two other fan shaped zones appear in the upper part of the image. These upper two dark blue zones are interpreted as early lowstand lobes associated with the active F1 growth fault. They would have been missed on the base of amplitude maps. Unfortunately, these two lowstand slope fans do not present gas related amplitude anomalies.

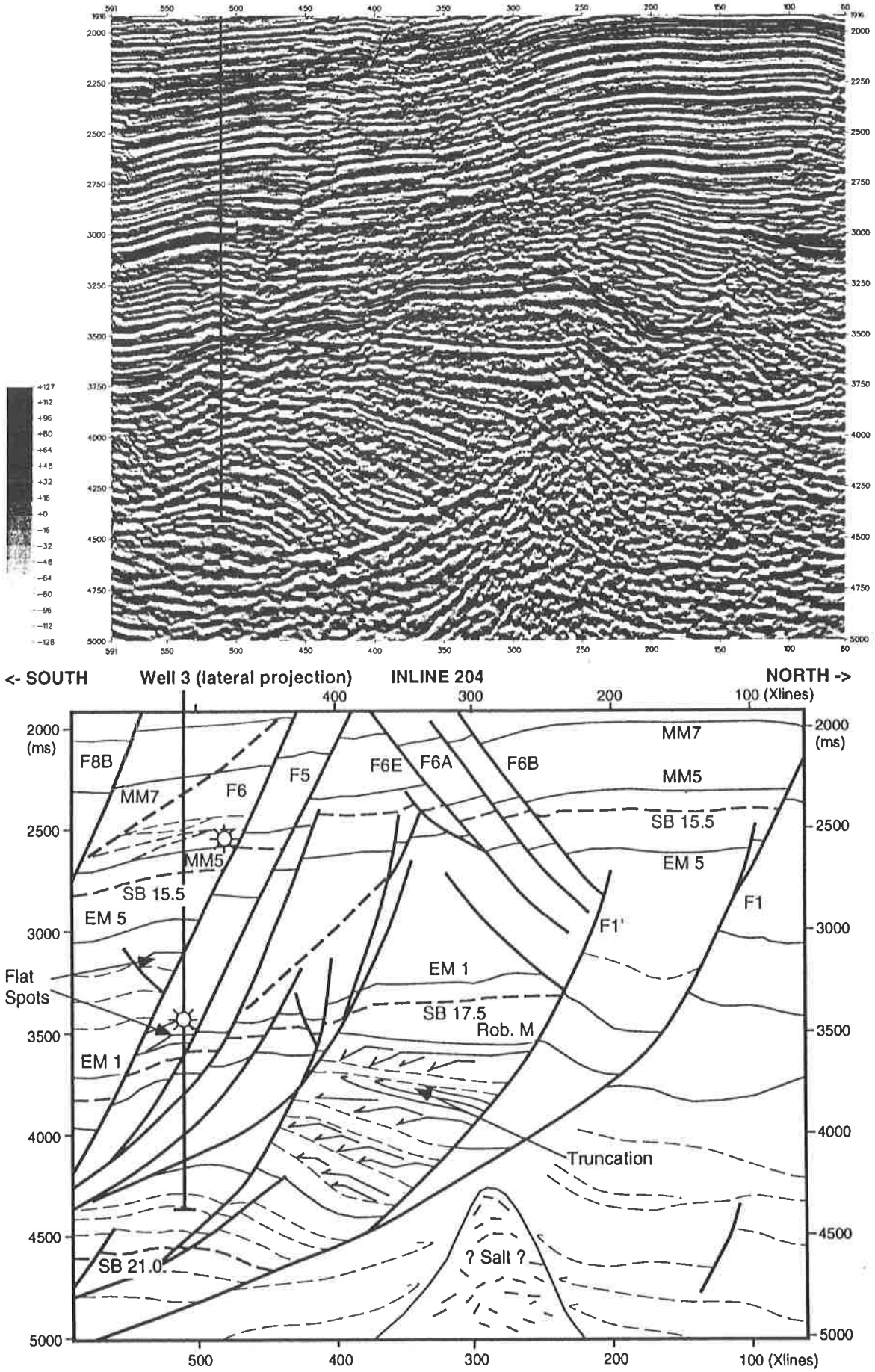

Fig. 6-8: North-south profile across the studied 3D data showing stacked gas accumulations (flat and bright spots) against the F5 /F6 growth faults. The triangular shaped dome below the major F1 growth fault is interpreted as a zone of high-pressure shale.

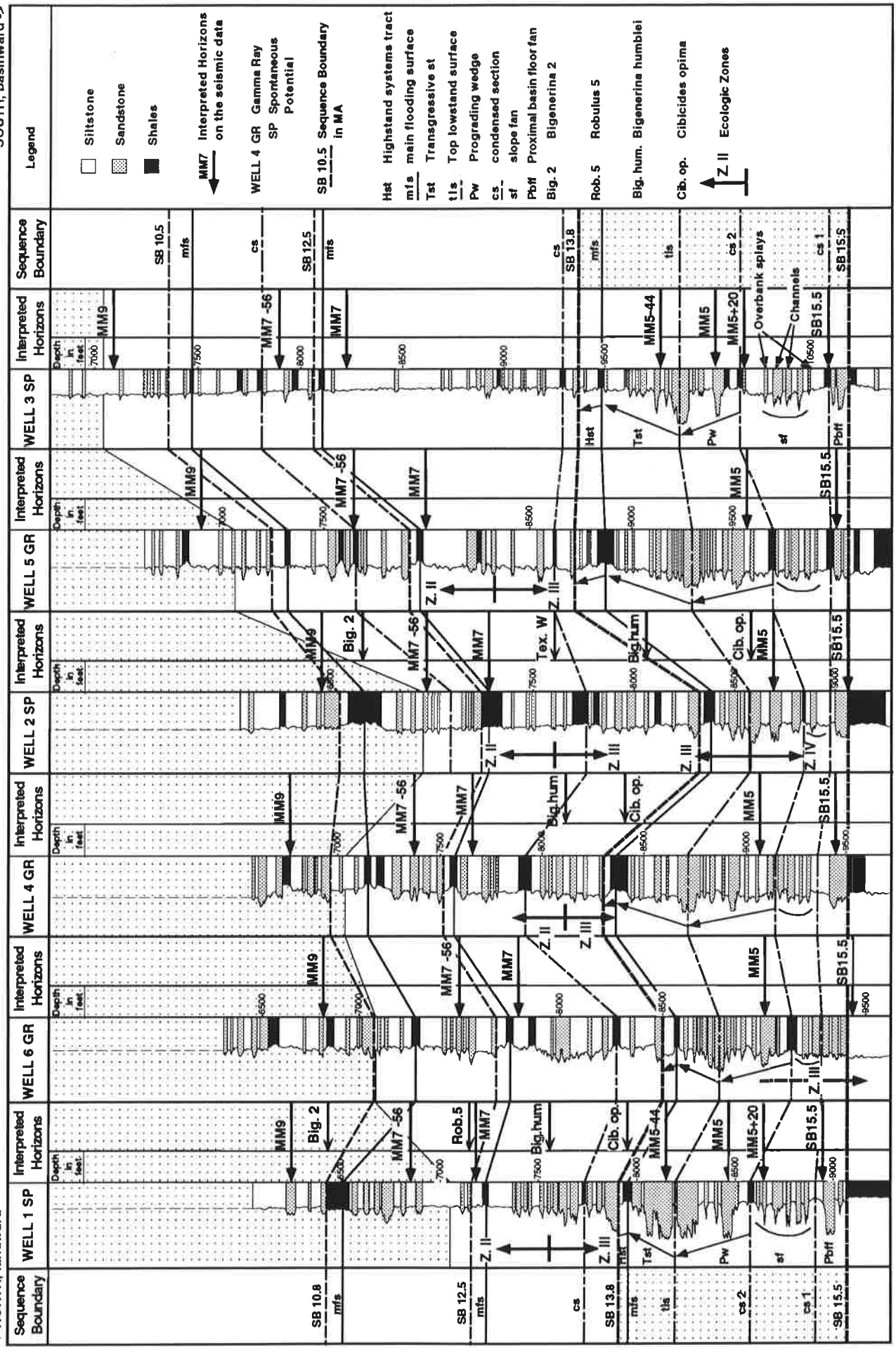

Fig. 6-9: Synoptic north-south well log transect for the Cibicides opima. interval (shaded, SB 15.5 to SB 13.8) and sequential analysis on logs. The wells are "flattened" along the SB 15.5 interpreted sequence boundary. Note the excellent lateral continuity of systems tracts.

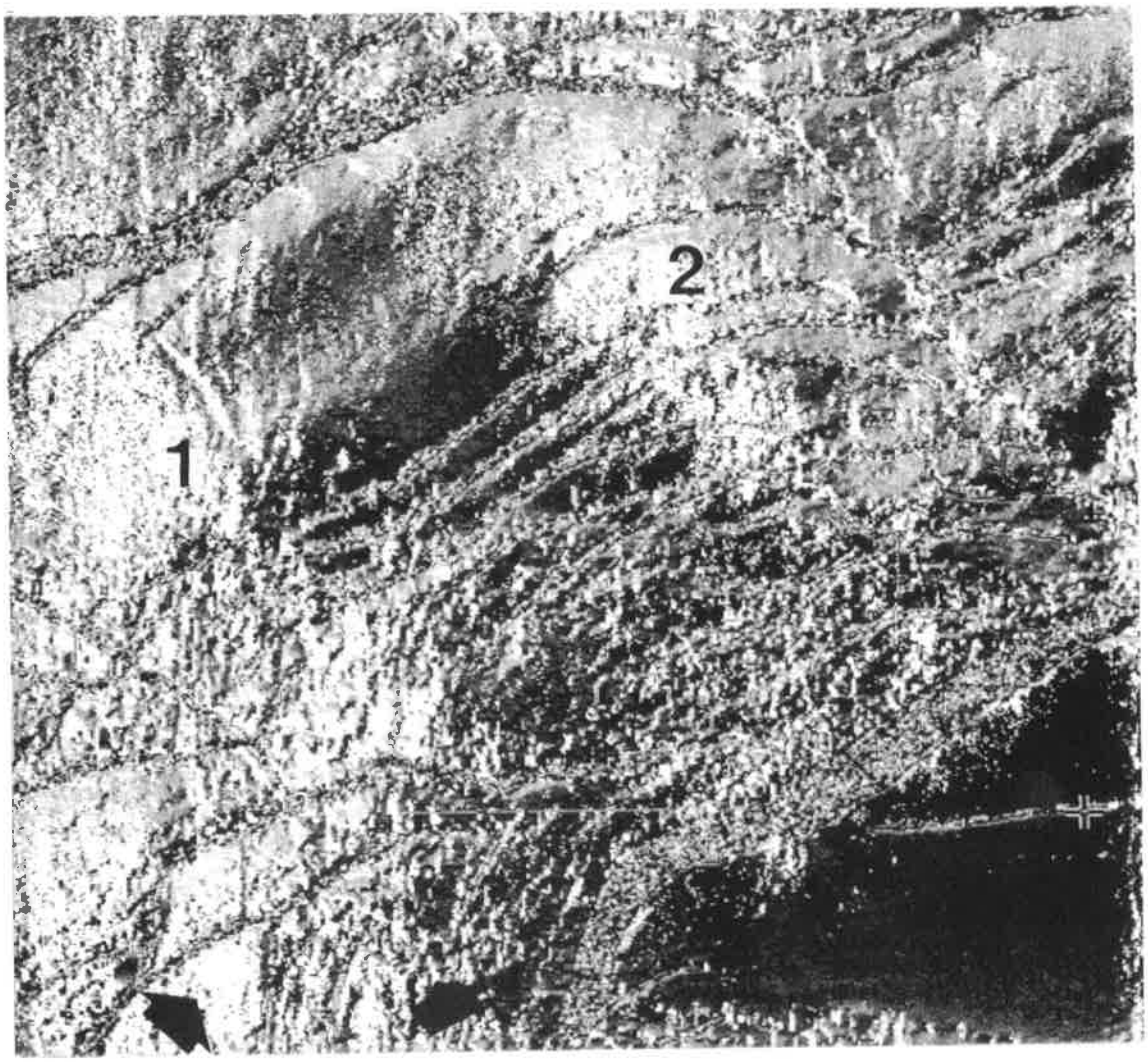

Fig. 6-10: Azimuth map of the MM5 interpreted horizon (Cib. op. top) showing the present shape of the two positive salt related structures below the F1 fault (pointers 1 and 2). The pointer indicates the southern part of the lowstand fan interpreted on figure 6-11 ***b****.*

A sharp sandy signal marked on the SP curve on Well 3 log data (fig. 6-9) at the base of the transgressive systems tract is characteristic for reworked sand bodies in this interval (Saxena, 1990 ; Pattison & Walker, 1992; Reymond & Stampfli, 1994a) . An amplitude map is calculated 44 ms above the MM5 interpreted horizon (fig.12) in order to intersect that sand body. At that level, about 70 m above the amplitude map on figure 6-11A the amplitude anomaly related to the distributary mouth bar is still visible due to interpretation artefacts but an elongated feature (strong negative amplitude anomaly in violet, pointer 1) is intersected along the F6 fault. From the comparison with the composite sequence presented above, this elongated feature is interpreted as the result of the transgressive reworking of the lowstand fan into a bar like sand body parallel to the paleoshoreline, related to the F6 growth fault. The lateral extension of this bar can be found further to the north-east on the hanging wall of the F7 growth fault (see pointer 2 on fig. 6-12). Another positive elongated amplitude anomaly is observed at the same level, a few kilometres landward of the bar intersected by Well 3 (NE-SW red-orange diagonal anomaly, pointer 3 on fig. 6-12). It is interpreted as a second reworked sand body associated with the progression of the transgressive phase. The strong positive anomaly in the centre right portion of the image has not been drilled (as far as we know) and could be of economical interest. It is well confined by faults and presents a surface and thickness comparable to the pay sand found in the transgressive bar on the footwall of the F6 growth fault.

Conclusions

Interdisciplinary sequential analysis on well log data, 2D regional lines and 3D seismic vertical and horizontal displays provide a potent tool for the search, location and understanding of the sedimentary processes at the origin of subtle traps. Horizontal sedimentary facies maps obtained along one interpreted reflector or calculated over a definite volume of rocks allow to precisely delimit the lateral extension of the productive sands within a structure limiting the chance to drill dry holes when looking for the shaling out area of the reservoir. On new prospects as well as on already producing fields the additional input of sequential analysis on logs and on 3D data enables to locate and identify new productive zones.

Most reservoirs in clastic shelf sediments are associated with lowstand incised valleys or lowstand fans developed down the shelf break or accumulated in platform depressions on the footwall of active growth faults. The course of lowstand channels are influenced by the underlying salt activity and the development of major fans are systematically intercalated between the salt positive structures in the offshore direction. The local transgressive reworking of the top lowstand sandy lobes can generate well sorted elongated sand bodies susceptible of being good reservoir rocks. Furthermore, the petrophysical characteristics of gas related amplitude anomalies or potential oil stratigraphic reservoirs can be estimated on the base of well log data (wireline curves and sequential analysis) and confirmed with the 3D volume related attributes. And finally, the evolution of reservoir potential, morphology and deformation during production can be followed using the same tools combination by re-shooting portions of 3D data sets providing the necessary data for reservoir detailed modelling.

6.4 Summary

3D sequence stratigraphy integrates sequential analysis of regional 2D lines, well log data, 3D horizontal sample and volume related attributes maps to locate, define and understand sedimentary facies of subtle stratigraphic traps. It is a potent tool for the discovery of stratigraphic traps, their exploration and development. It leads to the better understanding of reservoir morphology, heterogeneity and subtle stratigraphic trapping mechanisms. On new prospects as well as on already producing fields the additional input of sequential analysis on logs and on 3D data allows to identify and locate new potential productive zones.

The observed periodicity in sedimentary facies derived from sequential analysis in clastic rocks allows to look directly at the right place through time and space for the hidden potential stratigraphic traps associated with definite systems tracts:

- basal lowstand systems tract reservoirs associated with erosional surfaces or sequence boundaries are mainly found in the porous sands of the incised valley beds and associated lateral crevasse splays.
- upper lowstand (prograding complex) potential reservoir on the outer shelf are found in distributary mouth bars and proximal deltaic lobes. On the inner shelf, occasional productive lowstand fans are developed on the footwall of growth faults (increased accommodation space by locally higher tectonic subsidence rate).
- top lowstand sands and transgressive silts can be reworked during marine transgression in elongated sand bodies likely to become good reservoir rocks.
- inner shelf low angle highstand progradation rarely constitutes good reservoir.
- inner shelf shallow erosional surfaces interpreted as type 2 sequence boundary do not constitute deep and coarse enough material to present interesting reservoirs.

An application of 3D sequence stratigraphy to the Cibicides opima gas condensate productive interval in the studied area reveals that previously interpreted stacked structural traps associated with a faulted anticline are in fact deformed stratigraphic traps limited by definite sedimentary bodies organised in sequences. The sequential analysis of pay sands and the visualisation of their morphology and lateral extend on horizontal 3D images enables to avoid drilling dry holes that look for the lateral shaling out of the reservoirs.

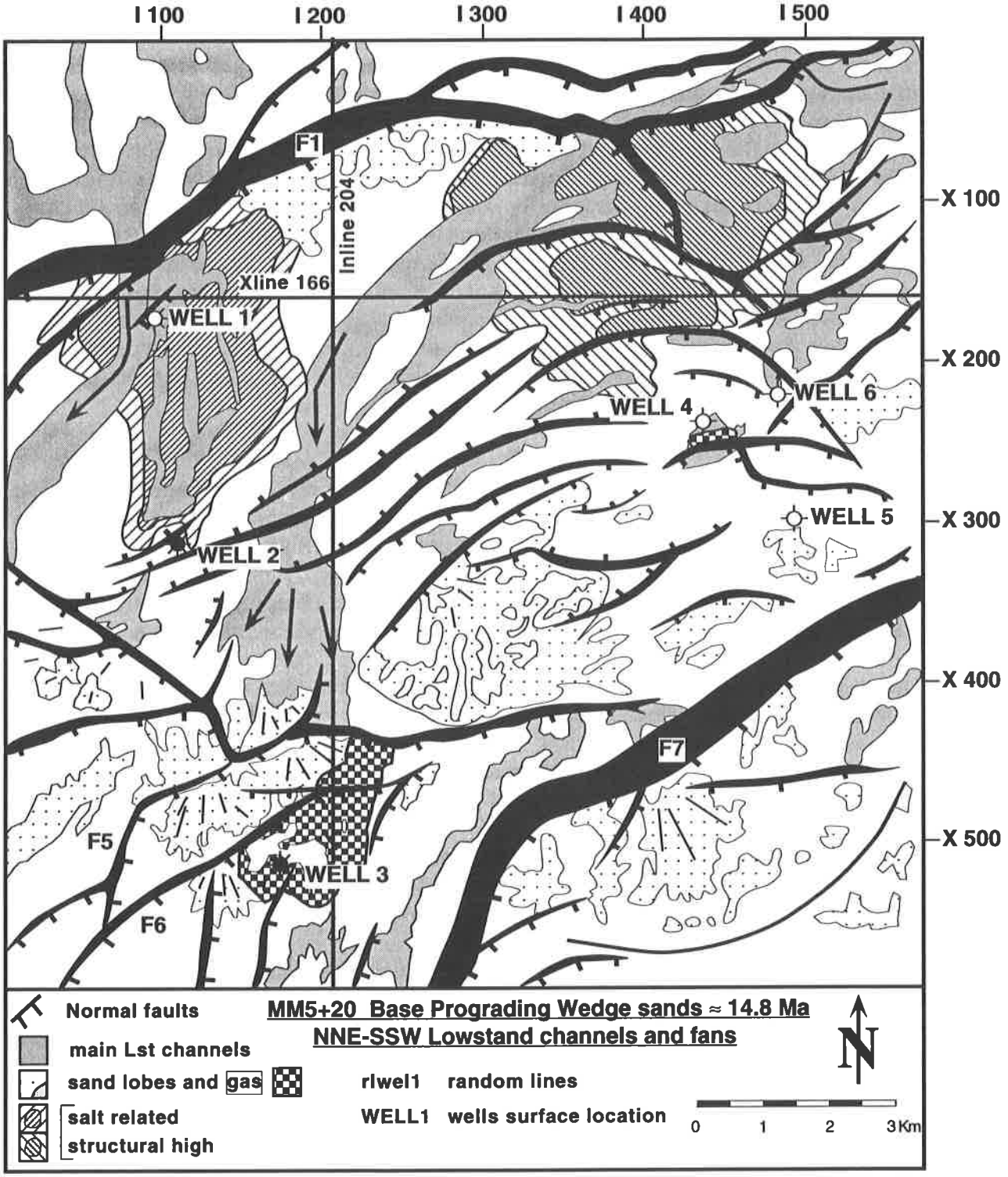

*Fig. 6-11: **b.** Sedimentary facies interpretation of figure 6-11: **a.** The lowstand channel course is deviated by the two domes and develops a distributary mouth bar and deltaic lobe down the F5 fault. F6 growth fault post-dates the deltaic deposition.*

*Fig. 6-11: **a.** Amplitude map calculated 20 ms below the MM5 horizon (NE-SW channel and fan).*

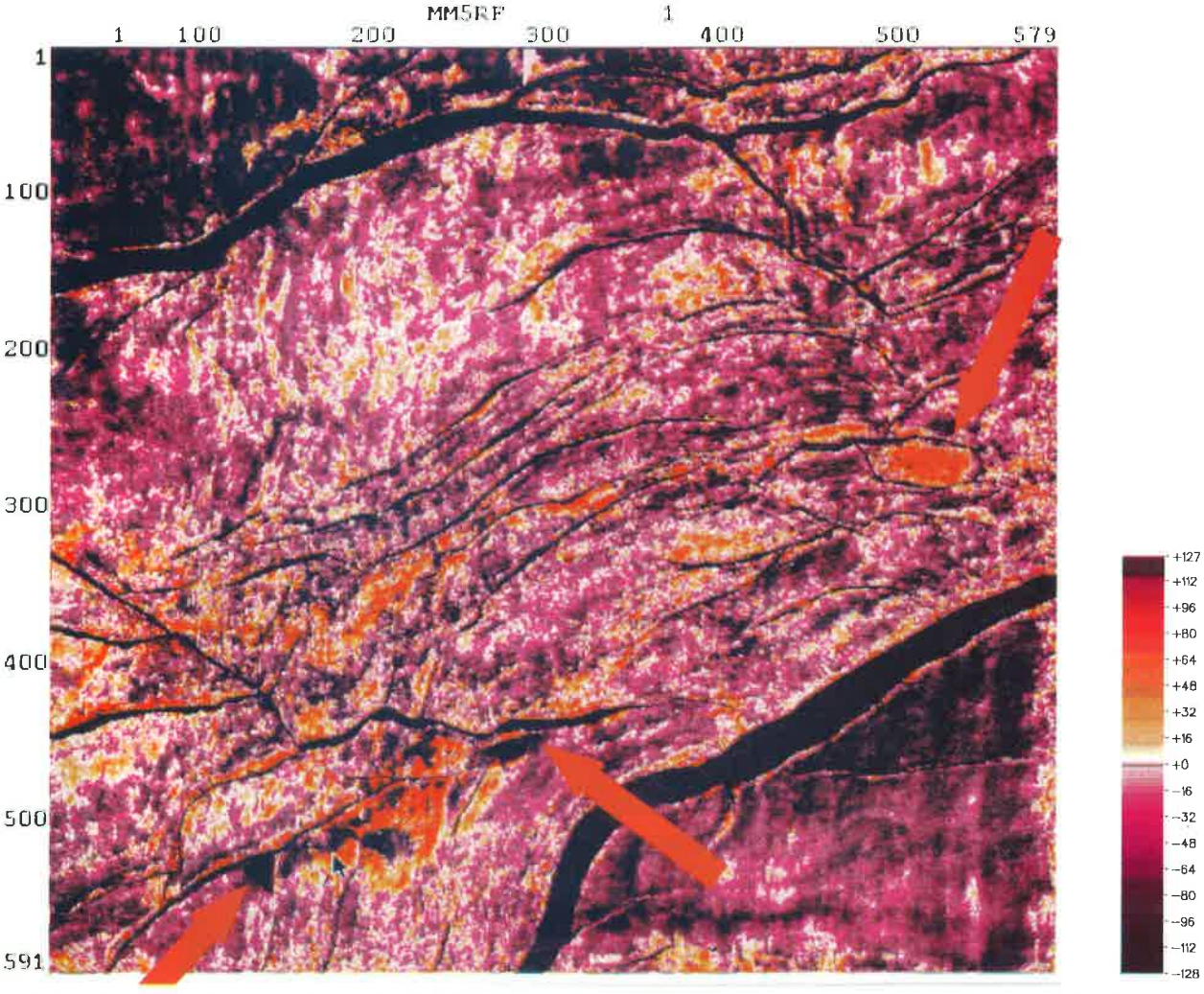

Fig. 6-12: Amplitude map along the MM5-44 horizon (NE-SW reworked sand bodies and bright spots).

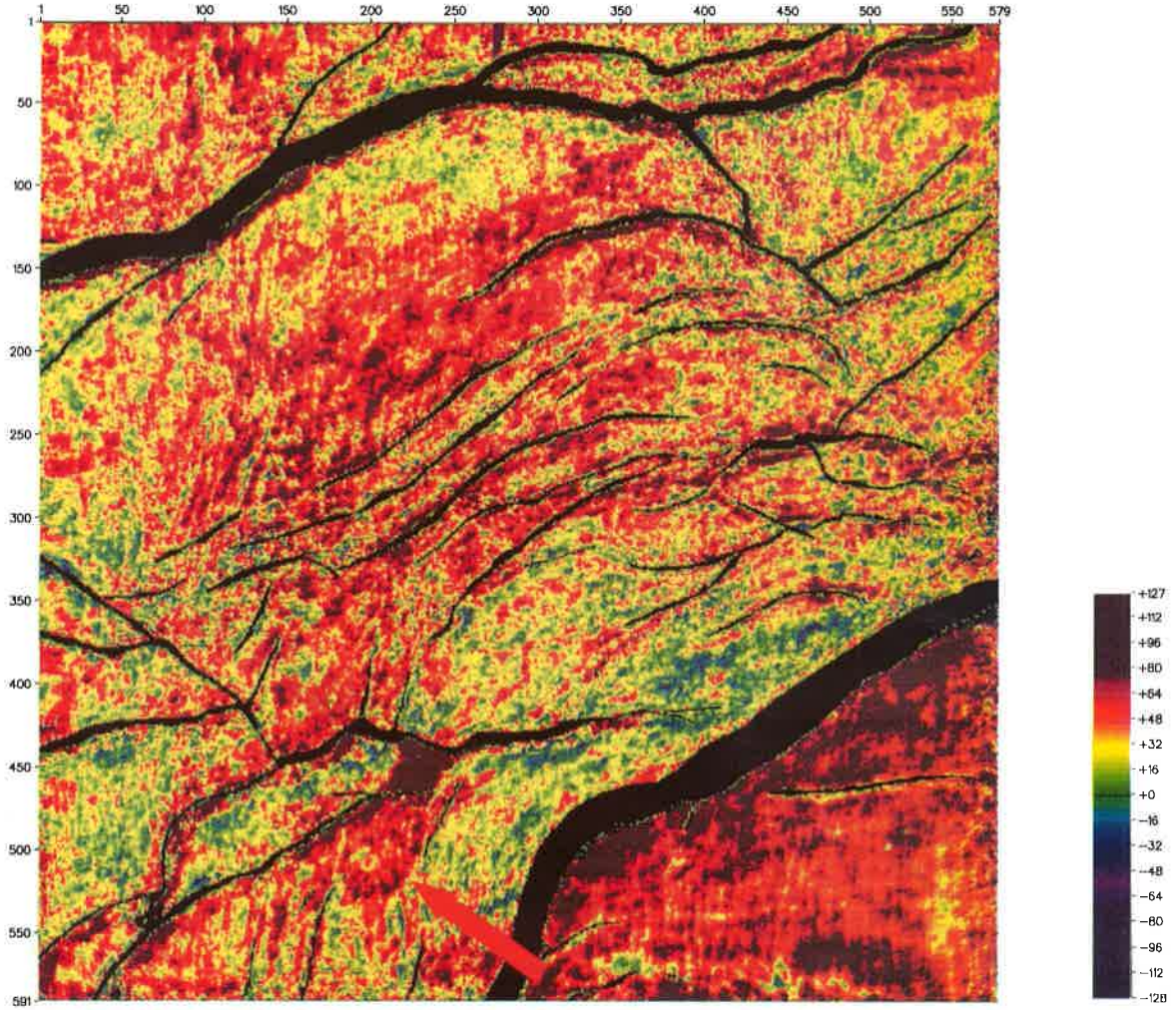

Fig. 6-13: Volume related reflection intensity attribute map (small channel and bright spot, dark red).

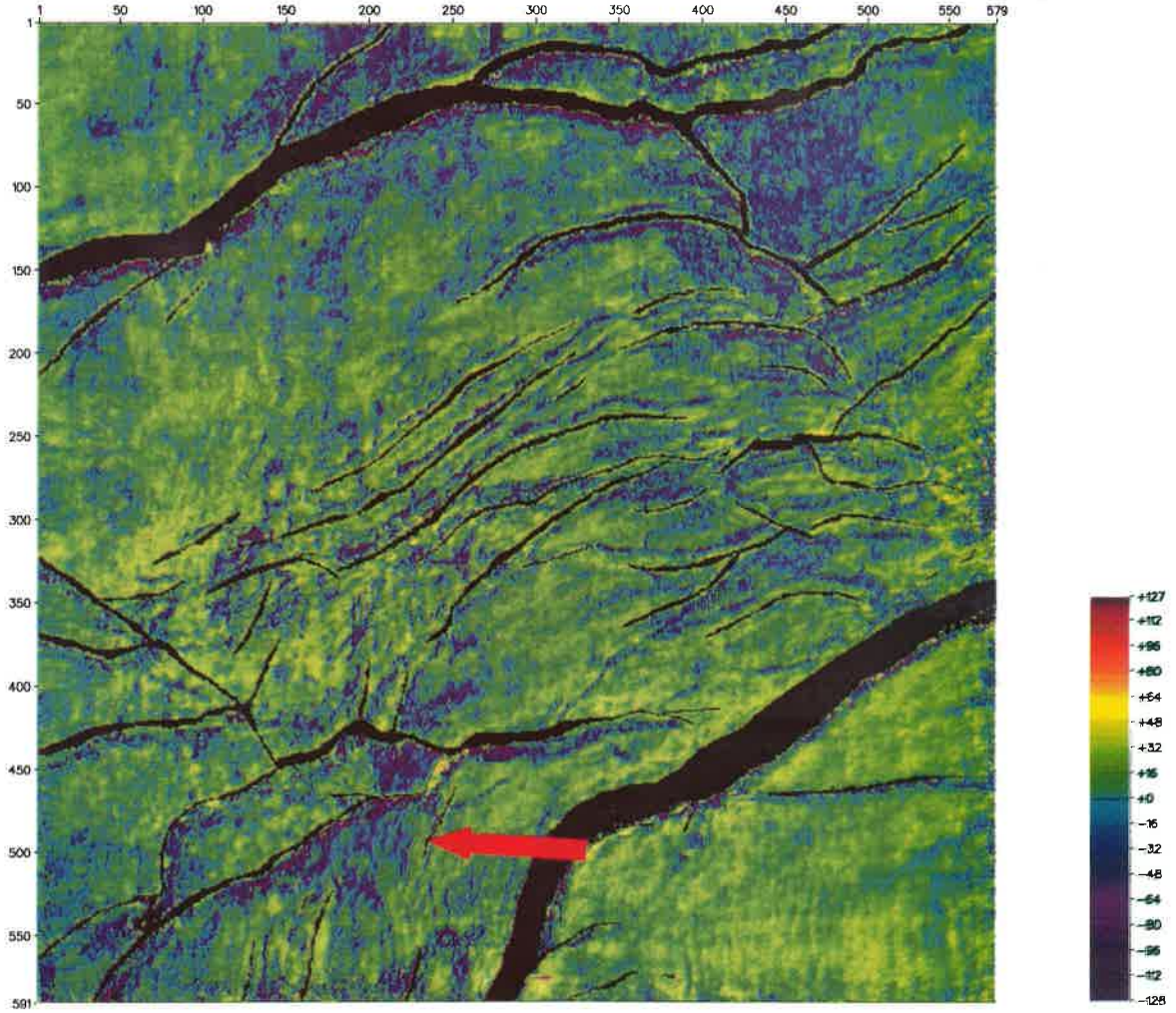

Fig. 6-14: Volume related acoustic impedance attribute map (dark blue zones=higher porosity).

7. Deformation, growth faults and associated sedimentation

7.1 Salt and growth faults in the Gulf of Mexico, history.

Since the beginning of the century, the Gulf of Mexico is well known for salt related deformation of sedimentary rocks. It all began when an exploratory well was drilled in 1905 over the Spindletop salt dome in southern Texas. The numerous discoveries of hydrocarbons related to salt uplifts led to an increasing interest and understanding of salt related positive structures.

The tectonic style in the Gulf of Mexico is governed by gravitational processes. The three different types of gravitational processes described by Ramberg (1981) have been successively mentioned as a possible cause for the salt related growth fault on the Gulf coast over a period of 50 years. In the early sixties, diapirism or upward movement of large salt masses by differences of density was thought to be at the origin of growth faulting in the central northern Gulf coast (Quarles, 1953 ; Ocamb, 1961) . At the end of the sixties and due to experimental analysis on clay modelling, it was thought that growth faults were generated at the shelf margin by gravity slide (Cloos, 1968) . Using the same concept of gravity sliding or gravitational gliding , Wilhelm and Ewing (1972) proposed that «growth faults use autochtonous salt as detachment surface». The idea of the detachment surface was adopted by most geologists working in the Gulf and the debate was to know if the gliding surface was based on salt or shale or both. But three years before that, Lehner in his outstanding synthesis of 1969, on the northern Gulf of Mexico demonstrates the predominance of salt as gliding surface. He wrote: «a flow of salt at depth away from the advancing clasting wedge, related to a zone of active down-to-the-ocean faults parallel to the Texas shelf edge». The gravitational gliding models (Ramberg, 1981) implied vertical continuous movement which required the presence of a deep heavy oceanic crust accommodating enough space for the shelf.

In the middle seventies, new ideas based on better and deeper seismic data appeared as it was discovered that many growth fault also dip landward and that smaller arcuate faults are directly related to the salt dome distribution. The notion of "mini-basin" or rim-syncline bordered by salt positive structures showing concentrated sedimentation appeared for the first time (Seglund, 1974 ; Spindler, 1977) . In 1978, Humphris evoked the idea of thick clastic masses of sediments (depocentres) displacing laterally large allochtonous salt nappes in the basinward direction (Humphris, 1978 ; Humphris, 1979) . The same year, Martin presents a cross section across the Texas-Louisiana shelf showing a "comb-like" arrangement of vertical ascending salt diapirs with no lateral displacement, even in the Sigsbee escarpement region (Martin, 1978) . The ideas were back to stage one: vertical diapirism. Concerning the origin of the Sigsbee escarpement (see location in fig. 1-1) Amery (1978) influenced by Martin's ideas denied the 10 km overthrust he had described in 1969 (Amery, 1969) . The concept of important lateral displacement of salt masses below the Central Gulf coast shelf proposed by Humphris in 1978 (taken from Lehner 1969) was later confirmed by more detailed studies on the Sigsbee escarpment (Watkins *et al.*, 1978 ; Buffler *et al.*, 1979) . In 1981, Bally proposed a complete detached origin for the Sigsbee escarpment based on the observation that the salt beneath the upper continental slope of the northern Gulf of Mexico was separated from the original salt depositional level (Bally, 1981) .

During the eighties, numerous higher quality and deeper (down to 13 s TWT) seismic data shot across the Gulf coast enabled Worral and Snelson to produce a synthesis on the salt related deformation, confirming the idea of the presence of a true northward thickening salt nappe below the lower slope offshore Texas and Louisiana at the origin of the Sigsbee escarpment (Worral & Snelson, 1989) . They describe an overthrust of at least 80 km for the salt tongue which reaches a thickness of 7 km in its northern part. This salt nappe intersects and overthrusts Eocene sediments in its inner northern part and actively overthrusts present deposits in the Sigsbee escarpment region (see fig. 7-1). The size of this large salt nappe is compared to a modern cross section through the western Swiss Alps based on the interpretation of recent deep seismic data (fig. 7-1, Marchant, 1993) . The size of the northern Gulf coast margin and the Sigsbee salt nappe is put in perspective when comparing it to the size of the central penninic Alps !

Most salt ridges and domes near the central Gulf slope are rooted on allochtonous salt masses inserted in the Cenozoic sediment pile and partially detached form their Late Jurassic original beds (Wu *et al.*, 1990a ; Wu *et al.*, 1990b) . These author defines three successive major phases of salt movement in the north-eastern Gulf of Mexico: 1) from the time of deposition (Middle to Late Jurassic, see chap.1) up to the Early Cretaceous, the Louann Salt was loaded by clastic and carbonated sediments causing episodic basinward movement of salt leading to large concentrations of salt in the slope environment

(autochtonous salt). 2) Reduced sedimentation rate during Late Cretaceous and Early Oligocene causes the stabilisation of the salt masses (allochtonous salt). 3) Extensive Neogene and Pleistocene seaward migrating thick depocentres formed large allochtonous salt sheets by gravity spreading within the younger sediments (possible detached allochtonous salt). Proposing an explanation for the Sigsbee escarpement, Wu et al. (1990) demonstrated that the amount of extension generated by the master growth faults is mainly compensated by salt withdrawal and partly by basinward shortening (see geological framework description, chapter 1).

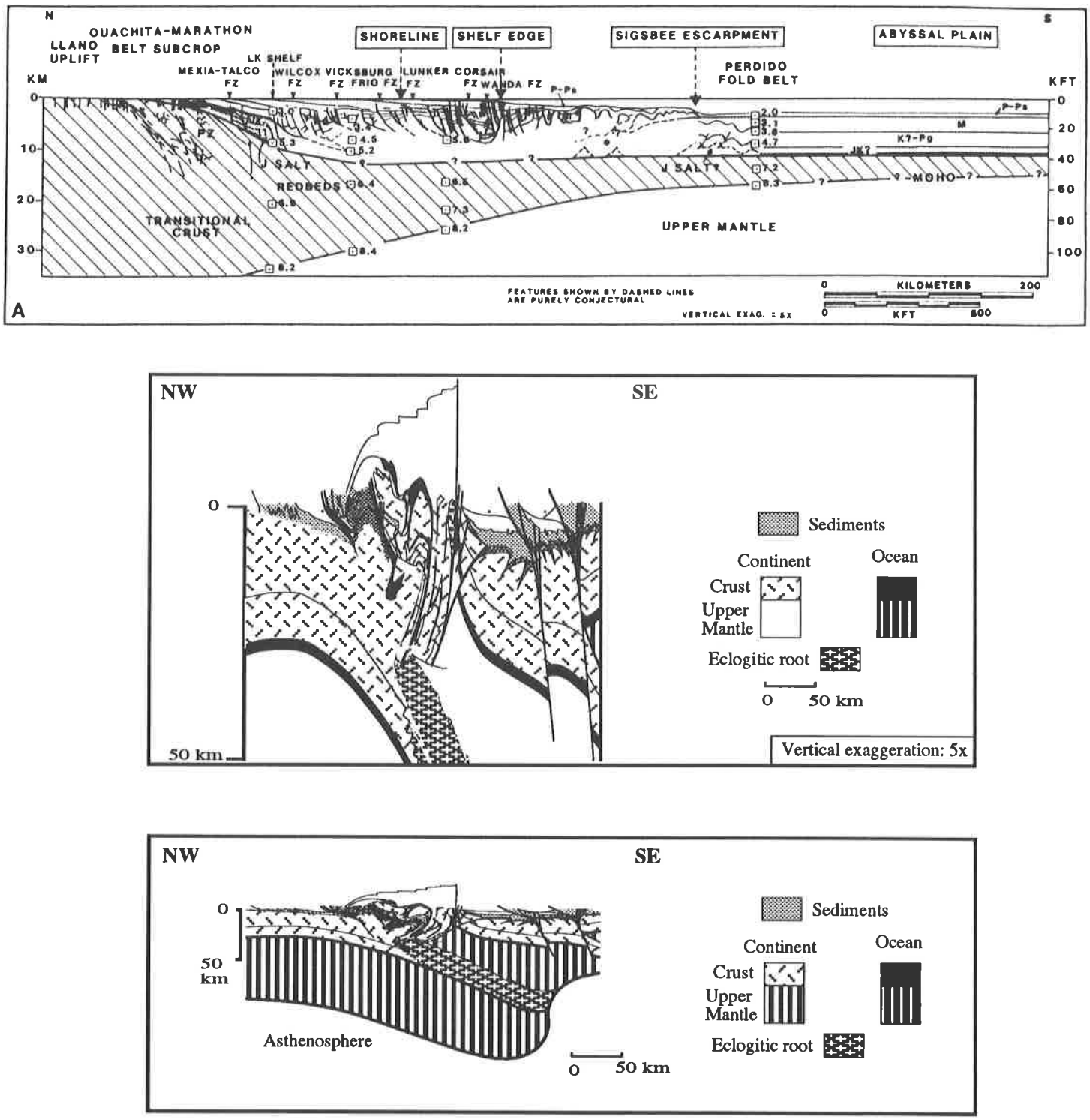

*Fig. 7-1: Interpretative same scale cross sections across the Texas Gulf margin (**a**) and the western Alps (**b**). Modified from Worral and Snelson (1989) and Marchant (1993). The Sigsbee escarpment salt overthrust is larger that the entire penninic nappes !*

7.2 Deformation versus sedimentation

At a smaller mini-basin scale, such as the one studied here, what are the causes for initiation of growth faults and associated salt movements ? Are the diapirs initiating growth faulting or vice versa ? Many papers have been written on the subject describing the morphology of growth faults in the Gulf coast, their relationships to the shelf margin deposits and migration of depocentres, the internal mechanism of salt diapirs formation and morphology and the modelling of the growth faults in relation to diapirs. The list below includes some of the main references on the subject and is followed by a synthesis of the main factors affecting the diapir/growth fault relationship mainly from the sedimentary point of view developed in this study (Jux, 1961 ; Lehner, 1969 ; Kirkland & Gerhard, 1971 ; Woodburry & Murray, 1973 ; Seglund, 1974 ; Schwarzacher, 1975 ; Watkins *et al.*, 1978 ; Halbouty, 1979 ; Humphris, 1979 ; Buffler *et al.*, 1980 ; Crans *et al.*, 1980 ; Winker, 1982 ; Coleman *et al.*, 1983 ; Jackson & Seni, 1983 ; Winker & Edwards, 1983 ; Suter & Berryhill, 1985 ; Jenyon, 1986 ; White et al. 1986; Curtis, 1987 ; Lerche & O'Brien, 1987 ; Suter *et al.*, 1987 ; Jackson *et al.*, 1988 ; Kupfer & Fails, 1989 ; Talbot & Jackson, 1989 ; Worral & Snelson, 1989; Jackson, 1990 ; Wu *et al.*, 1990a ; Wu *et al.*, 1990b ; Xiao, 1990 ; Swift *et al.*, 1991 ; Kern, 1992 ; Xiao & Suppe, 1992 ; Darros de Matos, 1993 ; Jackson & Vendeville, 1994) .

Two dimensional models of gravitational sliding related to extension have been developed by Crans and Mandl (Crans et al. 1980; Crans &Mandl, 1980 a and b). They describe the growth faults and "toe"-thrust morphology and mode of creation in idealised deltaïc sediments. Two parameters control the synsedimentary development of slide structures: the sedimentation rate and the rate of overpressure relaxation (restrengthening the basal slip plane; Mandl, 1987, 1988).

The causes or driving forces for salt tectonic can be separated into four interactive domains: depositional (and erosional), physical, tectonic and eustatic. The timing of salt movement at any scale is mainly related to deposition (loading) and erosion (unloading). Other physical factors such as large scale thermal convection of salt or local heat sources (magmatic intrusions) have also been evoked . Similarly, pure tectonic factors such as gravity gliding and spreading, sub-salt deformation and thin skinned extension and contraction are also thought to be possible independent causes for large salt masses displacement (Woodburry *et al.*, 1980) . The fourth point to consider is eustasy and related changes in sediment influx or the recurring changes in water column differential loading associated with eustatic cycles (Lowrie, 1986) . Although all these factors interact to initiate growth faulting and salt movement, sedimentary differential loading seems to be the essential cause of salt displacement. Two types of sedimentary loading conditions and associated underground responses can be distinguished:

- outer shelf **lowstand** related deltaic influences bringing large volume of fine sorted sands provoking shelf edge instabilities and initiation of growth faults (Winker, 1982 ; Coleman *et al.*, 1983 ; Winker & Edwards, 1983 ; Suter & Berryhill, 1985 ; Berryhill, 1987) . The gravity loading is accommodated by salt displacement mainly in the basinward direction (down-building, Barton, 1933; Bally, 1981; Bally *et al.*, 1981; Worral & Snelson, 1989 ; Wu *et al.*, 1990a). In the studied area, outer shelf conditions are encountered during the late Early Miocene (see, fig. 1-5b). and coincide with the Early-Middle Miocene depocentre and the highest rates of total subsidence (fig. 7-4). Similar sedimentary environments are described by Berryhill (1987, see fig. 5-5) in the modern northern Gulf of Mexico shelf break region and have been used for comparison with the studied Middle Miocene depocentre. We believe that most master growth faults presently observed on the shelf were initiated in shelf edge condition.

- The second type of sedimentary differential loading found on the inner shelf is associated with relative **highstand** proximal progradation. Development of large low angle thin proximal highstand fans as exemplified in chapter 5 (fig. 5-9, 5-11, 5-12, 5-17, 5-21, 5-24, 5-51). Such fans take advantage of already active growth faults on the inner shelf to accentuate lateral differential loading causing salt mainly basinward but also lateral movements. The lateral disposition of highstand fans is not only influenced by the pre-existing tectonic framework on the shelf (growth faults associated depressions) and positive salt related features (fig. 6-7 and 6-8) but also by the anterior depositional highs (lateral lobe shifting similar at a smaller scale, to the Holocene impressive migration of the Mississippi delta; Kolb & Van Lopik, 1958 ; Coleman, 1976) . Evidences for secondary arcuate growth fault creation by highstand differential loading can be found in the inner shelf environment (fig. 5-12) and we believe that major growth fault are difficult to generate in the inner shelf environment but that the pre-existing faults triggered during relative lowstand conditions are "nourished" and locally accelerated by highstand progradation.

The effect of differential erosional loading/unloading can be presented as distinct from the lateral

differential sedimentary loading factor. Differential erosional unloading on the shelf is mainly related to periods of relative low sea level. In continental or inner to middle neritic environment, fluvial erosion can differentially unload large portions of the shelf so that diapiric walls can rise along the main incised valley floor (Huntoon, 1982) ! On the inner shelf, differential erosional loading can thin and locally flatten pre-existing positive morphologies such as salt related domes and footwalls of active growth faults (an example of erosion on top of a salt related positive structure observed in the studied area is described in chapter 4, figure 4-7). During periods of lowstand on the inner shelf and mainly at the beginning of the relative fall of sea level (see ie figs. 5-16, 5-27, 5-33 and 5-50) the footwall of active growth faults is partially levelled and incised by streams developing proximal fans on the hanging wall (fig. 7-2 B). This small scale differential loading and unloading configuration that can be repeated for each eustatic cycle recorded on the platform has an extremely dynamic effect on the possible downward and basinward shifting salt masses. If the relative sea level fall is greater than the rate of total subsidence on the inner shelf then a portion of the shelf is levelled and the vertical throw of active growth fault is partially or entirely eroded (see chap. 7-3 for further details). In such a setting, major incised valleys developed during the maximum of relative sea level fall, are mostly along the traces of the main growth faults.

This situation is illustrated in figures 5-35, 5-39, 5-44, 5-47 and 5-56 and is schematically represented in figure 7-2 A. The early lowstand shallow channels and associated fans can be partially or entirely removed according to the importance of erosion occurring at the peak of relative sea level fall. The formation of mini-basins by concentrated sedimentation on the inner shelf over a long period of time is therefore likely to be generated by the systematic erosion of the footwall and correlative loading of the hanging wall of major growth faults during periods of relative lowstand (differential erosional loading / unloading). This local high subsidence rate of the hanging wall of major growth faults can be rapid enough to lower the overpressure zone and thereby prevent the accumulation of hydrocarbons in large portions of the shelf (exemple of Borneo Pleistocene delta, Stampfli, oral comm.).

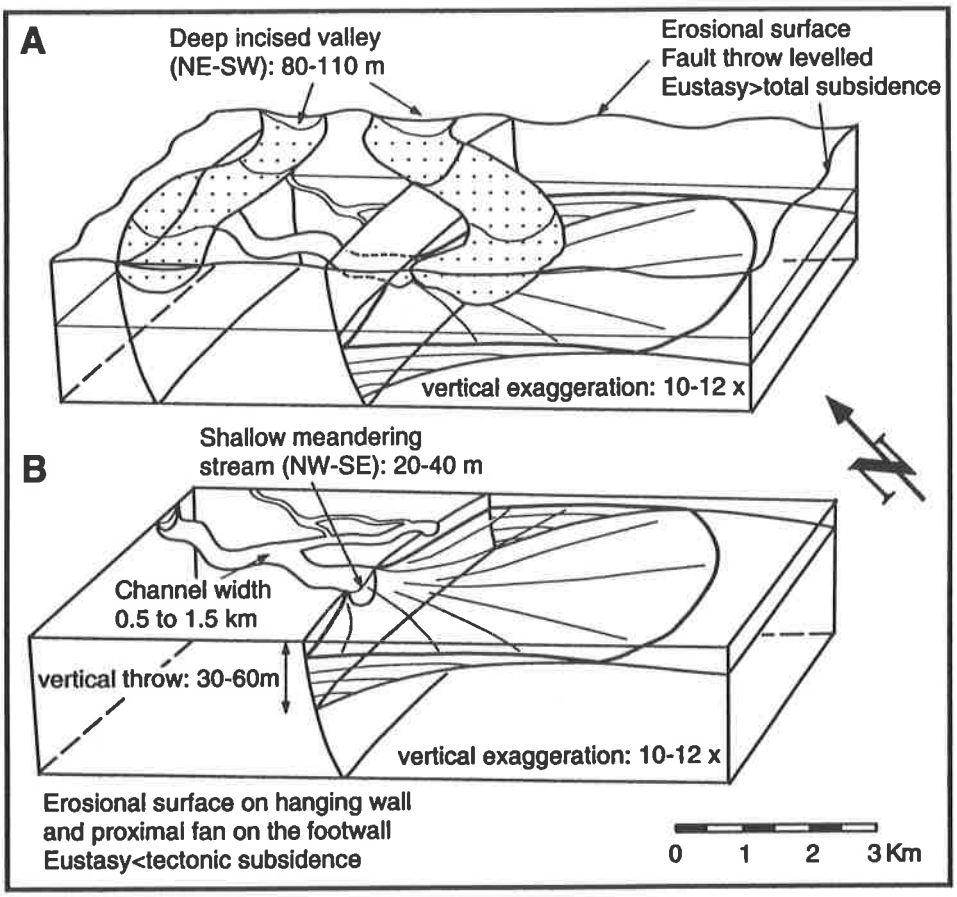

Fig. 7-2: Inner shelf deformation versus sedimentation in period of relative lowstand. ***b.*** *Onset of relative sea level fall, shallow erosion on the hanging wall (unloading) and proximal top highstand and base lowstand fan progradation on the foot wall depression.* ***a.*** *Maximum lowstand erosion, incised valleys and worn down shelf (vertical throw of active growth faults eroded, eustatic fall > total subsidence.*

The additional input or overload associated with periods of relative highstand will not systematically contribute to mini-basin formation as the highstand fans are less influenced by the pre-existing fault geometry (differential depositional loading, important lateral deltaic lobe migration from cycle to cycle).

In conclusion, eustasy is not the dominant factor controlling the formation of mini-basins on the inner shelf. The main factors or agent are gravitational loading; sedimentary loading on the outer shelf and differential loading on the inner shelf. These two factors are partially influenced by eustasy. Eustatic cycles can manifest themselves on the shelf and locally accentuate gravitational processes caused by master growth faults genetically related to major depocentres deposited in outer shelf conditions. These depocentres themselves are more related to the general tectonic framework of the hinterland than to eustasy (Bally, a course note). If total and local tectonic subsidence rates are propitious then sedimentation influenced by eustasy will contribute to differential loading on the shelf. This relation is further discussed in the next chapter.

7.3 Total subsidence, relation to sedimentation and eustasy.

Total subsidence calculation: introduction

The total subsidence curve indicates the history of the burial of a given rock formation through time. This curve is the sum of all vertical movements at a given time. It is obtained on the basis of a t/z curve corrected for compaction, paleobathymetry and eustasy. The tectonic subsidence is obtained by removing the effect of the sediment load increasing through time. This is based on an Airy type of isostatic re-equilibration. Tectonic subsidence curves are difficult to interpret based on the data available in this study as no eustatic corrections could be realised for the 3rd and 4th order sequences dominating the sediment record in the studied area (see decompaction principle point 4). The global tectonic curve provides information on the basement response to vertical loading and horizontal stresses through time. In this study, the basement taken as a reference is the base of the Middle Miocene sediments which is much more subject to salt displacement than isostatic readjustment of the Gulf coast passive margin basement. This excludes the possibility of any simple modelling of crustal response to the sediment load in the Gulf coast region.

Decompaction principle

Subsidence analysis is divided in six steps:

1) Construction of the t/z curve based on age and depth of sediment packages. In this study (fig. 7-3, annexe A-4-1), this curve is constructed from the interpreted horizons on the 3D data calibrated in time from benthic foraminifers zones in the productive interval (Miocene) and from sequential analysis and correlation with published sources (Courtney Reed & Layendecker, 1987)

2) Decompaction based on the curve of porosity loss with depth. This curve is expressed by:

$$\emptyset = \emptyset o \exp(-c\, z)$$

where Øo is the surface porosity value and c the coefficient of porosity loss with depth (z) dependant on lithology .

The thickness of one formation after decompaction is :

$$y'2-y'1 = y2-y1-(\emptyset o/c)\{\exp(-c\, y1)\}-\exp(-c\, y2)+(\emptyset o/c)\{\exp(-cy'1)\}-\exp(-cy'2)$$

The solution to this equation is found by iteration based on the program from Allen and Allen, (1990) . The Øo, c and density values used in the program developed by Favre (under press) are listed in the table below:

Lithology	Øo (%)	c (km-1)	d (g/cm3)	References
Shale	63	0.51	2.72	(Sclater & Christie, 1980)
Silt	56	0.39	2.685	(Sclater & Christie, 1980)
Sandstone	49	0.27	2.65	(Sclater & Christie, 1980)
Chalk	45	0.54	2.71	(Sawyer et al., 1982)
Dolomite	31	0.22	2.8	(Heidlauf et al., 1986)

In this study, the lithology of each interval has been estimated from the well log data and expressed as the weighed mean of the above values. The mean decrease in porosity trend with depth have been taken from the synthesis for the Gulf coast sediments by Gregory (1977) and Schluger (1979) and porosity values obtained in this study on Well 4 (see fig. 3-14a).

3) Paleobathymetric corrections take into account the paleo-water-depth condition of each formation. In this study they are estimated on the basis of:

- the sedimentary facies interpreted from the seismic facies displayed on the horizontal ampli tude map.
- the lithology indication on well log data.
- the content in benthic foraminifers in the productive interval (See annexe A-4-2).

4) Eustatic corrections: the existing programs apply eustatic corrections based on the global 2nd order cycles (Haq et al, 1988) which would be irrelevant on the period of 17 Ma considered in this study. A new program taking into account the shorter cycles observed on the Plio-Pleistocene will soon be available.

5) True tectonic curve and sediment unloading: total subsidence is the sum of the basin tectonic driving force (crustal thinning, rifting, salt related down-building etc...) and of the sediment and water load. It is therefore necessary to suppress the effects of the sedimentary load to obtain the pure tectonic component. This isostatic equilibration (Airy model) needs the evaluation of the water depth through time and of the porosity changes of the formations with increasing depth. In this research, the tectonic subsidence calculated for Well 3 is very delicate to interpret as it shows the combined effects of at least four distinct factors:

- eustatic changes in water load.
- salt tectonic related to changes in sediment loading through time.
- Gulf coast basement tectonic subsidence in response to loading at basin scale.
- lithospheric thermal subsidence (Wernicke, 1984) .

More data over a wider time interval, accurate eustatic corrections and detailed understanding of the salt tectonic timing would be required to be able to interpret correctly a tectonic subsidence curve which cannot be considered at this stage.

6) Modelling: basin tectonic subsidence modelling aims at determining the amount of crustal thinning and defining the type of passive margin evolution below a given basin. This requires an exhaustive study of the sediment record from the basement up to the present over a large area which is definitively not the case in this research.

Total subsidence versus sedimentation and eustasy.

The curve of cumulated thicknesses (t/z, fig. 7-3), obtained by the transformation of the time depth of every interpreted horizon with the velocity law on Well 2, indicates three distinct trends of apparent subsidence. The two curves on figure 7-3 are displayed without bathymetric nor eustatic corrections and no decompaction is applied. The table below compares the values obtained for the three observed trends on the two type of curves (t/z, fig. 7-3 and subs. tot. on fig. 7-4). The first (younger) trend (1 on fig. 7-4) covers the entire Gulf coast Pleistocene between 2.7 Ma (MPLIO horizon, base Gulf coast Pleistocene) and the present (HP6 horizon at ≈ 0.2 Ma). The second trend marked by two kinks at LM1 and TOPMIODL spreads over the Middle and Late Miocene and base Pliocene (MM5 at 15.2 Ma and MPLIO at 2.7 Ma, see annexe 4, table A-4-1 for age and depth of every horizon). The third and steeper trend corresponds to the top Early Miocene (from MM5 to EM1 at 17.3 Ma).

Trends	Well 2 t/z	Well 3 t/z	Well 2 subs.tot	Well 3 subs tot
Plio-Pleist.	360	374	224(ci:0.994)	205(ci:0.995)
Late-Mid. Mio	134	165	127(ci:0.999)	138(ci:0.993)
Early Mio.	626	589	747(ci:0.987)	630(ci:0.984)

(trends in m/Ma and ci: correlation index)

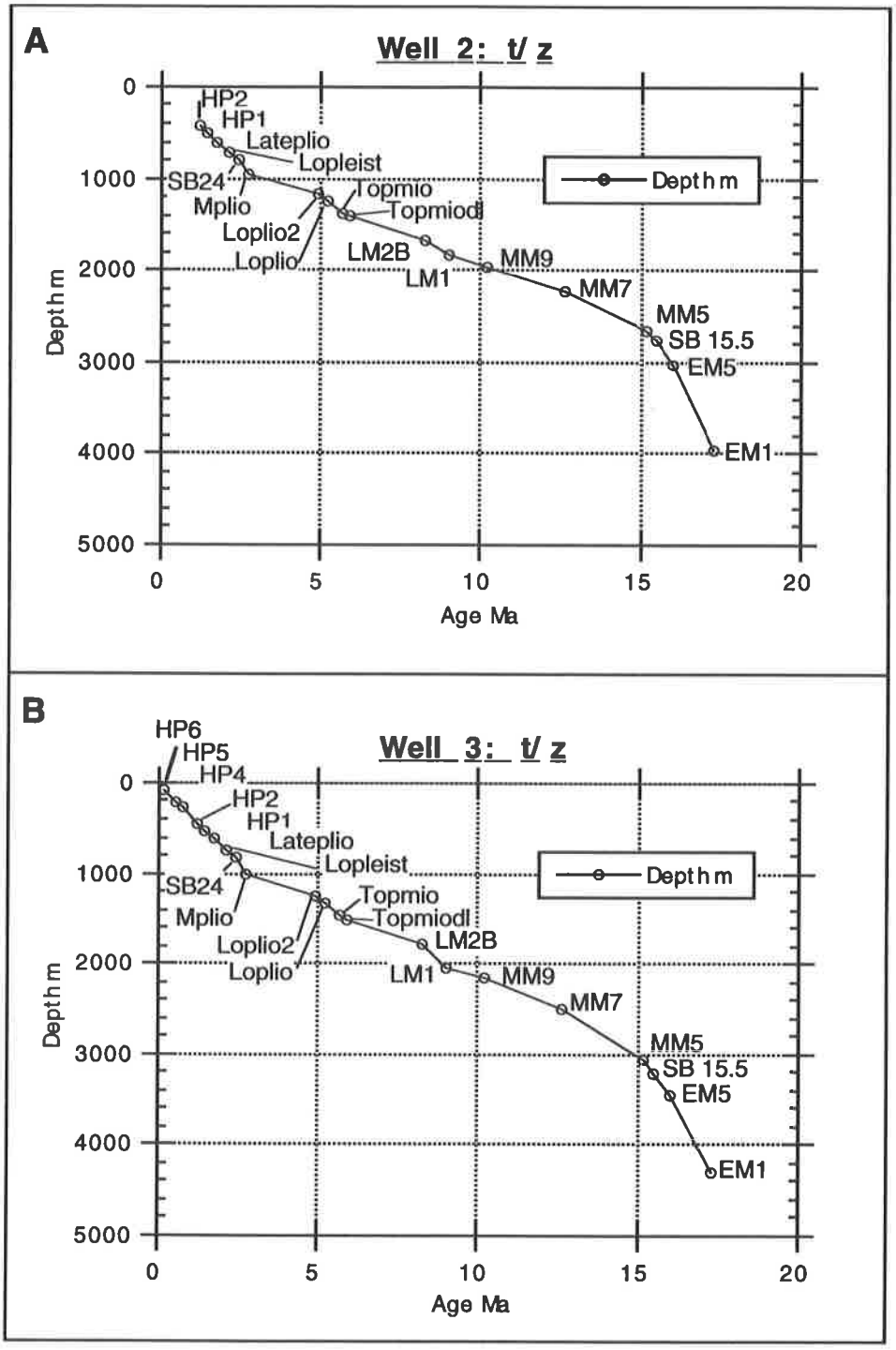

Fig. 7-3: Time /depth (t/z) curves for Well 2 and Well 3 (depth in m from velocity law calculated on Well 2). Three trends visible (HP6-Mplio, Mplio-MM5, SB15.5-EM1).

The mean subsidence rate has been calculated by linear approximation and the correlation index is indicated. Cautious interpretation must be proposed as many factors can be at the origin of distinct trends observed on a curve of decompacted total subsidence. The position of the main depocentres through time, the local response of tectonic subsidence to differential loading related to eustasy and tectonic, the crustal north Gulf coast subsidence, inaccuracy in horizon age and depth, intersection of well logs with major faults, etc... must be considered for each trend.

Trend 3 (Early Miocene, ≈700 m/Ma) is clearly related to the Early Miocene depocentre situated in the studied area at that period (fig. 5-2). The signs of the late Early Miocene shelf break are found in the studied region below the EM5 horizon (see fig. 1-9, PLATE 1). We believe that the major growth faults present in this survey (F1 and F7) were initiated at that time in upper bathyal conditions (see fig. 7-6, Coleman *et al.*, 1983 ; Winker & Edwards, 1983) . It is difficult to say if any kinks are observed on this

trend represented by only three points. But with a total subsidence rate of 70 m / 0.1 Ma, which is the time duration of the 4th order cycles observed in the Plio-Pleistocene, little chance is given to eustasy to manifest its effect on the outer shelf during the Early Miocene. The observed disappearance of erosional features on amplitude maps on the 3D survey, below the MM5 horizon is related to the marine environment of deposition and to the high rate of total subsidence.

Trend 2 on figure 7-4 b shows an average rate of total subsidence of 13 m /0.1 Ma. The corresponding depocentres (Late and Middle Miocene) are found respectively 40 to 150 km away from the region of interest (fig. 5-2). With such a low rate of total subsidence, all 4th and 3rd order eustatic cycles have a chance to erode part of the middle to outer shelf in that region during that period. On the seismic data, only major 3rd order erosions marked by important hiatuses and large incised valleys are visible during this interval (SB 5.5, 6.3, 7.1, etc..., down to 15.5, fig. 5-65). No trace of shorter cycles are recorded or preserved (chap. 5.6/7). All three kinks on the curve (rapid increase of subsidence, before LM1, TOPMIODL and MPLIO) correspond to period of drastic lowstand correlated to the maximum of cold periods (see fig. 5-40, PLATE 3, from LM1 to LM2B, TOPMIODL to LOPLIO, MPLIO to SB 24). The curve of total subsidence is not corrected for eustatic variations which means that the lowstand erosional unloading (water and sediments) are even stronger than mentioned here. Important erosional differential loading / unloading and massive sedimentation on the shelf break (40 to 150 km away) provoke an almost instantaneous down-building response in the underlying salt bodies which causes a rapid increase in the tectonic component of the total subsidence curve.

Trend 1 shows an average total subsidence rate of 21 m /100kyrs recorded in inner to middle neritic marine environments (Pleistocene depocentre 250 to 300 km offshore from the studied area). With such a subsidence rate, most 0.1 Ma erosional phases can be recorded and identified on the seismic data (chap. 5-2 to 5-5). Only one kink (rapid increase of subsidence) is observed between the HP4 and the HP2 horizons on the curve of total subsidence for that interval. This period coincides with the peak of maximum cold registered in the Pleistocene (sensus stricto) between 0.8 and 1.2 Ma (see fig. 5-6, PLATE 3). The impossibility to observe the totality of 0.1 Ma cycles over that interval is explained by the local increase in subsidence rate and by the strong lowstand erosions recorded at 0.8, 1.65-1.85 and 2.4-2.6 Ma.

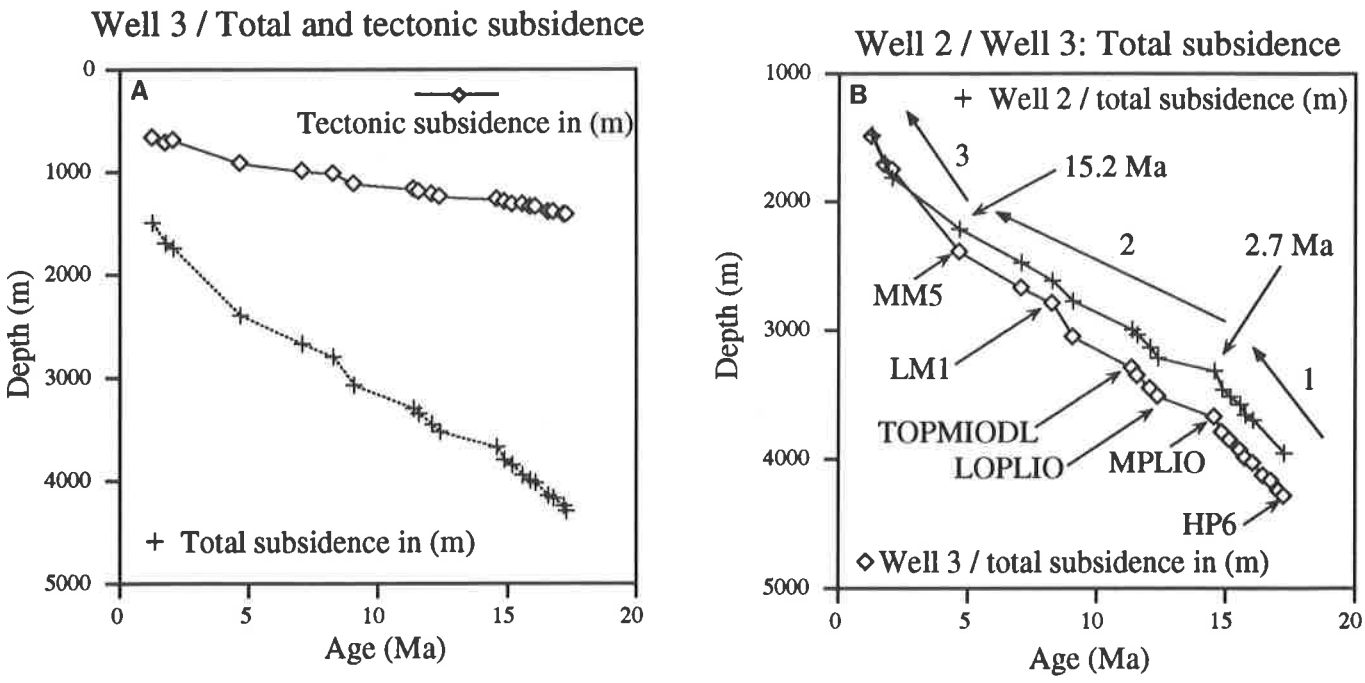

*Fig. 7-4: **a.** Total and tectonic subsidence curves for Well 3. Kink on curves due to the absence of eustatic corrections. **b.** Superposed total subsidence curves for Well 2 and 3. Three trends also identified after decompaction from t/z curves (fig. 7-3).*

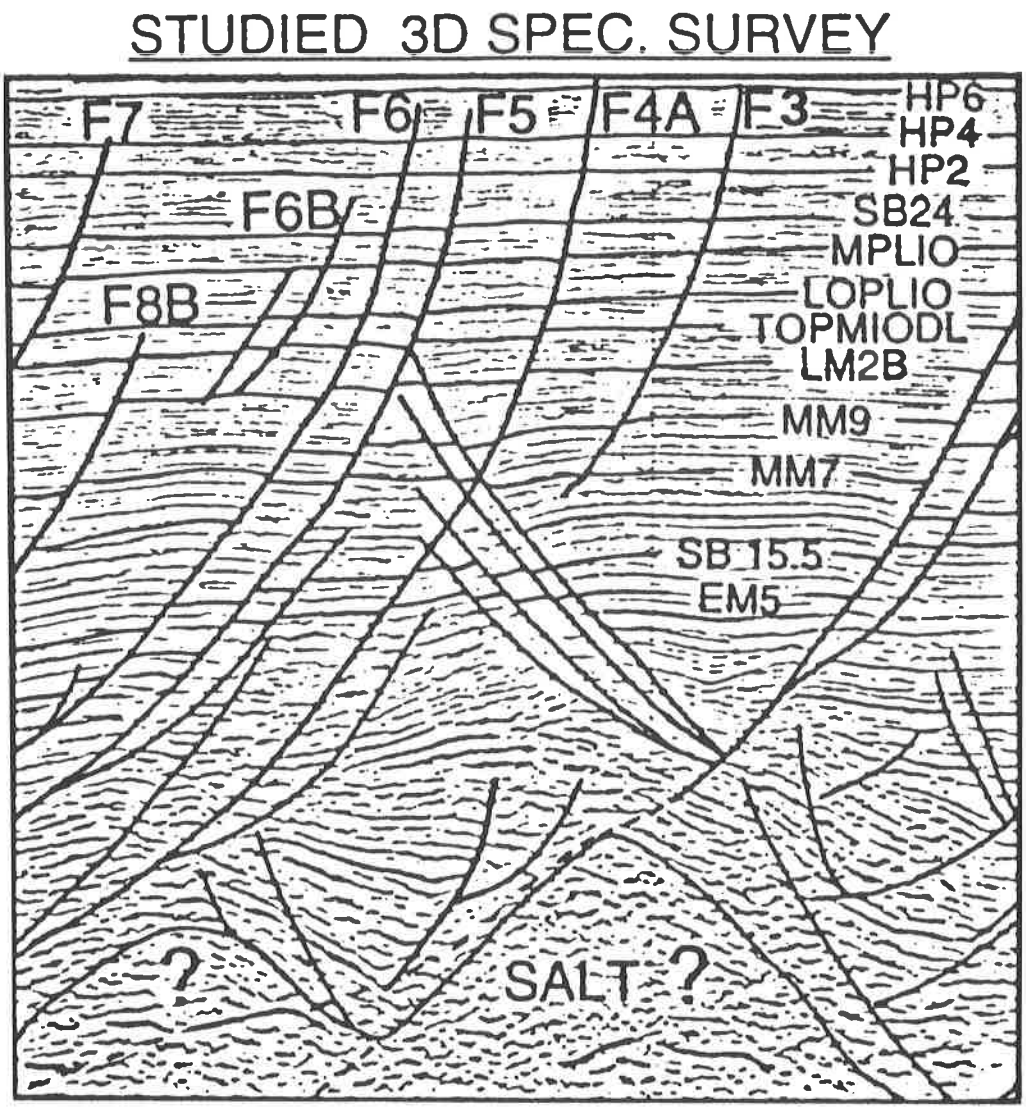

Fig. 7-5: Magnified interpreted portion of the north-south regional transect (fig. 1-9) across the studied 3D survey. Location of major growth faults F1 and F7.

Conclusion

At the shelf scale, the rate of total subsidence (decompacted, without backstripping, Allen & Allen, 1990) and not corrected for eustatic 2nd order cycles shows the regional impact of depocentres offshore migration through time. The depocentre major shifts over the Cenozoic are related to the tectonic of the hinterland and not to 2nd order eustatic cycles (Bally, oral communication). Considering the shorter eustatic cycles (0.1 to 0.5 Ma cycles over the Plio-Pleistocene), the combined effects of the rate of total subsidence and the marine environments constrain the development of 4th order sequence boundaries on the shelf. On the inner shelf (inner to middle neritic) when the total subsidence rate is low (trend 2), major (3rd order) lowstand events develop important hiatuses partially eroding the shorter cycles (4th order sequences) marked by shallower erosions. When the rate of total subsidence is high enough, most shorter cycles can be recorded and preserved on the inner shelf (trend 1). Total subsidence rate superior to 500 m/Ma are typical of the shelf break area (important sediment loading) where even erosional surfaces related to extreme changes in sea level (up to 200 m) have no chance to be recorded.

Total subsidence versus local deformation and sedimentation

The formation of small rim synclines on a clastic shelf bordered by arcuate growth faults is mainly governed by allochtonous salt sheet movements in response to sediment loading (fig. 1-9, PLATE 1). The local sedimentation facies on the shelf is a function of the complex interaction of the total subsidence rate, the local tectonic subsidence, the rate of sediment input and eustasy (Posamentier & Allen, 1993). At the scale of the mini-basin, the tectonic component can be estimated in detail for each fault block. The high density of information provided by 3D seismic data allows to locate and precisely quantify the timing and displacement along normal and antithetic faults. The two modes that determine the periods and rates of activity of growth faults on seismic data are the measurement of the fault vertical throw between two isotime reflectors and the calculation of isopach maps. Differential rate of growth fault activity can be visualised by mapping the fault throw on the fault plane. Figure 7-6 (A and B) shows the curve of total fault throw measured in the zone of maximum activity of the two major growth fault observed in the 3D data (F1 and F7, see fig. 7-7 B for location).

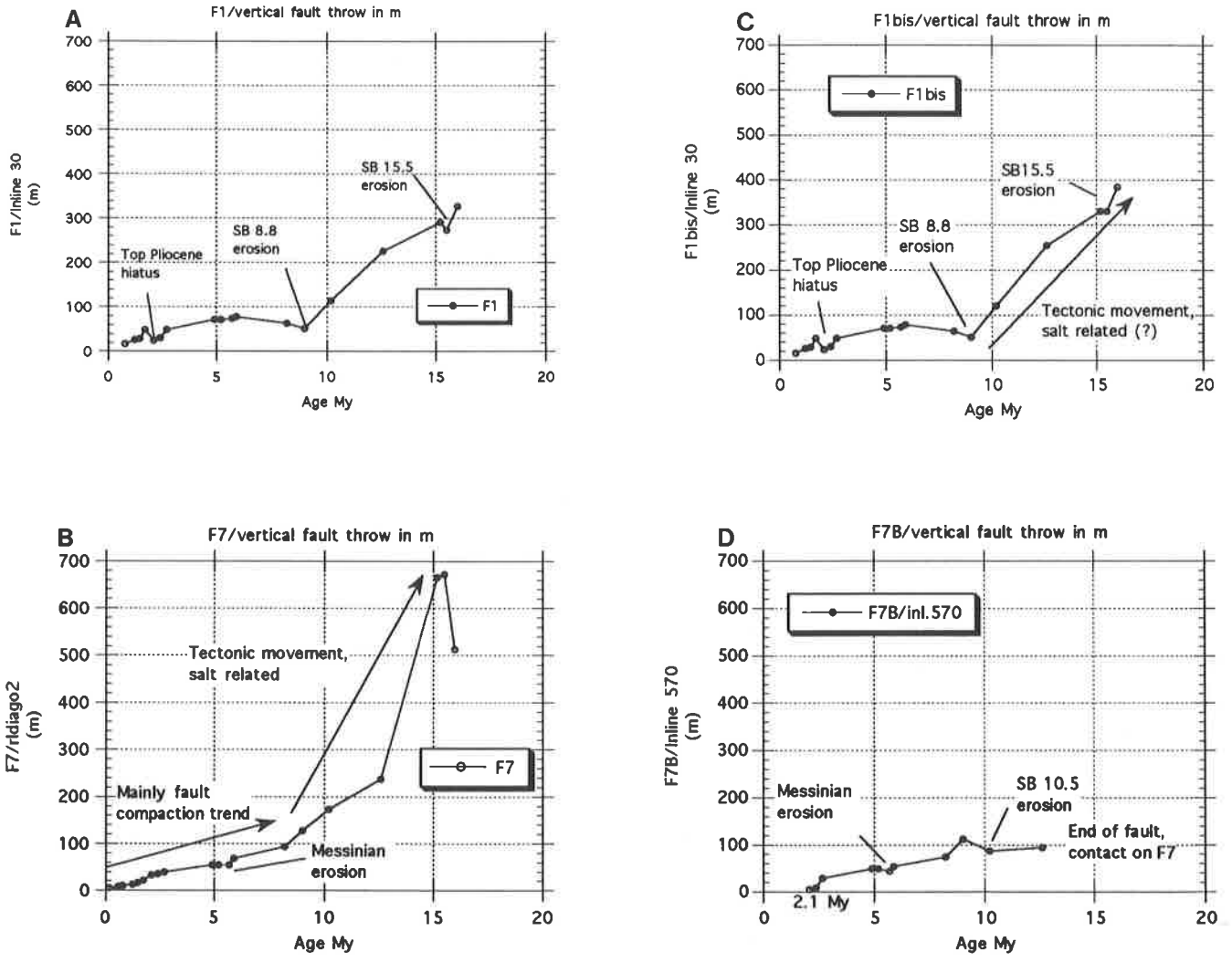

*Fig. 7-6: Growth fault throw (in m) measured on interpreted horizon. **a.** F1 **b.** F7 **c.** F1B and **d.** F7B (see fig. 7-7 b for location). Two trends are visible: slow rate (100 m /10 Ma, compaction) and rapid activity (≈500m / 5Ma, salt related down-building). Major hiatuses recorded by the fault throw history.*

Two trends are visible and express a common history on the two major growth faults on the inner shelf:

-the phase of major activity is recorded from the onset of the fault activity (late Early Miocene) to the middle Late Miocene (≈8 Ma). This rapid growth rate of 100 m /Ma is related to salt down building processes below the studied area partially accommodated by the basinward movements of the allochtonous salt sheet situated 40 km offshore from the studied area (see, PLATE 1). As the depocentre moves further offshore from the studied area, the rate of growth fault activity starts to decline (around 8 Ma before present the main depocentre was located 60 to 80 km offshore from the studied area, approximately 20 km basinward of the allochtonous salt tongue seen on fig. 1-9).

- the second trend (10 m /Ma) is the average rate of growth activity moved by the combined effects of differential loading on the shelf related to eustasy and of sediment differential compaction between the footwall and the hanging wall of major growth faults. The far distant depocentre (>150 km) does not influence the local tectonic subsidence anymore. Differential loading / unloading becomes the predominant driving force on the inner shelf.

Period of major lowstand can be recorded on the fault throw curves when the degree of erosion is high enough to partially level the fault related pre-existing topography on the shelf (see fig. 7-2 a). Figure 7-6(a and b) shows the deflection of the fault throw curve at the top Pliocene hiatus (2.4-2.6 Ma), the Messinian lowstand (5.5 Ma), the erosion related to the cold peak at 8.8 Ma (see fig. 5-40, Plate 3) and the basal Middle Miocene lowstand (SB 15.5). These major erosional surfaces are recorded on all the faults in the studied area confirming important erosions levelling the entire shelf and the basinward reworking of important masses of sediments during phases of major lowstand.

7.4 An application of 3D fault analysis to subtle potential traps.

3D seismic data high density of information allows to observe transfer zones between juxtaposed growth fault. The example below shows the local splitting in two of a normal growth fault developed in front of an older antithetic fault. The dome like structure created in the triangle between the termination of three faults is presented as a potential tectonic subtle trap sealed on each side by a normal fault.

Figure 7-7 b presents the fault configuration of the studied area at the level of the LOPLIO interpreted horizon. In the centre of the image three antithetic faults dip landward and are associated with the major F1 and secondary F3 basinward dipping growth faults (F6B is the oldest of the three antithetic faults). The southern termination of the younger F5B fault is split into two branches, by the presence of the F6B fault. Figure 7-7 a and the interpretation of three parallel inlines on figure 7-7 c show that the F5B2 branch is added to the main F5B fault to match the transfer of vertical throw to the F6B fault. The precedence of the antithetic faults rooted on the F3 fault versus the F5B fault is demonstrated at the bottom of the inlines on figure 7-7 c showing the shifted F6A by the younger F5B. Inline 340 intersects the F5B and F6B faults and presents a local roll-over like feature against the F5B fault. A strong negative amplitude anomaly is observed at the level of LOPLIO (see pointer on fig. 7-7 c). Laterally, 250 m to the east, Inline 350 intersects the F5B, F5B2 and F6B faults. This section shows the creation of the secondary F5B2 fault parallel to the main F5B fault to accommodate the diminution of normal throw lost by the F6B antithetic fault. Further to the east, on Inline 360, the antithetic fault is transferred entirely to the F5B and F5B2 normal faults. 500 meters more to the east the F5B2 fault is merged with the major F5B fault.

The negative amplitude anomaly contained within half a loop (dashed ovoid on fig. 7-7 a) has a diameter of more than a kilometres and is associated to the positive tectonic dome in the triangle transfer zone between an antithetic and a younger normal fault. When situated at the right depth, such structures (common on the Louisiana shelf, Louisiana style, Worral & Snelson, 1989) could be of economical interest.

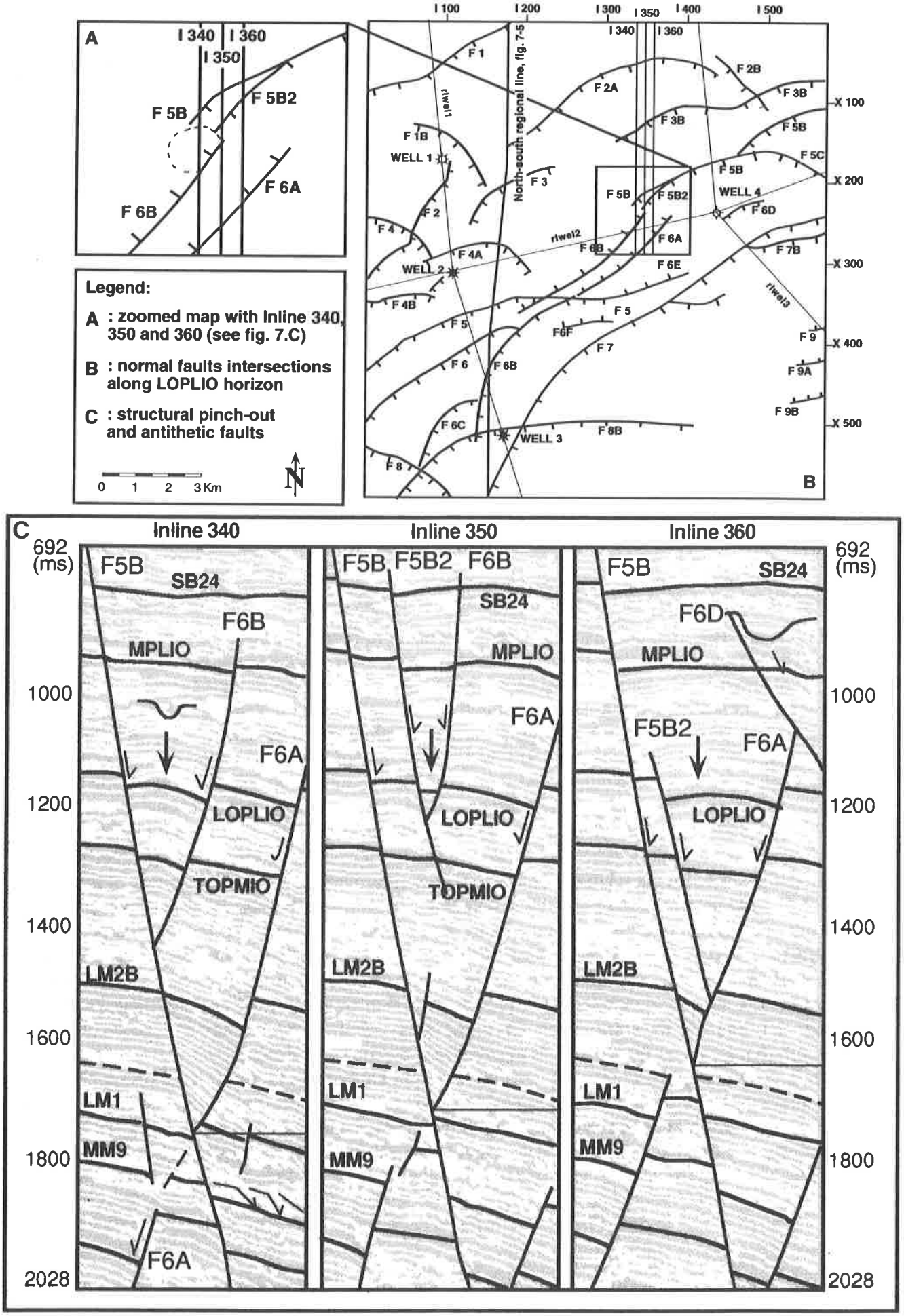

Fig. 7-7: Growth faults and subtle tectonic traps. ***a.*** *Zoomed plan-view on the transfer zone between a normal (F5) and an antithetic fault (F6B).* ***b.*** *Plan view of the total surface of the studied area and fault location along LOPLIO horizon (see fig. 7-7 a).* ***c.*** *Three zoomed north-south inlines across the transfer zone from F5 to F6B growth faults (location on fig. 7-7 a and b).*

7.5 Conclusions

The process of growth fault interaction with sedimentation and salt movements is related to an important number of synergistic interrelating factors. Lowrie in 1986 has proposed that growth faults are most likely developing on the shelf break, and during periods of low sea level (Lowrie, 1986) . During a global cold event, the total free water volume in the oceans is lowered and transferred onto the continents. The reduction in the ocean surface can reach 20 % and the ice coverage can increase up to 50 % (Fairbridge, 1983). Thus, water is removed from the shelf and isostatic compensation occurs differentially. The depletion of up to 160 meters of water on the shelf induces a discharge (unloading) producing a vertical readjustment of around 40 m (Lowrie, 1986) . Almost the totality of the shelf is above water level and the shoreline is close to the shelf break. The total sedimentation organised in prograding wedges is concentrated on the outer shelf and upper slope. Lateral differences in compaction rates between the shelf and the slope increases the angle between them and accentuates the instability. Once a growth fault system is initiated on the shelf break it creates a depression that will possibly deviate the alluvial system and serve as a trap for further sedimentation. Lateral differences in pore expulsion rates under the shelf zone and under the thicker prograding package on the upper slope (Fairbridge, 1983) will liberate water in the fault plane enabling easier movement along the fault plane.

Therefore, the combined effects of isostatic readjustment, aquatic overburden lateral differences, concentrated sedimentation and increased pore fluid expulsion, tend to generate growth faults near the shelf break during low sea level periods. Eustatic periodic influences (differential loading related to pre-existing topography) are predominant on the inner shelf to accentuate or perpetuate the fault growth rates. On the Gulf coast Pleistocene of the proximal central northern Gulf of Mexico margin, the rate of total subsidence is increasing (trend 1 on fig. 7-4 a) even if the corresponding depocentre is located 300 km further offshore. This is due to the fact that ever larger quantities of sediments are trapped in the mini-basins depressions on the inner shelf provoking a third major Plio-Pleistocene phase of salt activity and allochtonous sheet emplacement on the inner shelf. The offshore equivalent of this Plio-Pleistocene phase observed on the inner shelf is described by Wu *et al.*, (1990b) on the present north-eastern Gulf of Mexico slope.

The sedimentation on the inner shelf is related to total subsidence, local fault related tectonic subsidence, volume of sediment influx and eustasy. The following summarised conclusions on the relation between sedimentation and deformation on the inner shelf of the central Gulf of Mexico are proposed:

-sedimentary loading does not require a density inversion but rather a constant place for erosion and deposition (growth fault).

-differential loading can initiate growth fault on the shelf break mainly during lowstand periods.

- on the inner shelf, differential loading and unloading are the dominant factor affecting tectonic local subsidence. Lowstand sedimentation on the inner shelf is **concentrated** on the footwalls of major growth faults (superposition of lobes).This perpetuates and even increases their rate of activity. Highstand progradation on the inner shelf spreads over large areas and deposit thin large mainly juxtaposed lobes not affecting tectonic local subsidence but rather global total subsidence.

-Delta lobes shift laterally on the shelf break during period of lowstand and migrate laterally on the inner shelf during period of highstand.

- Faults possibly trigger salt tectonic rather than the contrary.

- Secondary normal and antithetic faults parallel to major growth faults develop progressively in the basinward direction. Pre-existing antithetic faults of a major growth fault can be shifted by a second generation of faults (see below).

8. Discussion and conclusions.

Aristotle was right: The Whole is really much more than the sum of the parts.
The amount of geological information contained into a set of closely spaced parallel seismic lines is simply astounding, provided the data are correctly transformed into a full 3D data volume (3D migration) and consistently interpreted. The objective of this concluding chapter is not to repeat the extensive conclusions written at the end of the 7 preceding chapters but rather to integrate them into a perspective view for further researches and draw more general inferences applicable outside of the studied area.

Initially, sequence stratigraphy and global eustatic curves were severely attacked because of the lack of biostratigraphic data and because sequences or systems tracts are not time consistent stratigraphic units but only stratigraphic packages not bounded by isotimes. In this sense, this research remains open to criticism but it is important to mention that coherent lateral systems tracts correlation can be done within a single basin provided they are made by correlating systems tracts successions rather than single isolated events. This precaution takes care of the natural lateral facies changes within a single time unit. The resulting eustatic curve is not global but limited to a basin and traces nothing but the relative movements of sea level at one place, taking into account the local tectonic component. This is why it remains a fundamental prerequisite to be a geologist in front of a 3D seismic interpretation workstation in order to be able to interpret seismic facies into sedimentary facies then leading to the evaluation of a complete depositional environments (including paleobathymetry, rate of sediment supply and total and tectonic subsidence). To unveil the original depositional setting and find out the history of deformation is the only way to find and circumscribe subtle stratigraphic traps. This is much easier with 3D seismic data.

The procedure of how to apply 3D sequence stratigraphy to a new prospect (new 3D survey) to rapidly test the presence of subtle stratigraphic traps is summarised below:

- consult literature on the region looking for the predominant type of reservoir, location, age and association with systems tracts.
- find local eustatic curves, regional seismic cross sections and well log data ifany. Apply gross sequential analysis to regional cross sections and to well log data (see Annexe 3).
- rapidly interpret major unconformities and main flooding continuous events on the potentially productive interval on the 3D data set.
- compare the regional sequential analysis with the 3D survey and initial local sequential analysis.
- apply detailed sequential analysis to the 3D data set and to the eventually available well log data on the productive interval.
- have a rapid overview on the vertical and horizontal seismic sections on the 3D data looking for strong lithofacies amplitude anomalies (channels, sand bars, sandy progradation on shale) and gas related bright spots
- conduct a detailed interpretation of enough continuous horizontal datum (condensed sections, main flooding surfaces and sequence boudaries) to be able to extract consistent horizontal attributes maps in the zone of interest.
- interpret seismic facies (from various attribute maps) into sedimentary facies and deduce depositional environment.
- if any, delimit and estimate lithology, porosity and volume of potential reservoirs related to a particular systems tract and drill !

This succinct flow chart demonstrates the enormous advantage of 3D seismic data compared to 2D lines. An isolated polarity inversion or a an eventual water/hydrocarbon contact on a 2D line can be perfectly delimited and visualised on a 3D survey. Furthermore its lithological content and origin can be directly assessed thus reducing considerably the eventuality of misinterpretation leading to dry holes.

The main theoretical inputs of this research are reviewed below to orientate further researches. It is true that major Cenozoic deltaic progradations in the Gulf coast region are related to regional tectonic events and not to 2nd order eustatic influences (Rock Dale Deltas of the late Palaeocene Wilcox formation corresponds to the Laramide uplifts; the mid-Oligocene Frio formation coincides with the Sierra Madre ash flows; the Mississippi Neogene progradation is related to the Southern Rockies reactivation). But it is also true and demonstrated by this study that rapid eustatic changes (4th and 5th order) are influencing local sedimentation and deformation rates. The relative importance of tectonic and eustasy at a given place is then just a matter of scale.

Going back in time at a given spot looking at eustatic events gives the impression that registered sedimentary cycles are only getting larger and larger. The eight 0.1 Ma eustatic cycles of the top Pleistocene are clearly demonstrated today and seem to represent the shorter eustatic cycles that will be found on that interval. But in 1987, based on high resolution shallow seismic data, Berryhill wrote :« at least twice and perhaps three times during the late Wisconsinian regression and before the Holocene transgression, sea level oscillated sufficiently to cause retrenchment...» implying shorter cycles within shorter cycles.

Thus, the keyword to the understanding of natural cycles back in time is *vertical resolution.* Comparing 2D seismic lines and 3D data sets presenting the same range of frequencies shows that the vertical resolution provided by 3D data is at least 8 times superior to 2D lines. On an interval of 200 milliseconds (≈ 200 m), 5 to 6 distinct seismic events can be recognised on 2D vertical sections but 50 successive horizontal maps are obtained from 3D data sets ! This allows the observation of shorter order cycles on clastic shelves as recorded in inner to middle neritic environments deeper in the sediment record. Superposed erosive phases missed by 2D seismic data sets and the associated coastal onlap curves can be distinguished on 3D horizontal images by the differences in depth, size, orientation and degree of sinuosity of successive erosional events.

We demonstrate in this study that 0.1 Ma cycles extend at least over the entire Gulf coast Pleistocene (0 to 3.0 Ma) and that they correspond to the record of the eccentricity period of the Earth orbit around the Sun (96'000 years). Furthermore, a 0.8 Ma periodicity marked by the recurrence of stronger falls in relative sea level becomes apparent from the upper Neogene to the present (0 to 10.5 Ma). These cycles coincide surprisingly with major inversions of the magnetic field around the planet.

The sedimentation on the inner shelf is mainly governed by total subsidence, local tectonic subsidence, volume of sediment influx and eustasy. Salt basinward and lateral displacement under the northern Gulf coast shelf is controlled by growth faults generation near the shelf break and by rim-synclines formation on the inner shelf. The initiation of major growth faults occurs near the shelf break during periodes of lowstand.

3D sequence stratigraphy and the reconstruction of paleosurfaces of sedimentation will rapidly extend laterally as ever larger surfaces of continental shelves get covered with 3D data sets and ever more potent computing facilities become available. At the same time, new development in seismic reflection and other geophysical techniques will provide ever finer vertical resolution to ever greater depth improving the recognition of natural cycles back in time.

Considering this, how would it be possible to claim any research as the final Truth as truth is but how we see Truth. This work is a truth as seen today but surely not the truth of tomorrow. And I am already looking forward to it.

REFERENCES:

Abdulah, K.C. & Anderson, J.B. (1991). Eustatic controls on the evolution of the Pleistocene Brazos-Colorado Deltas, Texas. GCSSEPM Foundation Eleventh Annual Research Conference Program and Abstracts, 1-7.

Aharon, P., Goldstein, S.L., Wheeler, C.W. & Jacobson, G. (1993). Sea-level events in the South Pacific linked with the Messinian salinity crisis. Geology 21. 771-775.

Albritton, C.C. (1980). The Abyss of time. Freeman (Eds.). San Francisco. 251 p.

Allen, A.A. & Allen, J.R., (1990). Basin Analysis, principles and application. Blackwell Scientific Publications, Oxford. 451 p.

Amery, G.B., (1969). Structure of Sigsbee scarp, Gulf of Mexico. APPG Bull. 53. 2480-2482.

Amery, G.B., (1978). Structure of continental slope, northern Gulf of Mexico. - In Bouma, A.H. Moore, G.T. & Coleman, J.M. (Eds.), Framework, facies and oil-trapping characteristics of the upper continental margin: 141-153. Tulsa.

Anderson, J.B., Siringan, F.P., Taviani, M. & J., L., (1991). Origin and evolution of Sabine Lake, Texas-Louisiana. TGCAGS, XLI 12-16.

Anderson, J.B., Siringan, F.P. & Thomas, M.A., (1990). Sequence stratigraphy of the late Pleistocene-Holocene Trinity/Sabine valley system : relationship to the distribution of sand bodies within the transgressive systems tract. GCSSEPM Foundation Eleventh Annual Research Conference Program and Abstracts, 15-20.

Anstey, N.A. (1973): The significance of color displays in the direct location of hydrocarbons. - In 43rd Annual International Meeting of the Society of Exploration Geophysicists. Mexico City. Abstract.

Armentrout, J.M. (1994): Sequence stratigraphic biostratigraphy: surface recognition, facies definition and cycle correlation; examples from the Gulf of Mexico Plio-Pleistocene. - High resolution sequence stratigraphy: innovations and applications: 189-193, 265-269. Liverpool.

Balch, A.H. (1971). Color songrams-a new dimension in seismic data interpretation. Geophysics, 36 (6): 1074-1098.

Bally, A.W. (1981). Thoughts on the tectonics of folded belts. - In McClay, K.R. & Price, N.J. (Eds.) Thrust and nappe tectonics: 13-32. London: The Geological Society of London.

Bally, A.W. (1989). Atlas of seismic stratigraphy. AAPG Studies in Geology, Memoir 27 (Vol. 3).

Bally, A.W., Bernoulli, D., Davis, G.A. & Montadert, L., (1981). Listric normal faults. Oceanol. acta, Actes 26ème Congrès International de Géologie (colloque Géologie des Marges Continentales, Paris, 7-17 juillet 1980): 87-101.

Bally, A.W., Catalano, R. & Oldow, J., (1985). Elementi di tettonica regionale. Pitagora Editrice, Bologna. 256 p.

Bally, A.W. (1988). A course note. Rice University, Houston, Texas.

Barber, P.M., (1981). Messinian subaerial erosion of the Proto-Nile Delta. Marine Geology, 44. 253-272.

Barton, D.C., (1933). Mechanics of formation of salt domes with special references to Gulf coast salt domes of Texas and Louisiana. AAPG Bull., 17. 1025-1083.

Bates, R.L. & Jackson, J.A., (1987). Glossary of Geology. American Geological Institute. Alexandria. 788 p.

Beard, J.H. & Lamb, J.L., (1968). The lower limit of the Pliocene and Pleistocene in the Caribbean and Gulf of Mexico. TGCAGS, XVII, 174-186.

Beard, J.H., Sangree, J.B. & Smith, L.A., (1982). Quaternary chronology, paleoclimatic depositional sequences and eustatic Cycles. AAPG Bull., 66. 158-169.

Bentz, F.P. & Hudges, J.B., (1981). New reflection seismic evidence of a Late Miocene Nile canyon. - In Said, R. Eds., The geological evolution of the River Nile: 131-138. New York: Springer Verlag.

Berggren, W.A., Kent, D.V. & Van Couvering, J.A., (1985). Neogene geochronology and chronostratigraphy: Part 2. - In Snelling, N.J. (Eds.), The chronology of the geological record. 211-260. Geological Society of London.

Berryhill, H.L.J., (1987). Late Quaternary facies and structure northern Gulf of Mexico. AAPG, Studies in Geology. Memoir 23.

Berryman, L.H., Goupillaud, P.L. & Waters, K.H., (1958). Reflections from multiple transition layers. Geophysics, 23. 223-243.

Berven, R.J., (1966). Cardium sandstones bodies, Crossfield-Garrington area, Alberta. Bull. of Canadian Petroleum Geology, 14. 208-240.

Blum, M.D. (1994). Glacio-eustatic and climatic controls on quaternary alluvial plain depositional sequences, Texas gulf coastal plain (USA). - In High resolution sequence stratigraphy: innovations and applications. Abstract. 295-299. Liverpool.

Bone, M.R., Giles, B.F. & Tegland, E.R. (1976): 3-D high resolution data collection, processing and display. - In 46th Annual SEG Meeting. Houston, Texas.

Bone, M.R., Giles, B.F. & Tegland, E.R., (1983). Analysis of seismic data using horizontal cross-sections. Geophysics. 48/9. 1172-1178.

Bouma, A.H. & Coleman, J.M., (1986). Intraslope basin deposits and potential relation to the continental shelf, northern Gulf of Mexico. TGCAGS, 36. 419-428.

Bracewell, R.N., (1965). The Fourier transform and its applications. New York. Mc.Graw-Hill. 268-271

Brown, A.R., (1979). 3-D seismic survey gives better data. Oil and gas journal, November 5. 57-71.

Brown, A.R., (1983). Structural interpretation from horizontal seismic sections. Geophysics. Vol. 48/9. 1179-1194.

Brown, A.R., (1983b). Discussion on Seismic data display and reflection perceptibility. Geophysics. Vol. 48/2. 1291-1292.

Brown, A.R., (1985). The role of horizontal seismic section in stratigraphic interpretation. In: Seismic stratigraphy II-An integrated approach to hydrocarbon exploration. Berg. O.R. & Wolverton, D.G. (Eds.) AAPG Memoir 39. Tulsa.

Brown, A.R., (1986). Interpretation of three-dimensional Seismic Data. Tulsa. AAPG Memoir 42, Tulsa. 194 p.

Brown, A.R., (1986b). The role of horizontal seismic sections in stratigraphic interpretation. In: Seismic stratigraphy II-An integrated approach to hydrocarbon exploration. Berg. O.R. & Wolverton, D.G. (Eds.) AAPG Memoir 39. Tulsa.

Brown, A.R., (1990). Horizon slices over reservoir interfaces. AAPG Bull. Vol. 74. Abstract. 619.

Brown, A.R., (1992). Seismic interpretation today and tomorrow. The leading edge, 11 (11). 10-15.

Brown, A.R. & McBeath, R.G. (1980). Three-D seismic surveying for field development come of age. Oil and Gas Journal. Vol. 68. 63-65.

Brown, A.R., Dahm, C.G. & Graebner, R.J., (1981). A stratigraphic case history using three-dimensional seismic data in the Gulf of Thailand. Geophysical prospecting. 29. 327-341.

Brown, A.R., Graebner, R.J. & Dahm, C.G., (1982). Use of horizontal seismic sections to identify subtle traps. - In Halbouty, M.T. (Eds.), The deliberate search for subtle traps. 47-56. AAPG Memoir 32.

Brown, A.R., Serpell Edwards, G. & Howard, R.E., (1987). Fault slicing - A new approach to the interpretation of fault detail. 52/10. 1319-1327.

Brown, A.R., Wright, R.M., Burkart, K.D. & Agbriel, W.L., (1984). Interactive seismic mapping of net productible gas and sand in the Gulf of Mexico. Geophysics. 49/6. 686-714.

Brown, L.F. & Fisher, W.L. (1980). Seismic stratigraphy interpretation of depositional systems: examples from Brazil rift and pull-apart basins. In: Seismic stratigraphy-Apllications to hydrocarbon exploration. C.E. Payton (Eds.). AAPG Memoir 26. Tulsa. 213-248.

Bryant, I.D. & Flint, S.S., (1993). Quantitative clastic reservoir modelling problems and perspectives. In: Flint, S.S. & Bryant, I.D. (Eds.). The geological modelling of hydrocarbon reservoirs and outcrop analogues. Spec. Public. International Assoc. of Sedimentologists. Blackwell Scientific Publications. Vol. 15. 3-20.

Buffler, R.T., Schaub, F.J., Huerta, R. & Ibrahim, A.K. (1980). A model for the evolution of the Gulf of Mexico Basin. - In International geological congress, geology of continental margins symposium. 129-136. Paris. Oceanologica Acta.

Buffler, R.T., Shaub, F.J., Watkins, J.S. & Worzel, J.L., (1979). Anatomy of the Mexican Ridges, southwetern Gulf of Mexico. - In Watkins, J.S. Montadert, L. & Dickerson, P.W. (Eds.), Geological and geophysical investigations of continental margins: 319-327. Tulsa. AAPG Memoir 29.

Bullard, S.C., Everett, J. & Smith, A., (1965). The fit of the continents around the Atlantic. Royal Society of London, Philosophical Transactions, 1088. 41-51.

Buffler, R.T. (1989). Distribution of crust, distribution of salt and the early evolution of the Gulf of Mexico basin, program and extended and illustrated abstracts. SEPM Foundation (Eds.), Tenth annual conference, Gulf coast section. Houston. 25-27.

Campbell, C.V. (1967). Lamin, Laminaset, bed and bedset. Sedimentology. Vol. 8 7-26.

Caron, J.M., Gauthier, A., Schaaf, A. Ulysse, J. and Wozniak, J., (1992). Comprendre et enseigner la planète Terre. Ophrys (Eds.) Paris. 271 p.

Chaline, J., (1985). Histoire de l'homme et des climats au Quaternaire. Paris.

Chiocci, F.L., (1994). Very High-resolution seismics as a tool for sequence stratigraphy applied to outcrop scale-Examples from Eastern Tyrrhenian Margin Holocene/Pleistocene deposits. AAPG Bull, 78 (3). 378-395.

Cita, M.B., (1975). The Miocene/Pliocene boundary: history and definition. - In Saito, T. & Burckle, L.H. (Eds.). Late Neogene epoch boundaries: 1-30. New York. Micropaleontology Press.

Cita, M.B. & Ryan, W.B.F., 1978. Messinian erosional surfaces in the Mediterranean. Marine Geology, 27. 193-363.

Cloos, E., (1968). Experimental analysis of Gulf coast fracture patterns. AAPG Bull., 52. 420-444.

Coffeen, J.A., (1990). Seismic on screen. An introduction to interactive interpretation Tulsa: Penwell Books. 284 p.

Coleman, J.M., (1976). Deltas: processes of deposition and models for exploration (Champain III, Continuing Education Publishing).

Coleman, J.M., Prior, D.B. & Linsay, J.F., (1983). Deltaïc influences on shelfedge instability processes. SEPM, Special communication, 33. 121-137.

Courtney Reed, J. & Layendecker, C.L., (1987). Correlation of Cenozoic Sediments. Gulf of Mexico Outer Continental shelf. New Orleans. MMS Report, US Department of the Interior.

Crans, W., Mandl, G. & Haremboure, J., (1980). On the theory of growth faulting : a geomechanical delta model based on gravity sliding. Journal of Petroleum Geology. Vol. 2/3. 265-307.

Crans, W. and Mandl, G. (1980). On the theory of growth faulting. Part II(a): Genesis of the "Unit". Journal of Petroleum Geology. Vol.3/2. 209-236.

Crans, W. and Mandl, G. (1981). On the theory of growth faulting. Part II(b): Genesis of the "Unit". Journal of Petroleum Geology. Vol.3/3. 333-355.

Curtis, M.D., (1987). The northern Gulf of Mexico basin. Episodes, 10. 267-270.

Dalley, R.M., Gevers, E.C.A., Stampfli, G.M., Davies, D.J., Gastaldi, C.N., Ruijtenberg, P.A. & Vermeer, G.J.O., (1989). Dip and azimuth displays for 3D seismic interpretation. First Break. Vol. 7/3. 86-95.

Darros de Matos, R.M., (1993). Geomotry of the Hanging wall above a system of Listric normal faults-A numerical solution. AAPG Bull., 77 (11). 1839-1859.

Dooley, R.E. & Wampler, R.E. (1983). Potassium Argon relations in the base dikes of Georgia; The influence of excess 40 Ar on the geochronology of early Mesozoic igneous and tectonic events. US Geological survey, Prof. Paper. 1313-M. 24 p.

Duff, P. Hallam, A. and Walton, E.K. (1967). Cyclic sedimentation, developments in sedimentation, develpments in sedimentology. Elsevier. Amsterdam. 280 p.

Duval, B. & Cramez, C. (1990). Sequence stratigraphy workshop: A course note - Total (Eds.).

Enachescu, M.E., (1990a). 4D interpretation of 3D data. 52nd Mtg., Eur. Assn. Expl. Geoph., Technical program. 30-31.

Enachescu, M.E., (1992). Workstation resolution: Four-Dimensional interpretation of three-dimensional reflection data. CSEG Recorder. 4-10.

Enachescu, M.E., (1993). Amplitude interpretation of 3-D data. Geophysics.

Fairbridge, R.W., (1976). Convergence of evidences on climatic change and ice age. Ann. N.Y. Sci. Vol. 91/1. 542-579.

Fairbridge, R.W., (1983). Syn-diagenesis-anadiagenesis-epidiagenesis: Diagenesis in Sediments and sedimentary rocks. - In Chilingar, G.L.a.G.V. (Eds.) Developments in sedimentology: Elsevier scientific publishing company.17-113.

Favre, P. (1992): Géologie des massifs calcaires situés au front sud de l'unité de Ketama (Rif, Maroc). - PhD, Geneva.

Favre, P., (1995). Relations entre rifting et inversion de la marge transformante N africaine: Exemple du Rif Externe (Maroc). Geodynamica Acta, (under press).

Fisk, H.N. (1944). Geological investigations of the alluvial valley of the lower Mississippi river. US Army, War Dept. Corps of Engineers. 78 p.

Foote, R.Q. & Martin, R.G., (1981). Petroleum geology of the Gulf of Mexico maritime boudary assessment area. - In: Powers, R.B. (Eds.). Geologic framework, petroleum geology, petroleum resource estimates, mineral and geothermal resources, geologic hazards and deep water drillings technology in the maritime boundary region in the Gulf of Mexico: U.S. Geological Survey Open file report. 68-79.

Forrest, M.C., (1986). Deep water Gulf of Mexico exploration geology, hydrocarbons and economics. TGCAGS, 36. 45-47.

French, W.S., (1992). Where are we going ? The Leading edge, 11 (10). 6-9.

Galloway, W.E., (1986). Growth faults and fault-related structures of prograding terrigenous clastic continental margins. TGCAGS, 36. 121-128.

Gerhardstein, A.C. & Brown, A.R., (1984). Interactive interpretation of seismic data. Geophysics. 49/4 353-363.

Gordon, P.T. (1982). Devillier field, Chamber County, Texas - Effects of growth faults and deltaic sedimentation on hydrocarbon accumulation in a stratigraphic trap. In: Halbouty, M.T. (Eds). The deliberate search for subtle trap. AAPG Memoir 32. Tulsa. 115-130.

Gregory, A.R., (1977). Aspects of rock physics from laboratory and log data that are important to seismic interpretation. - In Payton, C.E. (Eds.). Seismic stratigraphy- Applications to Hydrocarbon Exploration. Tulsa. AAPG Memoir 26.15-46.

Haddad, G.A. & Vail P.R., (1992). Pliocene and quaternary sea-level change: linking eustasy (from

sequence stratigraphy) to the oxygen isotope record of global ice volume. Sequence stratigraphy of European basins. Abstract. Institut français du pétrole (Eds). Dijon, France. 450-451.

Halbouty, M.T., (1979). Salt domes. Gulf Region, United States and Mexico. Houston, Texas. Gulf publishing Company.

Halbouty, M.T., (1982). The time is now for all explorationists to purposefully search for the subtle trap. - In Halbouty, M.T. (Eds.), The deliberate search for subtle trap. Tulsa. AAPG Memoir 32. 1-10.

Hale, D., N., R.H. & Stefani, J., (1992). Imaging salt with turning seismic waves. Geophysics, 57 (11). 1453-1462.

Haq, B.U., Hardenbol, J. & Vail, P.R., (1988). Mesozoic and Cenozoic chronostratigraphy and cycles of sea-level change. - In Sea-Level changes. An integrated approach.: 71-108. SEPM Spec. Publ. Tulsa.

Harland, W.B., Armstrong, R.L., Cox, A.V., Craig, L.E., Smith, A.G. & Smith, D.G., (1989). A geologic time scale. Cambridge.

Harms, J.C. & Tackenberg, P., (1972). Seismic signatures of sedimentation models. Geophysics, 37. 45-58.

Hays, J.D., Imbrie, J. & Shackelton, N.J., (1976). Variations in the Earth's orbit: pacemaker of the ice ages. Science, 194. 1121-1132.

Heidlauf, D.T., Hsui, A.T. & Klein, G., (1986). Tectonic subsidence analysis of the illinois basin. J.Geology, 94 (6). 779-794.

Hilterman, F.J., (1982). Interpretative lessons from three-dimensional modeling. Geophysics. 47/5. 784-808.

Hoetz, H.L.J.G. & Watters, D.G., (1992). Seismic horizon attribute mapping for the Annerveen Gasfield, The Nederlands. First Break, 10 (2). 41-51.

Humphris, C.C., Jr., (1978). Salt movement on continental slope, northern Gulf of Mexico. - In Bouma, A.H. Moore, G.T. & Coleman, J.M. (Eds.). Framework, facies and oil-trapping characteristics of the upper continental margin. Tulsa. AAPG Studies in Geology. 69-86.

Humphris, C.C.Jr., (1979). Salt movement in continental slope, Northern Gulf of Mexico. AAPG Bull., 63. 782-798.

Huntoon, P.W., (1982). The Meander anticline, Canyonlands, Utah, an unloading structure resulting from horizontal gliding on salt. Geological Society of America Bull., 93. 941-950.

Jackson, M.P.A., (1990). Salt diapirs of the Great Kavir, Central Iran. Geol. Soc. of America, Memoir 177.

Jackson, M.P.A. & Seni, S.J., (1983). Geometry and evolution of salt structures in a marginal rift basin in the Gulf of Mexico, east Texas. Geology. 11. 131-135.

Jackson, M.P.A., Talbot, C.J. & Cornelius, R.R., (1988). Centrifuge modeling of the effects of aggradation and progradation on syndepositionnal salt structures. University of Austin, Texas. Bureau of economic geology.

Jackson, M.P.A. & Vendeville, B.C., (1994). Regional extension as a geologic trigger for diapirism. Bull. Geological Society of America, 106. 57-73.

Jenyon, M.K., (1986). Salt tectonics. Elsevier. New York. 191 p.

Jux, U., (1961). The palynologic age of diapiric and bedded salt in the Gulf Coastal Province. Louisiana Geological Survey Bull., 8. 1-46.

Kern, G., (1992). Interprétation des structures salifères: difficultés et progrès (cas pétroliers de Hollande). Mém. Soc. géol. France. Journées de géophysique appliquée, 161. 103-118.

Keskes, N. & Camy-Peyret, J., (1992). Les techniqus d'analyse d'images au service de l'interpretation structurale des données sismiques 3D et 2D. Mem. Soc. Géol. France. Journées de géophysique appliquée. 161. 133-140.

Kirkland, D.W. & Gerhard, J.E., (1971). Jurassic salt, central Gulf of Mexico, and its temporal relation to circum-Gulf evaporites. AAPG Bull, 55. 680-686.

Kohonen, T., 1984. Self-Organization and associative memory. Berlin. Springer-Verlag.

Kolb, C.R. & Van Lopik, J.R. (1958). Geology of the Mississippi river deltaic plain. Report No. 3-4. US Corps Engrs. Waterways Expt. Sta. Tech. Reports.

Kupfer, D.H. & Fails, T.G., (1989). Internal kinematics of salt diapirs. Discussion. AAPG Bull., 73. 939-945.

Leeder, M. (1994): Fluvial systems and sequence stratigraphy. - In High resolution sequence stratigraphy: innovations and applications. Abstract. 19. Liverpool.

Leeder, M.R., (1985). Sedimentology : Process and product. London: ALLEN, G. & UNWIN. 344 p.

Legget, M., Sandham, W.A. & Durrani, T.S. (1994): 3D seismic Horizon tracking using artificial Neural network. - In 56th meeting of the European association of exploration geophysicists. Abstract B049. Vienna, Austria.

Lehner, P., (1969). Salt tectonics and Pleistocene Stratigraphy on Continental Slope of Northern Gulf of Mexico. AAPG Vol. 53/12, 2431-2479.

Lerche, J. & O'Brien, J.J., (1987). Dynamical geology of salt and related structures. Academic Press of the US.

Lindseth, R.O., (1979). Synthetic sonic logs-a process for stratigraphic interpretation. Geophysics, 44. 3-26.

Lowrie, A., (1986). Model for fine-scale movements associated with climate and sea level changes along Louisiana shelfbreak growth faults. TGCAGS, XXXVI 497-509.

Mandl, G. (1987). Short notes: Discontinuous fault zones. Journal of Structural geology. Vol. 9/1. 105-110.

Mandl, G. (1988). Extensional faulting. In: H.J. Zwart (Eds.). Mechanics of tectonic faulting. Models and basic concepts. Elsevier - Amsterdam. Development in Structural Geology 1. 95-133.

Mann, C.J. & Thomas, W.A., (1964). Cotton Valley goup nomenclature, Louisiana and Arkansas. TGCAGS. 31. 143-152.

Marchant, R.H. (1993): The Underground of the Western alps. - PhD, Lausanne. Mémoires de Géologie Vol. 15.

Martin, R.G., (1978). Northern and eastern Gulf of Mexico continental margin: stratigraphy and structural framework. - In Bouma, A.H. Moore, G.T. & Coleman, J.M. (Eds.), Framework, facies and oil-trapping characteristics of the uppercontinental margin: 21-42. AAPG Studies in Geology.

Martin, R.G. & Bouma, A.H., (1978). Physiography of the Gulf of Mexico. In: Framework, facies and oil-trapping characteristics of the upper continental margin. AAPG Studies in Geology. Vol. 7. Tulsa. 3-19.

Martin, R.G. & Bouma, A.H., (1982). Active diapirism and slope steepening, northern Gulf of Mexico continental slope. Marine geotechnology, 5 (1): 63-91.

Mastoris, S., 1989. 3D seismic interpretation techniques define shallow gas sand reservoirs. Oil and Gas Journal, 87. 69-73.

McGoockey, D.P., (1975). Gulf coast Cenozoic sediments and structure; an excellent example of extra-continental sedimentation. TGCAGS. 25. 104-120.

McGowen, M.K. & Harris, D.W., (1984). Cotton Valley (Upper Jurassic) and Hosston (Lower Cretaceous) depositional systems and their influences on salt tectonics in the East Texas basin. - In Ventress, P.S.a.o. (Eds.), The Jurassic of the Gulf Rim: 213-249. GCSSEPaleont. and mineral. Foundation.

Merriam, D.F. (1964). Symposium on cyclic sedimentation. Kansas geological survey Bull. Vol. 169/1-2. 636p.

Merriam, D.F. & Allen, B.M., (1991). Color unlocks perspective for 3-D stratigraphic models. Geotimes. 19-21.

Milankovitch, M., 1941. Kanon der Erdbestrahlung und seine Anwendung auf das Eiszeitenproblem. Acad. Roy. Serbe (Eds). Vol. 133. 633 p.

Mitchum, R.M., 1977. Seismic stratigraphy and global changes of sea level, Part 11: Glossary of terms used in Seismic stratigraphy. - In Payton, C.E. (Eds.). Seismic stratigraphy-application to hydrocarbon exploration. Tulsa: AAPG Memoir 26. 205-212.

Mougenot, D. (1994): Why use seismic in 3 dimensions? Report - CGG/Geotop, Massy, France.

NAGRA (1994). Untersuchungen in der Nordscchwiez für den Entsorgungsnachweis. Report.

Neff, D.B., (1993). Amplitude map analysis usinf forward modeling in sandstone and carbonate reservoirs. Geophysics, 58 (10). 1428-1441.

Neidell, N.S., (1985.) Seismic visibility of stratigraphic objectives. Society of Petroleum Engineers, Paper 14175.

Nestvold, E.O., (1992). 3-D seismic: Is the promise fulfilled? The leading edge, 11 (6). 12-19.

Nur, A.M., (1989). Four-dimensional seismology and (true) direct detection of hydrocarbons:the petrophysical basis. The leading edge, 9. 30-36.

Ocamb, R.D., (1961). Growth faults in south Louisiana. Transactions, Gulf coast association of geological societies, 11. 139-173.

Odin, G.-S. & Odin, C., (1990). Echelle numérique des temps géologiques, mise à jour 1990. Géochronique, 35. 12-23.

Pattison, S.A.J. & Walker, R.G., (1992). Deposition and interpretation of long, narrow sandbodies underlaine by a basinwide erosion surface: Cardium formation, Cretaceous western interior seaway, Alberta, Canada. J. Sed. Petr., 62 (2): 292-309.

Peterson, F.M. & Reynish, W.C., (1989). Three-dimensional seismic exploration - A cost effective approach. Geophysics. 54/7 815-823.

Peterson, R.A., Filipone, W.R. & Coker, F.B., (1955). The synthesis of seismograms from well log data. Geophysics, 26. 138.

Pillevuit, A., (1993). Les blocs exotiques du Sultanat d'Oman. Mémoire de Géologie de Lausanne, Vol. 17. 249 p.

Pindell, J.L., (1985). Alleghenian reconstruction and subsequent evolution of the Gulf of Mexico, Bahamas and Proto-Caribbean. Tectonics. 4. 1-39.

Posamentier, H.W., Jervey, M.T. & Vail, P.R., (1988). Eustatic controls on clastic deposition I - Conceptual Framework. - In: C.K.W.e.a. (Eds.). Sea-level changes: An integrated approach. Tulsa. SEPM Spec. Publ. 109-124.

Posamentier, H.W. & Vail, P.R., (1988). Eustatic controls on clastic deposition. II-sequence and systems tracts models. - In: C.K.W.e.a. (Eds.). Sea-level changes: An integrated approach. Tulsa. SEPM Spec. Publ.125-154.

Posamentier, H.W. & Weimer, P., (1993). Siliclastic sequence stratigraphy and Petroleum Geology-Where to from here ? AAPG Bull. Vol. 77/5. 731-742.

Posamentier, H.W., (1993). Variability of the sequence stratigraphic model: effects of local basin factors. Sedimentary geology. Vol. 86. 91-109.

Prosser, S., (1993). Rift related depositional squences and their seismic expression. In: Williams, G.D. & Dobb, A. (Eds.). Tectonics and seismic stratigraphy. London: Special Publication of the Geological Society of London. 35-66.

Quarles, M.J., (1953). Salt ridge hypothesis on the origin of Texas Gulf fault type of faulting. AAPG Bull., 37. 489-508.

Ramberg, H., (1981). Gravity, deformation of the earth's crust. Academic Press, London. 452 p.

Reymond, B. & Stampfli, G.M. (1992a): 3D seismic analysis of sedimentary facies and cyclo-stratigraphy from early Miocene to Present in the offshore West-Cameron region (Louisiana, Gulf of Mexico). - In 29th international geological congress,Vol. 2. 299. Kyoto, Japan.

Reymond, B. & Stampfli, G.M. (1992b): 3D seismic stratigraphic analysis of middle Miocene to present day sediments in the offshore West-Cameron region (Gulf of Mexico). - In: CNRS-IFP, Dijon meeting. Dijon. 465.

Reymond, B. & Stampfli, G.M. (1993): Interaction between 3D sesmic interpretation and sequence stratigraphy analysis on logs. - In: EAEG 55th annual meeting, Stavanger.

Reymond, B.A. & Stampfli, G.M., (1994a). Sequence stratigraphic interpretation of 3D seismic data offshore Louisiana-a case study. First Break. Vol. 13/8 453-462.

Reymond, B.A. & Stampfli, G.M. (1994b): Plio-Pleistocene cyclic sedimentation in the central northern Gulf of Mexico through 3D Seismic stratigraphy. In: High resolution sequence stratigraphy: innovations and applications. Liverpool.

Reymond, B.A. & Stampfli, G.M. (1994c): Detritic systems tracts horizontal morphology from 3D Sequence Stratigraphy. - In EAEG/EAPG 56th annual meeting, Vienna.

Reymond, B.A. & Stampfli, G.M., (1994d). La sismique tridimensionnelle: outil géologique pour l'analyse tectonique, géomorphologique et sédimentologique. Bull. Soc. Vaudoise Sciences Naturelles, 83 (1). 17-36.

Reymond, B.A. & Stampfli, G.M., (1995). 3D Sequence stratigraphy and subtle stratigraphic traps identification (West-Cameron region, offshore Louisiana, Gulf of Mexico). Marine and petroleum geology (under press).

Reynolds, A.D. (1994): Sequence stratigraphy and the dimensions of paralic sandstones bodies. - In High resolution sequence stratigraphy: innovations and applications. 69-72. Liverpool: University of Liverpool.

Russel, B.H., (1992). Using color in seismic displays. The Leading Edge, 11 (9). 13-18.

Ryan, W.B.F., (1976). Quantitative evaluation of the depth of the western Mediterranean before, during and after the Late Miocene salinity crisis. Sedimentology, 23. 791-813.

Salvador, A., (1987). Late Triasic-Jurassic paleogeography and origin of Gulf of Mexico basin. AAPG Bull. Vol. 71/4. 419-451.

Sassen, R. & Moore, C.H., (1988). Framework of hydrocarbon generation and destruction in the eastern Smackover trend. AAPG Bull, 72. 649-663.

Savit, C.H. & Wu, C., (1982). Geophysical characterisation of Lithology - Application to subtle traps. - In Halbouty, M.T. (Eds.). The deliberate search for subtle trap.Tulsa. AAPG Memoir 32. 11-30.

Sawyer, D.S., Toksöz, M.N., Sclater, J.G. & Swift, B.A., (1982). Thermal evolution of the Baltimor Canyon trough and Georges Bank basin. - In Watkins, J.S. & Drake, C.L. (Eds.). Studies in continental margin geology. AAPG Memoir 34. 743-764.

Sawyer, D.S., (1985). Total tectonic subsidence, a parameter for distinguishing crust type at the U.S. Atlantic continental margin. Journal of Geophysical Research. Vol. 90. 7751-7769.

Saxena, R.S., (1990). Model for reworked deltaic sands-exemples from south Lake Arthur, Bayou Gentily and Bayou Leary Field. Gulf Coast Assoc. Geol. Socs., Trans., XL 757-768.

Schaffer, B.L., (1990). The nature and significance of condensed sections in Gulf Coast late Neogene sequence stratigraphy. Gulf Coast Assoc. Geol. Socs., Trans, XL 767-776.

Schaub, F.J., Buffler, R.T. & Parsons, J.G., (1984). Seismic stratigraphic framework of the deep central Gulf of Mexicobasin. University of Texs Institute for Geophysics Contribution, 56 1-22.

Schlager, W. (1994): Reefs and carbonate platforms in sequence stratigraphy. - In High reolution sequence stratigraphy: innovations and applications. 143-149. Liverpool.

Schalger, W. (1993). Accommodation and supply- a dual control on stratigraphic sequences. Sedimentary Geology. Vol. 86. 111-136.

Schalger, W. & Buffler, R.T., (1984). Deep sea drilling project, leg 77. GSA Bull. Vol. 95. 226-236.

Schluger, P.R., (1979). (Eds). Diagenesis as it affects clastic reservoirs. Spec. Publ. Soc. econ. Paleont. Mineral. Vol. 26. 443 p.

Schwarzacher, W., (1975). Sedimentation models and quantitative stratigraphy. Developments in sedimentology 19. Amsterdam. Elsevier.

Sclater, J.G. & Christie, P.A.F., (1980). Continental streching: an explanation of the post-mid-Cretaceous subsidence of the Central North Sea basin. 87 (B7). 3711-3739.

Scott, K.R., Hayes, W.E. & Fietz, R.P., (1961). Geology of the Eagle Mills formation. TGCAGS. 11. 1-14.

Seglund, J.A., (1974). Collpase-fault systems of Louisiana Gulf Coast. AAPG Bull., 58 (12). 2389-2397.

Selby, E.G., (1978). Three-Dimentional data collection and processing. APEA Journal, 18. 116-123.

Sheriff, R.E., (1976). Inferring stratigraphy from seismic data. AAPG Bull., 60. 528-542.

Sloss, L.L., (1963). Sequences in the cratonic interior of North America. Bull. of Geological Society of America, 74. 93-113.

Sloss, L.L., (1972). Synchrony of Phanerozoic sedimentary-tectonic events of the north-American craton and the Russian plateform. 24th International Geological Congress.

Sonneland, L. (1994): 3D model based Bayesian classification. - In 56th meeting of the European association of exploration geophysicists. P137. Vienna, Austria.

Sonneland, L., Barkved, O. & Hagenes, O., (1991). Construction and interpretation of seismic classifier maps. Geco-Prakla Report, Stavanger.

Sonneland, L., Barkved, O., Olsen, M. & Snyder, G. (1990). Application of seismic wavefield attributes in reservoir characterisation. Geco-Prakla Report, Stavanger.

Soreghan, G.S. & Dickinson, W.R. (1994). Variable stratigraphic expression of high-frequency eustatic cycles: implications for interpretation of accommodation. - In: Johnson, S.D. (Eds.). High resolution sequence stratigraphy: innovations and applications. Liverpool. Abstract. 164-165.

Spindler, W.M., (1977). Structure and Stratigraphy of a small Plio-Pleistocene Depocenter, Louisiana Continental Shelf. TGCAGS. 27. 180-196.

Stampfli, G.M. & Höcker, C.W.F., 1989. Messinian palaeorelief from a 3-D seismic survey in the Tarraco concession area (Spanish Mediterranean Sea). Geologie in Mijnbow. 68. 201-210.

Strahan, C.V. (1986): West Cameron block 294 Field, offshore Louisiana. Report: Amoco production company.

Suter, J.R. & Berryhill, H.L., (1985). Late quaternary shelf-margin deltas. Northwest Gulf of Mexico. AAPG Bull., 69. 77-91.

Suter, J.R., Berryhill, H.L. & Penland, S., (1987). Late quaternary sea-level fluctuations and depositional sequences, southwest Louisiana continental shelf. - In Nummedal, D. (Eds.), Sea-level fluctuation and coastal evolution. Soc. of Economic Paleonto and Mineralo. 198-219.

Swift, D.J.P., Oertel, G.F., Tillman, R.W. & Thorne, J.A., (1991). Shelf sand and sandstones bodies. Geometry facies and sequence stratigraphy. Oxford. Blackwell Scientific Publications.

Talbot, C.J. & Jackson, M.P.A., (1989). Internal kinematics of salt diapirs. Reply. AAPG Bull., 73. 946-950.

Taner, M.T., Koeler, F. & Sheriff, R.E., (1979). Complex trace analysis. Geophysics, 44. 1041-1063.

Taner, M.T. & Sheriff, R.E., (1977). Application of Amplitude, Frequency, and other attributes to stratigraphic and hydrocarbon determination. - In Payton, C.E. (Eds.), Seismic Stratigraphy-applications to hydrocarbon exploration. Tulsa. AAPG Memoir 26. 301-328.

Tegland, E.R., (1977). 3-D seismic techniques boost field development. Oil and gas journal, 75 (37). 79-82.

TGS (1990): Gulf of Mexico chronostratigraphic correlation chart. TGS, offshore geophysical company. Houston, Texas.

Vail, P.R., Mitchum, R.M. & Thompson, S., (1977). Seismic stratigraphy and global changes of sea level, seismic stratigraphy- part 3: Relative changes of sea level from coastal onlap. Tulsa. AAPG Memoir 26.

Vail, P.R. & Wornardt, W.J., (1991). An integrated approach to exploration and development in the 90s : well log-seismic sequence stratigraphy analysis. TGCAGS, 41. 630-650.

Vail, P.R. & Wornardt, W.W., (1990). Well log-seismic sequence stratigraphy : an integrated tool for the 90's. GCSSEPM Foundation Eleventh Annual Research Conference Program and Abstracts. 379-388.

Van Wagoner, J., Mitchum, R.M.J., Posamentier, H.W. & Vail, P.R., (1987). Seismic stratigraphy

interpretation using sequence stratigraphy, Part 2: Key definitions of sequence stratigraphy. - In Bally, A.W. (Eds.). Atlas of seismic stratigraphy. AAPG Studies in Geology, No 27. 11-14.

Vogler, D.M. & Robinson, B.A., (1987). Exploration of deep Geopressured gas : Corsair trend, Offshore Texas. AAPG Bull., 73. 777-787.

Walton, G.G., (1972). Three-dimentional seismic method. Geophysics, 37. 417-430.

Warrick, R.A., (1993). Climate and sea level: a synthesis. - In Warrick, R.A. (Eds.). Climate and sea level change: observations, projections and implications. Cambridge. Cambridge University press. 3-21.

Warrick, R.A., Barrow, E.M. & Wigley, M.L., (1993). Climate and sea level change: observations, projections and implications. Cambridge: Cambridge University Press.

Waters, K.H., (1986). Reflection seismology. A tool for energy resource exploration (Third edition). New York. John Willey &sons Inc. (Eds.) 538 p.

Watkins, J.S., Ladd, J.W., Buffler, R.T., Shaub, F., Houston, M.H. & Worzel, J.L., (1978). Occurence and evolution of salt in deep Gulf of Mexico. - In Bouma, A.H. Moore, G.T. & Coleman, J.M. (Eds.), Framework, facies and oil trapping characteristics of the upper continental margin. Tulsa. AAPG Studies in Geology. Vol. 7. 43-65.

Wehr, F.L. & Brasher, L. (1994): Impact of sequence based correlation style on reservoir model behaviour, lower Brent group, North Cormorant field, UK North sea. - In High resolution sequence stratigraphy: innovations and applications. Liverpool. Abstract 55-56.

Wernicke, B., (1984). Uniform-sense normal simple shear of the continental lithosphere. Canadian journal of earth sciences, 22. 108-125.

Wernli, R., (1987). Micropaléontologie du Néogène post-nappes du Maroc septentrional et description systématique des foraminifères planctoniques. Notes et mémoires du service géologifque du Maroc, 331 p.

Wheeler, H.E., (1963). Post-Sauk and pre-Absaroka Paleozoic stratigraphic patterns in North America. AAPG Bull. Vol. 47. 1497-1526.

White, N.J., Jackson, J.A. and McKenzie, D.P. (1986). The relationship between the geometry of normal faults and that of the sedimentary layers in their hanging walls. Journal of Structural geology. Vol. 8/8. 897-909.

Widess, M.B., (1973). How thin is a thin bed ? Geophysics. 38. 1176-1180.

Wilhelm, O. & Ewing, M., 1972. Geology and History of the Gulf of Mexico. Bull. geol. Soc. Am., 83. 575-600.

Winker, C.D., (1982). Cenozoic shelf margins, northwestern Gulf of Mexico. TGCAGS, 32. 427-448.

Winker, C.D. & Buffler, R.T., (1988). Palaeogeographic evolution of early deep-water Gulf of Mexico and margins, Jurassic to Middle Cretaceous. AAPG Bull., 72. 318-346.

Winker, C.D. & Edwards, M.B., 1983. Unstable progradational clastic shelf margins. - In: Stanley, D.J.a.M., G.T. (Eds.). The shelfbreak : a critical interface on continental margins. Tulsa. SEPM, Special Publication No. 33.

Witka, T. & Krummel, H. (1994): High resolution 3D seismic survey over a waste site. Field layout and data acquisition. - In: EAEG/EAPG 56th annual meeting. Vienna.

Woodburry, H.O. & Murray, I.B., (1973). Pliocene and Pleistocene Depocenters. Outer Continental Shelf, Louisiana and Texas. AAPG Bull., 57. 2428-2439.

Woodburry, H.O., Murray, I.B. & Osborne, R.E., (1980). Diapirs and their relation to hydrocarbon accumulation. - In Miall, A.D. (Eds.). Facts and principles of world petroleum occurence. Canadian Society of Petroleum Geologists. 119-142.

Wornardt, W.W. & Vail, P.R., (1991). Revision of the Plio-Pleistocene cycles and their application to sequence stratigraphy and shelf and slope sediments in the Gulf of Mexico. TGCAGS. 41. 719-744.

Worral, D.M. & Snelson, S., (1989). Evolution of the northern Gulf of Mexico, with emphasis on Cenozoic growth faulting and the role of salt. - In: Bally, A.W. and A.R. Palmer. (Eds.). The Geology of North America. An overview. GSA - Washington. 97-138.

Wright, L.D., (1977). Sediment transport and deposition at river mouths: a synthesis. Bull. Geol. Soc. Am. Vol. 88. 857-68.

Wu, S., Bally, A.W. & Cramez, C., (1990a). Allochtonous salt, structure and stratigraphy of the north-eastern Gulf of Mexico. Marine and Petroleum Geology. Part II : Structure. 7 (4): 334-370.

Wu, S., Vail, P.R. & Cramez, C., (1990b). Allochtonous salt, stucture and stratigraphy of the north-eastern Gulf of Mexico. Marine and Petroleum Geology Part I : Stratigraphy. 7 (4): 318-333.

Wyllie, M.R.J., Gregory, A.R. and Gardner, L.W., (1956). Elastic wave velocitites in heterogeneous and porous media. Geophysics. Vol. 21/1. 41-70.

Xiao, H. & Suppe, J., (1992). Origin of rollover. AAPG Bull., 76 (4). 509-529.

Xiao, H.-B. (1990). Kinematics and Mechanics of Normal faulting and associated folding, with apllications to the Gulf of Mexico. - PhD, Princeton University.

ANNEXE 1

Interpretation GRID rotation and inversion procedure in 7 steps.

Seismic data loading on interpretation systems is quite complex and errors in orientation may occur. A 3D survey is defined by its number of inlines, crosslines (with a regular interval), point of origin (intersection between inline or row 1 and crossline or column 1) and orientation (angle of rotation). Three directions are possible for the orientation of the Inlines in a 3D grid

- Inlines can be shot in the north/south direction
- They can be shot in the east/west direction
- or at some angle from the 0 North direction (see Fig. A1, a)

The CHARISMA^{TM} software sees the Inlines as loaded either in the north/south or east/west direction and the "1,1 Origin" point can be assigned to one of the four corners of the grid, providing 8 possibilities of orientation (4 with vertical Inlines and 4 with horizontal inlines). On top of that is added the eventual rotation angle when the true orientation of acquisition was not north/south or east/west (see Data Loading Manual for more references). Being aware of that, it is no problem to change the orientation of the 3D survey at any time by reloading it from the original tapes with the desired orientation.It is not so obvious with interpretation grids. We will briefly expose the procedure followed to operate the mirror inversion and rotation needed in our case, to save and reload interpretation grids (see Fig. A1, b). The two successive operations of mirror inversion and 90° rotation is equivalent to a permutation of the X and Y and Z conservation co-ordinates in a given XYZ matrix.

Interpretation grids are in Grid format on CHARISMA^{TM} (File.GRID) and can transformed in standard XYZ or ASCII format with the GRIDXYZ utility provided in the software. This facilities allows direct importing or exporting of CHARISMA grids to other software. The transformation of a grid through this process is realised in reference to the true (X;Y) origin co-ordinate in one of the international system (UTM). In our case and as depicted on figure A1, b, the origin location will be shifted from its original position after inversion of the matrix. That it is the reason why it is needed to reload the seismic data with an artificial (0;0 geographical co-ordinate) and to change the grid header of each interpreted horizon prior to operating the matrix inversion, in order to fit the inverted interpretation on the reloaded seismic data.Thus, the successive steps to switch a grid orientation are as follows :

0. Reload the seismic data with orientation and rotation angle to zero.
1. Change the grid header file (chgrhead utility). Put the orientation and rotation angle to zero.
2. Transform file format (from file.GRID to newfile.XYZ, gridxyz utility)
3. Invert XYZ matrix with the following UNIX function :

```
% awk '{printf "%s\t-%s\t...%s\n",substr($2,2,length($2-1),
  $1,$3,$4,$5,$6,$7 }' newfile.XYZ >invertfile.XYZ  (with n=7)
```

Assigning the function to a label (fb), it can be reduced to :

```
% awk -f fb newfile.XYZ >invertfile.XYZ
```

4. The output grid (newgrid.GRID) must already exist to be able to copy the new file =>
   - create a new horizon with Idbmaint utility
   - apply Idbback utility to generate newgrid.GRID file
5. Transform "invertfile.XYZ" obtained under 3, into "invertfile.GRID" format with xyzgrid utility).
6. copy invertfile.GRID to the newgrid.GRID generated under 4.
7. Have a drink, because you just saved at least one week of interpretation !

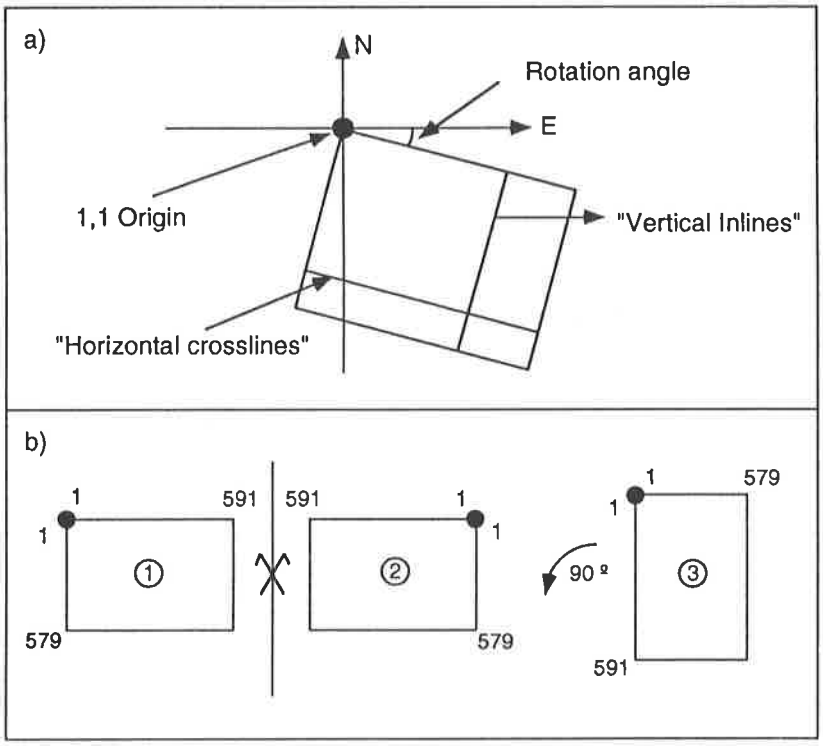

A-1-1: ***a.*** *Co-ordinate system for positioning a 3D survey in space.* ***b.*** *Mirror symmetry and rotation applied to all interpretation grids due to an orientation error during the loading of the 3D survey.*

ANNEXE 2

Biostratigraphic horizons (Neogene-Pleistocene) in the Gulf of Mexico and marine plaeoenvironments offshore Louisiana for the productive interval (11.6 to 21.0 Ma).

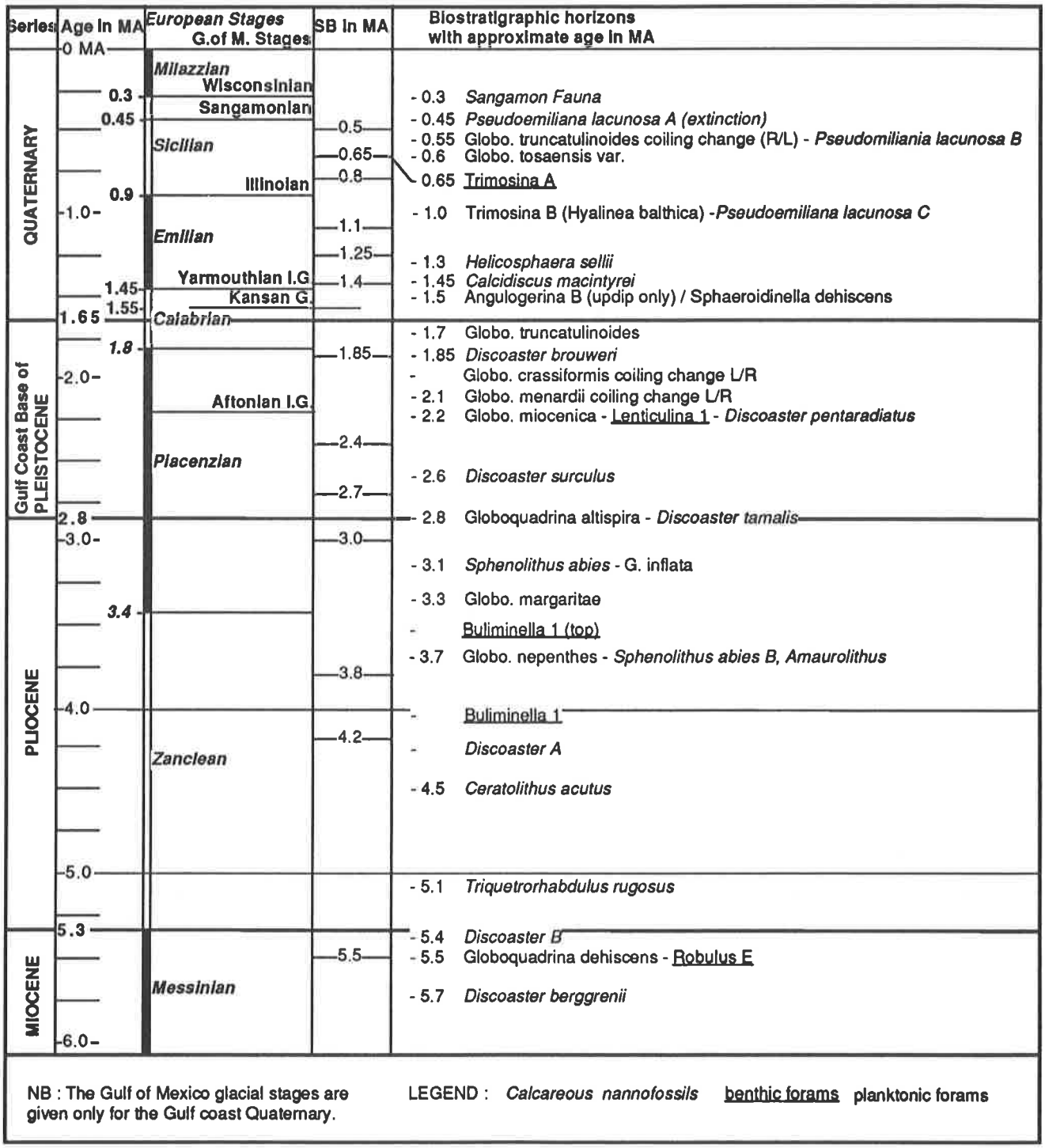

A-2-1: Synthetic table for the Plio-Pleistocene (with European and Gulf of Mexico stages) of all major biostratigraphic horizons (Calcareous nannofossils, benthic forams and planktonic forams) used for correlation and paleoenvironment definition in the Gulf of Mexico (Integration of a long list of published and unpublished data).

Series	Age in MA	European Stages	SB in MA	Biostratigraphic horizons with approximate age in MA
PLIOCENE	3.4 -	Placenzian		See on Plio-Pleistocene chart
	5.0	Zanclean		- 5.4 *Discoaster B* - 5.5 Globoquadrina dehiscens - Robulus E
	5.3		5.5	- 5.7 *Discoaster berggrenii*
MIOCENE Late	6.5 -	Messinian	6.3	- 6.2 Bigenerina A - 6.5 *Discoaster neohamatus-Discoaster calcaris* - 6.7 Cristellaria K
		Tortonian	8.2 8.8	- 6.9 Globo. acostaensis coiling change R/L - 7.3 *Discoaster prepentaradiatus*- Spaeroidinellopsis seminullina - 7.8 Cyclammina 3 - 8.2 *Discoaster bollii* - Discorbis 12 - 8.8 *Catinasteer spp.* - Textularia L - 9.0 *Discoaster Hamatus*
	10.0		10.5	- 10.5 Cibicides carstensi - Bigenerina 2 - Globorotalia mayeri
	11.0			- 10.6 *Coccolithus miopelagicus* - 10.8 Uvigerina 3
Middle		Serravallan	12.5	- 11.5 Textullaria W - Globo. foshi robusta *Discoaster berggrenii* - 11.7 *Discoaster deflandrei*
	14.5 -		13.8	- 13.4 Bigenerina humblei - Globo. foshi foshi
	15.0	Langhian		- 14.3 Cristellaria I - Globo. foshi barisanensis - 14.4 *Sphenolithus heteromorphus*
	16.0		15.5	- 15.5 Cibicides opima - 15.8 Praeorbulina glomerosa
Early		Burdigalian	16.5 17.5	- 15.9 Amphistegina B -*Helicosphaera ampliaperta* - 16.3 Robulus L - 16.7 Robulus mayeri - 17.1 Gyroidina 9 - 17.4 Cristellaria A *Sphenolithus belemnos* - 18.0 Marginulina A
	20.0			- 20.5 Siphonina davisi
		Aquitanian	21.0 22.0	- 21.5 Planulina palmerae
				- 22.7 *Cyclicargolithus abisectus* - 23.0 Lenticulina hanseni
	23.5			- 23.5 Cristellaria R - Globo. kugleri
	24.0	Chattian		- 23.8 Robulus A - Dictyococcites bisectus - Globo. ciperoensis

LEGEND : *Calcareous nannofossils* benthic forams planktonic forams

A-2-2: Neogene synthetic table (European stages) of all major biostratigraphic horizons (Calcareous nannofossils, benthic forams and planktonic forams) used for correlation and paleoenvironment definition in the Gulf of Mexico (Integration of a long list of published and unpublished data).

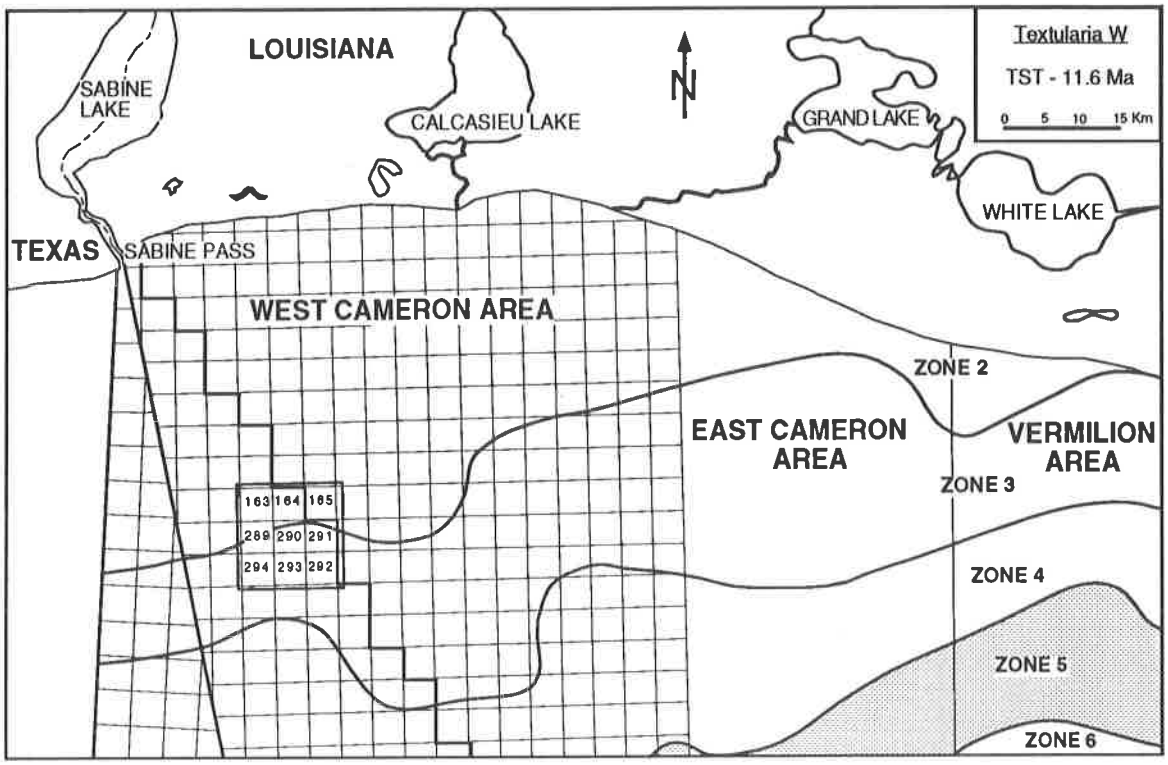

A-2-3: Textularia W (Tst, 11.6 Ma) marine environments map offshore Louisiana reconstructed from the OCS MMS Report (wells and seismic sections, 1987) and unpublished data. See fig. 2-4 for marine environments nomenclature.

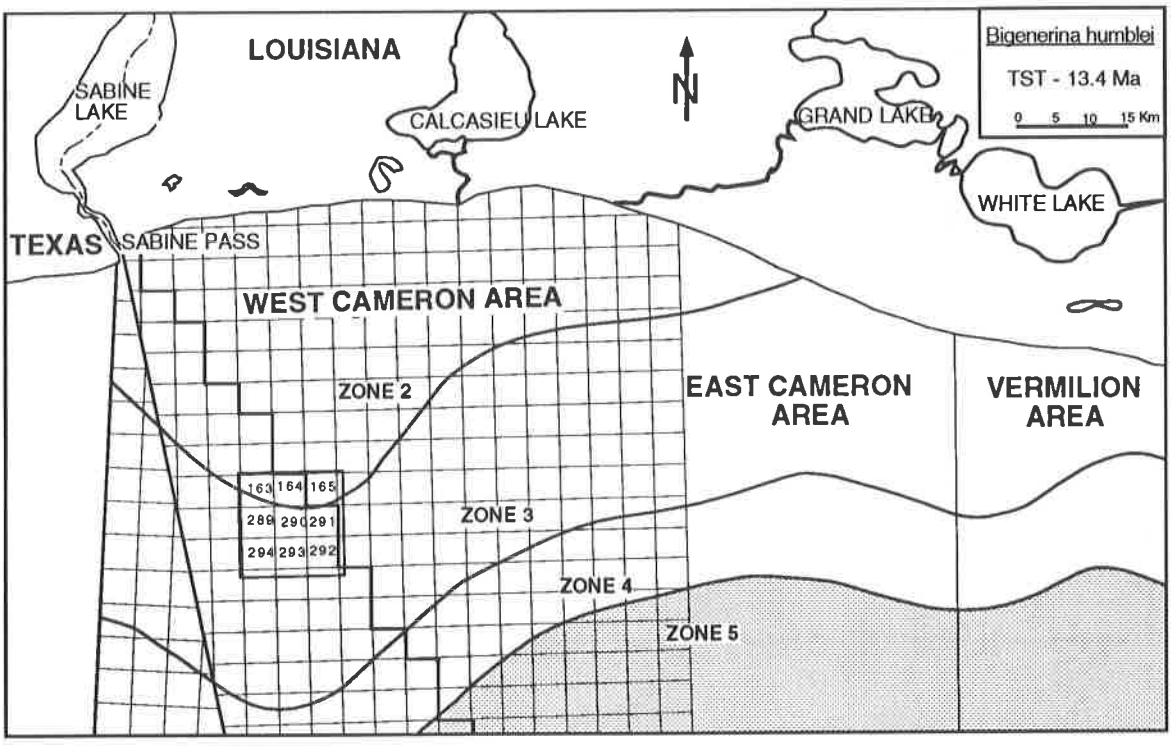

A-2-4: Bigenerina H. (Tst, 13.4 Ma) marine environments map offshore Louisiana reconstructed from the OCS / MMS Report (wells and seismic sections, 1987) and unpublished data. See fig. 2-4 for marine environments nomenclature.

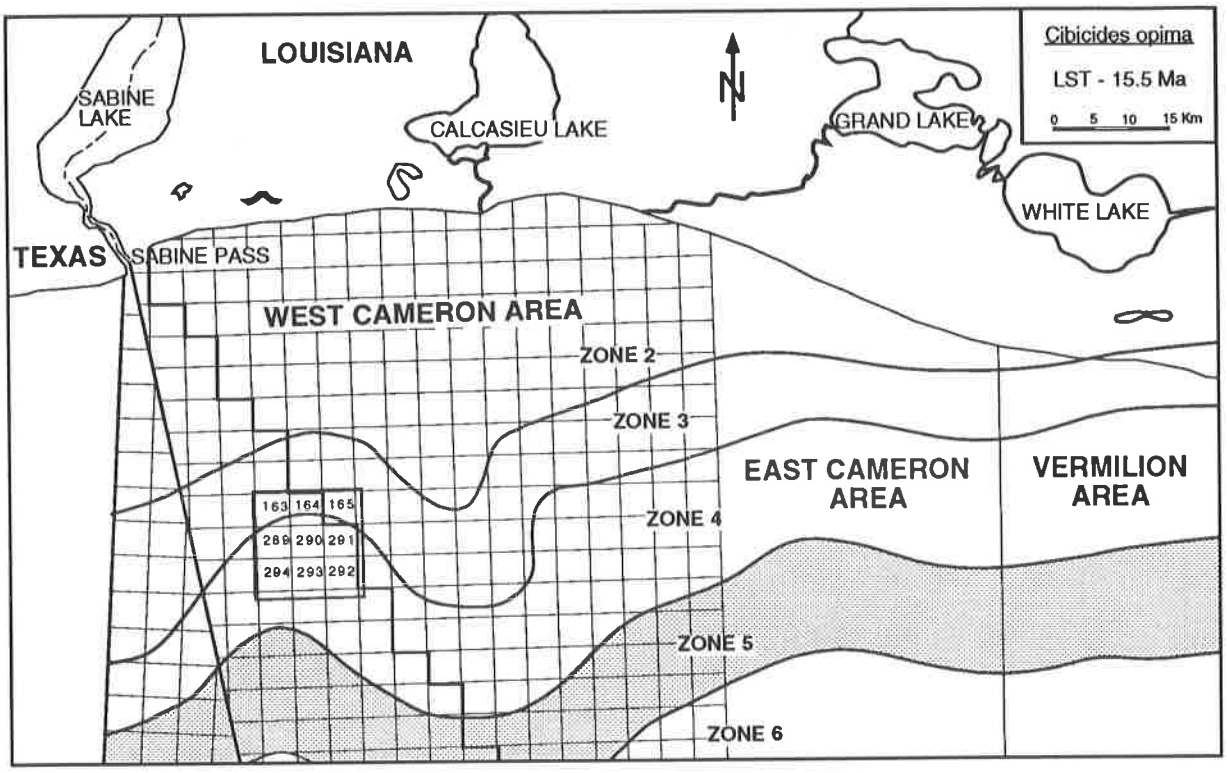

A-2-5: Cibicides op. (Lst, 15.5 Ma) marine environments map offshore Louisiana reconstructed from the OCS MMS Report (wells and seismic sections, 1987) and unpublished data. See fig. 2-4 for marine environments nomenclature.

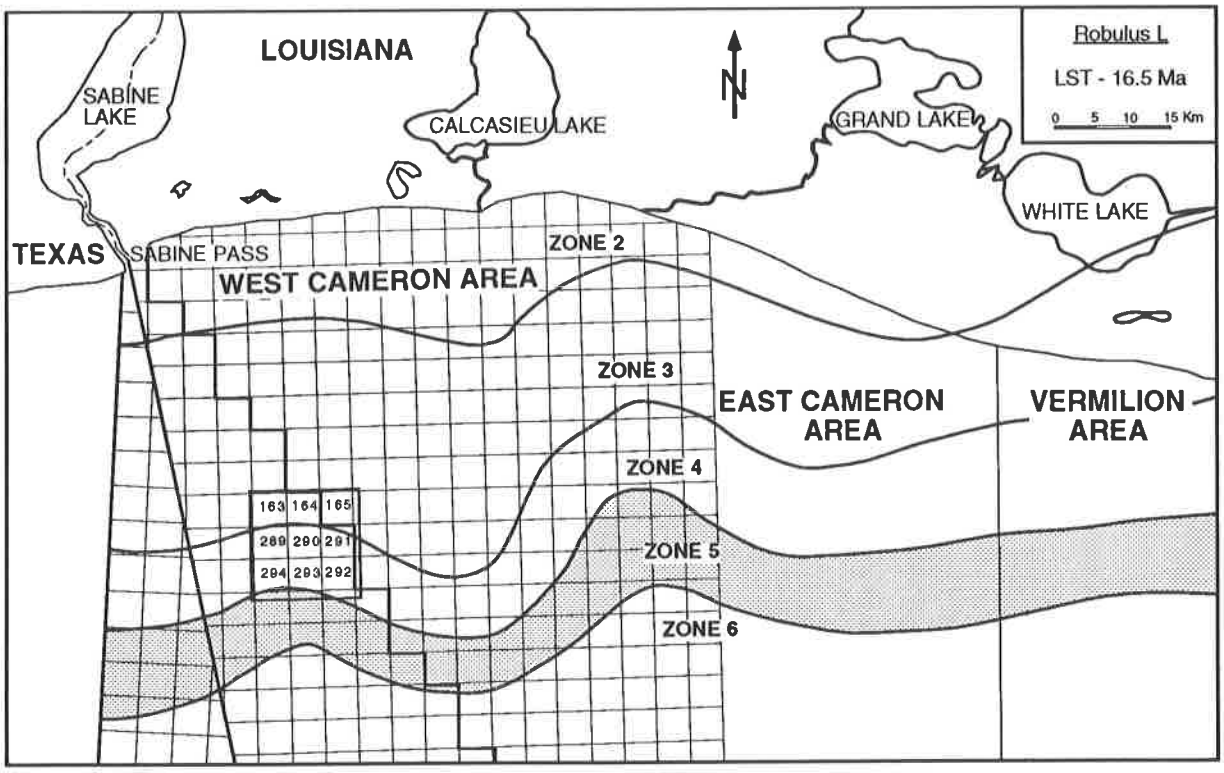

A-2-6: Robulus L. (Lst, 16.5 Ma) marine environments map offshore Louisiana reconstructed from the OCS MMS Report (wells and seismic sections, 1987) and unpublished data. See fig. 2-4 for marine environments nomenclature.

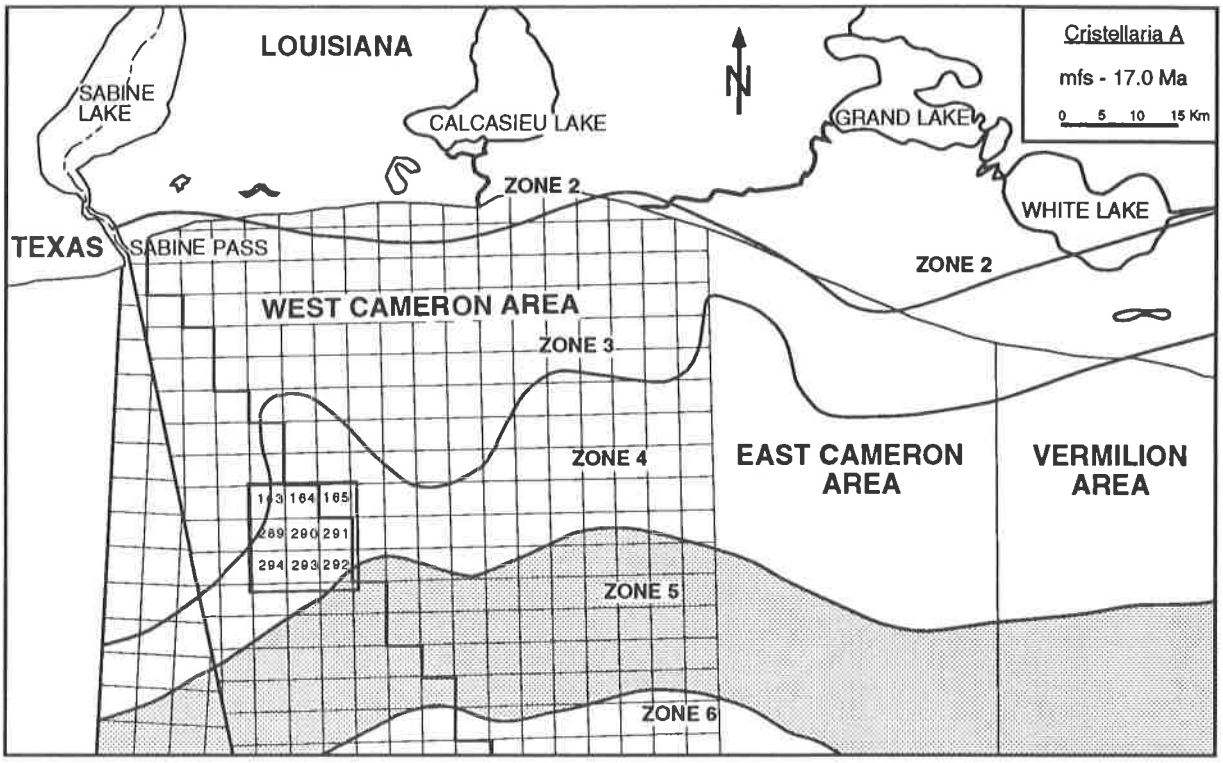

A-2-7: Cristellaria A (mfs, 17.0 Ma) marine environments map offshore Louisiana reconstructed from the OCS MMS Report (wells and seismic sections, 1987) and unpublished data. See fig. 2-4 for marine environments nomenclature.

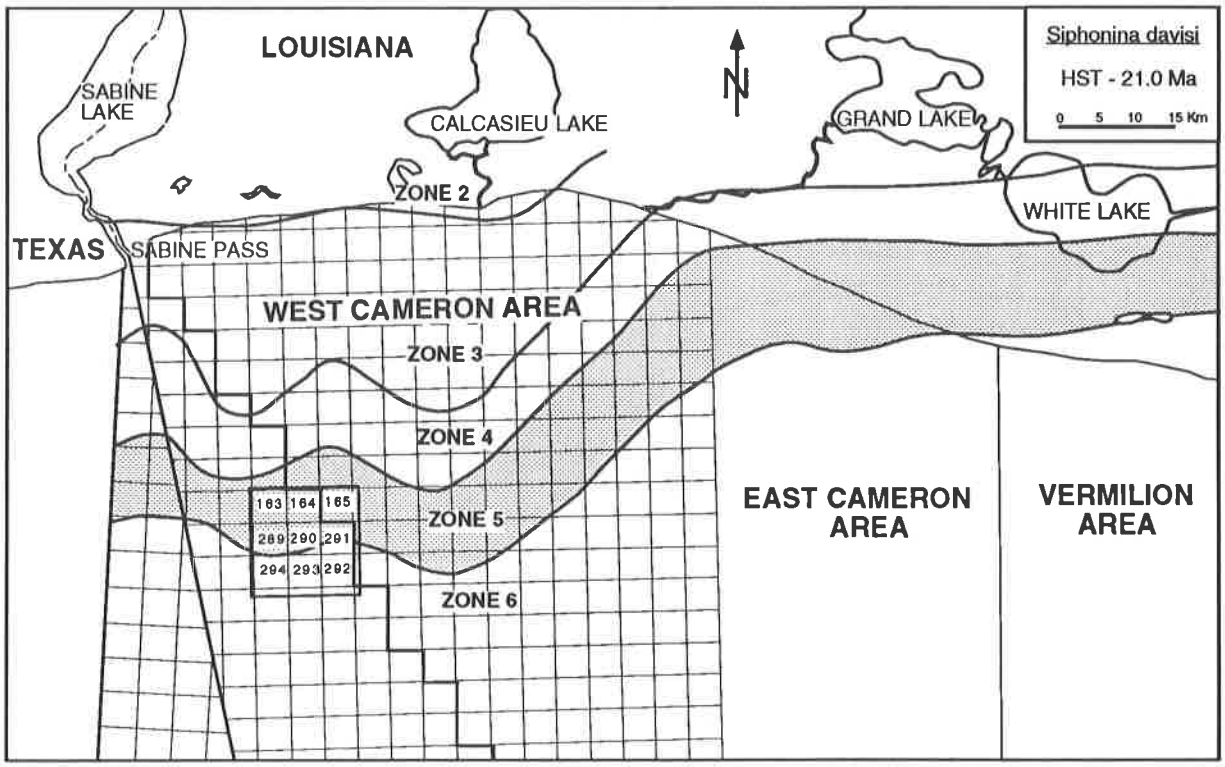

A-2-8: Siphonina davisi (Hst, 21.0 Ma) marine environments map offshore Louisiana reconstructed from the OCS MMS Report (wells and seismic sections, 1987) and unpublished data. See fig. 2-4 for marine environments nomenclature.

ANNEXE 3

Well log interpretation procedure and correlation to 2D and 3D seismic data (modified from Vail, 1992).

Data needed:
- Well logs, dipmeter logs
- Biostratigraphy regional tables, microfossils checklists
- 2D and 3D seismic sections
- Synthetics seismograms, time-depth conversion charts
- Well logs cross sections (random lines through wells)

Step 1: Interpret rock type from well logs (shale / silt / sands).

- Gamma ray, Spontaneous potential.
- Sonic, Resistivity
- Porosity logs

Step 2: Interpret depositional environments from well logs.

- Palaeontology (cores and cuttings)
- Well log patterns

Step 3: Interpret major transgressive / regressive facies cycles on well logs.

- 2nd - 3rd Order cycles (3-50 Ma and 0.5-3 Ma, respectively)

Step 4: Identify condensed sections and locate on well logs (based on Biostratigraphy).

- Abundance peaks and diversity peaks
- Total organic matter peaks

Step 5: Date condensed sections with Biostratigraphy.

- attribute an age to each condensed sections
- tie to global and local cycle chart
- check for missing or stacked condensed sections for indicators of faults, slump scars, canyons or multiple sequence starvation

Step 6: Identify discontinuities from dipmeter logs.

Step 7: Interpret sequences and systems tracts on well logs.

Step 8: Interpret sequences, systems tracts and faults on seismic data from reflector termination patterns (on 2D) and seismic vertical and horizontal facies (on 3D, seismic attributes and volume attributes).

- Identify discontinuities, sequences and systems tracts
- Tie sequences and systems tracts boundaries to wells with synthetics seismograms or/and time-depth conversion charts
- Check the interpretation with closing loops on seismic data

Step 9: Correlate well logs by parasequences / marker bed correlation.

- On individual wells, identify parasequences and marker beds within systems tracts
- Correlate sequences and systems tracts between well logs following seismic correlation and biostratigraphic age
- Correlate parasequences and marker beds between wells, starting near the main flooding surfaces

Step 10: Transfer sequences, systems tracts and parasequences boundaries to well log cross sections and extend to the rest of seismic data.

- Mark porous clean sands, porous carbonate beds, amplitude anomalies, erosional features.

Step 11: Make summary, local chronostratigraphic chart showing sequences and systems tracts.

Step 12: Make sequence boundary based tectonic subsidence curves.

- Relate changes in ratio of tectonic subsidence to major transgressive/regressive facies cycles
- Calculate eustatic variations
- Plot summary curves on chronostratigraphic chart

Step 13: Map sequences and systems tracts for interpreting paleogeography and geologic history.

- 2D =>regional contour map with facies superposed
- 3D =>local amplitude maps on systems tracts interface or on sediments volumes.

Step 14: Identify and map resource plays and prospects.

References:

Vail, P.R. (1992): A course note on sequence stratigraphy. Rice University-Houston Texas.

GMA LOGM
KB ELEVATION=77.0 FT

TIME DATUM	=0.0 FT	LOGS USED IN RC CALC.	=SONIC ONLY	SAMPLE INTERVAL	=0.5 MS
AGC LENGTH	=500.0 MS	AMPLITUDE	=1.0	TRACES PER INCH	=18.0
# OF TRACES	=10	INCHES PER SEC	=5.00	CHECK SHOT APPLIED	=Y
MULTIPLES	=NONE				

WAVELET # 1 TIME VARIANT WAVELET :
3 Component Wavelets

T.V.WAVELET #1.1 ORMSBY :
FREQ. 1 =10.0 Hz
FREQ. 2 =20.0 Hz
FREQ. 3 =50.0 Hz
FREQ. 4 =70.0 Hz
PHASE =MINIMUM

T.V.WAVELET #1.2 ORMSBY :
FREQ. 1 =10.0 Hz
FREQ. 2 =20.0 Hz
FREQ. 3 =45.0 Hz
FREQ. 4 =50.0 Hz
PHASE =MINIMUM

T.V.WAVELET #1.3 ORMSBY :
FREQ. 1 =8.0 Hz
FREQ. 2 =16.0 Hz
FREQ. 3 =30.0 Hz
FREQ. 4 =35.0 Hz
PHASE =MINIMUM

FORMATION	DEPTH ft(KB)	DEPTH ft(ASL)	TIME Seconds	AVG VEL ft/s	RMS VEL ft/s	INT VEL ft/s	INT TIME Seconds	INT DEN g/cc
Big A	5292	-5215	1.478	7057	7099			
Fault	5670	-5593	1.577	7091	7131	7594	0.100	0.000
Disc 12	5998	-5921	1.665	7111	7150	7477	0.088	0.000
Tex L	6338	-6261	1.754	7140	7178	7678	0.089	0.000
Big 2	6711	-6634	1.850	7170	7207	7724	0.097	0.000
Tex M	7585	-7508	2.063	7279	7320	8225	0.213	0.000
HST WC153	7700	-7623	2.090	7294	7335	8418	0.027	0.000
Big Hum Sd	7845	-7768	2.122	7320	7364	8994	0.032	0.000
Big Hum	8050	-7973	2.163	7371	7423	10000	0.041	0.000
Cib Op	8612	-8535	2.278	7494	7563	9824	0.114	0.000
Fault	8626	-8549	2.281	7496	7565	9543	0.003	0.000
Fault	8730	-8653	2.303	7516	7587	9573	0.022	0.000
Cib Op Sd	9002	-8925	2.358	7570	7647	9801	0.056	0.000
Cib Op E	9810	-9733	2.530	7694	7779	9391	0.172	0.000
LKG	9896	-9819	2.547	7710	7797	10126	0.017	0.000
Fault	10170	-10093	2.607	7743	7830	9131	0.060	0.000
Amph B	10236	-10159	2.622	7750	7838	9026	0.015	0.000
10500 Sd	10422	-10345	2.663	7771	7859	9126	0.041	0.000
Rob L	10534	-10457	2.687	7784	7873	9212	0.024	0.000
Regional 90	10623	-10546	2.706	7794	7883	9181	0.019	0.000
11100 Sd	10940	-10863	2.775	7829	7918	9192	0.069	0.000
10650 Sd	11131	-11054	2.817	7847	7937	9048	0.042	0.000
Fault	11195	-11118	2.831	7853	7943	9128	0.014	0.000
Perf	11224	-11147	2.838	7855	7945	8783	0.007	0.000
thru	11294	-11217	2.853	7863	7954	9385	0.015	0.000
Deep Pay	11423	-11346	2.880	7878	7969	9372	0.028	0.000
Zone 5	11534	-11457	2.905	7888	7979	9153	0.024	0.000
Rob May eq.	11650	-11573	2.931	7898	7989	8955	0.026	0.000
Rob May 1	11862	-11785	2.978	7914	8004	8905	0.048	0.000
Fault?	12089	-12012	3.028	7933	8023	9043	0.050	0.000
12800 Sd	12770	-12693	3.180	7984	8073	9002	0.151	0.000
14100 Sd	14024	-13947	3.440	8110	8204	9651	0.260	0.000

A-3-1: Information for synthetic log calculation on Well 2.

TWT ms	Depth ft	Depth m	TWT ms	Depth ft	Depth m	TWT ms	Depth ft	Depth m	TWT ms	Depth ft	Depth m	TWT ms	Depth ft	Depth m	TWT ms	Depth ft	Depth m
0.5	1504	458	1	3328	1014	1.5	5300	1615	2	7246	2209	2.5	9600	2926	3	11887	3623
0.51	1540	469	1.01	3368	1027	1.51	5338	1627	2.01	7288	2221	2.51	9646	2940	3.01	11932	3637
0.52	1575	480	1.02	3408	1039	1.52	5375	1638	2.02	7330	2234	2.52	9692	2954	3.02	11977	3651
0.53	1611	491	1.03	3449	1051	1.53	5413	1650	2.03	7372	2247	2.53	9738	2968	3.03	12022	3664
0.54	1647	502	1.04	3489	1063	1.54	5451	1661	2.04	7414	2260	2.54	9784	2982	3.04	12067	3678
0.55	1683	513	1.05	3529	1076	1.55	5489	1673	2.05	7456	2273	2.55	9830	2996	3.05	12112	3692
0.56	1718	524	1.06	3569	1088	1.56	5526	1684	2.06	7498	2285	2.56	9875	3010	3.06	12156	3705
0.57	1754	535	1.07	3609	1100	1.57	5564	1696	2.07	7540	2298	2.57	9921	3024	3.07	12201	3719
0.58	1790	546	1.08	3650	1113	1.58	5602	1707	2.08	7582	2311	2.58	9967	3038	3.08	12246	3733
0.59	1825	556	1.09	3690	1125	1.59	5639	1719	2.09	7624	2324	2.59	10013	3052	3.09	12291	3746
0.6	1861	567	1.1	3730	1137	1.6	5677	1730	2.1	7666	2337	2.6	10059	3066	3.1	12336	3760
0.61	1897	578	1.11	3770	1149	1.61	5715	1742	2.11	7715	2352	2.61	10105	3080	3.11	12382	3774
0.62	1932	589	1.12	3810	1161	1.62	5753	1754	2.12	7763	2366	2.62	10151	3094	3.12	12428	3788
0.63	1968	600	1.13	3850	1173	1.63	5790	1765	2.13	7812	2381	2.63	10197	3108	3.13	12474	3802
0.64	2004	611	1.14	3890	1186	1.64	5828	1776	2.14	7860	2396	2.64	10243	3122	3.14	12520	3816
0.65	2040	622	1.15	3930	1198	1.65	5866	1788	2.15	7908	2410	2.65	10289	3136	3.15	12566	3830
0.66	2075	632	1.16	3970	1210	1.66	5904	1800	2.16	7957	2425	2.66	10334	3150	3.16	12611	3844
0.67	2111	643	1.17	4010	1222	1.67	5942	1811	2.17	8005	2440	2.67	10380	3164	3.17	12657	3858
0.68	2147	654	1.18	4050	1234	1.68	5979	1822	2.18	8054	2455	2.68	10246	3123	3.18	12703	3872
0.69	2182	665	1.19	4090	1247	1.69	6017	1834	2.19	8102	2469	2.69	10472	3192	3.19	12749	3886
0.7	2218	676	1.2	4130	1259	1.7	6055	1846	2.2	8151	2484	2.7	10518	3206	3.2	12795	3900
0.71	2254	687	1.21	4170	1271	1.71	6094	1857	2.21	8200	2499	2.71	10564	3220	3.21	12841	3914
0.72	2289	698	1.22	4210	1283	1.72	6132	1869	2.22	8249	2514	2.72	10610	3234	3.22	12887	3928
0.73	2325	709	1.23	4250	1295	1.73	6171	1881	2.23	8298	2529	2.73	10656	3248	3.23	12933	3942
0.74	2360	719	1.24	4290	1308	1.74	6209	1893	2.24	8347	2544	2.74	10702	3262	3.24	12979	3956
0.75	2396	730	1.25	4330	1320	1.75	6248	1904	2.25	8396	2559	2.75	10748	3276	3.25	13025	3970
0.76	2431	741	1.26	4370	1332	1.76	6286	1916	2.26	8444	2574	2.76	10793	3290	3.26	13070	3984
0.77	2467	752	1.27	4410	1344	1.77	6325	1928	2.27	8493	2589	2.77	10839	3304	3.27	13116	3998
0.78	2502	763	1.28	4450	1356	1.78	6363	1939	2.28	8542	2604	2.78	10885	3318	3.28	13162	4012
0.79	2538	774	1.29	4490	1369	1.79	6402	1951	2.29	8591	2619	2.79	10931	3332	3.29	13208	4026
0.8	2573	784	1.3	4530	1381	1.8	6440	1963	2.3	8640	2633	2.8	10977	3346	3.3	13254	4040
0.81	2609	795	1.31	4569	1393	1.81	6479	1975	2.31	8688	2648	2.81	11023	3360	3.31	13304	4055
0.82	2644	806	1.32	4607	1404	1.82	6517	1986	2.32	8736	2663	2.82	11069	3374	3.32	13353	4070
0.83	2680	817	1.33	4646	1416	1.83	6556	1998	2.33	8784	2677	2.83	11115	3388	3.33	13403	4085
0.84	2715	828	1.34	4684	1428	1.84	6595	2010	2.34	8832	2692	2.84	11161	3402	3.34	13452	4100
0.85	2751	839	1.35	4723	1440	1.85	6634	2022	2.35	8880	2707	2.85	11207	3416	3.35	13502	4115
0.86	2787	849	1.36	4761	1451	1.86	6672	2034	2.36	8928	2721	2.86	11252	3430	3.36	13552	4131
0.87	2822	860	1.37	4800	1463	1.87	6711	2046	2.37	8976	2736	2.87	11298	3444	3.37	13601	4146
0.88	2858	871	1.38	4838	1475	1.88	6750	2057	2.38	9024	2751	2.88	11344	3458	3.38	13651	4161
0.89	2893	882	1.39	4877	1487	1.89	6788	2069	2.39	9072	2765	2.89	11390	3472	3.39	13700	4176
0.9	2929	893	1.4	4915	1498	1.9	6827	2081	2.4	9120	2780	2.9	11436	3486	3.4	13750	4191
0.91	2969	905	1.41	4954	1510	1.91	6869	2094	2.41	9168	2794	2.91	11481	3499	3.41	13800	4206
0.92	3009	917	1.42	4992	1522	1.92	6911	2106	2.42	9216	2809	2.92	11526	3513	3.42	13850	4221
0.93	3049	929	1.43	5031	1533	1.93	6953	2119	2.43	9264	2824	2.93	11571	3527	3.43	13900	4237
0.94	3089	942	1.44	5069	1545	1.94	6995	2132	2.44	9312	2838	2.94	11616	3541	3.44	13950	4252
0.95	3129	954	1.45	5108	1557	1.95	7037	2145	2.45	9360	2853	2.95	11662	3555	3.45	14000	4267
0.96	3168	966	1.46	5146	1569	1.96	7078	2157	2.46	9408	2868	2.96	11707	3568			
0.97	3208	978	1.47	5185	1580	1.97	7120	2170	2.47	9456	2882	2.97	11752	3582			
0.98	3248	990	1.48	5223	1592	1.98	7162	2183	2.48	9504	2897	2.98	11797	3596			
0.99	3288	1002	1.49	5262	1604	1.99	7204	2196	2.49	9552	2911	2.99	11842	3609			

A-3-2: Velocity law table for correlation of the five other wells to the synthetic on Well 2.

ANNEXE 4

Total subsidence calculation and growth fault throw table.

A	Well 2/Horizons	Ancient names	Depth ms	Depth ft	Depth m	Age Ma
0	HP 2	HP2	476.00	1432.0	436.00	1.2200
1	HP 1	HP1	544.00	1661.0	506.00	1.4700
2	LOPLEIST	MPM2 (Pleist1)	640.00	2004.0	611.00	1.7200
3	LATEPLIO	MPM1 (Pleist 2)	736.00	2346.0	715.00	2.1000
4	SB 2.4	new	816.00	2630.0	802.00	2.4000
5	MPLIO0	LPM1 (UPPLION)	964.00	3184.0	970.00	2.7000
6	LOPLIO2	UPLIOM	1128.0	3842.0	1171.0	4.9000
7	LOPLIO	LOPLIOM2 (loplio)	1196.0	4114.0	1254.0	5.2000
8	TOPMIO	new	1304.0	4545.0	1385.0	5.7000
9	TOPMIODL	LPLIOM1 test2	1336.0	4669.0	1423.0	5.9000
10	LM2B	UMM2B	1552.0	5496.0	1675.0	8.2000
11	LM1	UMM1	1688.0	6010.0	1832.0	9.0000
12	MM9	MM9	1804.0	6455.0	1967.0	10.200
13	MM7	MM7	2012.0	7296.0	2224.0	12.600
14	MM5	MM5	2312.0	8698.0	2651.0	15.200
15	SB 15.5b	new	2388.0	9062.0	2762.0	15.500
16	EM5	EM5	2580.0	9967.0	3038.0	16.000
17	EM1	EM1	3248.0	13015	3967.0	17.300

B	Well 3/Horizons	Depth ms	Depth ft	Depth m	Age Ma
0	HP6	92.000	226.00	69.000	0.16000
1	HP5	260.00	702.00	214.00	0.55000
2	HP 4	340.00	919.00	280.00	0.77000
3	HP 2	504.00	1518.0	463.00	1.2200
4	HP 1	568.00	1747.0	532.00	1.4700
5	LOPLEIST	644.00	2018.0	615.00	1.7200
6	LATEPLIO	756.00	2417.0	737.00	2.1000
7	SB 2.4	836.00	2701.0	823.00	2.4000
8	MPLIO0	996.00	3312.0	1009.0	2.7000
9	LOPLIO2	1188.0	4082.0	1244.0	4.9000
10	LOPLIO	1252.0	4338.0	1322.0	5.2000
11	TOPMIO	1364.0	4776.0	1456.0	5.7000
12	TOPMIODL	1416.0	4977.0	1517.0	5.9000
13	LM2B	1652.0	5874.0	1790.0	8.2000
14	LM1	1872.0	6719.0	2048.0	9.0000
15	MM9	1964.0	7095.0	2163.0	10.200
16	MM7	2216.0	8229.0	2508.0	12.600
17	MM5	2604.0	10077	3071.0	15.200
18	SB 15.5b	2712.0	10573	3223.0	15.500
19	EM5	2884.0	11363	3463.0	16.000
20	EM1	3464.0	14136	4308.0	17.300

A-4-1: Age in Ma and depth (in ms, in feet and meter from the velocity law on Well 2) for the main interpreted horizons. ***a.*** *On Well 2.* ***b.*** *On Well 3.*

Interval	Age Ma	Thickness W3	ecolog. zone	lithology	Thickness/W2	lithology
0-HP6	0 M a	69	IN	sa+si		
HP6-HP5	0.16	145	IN	sa+si		
HP5-HP4	0.55	66	IN	sa		
HP4-HP2	0.77	183	IN	sa+a		
HP2-HP1	1.22	69	IN	sa	70	sa
HP1-LOP	1.47	83	IN	si+a	105	si+a
LOP-LAT	1.72	122	IN	sa+si	104	sa+si
LAT-SB	2.1	86	IN	sa+si	87	sa+si
SB-MP	2.4	186	IN	si	168	si
MP-LOP2	2.7	235	IN	si	201	sa
LOP2-LOP	4.9	78	MN	sa+a	83	sa+si
LOP-TOP	5.2	134	MN	sa+si	131	sa+si
TOP-TOPD	5.7	61	MN	si+a	38	si+a
TOPD-LM2	5.9	273	MN	si	252	si
LM2-LM1	8.2	258	MN	si+a	157	si+a
LM1-MM9	9	115	MN	sa+si	135	sa+si
MM9-MM7	10.2	345	MN	sa+si	257	sa+si
MM7-MM5	12.6	563	ON	sa+si	427	sa+si
MM5-SB15	15.2	152	ON	sa	111	sa
SB15-EM5	15.5	240	ON-UP	sa+si	276	sa+si
EM5-EM1	16	845	UP	sa	929	sa
EM1	17.3					
Paleodepth	0 m	25 m	80m	200 m	300 m	
Age Ma	2.7 Ma	10.2 Ma	15.2 Ma	15.5 Ma	16.0 Ma	

A-4-2: Table for total subsidence calculation on Well 2 and Well 3. Initial water column on Well 2: 300 m and 500 m on Well 3. Sa, sand; Si, silt; A, Shale. Depositional environment: IN, inner neritic; MN, Middle neritic; ON, Outer neritic; UPB, upper bathyal.

Horizons	Age My	F1	F1bis	F2A	F2A/riwel3	F3B/riwel3	F4A/riwel1	F5/riwel1	F5B/riwel3	F6/riwel1	F6Bn/riwel1
HP6 m	0.16						channel		4		
HP5 m	0.55			channel			4		4		
HP4 m	0.77	16	16	4		channel	4		9		
HP2 m	1.22	26	26	9		4	22	17	13		
HP1 m	1.47	28	28	9		4	35	22	26	4	
LOPLEIST m	1.72	48	48	9		18	35	31	22	9	
LATEPLIO m	2.1	24	24	24		38	38	38	5	24	
SB2.4 m	2.4	30	30	22	14	5	43	53	19	24	
MPLIO m	2.7	49	49	39	15	49	49	24	39	24	10
LOPLIO2 m	4.9	71	71	49	25	49	69	49	49	49	25
LOPLIO m	5.2	71	71	54	49	54	69	49	69	54	30
TOPMIO m	5.7	74	74	54	30	39	79	54	69	49	25
TOPMIODL m	5.9	78	78	49	34	49	78	49	73	54	34
LM2B m	8.2	64	64	59	39	66	84	64	89	69	34
LM1 m	9	51	51	66	41	66	81	91	109	102	46
MM9 m	10.2	113	120	70	49	76	32	92	130	97	54
MM7 m	12.6	226	254	83	55	75	44	116	155	110	6
MM5 m	15.2	291	330	73	84	84	0		179	118	0
SB15.5b m	15.5	274	330	62	45	95	39		162	118	0
EM5 m	16	327	384	59	73	90	85		178	152	0
Horizons	Age My	F6B/ant	F6A/ant	F6E/ant	F7	F7B/lnl.570	F8/lnl.5	F8B/lnl.570	F9/l.570	F9A/l.570	F9B/l.570
HP6 m	0.16				5						
HP5 m	0.55				8						
HP4 m	0.77				11						
HP2 m	1.22	channel			13						
HP1 m	1.47	4			17						
LOPLEIST m	1.72	9	4		22		channel				
LATEPLIO m	2.1	14	5		34	5	5	channel			
SB2.4 m	2.4	14	10		36	10	5	5	0	5	
MPLIO m	2.7	20	24		39	29	15	20	5	20	
LOPLIO2 m	4.9	34	30	30	54	49	44	30	10	34	5
LOPLIO m	5.2	34	34	30	54	49	54	32	20	37	20
TOPMIO m	5.7	34	39	42	54	44	39	34	15	20	25
TOPMIODL m	5.9	39	44	34	68	54	44	39	20	29	24
LM2B m	8.2	44	49	39	93	74	39	42	30	44	34
LM1 m	9	51	51	56	127	112	41	56	5	18	30
MM9 m	10.2	38	54	65	173	86	59	65	5	22	43
MM7 m	12.6	61	55	72	237	94		77		11	52
MM5 m	15.2	50	45	76	666						
SB15.5b m	15.5	39	50	84	672						
EM5 m	16	68	62	147	513						

A-4-3: Table of measured fault throw (in m, calculated from ms) along major interpreted horizons.

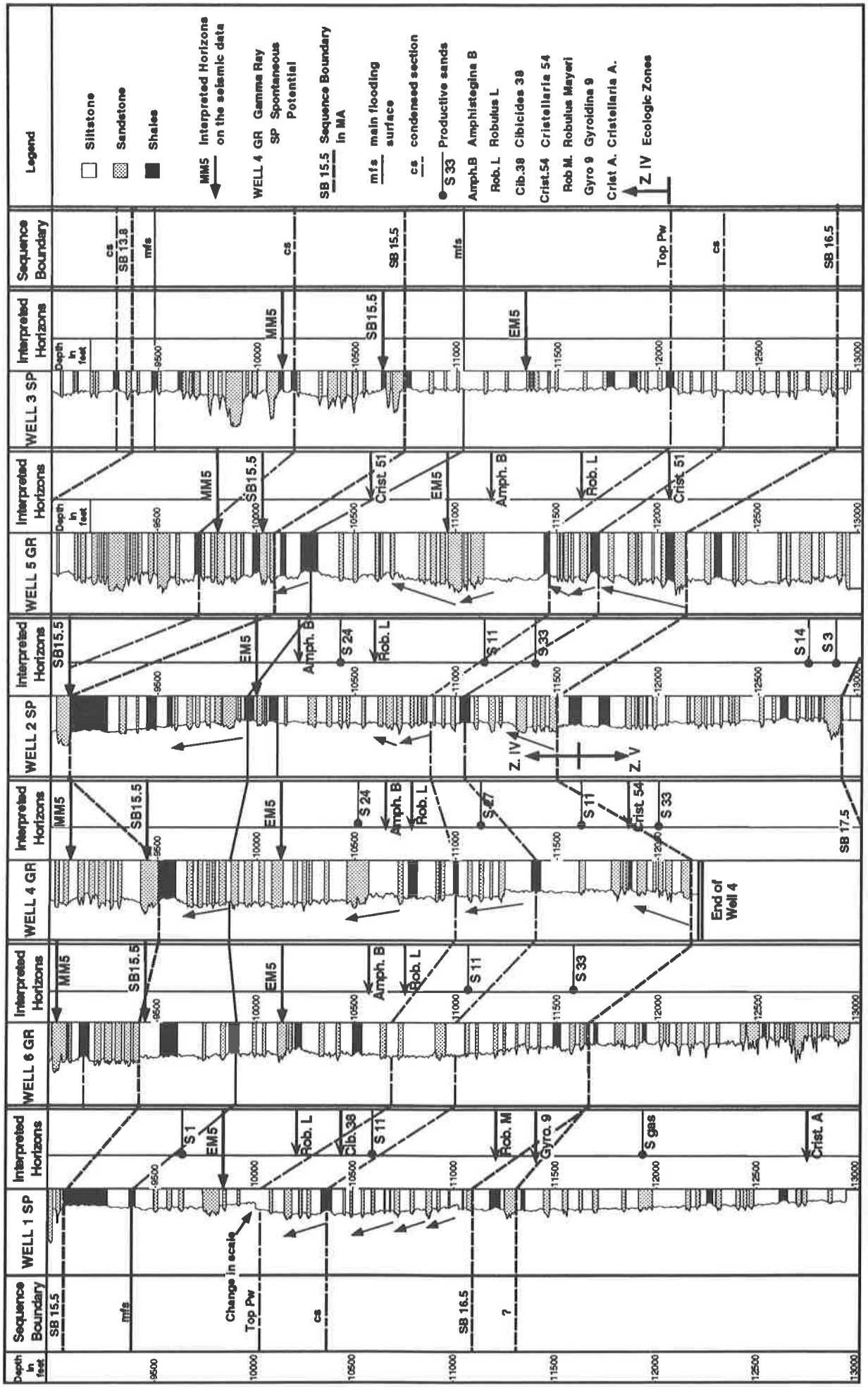

A-4-4: North-south well log interpreted transect for the basal Middle Miocene productive sequences (not discussed in Chapter 5).

PLATE 1

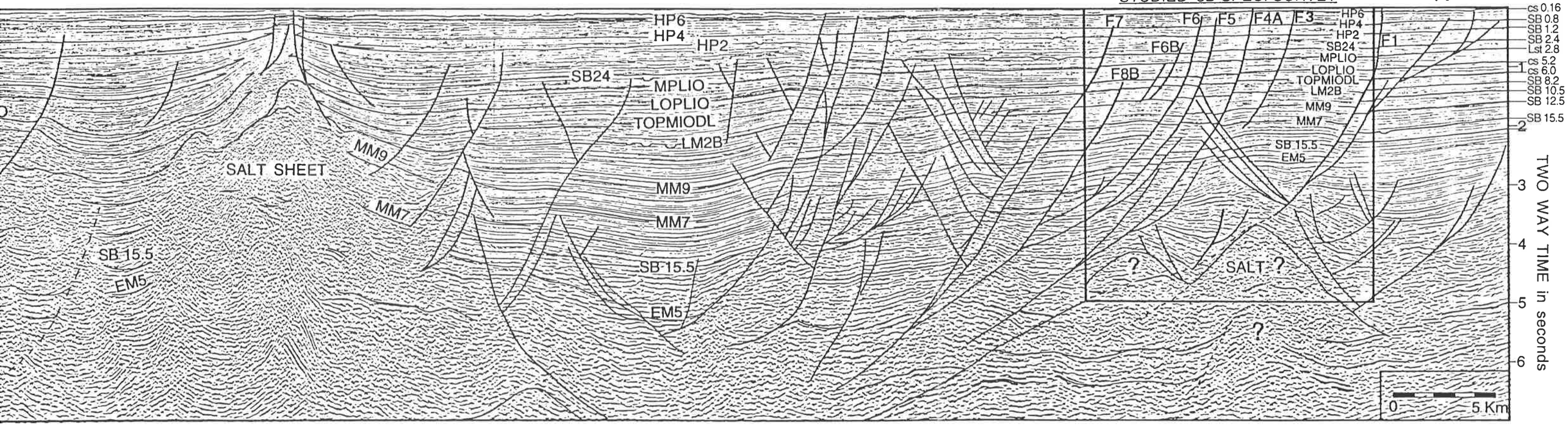

Fig. 1-9 (PLATE 1): Regional north-south cross section across the studied area. Extrapolation of the major interpreted horizon from the 3D survey to the entire offshore Louisiana shelf. Tectonic and total subsidence in the studied area is controlled by the large allochtonous salt sheet 40 km offshore (published with the permission of TGS-CALIBRE Geophysical Company and GECO-PRAKLA).

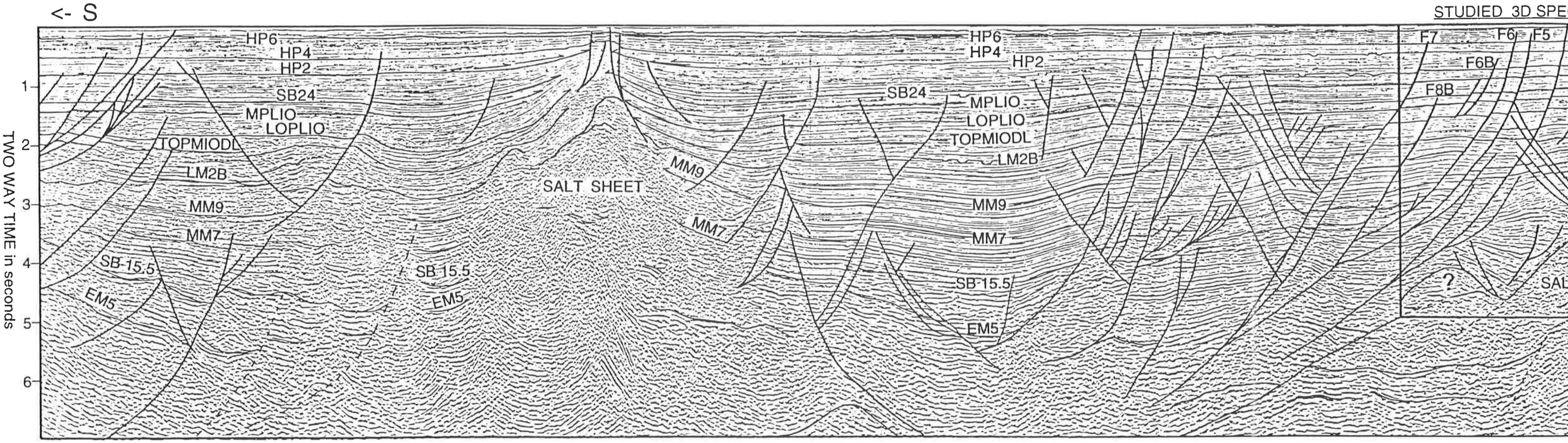

Fig. 1-9 (PLATE 1): Regional north-south c
Extrapolation of the major interpreted horizon fr
Louisiana shelf. Tectonic and total subsidence in
allochtonous salt sheet 40 km offshore (published
Geophysical Company and GECO-PRAKLA).

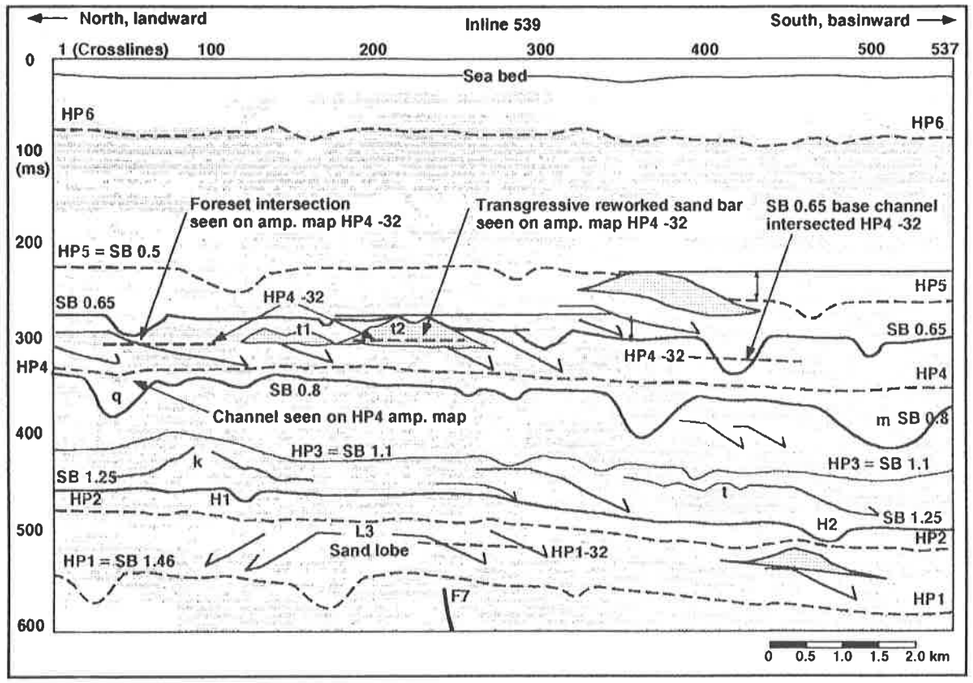

Fig. 5-7: North-south vertical seismic section (Inline 539, see fig. 5-5 for location) showing facies and sequence stratigraphic interpretation superposed on seismic data for the Upper Pleistocene.

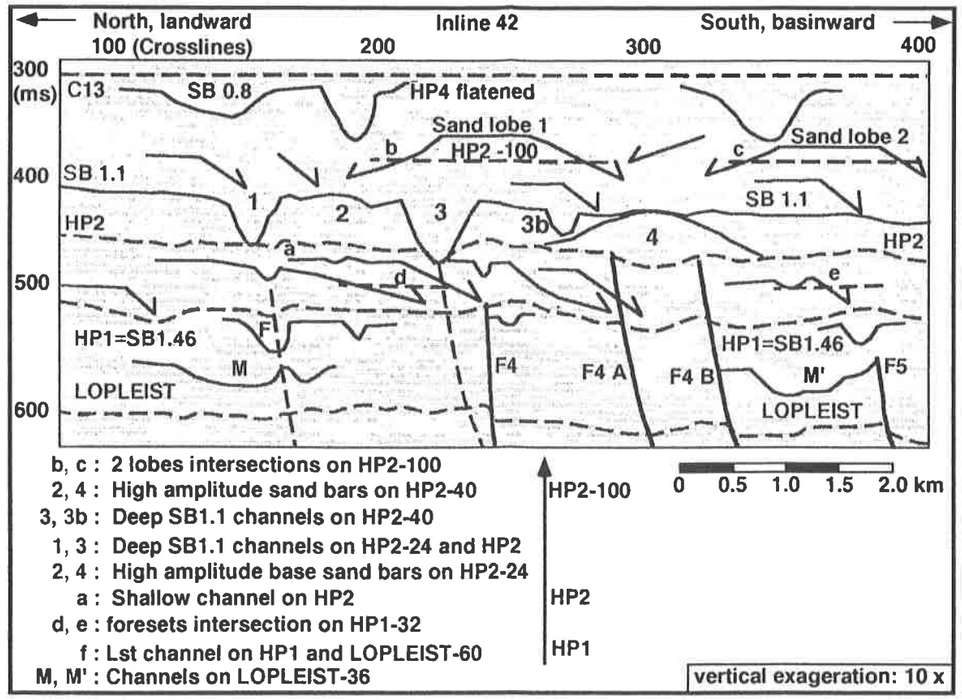

Fig. 5-14: North-south seismic section (data and interpretation) in the western part of the 3D survey (Inline 42). Interpreted horizons are dashed lines. HP4 horizon is flattened to restore the subjacent sediment morphology.

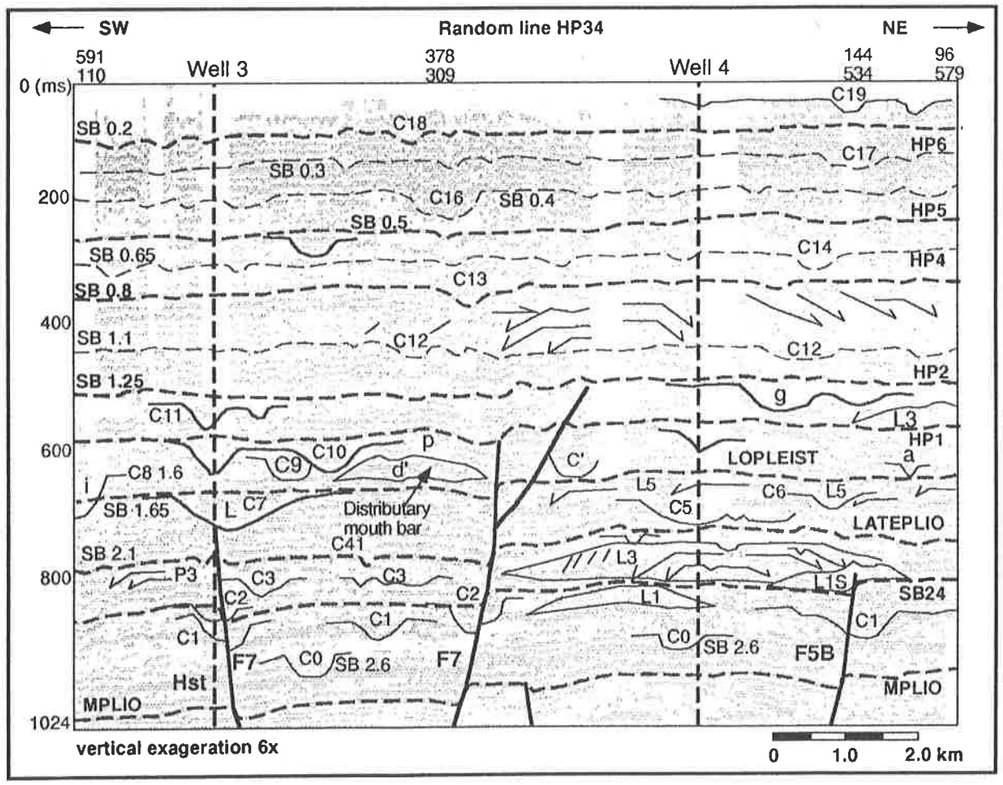

Fig. 5-22: NE-SW random seismic section (HP34), connecting Well 3 to Well 4 (shaded seismic data with superposed interpretation , see fig. 5-25 for location). This line is perpendicular to the main direction of sediment input and intersects most main channels.

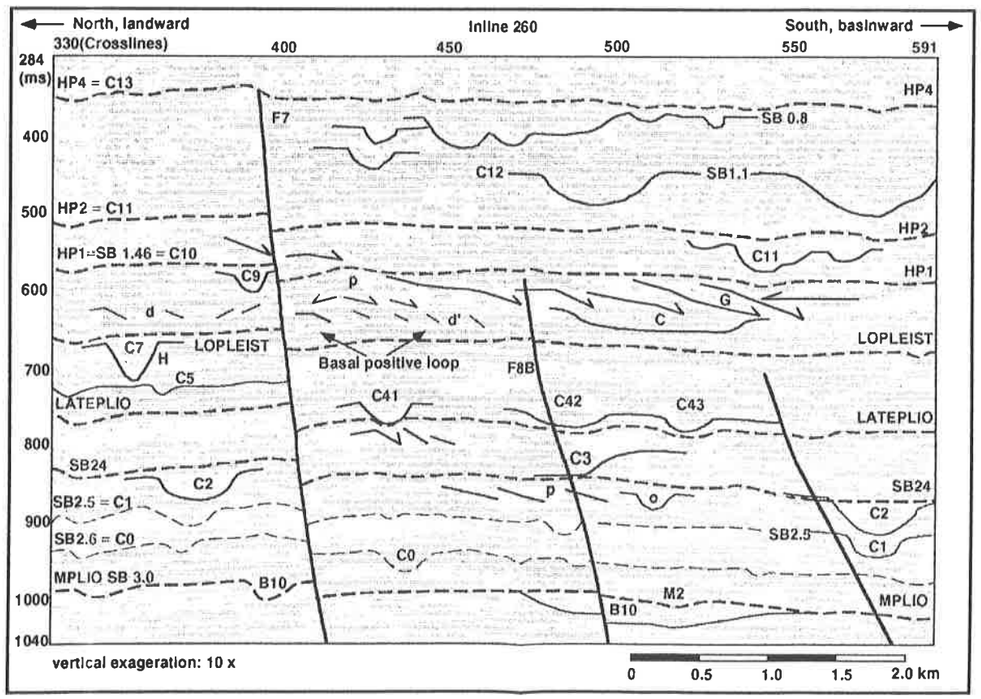

Fig. 5-23: Offshore portion of the North-south Inline 260, across the F7 main growth fault (see fig. 5-25 for location). Raster density seismic data with superposed interpretation and location of erosional surfaces (C = Gulf coast Pleistocene, B = Middle and Late Miocene).

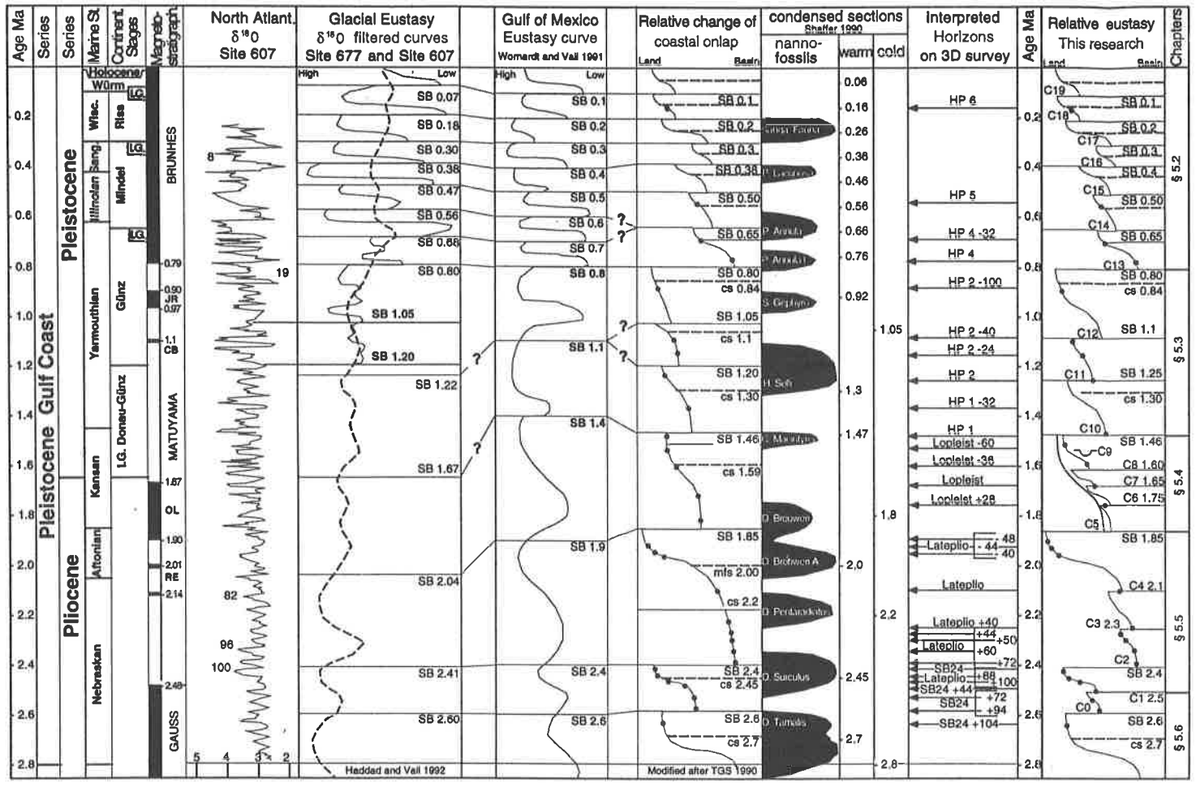

Fig. 5-6: Synthetic Pleistocene chart with series and continental stages, oxygen isotopes reference curve, eustatic and coastal onlap curves in the Gulf of Mexico, histogram of faunal abundance and presented amplitude maps(black dots). Note the four chapters: **a.** §5.2 Upper Pleistocene 4th Order sequences discussion; **b.** §5.3 Lower Pleistocene, one or two 3rd Order sequence; **c.** §5.4 Plio-Pleistocene limit; **d.** §5.5 One large 3rd Order sequence.

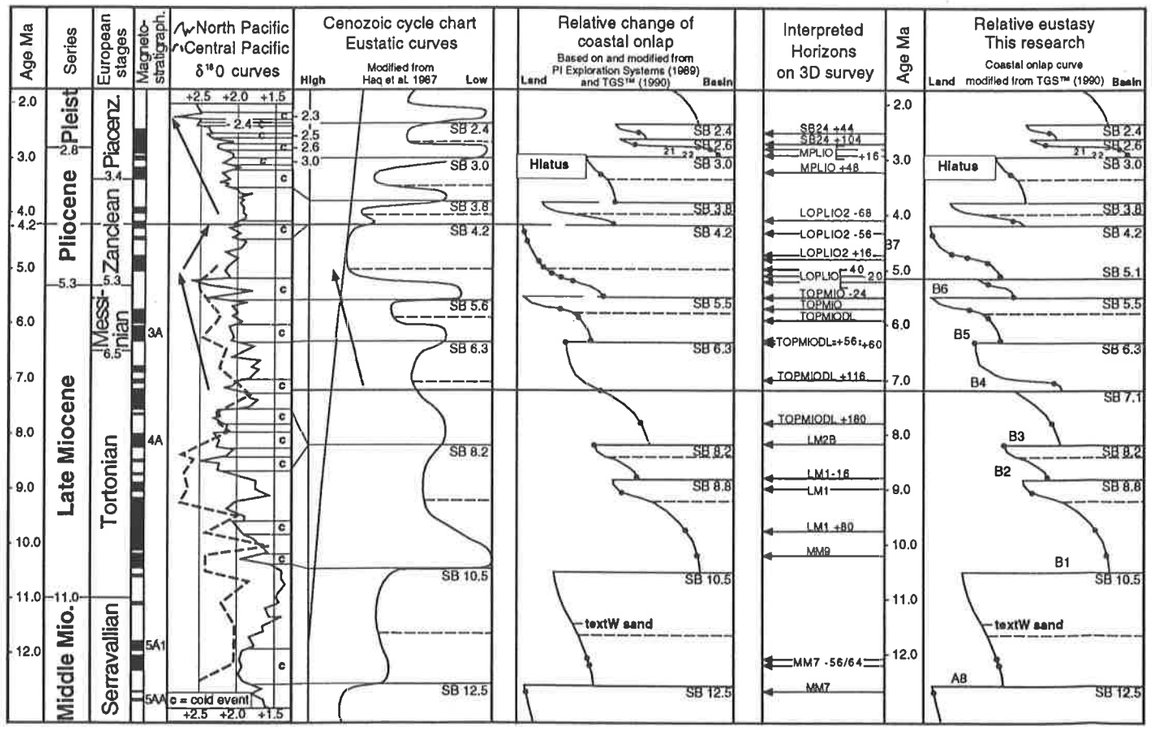

Fig. 5-40: Neogene synthetic chart with comparison of oxygen isotopes curves in the Pacific, global eustatic curves (Haq et al. 1987), a curve of relative coastal onlap for the Gulf of Mexico from PI Exploration Systems, (1989) and TGS™ (1990) and the curve of relative coastal onlap proposed by this study. Interpreted horizon on the 3D seismic data are indicated by black dots on the coastal onlap curve.

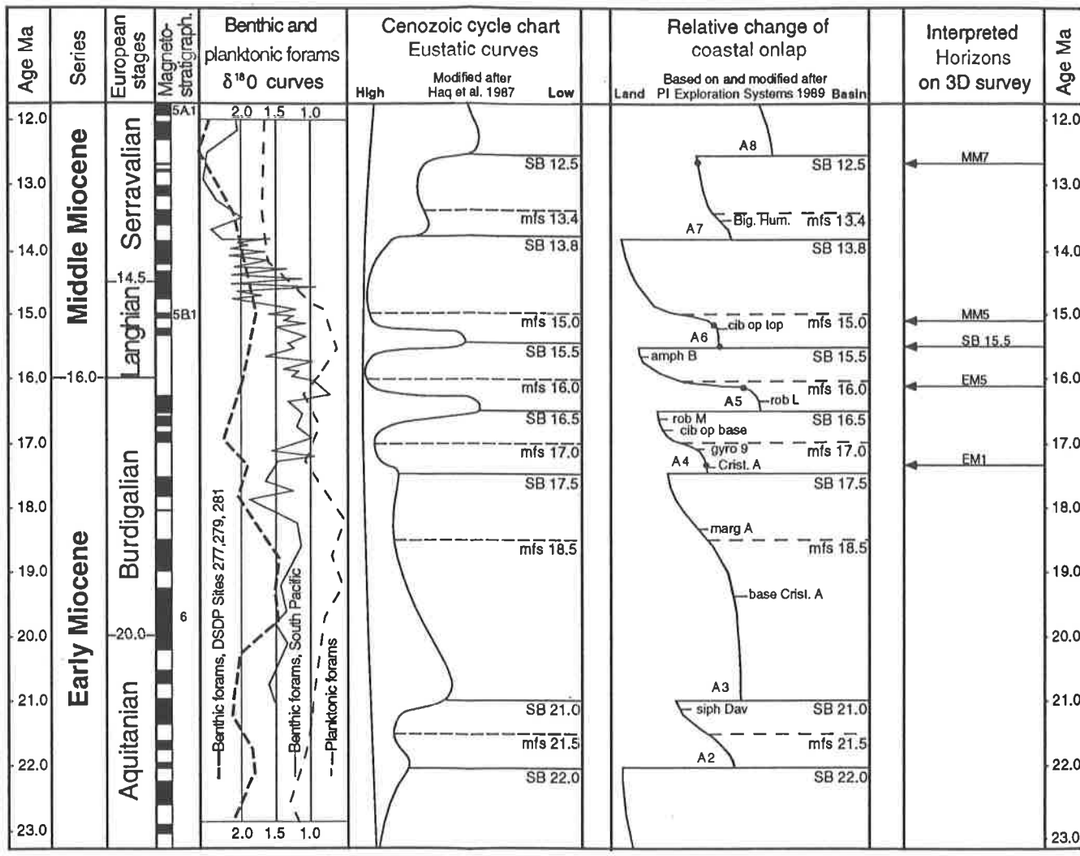

Fig. 5-58: Synthetic Early and Middle Miocene chart with series and continental stages, oxygen isotopes reference curve, eustati and coastal onlap curves in the Gulf of Mexico, and interpreted horizons (black dots).

Mémoires de Géologie (Lausanne)

No. 1 BAUD A. 1987. Stratigraphie et sédimentologie des calcaires de Saint-Triphon (Trias, Préalpes, Suisse et France). 202 pp., 53 text-figs., 29 pls.

No. 2 ESCHER A, MASSON H. and STECK A. 1988. Coupes géologiques des Alpes occidentales suisses. 11 pp., 1 text-figs., 1 map

No. 3 STUTZ E. 1988. Géologie de la chaîne Nyimaling aux confins du Ladakh et du Rupshu (NW-Himalaya, Inde). Evolution paléogéographique et tectonique d'un segment de la marge nord-indienne. 149 pp., 42 text-figs., 11 pls. 1 map.

No. 4 COLOMBI A. 1989. Métamorphisme et géochimie des roches mafiques des Alpes ouest-centrales (géoprofil Viège-Domodossola-Locarno). 216 pp., 147 text-figs., 2 pls.

No. 5 STECK A., EPARD J.-L., ESCHER A., MARCHANT R., MASSON H. and SPRING L. 1989 Coupe tectonique horizontale des Alpes centrales. 8 pp., 1 map.

No. 6 SARTORI M. 1990. L'unité du Barrhorn (Zone pennique, Valais, Suisse). 140 pp., 56 text-figs., 3 pls.

No. 7 BUSSY F. 1990. Pétrogenèse des enclaves microgrenues associées aux granitoïdes calco-alcalins: exemple des massifs varisque du Mont-Blanc (Alpes occidentales) et miocène du Monte Capanne (Ile d'Elbe, Italie). 309 pp., 177 text-figs.

No. 8 EPARD J.-L. 1990. La nappe de Morcles au sud-ouest du Mont-Blanc. 165 pp., 59 text-figs.

No. 9 PILLOUD C. 1991 Structures de déformation alpines dans le synclinal de Permo-Carbonifère de Salvan-Dorénaz (massif des Aiguilles Rouges, Valais). 98 pp., 59 text-figs.

No. 10 BAUD A., THELIN P. and STAMPFLI G. 1991. (Eds.) Paleozoic geodynamic domains and their alpidic evolution in the Tethys. IGCP Project No. 276. Newsletter No. 2. 155 pp.

No. 11 CARTER E.S. 1993 Biochronology and Paleontology of uppermost Triassic (Rhaetian) radiolarians, Queen Charlotte Islands, British Columbia, Canada. 132 pp., 15 text-figs., 21 pls.

No. 12 GOUFFON Y. 1993. Géologie de la "nappe" du Grand St-Bernard entre la Doire Baltée et la frontière suisse (Vallée d'Aoste -Italie). 147 pp., 71 text-figs., 2 pls.

No. 13 HUNZIKER J.C., DESMONS J., and HURFORD AJ. 1992. Thirty-two years of geochronological work in the Central and Western Alps: a review on seven maps. 59 pp., 18 text-figs., 7 maps.

No. 14 SPRING L. 1993. Structures gondwaniennes et himalayennes dans la zone tibétaine du Haut Lahul-Zanskar oriental (Himalaya indien). 148 pp., 66 text-figs, 1 map.

No. 15 MARCHANT R. 1993. The Underground of the Western Alps. 137 pp., 104 text-figs.

No. 16 VANNAY J.-C. 1993. Géologie des chaînes du Haut-Himalaya et du Pir Panjal au Haut-Lahul (NW-Himalaya, Inde). Paléogéographie et tectonique. 148 pp., 44 text-figs., 6 pls.

No. 17 PILLEVUIT A. 1993. Les blocs exotiques du Sultanat d'Oman. Evolution paleogeographique d'une marge passive flexurale. 249 pp., 138 text-figs., 7 pls.

No. 18 GORICAN S. 1994. Jurassic and Cretaceous radiolarian biostratigraphy and sedimentary evolution of the Budva Zone (Dinarides, Montenegro). 120 pp., 20 text-figs., 28 pls.

No. 19 JUD R. 1994. Biochronology and systematics of Early Cretaceous Radiolaria of the Western Tethys. 147 pp., 29 text-figs., 24 pls.

No. 20 DI MARCO, G. 1994. Les terrains accrétés du sud du Costa Rica. Evolution tectonostratigraphique de la marge occidentale de la plaque Caraïbe. 166 pp., 89 text-figs., 6 pls.

No. 21 O'DOGHERTY L. 1994. Biochronology and paleontology of Mid-Cretaceous radiolarians from Northern Apennines (Italy) and Betic Cordillera (Spain). 415 pp., 35 text-figs., 73 pls.

No. 22 GUEX J. and BAUD A. (Eds.) 1994. Recent Development on Triassic Stratigraphy. 184 pp.

No. 23 INTERRAD Jurassic -Cretaceous Working Group. BAUMGARTNER, P.O. et al. (Eds.) 1994. Middle Jurassic to Lower Cretaceous Radiolaria of Tethys: Occurrences, Systematics, Biochronolgy. env. 900 pp., 400 pls.

No. 24 REYMOND, B. 1994. Three-dimensional sequence stratigraphy offshore Louisiana, Gulf of Mexico (West Cameron 3D seismic data). 215 pp., 169 text-figs., 49 pls.

Order from **Institut de Géologie et Paléontologie,**
Université de Lausanne. BFSH-2. CH-1015, SWITZERLAND.
Bank Transfer: Banque Cantonale Vaudoise 1002 Lausanne
Account Number: **C. 323.52.56** Institut de Géologie, rubrique: Mémoires

Price $ 20 or CHF 30 per volume (volume 23 price on request) includes postage and handling.
Payment in U.S. Dollars or Swiss Francs

- Please do not send check -